ACTA POLONIAE PHARMACEUTICA

VOL. 71 No. 6 November/December 2014 ISSN 2353-5288

Drug Research

This Journal is published bimonthly by the Polish Pharmaceutical Society (Issued since 1937)

The paper version of the Publisher magazine is a prime version.
The electronic version can be found in the Internet on page
www.actapoloniaepharmaceutica.pl

An access to the journal in its electronics version is free of charge

Impact factor (2013):	0.693
MNiSW score (2013):	15 points
Index Copernicus (2012):	13.18

Charges

Annual subscription rate for 2015 is US $ 210 including postage and handling charges. Prices subject to change.
Back issues of previously published volumes are available directly from Polish Pharmaceutical Society, 16 Długa St., 00-238 Warsaw, Poland.
Payment should be made either by banker's draft (money order) issued to „PTFarm" or to our account Millennium S.A. No. 29 1160 2202 0000 0000 2770 0281, Polskie Towarzystwo Farmaceutyczne, ul. Długa 16, 00-238 Warszawa, Poland, with the memo Acta Poloniae Pharmaceutica - Drug Research.

Warunki prenumeraty

Czasopismo Acta Poloniae Pharmaceutica - Drug Research wydaje i kolportaż prowadzi Polskie Towarzystwo Farmaceutyczne, ul. Długa 16, 00-238 Warszawa.
Cena prenumeraty krajowej za rocznik 2015 wynosi 207,90 zł (w tym 5% VAT). Prenumeratę należy wpłacać w dowolnym banku lub Urzędzie Pocztowym na rachunek bankowy Wydawcy:

Millennium S.A.
29 1160 2202 0000 0000 2770 0281
Polskie Towarzystwo Farmaceutyczne
ul. Długa 16, 00-238 Warszawa

z dopiskiem: prenumerata Acta Poloniae Pharmaceutica - Drug Research.
Warunki prenumeraty zagranicznej - patrz tekst angielski.

Typeset by RADIUS, Warszawa; Printed by MCP, Marki

Acta Poloniae Pharmaceutica – Drug Research

Volume 71, Number 6 November/December 2014

CONTENTS

NINTH MULTIDISCIPLINARY CONFERENCE ON DRUG RESEARCH

REVIEWS

FULL PAPERS

APPHAX 71 (6) 883 – 1118 (2014)

SHORT COMMUNICATIONS

Editorial

The ninth Multidisciplinary Conference on Drug Research took place in very nice but somewhat isolated hotel and spa "Cztery Wiatry" ("Four Winds" on Chańcza artificial lake), near Szydłów, in Świętokrzyskie region, between 12 - 14 May, 2014. The conference gathered ca. 150 participants from many Polish scientific centers; most of them took active part in the program, which comprised 14 invited lectures, 19 short lectures and 134 poster presentations, arranged into two consecutive sessions. The opening lecture, devoted to the position of generic drugs in the present situation and future development of pharmaceutical sector, was delivered by prof. Łukasz Kaczmarek, CEO of Pharmaceutical Research Institute (IF). Details of the scientific program, which traditionally covered all aspects of drug research - from theory and design, through synthesis, to preclinical and clinical evaluation, published as Book of Abstracts (ISBN 83-89585-40-5), are also available on the website of PRI Pharmaceutical Research Institute - Instytut Farmaceutyczny). The organizers, considering informal obligation to consolidate drug research environment across various specialties and different affiliations their lasting duty, designated a panel discussion devoted to the future of the conference, in view of participants needs. It turned out that the majority would like to see continuation of MKNOL as an multidisciplinary event, supporting present design and format of the conference. Well, it certainly does not mean that everything is perfect. As we all know from everyday life - the economy is not. In the past, the organizers of MKNOL declared their support to participants, who wished to publish their proceedings in Acta Poloniae Pharmaceutica - Drug Research, in a dedicated issue. The journal, which is doing well in terms of impact factor and overall scientific trademark, has recently introduced dramatic publication policy changes, which resulted in introduction of publication charge. Under these rather suddenly declared new conditions, Pharmaceutical Research Institute (IF) is unable to continue unconditional support to all prospective authors of post - MKNOL publications. This time, from nearly 60 submitted contributions, only half could be qualified, based on the quality merit, to the sponsored pool of APP-DR November-December 2014 issue. Please accept our apologies. We will do our best to come to terms with the Editors of APP-DR over a new, clear policy concerning future publications of the MKNOL participants. Thank you for your continuing interest!

June 2014

Grzegorz Grynkiewicz, Guest Editor

Acta Poloniae Pharmaceutica – Drug Research, Vol. 71 No. 6 pp. 887–899, 2014 ISSN 0001-6837
Polish Pharmaceutical Society

REVIEWS

LYSOPHOSPHATIDYLCHOLINE AND LYSOPHOSPHATIDYLINOSIOL – NOVEL PROMISSING SIGNALING MOLECULES AND THEIR POSSIBLE THERAPEUTIC ACTIVITY

ANNA DRZAZGA, AGATA SOWIŃSKA and MARIA KOZIOŁKIEWICZ*

Lodz University of Technology, Institute of Technical Biochemistry,
Stefanowskiego 4/10, 90-924 Łódź, Poland

Abstract: For many years the role of lysophospholipids (LPLs) was associated only with structural and storage components of the cell without any informational function. Today, based on many research projects performed during the last decades, it is clear that some of the LPLs act as hormone-like signaling molecules and thus are very important inter- and intracellular lipid mediators. They can activate specific membrane receptors and/or nuclear receptors regulating many crucial physiological and pathophysiological processes. The LPLs were identified as involved in a majority of cellular processes, including modulation of disease-related mechanisms observed, for instance, in case of diabetes, obesity, atherosclerosis and cancer. Among LPLs, lysophosphatidylcholine (LPC) and lysophosphatidylinositol (LPI) are becoming attractive research topics. Their recently revealed activities as novel ligands of orphan G protein-coupled receptors (i.e., GPR55 and GPR119) involved in modulation of tumor physiology and insulin secretion seem to be one of the most interesting aspects of these compounds. Moreover, the most recent scientific reports emphasize the significance of the acyl chain structure bound to the glycerol basis of LPL, as it entails different biological properties and activities of the compounds.

Keywords: lysophospholipids, lysophosphatidylcholine, lysophosphatidylinositol, GRP55, GPR119, diabetes, cancer

Abbreviations: AMD – age-related macular degeneration, ATX – autotaxin, cAMP – 3'-5'-cyclic adenosine monophosphate, CMC – critical micelle concentration, cPA – cyclic phosphatidic acid, DDHD1 – DDHD domain-containing protein 1, ERK – extracellular signal-regulated kinase, GAPDH – glyceraldehyde 3-phosphate dehydrogenase, GIP – glucose-dependent insulinotropic peptide, GLP-1 – glucagon-like peptide 1, GM-CSF – granulocyte macrophage colony-stimulating factor, GPCR – G protein-coupled receptors, GPLs – glycerolysophospholipids, IFN-γ – cytokine-induced interferon γ, IL – interleukin, LCAT – lecithin:cholesterol acyltransferase, LDH – lactate dehydrogenase, LDL – low-density lipoprotein, LPA – lysophosphatidic acid, LPE – lysophosphatidylethanolamine, LPG – lysophosphatidylglycerol, LPS – lysophosphatidylserine, LSPL – lysosphingophospholipid, lysoPLD – lysophospholipase D, NADPH – nicotinamide adenine dinucleotide phosphate, PC – phosphatidylcholine, PGE_2 – prostaglandin E_2, PGF1α – 6-keto-prostaglandin $F_{1\alpha}$; PGI2 – prostaglandin I_2 (prostacyclin), PI – phosphatidylinositol, PLA_1 – phospholipase A_1, PLA_2 – phospholipase A_2, PLC – phospholipase C, PPARγ – proliferator-activated receptor γ, ROS – reactive oxygen species, S-1-Ps – sphingosine-1-phosphates, SPC – sphingosylphosphatidylcholine, T1DM – type 1 diabetes mellitus, T2DM – type 2 diabetes mellitus, TGF-β1 – transforming growth factor β1, TRPM8 – transient receptor potential cation channel subfamily M member 8, TRPV2 – transient receptor potential cation channel subfamily V member 2, TXA2 – thromboxane A2

Lysophospholipids (LPLs) for a long time were considered only as membrane components necessary to mediate synthesis of various phospholipids and to embed proteins into cell membranes. Thanks to the rapid advance in chemistry and biology of LPLs during the last decades, the group of ''bioactive lysophospholipids'' of hormone-like signaling properties was revealed. Most popular in this area are LPLs with glycerol (glycerolysophospholipids, GPLs) or sphingoid (lysosphingophospholipids, LSPLs) backbones, where families of lysophosphatidic acids (LPAs) and sphingosine-1-phosphates (S-1-Ps) have been investigated to the greatest extent so far. Much less information is

* Corresponding author: e-mail: maria.koziolkiewicz@p.lodz.pl, phone: (0-42) 631 34 03, fax: (0-42) 636-66-18

available considering the remaining LPLs, such as cyclic phosphatidic acid (cPA), lysophosphatidylglycerol (LPG), sphingosylphosphatidylcholine (SPC), lysophosphatidylserine (LPS), lysophosphatidylethanolamine (LPE), lysophosphatidylcholine (LPC) and lysophosphatidylinositol (LPI). Glycerol derivatives of lysophospholipids are a diverse group of molecules bearing both saturated (e.g., 16:0, 18:0) and unsaturated (e.g., 18:1, 18:2, 20:4) fatty acid chains, contrary to S1P (2*S*-amino-1-(dihydrogen phosphate)-4E-octadecene-1,3*R*-diol), which is a single molecular species. Common structural features of GPLs is a glycerol backbone, a phosphate head group at the *sn-3* position, a hydroxyl group at the *sn-2* (or *sn-1*) position and a single fatty acid chain at the *sn-1* (or *sn-2*) position. Besides, the acyl chain at the *sn-2* position of the 2-acyl-lysophospholipid has a tendency to migrate to the *sn-1* position, thus resulting in the creation of the 1-acyl-lysophospholipid (1, 2).

Lysophospholipids are necessary to maintain homeostasis of many physiological processes including reproduction, vascular development, and functioning of the nervous system. The majority of the studies have demonstrated beneficial effects of particular lysophospholipids towards health. The famous example of a brain permeant LPL, which was officially approved by US Food and Drug Administration and European Medicines Agency as the first orally administered drug in multiple sclerosis treatment, is 2-amino-2-[2-(4-octylphenyl)ethyl]-1,3-propanediol (FTY720, the S1P analogue known as *fingolimod* and, recently, *Gilenya*) (3). Another example is *edelfosine* (1-octadecyl-2-O-methyl-glycero-3-phosphocholine, 2-LPC) which is a drug proposed in treatment of multiple sclerosis and other neurodegenerative diseases (4). The pharmacological research results are the best proof of favorable activities of LPLs and their great potency in disease therapy.

Currently, LPC and LPI seem to be the most attractive research goals in terms of biological activity and possible application. In serum plasma both of the compound groups function mainly as substrates for autotaxin (ATX). Enzymatic digestion of LPC and LPI leads to formation of various forms of LPA and cPA, which are involved i.a., in modulation of cardiovascular system physiology, wound healing, metabolism of lipids and carbohydrates, mediated by membrane and nuclear receptors (respectively: receptors of LPA family and nuclear peroxisome proliferator-activated receptor γ, PPARγ) (5). However, according to recent findings, both LPC and LPI are capable of modulation of significant physiological processes directly due to interaction with respective G protein-coupled receptors (GPCRs), which at the same time identifiy them as novel ligands of "orphan receptors".

LPC (1-acyl-glycero-3-phosphocholine) is known for its favorable effects towards health in terms of indirect promotion of internal and external wound healing and organ regeneration (5, 6), therapy of autoimmune and neurodegenerative diseases (4, 7–9) or even treatment of age-related macular degeneration (AMD) (10). Moreover, recent reports have shown that LPC induces insulin secretion from pancreatic β-cells. It has been also found that LPC activates glucose uptake and effectively lowers blood glucose levels in mouse models of type 1 and 2 diabetes mellitus (T1DM and T2DM, respectively) (11, 12). Unfortunately, up to date, the precise mechanism of this phenomenon has remained unknown. On the other hand, oleoyllysophosphatidylcholine (LPC 18:1) was reported to bind to one of membrane receptors known as GPR119, which is responsible for increase in glucose stimulated insulin secretion in murine NIT-1 insulinoma cells due to protein kinase A (PKA) related signaling pathway (12, 13). The nature of the endogenous ligands to GPR119, and whether this GPCR plays a physiological role in direct regulation of insulin secretion by pancreatic β cell, is currently under investigation.

When it comes to LPI (1-α-lysophosphatidylinositol), there is a strong evidence that it is involved in tumor cell proliferation and migration. Clinical data identified LPI as a biomarker for poor prognosis in cancer patients, whereas *in vitro* studies demonstrated significantly elevated levels of LPI in highly proliferative cancer cells (14). In 2007, Oka et al. documented for the first time that LPI is an agonist of GPR55 expressed to high extent by tumor cells. The team found LPI to induce rapid phosphorylation of the extracellular signal-regulated kinase (ERK) and an increase in intracellular Ca^{2+} in GPR55-expressing cells. On the other hand, there is a lot of controversies about natural ligands for GPR55, which need to be clarified.

All known LPLs characterized by various biological activities need to be further studied in detail. One of the issues to be clarified is the mechanism of action of the biomolecules with respect to their specific chemical structure. This review is especially devoted to activities and mechanisms of action of LPC and LPI species recently discovered as meaningful signaling molecules. The subject is being intensively studied by the research team of the Institute of Technical Biochemistry, Lodz

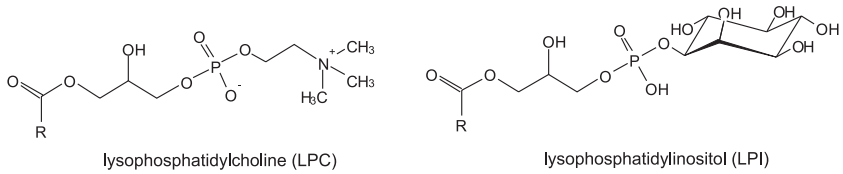

Figure 1. Structure of lysophosphatidylcholine (LPC) and lysophosphatidylinositol (LPI). „R" represents a fatty acid residue

University of Technology (IBT LUT) in Poland (2, 15).

Lysophosphatidylcholine

LPC is the most abundant LPL with relatively high concentration in human blood (approximately 150 mM), however, showing significant level variations with respect to gender and age (16). To some extent, it is available in dietary products (i.e., eggs, soya, oilseeds and fish). Most of the circulating LPC molecules are associated with albumin. They are also the major phospholipid component of oxidized low-density lipoproteins (17, 18). Several types of LPC molecules with various acyl chains, such as palmitoyl (16:0), stearoyl (18:0), oleoyl (18:1), linoleoyl (18:2), arachidonoyl (20:4) and docosahexanoyl (22:6), have been found in human plasma (19). The compounds are derived from phosphatidylcholine due to transacylation of the sn-2 fatty acid residue of lecithin to free cholesterol catalyzed by lecithin:cholesterol acyltransferase (LCAT), which finally results in the formation of cholesterol ester and LPC (1, 20). The rate of ester formation by LCAT depends on the nature of the head group, fatty acid residues and the macromolecular properties of the lipid (1). It is also generated by the action of phospholipases A_2 (PLA_2) and phospholipases A_1 (PLA_1), which are able to cleave the sn-2 and sn-1 ester bond, respectively (21). Appreciable amounts of LPC are also formed in plasma by endothelial lipase (1, 17).

Structurally different LPCs were recognized as carriers of fatty acids, phosphatidylglycerol and choline between tissues (22). As a representative of pro-inflammatory LPLs, LPC is involved in modulation of T cell functions and immunity. In activated microglia (brain macrophages) LPC was found to trigger interleukin-1 β (IL-1β) processing and release (23). It was also reported to enhance the expression of cytokine-induced interferon γ (IFN-γ) (1) and transforming growth factor β1 (TGF-β1) (24). Moreover, LPC-dependent NADPH oxidase stimulation and production of reactive oxygen species (ROS) was documented to activate caspase-1 that converts pro-cytokines to their mature, biologically active forms (IL-1β, IL-18 and IL-33) (25). LPC is also involved in the production of prostaglandin I_2 (PGI2 also known as prostacyclin) *in vitro* in primary human aortic endothelial cells and *in vivo* in murine model. A stable degradation product of PGI2, 6-keto-prostaglandin F_{1a} (PGF1α) was also found induced by LPC species (namely 18:1 and 20:4) (1).

In addition, it was recently found out that polyunsaturated LPC variants, such as LPC 20:4 and LPC 22:6, may serve as successful anti-inflammatory agents, opposing the activity of saturated acyl LPCs known to induce the response of immunological system (i.e., LPC 16:0) (8, 26, 27). As presented by Jin et al., LPC 22:6 as well as 17-hydroxy-LPC 22:6 exert anti-inflammatory effect in mice treated with lipopolysaccharide. It was detected that administration of these compounds before injection of lipopolysaccharide reduces increase in weight of spleen dose-dependently, where 17-hydroxy-LPC 22:6 appears to be more effective (9). Another example of anti-inflammatory polyunsaturated LPC is 15-hydroxy-docosapentanoyl-LPC (15-hydroxy-LPC 20:5) that inhibits formation of leukotrienes and cytokines in zymosan A-induced peritonitis of mice (28). Similar observation was made in case of LPC 20:4 and its derivative (15-hydroxy-LPC 20:4) (29). The anti-inflammatory effects were related to down-regulation of leukocyte extravasation, plasma leakage, and formation of pro-inflammatory mediators (IL-5, IL-6, nitric oxide, 12-hydroxyeicosatetraenoic acid and PGE_2 stimulated by LPC 16:0), and up-regulation of anti-inflammatory mediators (IL-4 and IL-10) (27). This evidence suggests that LPCs could be regarded as major modulators of inflammation process. LPC, together with LPS and LPE, is also found to be a natural agonist of G2A receptor, which in this case serves as suppressor of autoimmunity (1, 30). LPC, LPS and LPE, regard-

less of differences in structure, induce mobilization of intracellular Ca^{2+} ions through G2A signaling-dependent pathway. However, it resulted from amphipatic nature and detergent-like properties of the compounds and their interaction with lipid bilayer of the cellular membrane rather than direct interaction of the LPLs with the receptor. As originally described by Ben-Zeev et al., the process leads to $G_{\alpha i}$-related activation of phospholipase C (1, 31). On the other hand, direct, receptor mediated release of $G_{\alpha q/11}$ subunit without the membrane permeabilization effect was also observed (1, 32).

The problem of membrane permeabilization can be a matter of cytotoxicity. LPC above critical micelle concentration (CMC) can lead to rapture of cellular membrane resulting in hemolysis (1). However, there can be over 200-fold difference in CMC/toxic value depending on the structure of the LPC's acyl residue (33, 34). The issue was studied for the first time for hexanoyl (6:0), octanoyl (8:0), decanoyl (10:0), 12:0, 14:0, 16:0, 18:0, 18:1, nonadecanoyl (19:0), arachidoyl 20:0, and lignoceroyl 24:0 LPC species by Kim et al. in 2007 (Jurkat cell model) (35). The research led to identification LPC with palmitoyl residue as the most toxic. Yet, applied concentration of all tested LPCs was 20 μM, which is much higher than estimated CMC values of these compounds (33, 34). It was also found that serum albumin is capable of reduction of any cytotoxic effects caused by LPLs (35).

Six years later, Rytczak et al. at IBT LUT performed synthesis of novel phosphorothioate and phosphorodithioate analogues of 2-methoxy-lysophosphatidylcholine 12:0, 16:0, 18:0 and 18:1, which was followed by assessment of their influence on viability and cell membrane integrity of β-TC3 murine insulinoma cell model (2). The biological studies addressed possibility of engagement of LPC species in modulation of insulin secretion. Diversity of investigated LPC structures allowed the team to indicate the dependence of strength of the observed biological effects on chemical modification and acyl chain bound to the glycerol backbone (sample results in Table 1). The cytotoxicity assessment involved only a 10-μM concentration, which for some of the tested species was very distant from the expected CMC (i.e., $CMC_{LPC\ 12:0}$ = 740 μM, $CMC_{LPC\ 18:0}$ = 0.4 μM) (2, 33, 34). Surprisingly, it was clearly depicted that none of the tested compounds caused any significant decrease in cell viability, where the strongest toxic effect (relative cell viability > 72%) was observed for native LPC 14:0 and LPC 16:0, which is in contrast to results obtained by Kim et al. (2). It is worth noticing that the experiments were based on serum-free culture media. What is more, some of the compounds were found promoting cell survival (i.e., LPC 12:0, LPC 18:1), which was also observed in case of some methoxy-LPC's modified with one or two sulfur atoms, which native counterparts are toxic (LPC 14:0 and LPC 16:0). Additionally, the possibility of membrane perturbation by LPC molecules was controlled by assessment of lactate dehydrogenase (LDH) release, which led to a conclusion that the tested LPC analogues at 10 μM do not rapture lipid bilayer regardless of their structure and chemical modification and/or expected toxic CMC (Table 1) (2).

Research group of Rao et al. was also interested in activity of different LPCs with respect to their specific structure. The group investigated LPC 16:0, 18:1, 18:2 and 20:4 in terms of their influence on vasorelaxation. Table 1 presents sample data on prostanoid release from LPC-treated (10 μM concentration) aortic rings. Detection included $PGF_{1\alpha}$, PGE_2, PGI_2 and thromboxane A2 (TXA2) (36). As can be noticed from Table 1. different forms of LPC caused significantly different effects on the same experimental model. For instance, LPC 20:4 was capable of prostanoid release induction at 5-fold greater level than LPC 16:0. Taking into account all the stated research on varied LPC activities, it can be surely stated that there are plenty of distinct biological effects exerted by LPCs depending on their specific structure. (2, 35, 36).

Despite obvious connection between acyl chain structure and biological impact of LPC species, the concept of research regarding this issue is neglected in many cases. As far as the role of LPC in diabetes is concerned, the only documented activity concerns LPC 18:1 (13). This LPC species was defined as a novel ligand of GPR119 – a key receptor responsible for regulation of insulin secretion from β cells of pancreatic islets (13, 37), which is also engaged in reduction of fat deposition and food intake. GPR119 is expressed in the human Langerhans islets at the level of 8% relatively to glyceraldehyde 3-phosphate dehydrogenase (GAPDH) (38). Its activation entails intracellular cAMP accumulation connected to release of $G_{\alpha s}$ protein (12, 13). Expression of this receptor was also documented in case of enteroendocrine cells of the gut (12, 39–41), where its activation was related to stimulation of glucagon-like peptide 1 (GLP-1) and glucose-dependent insulinotropic peptide (GIP). This clearly shows that GPR119 is involved both directly and indirectly in the process of insulin secretion. What is more, since GLP-1 promotes expansion of β-cell mass, it is possible that agonists

Table 1. Comparison of biological impact of structurally different LPCs. Assessment of cytotoxicity, membrane perturbation potential (2) and prostanoid release stimulation (36). ? – no available data.

LPC modification	*In vitro* cell viability assessment (βTC3 model, 24-hour incubation with 10 μM of LPC, relative %)				LDH release (native)		CMC of native LPC (μM) (33, 34)	Prostanoid release from aortic rings (1-hour incubation with 10 μM of LPC, approximate relative fold of release)			
	native	2-metoxyphosphoro-		2-metoxyphosphoro-				6-keto-PGF_{1a}	TXB_2	$PGF_{2\alpha}$	PGE_2
		-thioate	-dithioate	-thioate	-dithioate						
LPC 12:0	~106	~90	~87	< 0	< 5	740	?				
LPC 14:0	~75	~112	~104	< 0	< 5	45	?				
LPC 16:0	~73	~105	~113	< 0	< 5	7	4	1.67	1	1.5	
LPC 18:0	~89	~90	~86	< 0	< 0	0,4	?				
LPC 18:1	~130	~121	~91	< 0	< 0	10	4.5	2.67	1.67	3	
LPC 18:2	?						5	2	1	3	
LPC 20:4	?						21	5	4.83	7	

of GPR119 may influence both the secretory activity and the viability of β-cells at the same time (40, 41). Properly chosen ligand of GPR119 may thus lead to improved glucose homeostasis in patients with T2DM, which is currently affecting over 90% of the patients due to severe insulin resistance and defective insulin secretion (42, 43).

Apart from obviously favorable effects towards T2DM patients, LPC was also found to improve glucose uptake in mouse models of T1DM, which is an insulin independent form of the disease due to autoimmune destruction of pancreatic β cells (11, 42, 43). This means that induction of insulin secretion from β cells, which are destroyed in case of T1DM, is not the only activity of LPC involved in modulation of metabolism.

LPC is the most abundant lysophospholipid in human blood. Significant decrease of its serum concentration was found to be related with high fat diet and T2DM condition (44, 45). These observations are consistent with the previous findings of Soga et al., whose publication clearly shows that LPC is involved in modulation of cellular glucose uptake (13). However, there are also opposite findings where high-fat diet related obesity was correlated with increase of palmitoleyl LPC (LPC 16:1) and LPC 22:4 serum concentration (46) and LPC 18:0 could be even regarded as a biomarker positively related to pathological gain in weight (47).

In the context of regulation of pancreatic hormonal secretion it is worth to pay attention to α cells of Langerhans islets, which are also reported to express GPR119 receptor (48). As far as α cells are responsible for glucagon secretion, activity of which is antagonistic to insulin, it suggests crucial role of GPR119 in maintenance of carbohydrate metabolism, as well as possibly bipolar biological activity of its ligands (38). So far, the potential role of LPC species in glucagon secretion modulation remains unknown.

When regulation of insulin secretion is concerned, GPR55 is another current research topic. Romero-Zerbo in 2011 (49) proposed GPR55 as a novel target for

treatment of T2DM as it was found directly involved in regulation of insulin secretion from β cells. This receptor is found commonly expressed in various tissues of the body, including the islets of Langerhans, however, it is not distributed on α cells of pancreas (50). Oleoylethanolamide (OEA), which is common also for GPR119, is one of the ligands of GPR55 causing enhanced secretion of insulin in *in vitro* cell models (51). There are very little literature data on possible interaction of GPR55 with LPC (1).

Both diabetes types remain incurable to a high extent resulting in indispensable life-long treatment and commonly occurring disease complications (such as hyperglycemia, obesity, cardiovascular and gastrointestinal disorders). This devastating disease affects over 371 million people in the world and is predicted to be the 7th leading cause of death in 2030 (WHO data). When it comes to Poland, it is the fourth European country with the highest epidemiological rates with 3 million people suffering from diabetes, where over one-third is not even aware of the fact. The obvious need of novel diabetes treatment and prophylaxis methods cause the GPR119-LPC interaction an important research area and are expected to expand in the future. It is also a significant matter of studies performed by research teams of IBT LUT.

Beneficial effects of LPC involve regulation of intestinal uptake of nutritional substances. Research results from *in vitro* (e.g., human intestinal Caco-2 cell model) and *in vivo* studies (rat plasma analysis) indicate that mixed micelles containing LPLs significantly influence intestinal uptake of β-carotene and lutein (10, 52). Particularly, micelles containing PC and LPC predominant within the composition cause meaningful increase in uptake of these substances. This is especially important from the point of view of treatment of diseases resulting from nutritional deficiencies, such as age-related macular degeneration (AMD). In this case, an inadequate intake of animal- and plant-based foods with low-fat content was considered to be the major cause of this disease. It was clinically tested that an increased intake of lutein is positively correlated to increased macular lutein density and inversely correlated to the progress of AMD pathogenesis (10). Rodriguez-Navarro et al. emphasize that chronic exposure to high-fat, LPL-rich diet can significantly influence the process of aging and related pathogenesis as dietary lipids are found to modulate the process of chaperone-mediated autophagy, involved in intracellular quality control and response to stress conditions (53).

Dietary available LPC was also found favorable to human health as it was recently published that LPC species administered to diabetic patients of high risk of cardiovascular disease development successfully decreases serum concentration of LPA responsible for platelet aggregation and vein clogging (54).

Moreover, impaired synthesis of LPC and PC in case of Alzheimer's patients suggests beneficial effects of these lipids in the disease therapy (7). It was also revealed that schizophrenic patients are characterized by significantly diminished levels of LPCs in blood plasma, which may influence the psychosis development as well as result in enhanced susceptibility to infections (55).

From the point of view of animal husbandry, activity of dietary-uptaken LPC is particularly favorable. It is known, that supplementation of fat-based forage for broiler chickens with LPC as an emulsifier improves the gain of their body weight during the starter period (56, 57). Next to increase of total tract apparent digestibility of fatty acids, LPC is also found to cause no adverse effects on the animals' physiology. Focusing on molecular mechanisms associated with the process, LPC is found to induce secretion of enzymes responsible for absorption and transport of dietary lipids. Nakano and co-workers present that oil-feeding accompanied by mixed lipid micelles build of LPC molecules result in 10-fold increase in production of intestinal alkaline phosphatase by the brush border microvilli as compared to the enzyme release in regular high-fat diet conditions (experiments *in vitro*, Caco2 cell line) (58).

LPC was also found to be connected to pathological conditions related to atherosclerosis. It is thought to play a significant role in the atherogenic disease, being a component of oxidized low-density lipoprotein (LDL) in atherosclerotic lesions. LPC 16:0 also induces human umbilical vein endothelial cells (HUVECs) and vascular smooth muscle cells (VSMCs) cell apoptosis processes, which can be associated with atherogenesis (59). On the other hand, there are some evidence suggesting that LPC could be directly engaged in tissue regeneration, as it interacts with LPC GPR4 receptor, which is widely expressed in various endothelial cells and involved in stimulation angiogenesis and cellular migration (30).

Among other properties, LPC is being a natural airway surfactant (60, 61), enabling to enhance viral gene transfer in animal models. Cmielewski and co-workers examined the effect of airway pretreatment with variants of LPC on lentiviral vector gene transfer efficiency in murine nasal airways *in vivo*. Only one hour after administration of LPC

variants was enough to induce an airway barrier function. It can be correlated to the effectiveness of gene expression, where the variants with longer acyl chains appeared to be more effective. The enhanced expression correlated with LPC could provide new options for preclinical development of efficient airway gene transfer techniques.

Lysophosphatidylinositol

LPI is a subspecies of LPL containing an inositol head group. It was found present in different ranges in normal human cells (i.e., endothelial cells (62), platelets (63), peripheral blood neutrophils (64)), various cancer cell lines (65–72), and animal cells (i.e., mouse fibroblasts (73) and macrophages (74), rat brain cells (75)). Concentration of LPI is different in various tissues (37.5 nM per gram of tissue in rat brain, 2.5 μM in mouse serum and 1.5 μM in samples of plasma from healthy women (1)) but the fatty acid composition of LPI is distinctive in every mammalian cell type. Derivatives of stearic and arachidonic acids are supposed to be the most active and abundant species. For instance, 2-arachidonoyl (2-20:4) LPI has been reported to have the highest level of biological activity (75).

LPI is a product of phosphatidylinositol (PI) degradation, which is catalyzed by phospholipase PLA_2 (1). Moreover, it was reported that PLA_1 can be also involved in formation of LPI. Yamashita et al. identified phospholipase DDHD domain-containing protein 1 (DDHD1, one of members of the mammalian intracellular PLA_1 family) as a candidate enzyme involved in LPI formation. It was demonstrated that purified DDHD1 is capable of generating 2-arachidonoyl LPI (76).

Up to date, little is known about the export system of LPI. According to the report of Yamashita et al., most of LPI produced by DDHD1 is released into the medium but it was impossible to identify the mechanism of this process (76). However, it has been already found that the ATP-binding cassette ABCC1 transporter is engaged in export of LPI into the extracellular media in case of human prostate cancer PC3 cell line (71).

Deacetylation of LPI by lysophospholipase A (lysoPLA) was the first known degradation pathway of this compound species. The process has been observed in porcine platelets membranes (77). It was also found that degradation of LPI may be catalyzed by phospholipase C (PLC) with specificity for LPI (lysoPI-PLC) (77, 78). Another enzyme involved in LPI metabolism is lysophospholipase D (lysoPLD, autotaxin), which is present in blood plasma and serum and converts LPI to LPA (1, 79). Physiological role of LPI is still poorly understood. Even though the first publications concerning plausible biological activity of LPI were published in the mid-80s (80, 81), little attention was drawn to this bioactive lipid comparing to LPA or S1P. The research group of Oka was the first to demonstrate significant biological activity of LPI, which only in 2007 was described as the most active endogenous agonist of orphan GPR55 – the intrinsic receptor for LPI (82). At present, LPI is suggested to be able to activate other GPCRs as well. For instance, LPI was reported as an activator of human GPR119 in RH7777 rat hepatoma cells stably expressing this receptor (13).

First reports devoted to biological activity of LPI suggested that the compound is involved in stimulation of insulin release from pancreatic islets. Metz et al. found that the process was mediated *via* intracellular Ca^{2+} ions mobilization (80, 81). These results have indicated that LPI may play an important role in regulation of the whole body metabolism, also in case of diseases such as obesity and T2DM. The thesis was verified during further studies showing increased level of LPI in plasma of obese patients. Moreover, GPR55 expression is enhanced in adipose tissue of obese subjects. Correlation between expression of GPR55 and weight, body mass index and percentage fat mass was also found, which was particularly noticeable in case of women (83). LPI was also reported to increase intracellular calcium level and expression of lipogenic genes in visceral adipose tissue explants and in differentiated visceral adipocytes (1).

Other biological activities of LPI are related to artery contraction, cell proliferation and migration (84). LPI impact on intracellular free Ca^{2+} concentration was analyzed by Oka et al. using GPR55-expressing HEK293 cell model. What is more, Monet et al. demonstrated that application of LPI induces sustained cytoplasmic Ca^{2+} concentration increase in CHO cells, which stably express murine transient receptor potential cation channel subfamily V member 2 (TRPV2) (85). LPI was also reported to activate Akt and enhance intracellular Ca^{2+} levels in prostate and ovarian cancer cells (86). Degradation products of LPI were not observed to induce mobilization of Ca^{2+} or phosphorylation of ERK in GPR55-expressing cells. This proves that the effects of LPI are due to itself, not its metabolites (82). Some recent studies have reported possibility of Ca^{2+} influx induction by LPI through ion channels belonging to the transient receptor potential (TRP) family (87, 88). LPI was found to evoke an increase in intracellular Ca^{2+} in CHO cells expressing murine

transient receptor potential cation channel subfamily M member 8 (TRPM8). The receptor is mainly expressed in a subpopulation of dorsal root ganglion (DRG) neurons that also express GPR55 (89). Other studies have shown that LPI induces Ca^{2+} entry in PC3 cells expressing TRPV2. Induction was observed even in the presence of capsazein, an inhibitor of TRPV1, which proves that LPI directly interacts with endogenous TRPV2 channel of the PC3 model. This observation suggests that LPI influenced Ca^{2+} influx due to translocation of TRPV2 protein to plasma membrane. However, Ca^{2+} increase induced by LPI *via* TRPV2 channel was observed after some delay, which implies that LPLs are involved in indirect activation of TRPV2 channels, unlike in case of lipid ionotropic receptors (85). On the other hand, it was demonstrated that LPI/GPR55-exerted effects of sustained, oscillatory Ca^{2+} release stimulation are dependent on $G\alpha_{13}$ and require activation of rhoA (90). It was also reported that effect of LPI in mobilization of intracellular Ca^{2+} in PC3 cells entails migration and proliferation of these cells (71, 85).

The role of LPI is not limited to stimulation of Ca^{2+} mobilization pathway. The compound was observed to be secreted at high concentrations by fibroblasts and epithelial cancer cells, in case of which it showed mitogenic activity (91). LPI was proposed to play an important role in bone physiology due to regulation of osteoclast number and function. Whyte et al. confirmed high level of GPR55 expression in murine and human osteoclasts, implying involvement of LPI in stimulation of osteoclast polarization and bone resorption (92). It was also proven that under inflammatory conditions LPI is produced by immune cells (i.e., macrophages) and involved in stimulation of immunological response (91). High levels of GPR55 expression were observed in spleen (93, 94), neutrophils (91) and mast cells (72).

Interestingly, LPI was recognized as a regulator of peripheral sensory neuron function as well as pathological pain (95). As previously mentioned, LPI stimulates the increase in intracellular Ca^{2+} concentration in DRG neurons and activates TRPM8 channel expressed in this group of neurons. Therefore, it is able to affect DRG neurons involved in nociception, associated with neuropathic or inflammatory pain (89). The same conclusions were drawn by studies on GPR55 knock-out mice, which served as models of inflammatory mechanical hyperalgesia achieved by injection of Freund's complete adjuvant and partial nerve ligation. In this case, the knock-out murine model response to LPI stimulations was found attenuated, which was further attributed to increase in levels of IL-4, IL-10, IFNγ and granulocyte macrophage colony-stimulating factor (GM-CSF). GPR55 knock-out mice also failed to develop mechanical hyperalgesia in the model of neuropathic hypersensitivity (96). What is more, LPI is supposed to possess neuroprotective activity, as it can activate the 2-pore domain K^+ channels TREK-1 and TRAAK, which are important in terms of synaptic function modulation due to regulation of the neuron membrane potential. This activity does not seem to involve GPCR associated signaling, suggesting a non-receptor mediated activity of LPI. Similar effects were also observed in case of LPC (86).

Detection of GPR55 in various human cancer cell lines, including the ones obtained from breast (68, 70), brain, cervix, skin, pancreas, liver (70), ovaries, prostate (71) and hematological tumors (69, 70, 72), caused increased interest in the role of LPI/GPR55 in cancer progression. Clinical data implicated engagement of LPI in cancer progression and recurrence (84), which was additionally supported by research results showing increased LPI levels in plasma and ascites from ovarian cancer patients as compared to samples from healthy controls or patients with non-malignant diseases (97). Correlation between GPR55 expression in breast cancer tissue and tumor aggressiveness is also known (70). Moreover, similar observation was made during analysis of microarray data concerning pancreatic tumors and glioblastomas (76).

It has been already proven that LPI induces cell migration present in case of physiological and pathophysiological processes, such as embryonic development, immune system activities, inflammatory processes, wound healing, angiogenesis, cancer progression and metastasis (98, 99). Among other activities LPI enhances motility of sperm cells (100), induces directional migration of human peripheral blood neutrophils with improvement to their migratory capacity towards 2-AG (the CB_2R agonist) (91) and exerts pro-migratory influence on human coronary artery smooth muscle cells (SMC) (101). The compound is also found to induce an increase in migration of PC3 cells after activation of TRPV2 channel (85). Migration of highly metastatic MDA-MB-231 human breast adenocarcinoma cells was found significantly enhanced due to LPI treatment as well (68). Interestingly, Ford et al. observed that GPR55 expression in MDA-MB-231 cells is relatively high as compared with poorly metastatic MCF-7 human breast adenocarcinoma cells, however, GPR55 overexpression in MCF-7

cells results in acquirement of their migration ability. Further addition of exogenous LPI enhanced the observed effect even more. The results described here suggest that GPR55 overexpression induced a pro-migratory phenotype in breast cancer cells and that LPI may mediate pro-migratory effects *via* GPR55 activation. Beside the evidence that LPI enhanced breast cancer cell chemotaxis, it was also reported that it can increase cellular polarization and orientation of nanogrooved substratum (68). Nevertheless, there are some contradictory findings on LPI considered as a negative regulator of migration, which was demonstrated in case of endothelial cells (EC) (102). LPI was also shown to stimulate expression of adhesion molecules by endothelial cells (i.e., VCAM-1 in rabbit aortic EC and ICAM-1 in human umbilical vein cells) (103).

The first report indicating the role of LPI in cell proliferation was based on studies devoted to transformation of rodent fibroblasts with cytoplasmic and membrane-associated oncogenes. The process was followed by an increase in intracellular levels of glycerophosphoinositol (GPI), which is a product of LPI deacetylation catalyzed by PLA2 (104). However, the first evidence of direct impact of LPI on cell proliferation was demonstrated by Piñeiro et al., who described mitogenic activity of LPI inducing proliferation of FRTL5 differentiated epithelial thyroid cells. Moreover, comparison of LPI levels in differentiated FRTL5 cells and Kiki cells stably transformed with the k-ras oncogene showed increased concentration of the compound in the latter model (71). Similar results were obtained by Ross et al., who observed highly elevated levels of LPI species and LPI metabolites in cells transformed to overexpress ras-p21 (84). Importantly, enhanced level of LPI was proven to be a consequence of activation of enzymes involved in the Ras pathway, not a transformation itself (105). LPI was also detected in the extracellular medium of ras-transformed fibroblasts, which proves the cells to be capable of both synthesis and release of the lipid (106). Increased levels of intracellular and extracellular LPI were observed in k-ras transformed KiKi cells as well. These results indicate that cancer cells are able to promote their own proliferation by synthesis and release of LPI. The observation is additionally supported by the data on the mechanism of LPI export in PC3 cells, which was found to be mediated by the ABCC1 transporter (71).

Altogether, LPI is a mitogen stimulating proliferation of normal and oncogene-transformed cells. Furthermore, LPI/GPR55 interaction is found pivotal in maintenance of autocrine loop that sustains prostate cancer cell proliferation (71). The observation is consistent with data on overexpression of GPR55 regarded as a strategy of cancer cells to increase their proliferation, which was demonstrated both *in vitro* and *in vivo* (70). No certain explanation for the proliferation-inducing effects of GPR55 overexpression is available so far. However, there are some data connecting these effects with the presence of LPI in experimental settings. Andradas et al. demonstrated that inhibition of cytosolic phospholipase A_2 ($cPLA_2$) activity with pyrrophenone in HEK293 cells blocks proliferation induced by GPR55 overexpression (70). Piñeiro et al. achieved the same effect after genetic ablation of $cPLA_2$. Importantly, cell proliferation decreased due to $cPLA_2$ silencing was recovered by addition of exogenous LPI (71) indicating that cancer cells generate mitogenic LPI through the action of $cPLA_2$. According to previously mentioned data concerning elevated levels of LPI in ascites and plasma from patients with ovarian cancer, the same proliferation induction strategy could be used, for instance, by human gynecological tumors.

CONCLUSIONS

Research conducted in past years has demonstrated that many important physiological and pathophysiological processes are regulated by LPC and LPI. LPC is identified as a ligand of GPR119 receptor expressed at high level by cells of Langerhans islets. The compound is proposed to be involved in carbohydrate metabolism modulation due to documented stimulation of insulin secretion and cellular glucose uptake. There are also some contradictory reaserch leading to conlusion that LPC is either promoting or attenuating development of obesity and related metabolic disorders. Yet, it was described as a favorable means of weight gain promotion in case of animal husbandry. Apart from metabolism-related issues, LPC was found to promote would healing, neuroregeneration processes and nervous system regulation, macular regeneration, and attenuation of autoimmune response. Molecular mechanisms of these activities remain poorly understood so far. However, there appeared several attempts to prove and explain the dependence of particular LPC activity on its species and chemical modifications.

LPI is defined as endogenous natural ligand for GPR55. The species is known as intracellular and cytoplasmic Ca^{2+} concentration regulator. LPI/GPR55 system was also demonstrated to be positively associated with obesity in human. Recent

Table 2. Update on recognized activities and mechanisms of action of LPC and LPI.

LPL	Non-receptor mediated effects	Influenced receptor	Receptor distribution	Identified LPL mediated G protein release	Main signaling pathways	Receptor mediated effects	References
LPC	• Counteracting neurodegeneration • Anti-inflammatory activity (polyunsaturated fatty acid residues) • Promotion of intestinal uptake of β-carotene and lutein (applicable in therapy of AMD and age-related diseases) • Reduction of aging process due to dietary uptake • Natural airway surfactant, medium for efficient airway gene transfer techniques • Synaptic function modulation due to regulation of the neuron membrane potential (activation of TREK and TRAAK K^+ channels)	GPR4	Ubiquitous, mainly vascular endothelial cells, smooth muscle cells, lung, heart, kidney	$G_{\alpha i/o}$?	$[Ca^{2+}]\uparrow$, ERK$\uparrow$	Cell migration, angiogenesis	
		G2A	Inflammatory cells, lymphoid tissues, hematopoietic cells, keratinocytes	$G_{\alpha i/o}$, $G_{\alpha q/11}$, $G_{\alpha s}$, $G_{\alpha 13}$	$[Ca^{2+}]\uparrow$, ERK$\uparrow$, p38 MAPK$\uparrow$, JNK$\uparrow$	Suppression of auto-inflammatory response, cell migration (especially LPC20:4/22:6, 17-hydroxy-LPC22:6, 15-hydroxy-LPC20:4/20:5), apoptosis	1–61
		GPR119	Major in pancreatic Langerhans islets, enteroendocrine cells of the gut, brain	$G_{\alpha s}$	AC$\uparrow$, PKA$\uparrow$	Regulation of insulin secretion from pancreatic β cells	
		GPR55 (weak interaction)	Central nervous system, adrenal glands, testis, spleen, gastrointestinal tract, breast adipose tissues, endothelium (i.e., human vein endothelial cells)	$G_{\alpha 12}$, $G_{\alpha q}$	$[Ca^{2+}]\uparrow$, ERK$\uparrow$, PLC$\uparrow$, rhoA$\uparrow$, cdc42$\uparrow$, rac1$\uparrow$	Regulation of nervous system and bone morphogenesis, cell migration	
LPI	• Synaptic function modulation due to regulation of the neuron membrane potential (activation of TREK and TRAAK K^+ channels)	GPR55 (possibly also GPR119)	Endothelial cells, platelets, peripheral blood neutrophils, mouse fibroblasts and macrophages, rat brain cells, spleen, neutrophils, mast cells, DRG neurones, cancer cell lines including ones obtained from breast, brain, cervix, skin, pancreas, liver, ovaries, prostate, hematological tumors	$G_{\alpha 13}$	$[Ca^{2+}]\uparrow$, ERK$\uparrow$, rhoA$\uparrow$, Akt$\uparrow$	Insulin release from pancreatic islets, artery contraction, regulation of osteoclasts number and function, regulation of peripheral sensory neuron function and pathological pain, regulation the immune system response during inflammatory condition, modulation of proliferation, differentiation, motility and tumorigenesis in diverse cell types	1, 62–110

studies strongly suggest that LPI/GPR55 plays an important role in processes related to inflammatory and neuropathic pain. Moreover, it was shown that LPI may be involved in the immune system response during inflammatory condition, as well as modulation of osteoclast physiology. LPI is also emerging as a key modulator of proliferation, differentiation, motility and tumorigenesis in diverse cell types.

The past decade was rich in new findings on various biological activities as well as associated physiological and pathophysiological roles of LPC and LPI. Despite the fact, numerous questions still need to be answered and further studies are necessary.

Acknowledgment

This work was supported by grants from the National Science Centre (grant no. 2011/01/B/ST5/06383 and grant no. 2013/11/N/NZ5/00270).

REFERENCES

1. Grzelczyk A., Gendaszewska-Darmach E.: Biochimie 95, 667 (2013).
2. Rytczak P., Drzazga A., Gendaszewska-Darmach E., Okruszek A.: Bioorg. Med. Chem. Lett. 23, 6794 (2013).
3. Di Menna L., Molinaro G., Di Nuzzo L., Riozzi B., Zappulla C., Pozzilli C., Turrini R. et al.: Pharmacol. Res. 67, 1 (2013).
4. Abramowski P., Otto B., Martin R.: PLoS One 9, e91970 (2014).
5. Gendaszewska-Darmach E.: Acta Biochim. Pol. 55, 227 (2008).
6. Benesch M.G., Ko Y.M., McMullen T.P., Brindley D.N.: FEBS Lett. (2014).
7. Grimm M.O., Grosgen S., Reimenschneider M., Tanila H., Grimm H.S., Hartmann T.: J. Chromatogr A 1218, 7713 (2011).
8. Riederer M., Ojala P.J., Hrzenjak A., Graier W.F., Malli R., Tritscher M., Hermansson M. et al.: J. Lipid Res. 51, 2957 (2010).
9. Jin M.C., Hung N.D., Yoo J.M., Kim M.R., Sok D.: J. Lipid. Sci. Technol. 114, 114 (2012).
10. Mamatha B.S., Baskaran. V.: Nutrition 27, 960 (2011).
11. Yea K., Kim J., Yoon J.H., Kwon T., Kim J.H., Lee H.J, Kim J.I. et al.: J. Biol. Chem. 284, 33833 (2009).
12. Overton H.A., Fyfe M.C.T., Reynet C.: Br. J. Pharmacol. 153, 76 (2008).
13. Soga T., Ohishi T., Matsui T., Saito T., Matsumoto M., Takasaki J., Matsumoto S. et al.: Biochem. Biophys. Res. Commun. 326, 744 (2005).
14. Oka S., Nahajima K., Yamashita A., Kishimoto S., Sugiura T.: Biochem. Biophys. Res. Commun. 362, 928 (2007).
15. Gendaszewska-Darmach E., Laska E., Rytczak P., Okruszek A.: Bioorg. Med. Chem. Lett. 22, 2698 (2012).
16. Ishikawa M., Maekawa K., Saito K., Senoo Y., Urata M., Murayama M., Tajima Y.et al.: PLoS One 9, 91806 (2014).
17. Schmitz G., Ruebsaamen K.: Atherosclerosis 208, 10 (2010).
18. Guo Z., Vikbjerg A.F., Xu X.: Biotechnol. Adv. 23, 203 (2005).
19. Lee J.Y., Min H.K., Moon M.H.: Anal. Bioanal. Chem. 400, 2953 (2011).
20. Akoi J., Taira Y., Takanezawa Y., Kishi Y., Hama K., Kishimoto T., Mizuno K. et al.: J. Biol. Chem. 277, 48737 (2002).
21. Murakami M., Taketomi Y., Miki Y., Sato H., Hirabayashi T., Yakamoto K.: Prog. Lipid. Res. 50, 152 (2011).
22. Xu Y.: Biochim. Biophys. Acta. 1582, 81 (2002).
23. Stock C., Schilling T., Schwab A., Eder C.: J. Immunol. 177, 8560 (2006).
24. Hasegawa H., Lei J., Matsumoto T., Onishi S., Suemori K., Yasukawa M.: Biochem. Biophys. Res. Commun. 415, 526 (2011).
25. Schilling T., Eder C.: Cell. Immunol. 256, 87 (2010).
26. Lucas A., Grynberg A., Lacour B., Goirand F.: Metabolism 57, 233 (2008).
27. Hung N.D., Sok D.E., Kim M.R.: Inflamm. Res. 61, 473 (2012).
28. Hung N.D., Kim M.R., Sok D.E.: Br. J. Pharmacol. 165, 1119 (2011).
29. Hung N.D., Kim M.R., Sok D.E.: Prostoglandins Other Lipid Mediat. 90, 105 (2009).
30. Meyer zu Heringdorf D., Jakobs K.H.: Biochim. Biophys. Acta 1768, 923 (2007).
31. Ben-Zeev G., Telias M., Nussinovitch I.: Cell Calcium 47, 514 (2010).
32. Eckels P., Gamboni-Robertson F., Banerjee A., Silliman C.C.: Biochem. J. 432, 35 (2010).
33. Matsuzaki K., Hanola T., Miyajima K., Mikura Y., Shimizu H., Toguchi H.: Chem. Pharm. Bull. 36, 4253, (1988).
34. Heerklotz H., Epand R. M.: Biophys. J. 80, 271 (2001).
35. Kim Y.L., Im Y.J., Ha N.C., Im D.S.: Prostaglandins Other Lipid Mediat. 83, 130 (2007).

36. Rao S.P., Reiderer M., Leichleitner M., Hermansson M., Desoye G., Hallstrom S., Graier W.F., Frank S.: PLoS One. 8, 65155 (2013).
37. Overton H.A., Babbs A.J., Doel S.M., Fyfe M.C.T., Gardner L.S., Griffin G., Jackson H.C. et al.: Cell Metabol. 3, 167 (2006).
38. Amisten S., Salehi A., Rorsman P., Jones P.M., Persaud S.J.: Pharmacol. Ther. 139, 359 (2013).
39. Sakamoto Y., Inoue H., Kawakami S., Miyawaki K., Miyamoto T., Mizuta K., Itakura M.: Biochem. Biophys. Res. Commun. 351, 474 (2006).
40. Ahlkvist L., Brown K., Ahren B.: Ahlkvist. Endocr. Connect. 2, 69 (2013).
41. Zhu X., Huang W., Qian H.: GPR119 Agonists: A Novel Strategy for Type 2 Diabetes Treatment, in Diabetes Mellitus – Insights and Perspectives., Oguntibeju O. O. Ed., InTech, Rijeka 2013.
42. Lipina C., Rastedt W., Irving A.J., Hundal H.S.: Bioessays 34, 681 (2012).
43. Sena C.M., Bento C.F., Pereira P., Seiça R.: EPMA J. 326, 744 (2010).
44. Barber M.N., Risis S., Yang C., Meikle P.J., Staples M., Febbraio M.A., Bruce C.R.: PLoS One 7, 41456 (2012).
45. Wang-Sattler R., Yu Z, Herder C, Messias AC, Floegel A, He Y, Heim K, et al.: Mol. Syst. Biol. 8, 615 (2012).
46. Esinger K., Liebisch G., Schmitz G., Aslanidis C., Krautbauer S., Buechler C.: Int. J. Mol. Sci. 15, 2991 (2014).
47. Li F., Jiang C., Larsen M. C., Bushkofsky J., Krausz K. W., Wang T., Jefcoate C. R., Gonzalez F. J.: J. Prot. Res. (2014).
48. Odori S., Hosoda K., Tomita T., Fujikura J., Kusakabe T., Kawaguchi Y., Doi R. et al.: Metabolism 62, 70 (2013).
49. Romero-Zerbo S.Y., Rafacho A., Diaz-Arteaga A., Suarez J., Quesada I., Imbernon M., Ross R.A. et al.: J. Endocrinol. 211, 177 (2011).
50. McKillop A.M., Moran B.M., Abdel-Wahab Y.H., Flatt P.R.: Br. J. Pharmacol. 170, 978 (2013).
51. Godlewski G., Offertaler L., Wagner J.A., Kunos G.: Prostaglandins Other Lipid Mediat. 89, 105 (2009).
52. Kotake-Nara E., Nagao A.: Biosci. Biotechnol. Biochem. 76, 875 (2012).
53. Rodriguez-Navarro J.A., Kaushik S., Koga H., Dall'Armi C., Shui G., Wenk M.R., Di Paolo G., Cuervo A.M.: Proc. Natl. Acad. Sci. USA 109, 705 (2012).
54. Abdolahi A., Georas S.N., Brenna J.T., Cai X., Thevenet-Morrison K., Phipps R.P., Lawrence P. et al.: Prostaglandins Leukot. Essent. Fatty Acids 90, 61 (2014).
55. Oresic M., Seppanen-Laakso T., Sun D., Tang J., Therman S., Viehman R., Mutsonen U. et al.: Genome Med. 4, 1 (2012).
56. Zhang B., Haitao L., Zhao D., Guo Y., Barri A.: Anim. Feed Sci. Technol. 163, 177 (2011).
57. Raju M.V., Rao S.V., Chakrabatri P.P., Rao B.V., Panda A.K., Devi B., Sujatha V. et al.: Br. Poult. Sci. 52, 769 (2011).
58. Nakano T., Inoue I., Alpers D.H., Akiba Y., Katayama S., Shinozaki R., Kaunitz J.D. et al.: Am. J. Physiol. Gastrointest. Liver Physiol. 297, 207 (2009).
59. Kogure K., Nakashima S., Tsuchie A., Tokumura A., Fukuzawa K.:. Chem. Phys. Lipids.126, 29 (2003).
60. Cmielewski P., Anson D.S., Parson D.W.: Respir. Res. 11, 84 (2010).
61. Kitsiouli E., Nakos G., Lekka M. E.: Biochim. Biophys. Acta 1792, 941 (2009).
62. Bondarenko A., Waldeck-Weiermair M., Naghdi S., Poteser M., Malli R., Graier W.F.: Br. J. Pharmacol. 161, 308 (2010).
63. Billah M.M., Lapetina E.G.: J. Biol. Chem. 257, 5196 (1982).
64. Smith D.M., Waite M.: J. Leukoc. Biol. 52, 670 (1992).
65. Xiao Y., Chen Y., Kennedy A.W., Belinson J., Xu Y.: Ann. N.Y. Acad. Sci. 905, 242 (2000).
66. Xiao Y.J., Schwartz B., Washington M., Kennedy A., Webster K., Belinson J., Xu Y.: Anal. Biochem. 290, 302 (2001).
67. Xu Y., Xiao Y.J., Baudhuin L.M., Schwartz B.M.: J. Soc. Gynecol. Investig. 8, 1 (2001).
68. Ford L.A., Roelofs A.J., Anavi-Goffer S., Mowat L., Simpson D.G., Irving A.J.,Rogers M.J. et al.: Br. J. Pharmacol. 160, 762 (2010).
69. Oka S., Ota R., Shima M., Yamashita A., Sugiura T.: Biochem. Biophys. Res. Commun. 395, 232 (2010).
70. Andradas C., Caffarel M.M., Perez-Gomez E., Salazar M., Lorente M., Velasco G., Guzman M., Sanchez C.: Oncogene 30, 245 (2011).
71. Pińeiro R., Maffucci T., Falasca M.: Oncogene 30, 142 (2011) .
72. Cantarella G., Scollo M., Lempereur L., Saccani-Jotti G., Basile F., Bernardini R.: Biochem. Pharmacol. 82, 380 (2011).
73. Hong S.L., Deykin D.: J. Biol. Chem. 256, 5215 (1981).

74. Zoeller R.A., Wightman P.D., Anderson M.S., Raetz C.R.: J. Biol. Chem. 262, 17212 (1987) .
75. Oka S., Toshida T., Maruyama K., Nakajima K., Yamashita A., Sugiura T.: J. Biochem. 145, 13 (2009).
76. Yamashita A., Oka S., Tanikawa T., Hayashi Y., Nemoto-Sasaki Y., Sugiura T.: Prostaglandins Other Lipid Mediat. 107, 103 (2013).
77. Murase S., Okuyama H.: J. Biol. Chem. 260, 262 (1985).
78. Tsutsumi T., Kobayashi T., Ueda H., Yamauchi E., Watanabe S., Okuyama H.: Neurochem. Res. 19, 399 (1994).
79. Umezu-Goto M., Kishi Y., Taira A., Hama K., Dohmae N., Takio K., Yamori T. et al.: J. Cell Biol. 1508, 227 (2002).
80. Metz S.A.: Biochem. Biophys. Res. Commun. 138, 720 (1986).
81. Metz S.A.: J. Pharmacol. Exp. Ther. 238, 819 (1986).
82. Oka S., Nakajima K., Yamashita A., Kishimoto S., Sugiura T.: Biochem. Biophys. Res. Commun. 362, 928 (2007).
83. Moreno-Navarrete J.M., Catalan V., Whyte L.: Diabetes 61, 281 (2012).
84. Ross R.A.: Trends Pharmacol. Sci. 32, 265 (2011).
85. Monet M., Gkika D., Lehen'kyi V., Pourtier A., Abeele F.V., Bidaux G., Juvin V. et al.: Biochim. Biophys. Acta 1793, 528 (2009) .
86. Piñeiro R., Falasca M.: Biochim. Biophys. Acta 1821, 694 (2012) .
87. Andersson D.A., Nash M., Bevan S.: J. Neurosci. 27, 3347 (2007).
88. Vanden Abeele F., Zholos A., Bidaux G., Shuba Y., Thebault S., Beck B., Flourakis M. et al.: J. Biol. Chem. 281, 40174 (2006).
89. Lauckner J.E., Jensen J.B., Chen H.Y., Lu H.C., Hille B., Mackie K.: Proc.Natl. Acad. Sci. USA 105, 2699 (2008).
90. Henstridge C.M., Balenga N.A., Ford L.A., Ross R.A., Waldhoer M., Irving A.J.: FASEB J. 23, 183 (2009).
91. Balenga N.A., Aflaki E., Kargl J.: Cell Res. 21, 1452 (2011).
92. Whyte L.S., Ryberg E., Sims N.A., Ridge S.A., Mackie K., Greasley P.J.: Proc. Natl. Acad. Sci. USA 106, 16511 (2009).
93. Ryberg E., Larsson N., Sjogren S., Hjorth S., Hermansson N.O., Leonova J.: Br. J. Pharmacol. 152, 1092 (2007).
94. Sawzdargo M., Nguyen T., Lee D.K., Lynch K.R., Cheng R., Heng H.H., George S.R., O'Dowd B.F.: Brain Res. Mol. Brain Res. 64, 193 (1999).
95. Gangadharan V., Selvaraj D., Kurejova M., Njoo C., Gritsch S.: Pain 154, 2801 (2013).
96. Staton P.C., Hatcher J.P., Walker D.J.: Pain 139, 225 (2008).
97. Xu Y., Xiao Y.J., Baudhuin L.M., Schwartz B.M.: J. Soc. Gynecol. Investig. 8, 1 (2001).
98. Raftopoulou M., Hall A.:. Dev. Biol. 265, 23 (2004).
99. Ridley A.J., Schwartz M.A., Burridge K., Firtel R.A., Ginsberg M.H., Borisy G.: Science 302, 1704 (2003).
100. Wheeler M.B., Seidel Jr. G.E.: Gamete Res. 22, 193 (1989).
101. Kohno M., Yokokawa K., Yasunari K., Minami M., Kano H., Hanehira T., Yoshikawa J.: Circulation 98, 353 (1998).
102. Murugesan G., Fox P.L.: J. Clin. Invest. 97, 2736 (1996).
103. Kume N., Cybulsky M.I., Gimbrone Jr M.A.: J. Clin. Invest. 90, 1138 (1992).
104. Alonso T., Santos E.: Biochem. Biophys. Res. Commun. 171, 14 (1990) .
105. Falasca M., Iurisci C., Carvelli A., Sacchetti A., Corda D.: Oncogene 16, 2357 (1998).
106. Eichholtz T., Jalink K., Fahrenfort I., Moolenaar W.H.: Biochem. J. 291, 677 (1993).
107. Labonte E.D., Pfluger P.T., Cash J.G., Kuhel D.G., Roja J.C., Magness D.P., Jandacek R.J. et al.:. FASEB J. 24, 2516 (2010).
108. Labonte E.D., Kirby R.J., Schildmeyer N.M., Cannon A.M., Huggins K.W., Hui D.Y.: Diabetes 55, 935 (2006).
109. Kim H.J., Kim H.J., Noh S., Hur H.J., Sung M.J., Hwang J.T., Park J.H. et al.: J. Proteome Res. 10, 722 (2011).
110. Fox T.E., Bewley M.C., Unrath K.A., Pedersen, M.M., Anderson R.E., Jung D.Y., Jefferson L.S. et al.: J. Lipid Res. 52, 509 (2011).

Acta Poloniae Pharmaceutica – Drug Research, Vol. 71 No. 6 pp. 900–916, 2014 ISSN 0001-6837
Polish Pharmaceutical Society

AMD – THE RETINAL DISEASE WITH AN UNPRECISED ETIOPATHOGENESIS: IN SEARCH OF EFFECTIVE THERAPEUTICS

JERZY Z. NOWAK

Department of Pharmacology and Toxicology, Interfaculty Chair of General and Clinical Pharmacology, Medical University of Lodz, Poland
Institute of Pharmacology, Polish Academy of Sciences (Scientific Board) in Kraków, Poland

Abstract: AMD (age-related macular degeneration) is a progressive vision-threatening ocular disease, affecting central region of the retina – the macula – and manifesting in the elderly. AMD is a degenerative disease, and the degeneration affects primarily the retinal pigment epithelial (RPE) cells and secondarily the photoreceptors, leading consequently to disturbances or partial loss of central vision and legal blindness. Clinically, the disease is classified as: atrophic – dry AMD (in majority of cases), and neovascular – wet AMD (with choroidal neovascularization – CNV; 10–15% of all AMD cases). Pathogenesis of AMD is complex, multifactorial and only poorly recognized. Main risk factors include: advanced age, genetic predispositions, environmental determinants, history of exposure to intensive light and smoking. At least four molecular processes contribute to the development of AMD pathology: lipofuscinogenesis, drusogenesis, inflammation and choroidal neovascularization (in wet AMD). Since vascular endothelial growth factor (VEGF) is a predominant proangiogenic factor in CNV, the wet AMD can be treated with intravitreous application of „anti-VEGF" agents (Avastin, Lucentis, Eylea). Till now, there is no approved therapy for dry AMD, although several agents/treatments are currently in clinical trials. This paper briefly describes major molecular and cellular events leading to AMD, and presents currently used and new experimental therapeutic strategies against AMD.

Keywords: AMD, age-related macular degeneration, pathogenesis, lipofuscin, drusen, oxidative stress, inflammation, retina, vision, therapeutic strategies

Age-related macular degeneration (AMD) is one of the most common irreversible causes of severe loss of vision, including legal blindness. In its course the disease inevitably leads to serious compromise of quality of life. AMD affects several dozen millions of people over the age of 60 worldwide, with hundreds of thousands of new cases diagnosed each year. Clinically, the disease is classified into slowly progressing atrophic – dry AMD (~85% of all AMD cases), with advanced or late stage named geographic atrophy (~35%), and rapidly progressing neovascular (exudative) – wet AMD (10–15% of all AMD cases) (1, 2). The mentioned clinically distinct two forms of AMD (dry and wet) have however common molecular and cellular "roots", which are often referred to as the early-intermediate stage AMD or age-related maculopathy (ARM). At early stages, the pathology is developing asymptomatically; however, later on – at certain moment of the disease progression – the patients start to experience some problems with vision (non-specific mild signs decreasing the comfort of vision), which force them to contact an ophthalmologist. With time, the symptoms tend to become more pronounced – in such patients an ophthalmologist, after detecting in addition the presence of drusen in the macula region, as well as hypo- and/or hyperpigmention of the RPE, or the presence of newly formed subfoveal blood vessels originating from the choroid, properly diagnoses the disease as the dry or the wet form AMD – in one eye or both eyes.

As already stated, the wet form AMD, characterized by subretinal extravasations of the choroid-derived neovessels (choroidal neovascularization – CNV) and hemorrhage under and into the photoreceptor cell layer in the macula region, is a rapidly developing and devastating phenomenon diagnosed in relatively small portion of all AMD cases; thus, a question arises as to whether the rapidly developing

* Corresponding author: e-mail: jznowak07@gmail.com

"macular" CNV, manifesting the presence of the wet form AMD, is a complication of the dry AMD, or it represents an independent from atrophic form (including geographic atrophy – GA), macular disease? An answer to this question may have important therapeutic and prognostic implications. Our knowledge concerning AMD pathogenesis, from its early stages to advanced pathology, is still incomplete, which makes problems in proper interpretation of many molecular, cellular and clinical phenomena together with their underlying mechanisms, as well as functional consequences, occurring during the course of the disease. And this is the reason why therapeutic approaches used in the past and at present were/are of limited efficacy, which particularly is the case with atrophic – dry AMD. Since vascular endothelial growth factor (VEGF) is a predominant proangiogenic factor in CNV, the wet AMD can be treated with intravitreous application of „anti-VEGF" agents (Avastin, Lucentis, Eylea). Till now, there is no approved therapy for dry AMD; yet, many chemically different agents showing different mechanisms of action are currently in clinical trials (see last paragraph).

The aim of this article is twofold: 1. to provide current knowledge on AMD pathogenesis, with deeper insight into the early stages of the disease, and the dilemma on real status of the wet-neovascular AMD *versus* the dry-atrophic form, and 2. to summarize latest efforts on potential therapeutics for AMD, with emphasis on therapies for the dry form AMD.

AMD – non-modifiable and modifiable risk factors

There are many various risk factors that may predispose or facilitate the pathogenesis of AMD. Such factors are usually classified as non-modifiable and modifiable ones. The former group includes genetic predispositions and age, while the latter group includes a number of environmental, behavioral or other factors that possibly may, to varying degree (depending on individual characteristics and sensitivity), influence molecular mechanisms or cellular processes underlying the disease development (3).

Genetic risk factors

Genetic predispositions seem likely to occur, as much evidence points to a familial component of AMD. Several genes were earlier identified that cause diseases with clinical features that overlap with AMD, e.g., *ABCA4*, *ELOVL4*, *FIBL-6*, *APOE*, *SOD2*. Although mutations in the mentioned genes may to some extent contribute to the development of particular features of AMD, they obviously are not responsible for the advanced and complex AMD pathology. In 2005, the pioneering discovery of complement factor H (*CFH*) as a major AMD susceptibility gene showed that there is a gene, whose polymorphism (Y402H), leading to increased activity of the complement system, likely contributes to the AMD pathology. Further extensive investigations, including genome-wide association studies (GWAS), have confirmed a number of additional genetic risk loci – a total of 20 susceptibility loci, which considered together can explain up to 60–70% of the disease heritability (4). Based on common SNP (single nucleotide polymorphism) associations, two loci seem to contribute to the greatest AMD risk: 1q31 and 10q26, the former related to already mentioned Y402H variant in the *CFH* gene encoding CFH (a negative regulator in the alternative complement pathway), the latter representing non-complement related genes involved in AMD, i.e., *ARMS2* (*age-related maculopathy susceptibility 2*) / *HTRA1* (*high-temperature requirement A serine peptidase 1*) (5). At present, we know that a number of other genes within the alternative complement pathway may be associated with AMD in both a non-protective and protective manner, these include genes encoding CFI, C3, C2/CFB, C7 (4, 6).

Aging as a risk factor

Aging favors the development of AMD, particularly in predisposed individuals (due to concomitant presence of some additional risk factors). The term "age-related" in the disease name – AMD is fully justified, as the age is the major (albeit individual, i.e., specific to each subject) and unavoidable determinant of various dysfunctions at the cellular and organ level. The term "age-related physiology" covers several changes or dysfunctions that may appear important for AMD pathology, such as: extracellular drusen formation, Bruch's membrane stiffening (including increasing thickness of Bruch's membrane and lipid accumulation), intracellular debris (resulting from oxidative stress-induced cell/tissue damage, lipofuscin, advanced glycation end products – AGEs), mitochondrial defects, cell loss and tissue degeneration. Some sort of age-related changes may be associated with the deficiency of necessary microelements/nutrients or with the loss of function in the aging cells – particularly postmitotic, i.e., non-regenerable cells as, for example, the retinal pigment epithelium cells – RPE or photoreceptors. While the lacking microelements/nutrients

may be supplied from the outside, thus attempting to compensate for their deficiency in particular cells/tissues, we are unable until now to stop the systemic aging process. Considering AMD pathology, it is however important to precisely differentiate between age-related "physiologic" changes from already pathologic events/symptoms (7) – such task may sometimes be really difficult to perform, as in patients with a risk of AMD development, physiology, including that related to aging, seems to smoothly shift into pathology.

Modifiable risk factors

There is an array of environmental and behavioral factors that may increase the risk of AMD development, their role(s) being likely dependent on individual sensitivity and functional tissue/organ characteristics; among them are:

- cigarette/tobacco smoking – this has been identified as the most consistently reported modifiable risk factor for the development of AMD, and increasing the risk of progression to advanced AMD (8, 9).
- light (exposure to intensive light in the past) – depending on environmental lighting conditions, each day the human retina absorbs approximately 10^{12} to 10^{15} photons. Although perception of light (visible spectrum: 400–700 nm) by retinal photoreceptors is a physiological process, excess of visible light, especially in the range of shorter wavelengths, may show toxic effects (10). The blue region (400–500 nm) of the visible spectrum is of particular importance since it has a relatively high energy and can easily penetrate ocular tissues, including the neural retina with photoreceptors (11). In addition, ambient radiation from the sun or from artificial light sources contains varying amounts of UV irradiation from A to C range (220–400 nm). The shorter the wavelength, the greater energy and therefore the greater the potential for photochemical cell/tissue damage. However, although the longer wavelengths are less energetic, they can penetrate the eye more deeply (12). Concerning possible toxic effects: brief exposure to bright light can cause immediate thermal injury, whereas exposure to light for an extended period of time may lead to photochemical damage, including RPE monolayer disruption (10, 11).
- improper diet (fatty, vegetable-poor) – specific dietary recommendations are therapeutically crucial in many ailments and diseases (e.g., diabetes, arterial hypertension); this may also apply to AMD, however the expected preventive/therapeutic results in AMD patients may be poor and varying, despite the fact that there is a vast literature on that topic suggesting the importance of a proper diet or dietary supplements (13). Dietary supplements, containing macular pigments (lutein and zeaxanthin), selected vitamins (E and C) and/or metal salts (zinc, selenium) – all directed to prevent or fight oxidative stress, are widely marketed as a strategy for AMD, but clinical data are inconclusive, giving no firm clues concerning their real efficacy against the disease (13–15).

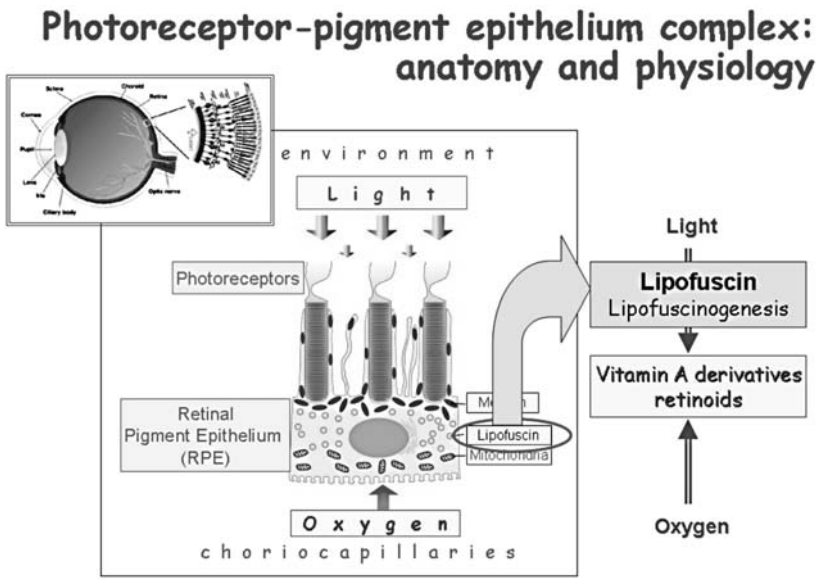

Figure 1. Physiologic aspects of photoreceptor-pigment epithelium (RPE) functional complex. For explanations see text

- Hypertension – possible, but less defined risk factor.

AMD – the origin and development of the pathology

Although the role of at least five processes (oxidative stress, lipofuscinogenesis, drusogenesis, inflammation and neovascularization in wet AMD) in AMD pathogenesis is commonly accepted, the onset of the disease remains elusive since the mechanism triggering the pathology remains unknown. It is practically impossible to detect any sign/change at the very beginning of AMD since, as mentioned earlier, the disease develops inconspicuously over many years. In order to understand the arising pathology it is reasonable to enter physiological events underlying vision, and to analyze those processes whose course may be deteriorated either spontaneously or as a result of the action of at least some risk factors. Figure 1 depicts anatomy and physiology of the photoreceptor-retinal pigment epithelium (RPE) complex, showing also possible propathogenic mechanisms related to light exposure and oxygen supply.

AMD is a slowly progressing disease of degenerative characteristics, with meaningful clinical symptoms occurring many years later, usually in the elderly (60+ years) population. The evidence shows that the degeneration affects primarily the retinal pigment epithelium (RPE) cells and secondarily photoreceptors; early changes in the Bruch's membrane and the choroid are also possible.

The AMD pathology takes place within functional anatomic complex of the macula region embracing: photoreceptors, the retinal pigment epithelium cells (RPE), the Bruch's membrane and the choroid.

Photoreceptors and RPE cells. Physiological roles of the last three structures listed above are to create optimal conditions for work and activity of photoreceptors (rods and cones), whose principal role is to absorb photons of light and thus detect visual signals from surrounding environment. RPE cells, forming monolayer, are in tight contact with photoreceptor inner segments (PIS) containing densely packed molecules of visual pigments – their function is crucial for activity and survival of photoreceptors. RPE cells are multifunctional and take part in the blood-retina barrier structure and function, delivery of nutrients (including oxygen) to photoreceptors, collection of metabolic products from photoreceptors, the role – together with photoreceptors – in the visual (retinoid) cycle, phagocytosis and enzymatic metabolism of constantly shed apical fragments of PIS during the vision process. All the mentioned RPE functions are interrelated and indispensable for maintaining photoreceptors' physiology (see Fig. 1).

The Bruch's membrane is built from 5 layers containing collagen and elastin; its role is to physically separate neural retina from vascular bed consisting of choroidal microvessels. Changes in the structure and function of the Bruch's membrane can facilitate and underlie the CNV phenomenon.

The choroid represents one of the two circulatory systems delivering blood to the retina; the choroid or choroidal system, *via* its choriocapillaries, is responsible for supplying the outer third part of the retina (containing photoreceptors and RPE cells; which physiologically remains completely avascular) with necessary microelements and oxygen.

It seems highly unlikely that there is only one signal/mechanism responsible for initiation of the pathology. A widely accepted scenario takes into consideration an interactive role of two, three, or even more factors. Thus, due to interplay of plurality of risk factors, both endogenous and exogenous or behavioral, which might predispose, or even contribute to the development of the disease, some important physiological processes underlying vision may become irreversibly deteriorated. In other words, the critical physiological processes responsible for the vision process (including the visual excitation cascade) move beyond the limits of homeostasis, creating a biochemical platform for the future pathology. This involves: uncontrolled and non-neutralizable oxidative stress, intensified lipofuscinogenesis in the retinal pigment epithelium (RPE) cells, formation of drusen under the RPE monolayer (i.e., in the direction of Bruch's membrane) – the process called drusogenesis, low grade chronic inflammatory process known as parainflammation, and enhanced activity of the complement alternative pathway (as a result of e.g., Y402H mutation in *CFH* gene); some additional less recognized factors/phenomena may also play in concert in building future pathology (16–19).

RPE – the primary site of AMD pathology

Our bodies contain many non-regenerable (postmitotic) cells, particularly within the central nervous system. These include the photoreceptors (only the external segments that contain photopigments, i.e., photoreceptors outer segments (POS), are subject to regeneration) and retinal pigment epithelium (RPE) cells. In the pathogenesis of

AMD, RPE cells are the first cells that become metabolically inefficient and thus undergo degeneration; dysfunction and atrophy of photoreceptors is secondary, as they are unable to function and survive without functionally efficient RPE cells, and therefore also undergo degeneration. The pathological process involves mostly a small region of the retina, known as the macula, where the cone photoreceptors, responsible for acute and color vision, are predominant. Therefore, first clinical symptoms of AMD include several nonspecific symptoms resembling malfunction of the vision process, e.g., blurred vision, defects with central vision of various intensity or gradual loss of color vision, "warping" of perceived images (1, 20).

When the eyes are open, photoreceptors are continuously working, absorbing light photons and "recording" the image of the environment. In other words, eyes permanently record this image in an automatic fashion, generating the first signal of a complex, multisynaptic vision process. POS, filled with visual pigment molecules, are characterized by significant functional dynamics; they wear off upon continuous function and, as a consequence, the apical fragments are constantly shed and captured by neighboring RPE cells. At the same time, POS are being rebuilt in order to maintain appropriate size (which is an important parameter determining the efficacy and survival of photoreceptors). Regeneration proceeds from the perikaryon, i.e., the photoreceptor inner segment (PIS), and requires numerous building blocks, including docosahexaenoic acid (DHA). These building blocks are supplied by the RPE cells and originate partly from the captured POS fragments and partly from circulation (consumed food) (19).

One of the many important roles played by the RPE cells is "digestion" of the absorbed (and continuously being absorbed) photoreceptor material stored in phagolysosomes. Despite the fact that phagocytosis and enzymatic degradation occurring as a result of the activity of numerous lysosomal enzymes and physiological processes that had developed over thousands of years in creatures dwelling on Earth and making use of the visual organ system (retinal processes that govern visual perception in many vertebrates, including humans, are generally similar), they seem to be of limited efficacy, at least in humans. This claim is supported by systemic accumulation of lipofuscin, known as the age pigment, in RPE cells (Fig. 1).

Lipofuscinogenesis – age-related physiology or pathologic event?

Lipofuscin and the process of its formation, i.e., lipofuscinogenesis, are not the attributes of RPE

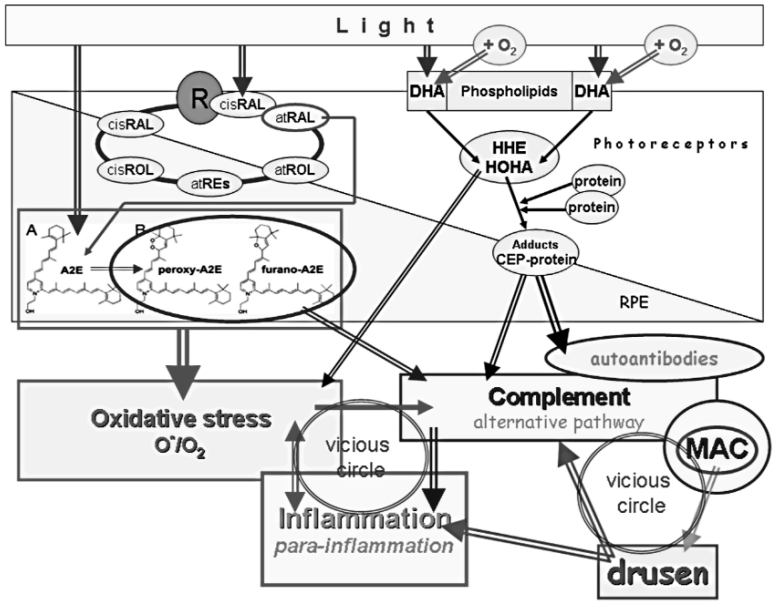

Figure 2. Interrelations between molecular and cellular processes occurring at early-moderate stages of AMND pathogenesis. For explanations see text. Note that some mechanisms may form a kind of vicious circuses. Abbreviations: RAL – retinal, ROL – retinol, at-RAL – all-trans-retinal, atREs – retinyl esters, DHA – docosahexaenoic acid, HHE – 4-hydroxy-2-hexenal, HOHA – 4-hydroxy-7-oxyhept-5-ene acid, MAC – membrane attack complex

cells and connections between photoreceptors and RPE, as they are also present in other non-renewable cells, such as neurons, cardiomyocytes or skeletal muscle cells. Lipofuscin, being accumulated in various cells in the course of aging, is also known as "age pigment". As such, lipofuscinogenesis, together with accumulated lipofuscin, could be considered as events lying within frames of physiology or "extended" or age-dependent physiology.

However, there is an important compositional difference between the retinal lipofuscin and the pigment accumulated in other body cells. The retinal lipofuscin has a unique characteristics because of the presence of retinoids (vitamin A derivatives), originating from the visual cycle, particularly bisretinoids – products of spontaneous fusion of two molecules of all-*trans*-retinal, generated *via* photoreaction (i.e., by absorption of photons) by 11-*cis*-retinal, a cofactor of the visual pigment. Taking into account that bisretinoids are photocytotoxic compounds, an important issue deals with conditions promoting their formation – do they represent "extended" (and likely reversible) physiological reactions, or they, after reaching certain level of activity, direct pathological pathway/s? (see Fig. 2). In order to answer such questions, it is necessary to follow reactions/pathways underlying first steps of vision physiology.

The cis→trans retinal transformation is the crucial first step of visual cycle, initiating further conformational transformations of opsin (i.e., the visual pigment protein) into its active forms (e.g., meta-rhodopsin II), capable of progressing the visual cycle with the final effect consisting in the closure of cGMP-dependent cation channel in the cellular membrane of photoreceptors and quenching the so-called darkness current. In this time, the cellular membrane of photoreceptors is hyperpolarized only to regain the state of being ready to absorb another photon, i.e., the depolarization state; the active pigment, capable of absorbing photons, is a molecule, e.g., rhodopsin, that contains a light sensitive co-factor, 11-*cis*-retinal (21).

The all-*trans*-retinal (at-RAL) formed, following photon absorption, is completely dissociated from the visual pigment and undergoes further physiological transformations in the retinoid cycle that takes place in both photoreceptors and RPE cells (Fig. 2). However, part of at-RAL that does not bind the ABCA4 (ATP-binding cassette [transporter] A4 type, also known as ABCR), transporting the retinoid into the sites with all-*trans*-retinal dehydrogenase activity, "falls out" the cycle and spontaneously dimerizes (using often ethanolamine as a "linker") into phototoxic bisretinoids, including A2E (N-retinylidene-N-retinylethanolamine) (Fig. 2). Till now, at least 25 bisretinoid fluorophores originating in photoreceptor cells and resulting from reactions of all-*trans*-retinal have been indentified (22, 23). A2E, which is the best characterized lipofuscin component, seems to represent a thoroughly established stress-inducing product (24–26). Among various biological features of A2E is its, and especially furano- and peroxy- metabolites, significant ability to activate the complement system (an alternative pathway) (27, 28), which is an effector mechanism of the innate immunity, capable of efficiently and automatically acting in system's defense, including destruction of "own" cells (29–31).

Accumulation of lipofuscin deposits in RPE cells is a hallmark of aging in the eye, and in fact is manifestation of metabolic inefficacy of their lysosomal compartment, characterized by reduced autophagy (32–34). The reason for this inefficacy remains unknown, although considering molecular complexity of autophagic processes, the reasons may be multiple, including hypofunction or insufficient quantity/activity of lysosomal enzymes – cathepsins being most predominant in normal conditions. Lipofuscin deposits accumulate with age, and the adverse effects of accumulating products of oxidative stress that accompanies lipofuscinogenesis are intensified. Local inflammatory reaction that develops at certain moment, being manifested by an atypical process referred to as para-inflammation, drusogenesis (drusen, pesudodrusen), and peroxidation of polyunsaturated fatty acids (PUFAs) and PUFA-derived oxidative protein modifications, become the driving forces of the developing AMD pathology (Figs. 2 and 3).

Recently, however, using imaging mass spectrometry, a lack of correlation between the spatial distribution of A2E and lipofuscin fluorescence in the human retinal pigment epithelium (RPE) has been reported (35), an observation rising some doubts on the role of this bisretinoid in increasing lipofuscin fluorescence observed in the central RPE with aging. This potentially important observation needs further verification and, when confirmed, requires rethinking the A2E in relation to both aging and AMD retina.

Long-chain PUFAs – oxidative modifications and formation of carboxyalkylpyrrole-protein adducts

Fatty acids are present in the most diverse forms of life and perform important functions as lipid components in the structure of the

plasmatic/cellular membranes, being responsible for e.g., membrane fluidity, and involved in metabolic/signaling processes; they are important sources of energy and precursors of signaling molecules (including pro-inflammatory, anti-inflammatory, vasoactive, and many other mediators). The vast family of fatty acids comprise saturated and unsaturated compounds, the latter containing one or more double bonds between carbon atoms, C=C, in a hydrocarbon chain, referring to, respectively, monounsaturated or polyunsaturated fatty acids (PUFAs). Long-chain PUFAs include such compounds as: arachidonic acid (AA or ARA; four C=C bonds), eicosapentaenoic (EPA; five C=C bonds), or docosahexaenoic acid (DHA; six double C=C bonds).

PUFA residues of membrane phospholipids are very sensitive to oxidation and the action of reactive oxygen species (ROS), the process known under the term of "lipid peroxidation". Peroxidation of highly unsaturated lipids (e.g., AA, EPA, DHA) leads to complex mixtures of harmful products, including malondialdehyde, acrolein, 4-hydroxy-2-nonenal, 4-hydroxyhexenal, as well as a number of hydroxy-ω-oxoalkenoic acids. The latter compounds, together with their derivatives of the carboxyalkylpyrrole type, are produced in the central nervous system, including the retina. Although structural unsaturation predisposes long-chain PUFAs for peroxidation with resultant harmful compounds, it should be emphasized that these unsaturated fatty acids play many important physiological roles, which, ironically, are related just to their structural unsaturation.

Photoreceptor cell membranes contain exceptionally large amounts of long-chain PUFAs in general, and particularly the most unsaturated docosahexaenoic acid (DHA). It is this high unsaturation which makes DHA particularly susceptible to spontaneous peroxidation and fragmentation into cytotoxic compounds, e.g., 4-hydroxy-2-hexenal (HHE) and 4-hydroxy-7-oxyhept-5-enoic acid (HOHA), the latter being a member of hydroxy-ω-oxoalkenoic acids. HOHA may additionally fuse with protein molecule (e.g., albumin) to form immunogenic carboxyethylpyrrole-protein adducts, e.g., CEP-albumin adduct (Fig. 2) (23, 36–39).

It has been shown that CEP-protein adducts are formed more abundant in ocular tissues (drusen, Bruch's membrane) from AMD patients than from normal human donors, an observation suggesting their role in the pathogenesis of AMD (36, 40). CEP immunoreactivity was detected not only in human retina, but also in human plasma, with values being again significantly higher in the plasma of AMD donors than in the plasma samples of healthy donors (41). Interestingly, the plasma CEP immunoreactivity positively correlated with CEP autoantibody titer (41), indicating that CEP behaves as an antigen

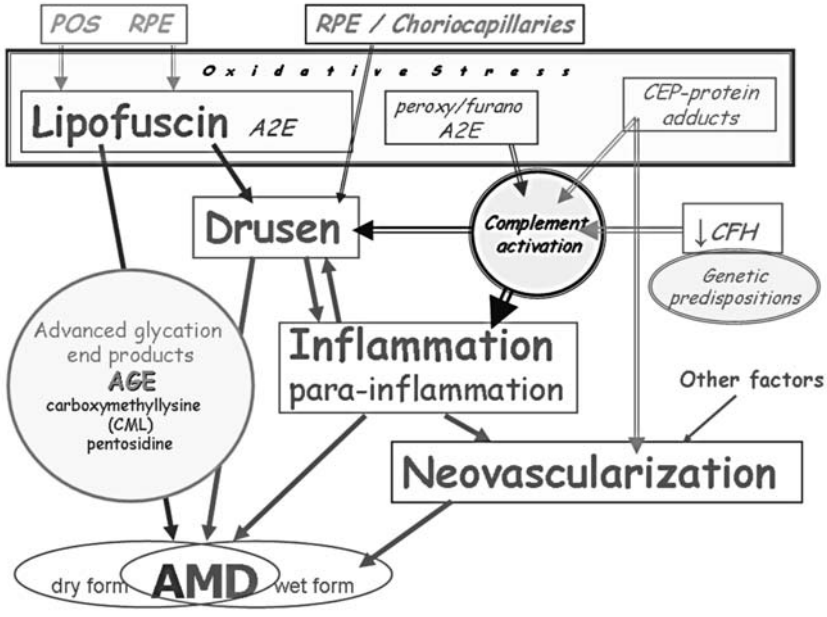

Figure 3. Principal molecular events underlying the development of AMD pathology. For explanations see text

which generates production of specific anti-CEP antibodies (Fig. 2). The immune-mediated events related to immunogenic CEP-protein adducts, which in AMD patients are probably generated through many decades, may contribute as one of many molecular links to the development of AMD pathology. Although direct evidence of the role of CEP-protein adducts in AMD pathogenesis in humans is lacking, recent experiments carried out on mice immunized with CEP-modified mouse serum albumin (CEP-MSA) and Freund's adjuvant (used in an attempt to rise the level of sensitivity to endogenously generated CEP) have shown that the retinas of such animals produced changes similar to those seen in retinas of AMD-suffering peoples; they included: accumulation of drusen, swollen Bruch's membrane, fixation of complement-C3d product in Bruch's membrane, lesions in the RPE cells, decreased electrophysiological responses to light (42, 43). In addition, in mice with laser-induced rupture of Bruch's membrane (an accepted experimental model of CNV), subretinal injection of CEP-MSA significantly augmented CNV, the effect being similar to that produced by injections of VEGF, a major proangiogenic factor (37).

Concerning oxidative stress and the retina, one should not forget that the supply of oxygen (and microelements/nutrients) *via* the choriocapillary system into photoreceptors-RPE cells complex is one of the largest in primates. Taking into account the functional specificity of the retina, particularly of photoreceptors (photosensitivity, extensive metabolism, high partial pressure of oxygen being the substrate for the formation of oxygen-derived radicals), one may suspect that the retina is particularly well predisposed for formation of ROS (39).

The nature must have predicted the potentially adverse, propathogenic processes, such as oxidative stress or lipofuscinogenesis, in the retina, as the tissue, and particularly the macular region – very important for acute and color vision in primates – has been equipped with an array of antioxidative defense systems, including specific macular pigments (MPs): lutein, zeaxanthin and meso-zeaxanthin (44).[1]

Proper functioning of retinal antioxidation defense systems is believed to avert potential early propathogenic changes that may lead to AMD. These propathogenic changes are in fact physiological reactions that become functionally (chemically) impaired due to their intensity and the accompanying overproduction of ROS, crucial transformations of "visual" retinoids into byproducts – bisretinoids, and peroxidation and fragmentation of long-chain PUFAs (Figs. 2 and 3). This may be generally due to indisposition of the aging body – its organs, tissues and cells, and hypofunction of the aforementioned antioxidative defense systems, both enzymatic and non-enzymatic. Since these systems are dependent on the supply of exogenous nutrients, thus their activity is diet-dependent (13) – hence the idea of the role of diet and dietary supplements as preventive/therapeutic modalities for AMD (read further).

Drusen and drusogenesis

Another pathogenic component of AMD are drusen that are amorphous deposits accumulating extracellularly in the area between RPE and the inner collagenous zone of Bruch's membrane (1, 45–47). Drusen are considered the hallmark of AMD (1, 20). Clinically, they are divided into two main phenotypes, "hard" and "soft", depending on their relative size and shape. Although a few small (< 63 μm) hard drusen can be found in at least 95% of the aged populations (1), the presence of numerous larger (≥ 125 μm) hard drusen, and especially soft drusen (≥ 125–250 μm) in the macula is considered – particularly when accompanied by pigment irregularities or depigmentation – a major visible risk factor for developing the advanced forms of AMD. In fact, it was shown that degenerative changes, with either impending or executed photoreceptor cell death, occur in populations of photoreceptors overlying drusen (with a tendency to extend laterally to drusen) of all sizes, including even small subclinical structures (< 63 μm) (45, 46).

[1] It should also be mentioned that the classical antioxidative systems present within the body are classified as either enzymatic or non-enzymatic. Enzymatic systems include three basic enzymes: superoxide dismutase (SOD), catalase and glutathione peroxidase, which are dependent on metal ions, such as zinc, copper, manganium or selenium. The non-enzymatic system consists of carotenoids (including the mentioned macular pigments – lutein, zeaxanthine, meso-zeaxanthine), vitamins E and C and glutathione. The enzymatic system is endogenous; however, the metal ions that are required for its proper function are exogenous, i.e., must be supplied with food. As far as the non-enzymatic is concerned, only glutathione is an endogenous antioxidant. The remaining elements of the system, i.e., carotenoids and vitamins E and C are exogenous factors supplied with food or appropriate dietary supplements. The role of carotenoids is to neutralize singlet oxygen and reactive free radicals. What's interesting, the mechanism underlying these two activities of carotenoids are different and neutralization of free radicals may, in certain conditions (e.g., those when excessive amounts of radicals are present), change the antioxidative activity of these compounds into prooxidative activity.

Drusogenesis is a complex and multifactorial process taking place slowly over many years, and the idea is that the negative impact of the forming drusen on overlying (and neighboring) RPE-photoreceptor cells relies not only on the physical displacement of the RPE monolayer and photoreceptors by them, but also on their indirect influence, most probably *via* the activation of the immune system and local inflammation (48). Proteomic and immunohistochemical analysis of drusen has revealed many protein constituents, including – in addition to RPE remnants – a number of immune-associated elements/molecules, such as dendritic cell processes, immunoglobulins, class II antigens, and components of the complement cascade, e.g., activators, inhibitors (notably CFH), activation-specific complement fragments, and terminal pathway components, including the membrane attack complex (MAC; C5b-9), the latter being lethal not only to foreign pathogens but also to local host cells and tissues (such as RPE, photoreceptors, and other ocular structures) (36, 48, 49).

The complement system is the key element of the innate immune system in host defence (50, 51). It seems likely that local inflammation and activation of the complement cascade, with uncontrolled generation of MAC, may actively contribute to drusogenesis, RPE/photoreceptor degeneration, and Bruch's membrane disruption (associated with neovascular – wet AMD) (17, 47). And *vice versa*, at least some material collected in drusen is endowed with immunogenic properties (e.g., CEP – the lipid peroxidation product), which activate T-cells and macrophages, leading thus to stimulation of the immune responses of both innate and adaptive immune systems that in AMD work in concert (31, 52).

Although drusen constitute an established link in the pathogenesis of AMD (drusen are in fact a hallmark of AMD), they alone do not seem to be sufficient to drive the AMD pathology.

Inflammation

Although the role of inflammation in the pathogenesis of AMD is widely accepted, obviously AMD is not a classic inflammatory disease (31, 53, 54). The state that resembles in some aspects inflammation and may apply to the process taking place in AMD neurodegenerative pathology is named parainflammation (55). This process is thought to be a tissue response to noxious stress induced by various stressors, including oxidative stress. It usually has slow course and characteristics of low grade chronic process which intensifies with age (56). Inflammation – parainflammation plays in concert with the complement system (54).

In consequence, parainflammation, together with microglia activation and macrophage infiltration, as well as activation of the complement cascade, especially alternative pathway, with uncontrolled generation of MAC, may actively contribute to AMD development by increasing drusogenesis, RPE/photoreceptor damage, leading to their degeneration, and Bruch's membrane disruption (associated with the late-stage neovascular AMD).

Lipofuscinogenesis, oxidative stress, drusogenesis, PUFAs peroxidation-fragmentation and inflammation – how far to AMD?

All the mentioned processes – lipofuscinogenesis, oxidative stress, drusogenesis, PUFAs peroxidation-fragmentation and parainflammation – can be formed in different tissues to varying extent even in physiology, and more intensively in age-related physiology (without obvious pathological symptoms); however, their pathogenic potential reveals when they are overactive for years and their products formed in excess, and/or in the presence of some additional factors favoring or strengthening propathogenic mechanisms.

The retina lipofuscin contains an array of visual/retinoid cycle-derived retinoids (which are absent from other age pigments – lipofuscins accumulated in e.g., neurons, cardiomyocytes, skeletal muscle cells), and just their presence, and especially the presence of various bisretinoids (e.g., A2E) endowed with photocytotoxic potential, renders the ocular age-pigment (lipofuscin) into a group of endogenous material with a high pathogenic risk. The process of lipofuscinogenesis is tightly linked with oxidative stress, the latter having an impact on PUFAs peroxidation and fragmentation, as well as formation of immunogenic carboxyalkylpyrrole-protein adducts that accumulate in drusen and blood. Thus again, concerning PUFAs-derived oxidative protein modifications, the retina, due to intensive supply of oxygen, high levels of light exposure, and distinctly high levels of a given fatty acid such as most unsaturated DHA, results in its natural predisposition to ROS generation and PUFAs peroxidation. These phenomena, together with chronic low grade inflammation (parainflammation) related with activated immune system and drusen-containing ingredients with different propathogenic – immunogenic potential, are prone to generate pathologic responses, whose intensity rises with aging, culminating in the gradual appearance of clinically-relevant visual symptoms typical for early-intermediate stages of AMD.

Interestingly, there are more and more experimental data which strengthen the role not only of innate immunity, but also of adaptive immunity in AMD development (52, 54, 57–59). A question whether AMD should be renamed into autoimmune macular disease becomes a vivid issue (59), as genetic predispositions include genes, whose SNPs lead to enhanced immune responses (6) – the risk factors that may be active from the very beginning of our existence.

Choroidal neovascularization

The presence in the macula region of subfoveal newly formed blood vessels originating from choroidal circulatory system (choroidal neovascularization – CNV) in AMD patients is nearly automatically diagnosed as the wet AMD. CNV is an example of neoangiogenesis or angiogenesis and is a process of blood vessel formation (angiogenesis) based on existing vessels.

Blood vessels formed during vasculogenesis, mainly in embryonic life, do not undergo further growth but are stable. The processes which require periodic blood vessel reconstruction, e.g., menstruation, placenta formation or changes in the mammary gland during lactation, form an exception – they represent physiologic neoangiogenesis. Another type of physiological angiogenesis is the formation of vessels in a damaged tissue/organ requiring repair (e.g., wound healing). Neoangiogenesis may also occur as an unwanted phenomenon – pathologic angiogenesis, as is the case for example during tumor growth, or its occurrence in physiologically avascular tissues, such as cornea, vitreous body or the retina macula region. Principal mechanisms underlying physiologic and pathologic angiogenesis are generally similar (although some differences is vessel quality may exist); different may be causing factors, although hypoxia is a major direct proangiogenic condition. A simplified sequence of hypoxia-driven angiogenic pathway may be as follows: hypoxia →HIF-1 (hypoxia-inducible factor) → [gene expression] VEGF-A (vascular endothelial growth factor) → VEGFR-2/VEGFR-1/NRP-1 driven signaling → angiogenesis.

Neovascularization results from a functional dominance of angiogenic factors (e.g., vascular endothelium growth factor – VEGF) over antiangiogenic/angiostatic factors (e.g., pigment epithelium growth factor – PEDF), despite whether the primary event is an increase of angiogenic activity or a decrease of antiangiogenic activity. Molecularly, angiogenesis-neovascularization is a highly complex process involving numerous specific molecules, receptors and signaling pathways (60, 61). Many of them have been recognized and some are targets for modern therapeutics.

Regarding CNV in AMD, an initiation of subfoveal process of neovascularization originating from microcapillary blood vessels of the choroid is still unclear, particularly when the causing factor(s) and primary molecular/cellular events are concerned (62–64).

One of the postulated proangiogenic mechanisms may be linked to the existence of drusen between RPE monolayer and Bruch's membrane. The growing number and size of drusen, as well as the appearance of soft drusen, may lead to local detachment of RPE from Bruch's membrane and choriocapillaries (the latter supplying blood, oxygen and nutrients to external retina layers) and, in consequence, to the appearance of local hypoxia. Hypoxia subsequently provokes the expression of hypoxia-inducible factor-1α – HIF-1α, which, after binding with HIF-1β, becomes an active molecule (HIF-1) capable of promoting expression of several genes, including gene encoding VEGF-A family of proangiogenic factors stimulating the initiation of choroidal neovascularization – CNV (wet AMD).

Oxidative stress and chronic low grade inflammatory process – parainflammation (both taking part in the AMD pathogenesis) may also contribute to the initiation of CNV, because in the course of these processes many factors of various biological activity are expressed, including proangiogenic factors, e.g., VEGF-A (but not only). It is worth of mentioning that recently published experimental data have documented that oxidative stress is in fact able to promote ocular neovascularization (65).

Experiments carried out on mice with laser-induced rupture of Bruch's membrane (an animal model of CNV) have shown that subretinal injection of CEP-MSA (mouse serum albumin) significantly augmented CNV (37). Further experiments utilizing the "human" adduct CEP-HSA (human serum albumin) have documented angiogenic properties of the adduct in two widely used angiogenesis model systems, namely the chick chorioallantoic membrane and rat corneal micropocket assay. The obtained results showed CEP-HSA to be highly potent (active in picomolar amounts) inducer of neovascularization that utilized VEGF-independent pathways (37). While VEGF realizes its action *via* specific VEGF receptor-mediated signaling pathway, CEP-induced angiogenesis probably involves activation of toll-like receptor type 2 (TLR2) (66).

The mechanisms (depicted above) possibly underlying the initiation of CNV in AMD patients

strongly suggest that the CNV phenomenon can be considered a complication of the dry-atrophic form AMD (see Fig. 3).

The cited observations referring to VEGF-independent CNV may have important practical consequences, since CNV occurring in wet AMD is currently treated with anti-VEGF drugs (read later). Yet, CNV resistant to anti-VEGF therapy is not unusual in AMD patients, indicating in such cases the role of VEGF-independent mechanism(s). Therefore, it is not unlikely that in such VEGF-independent CNV in AMD patients, CEP oxidative protein modifications and TLR2-directed signaling pathway may operate – a suggestion that is possible (based on animals' data), yet requiring experimental support for its validity in humans.

Detailed molecular and clinical analysis of and discussion on ocular neovascularization, including CNV, is presented in recently published articles (60, 61, 63).

Therapeutic approaches

Although the symptomatology of AMD is relatively straightforward, there is evidently many various pathogenetic factors, and thus complex mechanisms underlying the disease. Some mechanisms lie within frames of aging physiology, some touch the level of pathology, and some represent already irreversible pathology – everything with a tendency to increase its activity as a function of age. Furthermore, not all molecular links in the disease pathogenesis are recognized. For these reasons, available therapies are not causal treatments but, generally, they help to avoid or, what happens more frequently, to retard further vision loss rather than to substantially improve vision. None of up-to-now used treatments can definitely "cure" the disease or reverse its course. The use of anti-VEGF agents in patients with the wet form AMD may be considered a therapeutic breakthrough, due to their positive effects on quality of vision at least in some patients, yet currently much effort is still done in searching new more effective approaches. The situation concerning therapy of the dry – atrophic AMD is really depressing, as there is no approved strategy for this condition; however, an intensive research to find acceptable remedy is in progress.

Wet – neovascular AMD

Photodynamic therapy

Not far ago, in 2000, an approval of the photodynamic therapy (PDT) using an intravascular photosensitizer verteprofin (a benzoporphyrin derivative monoacid, BPD; Visudine) and low energy visible red laser (689 nm), has at that time revolutionized the treatment of rapidly progressing and devastating subfoveal CNV. The verteporfin-based PDT or vPDT procedure works by inducing occlusion of new vessels – this effect is achieved by light-evoked activation of verteporfin with a subsequent transfer of its energy to molecular oxygen, resulting in the formation of highly reactive singlet oxygen capable of producing direct damage of endothelial cells. Although vPDT has become increasingly prevalent, its effect on the patients' vision is limited – there is a large number of CNV recurrences after PDT and the unpredictable repetition of treatments in 3-months intervals in PDT treatment (67, 68). At present, verteporfin-based PDT alone is rather rarely used in the clinic; it can be used however in combination with anti-VEGF agent and/or steroid as a second line therapy in patients not responding to monotherapy with anti-VEGF agents (68, 69).

Anti-VEGF therapy

Currently, three anti-VEGF agents are in use in ophthalmology: bevacizumab (Avastin), ranibizumab (Lucentis) and aflibercept (Eylea). All agents are injected intravitreously under sterile conditions and require proper treatment schedule.

Avastin – bevacizumab, a full-length humanized monoclonal antibody (MW ~149 kDa) that targets all isoforms of VEGF-A family. Its basic characteristics is: bioavailability: 100%, half-life ($T_{\frac{1}{2}}$): 20 days (range: 11–50 days), dissociation constant: 0.5–1 nM, it binds with two VEGF molecules. Avastin is a drug approved in 2004 (FDA) for intravenous use in oncology. Soon, in 2005, commercially available Avastin applied intravitreously was tested in AMD patients with CNV and appeared an effective drug, becoming since then and until now the most widely used anti-VEGF agent throughout the world (due to its low cost and good efficacy comparable to Lucentis and Eylea). Avastin has no official registration for its use in wet AMD and is used on an "off-label" basis. One intravitreous injection contains 1.25 mg of bevacizumab in 50 µL of the original commercially available sterile solution (vials containing 100 mg bevacizumab in 4 mL solution).

Lucentis – ranibizumab is a recombinant humanized monoclonal antibody fragment (MW ~48 kDa) that inhibits all isoforms of VEGF-A. Basic charcteristics of ranibizumab: bioavailability: 100%, $T_{\frac{1}{2}}$ (vitreous): ~10 days, dissociation constant: 0.14 nM; it binds one VEGF molecule. In fact, ranibizumab is a modified fragment of bevacizumab showing spectrum of clinical activity similar to that

of bevacizumab. Lucentis was approved as a therapy for wet AMD in 2006 (FDA) and in 2007 (EMA). One intravitreous injection contains 0.5 mg ranibizumab in 50 µL volume.

Monthly injections of ranibizumab and bevacizumab are the current "gold standard" therapy in the management of CNV associated with AMD. The treatment schedule includes three monthly injections followed by individualized treatment regimens, including traditional PRN (pro-re-nata) and "treat-and-extend". However, as shown in preclinical studies carried out on monkeys, repeated anti-VEGF therapy strongly reduced the diameter of the choriocapillaries (70) what in consequence may lead to some undesirable effects, including atrophy of RPE-photoreceptor complex (71).

Eylea – aflibercept (also known as VEGF-Trap or VEGF-Trap-Eye) – is a soluble fusion protein (MW ~110 kDa) containing fragments of two types of VEGF receptors, VEGFR-1 (domain 2) and VEGFR-2 (domain 3), linked with the Fc fragment of human immunoglobulin G (IgG). Aflibercept behaves as a soluble decoy receptor with a dissociation constant ~0.5 pM, recognizing and neutralizing all members of VEGF-A family, VEGF-B and placenta growth factor (PlGF). It was registered for wet AMD in 2011/2012. One intravitreous dose of Eylea containins 2 mg aflibercept (50 µL), and the recommended schedule is as follows: three monthly injections followed by additional bimonthly injections (if needed); another possible variant includes bimonthly injections from the beginning of the therapy.

Macugen – pegaptanib sodium (containing polyethylene glycol – PEG). Pegaptanib is a 28-base RNA aptamer (MW ~50 kDa) that binds and neutralizes selectively only one member of VEGF-A family, i.e., VEGF-A_{165} – the most active proangiogenic VEGF-A isomer. Macugen is in fact the first drug officially registered for wet AMD (FDA, 2004; EMA, 2006). Actually, because of preferable "position" of Avastin, Lucentis and Eylea, clinical importance of Macugen substantially decreased, being in many countries not used against CNV in AMD patients. The recommended intravitreous dose of Macugen is 0.3 mg applied every 6 weeks.

Emerging therapies: ongoing or discontinued clinical trials

- Small interfering RNAs:
  siRNA-027 (bevasiranib), **PF-04523655** (REDD14). In general, siRNAs are capable of blocking protein synthesis (posttranscriptional gene silencing) for specific proteins encoded by mRNAs whose target sequences are homologues to the siRNAs.

  Bevasiranib is a double-stranded siRNA directed directly against VEGF, whereas REDD14 indirectly leads to reduction of VEGF-A production (involving a primary inhibition of hypoxia-induced gene RTP801). Bevasiranib went positively through Phases I and II of clinical trials in patients with wet AMD, but did not overcome Phase III and in March 2009 the producer announced that "OPKO Health Pharmaceuticals terminates late-stage trial of bevasiranib for treatment of wet age-related macular degeneration". Concerning REDD14, no clear-cut and definitive clinical results are available until now.
- **Squalamine lactate** (Evizon) – a naturally occurring steroidal compound conjugated to spermidine at position C-3. It prevents angiogenesis by blocking the action of VEGF and integrin expression when bound to calmodulin. In earlier clinical studies (Phase I/II) the drug's intravenous formula was used; currently, the topical squalamine lactate undergoes clinical testing in the wet form AMD.
- **Palomid 529** – an investigational medicine targeting Akt/mTOR pathway (it dissociates both targets of rapamycin complexes TORC1 and TORC2). The agent reduces tumor growth, tumor angiogenesis and vascular permeability. The drug was tested in patients with wet AMD *via* subconjunctival injections. Preliminary clinical results appeared promising, yet, no conclusive data are available.
- **KH902** – recombinant soluble VEGFR protein containing binding domains of VEGFR1 and VEGFR2 combined with the Fc portion of IgG; it shows similar properties as aflibercept.
- Tyrosine kinase inhibitors:
  Vatalanib – shows an activity against the platelet derived growth factor (PDGF) receptor and c-kit receptor kinases, and shows high oral bioavailibity. **Pazopanib** – shows slightly wider activity than vatalanib, inhibiting tyrosine kinases associated with VRGF-R, PDGF-R and c-kit. Although both drugs were clinically tested in patients with wet AMD, the results have not been published yet.

Dry – atrophic AMD

In contrast to neovascular-wet AMD, where three therapeutics are currently widely used throughout the world (Avastin, Lucentis, Eylea), there is no approved therapy for atrophic-dry AMD. Based on already accepted mechanisms underlying the dry form AMD, a number of agents were/are experimentally selected and then introduced into

clinical trials, hoping that they will be active in preventing or at least in slowing the disease course. However, many of the clinically verified compounds were withdrawn from testing for various reasons – either lack or poor clinical activity, or toxic effects, or other reasons uncovered by their producers (or distributors) – pharmaceutical company/ies. Yet, a great number of therapies proposed for atrophic AMD can be evaluated with optimism, showing continued efforts of scientists and physicians in looking for acceptable treatment of the AMD pathology. Below, some agents will be shortly presented; they include: drugs that decrease oxidative stress, visual cycle modulators, neuroprotectants, drugs that suppress inflammation, including anticomplement agents [according to: (72–75)].

- Drugs that decrease oxidative stress:
  AREDS-2 formula (Age-Related Eye Disease Study 2) – a composition of two macular xanthophylles (lutein, zeaxanthin), vitamins (E, C), copper, zinc (both in oxide form) – all ingredients possessing direct or indirect antioxidant activity A mixture contained also two ω-3 PUFAs: EPA and DHA, but their role in AMD is discussable (due to their both positive and possible negative potential (23, 61)); Phase III clinical study was completed at the end of 2013. Oral use.
  OT-551 (Tempol; a prodrug of tempol hydroxylamine – tempol-H) – SOD mimetic and NRF2 activator. Phase II. Topical application.

- Visual cycle modulators:
  ACU-4429 (Emixustat-HCl) – a small non-retinoid; it inhibits retinol isomerization by acting on RPE65 and thus slows the rod visual cycle. It is designed to prevent the generation of toxic by-products of the visual cycle. Phase II/III – the study is currently ongoing. Oral use.
  Fenretinide – a synthetic retinol analog; it inhibits retinol binding to retinol binding protein – RBP. The "positive" results of Phase II clinical trial were not statistically significant and the drug did not enter Phase III study. Oral use.

- Neuroprotectants:
  CNTF (ciliary neurotrophic factor; NT-501) – a neuroprotective cytokine that prevents photoreceptor degeneration. Phase III – ongoing. An intravitreal implant using "encapsulated cell technology".
  Brimonidine tartrate – an α_2-adrenergic receptor agonist with neuroprotective potential. It is an approval anti-glaucoma medicine (eye drops). Phase II study with AMD patients using a sustained delivery system is underway. Intravitreal implant.
  Tandospirone – a selective 5-HT_{1A} receptor agonist that as an oral version is used as anxiolytic and antidepressant; it protects photoreceptors and RPE cells from photo-oxidative stress. The drug completed Phase III trial in dry AMD in 2012, but the obtained results have not yet been released. Topical application.
  Glatiramer acetate (Copaxone) – an immunomodulatory drug currently used to treat multiple sclerosis; multifunctional agent: it suppresses T-cells, downregulates inflammatory cytokines, reduces amyloid-β-induced retinal microglial cytotoxicity. Phase II study is underway. Subcutaneous injection.

- Drugs that reduce toxic by-products:
  RN6G (PF-4382923) – a humanized monoclonal antibody against amyloid-β that accumulates in drusen. Phase II study is ongoing. Intravenous injection.
  GSK 933776 – a humanized monoclonal antibody against amyloid-β N-terminus. Phase II study is currently underway. Intravitreal injection.

- Drugs that suppress inflammation:
  ILuvien (fluocinolone acetonide) – an anti-inflammatory and immonosupressing corticosteroid. Phase II study with dry AMD patients is in progress (currently approved in Europe for diabetic macular edema). Intravitreal implant.
  POT-4 (Compstatin, AL-78898A) – a synthetic cyclic peptide that irreversibly inhibits complement C3 with resulting inhibition of complement pathways and prevention of membrane attack complex (MAC) formation. Phase II study completed, the results have not yet been released. Intravitreal injection.
  Soliris (Eculizumab) – a humanized IgG antibody against complement C5. It is the first FDA approved complement inhibitor for the treatment of paroxysmal nocturnal hemoglobinuria. It prevents lysis of erythrocytes and the formation of MAC. Phase II study with AMD patients – no clear-cut results are available. Intravenous injection.
  FCFD4514S (Anti-Factor D Fab; Lampalizumab) – a humanized monoclonal antibody (Fab fragment) against complement factor D; it inhibits complement activation and chronic inflammatory process in tissues. Phase II study

with dry AMD patients completed and Phase III trial is planned. Intravitreal injection.
LFG1905 – a fully human antibody against complement C5. Phase II study in progress.
Intravitreal injection.
ARC1905 – aptamer-based complement C5 inhibitor. Phase I clinical trial. Intravitreal injection.

- Vascular enhancers:
  MC-1101 – a facilitator of choroidal blood flow. Phase II/III study. Topical application.

- Stem cell replacement:
  MA09-hRPE – a human embryonic stem cell-derived RPE cells. Phase I/II study. Stem cell transplant.
  itMSC-DryAMD – an "ischemic tolerant" mesenchymal stem cells. Phase I/II study. Stem cell transplant.
  HuCNS-SC – a human central nervous system stem cells. Phase I/II study. Stem cell transplant.

Actually, many potential therapeutic strategies focused on complement modulation are in preclinical studies, they include (76):

- protease inhibitor (C1-INH; inhibition of C1q, C1r, C1s),
- factor B inhibitor (TA106 – Fab; inhibition of C3 convertase),
- C3-inhibitor (TT30/CR2-fH – fusion protein containing CFH and CR2; inhibition of C3 convertase),
- recombinant complement factor H (rCFH from human plasma; replacement of CFH and inhibition of C3 convertase),
- antagonist of C5aR (peptide JPE-1375/JSM-7717 and PMX53; binding C5a),
- gene therapies with: human CD46 (AdCAGCD46; inhibition of C4b and C3b) and human CD59 (AdCAGsCD59; inhibition of MAC).

Recent analysis published in the Cochrane Review series devoted to complement inhibitors for AMD provides a meaningful conclusion: "There is insufficient information at present to generate evidence-based recommendations on the potential safety and efficacy of complement inhibitors for prevention or treatment of AMD. However, we anticipate the results of ongoing trials." (77).

Comment on dietary supplement-based treatment for dry AMD

One of the mentioned therapies, i.e., AREDS-2 study/formula, needs comment, because it deals with an "antioxidant" dietary supplementation that in fact was and still is widely used by AMD patients, as well as by people being at risk of developing the disease. The concept that antioxidant agents may prevent the development and/or the course of AMD finds its rationale in the disease pathogenesis, where oxidative stress seems to be one of driving forces (see Figs. 2 and 3). Various antioxidant preparations were in the past and still are freely available on the market – such mixtures were recommended by ophthalmologists to their patients, becoming in fact the only modality with which to prevent or "cure" atrophic-dry form AMD. A "scientific" support for beneficial role of antioxidants in AMD came from AREDS (or AREDS-1) clinical trial whose primary aim was to evaluate the effect of pharmacological doses of nutritional supplements on the rate of progression to advanced AMD. The AREDS formula included: vitamin C (500 mg), vitamin E (α-tocopherol; 400 IU), β-caroten (15 mg), zinc (as zinc oxide; 25 or 80 mg) and copper (as cupric oxide; 2 mg) – the results were published late in 2001. According to the 2001 report, AREDS formula led to an overall 19–25% risk reduction in the disease progression in individuals who had a moderate risk of AMD development at five years' treatment (78). At that time, many enthusiastic opinions on clinical efficacy of AREDS formula announced on different occasions have appeared, including NEI Information Office – News and Events (October 2001): "Antioxidant vitamins and zinc reduce risk of vision loss from age-related macular degeneration". However, since then, a number of less enthusiastic opinions has also been published (13, 14). Interestingly, somewhat earlier it has been observed in ATBC (α-tocopherol, β-carotene cancer prevention) study that β-carotene contributes to the development of lung cancer in smokers (79). In addition, β-carotene is a precursor of vitamin A, and the visual cycle retinoids (vitamin A derivatives) may act as substrates for the formation of photocytotoxic bisretinoids (e.g., A2E). Beneficial effects of zinc have been known for a long time, however, a question arose with regard to the dose: 25 or 80 mg – which should be used? And, finally, recently there was a trend to supplement AMD patients with lutein and zeaxanthin – two naturally occurring macular pigments (xanthophylls), as well as ω-3 PUFAs (EPA, DHA), with a practical, although unproven idea: the more agents the better. Having this in mind, AREDS-2 large research project – clinical multicenter randomized study involving more than 4,000 participants (sponsored by National Eye Institute – NEI with collaboration from National Heart, Lung,

and Blood Institute – NHLBI) was initiated in 2007 and lasted till the end of 2012; its aim was to evaluate the effect of oral supplementation with macular xanthophylls (lutein, zeaxanthin) and ω-3 PUFAs (DHA, EPA) on AMD progression. The AREDS-2 formula consisted of: lutein (10 mg), zeaxanthin (2 mg), vitamin C (500 mg), vitamin E (400 IU), copper (as cupric oxide – 2 mg), EPA (650 mg), DHA (350 mg). Smaller studies (Secondary Randomization Agents – AREDS-Type Supplement) were also conducted to examine the effects of zinc (as zinc oxide) at doses of 25 and 80 mg, with particular focus on the lower dose, and elimination of β-carotene from the AREDS formula. The results of the AREDS-2 study were published in May 2013 (15) with general conclusion as follows: "Addition of lutein + zeaxanthin, DHA + EPA, or both, to the AREDS formulation in primary analysis did not further reduce risk of progression to advanced AMD. However, because of potential increased incidence of lung cancer in former smokers, lutein + zeaxanthin could be an appropriate carotenoid substitute in the AREDS formulation." In other words, there was some benefit to patients taking macular xanthophylls (instead of β-carotene), when the patients' diet was deficient in these pigments, ω-3 PUFAs did not improve the original AREDS formula, there was no difference between low dose and high dose of zinc.

In conclusion, there are still several unanswered questions concerning the described dietary supplementation, including, for example, the length of treatment necessary to see any improvement in patients' vision (whatever this means). And finally, based on recently published vast literature on diet and dietary supplements in AMD, as well as unpublished various (in terms of therapeutic output) observations of numerous ophthalmologists, one can say that pharmaceutical supplementation may, but does not have to help the AMD patients, leaving an open question on its effectiveness in practice (13). However, one should not cease being optimistic; optimism should be cherished by both the physicians when recommending appropriate dietary supplements to patients, and patients who would be regularly taking it; otherwise, the supplementation would serve no purpose whatsoever.

Yet, one should believe that the efforts of scientists – chemists, pharmacologists, physicians-ophthalmologists – will finally culminate in finding effective therapy for AMD, particularly for its widely occurring atrophic-dry form, that will find general acceptance as a therapeutic "gold standard".

REFERENCES

1. Fine S.L., Berger J.W., Maguire M.G., Ho A.C.: New Engl. J. Med. 342, 483 (2000).
2. Ferris III F.L., Wilkinson C.P., Bird A., Chakravarthy U., Chew E., Csaky K., Sadda S.R.: Ophthalmology 120, 844 (2013).
3. Chakravarthy U., Wong T.Y., Fletcher A., Piault E., Evans C., Zlateva G., Buggage R. et al.: BMC Ophthalmol. 10, 31 (2010).
4. Fritsche L.G., Fariss R.N., Stambolian D., Abecasis G.R., Curcio C.A., Swaroop A.: Annu. Rev. Genomics Hum. Genet. 15, 151 (2014).
5. Andreoli M.T., Morrison M.A., Kim B.J., Chen L., Adams S.M., Miller J.W., DeAngelis M.M., Kim I.K.: Am. J. Ophthalmol. 148, 869 (2009).
6. Gorin M.B.: Mol. Aspects Med. 33, 467 (2012).
7. Ardeljan D., Chan C.C.: Prog. Retin. Eye Res. 37, 68 (2013).
8. Cong R., Zhou B., Sun Q., Gu H., Tang N., Wang B.: Ann. Epidemiol. 18, 647 (2008).
9. Lawrensaon J.G., Evans J.R.: BMC Public Health 13, 564 (2013).
10. Hunter J.J., Morgan J.I.W., Merigan W.H., Sliney D.H., Sparrow J.R., Williams D.R.: Prog. Retin. Eye Res. 31, 28 (2012).
11. Algvere P.V., Marshall J., Seregard S.: Acta Ophthalmol. Scad. 84, 4, 2006.
12. Roberts J.E.: J. Photochem. Photobiol. 64, 136 (2001).
13. Nowak J.Z.: Mil. Pharm. Med. 4, 1 (2012).
14. Evens J.R., Lawrenson J.G.: Cochrane Database Syst. Rev. 11, CD000254 (2012)
15. Age-Related Eye Disease Study 2 Research Group (Chew E.Y., Clemons T.E., SanGiovanni J.P., Danis R., Ferris F.L. 3rd, Elman M., Antoszyk A. et al.): JAMA 309, 2005 (2013).
16. Nowak J.Z.: Pharmacol. Rep. 58, 353 (2006).
17. Anderson D.H., Radeke M.J., Gallo N.B., Chapin E.A., Johnson P.T., Curletti C.R., Hancox L.S. et al.: Prog. Retin. Eye Res. 29, 95 (2010).
18. Ambati J., Fowler B.J.: Neuron 75, 26 (2012).
19. Bhutto I., Lutty G.: Mol. Asp. Med. 33, 295 (2012).
20. McConnell V., Silvestri G.: Ulster Med. J. 74, 82 (2005).
21. Gross A.K., Wensel T.G.: in: Adler's Physiology of the Eye, Levin L.A., Nilsson F.E., Ver Hoeve J. et al. Eds., chapter 18, pp. 395–410, Elsevier/Saunders, Edinburgh 2011.
22. Sparrow J.R., Gregory-Roberts E., Yamamoto K., Blonska A., Ghosh S.K., Ueda K., Zhou J.: Prog. Retin. Eye Res. 31, 121 (2012).

23. Nowak J.Z.: Pharmacol. Rep. 65, 288 (2013).
24. Zhou J., Jang Y.P., Kim S.R., Sparrow J.R.: Proc. Natl. Acad. Sci. USA 103, 16182 (2006).
25. Schutt F., Bergman M., Holz F.G., Dithmar S., Volcker H.E., Kopitz J.: Graefes Arch. Clin. Exp. Ophthalmol. 245, 391 (2007).
26. Wu Y., Yanase E., Feng X., Siegel M.M., Sparrow J.R.: Proc. Natl. Acad. Sci. USA 107, 7275 (2010).
27. Sparrow J.R.: Adv. Exp. Med. Biol. 703, 63 (2010).
28. Ma W., Coon S., Zhao L., Fariss R.N., Wong W.T.: Neurobiol. Aging 34, 943 (2013).
29. Klaska I., Nowak J.Z.: Post. Hig. Med. Dosw. (online) 61, 167 (2007).
30. Calippe B., Guillonneau X., Sennlaub F.: CR Biol. 337, 178 (2014).
31. Nussenblatt R.B., Lee R.W.J., Chew E., Wei L,, Liu B., Sen H.N., Dick A.D., Ferris F.L.: Am. J. Ophthalmol. 158, 5 (2014).
32. Sparrow J.R., Boulton M.: Exp. Eye Res. 80, 595 (2005).
33. Mitter S.K., Rao H.V., Qi X., Cai J., Sugrue A., Dunn W.A. Jr, Grant M.B., Boulton M.E.: Adv. Exp. Med. Biol. 723, 83 (2012).
34. Salminen A., Kaarniranta K., Kauppinen A.: Aging (Albany NY) 4, 166 (2012).
35. Ablonczy D., Higbee D., Anderson D.M., Dahrouj M., Grey A.C., Gutierrez D.B., Koutalos Y. et al.: Invest. Ophthalmol. Vis. Sci. 54, 5535 (2013)
36. Crabb J.W., Miyagi M., Gu X., Shadrach K., West K.A., Sakaguchi H., Kamei M. et al.: Proc. Natl. Acad. Sci. USA 99, 14682 (2002).
37. Ebrahem Q., Renganathan K. Sears J., Vasanji A., Gu X., Lu L., Salomon R.G. et al.: Proc. Natl. Acad. Sci. USA 103, 13480 (2006).
38. Salomon R.G., Hong L., Hollyfield J.G.: Chem. Res. Toxicol. 24, 1803 (2011).
39. Nowak J.Z.: in: Oxidative Stress in Applied Basic Research and Clinical Practice, Dietrich-Muszalska A., Chauhan V., Grignon S. Eds., chapter 24; Springer 2014.
40. Hollyfield J.G., Salomon R.G., Crabb J.W.: Adv. Exp. Med. Biol. 533, 83 (2003).
41. Gu X., Meer S.G., Miyagi M., Rayborn M.E., Hollyfield J.G., Crabb J.W., Salomon R.G.: J. Biol. Chem. 278, 42027 (2003).
42. Hollyfield J.G., Bonilha V.L., Rayborn M.E., Yang X., Shadrach K.G., Lu L., Ufret R.L. et al.: Nat. Med. 14, 194 (2008).
43. Hollyfield J.G., Perez V.L., Salomon R.G.: Mol. Neurobiol. 41, 290 (2010).
44. Kijlstra A., Tian Y., Kelly E.R., Berendschot T.T.: Prog. Retin. Eye Res. 31, 303 (2012).
45. Bressler N., Silva J., Bressler S., Fine S.L., Green W.R.: Retina 14, 130 (1994).
46. Algvere P.V., Seregard S.: Acta Ophthalmol. Scand. 81, 427 (2003).
47. Nowak J.Z.: Mag. Okul. 3, 174 (2005).
48. Anderson D.H., Mullins R.F., Hageman G.S., Johnson L.V.: Am. J. Ophthalmol. 134, 411 (2002)
49. Crabb J.W.: Cold Spring Harb. Perspect. Med. (2014): doi: 10.1101/cshperspect.a017194.
50. Gasque P., Dean Y.D., McGreal E.P., VanBeek J., Morgan B.P.: Immunopharmacology 49, 171 (2000).
51. Zipfel P.F., Heinen S., Józsi M., Skerka C.: Mol. Immunol. 43, 97 (2006).
52. Cruz-Guilloty F., Saeed A.M., Duffort S. Cano M., Ebrahimi K.B., Ballmick A., Tan Y. et al.: PLoS One 9, e88201 (2014).
53. Donoso L.A., Kim D., Frost A., Callahan A., Hageman G.: Surv. Ophthalmol. 51, 137 (2006).
54. Weber B.H.F., Charbel Issa P., Pauly D., Herrmann P., Grassmann F., Holz F.G.: Dtsch. Arztebl. Int. 111, 133 (2014).
55. Xu H., Chen M., Forrester J.V.: Prog. Retin. Eye Res. 28, 348 (2009).
56. Medzhitov R.: Nature 454, 428 (2008).
57. Ambati J., Fowler B.J.: Neuron 75, 26 (2012).
58. Joseph K., Kulik L., Coughlin B., Kunchithapautham K., Bandyopadhyay M., Thiel S., Thielens N.M. et al.: J. Biol. Chem. 288, 12753 (2013).
59. Camelo S.: Autoimmune Dis. 2014, 532487 (2014).
60. Campochiaro P.A.: J. Mol. Med. 91, 311 (2013).
61. Nowak J.Z.: Mag. Lek. Okul. 7(1), 42 (2013).
62. Campochiaro P.A.: J. Cell Physiol. 184, 301 (2000).
63. Grossniklaus H.E., Kang S.J., Berglin L.: Prog. Retin. Eye Res. 29, 500 (2010).
64. Miller J.W., Le Couter J., Strauss E.C., Ferrara N.: Ophthalmology 120, 106 (2013).
65. Dong A., Xie B., Shen J., Yoshida T., Yokoi K., Hackett S.F., Campochiaro P.A.: J. Cell Physiol. 219, 544 (2009).
66. West X.Z., Malinin N.L., Merkulova A.A., Tischenko M., Kerr B.A., Borden E.C., Podrez E.A. et al.: Nature 467, 972 (2010).
67. Gaynes B.I., Fiscella R.G.: Expert Opin. Drug Saf. 3, 345 (2004)

68. Michels S., Hansmann F., Geitzenauer W., Schmidt-Erfurth U.: Invest. Ophthalmol. Vis. Sci. 47, 371 (2006).
69. Schmidt-Erfurth U., Richard G., Augustin A., Aylward W.G., Bandello F., Corcòstegui B., Cunha-Vaz J. et al.: Acta Ophthalmol. Scand. 85, 486 (2007).
70. Schraermeyer U., Julien S.: Expert Opin. Biol. Ther. 13, 157 (2013).
71. Rofagha S., Bhisitkul R.B., Boyer D.S., Sadda S.R., Zhang K.: Ophthalmology 120, 2292 (2013).
72. Damico F.M., Gasparin F., Scolari M.R., Pedral L.S., Takahashi B.S.: Arq. Bras. Oftalmol. 75, 71 (2012).
73. Evans J.B., Syed B.A.: Nature Rev. 12, 501 (2013).
74. Leung E., Landa G.: Expert Rev. Clin. Pharmacol. 6, 565 (2013).
75. Singer M.: F1000Prime Rep. 6, 29 (2014).
76. Troutbeck R., Al-Qureshi S., Guymer R.H.: Clin. Exp. Ophthalmol. 40, 18 (2012).
77. Williams M.A., McKay G.J., Chakravarthy U.: Cochrane Database Syst. Rev. 1:CD009300 (2014).
78. Age-Related Eye Disease Study Research Group: Arch Ophthalmol. 119, 1417 (2001).
79. Albanes D., Heinonen O.P., Taylor P.R., Virtamo J., Edwards B.K., Rautalahti M., Hartman A.M. et al.: J. Natl. Cancer Inst. 88, 1560 (1996).

Acta Poloniae Pharmaceutica – Drug Research, Vol. 71 No. 6 pp. 917–921, 2014 ISSN 0001-6837
Polish Pharmaceutical Society

FULL PAPERS

EFFECT OF VALPROIC ACID ON THE PROLIFERATION AND APOPTOSIS OF THE HUMAN MELANOMA G-361 CELL LINE

EWA CHODUREK, ANNA KULCZYCKA, ARKADIUSZ ORCHEL, EWELINA ALEKSANDER-KONERT and ZOFIA DZIERŻEWICZ

Medical University of Silesia in Katowice, School of Pharmacy with the Division of Laboratory Medicine, Department of Biopharmacy, Jedności 8, 41-200 Sosnowiec, Poland

Abstract: Melanoma malignant is characterized by a high malignancy and low susceptibility to treatment. Due to these properties, there is a growing interest in compounds that would have the ability to inhibit proliferation, induce differentiation of tumor cells and initiate the apoptotic pathway. *In vitro* and *in vivo* research indicate that valproic acid (a histone deacetylase inhibitor) may have anti-cancer properties. In our study, the role of VPA on proliferation and apoptosis in G-361 human melanoma cell line was examined. Obtained results indicated that administration of VPA at concentrations above ≥ 1 mM led to significant inhibition of cell growth. Simultaneously, it was observed that VPA at higher concentrations (5 and 10 mM) caused an increase in caspase-3 activity.

Keywords: malignant melanoma, G-361 cell line, valproic acid, proliferation, caspase-3 activity

Malignant melanoma (*melanoma malignum*) is the most dangerous form of skin cancer. Melanoma that arises from melanocytes is an aggressive, immunogenic and malignant tumor that spreads early *via* the blood and the lymphatics. It is most commonly found in the skin or mucous membranes of the mouth and genitals. Melanoma can arise from clinically normal skin or pigmented nevi (mainly atypical nevi) (1, 2). It can also occur in the eye or meninges. Rapid growth, early and multiple metastases and low susceptibility to treatment determine the significant malignancy of the melanoma. The etiopathogenesis of malignant melanoma is associated with malignant transformation of pigment cells – melanocytes (3). Melanocyte during ontogeny can transform into pigmented cell, which lacks of cytoplasmic projections, has the ability to hyperplasia, could accumulate in the groups within the epidermis and instil into dermis. Nevus cells form benign pigmented lesions, called acquired nevi. Benign nevi can be converted into atypical moles (dysplastic). Atypical/dysplastic nevus syndrome (ANS/DNS) can be passed from generation to generation and is associated with a high risk of developing melanoma in a family. Clark et al. proposed a model which implies a gradual transformation of melanocytes into dysplastic cells, and further into atypical cells with full malignant phenotype (1, 4, 5). More scientific papers point to the importance of tumor hypoxia in melanoma progression (6).

The acquisition of a malignant phenotype is caused by an imbalance between the action of two groups of genes – oncogenes and suppressors. Changes in these genes (during oncogenesis) result from the accumulation of mutations and epigenetic modifications. Extensive research in the field of melanoma etiopathology allowed identifying several of genes that mutation or inactivation contribute to the development of the disease (7).

In recent years, due to the low effectiveness of chemotherapy and radiotherapy in the anti-melanoma treatment, there is a growing interest in compounds that would have the ability to inhibit proliferation, induce differentiation of tumor cells and directing them to the apoptotic pathway. Scientific reports indicate a potential anti-cancer action of valproic acid (VPA), which belongs to the histone deacetylase inhibitors (HDACis) (8–11). It has been shown that VPA affects the activity of two of the four classes of HDAC, namely class I and II (subclass IIa). Exceptions in class IIa are HDAC 9, and HDAC 11, which are activated by VPA (12, 13).

* Corresponding author: e-mail: echodurek@sum.edu.pl

Cervoni and Szyf confirmed an indirect effect of VPA on the DNA demethylation, by increasing the availability of methylated nucleotides for DNA demethylases (14). VPA as a HDACi could form less condensed structure of chromatin, increase the DNA sensitivity to digestion with nucleases and increase the availability of DNA to intercalating agents. The compound also decreases the expression of proteins involved in the stabilization of chromatin, including SMC 1-6 (structural maintanance of chromosome), SMC binding proteins, DNA methyltransferase 1 (DNMT1), and heterochromatin protein 1 (HP1). Additionally, it may have an impact on transcription factors or other factors involved in important cellular processes, reduce the stability of the mRNA transcripts, and control proteasome-mediated protein degradation (15–18). All of these properties make probable the proapoptotic activity of this compound.

Different HDAC inhibitors, classified to short-chain fatty acids, benzamides, hydroxymates, cyclic tetrapeptides (19), may cause various changes at the molecular level (20, 21) resulting in various changes of the cellular phenotype. They may include e.g., downregulation of the antiapoptotic proteins, upregulation of the proapoptotic proteins, ROS generation or disruption of cell cycle checkpoints (22). One of the greatest challenge in developing the effective therapy is the precise evaluation of the effect of the compound on cell proliferation, differentiation and death.

The aim of the study was to investigate the influence of VPA on biology and function of human melanoma cell line (G-361).

EXPERIMENTAL

Cells

The malignant melanoma cell line (G-361) was purchased from ATCC-LGC Standards. To ensure proper proliferation, cells were grown in medium containing 90% McCoy's medium (Sigma-Aldrich), 10% fetal bovine serum (PAA), 100 U/mL penicillin and 100 µg/mL streptomycin (Sigma-Aldrich), and supplemented with 10 mM HEPES (Sigma-Aldrich). The culture flasks were incubated at 37°C in a humidified atmosphere containing 95% air and 5% CO_2.

Cell proliferation

To examine the proliferation activity, the *In Vitro* Toxicology Assay Kit based on reduction of the tetrazolium ring of XTT reagent (Sigma-Aldrich) was used. Melanocytes were cultured in 96-well plates (at initial density 8×10^3 cells/ well) in 200 µL of medium for 24 h. Subsequently, the cells were treated with VPA (Sigma-Aldrich) in a wide range of concentrations: 0.1–10 mM. After 72 h of incubation, medium was removed and RPMI medium without phenol red (Sigma-Aldrich) with XTT reagent (20% of medium volume) was added. After 4 h, the absorbance was measured at 450 nm

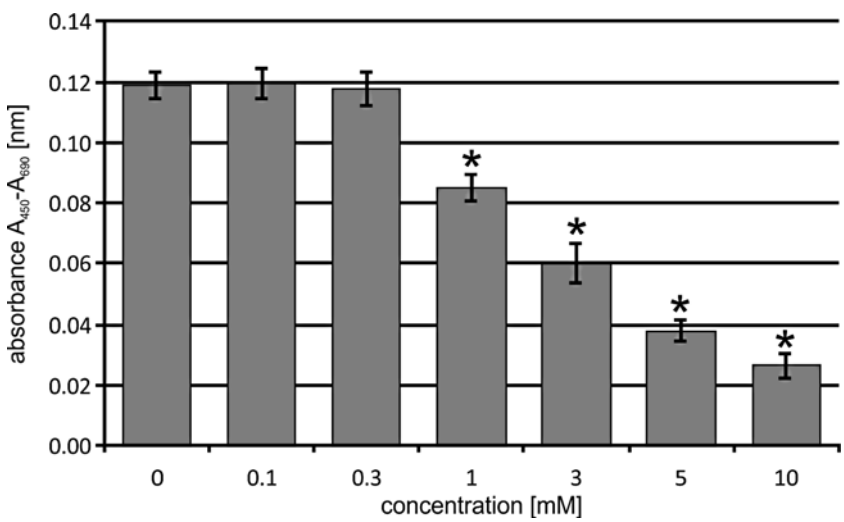

Figure 1. The effect of VPA on the proliferation of the human melanoma G-361 cell line. The cells were cultured for 72 h in the presence of various concentrations of VPA. Each bar represents the mean ± SD;* $p < 0.05$ *versus* control cells (untreated)

and 690 (reference wavelength) using the MRX Revelation plate reader (Dynex Technologies).

Caspase-3 activity

To evaluate the proapoptotic caspase-3 activity, the Colorimetric Caspase-3 Assay Kit (Sigma-Aldrich) was used. Cells were seeded into tissue culture dishes (21.5 cm^2) at the initial density of 2×10^6 cells/dish in 5 mL of culture medium. After 24 h cultivation, cells were incubated with VPA at 1, 3 and 10 mM for 2 days. Simultaneously, the control cells (untreated) and cells treated with 10 mM sodium butyrate (NaB) were cultivated. At the end of incubation, cells were lysed, centrifuged (16 000 × g; 10 min) and stored at –80°C. Activity of the active caspase-3 was determined using Ac-DEVD-pNA as substrate. Enzyme samples were incubated with substrate at 37°C for 2 h. Preincubation of some samples with caspase-3 inhibitor (Ac-DEVD-CHO) was done to confirm the assay specificity. The absorbance of released p-nitroaniline (pNA) was measured at 405 nm using the MRX Revelation plate reader (Dynex Technologies). The enzyme activity was calculated relative to cellular protein content (assessed using Bradford's method).

RESULTS

Cell proliferation

In order to determine the influence of the tested compound on cell proliferation, melanoma cells were incubated in the presence of a wide range of concentrations (0.1, 0.3, 1, 3, 5 and 10 mM) of VPA. The effect of 72 h of incubation is shown in Figure 1. The low concentrations of VPA (0.1 and 0.3 mM) did not exert a significant influence on the cell growth rate in a comparison to control group. At concentrations above 0.3 mM (1, 3, 5 and 10 mM), the concentration-dependent inhibition was seen. The higher the concentration the greater inhibition rate. The compound maximally inhibited cell proliferation at concentration of 10 mM.

Caspase-3 activity

In order to evaluate the influence of VPA on apoptosis in G-361 melanoma cell line, the activity of caspase-3 was tested. Cells were exposed to different concentrations of VPA (1, 5 and 10 mM) for 48 h. Preliminary studies with lower concentrations (0.1 and 0.3 mM) of VPA did not exert significant influence on cell apoptosis (data not shown). The effect of VPA on enzyme activity is presented in Figure 2. The increases in caspase-3 activity in cells treated with concentrations above 1 mM (compared to control cells) were statistically significant. Both concentrations of compound (5 and 10 mM) stimulated the enzyme activity at comparable level. At concentration of 1 mM of VPA, the activity of enzyme was slightly higher than in untreated control. To determine the apoptosis inducing power of VPA, the other histone deacetylase inhibitor –NaB, was used. Results showed that NaB exerted a

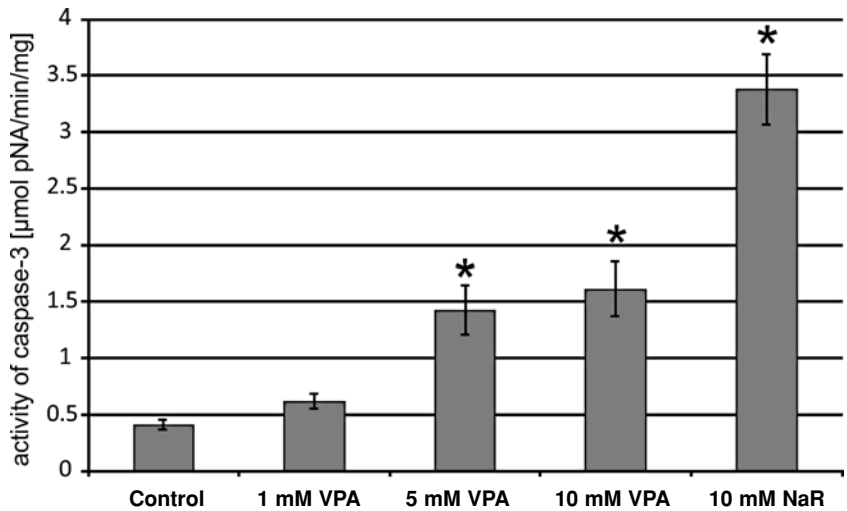

Figure 2. Effect of VPA and NaB on caspase-3 activity in G-361 cells. Each bar represents the mean ± SD; * $p < 0.05$

stronger effect on caspase-3 activity in G-361 than VPA (both compounds at 10 mM).

DISCUSSION

The malignant melanoma causes up to 80% of death from skin cancer (5). An increased proliferation, capacity to metastasize and broad spectrum of associated genetic and epigenetic changes contribute to resistance development of melanoma to conventional therapy. Lack of effectiveness of anti-melanoma therapies make it necessary to search for new drugs that improve or replace the standard chemotherapy. The new promising strategy is the administration of a histone deacetylase inhibitor (HDACi) – valproic acid (11, 13). The mechanism of anti-melanoma effect of VPA is based on induction of apoptosis in cancer cells by different mechanisms. The first utilizes the fact that VPA, as a histone deacetylase inhibitor (HDACi), leads to inhibition of histone deacetylases involved in formation of heterochromatin. Inhibition of histone deacetylation results in increased level of histone acetylation, euchromatin formation and re-expression of genes associated with cell cycle inhibition and apoptosis like *CDKN1A* encoding the p21 protein or *CDKN2A* encoding the p16 protein (8, 12, 23). HDAC inhibitors *via* both extrinsic and intrinsic apoptosis pathways contribute to the activation of the caspase cascade that degrades the cell structures and causes the cell death. Histone deacetylase inhibitors increase the expression of death receptors and their ligands in cancer cells and inhibit the antiapoptotic gene expression e.g., cFLIP, Bcl-2, Bcl-XL. In consequence, an imbalance in the level of proapoptotic and antiapoptotic genes leads to apoptosis (18, 24, 25).

To evaluate the inhibition of cell proliferation and proapoptotic properties of VPA, the XTT assay and caspase-3 activity test were performed. The results of XTT assay showed that VPA, at higher concentrations (1, 3, 5 and 10 mM) caused a statistically significant cell growth inhibition in the studied G-361 cell line. Similar results were obtained previously by determining the cytotoxicity (using *In Vitro* Toxicology Assay Kit, Sulforhodamine B based) mediated by valproic acid in G-361 and A-375 melanoma cell lines (10, 11, 23). Previous studies also showed that conjunction of 1 mM VPA with 5,7-dimethoxycoumarin significantly decreased the proliferation in A-375 melanoma cell line and could be useful in chemoprevention (10). In our studies, lower concentrations of VPA (0.1 and 0.3 mM) did not cause a significant reduction of cell growth.

Subsequently, the proapoptotic effect of VPA was examined. This assessment bases on measurement of released p-nitroaniline as a result of caspase-3 action. Caspase-3 is an effector caspase that cleaves cellular proteins and leads to cell death so its activity could be a good apoptosis marker. Incubation with higher concentrations of VPA – 5 and 10 mM caused an increase in enzyme activity (statistically significant). These results were compared with results obtained after incubation with another histone deacetylase inhibitor – sodium butyrate. In our studies, both substances stimulated the enzyme activity but NaB was much powerful inducer than VPA at the same concentration. The same findings were observed in A-375 line (26).

Summarizing, obtained results suggest that VPA seems to be a potent anti-melanoma agent, reducing proliferation of human melanoma G-361 cell line in a concentration-dependent manner. Currently, the possibility of synergistic action of VPA with known anti-cancer drugs should be tested.

Acknowledgments

This work was supported by SUM grant KNW-1-002/M/4/0 and KNW-2-023/D/3/K.

REFERENCES

1. Cockerell C.J.: Dermatol. Clin. 30, 445 (2012).
2. von Thaler A.K., Kamenisch Y., Berneburg M.: Exp. Dermatol. 19, 81 (2010).
3. Hyter S., Indra A.K.: FEBS Lett. 587, 529 (2013).
4. Volkovova K., Bilanicova D., Bartonova A., Letašiová S., Dusinska M.: Environ. Health 11, 12 (2012).
5. Miller A.J., Mihm M.C. Jr.: N. Engl. J. Med. 355, 51 (2006).
6. Olbryt M.: Postepy Hig. Med. Dosw. 67, 413 (2013).
7. Chodurek E., Gołąbek K., Orchel J., Orchel A., Dzierżewicz Z.: Ann. Acad. Med. Siles. 66, 44 (2012).
8. Wagner J.M., Hackanson B., Lübbert M., Jung M.: Clin. Epigenet. 1, 117 (2010).
9. Daud A.I., Dawson J., DeConti R.C.: Clin. Cancer Res. 15, 2479 (2009).
10. Chodurek E., Orchel A., Orchel J., Kurkiewicz S., Gawlik N., Dzierżewicz Z., Stępień K.: Cell. Mol. Biol. Lett. 17, 16 (2012).
11. Chodurek E., Dzierżęga-Lęcznar A., Kurkiewicz S., Stępień K.: J. Anal. Appl. Pyrolysis 104, 567 (2013).

12. Grabarska A., Dmoszyńska-Graniczka M., Nowosadzka E., Stepulak A.: Postepy Hig. Med. Dosw. 67, 722 (2013).
13. Chateauvieux S., Morceau F., Dicato M., Diederich M.: J. Biomed. Biotechnol. 6, 18 (2010).
14. Cervoni N., Szyf M.: J. Biol. Chem. 276, 40778 (2001).
15. Marchion D.C., Bicaku E., Daud A.I.: Cancer Res. 65, 3815 (2005).
16. Minucci S., Pelicci P.G.: Nat. Rev. Cancer 6, 38 (2006).
17. Chen P.S., Wang Ch-CH., Bortner C.D., Peng G-S., Wu X., Pang H., Lu R-B. et al.: Neuroscience 149, 203 (2007).
18. Gotfryd K., Skladchikova G., Lepekhin E.A., Berezin V., Bock E.: BMC Cancer 10, 14 (2010).
19. Hrabeta J., Stiborova M., Adam V., Kizek R., Eckschlager T.: Biomed. Pap. Med. Fac. Univ. Palacky, Olomouc, Czech Repub. 158, 2 (2014).
20. Ropero S., Esteller M.: Mol. Oncol. 1, 1 (2007).
21. Tang J., Yan H., Zhuang S.: Clin. Sci. (Lond) 124, 11 (2013).
22. Bose P., Dai Y., Grant S.: Pharmacol. Ther. 143, 323 (2014).
23. Papi A., Ferreri A.M., Rocchi P., Guerra F., Orlandi M.: Anticancer Res. 30, 535 (2010).
24. Kim H-J., Bae S-Ch.: Am. J. Transl. Res. 3, 166 (2011).
25. Schuchmann M., Schulze-Bergkamen H., Fleischer B.: Onkol. Rep. 15, 227 (2006).
26. Chodurek E., Orchel A., Gawlik N., Kulczycka A., Gruchlik A., Dzierzewicz Z. Acta Pol. Pharm. Drug Res. 67, 686 (2010).

Acta Poloniae Pharmaceutica – Drug Research, Vol. 71 No. 6 pp. 922–932, 2014 ISSN 0001-6837
Polish Pharmaceutical Society

TLC-DENSITOMETRIC METHOD FOR QUALITATIVE ANALYSIS OF BETAMETHASONE AND ITS RELATED COMPOUNDS IN PHARMACAUTICAL PREPARATIONS

MAŁGORZATA DOŁOWY* and ALINA PYKA

Department of Analytical Chemistry, Faculty of Pharmacy, Medical University of Silesia in Katowice, Jagiellońska 4, 41-200 Sosnowiec, Poland

Abstract: A new simple and rapid TLC-densitometric procedure for the separation and identification of betamethasone and its related substances, betamethasone-17,21-dipropionate, betamethasone-17-valerate, betamethasone-21-valerate and also betamethasone disodium phosphate was developed. One of the chromatographic systems proposed in this study, which has been satisfactory applied in separation of four pairs of examined compounds was silica gel $60F_{254}$ (E. Merck, Art. 1.05554) and a mixture containing chloroform-methanol-acetic acid (99.5%) in volume composition 28 : 5 : 0.5. Densitometric measurements were done using densitometer TLC Scanner 3 at 246 nm. The proposed method was checked in terms of its specificity for the determination of betamethasone-17,21-dipropionate and betamethasone disodium phosphate in commercially available products containing both compounds, separately, as active ingredients. The results showed that the method is suitable for qualitative analysis of betamethasone derivatives in simple and combined pharmaceuticals in various dosage forms e.g., lotion and injection solution. It also can be applied in quality control of pharmaceutical formulations of betamethasone and its related compounds in form of salts and esters.

Keywords: betamethasone, glucocorticoids, TLC-densitometry, NP-TLC, RP-TLC

Betamethasone (B) and its derivatives, betamethasone dipropionate, betamethasone disodium phosphate and also betamethasone valerate are synthetic glucocorticoids given orally in form of tablets, parenterally, by inhalation, by local injection, or administrated topically in the different disorders in which corticosteroids are indicated (1). B is a corticosteroid with anti-inflammatory and immunosuppressive properties, used especially to treat conditions such as arthritis, hormone and immune system disorders, allergic reactions, certain skin and eye conditions, breathing problems, and certain cancers. It is applied as a topical cream, ointment, lotion gel and tablets. As was reported by Pastuszka and Kaszuba in excellent review paper, the therapeutic effect of betamethasone derivatives depends mainly on potency of the drug, type of vehicle, application and also on the range of genetic factors describing individual sensitivity (2). It is well known that in order to achieve better therapeutic effect of glucocorticosteroids including betamethasone derivatives, they are often combined with other bioactive substances e.g., salicylic acid as keratolytic and antiseptic agent. Combination drugs containing betamethasone dipropionate and salicylic acid in form of ointment or liquid are widely used in dermatology in the therapy of skin diseases e.g., in plaque psoriaris, atopic dermatitis, seborrhoeic dermatitis, because it is well tolerated medication by patients and provides better penetration of betamethasone dipropionate into the skin. Moreover, B is available in a number of pharmaceutical preparations in combination with other steroids such as dexamethasone acetate, flumethasone pivalate or with antibacterial agents like, for instance, antibiotics (gentamicin) (2-8). Additionally, a mixture of B with its related compounds e.g., with betamethasone dipropionate, betamethasone disodium phosphate or with betamethasone valerate is present in various pharmaceutical formulations.

Official method recommended by United States Pharmacopoeia (USP) and by Polish Pharmacopoeia (FP) for the identification and assay

* Corresponding author: e-mail: mdolowy@sum.edu.pl

of B and its derivatives combined with other agents including antibiotics and preservatives in pharmaceutical dosage form is high performance liquid chromatography (HPLC) (9, 10). Numerous research papers reported applicability of this method in combination with UV, UV-DAD and MS/MS detectors in quality and quantity control of some dermatological products containing betamethasone derivatives and some cosmetics (11-15). Past study showed other analytical methods: spectrophotometry and voltammetry in analysis of betamethasone in biological samples (16-20). As was reported in above-mentioned papers (11-15), HPLC method is highly efficient for the determination of B but rather expensive and time consuming, because requires repeated solvent extraction of multicomponent pharmaceutical preparations containing B and its related compounds.

Therefore, it was tried to develop a simple and inexpensive TLC-densitometric method for separation and identification of B and some derivatives: betamethasone-17,21-dipropionate (BP), betamethasone-17-valerate (BV17), betamethasone-21-valerate (BV21) and also betamethasone disodium phosphate (BPh) in mixture. Additionally, the optimum chromatographic conditions, which were found for the separation of all examined compounds, were used for the separation and next identification of both, betamethasone-17,21-dipropionate and betamethasone disodium phosphate in their pharmaceutical formulations. According to our knowledge, until today there is only one TLC-densitometric procedure which was successfully applied in the quantification of betamethasone-17,21-dipropionate in combined pharmaceutical preparation (in the presence of salicylic acid and nipagin in a form of lotion) (21). Identification and quantification of betamethasone disodium phosphate in pharmaceutical dosage form by TLC-densitometry has not been yet officially published in research papers and also in both pharmacopoeias (9, 10).

Thus, the objective of this work was to develop a rapid, simple TLC-densitometric method for the separation and identification of the selected betamethasone derivatives including BPh and BP in mixture. The results of this study might be an indicator for further investigations concerning the quantitative analysis of examined betamethasone compounds.

EXPERIMENTAL

Chemicals and reference standards

The reference standards of betamethasone (CAS No. 378-44-9), betamethasone-17,21-dipropionate (CAS No. 5593-20-4), betamethasone-17-valerate (CAS No. 2152-44-5), betamethasone-21-valerate (CAS No. 2240-28-0) and also betamethasone disodium phosphate (CAS No. 151-73-5) were from commercial source - Sigma-Aldrich (St. Louis, MO, USA). The following mobile phase components: methanol, chloroform, acetone, n-hexane, ethyl acetate, acetic acid (99.5%) for liquid chromatography were purchased from POCh (Gliwice, Poland). Distilled water was obtained from Department of Analytical Chemistry (Medical University of Silesia, Sosnowiec, Poland). Standard solutions of five examined compounds at concentration of 5 mg/mL each were prepared in ethanol (96%, pure for analysis) from POCh (Gliwice, Poland). The reference standard mixtures: containing five examined compounds (M5) in quantity of 5 mg each in 1 mL: B, BP, BV17, BV-21 and also BPh were prepared. Other standard mixtures are consisted of B, BPh, and salicylic acid (M3) mixed at the same concentration like in the case of M5. The last variant of standard mixture was prepared by mixing both solutions of B and BPh at concentration of 5 mg/mL each (M2). Each solution (5 µL) was spotted on the chromatographic plates.

Pharmaceutical preparations

The commercially available pharmaceutical preparations of the combination: BPh + salicylic acid (0.5 mg + 20 mg) per mL in form of lotion and also marketed injection solution consisting of 5.3 mg of BPh per mL in form of an ampoule (5 mL) were used. A sample of lotion (1 mL) diluted with 200 µL of ethanol (96%) and also the commercial injection solution were spotted on TLC plates in quantity of 5 µL together with standards.

Materials

In preliminary study, in order to find the optimum chromatographic conditions for the complete separation of five examined compounds, different aluminum chromatographic plates (20 × 20 cm) were applied such as the chromatographic plates for NP-TLC precoated with with 0.20 mm layers of silica gel $60F_{254}$ without concentrating zone (E. Merck, Darmstadt, Germany, Art. 1.05554), with concentrating zone (E. Merck, Darmstadt, Germany, Art. 1.05583), and also the chromatographic plates used for RP-TLC analysis, silica gel 60 RP-$18F_{254}$ (E. Merck, Darmstadt, Germany, Art. 1.05559).

Apparatus

TLC Densitometer: Camag (Muttenz, Switzerland) equipped with TLC Scanner 3 con-

trolled by WinCATS 1.4.2 software. Deuterium lamp was as a source of radiation emitting continuous UV spectrum between 190 and 450 nm.

The 5 µL Camag micropipettes (Muttenz, Switzerland) were used to apply the solutions on the plates.

Chromatographic chamber: twin-trough chamber for 20 × 10 cm plates (Art. 0.222.5221, Camag, Muttenz, Switzerland).

Chromatography

A thin-layer chromatography was performed on aluminum plates (Art. 1.05554, Art. 1.05559, Art. 1.05583), which were cut from original plates into 10 × 10 cm before use. Next, the plates were activated at 120°C for 30 min. Micropipette (5 µL) was used for samples application. The plates were developed at room temperature (20°C) in a twin-trough chromatographic chamber with the use of several mobile phase systems:

- chloroform-acetone in volume composition 7 : 1;
- *n*-hexane-acetone-acetic acid (99.5%) in the volume compositions: 38.5 : 11 : 0.5, 38.5 : 11 : 0.7, 38.5 : 11 : 2, 38.5 : 11 : 1.2 and 38.5 : 11 : 4;
- *n*-hexane-ethyl acetate-acetic acid (99.5%) in volume composition 35 : 10 : 5;
- chloroform-ethyl acetate in volume composition 33.5 : 16.7;
- acetonitrile-water in volume compositions: 80 : 20, 65 : 35 and 50 : 50;
- chloroform-methanol-water in the volume compositions: 45 : 11 : 1, 38 : 11 : 1, 38 : 11 : 2, 30 : 11 : 1, 38 : 11 : 0, 38 : 9 : 1, 38 : 9 : 2 and 38 : 5 : 1;
- chloroform-methanol-acetic acid (99.5%) in volume composition 28 : 5 : 0.5.

The chamber was previously saturated with vapors of 50 mL of mobile phase for 30 min. In all experiments the migration distance was 80 mm. The distance between the tracks was 15 mm. After development, the plates were dried for 20 h at 20°C in a fume cupboard. Densitometric and spectrodensitometric analyses were carried out by Camag TLC Scanner 3 and controlled by WinCATS 1.4.2 software. To find the maximum absorbance of five examined steroids and also salicylic acid, the densitometric measurements were performed at multiwavelengths from $\lambda = 200$ to 400 nm, at the wavelength interval of 25 nm at each step. The optimum wavelength for all investigated steroids was $\lambda = 246$ nm. The identity of the salicylic acid spots were determined by scanning in absorbance mode at $\lambda = 300$ nm. The chromatographic bands were measured by spectrodensitometric analysis under the following conditions: the slit dimensions were 10.00 × 0.40 mm, Macro; the optimal optical system was light; the scanning speed was 20 mm/s and 20 nm/s; the data resolution was 100 µm/step and 1 nm/step, respectively, for densitometric and spectrodensitometric analysis. Each analysis was repeated three times.

The mean value of obtained R_F results and also average value of band width (w) of each examined compound were used to describe the efficacy of the separation and identification of betamethasone derivatives by the use of proposed TLC-densitometric method.

Calculating of separation factors

In order to estimate the results of the separation of four examined pairs of betamethasone derivatives: BPh/B, B/BV17, BV17/BV21 and also BV21/BP (on the basis of obtained densitograms), the following separation factors for adjacent peaks were calculated: ΔR_F, α and also R_F^{α} according to the equations [1- 3]:

$$\Delta R_{F(1,2)} = R_{F1} - R_{F2} \quad [1]$$

$$R^{\alpha}_{F(1,2)} = \frac{R_{F1}}{R_{F2}} \quad [2]$$

where: R_{F1} and R_{F2} are the values of the two adjacent peaks, and $R_{F1} > R_{F2}$.

$$\alpha = \frac{\frac{1}{R_{F1}} - 1}{\frac{1}{R_{F2}} - 1} \quad [3]$$

where: R_{F1} and R_{F2} are the values of the two adjacent peaks, and $R_{F1} < R_{F2}$.

Specificity (selectivity) of the method

According to current guidelines of analytical methods applied in quality and quantity control of pharmaceuticals such as ICH guidelines (22) and also on the basis of other guides published by Ferenczi-Fodor et al. (23, 24), by Nagy-Turák (25) and by Kobyłka and Komsta (26), each analytical method including TLC requires evaluation of specificity which is a part of validation procedure. As was reported in the above presented guidelines, it must be proven that the developed method can separate a substance determined from the impurities, excipients and/or degradation products (related compounds).

In this work, the specificity of the proposed method in order to use it in qualitative analysis of BP in the presence of salicylic acid in commercial lotion and also BPh in another marketed product was checked on the basis of the results obtained for

the optimum chromatographic conditions, which enabled complete separation of the examined compounds from other excipients present in both pharmaceuticals such as their degradation products and related substances (e.g., B).

To confirm the specificity of the developed TLC-densitometric method, the comparison of obtained chromatographic bands from standard solution and also coming from respective pharmaceutical was made.

Moreover, to estimate the effect of resolution of examined betamethasone and its related substances, the separation factor (R_S) for all adjacent bands (on densitogram) coming from investigated compounds was calculated as (27):

$$R_S = \frac{2d}{w_{b1} + w_{b2}} \quad [4]$$

where: d = a distance between the centers of two adjacent chromatographic bands; w_{b1} and w_{b2} = bands width at the base line.

RESULTS AND DISCUSSION

The purpose of work reported herein was to develop a simple and rapid TLC-densitometric method for the separation and identification of B and its related compounds such as BP, BV17, BV21 and also BPh in mixture. The developed method was applied in further steps of this study for the qualitative analysis of some of the investigated steroid

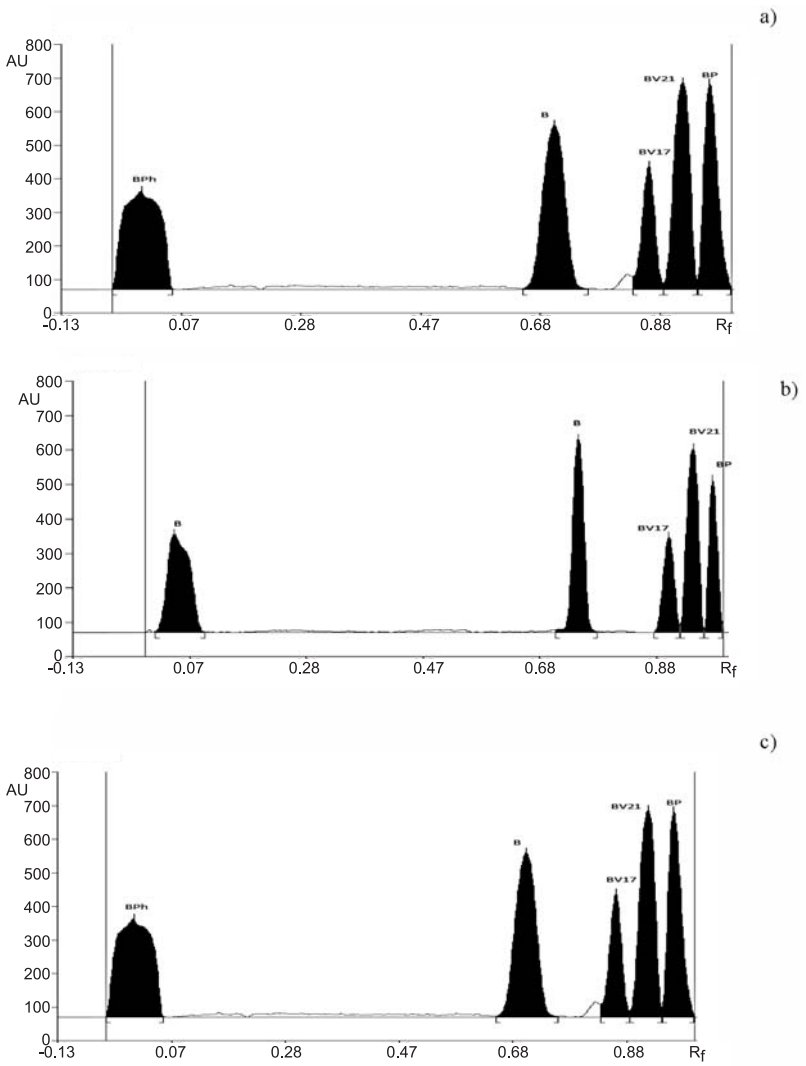

Figure 1. Densitograms registered from chromatograms of model mixture containing B, BV17, BV21, BP and BPh at 246 nm obtained on silica gel $60F_{254}$ (Art 1.05554) using the following mobile phase systems: chloroform-methanol-water 45 : 11 : 1 (v/v/v) (a), chloroform-methanol-water 38 : 11 : 2 (v/v/v) (b) and chloroform-methanol-acetic acid (99.5%) 28 : 5 : 0.5 (v/v/v) (c); for abbreviations see text

Table 1. Effect of resolution of betamethasone and its four examined derivatives obtained under selected chromatographic conditions.

Chromatographic conditions: mobile phase/chromatographic plates	Separated pairs of adjacent peaks on densitograms			
	BPh/B	B/BV17	BV17/BV21	BV21/BP
Chloroform-methanol-water 45 : 1 : 1 (v/v/v) silica gel 60F_{254} Art. 1.05554	+	+	+	+
Chloroform-methanol-water 38 : 11 : 1 (v/v/v) silica gel 60F_{254} Art. 1.05554	+	+	+	+
Chloroform-methanol-water 38 : 11 : 2 (v/v/v) silica gel 60F_{254} Art. 1.05554	+	+	+	+
Chloroform-methanol-acetic acid (99.5%) 28 : 5 : 0.5 (v/v/v) silica gel 60F_{254} Art. 1.05554	+	+	+	+
Chloroform-methanol-water 38 : 11 : 1 (v/v/v) silica gel 60 RP-18F_{254} Art. 1.05559	+	+	+	-
Chloroform-acetone 7 : 1 (v/v) silica gel 60 RP-18F_{254} Art. 1.05559	+	+	+	-
Chloroform-acetone 7 : 1 (v/v) silica gel 60F_{254} Art. 1.05554	-	+	+	+
n-Hexane-ethyl acetate-acetic acid (99.5%) 35 : 10 : 5 (v/v/v) silica gel 60 RP-18F_{254} Art. 1.05559	+	+	+	+/-
Acetonitrile-water 80 : 20 (v/v) silica gel 60F_{254} Art. 1.05554	+	+	+	-
Acetonitrile-water 80 : 20 (v/v) silica gel 60 RP-18F_{254} Art. 1.05559	+	+	+	-

Where: (+) = good separated , (-) = not separated, (+/-) = poorly separated, B = betamethasone, BV17 = betamethasone-17-valerate, BV21 = betamethasone-21-valerate, BP = Betamethasone-17,21-dipropionate, BPh = Betamethasone disodium phosphate.

compounds: BP and also BPh in pharmaceuticals containing BP in the presence of salicylic acid and BPh, respectively, as the active ingredients. As was reported above, many procedures (11-15), including HPLC were satisfactorily applied for the quality control of B derivatives in commercial products (e.g., cosmetics) and in biological samples. High-performance liquid chromatography is a very favorite analytical tool (accurate, precise) and widely used in separating the complex mixture of molecules including steroids in biological and also in pharmaceutical systems but in comparison with TLC, this technique is more expensive (price of columns) and required time consuming pre-treatment steps. Therefore, thin-layer chromatography (TLC) is still a very popular and frequently used analytical method in drug analysis because of its advantages: many samples can be analyzed quickly in one step without additional clean-up of samples and also solvents (28-31). For this reason, this technique is easy to perform and inexpensive in comparison with other chromatographic methods. As was described in the literature, a progress in TLC equipment and new developments in instrumentation of TLC e.g., densitometry, caused that modern TLC may in some cases be comparable to HPLC in terms of selectivity, precision and sensitivity (29). However, until today, both Pharmacopoeias (USP and FP) don't show the real possibilities of TLC in terms of its application in quantitative analysis of drugs including B and its derivatives (32). Pharmacopeial monographs describe only TLC semiquantitative purity test of these compounds in bulk substances and drugs (9, 10). A lack of the official pharmacopoeial TLC-densitometric procedure suitable for identification and quantification of B derivatives: BP, BV17, BV21 and also BPh in pharmaceuticals, shows that there is a need to develop a rapid and simple TLC-densitometric method for the separation and identification of these compounds in commercially available products. A special attendance was devoted to analysis of BPh in model mixture and in pharmaceutical product containing BPh.

According to obligatory validation procedures of analytical methods, the aim of the first step in this study was to find the optimum chromatographic conditions (proper mobile phase and kind of chromatographic plates), which allowed to achieve satis-

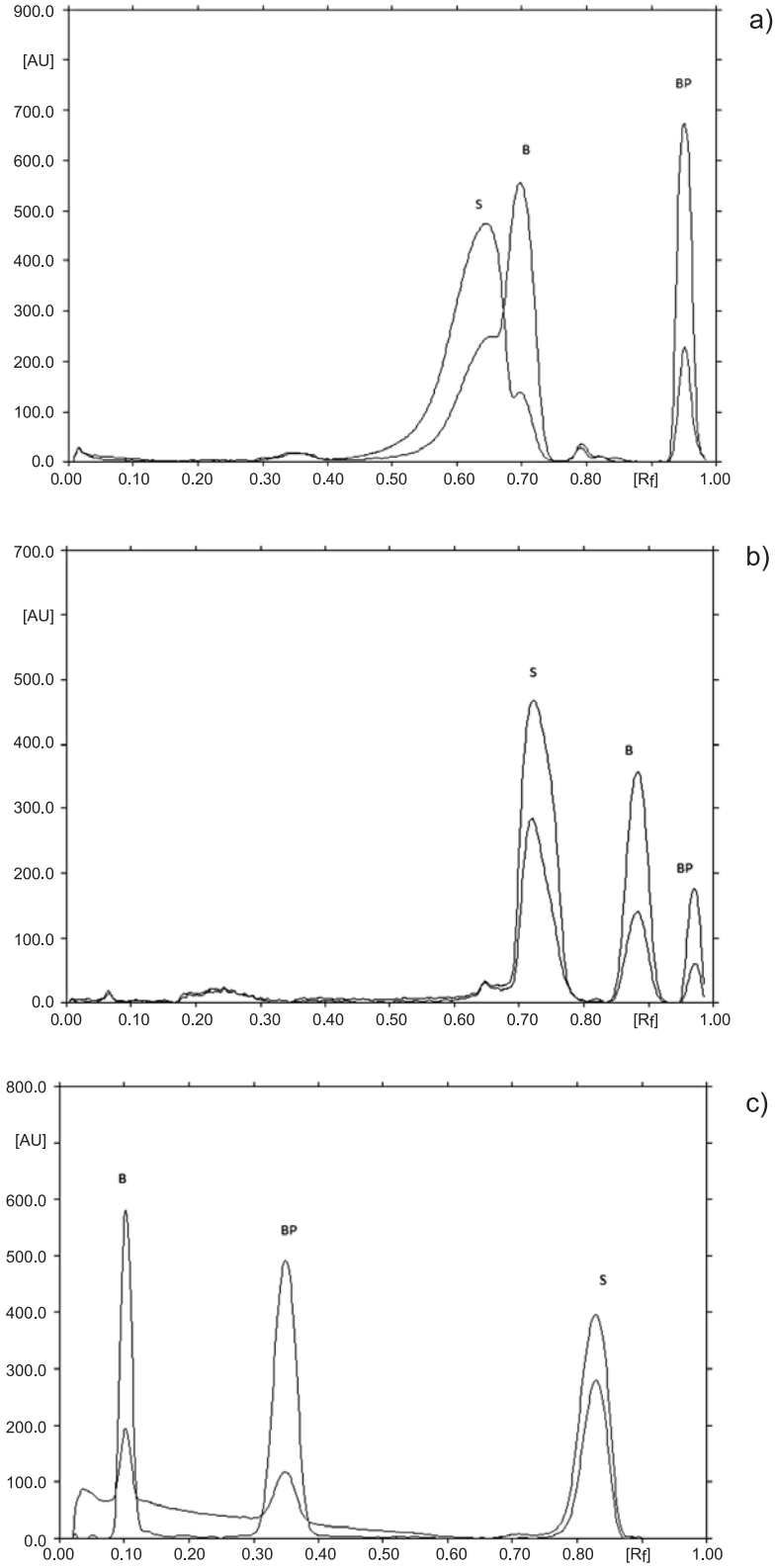

Figure 2. Densitograms registered from chromatograms of model mixture containing B, BP and S at 246 nm (for B and BP) and also at 300 nm for S obtained on silica gel $60F_{254}$ (Art 1.05554) using the following mobile phase systems: chloroform-methanol-acetic acid (99.5%) 28 : 5 : 0.5 (a), acetonitrile-water 80 : 20 (v/v) (b), and on silica gel $60F_{254}$ Art. 1.05583 and by *n*-hexane-ethyl acetate-acetic acid (99.5%) 35 : 10 : 5 (v/v/v) (c); for abbreviations see text

factory separation of B and four its derivatives mentioned above, including BP and BPh in mixture. In this preliminary study, various chromatographic conditions (different adsorbents and mobile phases) in normal and reversed phase system (NP-TLC and RP-TLC) were tested. The influence of some of them on efficacy of separation of five compounds was summarized in Table 1. On the basis of these data, it could be observed that among several chromatographic systems used (described in Experimental part) those which give satisfactory resolution of four pairs of examined compounds namely: BPh, B, BV17, BV21 and also BP in mixture are:

- chloroform-methanol-water 45 : 11 : 1 (v/v/v);
- chloroform-methanol-water 38 : 11 : 1 (v/v/v);
- chloroform-methanol-water 38 : 11 : 2 (v/v/v);
- and also chloroform-methanol-acetic acid (99.5%) in volume composition 28 : 5 : 0.5 and silica gel $60F_{254}$ Art. 1.05554 for all of them.

By the use of these chromatographic systems good resolution between each pair of five investigated compounds: BPh/B, B/BV17, BV17/BV21 and BV21/BP was achieved. Examples of densitograms of separated mixtures containing these compounds presented in Figure 1 confirm this fact. The choice of the presented chromatographic systems from all tested as the optimum for the separation and identification of five examined betamethasone compounds were done on the basis of the results of earlier studies focused on the separation and identification of seven bile acids (free and conjugated with respective amino acids) and some steroid hormones in mixture (33-38). In previous study, it was concluded that the following separation factors: ΔR_F, R_s, α and also R^{α}_F are very useful for estimation of the separation results of each pair of adjacent peaks on the densitogram. It was found that for each such pair obtained under above-mentioned chromatographic conditions the two important separation factors were satisfactory when: $\Delta R_F \geq 0.05$ and $R_s > 1.00$. It could be concluded that, similarly like in case of another group of steroids namely bile acids, $R_F \geq 0.05$ and $R_s > 1.00$ for each pair of betamethasone compounds resulted in their good separation. Moreover, based on the obtained results (Table 1), it could be observed that NP-TLC system is better than RP-TLC for separation of five examined compounds. However, it might be noted that the biggest problem in separation of all investigated mixtures referred to separation of BV21 from BP and also BPh from B (Table 1). The mobile phase: acetonitrile-water (80 : 20, v/v) recommended by US Pharmacopoeia for HPLC analysis of betamethasone derivatives was not satisfactory for the separation of BV21 from BP. Modification of mobile phase: chloroform-methanol-water by changing the water as a component of this mobile into acetic acid (99.5%) improved the resolution of examined compounds, especially BV21 from BP. Moreover, the obtained spots were compact in comparison with those formed by the use of mobile phase containing water. The second pair BPh/B, which was difficult to separate by the use of chloro-

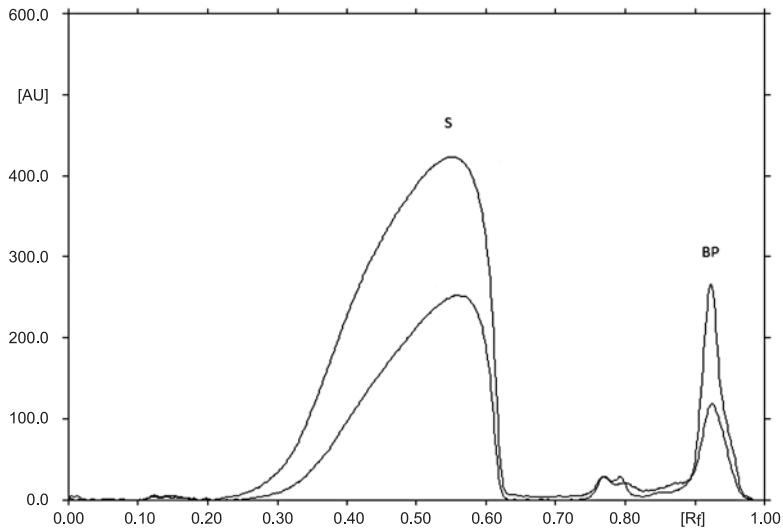

Figure 3. Densitogram obtained from commercial product containing BP and S (lotion) at 246 nm for BP and at 300 nm for S, developed on silica gel $60F_{254}$ (Art 1.05554) using mobile phase system: chloroform-methanol-acetic acid 28:5:0.5 (v/v/v); for abbreviations see text

Table 2. Separation factors of four pairs of examined compounds obtained by means of mobile phase: chloroform-methanol-acetic acid (99.5%) in volume composition: 28 : 5 : 0.5 on silica gel $60F_{254}$ (E. Merck, Art. 1.05554).

Separation factor	Pairs of adjacent peaks on densitograms obtained from standard mixtures (M2, M3 and M5) of examined compounds						
	BPh/B	B/BV17	BV17/BV21	BV21/BP	S/B	B/BP	S/BP
ΔR_F	0.69	0.14	0.06	0.05	0.05	0.25	0.30
α	119.50	2.28	1.80	2.36	1.27	10.00	10.80
R^{α}_F	35.50	1.20	1.07	1.05	1.08	1.35	1.46
R_S	8.23	2.78	1.25	1.11	0.70	3.21	7.12

form-acetone in volume composition 7 : 1 and silica gel $60F_{254}$ Art. 1.05554 could be successfully separated by the use of other mobile phase systems presented in Table 1, for example, containing a mixture chloroform-methanol-acetic acid (99.5%) 28 : 5 : 0.5 (v/v/v). Using these chromatographic conditions, the following R_F values for examined compounds were determined: $R_{F(BPh)} = 0.02 \pm 0.01$, $R_{F(B)} = 0.71 \pm 0.02$, $R_{F(BV17)} = 0.85 \pm 0.01$, $R_{F(BV21)} = 0.91 \pm 0.01$ and $R_{F(BP)} = 0.96 \pm 0.01$. The values of resolution factors (ΔR_F, R_s, α and also R^{α}_F) obtained for each examined pair, and also well separated and symmetric peaks of BPh, B, BV17, BV21, BP observed on densitogram (Fig. 1c) caused that the following chromatographic conditions: chloroform-methanol-acetic acid (99.5%) 28 : 5 : 0.5 (v/v/v) as a mobile phase and silica gel $60F_{254}$ (Art. 1.05554) were selected as the best (optimum) for the further steps regarding the qualitative analysis of pharmaceuticals containing: BP and BPh in form of lotion and injection solution, respectively.

TLC-densitometric analysis of pharmaceuticals containing BP and BPh, separately was evaluated with regard to obligatory analytical procedures designed for quality control of pharmaceutical preparations in term of its specificity and selectivity to determine BP and BPh as active ingredients in their commercial products in the presence of other components, like, for example, salicylic acid (in the case of BP) and including the substances related to both BP and BPh such as B (their degradation product). Densitogram registered from chromatograms of model mixture containing B, BP and salicylic acid (S) at 246 nm (for B and BP) and also at 300 nm for S obtained on silica gel $60F_{254}$ (Art 1.05554) using the mobile phase system: chloroform-methanol-acetic acid (99.5%) 28 : 5 : 0.5 (v/v/v) (Fig. 2a) indicates that according to previous suggestion this solvent mixture and silica gel $60F_{254}$ (Art. 1.05554) are optimum for the separation of BP (active ingredient) from its related compound B (potential degradation product). Moreover, this conclusion confirmed the values of ΔR_F, R_s, α and also R^{α}_F obtained for this separated pair B/BP from model mixture M3 (B + BP + S) presented in Table 2. Good resolution is observed between S and BP. Unfortunately, worse results of separation could be observed on the basis of both: densitogram and value of calculated separation factor R_s ($R_s < 1$) for S/B. To sum this part of study, it was suggested that the developed TLC-densitometric method will be also specific (allows to separate BP from B and S) by use of the same chromatographic plates (Art. 10.05554) and acetonitrile-water 80 : 20 (v/v) as mobile phase (Fig. 2b). Another optimum conditions are silica gel $60F_{254}$ plates (Art. 1.05583) developed by n-hexane-ethyl acetate-acetic acid (99.5%): 35 : 10 : 5 (v/v/v) (Fig. 2c). Under these conditions, it was possible to obtain satisfactory results of separation, comparable to those presented by Wulandari and Indrayanto by means of silica gel and ethanol (96%)-toluene-chloroform-glacial acid in volume composition: 6.0 : 20 : 14 : 0.5 (21). Thus, it could be said that the TLC procedure described in this paper could be an alternative to that presented by these authors. Additionally, applicability of developed chromatographic conditions are confirmed in Figure 3 obtained from commercially available preparation of BP and S.

The third step of this study included the application of developed TLC-densitometric procedure using silica gel $60F_{254}$ (Art. 1.05554) and mobile phase system: chloroform-methanol-acetic acid (99.5%) in volume composition: 28 : 5 : 0.5 to qualitative analysis of the second compound belonging to betamethasone group: BPh. According to our knowledge, there is no official TLC-densitometric procedure in pharmacopoeias and published in research papers. Therefore, the objective of this study was also to find the best conditions, which allowed to separate BPh from its related substance e.g., B and next, to apply them to verify the presence

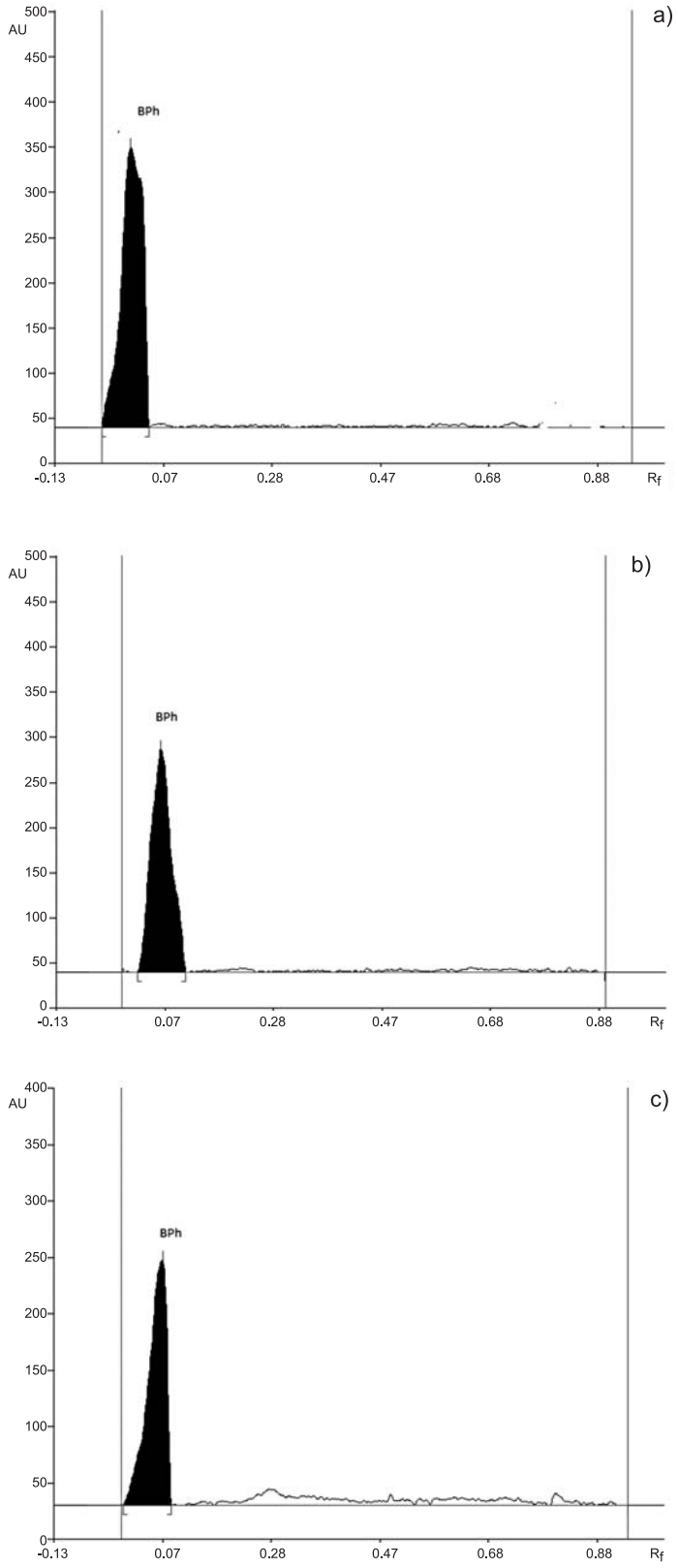

Figure 4. Densitograms from chromatograms of injection solution containing BPh, registered at 246 nm and obtained on silica gel $60F_{254}$ (Art 1.05554) using the following mobile phase systems: chloroform-methanol-acetic acid 28 : 5 : 0.5 (v/v/v) (a), chloroform-methanol-water 45 : 11 : 1 (v/v/v) (b) and by chloroform-methanol-water 38 : 11 : 2 (v/v/v) (c); for abbreviation see text

of BPh in commercially available product (injection solution). The separations factors obtained for this pair (BPh/B) by means of mobile phase system mentioned above, presented in Table 2, and also densitograms obtained from injection solution containing BPh (Fig. 4) confirm that the developed TLC procedure is suitable for qualitative analysis of BPh in commercial product. It allowed to separate BPh from its related substance e.g., B. Moreover, there are no additional peaks from excipients on densitogram obtained from the examined commercial product by use the optimum mobile phase (Fig. 4a). Next, densitograms presented in Figure 4, obtained on silica gel $60F_{254}$ (Art 1.05554) using the following mobile phase systems: chloroform-methanol-water 45 : 11 : 1 (v/v/v) (Fig. 4b) and also chloroform-methanol-water 38 : 11 : 2 (v/v/v) (Fig. 4c) indicate that besides the mixture of chloroform-methanol-acetic acid (99.5%) 28 : 5 : 0.5 (v/v/v) the two solvent mixtures give also good results of qualitative analysis of BPh in pharmaceuticals and could be applied alternatively to that one.

The study showed that the proposed TLC-densitometric procedure could be successfully applied for the determination of B and its related compounds such as BP, BV17, BV21 and also BPh in model mixture and in their selected pharmaceuticals e.g., lotion containing BP as active ingredient and also injection solution of BPh. Our study will be continued in terms of full validation of developed TLC-densitometric method in order to applied it in quantification of examined betamethasone derivatives in pharmaceuticals.

CONCLUSIONS

The results of this work show that a very simple and rapid TLC-method combined with densitometry for the separation and identification of B and its related substances: BP, BV17, BV21 and BPh was developed. The main advantage of this method is short time of analysis and possibility of analysis of five examined compounds in one step without additional clean-up of sample and solvents. It was stated that the proposed method is specific and acceptable for the detection of BP and BPh in commercially available products containing both compounds as active ingredients.

Acknowledgment

This research was financed by the Medical University of Silesia as part of statutory research project in 2014 year, No. KNW-1-006/N/4/0.

REFERENCES

1. Open Data Drug & Drug Target Database [Internet]. Available from: http://www.drugbank.ca/ DB00443drugs/ (2014).
2. Pastuszka M., Kaszuba A.: Postepy Dermatol. Alergol. 29, 196 (2012/13).
3. Furue M.: Br. J. Dermatol. 148, 128 (2003).
4. Juszkiewicz-Borowiec M.: Nowa Med. 11, 40 (2000).
5. Gottfried W.: Clin. Dermatol. 26, 229 (2006).
6. Yohn J.J., Weston W.L.: Curr. Probl. Dermatol. 2, 31 (1990).
7. Lagos B.R., Maibach H.J.: Br. J. Dermatol. 139, 763 (1998).
8. Ahluwalia A.: Med. Inflam. 7, 183 (1998).
9. Polish Pharmacopoeia, Polish Pharmaceutical Society, Warszawa, Poland 2011.
10. The United States Pharmacopoeia, Twinbrook Parkway, Rockville, USA 2011.
11. Xiong Y., Xiao K.P., Rustum, A.M.: J. Pharm. Biomed. Anal. 49, 646 (2009).
12. Shou M., Galinada W.A., Wei Y.Ch., Tang Q., Markovich R.J., Rustum A.M.: J. Pharm. Biomed. Anal. 50, 356 (2009).
13. Palwinder K., Galinada W.A., Wei Y.Ch., Tang Q., Rustum A.M.: Chromatographia 71, 805 (2010).
14. Gagliardi L., De Orsi D., Del Giudice R., Gatta F., Porra R., Chimenti P., Tonelli D.: Anal. Chim. Acta 457, 187 (2002).
15. Yu S. N., Il K.K., Kang-Bong L.: Forensic Sci. Int. 210, 144 (2011).
16. Singh D.K., Verma R.: IJPT 7, 61 (2008).
17. Assaleh F.H., Elosta S.G., Asseid F.M., Chandu B.R., Katakam P. JPSI 2, 13 (2013).
18. Amin A.S., Issa Y.M.: Anal. Lett. 1, 69 (1997).
19. Bahlul Z.A., Nagiat T.H., Babu R.C., Sreekanth N., Prakash K.: Int. J. Pharm. Biomed. Res. 1, 87 (2010).
20. Goyal R.N., Bishnoi S., Rana A.R.: Comb. Chem. High Throughput Screen. 13, 610 (2010).
21. Wulandari L., Indrayanto G. J.: Planar Chromatogr. Modern TLC 16, 438 (2003).
22. ICH Harmonized Tripartite Guideline (2005): http://www.ich.org Accessed 30 April 2014.
23. Ferenczi-Fodor K., Renger B., Végh Z.: J. Planar Chromatogr. Modern TLC 23, 173 (2010).
24. Ferenczi-Fodor K., Nagy-Turák A., Végh Z.: J. Planar Chromatogr. Modern TLC 8, 349 (1995).
25. Nagy-Turák A., Végh Z., Ferenczi-Fodor K.: J. Planar Chromatogr. Modern TLC 8, 188 (1995).

26. Kobyłka K., Komsta Ł.: Acta Chromatogr. 24, 433 (2012).
27. Ettre L.S.: Pure Appl. Chem.: 65, 819 (1993).
28. Ferenczi-Fodor K.; Végh Z., Renger B.: J. Chromatogr. A. 1218, 2722 (2011).
29. Ferenczi-Fodor K., Végh Z., Renger B.: Trends Anal. Chem. 25, 778 (2006).
30. Thin Layer Chromatography in Drug Analysis. Komsta Ł., Waksmundzka-Hajnos M., Sherma J. Eds., Boca Roton, USA 2013.
31. Bhawani S.A.; Sulaiman O., Hashim R., Mohamad M.N. Trop. J. Pharm. Res. 9, 301 (2010).
32. Nyiredy Sz., Ferenczi-Fodor K., Végh Z., Szepesi, G.: in Handbook of Chromatography, Sherma J., Fried B. Eds., p. 807, Marcel Dekker, Inc., New York 2003.
33. Pyka A., Dołowy M.: J. Liq. Chromatogr. Relat. Technol. 26, 1108 (2003).
34. Pyka A., Dołowy M.: J. Liq. Chromatogr. Relat. Technol. 28, 1383 (2005).
35. Pyka A., Dołowy M., Gurak D.: J. Liq. Chromatogr. Relat. Technol. 28, 631 (2005).
36. Pyka A., Dołowy M.: J. Liq. Chromatogr. Relat. Technol. 28, 1573 (2005).
37. Pyka A., Dołowy M.: J. Liq. Chromatogr. Relat. Technol. 27, 2613 (2004).
38. Babuśka-Roczniak M., Dołowy M., Janikowska G., Pyka A.: Curr. Top. Steroid Res. 9, 73 (2012).

Acta Poloniae Pharmaceutica – Drug Research, Vol. 71 No. 6 pp. 933–940, 2014 ISSN 0001-6837
Polish Pharmaceutical Society

COMPARISON OF ULTRAVIOLET DETECTION AND CHARGED AEROSOL DETECTION METHODS FOR LIQUID-CHROMATOGRAPHIC DETERMINATION OF PROTOESCIGENIN

KATARZYNA FILIP*, GRZEGORZ GRYNKIEWICZ, MARIUSZ GRUZA, KAMIL JATCZAK and BOGDAN ZAGRODZKI

Pharmaceutical Research Institute, Rydygiera 8 St., 01-793 Warszawa, Poland

Abstract: Escin, a complex mixture of pentacyclic triterpene saponins obtained from horse chestnut seeds extract (HCSE; *Aesculus hippocastanum L.*), constitutes a traditional herbal active substance of preparations (drugs) used for a treatment of chronic venous insufficiency and capillary blood vessel leakage. A new approach to exploitation of pharmacological potential of this saponin complex has been recently proposed, in which the β-escin mixture is perceived as a source of a hitherto unavailable raw material, pentacyclic triterpene aglycone – protoescigenin. Although many liquid chromatography methods are described in the literature for saponins determination, analysis of protoescigenin is barely mentioned. In this work, a new ultra-high performance liquid chromatography (UHPLC) method developed for protoescigenin quantification has been described. CAD (charged aerosol detection), as a relatively new detection method based on aerosol charging, has been applied in this method as an alternative to ultraviolet (UV) detection. The influence of individual parameters on CAD response and sensitivity was studied. The detection was performed using CAD and UV (200 nm) simultaneously and the results were compared with reference to linearity, accuracy, precision and limit of detection.

Keywords: protoescigenin, UHPLC, charged aerosol detection

Abbreviations: CAD – charged aerosol detection, HCSE – horse chestnut seeds extract, UHPLC – ultra-high performance liquid chromatography

Analysis of saponins is very challenging task because of high degree of structural complexity, multiplicity of similar functional groups and resulting physicochemical likeness of individual compounds, as well as the lack of chromophores, which hampers sensitivity of popular UV based detection systems. Although all analytical studies involving saponins – phytochemical, environmental, clinical and food research use contemporary separation techniques, the state of art in particular disciplines differs considerably: e.g., phytochemical research is mainly concerned with structural analysis of new compounds, while quantification and specification of plant materials seem to be a secondary issue. Therefore, even incremental improvements in qualitative and quantitative analysis of saponins come handy for pharmaceutical and clinical evaluation, as clearly reflected by regularly reported recent advancement (1, 2).

Escin (or aescin), a complex mixture of acylated pentacyclic triterpene saponins obtained from HCSE, is used as a phlebotropic drug for a treatment of chronic venous insufficiency and capillary blood vessel leakage. Recently, a new approach to exploitation of the escin mixture has been proposed (3). In this approach the saponin mixture was subjected to consecutive chemical transformations designed and developed as a scalable, validated technical processes, to afford hitherto unavailable material protoescigenin (**1**, **PES-01** see Scheme 1) in state of high chemical purity. Protoescigenin appears to be a suitable starting material for the design and further synthesis of various saponin mimetics (4). It was selected as the first candidate molecule, because although known as chemical entity from the classical period of triterpene saponin exploration (5, 6) and more recently confirmed as 3β,16α,21β,22α,24,28-hydroxyolean-12-ene by modern analytical and spectral tools (7), it is not commercially available and its chemistry is practically unexplored.

Analysis of the starting materials quality constitute a testing practice, that is essential for manu-

* Corresponding author: e-mail: k.filip@ifarm.eu

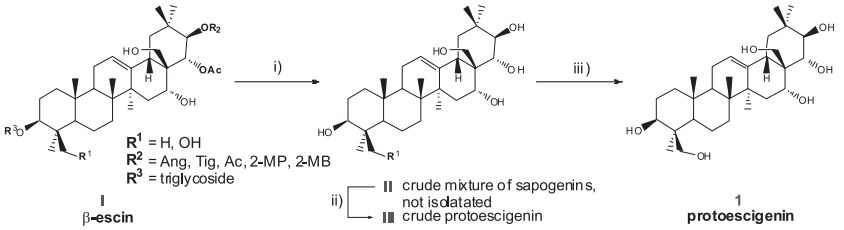

Scheme 1. Original method of preparation of protoescigenin (**1, PES-01**) from â-escin (**I**). Conditions: i) a) H_2SO_4, MeOH, reflux, b) KOH, H_2O; ii) MTBE, MeOH, H_2O; iii) a) *i*-PrOH, H_2O, b) *i*-PrOH, cyclohexane; Ang- angeloyl, Tig – tigloyl, Ac – acetyl, 2-MP – 2-methylpropanoyl, 2-MB – 2-methylbutanoyl (3)

facturing process development and helps to ensure product quality and consistency. Establishing of starting material specification, defined as a set of tests, references to analytical methods and appropriate acceptance criteria, is also the part of this practice. Among analytical methods, high performance liquid chromatography (HPLC) with UV detection has been commonly used as the technique for purity and assay control. However, traditional HPLC methods are frequently time- and solvent-consuming, especially in case of analysis of plant extracts samples (8). Additionally, for compounds lacking strong UV chromophores (like saponins) the most popular and widely used ultraviolet detection can be elusive. In such situations ultrahigh-performance liquid chromatography (UHPLC), accepted as a key approach to getting more analytic information in less time, with solvent reduction and waste minimization, can be a technique of choice. The solution to the detection problem may be the use of alternative detection method, like the charged aerosol detection, CAD. The response generated by CAD is independent of the chemical and spectral properties of non-volatile analytes but at the same time is mass-dependent, offering similar responses for the same mass of analyzed compounds (9–11). CAD system has many advantages, like broad dynamic response range up to 4 orders of magnitude, good precision, availability in a versions designed for both, classical HPLC and fast, UHPLC, as well as simple and reliable operation (9). However, CAD – as detector employing a nebulization process – has also some limitations: the response depending on the composition of the mobile phase and lack of possibility of certain peak identification or peak purity analysis (no spectral information is acquired).

Although many methods have been described in the literature for separation and analysis of saponins, HPLC coupled with various detectors being the most commonly used (12–15), none of them relates directly to the determination of protoescigenin. Additionally, applications of charged aerosol detection method for analysis of this group of compounds are still very rare. Until now, only several works and papers covering this subject have been published (12, 14, 16–19). The aim of our work was to fill the gap in this research area, and as a result a fast and universal method for quantitative analysis of protoescigenin was developed. A new UHPLC method with dual detection system, UV (200 nm) and CAD, was applied. The detection was performed using both systems simultaneously and the results were compared with reference to linearity, accuracy, precision and limit of detection and quantification. To the best of our knowledge, this work is the first in which dual detection system (UV/CAD) has been applied for protoescigenin determination.

EXPERIMENTAL

Chemicals and reagents

Samples of protoescigenin, including working standard (99.3%, UHPLC), as well as its main impurity barringtogenol C (BAC, 86.6% purity according to UHPLC) were manufactured and tested in Pharmaceutical Research Institute (Warszawa, Poland). Reference standards were fully characterized using the following techniques: UHPLC, ^{1}H NMR, ^{13}C NMR, IR, XRPD, MS, TG and DSC.

Acetonitrile (ACN) and methanol (MeOH) of HPLC grade were purchased from POCH S.A. (AVANTOR Gliwice, Poland). Acetic acid (HAc, ≥ 99.8%) was obtained from Fluka (Sigma-Aldrich, USA). Demineralized water (≥ 18.0 W/cm) from Barnstead system (Thermo Scientific, USA) was produced in the laboratory.

Chromatography

An UltiMate 3000RS UHPLC system (Thermo Scientific, Sunnyvale, CA, USA) was used to perform all of the analyses. The instrument was equipped with autosampler (WPS-3000TRS) and

column oven (TCC-3000RS), both enabled cooling. DAD-3000RS photodiode array and Corona charged aerosol (CAD) detectors (Thermo Scientific, Sunnyvale, CA, USA) were connected in this system. The data were analyzed using the Chromeleon software package.

The chromatographic separations were performed on an Acquity C18 BEH column (50 × 2.1 mm i.d., particle size 1.7 μm) manufactured by Waters (Waters Corporation, Milford Massachusetts, USA). The column oven temperature was set at 35°C and autosampler was kept at 20°C. The binary mobile phase, which composed of acetonitrile and 0.1% acetic acid (30 : 70, v/v), was pumped at flow rate of 0.4 mL/min. UV (DAD) detection was performed at 200 nm and the injection volume was set as 1 μL. Examined samples were dissolved in methanol (c ~ 2 mg/mL). CAD detection was performed with nitrogen pressure of 35 psi and range of 100 pA. The UV and CAD chromatograms were scanned concurrently.

Preparation of sample solutions

The stock solutions of standard and samples were prepared by dissolving 20.0 mg of substance into 10 mL of methanol. Stock solutions were further diluted by methanol to achieve a proper concentration for measurements and to get individual points of calibration curves for two ranges: (1) broad, from 0.002 mg/mL to 2.40 mg/mL and (2) narrow, for five concentration levels (i.e., from 1.60 to 2.40 mg/mL).

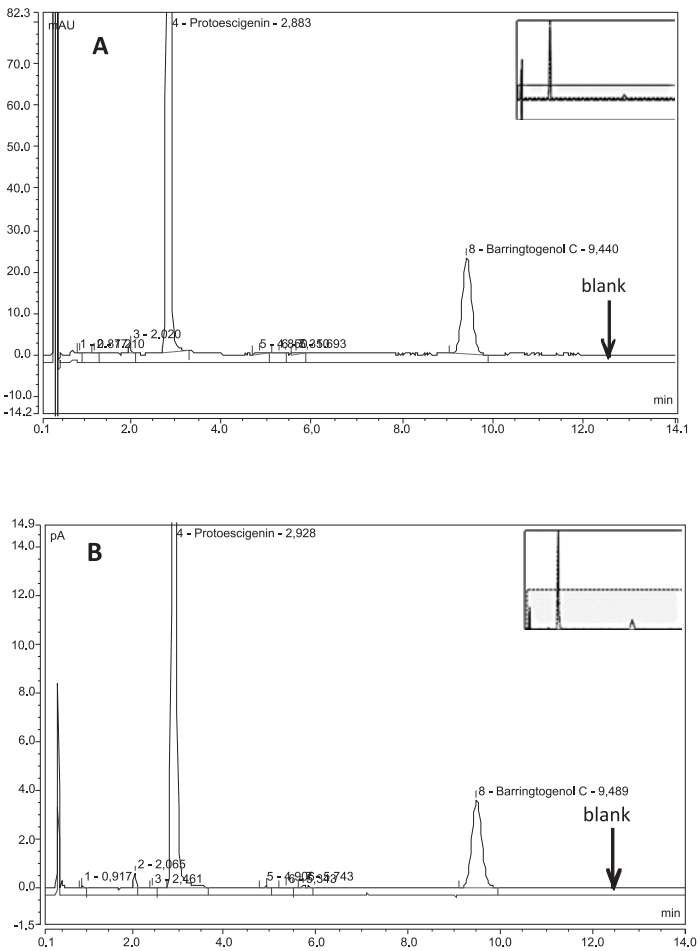

Figure 1 Example chromatogram of protoescigenin sample and blank: **A**. UV detection (200 nm), **B**. CAD detection

RESULTS AND DISCUSSION

Optimization of chromatographic conditions – UV detection and charged aerosol detection

The separation of protoescigenin and its process-related impurities was achieved with 30% of acetonitrile (ACN) in the mobile phase. This ACN concentration was chosen as an optimal for a good resolution of all observed peaks within reasonable time period (see Fig. 1). Because volatile additives are recommended for CAD detection, a couple of various eluents were tested as the aqueous part of the mobile phase during method development. Due to the poor UV absorbance of triterpene glycosides, 200 nm as the optimal wavelength in UV (DAD) detection of protoescigenin was selected.

Mobile phase composition

Various additives in the aqueous part of the mobile phase and their influence on the main peak area was examined. Ammonium acetate buffer, trifluoroacetic acid, formic acid and acetic acid, all at different concentrations, were tested. The results are presented in Figure 2 (both, for UV and CAD).

In case of UV, detection 10 mM concentration of ammonium acetate resulted in the lowest peak areas, changing concentration of this buffer had also noticeable influence on the UV response. Using of 5 mM ammonium acetate gave almost similar results as in the case of 0.1% trifluoroacetic acid (TFA). For both, TFA and ammonium acetate, lower concentrations resulted in the higher peak areas. Changing the concentration of formic acid and

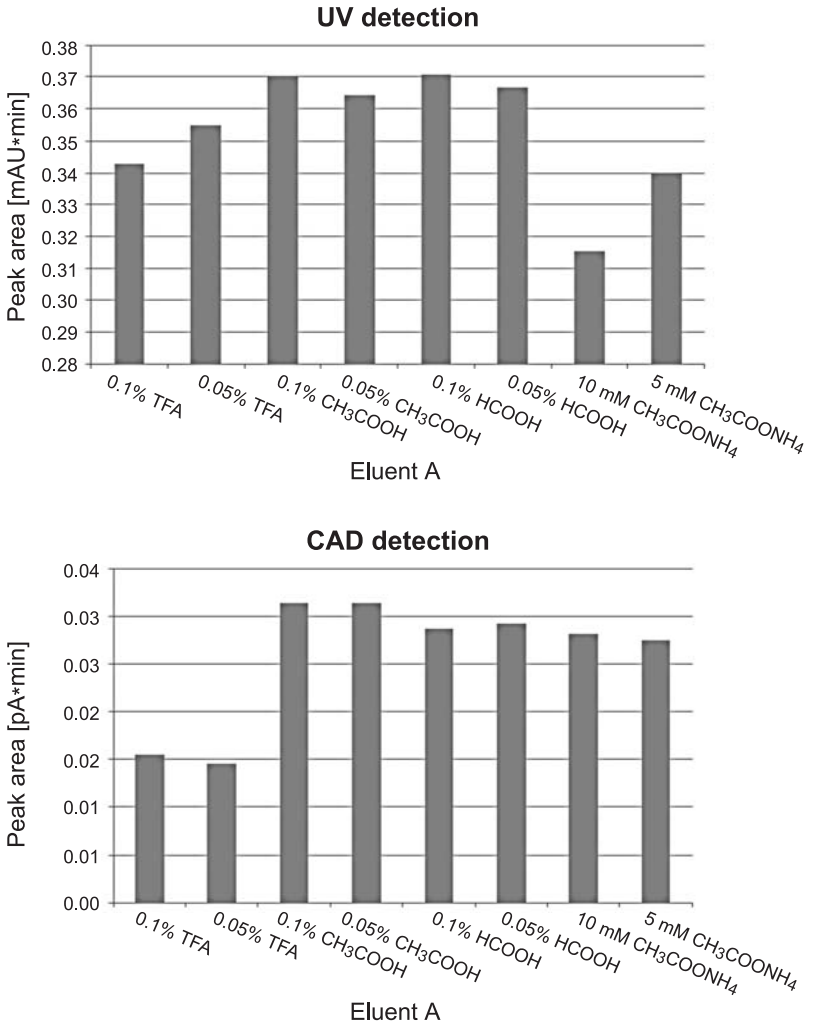

Figure 2 The influence of various additives to UV and CAD response (concentration of tested sample ~1 mg/mL, inj. vol. 1 µL)

acetic acid did not affect the UV detector response; in case of these two additives the highest peak areas of protoescigenin were observed.

Different results were obtained in case of CAD detection. TFA, in both concentrations (0.1 and 0.05%), had the strongest influence on the response (the lowest peak areas were observed); additionally a very strong increase of spike peaks was observed. On the other hand, using of ammonium acetate, as well as acetic and formic acid gave comparable CAD response, independent of the additive concentration, with acetic acid giving the highest peak areas.

Based on obtained results, as optimal component of the water part of the mobile phase, for both detection systems, 0.1% acetic acid was selected.

Influence of the flow rate on UV and CAD response

During the method development it was observed that for UV detection the protoescigenin peak area decreases with increasing mobile phase flow-rate, whereas CAD response remains flow rate-independent. This finding has been confirmed on two examples: (1) for 0.1% acetic acid/acetonitrile (70 : 30, v/v) and (2) 0.1% formic acid/acetonitrile (70 : 30 v/v) as a mobile phase. Example (1) is illustrated in Figure 3.

The explanations for the reduction of the signal intensity are described in the literature (20, 21). Because UV detector is concentration-sensitive, its signal follows the Lambert-Beer law (absorbance = concentration × molar abs. × optical path length).

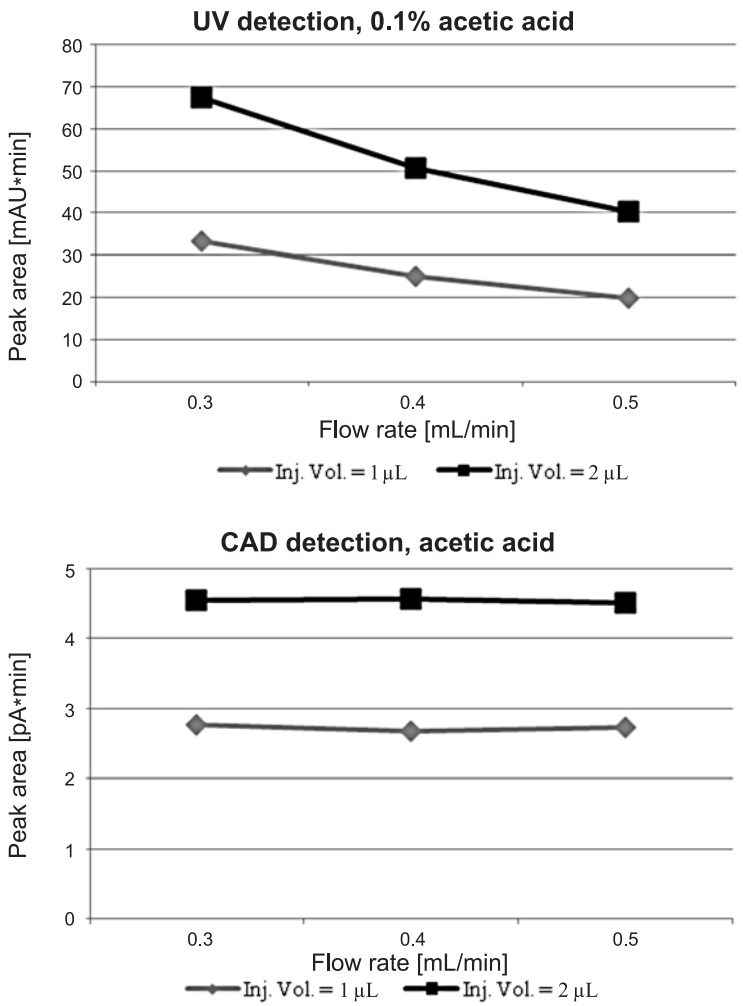

Figure 3 Correlation between the detector response and the mobile phase flow rates

When a peak reaches the cell of an UV detector its width is equal to its residence time, whereas its height is governed by the analyte concentration at the peak minimum. As a consequence, the peak area depends very strongly on the flow rate of the mobile phase (20, 21). On the other hand, charged aerosol detector as mass-sensitive is unaffected by this phenomena.

Influence of sample concentration and injection volume on S/N value in UV and CAD

Optimal sample concentration and injection volume was determined in both detection approaches. For protoescigenin concentration of 1 mg/mL and injection volume of 2 µL, S/N ratios for CAD were two times higher than for the UV detection.

Results are presented in Figure 4.

System suitability test (SST) and validation

The SST was performed by 7 subsequent injections of protoescigenin (PES-01) sample containing several process-related impurities, among them barringtogenol C (BAC) at the level of ~17% (normalization calculation method). Parameters such as peak asymmetry, resolution between critical peaks and repeatability (based on retention times and peak areas, the repeatability expressed as RSD %) were established. SST results were compared for both detection approach (see Table 1). Results are similar for both detection systems, but in case of CAD better symmetry of PES-01 peak was achieved.

A typical chromatogram is shown in Figure 1.

Limit of detection (LOD) and limit of quantitation (LOQ)

In analytical methods the detection limit (LOD) is defined as the minimum level at which the analyte can be reliably detected and quantitation limit (LOQ) as the minimum level at which the analyte can be quantified with acceptable accuracy and precision (22). Several approaches for determining the LOD and LOQ are possible – in this work, method based on signal-to-noise ratio (S/N) was used. Limits of detection and quantitation for both detection systems were established, assuming that S/N ratio for LOD should be not less than 3.3 and for LOQ not less than 10. The LOD criterion was fulfilled for the solutions at the concentration of 0.001 mg/mL for both, UV and CAD detection. In the case of CAD, S/N values were found to be almost two times higher than for the UV detection. The same was observed for LOQ, where the criterion was fulfilled for the solutions of protoescigenin with concentration of 0.002 mg/mL.

Linearity and calibration range

The linearity of methods (UV and CAD) was evaluated in two ranges of concentration: (1) broad, from LOQ to 120% of protoescigenin (i.e., from 0.002 mm/mL to 2.40 mg/mL) and (2) narrow, for five concentration levels (80% – 120%, i.e., from 1.60 to 2.40 mg/mL). Results are presented in Table 1. The obtained calibration curves were linear in both defined ranges. However, in the case of CAD, a log-log transformation for calibration curve, which

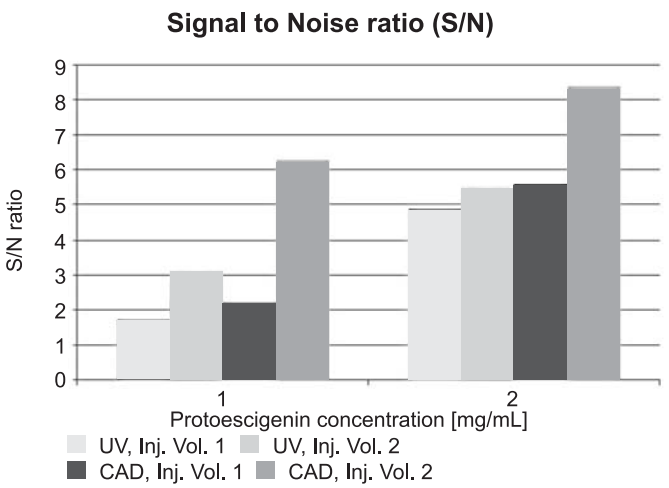

Figure 4. Influence of sample concentration and injection volume on S/N value in UV and CAD

Table 1. Method validation results.

	UV (200 nm)	CAD	Limits for pharmaceutical substances
Accuracy [%]	99.95	98.97	Recovery 98–101%
Precision [%RSD]	0.48	0.37	RSD ≤ 1.0%
Linearity – from LOQ to 120% (0.002 – 2.408 mg/mL)	R^2 = 0.9995 y = 0.4128x + 0.4000	R^2 = 0.9990 y = –0.044x + 1.042x + 0.713	$R^2 \geq 0.998$
Linearity – from 80–120% (1.616 – 2.408 mg/mL)	R^2 = 0.9996 y = 0.4297x – 1.4218	R^2 = 0.9986 y = 0.0347x + 0.5925	$R^2 \geq 0.998$
LOD S/N	0.001 mg/mL 4	0.001 mg/mL 7	S/N ≥ 3
LOQ S/N	0.002 mg/mL 11	0.002 mg/mL 21	S/N ≥ 10
System suitability results:			
Asymmetry	0.81	0.96	$0.8 \leq A_s \leq 1.5$
Resolution between PES-01 and the closest impurity	4.30	3.42	$R_s \geq 1.50$
PES-01 Peak area, RSD %	0.62	0.74	RSD ≤ 1.0%
PES-01 Retention time, RSD %	0.13	0.12	RSD ≤ 1.0%
BAC Retention time, RSD %	0.11	0.11	–

judgment concurred with those of other reports (23, 24), was necessary – but only for the broad concentration range. It was concluded that the developed method is appropriate for quantitative purposes for both UV and CAD detection, in broad concentration range.

Accuracy and precision

Method precision was tested using six protoescigenin samples at 100% of concentration (c = 2 mg/mL) and was expressed as % RSD. Accuracy was determined on three levels: 80%, 100% and 120%, three sample solutions per each level, and was expressed as % of recovery (see Table 1). All the results were in correspondence with the requirements for method validation.

CONCLUSIONS

Protoescigenin, the main genin of HCSE, was selected as a substrate for further exploratory chemistry. Physicochemical characterization of this compound has been recently described by Gruza et al. (3). As a complement to the aforementioned work, a new, fast and universal, ultra-high performance liquid chromatography (UHPLC) method for quantitative analysis of protoescigenin has been developed and validated. In the method dual detection system has been applied, with using UV (200 nm) and CAD simultaneously.

The results achieved in method optimization showed an influence of the mobile phase flow-rate on UV detector response, expressed as decrease of the protoescigenin peak area with increasing flow rate value. A relationship between the type of the additive to the aqueous mobile phase and both UV and CAD detectors response was also noticed. The best results were obtained when 0.1% acetic acid was used as the additive.

The SST and validation results were in good agreement with validation requirements for both detectors. UV and CAD detectors gave linear response, both for the narrow and the broad range of concentrations. The sensitivity of CAD detection was a little bit greater than the UV, when comparing achieved S/N values.

Combining of the two detection systems – classical UV (in version of DAD detector) and CAD is the big advantage of the developed method, because both detection approaches complement each other. CAD allows for slightly better detection of weakly UV active protoescigenin and on the other hand, the lack of possibility of peak purity analysis in case of CAD is solved by simultaneously employ-

ing of DAD detector. The results obtained for both detection approaches and their usefulness for protoescigenin quantification have been demonstrated.

Acknowledgment

The authors gratefully acknowledge financial support from European and Regional Funds under project POIG.0101.02-14-072/09-00.

REFERENCES

1. Zhang J., Qu F.: Methods for analysis of triterpenoid saponins in: Handbook of Natural Products, Ramawat K.G., Henry H., Merillon J.M. Eds., pp. 3311–3323, Springer-Verlag, Berlin, Heidelberg 2013.
2. Efferth T., Greten H.J.: Medicinal and Aromatic Plants 1, 7 (2012).
3. Gruza M., Jatczak K., Zagrodzki B., Łaszcz M., Cmoch P., Woźniak K., Malińska M. et al.: Molecules 18, 4389 (2013).
4. Jatczak K., Gruza M., Filip K., Cmoch P., Grynkiewicz G.: Centr. Eur. J. Chem. (2014), accepted for publication.
5. Kuhn R.; Löw I.: Tetrahedron 22, 1899 (1966).
6. Wulff G.; Tschesche R.: Tetrahedron 25, 415 (1969).
7. Agrawal P.K.; Thakur R.S.; Shoolery J.N.: J. Nat. Prod. 54, 1394 (1991).
8. Horse-Chestnut and Horse-Chestnut dry extract, standardized, Pharmeuropa 20, 478 (2008).
9. Vervoort N., Daemen D., Torok G.: J. Chromatogr. A 1189, 92 (2008).
10. Novakova L., Arnal Lopéz S., Dagmar Solichová D., Satínsk D., Kulichová B., Horna A., Solic P.: Talanta 78, 834 (2009).
11. Shaodong J., Lee W.J., Ee J.W., Park J.H., Kwon S.W., Lee J.: J. Pharm. Biomed. Anal. 51, 973 (2010).
12. Obreza A., Vehovec T.: J. Chromatogr. A 1217, 1549 (2010).
13. Oleszek W., Bialy Z.: J. Chromatogr. A 1112, 78 (2006).
14. Almeling S.: doctor thesis, Dissertation zur Erlangung des naturwissenschaftlichen Doktorgrades der Julius-Maximilians-Universität Würzburg, Würzburg 2011.
15. Negi J.S., Singh P., Pant G.J., Rawat M.S.: Pharmacogn. Rev. 5, 155 (2011).
16. CAD Bibliography, Thermo Scientific (2013). http://www.thermo.com.cn/Resources/201402/1711137765.pdf
17. Bai C.-C., Han S.-Y., Chai X.-Y., Jiang Y., Li P., Tu P.-F.: J, Liq. Chromatogr. Relat. Technol. 32, 242 (2009).
18. Eom H.Y., Park S.Y., Kim M.K., Suh J.H., Yeom H., Min J.W., Kim U. et al.: J. Chromatogr. A 1217, 4347 (2010).
19. Yeom H, Suh J.H, Youm J.R, Han S.B., Bull. Korean Chem. Soc. 31, 1159 (2010).
20. Meyer V.R.: Pitfalls and errors of HPLC in pictures, Wiley-VCH, Weinheim 2013.
21. Meyer V.R.: Practical High Performance Liquid Chromatography, Veronika R. Meyer, Wiley-VCH, Weinheim 2010.
22. ICH Harmonised Tripartite Guideline: Validation of analytical procedures: text and methodology Q2(R1); International Conference on Harmonisation of Technical Requirements for Registration of Pharmaceuticals for Human Use, Current Step 4 version, Parent Guideline dated 27 October 1994.
23. Vervoort N., Daemen D., Török G.: J. Chromatogr. A 1189, 92 (2008).
24. Górecki T., Lynen F., Szucs R., Sandra P.: Anal. Chem. 78, 3186 (2006).

Project co-financed by the European Regional Development Fund under the framework of the Innovative Economy Operational Programme.

POIG contract no 01.01.02-14-072/09 „Research on innovative endothelium medicine among novel escin analogues": www.ifarm.eu/poig/escyna/

Acta Poloniae Pharmaceutica – Drug Research, Vol. 71 No. 6 pp. 941–953, 2014 ISSN 0001-6837
Polish Pharmaceutical Society

PRELIMINARY STUDIES ON APPLICATION OF LIBRARY OF ARTIFICIAL RECEPTORS FOR DIFFERENTIATION OF METABOLITES IN URINE OF HEALTHY AND CANCER BEARING MICE

MAŁGORZATA WALCZAK[1], JUSTYNA FRĄCZYK[1*], ZBIGNIEW J. KAMIŃSKI[1], JOANNA WIETRZYK[2] and BEATA FILIP-PSURSKA[2]

[1] Institute of Organic Chemistry, Lodz University of Technology (TUL), Żeromskiego 116, 90-924 Łódź, Poland,
[2] Institute of Immunology and Experimental Therapy, Polish Academy of Science, Rudolfa Weigla 12, 53-114 Wrocław, Poland

Abstract: A library of artificial receptors formed by the self-organization of *N*-lipidated peptides attached to the cellulose *via m*-aminophenylamino-1,3,5-triazine was used for differentiation of metabolites in urine of healthy and cancer bearing mice. The interactions of urine metabolites with the receptors were visualized by using competitive adsorption-desorption of an appropriate reporter dye. Analysis of the binding pattern (fingerprint) of urine metabolites from healthy and from cancer suffering mice showed that there were several structures among 120-elements molecular receptors which were able to differentiate bonded ligands depending on the healthy state. For all three tested types of cancers two structures: Lipid-Pro-Ala-NH-C_6H_4-NH-DMT-cellulose and Lipid-Arg-Pro-NH-C_6H_4-NH-DMT-cellulose were selected as diagnostic.

Keywords: cancer marker, medical diagnostic, molecular receptor

Biomedical research is constantly challenged to clarify the relationship between health, disease and metabolism influenced by nutrition, pharmaceuticals and others. Biological fluids, such as urine, sweat, saliva, blood, contain a great number and variable metabolites that may offer valuable information on the metabolism of an organism, and consequently about its health status (1). In parallel with genomics, transcriptomics and proteomics, metabolomics will amplify our understanding of the pathophysiological processes involved and should be useful in an identification of potential biomarkers to develop new therapeutic strategies (2).

Indeed, metabolic fingerprinting, also referred to as metabolomics, metabonomics, metanomics (3) or associated terms, is a technique that allows identification and quantification of metabolites (low molecular weight molecules e.g., lipids, amino acids, and sugars)) in biological fluids and is useful in determining the phenotype of disease (4).

From a clinical point of view, the study of metabolic changes that occur in response to divergent physiological processes are helpful in the study of the mechanisms underlying the development of various diseases. In terms of personalized medicine, metabonomic approaches can provide the tool to predict the action of drugs in a particular individual based on the predose urinary metabolite profile (5). Analysis of complex metabolome is not a trivial task. There are several analytical strategies useful in analysis of metabolome (6): NMR (7) FT-IR (8), MS connected with separation techniques: HPLC, GC and CE. Only the combination of these analytical techniques offers analysis of complete metabolome. However, technological advances have increased the number of metabolites that can be quantified simultaneously (9).

Metabolic fingerprinting does not identify the whole set of metabolites but compare patterns or fingerprints of metabolites that change in response to a disease state, pharmacological therapies or environmental alterations. This approach is useful as a diagnostic tool to evaluate the disease state by comparing healthy controls and disease subjects, or to assay the success of a particular treatment (prognosis/recovery) (10). However, in the case of understanding the mechanisms underlying a disease, qualitative and quantitative analyses are necessary (11). Metabolite profiling focuses on the analysis of a group of metabolites related to a specific metabolic

* Corresponding author: e-mail: justyna.fraczyk@p.lodz.pl, phone: 48 42 6313221

pathway (12). Here we present preliminary studies on application of library of *N*-lipidated peptides immobilized on cellulose in fingerprinting of urine metabolites of healthy and tumor bearing mice.

MATERIALS AND METHODS

Immobilization of 2,4-dichloro-6-methoxy-1,3,5-triazine on Whatman 7 cellulose filter paper

One hundred thirty five (120 + 15) Whatman 7 cellulose filter plates (10 × 10 cm) were washed with hexane (200 mL) and ethyl acetate (200 mL). After drying in a vacuum desiccator, plates were treated with 1 M NaOH (400 mL) for 15 min. In the next step, alkaline solution was removed and plates were air dried for 10 min and then immersed in a suspension of 1 M solution of 2,4-dichloro-6-methoxy-1,3,5-triazine (DCMT) in THF (400 mL) and solid $NaHCO_3$ (42 g, 0.5 mol). Suspension with immersed cellulose plates was gently shaken for 45 min, then plates were washed successively with THF (250 mL), 50% solution THF in water (250 mL) and acetone (250 mL). DCMT functionalized plates were dried to constant weight in a vacuum desiccator. Loading of 2-chloro-4,-methoxy-1,3,5-triazine was calculated on the basis of the elemental analysis content of nitrogen and chlorine.

Elemental analysis: found: N 3.64%, Cl 2.66%; calculated from nitrogen content: 2.60 mmol N/1 g equivalent to 31.9×10^{-6} mol N/cm^2, corresponding to 31.9×10^{-6} mol triazine/cm^2; calculated from chlorine content: 0.75 mmol Cl/1 g equivalent to 9.2×10^{-6} mol Cl/cm^2, corresponding to 9.2×10^{-6} mol triazine/cm^2.

Functionalization of 2-chloro-1,3,5-triazine derivative immobilized on the cellulose support with 1,3-phenylenediamine

One hundred thirty (120 + 10) Whatman 7 cellulose plates modified with DCMT (10 × 10 cm) were immersed in 1 M solution of 1,3-phenylenediamine in THF (400 mL) and gently shaken for 15 h at room temperature. Solution was removed, plates were washed with CH_2Cl_2 (250 mL), THF (250 mL), DMF (250 mL) and CH_2Cl_2 (250 mL) and dried to constant weight in a vacuum desiccator.

Synthesis of library of N-lipidated dipeptides

Incorporation of N-Fmoc-protected amino acids (1st amino acids) on the surface of DMT-NH-C_6H_4-NH_2 functionalized cellulose sheets

Synthesis of N-Fmoc-Ala-NH-C_6H_4-NH-DMT-cellulose sheet {**1**}). General procedure

Forty two (40 + 2) DMT-NH-C_6H_4-NH_2 functionalized cellulose plates, labeled respectively with graphite pencil as **1**, were immersed in solution of 4-(4,6-dimethoxy-[1,3,5]-triazin-2-yl)-4-methylmorpholinium toluene-4-sulfonate (DMT/NMM/TosO$^-$) (4.13 g, 10 mmol) in DMF (40 mL), Fmoc-Ala-OH (3.29 g, 10 mmol) and NMM (2.5 mL, 23 mmol) and gentle shaking was continued for 12 h. The excess solution was removed and the modified cellulose plates were washed with DMF (3 × 50 mL) and methylene chloride (3 × 50 mL).

Synthesis of N-Fmoc-Trp(Boc)-NH-C_6H_4-NH-DMT-cellulose sheet {**2**}

Forty two (40 + 2) DMT-NH-C_6H_4-NH_2 functionalized cellulose sheets labeled as **2** were treated with DMF (40 mL) solution containing Fmoc-Trp(Boc)-OH (5.27 g, 10 mmol), DMT/NMM/TsO$^-$ (4.13 g, 10 mmol) and NMM (2.5 mL, 23 mmol).

Synthesis of N-Fmoc-Pro-NH-C_6H_4-NH-DMT-cellulose sheet {**3**}

Forty two (40 + 2) DMT-NH-C_6H_4-NH_2 functionalized cellulose sheets labeled as **3** were treated with DMF (40 mL) solution containing Fmoc-Pro-OH (3.38 g, 10 mmol), DMT/NMM/TsO$^-$ (4.13 g, 10 mmol) and NMM (2.5 mL, 23 mmol).

Deprotection of fluorenylmethyloxycarbonyl (Fmoc) group from amino acids incorporated on the surface of functionalized cellulose sheets {1-3}

Cellulose sheets {**1-3**} were treated with 25% solution of piperidine in DMF (200 mL) for 15 min. After removal of excess piperidine solution, {**1-3**} were washed with DMF (3 × 100 mL) and methylene chloride (1 × 100 mL).

Incorporation of the second N-Fmoc-protected amino acids on the surface of H_2N-amino acid-NH-C_6H_4-NH-DMT-celululose sheets. General procedure

To solution of DMT/NMM/TsO$^-$ (4.13 g, 10 mmol) in DMF (40 mL), Fmoc-protected amino acids (10 mmol) and NMM (2.5 mL, 23 mmol) were added. After obtaining homogeneous reaction mixture, H_2N-amino acid-NH-C_6H_4-NH-DMT-celululose sheets labeled with graphite pencil were immersed and gently shaken for 12 h. The excess solution was removed and the cellulose sheets were washed with DMF (3 × 50 mL) and methylene chloride (3 × 50 mL).

Incorporation of Fmoc-Ala-OH

Six (3 × 2) modified cellulose sheets {**1**, **2**, **3**} were treated with solution containing Fmoc-Ala-OH (3.29 g, 10 mmol), DMT/NMM/TsO$^-$ (4.13 g, 10

mmol) and NMM (2.5 mL, 23 mmol) and labeled as {**1.1**}, {**2.1**} and {**3.1**}.

Incorporation of Fmoc-Phe-OH

Six (3 × 2) modified cellulose sheets {**1**, **2**, **3**} were treated with solution containing Fmoc-Phe-OH (3.87 g, 10 mmol), DMT/NMM/TsO^- (4.13 g, 10 mmol) and NMM (2.5 mL, 23 mmol) and labeled as {**1.2**}, {**2.2**} and {**3.2**}.

Incorporation of Fmoc-Leu-OH

Six (3 × 2) modified cellulose sheets {**1**, **2**, **3**} were treated with solution containing Fmoc-Leu-OH (3.53 g, 10 mmol), DMT/NMM/TsO^- (4.13 g, 10 mmol) and NMM (2.5 mL, 23 mmol) and labeled as {**1.3**}, {**2.3**}, {**3.3**}.

Incorporation of Fmoc-Ile-OH

Six (3 × 2) modified cellulose sheets {**1**, **2**, **3**} were treated with solution containing Fmoc-Ile-OH (3.53 g, 10 mmol), DMT/NMM/TsO^- (4.13 g, 10 mmol) and NMM (2.5 mL, 23 mmol) and labeled as {**1.4**}, {**2.4**}, {**3.4**}.

Incorporation of Fmoc-Val-OH

Six (3 × 2) modified cellulose sheets {**1**, **2**, **3**} were treated with solution containing Fmoc-Val-OH (3.39 g, 10 mmol), DMT/NMM/TsO^- (4.13 g, 10 mmol) and NMM (2.5 mL, 23 mmol) and labeled as {**1.5**}, {**2.5**}, {**3.5**}.

Incorporation of Fmoc-Met-OH

Six (3 × 2) modified cellulose sheets {**1**, **2**, **3**} were treated with solution containing Fmoc-Met-OH (3.71 g, 10 mmol), DMT/NMM/TsO^- (4.13 g, 10 mmol) and NMM (2.5 mL, 23 mmol) and labeled as {**1.6**}, {**2.6**}, {**3.6**}.

Incorporation of Fmoc-Cys(Trt)-OH

Six (3 × 2) modified cellulose sheets {**1**, **2**, **3**} were treated with solution containing Fmoc-Cys(Trt)-OH (5.86 g, 10 mmol), DMT/NMM/TsO^- (4.13 g, 10 mmol) and NMM (2.5 mL, 23 mmol) and labeled as {**1.7**}, {**2.7**}, {**3.7**}.

Incorporation of Fmoc-Ser(tBu)-OH

Six (3 × 2) modified cellulose sheets {**1**, **2**, **3**} were treated with solution containing Fmoc-Ser(tBu)-OH (3.83 g, 10 mmol), DMT/NMM/TsO^- (4.13 g, 10 mmol) and NMM (2.5 mL, 23 mmol) and labeled as {**1.8**}, {**2.8**}, {**3.8**}.

Incorporation of Fmoc-Tyr(tBu)-OH

Six (3 × 2) modified cellulose sheets {**1**, **2**, **3**} were treated with solution containing Fmoc-Tyr(tBu)-OH (3.29 g, 10 mmol), DMT/NMM/TsO^- (4.13 g, 10 mmol) and NMM (2.5 mL, 23 mmol) and labeled as {**1.9**}, {**2.9**}, {**3.9**}.

Incorporation of Fmoc-Thr(tBu)-OH

Six (3 × 2) modified cellulose sheets {**1**, **2**, **3**} were treated with solution containing Fmoc-Thr(tBu)-OH (3.37 g, 10 mmol), DMT/NMM/TsO^- (4.13 g, 10 mmol) and NMM (2.5 mL, 23 mmol) and labeled as {**1.10**}, {**2.10**}, {**3.10**}.

Incorporation of Fmoc-Glu(OtBu)-OH

Six (3 × 2) modified cellulose sheets {**1**, **2**, **3**} were treated with solution containing Fmoc-Glu(OtBu)-OH (4.25 g, 10 mmol), DMT/NMM/TsO^- (4.13 g, 10 mmol) and NMM (2.5 mL, 23 mmol) and labeled as {**1.11**}, {**2.11**}, {**3.11**}.

Incorporation of Fmoc-Asp(OtBu)-OH

Six (3 × 2) modified cellulose sheets {**1**, **2**, **3**} were treated with solution containing Fmoc-Asp(OtBu)-OH (4.11 g, 10 mmol), DMT/NMM/TsO^- (4.13 g, 10 mmol) and NMM (2.5 mL, 23 mmol) and labeled as {**1.12**}, {**2.12**}, {**3.12**}.

Incorporation of Fmoc-Gln(Trt)-OH

Six (3 × 2) modified cellulose sheets {**1**, **2**, **3**} were treated with solution containing Fmoc-Gln(Trt)-OH (6.11 g, 10 mmol), DMT/NMM/TsO^- (4.13 g, 10 mmol) and NMM (2.5 mL, 23 mmol) and labeled as {**1.13**}, {**2.13**}, {**3.13**}.

Incorporation of Fmoc-Asn(Trt)-OH

Six (3 × 2) modified cellulose sheets {**1**, **2**, **3**} were treated with solution containing Fmoc-Asn(Trt)-OH (5.97 g, 10 mmol), DMT/NMM/TsO^- (4.13 g, 10 mmol) and NMM (2.5 mL, 23 mmol) and labeled as {**1.14**}, {**2.14**}, {**3.14**}.

Incorporation of Fmoc-His(Trt)-OH

Six (3 × 2) modified cellulose sheets {**1**, **2**, **3**} were treated with solution containing Fmoc-His(Trt)-OH (6.20 g, 10 mmol), DMT/NMM/TsO^- (4.13 g, 10 mmol) and NMM (2.5 mL, 23 mmol) and labeled as {**1.15**}, {**2.15**}, {**3.15**}.

Incorporation of Fmoc-Lys(Boc)-OH

Six (3 × 2) modified cellulose sheets {**1**, **2**, **3**} were treated with solution containing Fmoc-Lys(Boc)-OH (4.69 g, 10 mmol), DMT/NMM/TsO^- (4.13 g, 10 mmol) and NMM (2.5 mL, 23 mmol) and labeled as {**1.16**}, {**2.16**}, {**3.16**}.

Incorporation of Fmoc-Pro-OH

Six (3 × 2) modified cellulose sheets {**1**, **2**, **3**} were treated with solution containing Fmoc-Pro-OH (3.37 g, 10 mmol), DMT/NMM/TsO^- (4.13 g, 10 mmol) and NMM (2.5 mL, 23 mmol) and labeled as {**1.17**}, {**2.17**}, {**3.17**}.

Incorporation of Fmoc-Trp(Boc)-OH

Six (3 × 2) modified cellulose sheets {**1**, **2**, **3**} were treated with solution containing Fmoc-Trp(Boc)-OH (5.67 g, 10 mmol), DMT/NMM/TsO^- (4.13 g, 10 mmol) and NMM (2.5 mL, 23 mmol) and labeled as {**1.18**}, {**2.18**}, {**3.18**}.

Incorporation of Fmoc-Arg(Pbf)-OH

Six (3 × 2) modified cellulose sheets {**1**, **2**, **3**} were treated with solution containing Fmoc-Arg(Pbf)-OH (6.49 g, 10 mmol), DMT/NMM/TsO^- (4.13 g, 10 mmol) and NMM (2.5 mL, 23 mmol) and labeled as {**1.19**}, {**2.19**}, {**3.19**}.

Incorporation of Fmoc-Gly-OH

Six (3 × 2) modified cellulose sheets {**1**, **2**, **3**} were treated with solution containing Fmoc-Gly-OH (2.97 g, 10 mmol), DMT/NMM/TsO^- (4.13 g, 10 mmol) and NMM (2.5 mL, 23 mmol) and labeled as {**1.20**}, {**2.20**}, {**3.20**}.

Deprotection of fluorenylmethyloxycarbonyl (Fmoc) group from amino acids incorporated on the surface of functionalized cellulose sheets {1.1-3.20}

Functionalized cellulose sheets {**1.1**–**3.20**} were treated with 25% solution of piperidine in DMF (200 mL) for 15 min. After removal of excess piperidine solution, the cellulose sheets {**1.1**–**3.20**} were washed with DMF (3 × 100 mL) then methylene chloride (1 × 100 mL).

Incorporation of lipid fragment. Synthesis of triazine esters of fatty acids. General procedure

To a vigorously stirred and cooled to 0°C solution of DMM/NMM/TsO^- (6.20 g, 15 mmol) in methylene chloride (50 mL) *N*-methylmorpholine (NMM) (0.85 mL, 7.5 mmol) and fatty acid (15 mmol) were added. As a fatty acids were used 12-hydroxy-(cis)-9-octadecenoic acid (ricinoleic acid) (4.48 g, 15 mmol) or stearic acid (4.27 g, 15 mmol). The mixture was intensively stirred and cooled for additional 2 h. In the next step, the filtrate was concentrated to half volume by rotary evaporation. The residue was used for treating the H_2N-dipeptide-NH-C_6H_4-NH-DMT-cellulose sheets. After 12 h of coupling with triazine ester of fatty acids, modified cellulose sheets were washed successively with DMF (4 × 100 mL), CH_2Cl_2 (1 × 100 mL), MeOH (1 × 100 mL) and CH_2Cl_2 (1 × 100 mL).

Aminolysis of triazine ester of 12-hydroxy-(cis)-9-octadecenoic acid (ricinoleic acid)

Modified cellulose sheets labeled {**1.1**-**3.20**} were treated with solution of triazine ester of 12-hydroxy-(cis)-9-octadecenoic acid (ricinoleic acid). Final functionalized cellulose supports were labeled as {**1.1.A**} – {**1.20.A**}, {**2.1.A**} – {**2.20.A**} and {**3.1.A**} –{**3.20.A**}.

Aminolysis of triazine ester of stearic acid

Modified cellulose sheets labeled {**1.1**–**3.20**} were treated with solution of triazine ester of stearic acid. Final functionalized cellulose supports were labeled as {**1.1.B**} – {**1.20.B**}, {**2.1.B**} – {**2.20.B**} and {**3.1.B**} – {**3.20.B**}.

Deprotection of protecting groups in the side chains of dipeptides immobilized on cellulose supports

All modified cellulose sheets (120 sheets) were treated with mixture consisting of 50% (v/v) trifluoroacetic acid in methylenie chloride (250 mL) with 3% (v/v) water and 2% (v/v) triisopropylsilane for 3 h. In the next step, modified cellulose sheets were washed with methylene chloride (*2* × 200 mL), ethanol (2 × 200 mL) and individually dried in a vacuum desiccator.

Ten (9 + 1) sets of 6 mm diameter discs were cut from every one labeled plate and labeled with graphite pencil as plate label. Then, the discs were buffered with phosphate buffer pH 7 for 25 min. After removing solution of buffer, sets of discs were washed twice with water and with mixture MeOH : H_2O (1 : 1, v:v) for 15 min. Finally, the discs were dried to constant weight in the vacuum dessicator.

Selection of conditions for binding of urine to binding pockets of library N-lipidated peptides immobilized on cellulose

Method A

Set of discs was treated with solution of urine diluted with (1 : 1). After 15 min, the excess of the solution was removed and discs were washed three times with 0.9% NaCl solution. The library was dried in vacuum desiccator and then treated with solution of the reporter dye and scanned to investigate further mathematical analysis.

Method B

Set of discs was treated with urine solution under identical conditions as in the case of method

A. However, after docking the urine components, cellulose discs were drained to constant weight in vacuum desiccator and stored in the refrigerator for 3 days. Then, discs were washed three times with 0.9% NaCl solution to remove the excess of the analyte. The library was dried in vacuum desiccator and then treated with solution of the reporter dye and scanned to investigate further mathematical analysis.

Method C

Set of discs was treated with urine solution under identical conditions as in the case of method A, but after docking the urine components, wet

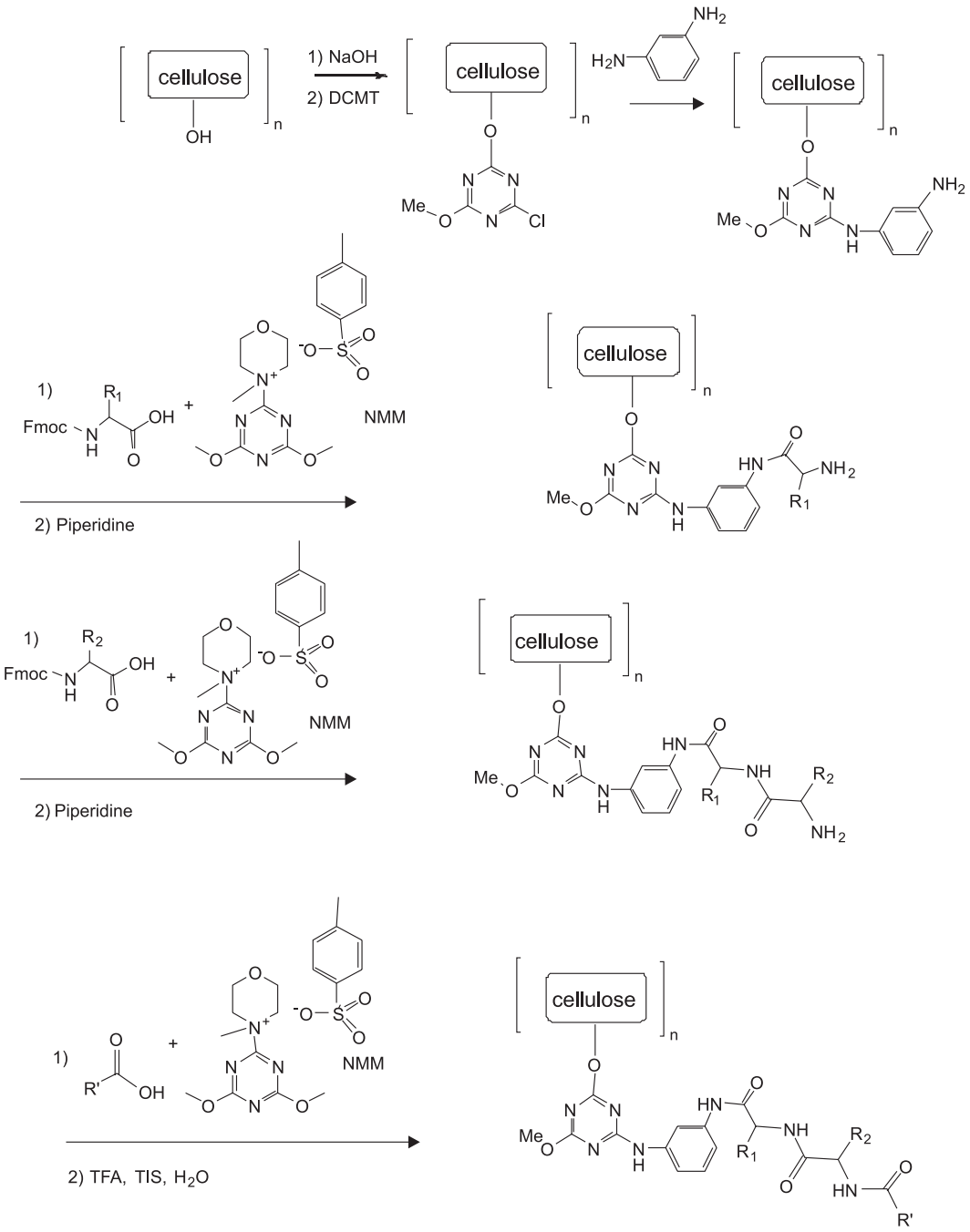

Scheme 1. The synthesis of library of *N*-lipidated peptides attached on the cellulose

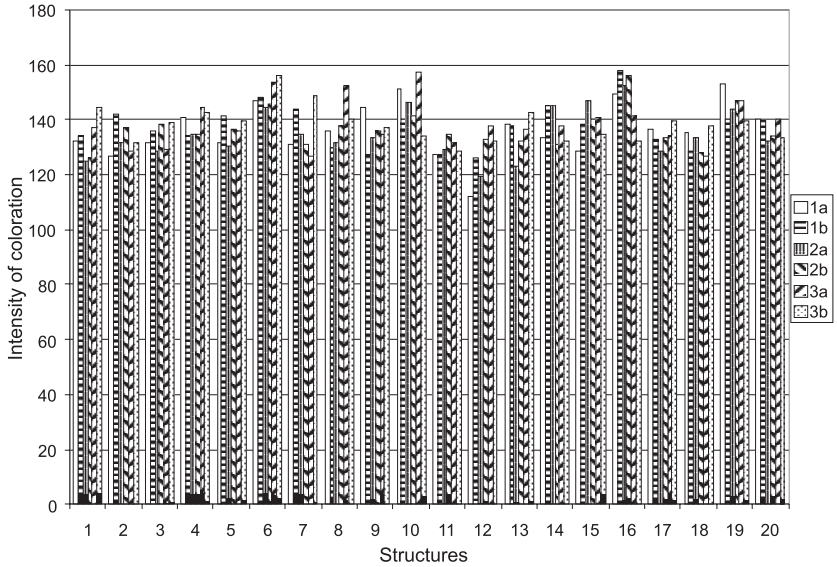

Figure 1. The binding profile of Brilliant Black by library of *N*-lipidated peptides {**1.1A – 3.20B**}. The numbers 1–20 code the second residue of amino acids of *N*-lipidated peptides. Numbers (1, 2, 3) code the first residue of amino acids of *N*-lipidated peptides and letters (a, b) code *N*-acyl residue. For every group of bars, signs refers to the same group of sub-structures

(without drying) cellulose discs were stored in the refrigerator for 3 days. In the next step, the discs were washed three times with 0.9% NaCl solution to remove the excess of the analyte. Then, the discs were washed three times with 0.9% NaCl solution to remove the excess of the analyte. The library was dried in vacuum desiccator and then treated with solution of the reporter dye and scanned to investigate further mathematical analysis.

RESULTS

The library of *N*-lipidated peptides was synthesized in a stepwise procedure involving immobilization of a 2,4-dichloro-6-methoxy-1,3,5-triazine (DCMT) scaffold on cellulose plate (13) followed by reaction with appropriate *meta*-phenylenediamine. Peptide fragment was attached under typical solid phase peptide synthesis (SPPS) using a quaternary *N*-triazinylamonium salt as coupling reagent (14) according to Fmoc/tBu strategy, after removing Fmoc group from immobilized dipeptides. Appropriate carboxylic acids, previously activated by means of a triazine coupling reagent (see Scheme 1), were attached. In order to obtain the same properties of every one element of library on the one cellulose plate it was prepared only one structure. Then, the library was cloned by cutting discs 6 mm in diameter an individually labeling every disc with the label of the respective library plate.

It has been expected that library of artificial receptors is able to bind ligands from mouse urine with efficiency comparable with those observed previously in the case of colored (15) or colorless (16) ligands. For monitoring the competitive adsorption-desorption mechanism of binding colorless ligands, a Brilliant Black as a reporter dyeing agent was used. Brilliant Black was selected as reporter dye, due to its high and very uniform affinity to binding (17) all elements of the library of *N*-lipidated peptides (see Fig. 1).

We expected that libraries of *N*-lipidated peptides immobilized on cellulose allow selective binding of metabolites from urine and will allow tracking changes in urine metabolites in the demand of health.

In view of the instability of urine, low concentrations of metabolites and the presence of structurally diversified mixture of chemical entities, in this preliminary study the peptide fragments of the binding pockets of the library components were prepared from all 20 coded amino acids. In spite of instability of urine, preliminary testing was performed to find optimal experimental condition of binding process.

In these studies, three different binding conditions of urine components by the library of *N*-lipidated peptides were tested (see Fig. 2). Selection of the conditions was aimed to check the influence of time and storage conditions of set discs. Under the

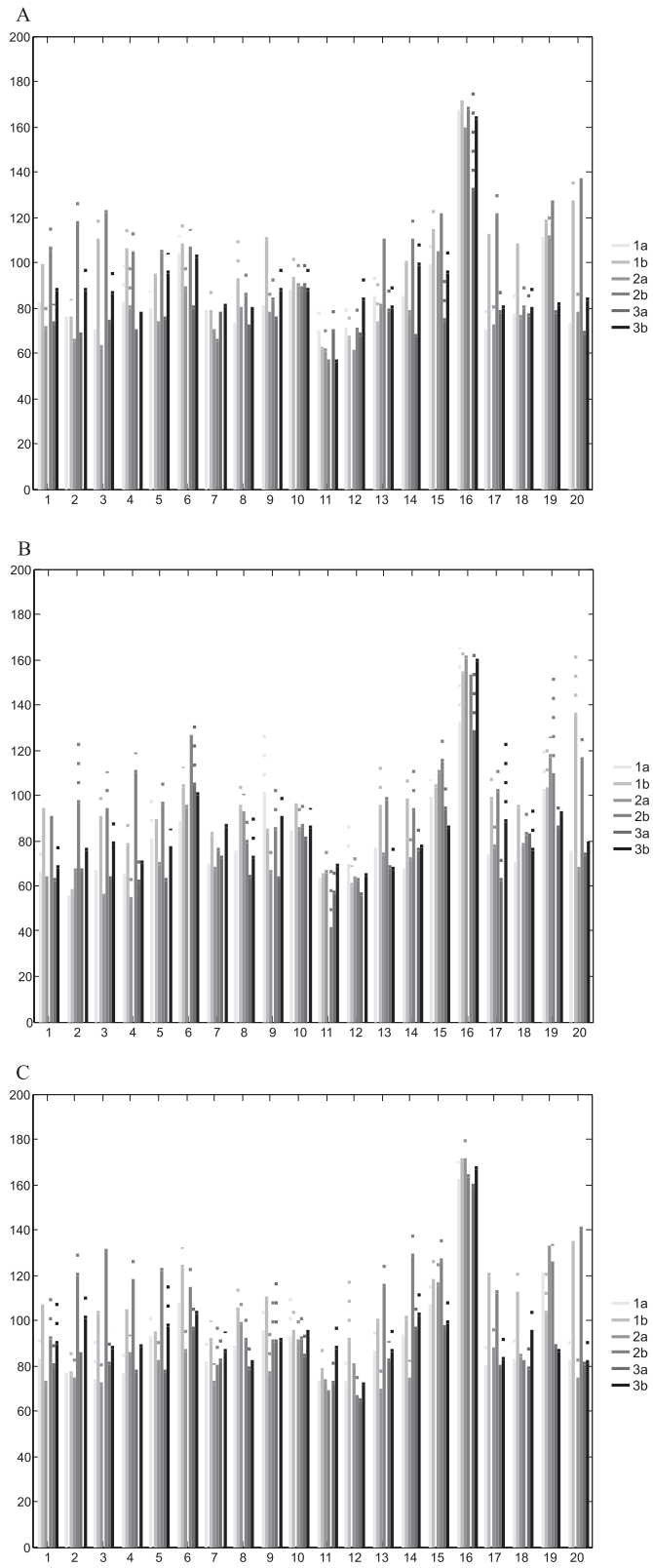

Figure 2. Intensity of coloration with standard deviations obtained for the library *N*-lipidated peptides treated urine by methods A–C. Arithmetic means (solid line) with standard deviations (dashed line). All experiments binding urine metabolites by the library of *N*-lipidated peptides were repeated five times. The numbers 1–20 code the second residue of amino acids of *N*-lipidated peptides. Numbers (1, 2, 3), in figure legend, code first residue of amino acids of *N*-lipidated peptides and letters (a, b) code *N*-acyl residue

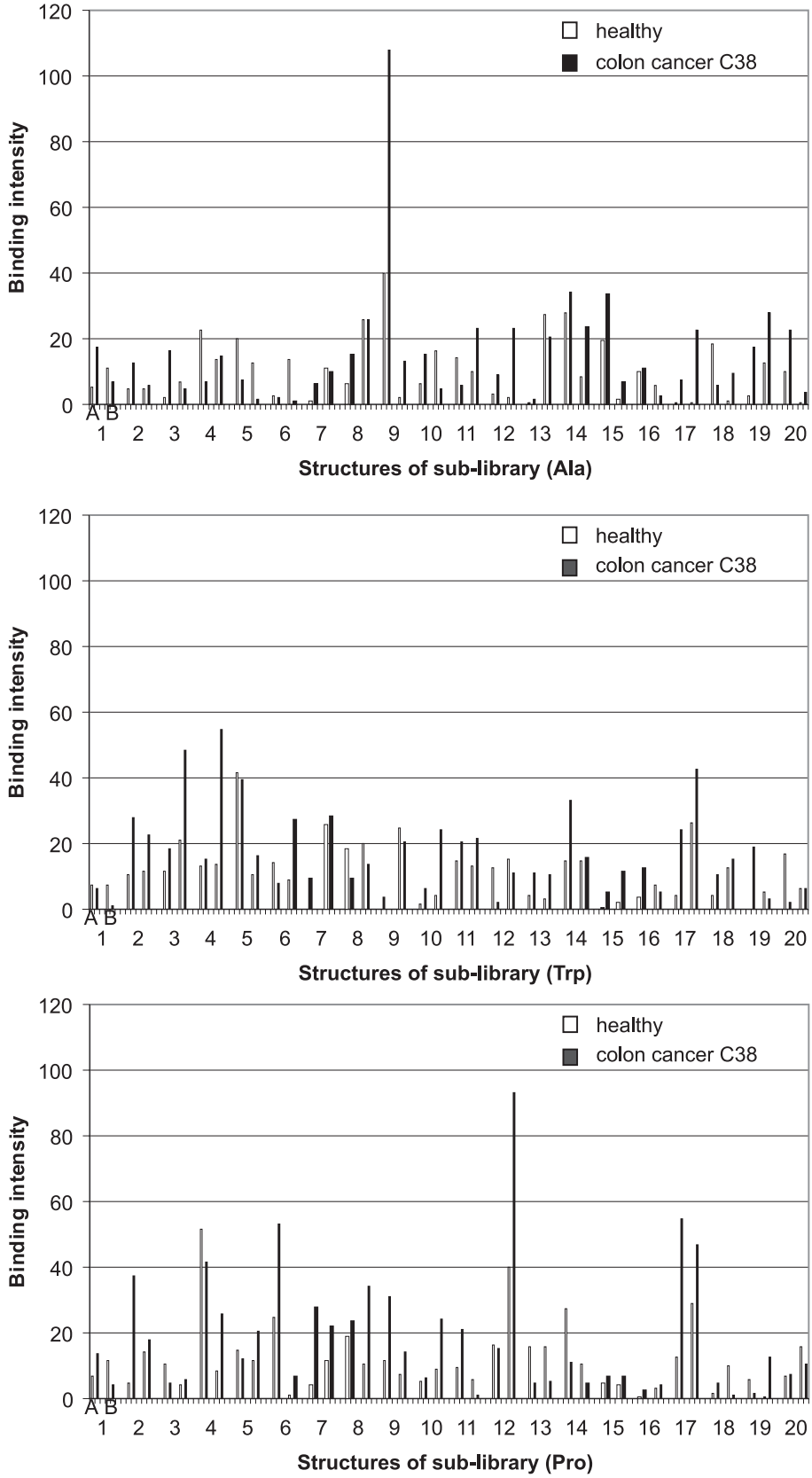

Figure 3. The binding profile of C57B1/6 mouse urine components for sub-libraries of *N*-lipidated peptides

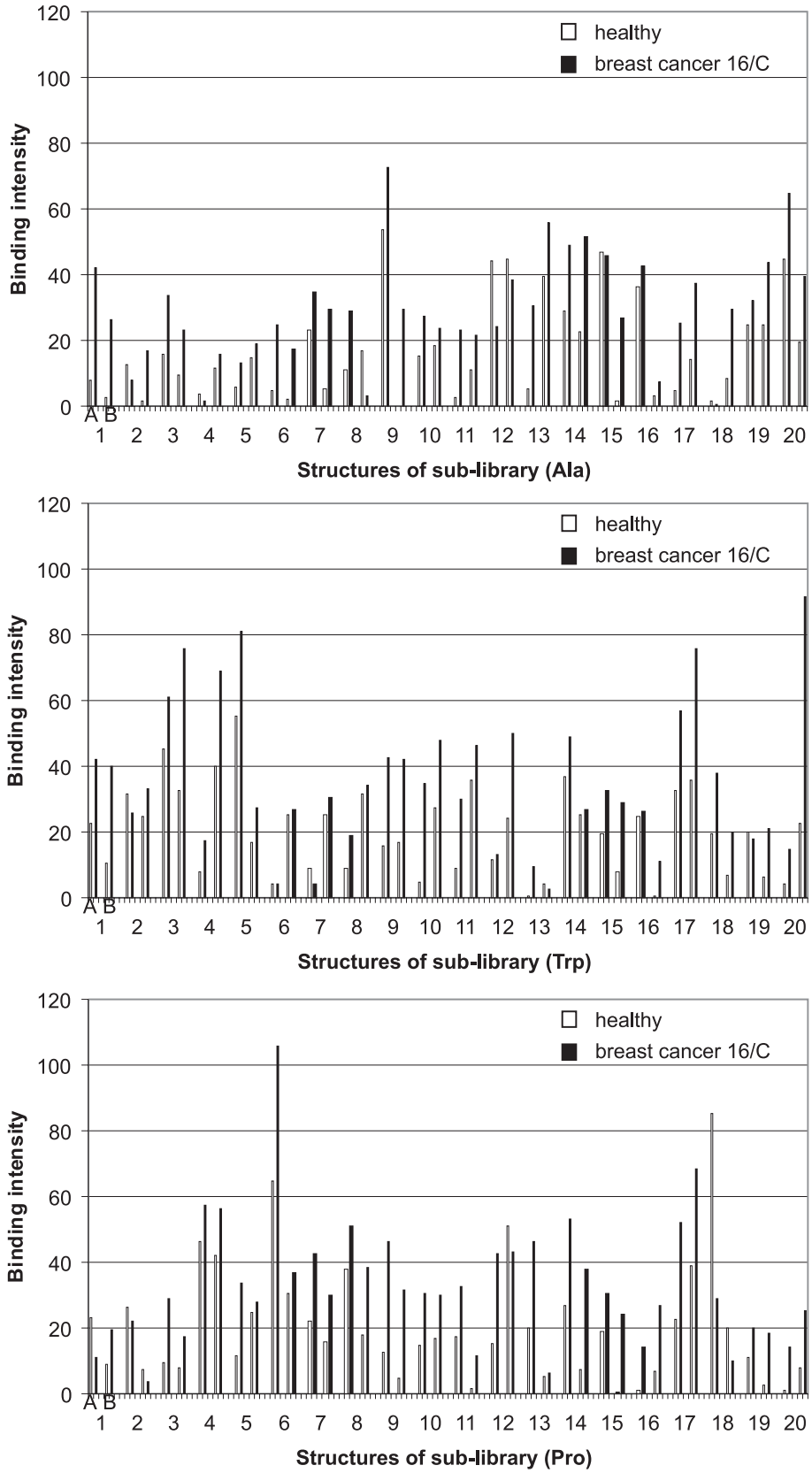

Figure 4. The binding profile of C3H mouse urine components for sub-libraries of *N*-lipidated peptides

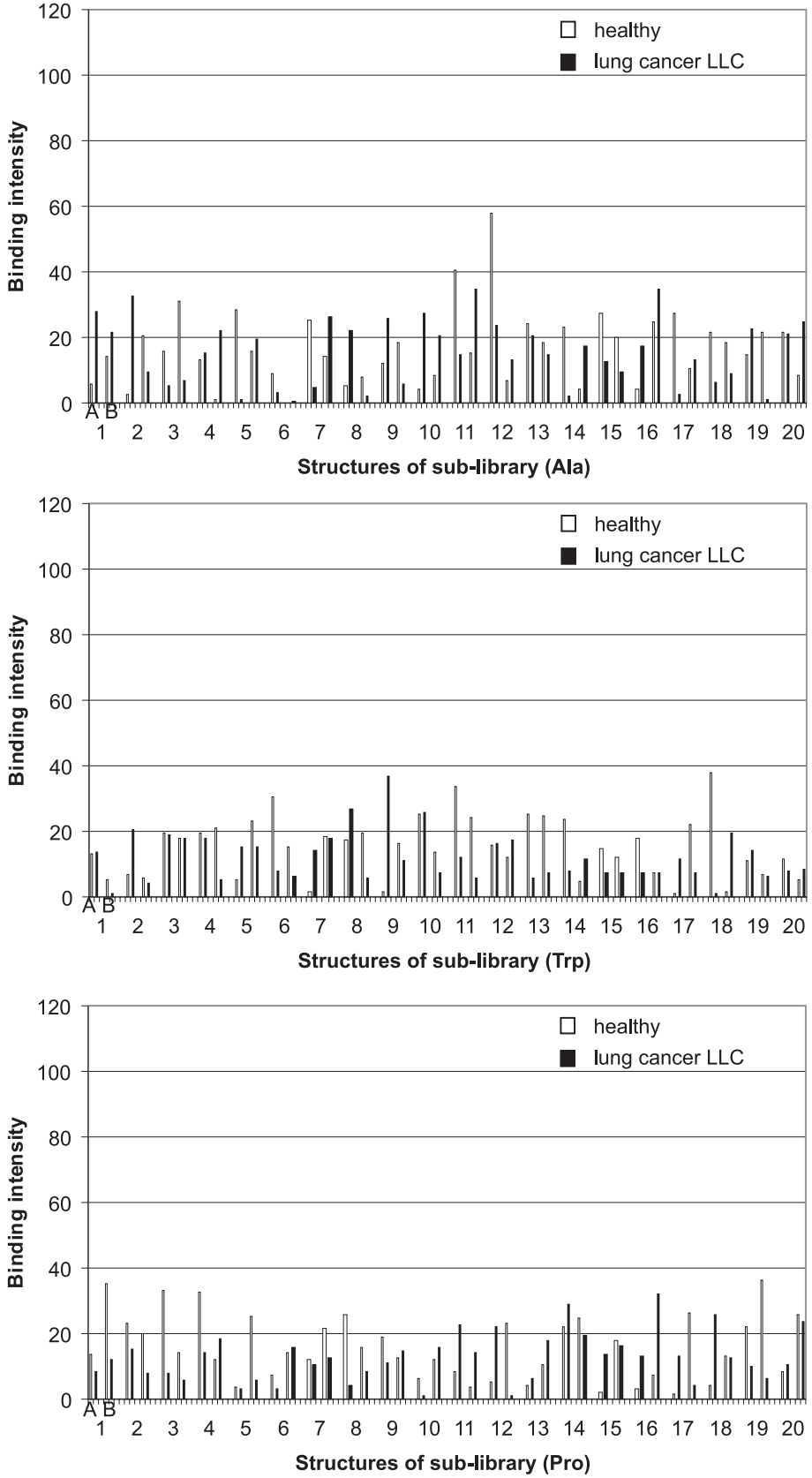

Figure 5. The binding profile of BDF1 mouse urine components for sub-libraries of *N*-lipidated peptides

Table 1. Elements of *N*-lipidated peptides library differentiating the urine of healthy mice and C57B1/6 mice with implanted colon cancer C38.

{**1**} (sub-Ala)	{**2**} (sub-Trp)	{**3**} (sub-Pro)
1.3A – ~AlaLeu-ricinoloyl	**2.4B** – ~TrpIle-stearoyl	**3.2A** – ~Pro-Phe-ricinoloyl
1.4A – ~AlaIle-ricinoloyl	**2.6B** – ~TrpMet-stearoyl	**3.4B** – ~ProIle-stearoyl
1.6B – ~AlaMet-stearoyl	**2.10B** – ~TrpThr-stearoyl	**3.7A** – ~ProCys-ricinoloyl
1.9A – ~AlaTyr-ricinoloyl	**2.17A** – ~TrpPro-ricinoloyl	**3.8B** – ~ProSer-stearoyl
1.12B – ~AlaAsp-stearoyl	**2.20A** – ~TrpGly-ricinoloyl	**3.9A** – ~ProTyr-ricinoloyl
1.17B – ~AlaPro-stearoyl		**3.12B** – ~ProAsp-stearoyl
		3.19B – ~ProArg-stearoyl

Table 2. Structures of elements of *N*-lipidated peptides library differentiating the urine of healthy mice and C3H mice with implanted breast cancer 16/C.

{**1**} (sub-Ala)	{**2**} (sub-Trp)	{**3**} (sub-Pro)
1.1A – ~AlaAla-ricinoloyl	**2.1A** – ~TrpAla-ricinoloyl	**3.3A** – ~ProLeu-ricinoloyl
1.1B – ~AlaAla-stearoyl	**2.1B** – ~TrpAla-stearoyl	**3.9A** – ~ProTyr-ricinoloyl
1.2B – ~AlaPhe-stearoyl	**2.3B** – ~TrpLeu-stearoyl	**3.9B** – ~ProTyr-stearoyl
1.6A – ~AlaMet-ricinoloyl	**2.9A** – ~TrpTyr-ricinoloyl	**3.14B** – ~ProAsn-stearoyl
1.6B – ~ AlaMet-stearoyl	**2.9B** – ~TrpTyr-stearoyl	**3.18A** – ~ProTrp-ricinoloyl
1.7B – ~AlaCys-stearoyl	**2.10A** – ~TrpThr-ricinoloyl	**3.19B** – ~ProArg-stearoyl
1.11A – ~AlaGlu-ricinoloyl	**2.15B** – ~TrpHis-stearoyl	**3.20A** – ~ProGly-ricinoloyl
1.13B – ~AlaGln-stearoyl	**2.19B** – ~TrpArg-stearoyl	
1.15B – ~AlaHis-stearoyl	**2.20B** – ~TrpGly-stearoyl	
1.17A – ~AlaPro-ricinoloyl		
1.18B – ~AlaTrp-stearoyl		

Table 3. Structures of elements of *N*-lipidated peptides library differentiating the urine of healthy mice and BDF1 mice with implanted lung cancer LLC.

{**1**} (sub-Ala)	{**2**} (sub-Trp)	{**3**} (sub-Pro)
1.1A – ~AlaAla-ricinoloyl	**2.4B** – ~TrpIle-stearoyl	**3.1B** – ~ProAla-stearoyl
1.2A – ~AlaPhe-ricinoloyl	**2.6A** – ~TrpMet-stearoyl	**3.3A** – ~ProLeu-ricinoloyl
1.3B – ~AlaLeu-stearoyl	**2.7A** – ~TrpCys-ricinoloyl	**3.4A** – ~ProIle-ricinoloyl
1.4B – ~AlaIle-stearoyl	**2.9A** – ~TrpTyr-ricinoloyl	**3.5B** – ~ProVal-stearoyl
1.5A – ~AlaVal-ricinoloyl	**2.11B** – ~TrpGlu-stearoyl	**3.8A** – ~ProSer-ricinoloyl
1.7A – ~AlaCys-ricinoloyl	**2.18A** – ~TrpTrp-ricinoloyl	**3.12B** – ~ProAsp-stearoyl
1.9B – ~AlaTyr-stearoyl	**2.18B** – ~~TrpTrp-stearoyl	**3.16B** –~ProLys-stearoyl
1.10A – ~AlaThr-ricinoloyl		**3.17B** – ~ProPro-stearoyl
1.14A – ~AlaAsn-ricinoloyl		**3.18A** – ~ProTrp-ricinoloyl
1.17A – ~AlaPro-ricinoloyl		**3.19A** – ~ProArg-ricinoloyl
1.18A – ~AlaTrp-ricinoloyl		

conditions of method A, set of discs after binding urine metabolites into the pockets was directly used to reporter dye binding. Under the conditions of method B, set of disks after binding urine metabolites was dried to constant weight and then stored in refrigerator for 3 days. In method C, set of discs after treatment with urine, without drying to a constant weight, was stored in the refrigerator for 3 days.

A comparison of graphs showed that the assay method and particularly conditions of storage of discs sets affects the binding profile. The highest spreads in the obtained results were observed in the case of method C, which indicates that the storage of wet set disks is undesirable. It turned out also that even in the case of storage of dry disks sets in the refrigerator (method B), it was observed scattering of results. These observations were taken into account during further experiments using murine urine. Thus, in all further tests method A was applied.

In experiments evaluating the utility of artificial receptors libraries for noninvasive medical diagnostics, urine derived from healthy mice and

mice with different types of cancer was used. In this studies, three different types of cancers were tested. The urine was collected from mice, when tumor volume reached ~ 700 mm^3. For each 120-elements molecular receptors library were obtained different binding profile (fingerprint) of mouse urine metabolites.

In the first test, a binding profile of urine from C57B1/6 healthy mice was compared with profile obtained using urine from C57B1/6 mouse suffering from colon cancer C38 (see Fig. 3).

In the next set of experiments, a binding profile obtained by treatment the library with urine of C3H healthy mouse was compared respectively with binding profile obtained with urine from C3H mouse bearing mouse mammary gland cancer 16/C (see Fig. 4).

The last studies involved binding metabolites from BDF1 (C57B1/6xDBA2) healthy mouse urine and urine from BDF1 mouse bearing lung cancer LLC (see Fig. 5).

Based on the graphs (Figs. 3–5), several characteristic changes in binding profile can be identified.

DISCUSSION AND CONCLUSIONS

A comparison of the binding profiles of healthy mice C57BL/6, C3H and BDF1 urine components (Figs. 3–5) shown that even in the case of standardized laboratory animals the results are varied. This is due to the fact that the composition of urine varies and depends on many factors including the species, diet and many others.

Comparative analysis of the binding profiles of urinary metabolites of healthy mice and mice with cancer enabled the selection of elements of the *N*-lipidated peptides library, where intensity of binding were mostly diversified, reflecting differentiation dependent upon the health.

Among the 120-element library of *N*-lipidated peptides immobilized on cellulose, there were found 18 structures differentiating the urine of healthy mice and C57BL/6 mice implanted with colon cancer C38 (see Table 1).

Analysis of three sub-libraries {**1.1**–**20.A-B**}, {**2.1**–**20.A-B**} and {**3.1**–**20.A-B**} (splitting up due to the structure of the amino acid connected with *m*-phenylenediamine residue) shown the strongest difference in coloration of field (**4** Ile residue attached to the first amino acid) is common to all sub-libraries. It should be emphasized that in this case the structure of the attached lipid does not affect the ability to discriminate between binding the urine of healthy mice and C57BL/6 mice bearing colon cancer C38. From the analysis emerges another dependency, namely, the impact of the "size" of the first amino acid residue.

In the case of sub-libraries comprising an alanine residue (small amino acid) in the first position and sub-libraries containing a proline residue (relatively small amino acid) were selected two additional common elements, namely, the field {**1.9**} and {**3.9**} (with Tyr residue), and {**1.12**} and {**3.12**} (with Asp residue). In the case of the last two library members, full compliance is observed in the structure of the lipid.

Analysis of the ability of binding of urinary metabolites from healthy C3H mouse and C3H mice bearing mammary gland cancer 16/C showed no presence of shared structures (see Table 2).

However, has been found the common correlation between the sub-libraries. For sub-library {**1**} with an alanine residue in the first position and the sub-library {**2**} containing a tryptophan residue it has been revealed the presence of up to three common structures: with Ala residue in the second position and with both lipid residues (**A** and **B**) and with His residue in the second position with the lipid **B**. In the case of sub-libraries {**2**} with tryptophan residue and sub-library {**3**} (proline in the first position) it has been found four common structures: {**2.3**} and {**3.3**} (with Leu residue), {**2.9**} and {**3.9**} (with Tyr residue), {**2.19**} and {**3.19**} (with Arg residue) and {**2.20**} and {**3.20**} (with Gly residue) (see Table 2). In the last case it has not been observed an influence of the lipid structure on binding selectivity.

Analysis of binding profile of urine BDF1 mice and BDF1 mice with implanted LLC lung carcinoma discovered the presence of two common elements for all three sub-libraries, e.g., with Ile residue and with Trp residue in the second position (see Table 3).

Furthermore, it has been found an additional correlation between the elements of two sub-libraries: {**1**} (sub-Ala) and {**2**} (sub-Trp). It has been selected an additional three common elements: with Cys, Tyr and Trp residue at the second position.

The analysis selected two structures: Lipid-Pro-Ala-NH-C_6H_4-NH-DMT-cellulose and Lipid-Arg-Pro-NH-C_6H_4-NH-DMT-cellulose diagnostic for all three tested types of cancers. In this case, the influence of the lipid on selectivity of receptors was found to be negligible compared to the peptide structure.

Acknowledgment

This work was supported by Ministry of Science and Education Poland N N 405 669540.

REFERENCES

1. (a) Nicholson J.K., Lindon J.C., Holmes E.: Xenobiotica 29, 1181 (1999); (b) Lamers R.J.A.N., DeGroot J., Spies-Faber E.J., Jellema R.H., Kraus V.B., Verzijl N., TeKoppele J. M. et al.: J. Nutr. 133, 1776 (2003).
2. (a) Kaddurah-Daouk R., Kristal B.S., Weinshilboum R.M.: Annu. Rev. Pharmacol. Toxicol. 48, 653 (2008); (b) Goonewardena S.N., Prevette L.E., Desai, A.A.: Curr. Atheroscler. Rep. 12, 267 (2010).
3. Watkins S.M.: Isr. Med. Assoc. J. 2, 722 (2000).
4. Waterman C.L., Kian-Kai C., Grifin J.L.: Biochim. Biophys. Acta 1801, 230 (2010).
5. Barderas M.G., Laborde C.M., Posada M., de la Cuesta F., Zubiri I., Vivanco F., Alvarez-Llamas G.: J. Biomed. Biotechnol. 2011, 790132 (2011).
6. Dunn W.B., Bailey N.J.C., Johnson H.E.: Analyst 130, 606 (2005).
7. Nicholson J.K., Wilson I.D.: Nat. Rev. Drug Discov. 2, 668 (2003).
8. (a) Harrigan G.G., LaPlante R.H., Cosma G.N., Cockerell G., Goodacre R., Maddox J.F., Luyendyk J.P. et al.: Toxicol. Lett. 146, 197 (2004); (b) Johnson H.E., Broadhurst D., Kell D.B., Theodorou M.K., Merry R.J., Grifith G.W.: Appl. Environ. Microbiol. 70, 1583 (2004).
9. Dettmer K., Aronov P.A., Hammock B.D.: Mass Spectrom. Rev. 26, 51 (2007).
10. Grifin J.L., Kauppinen R.A.: FEBS J. 274, 1132 (2007).
11. Watkins S.M., German J.B.: Curr. Opin. Biotechnol. 13, 512 (2002).
12. (a) Musiek E.S., Yin H., Milne G.L., Morrow J.D.: Lipids 40, 987 (2005); b) Cho H.J., Kim J.D., Lee W.Y., Chung B.C., Choi M.H., Anal. Chim. Acta 632, 101 (2009).
13. Kamiński Z.J., Kolesińska B., Cierpucha M.: PL Patent Appl. 08. 03. 2000 no. P-338931.
14. (a) Kamiński Z.J., Kolesińska B., Kolesińska J., Sabatino G., Chelli M., Rovero P., Błaszczyk M. et al.: J. Am. Chem. Soc. 127, 16912 (2005); (b) Kolesińska B., Frączyk J., Papini A.M., Kamiński Z.J.: Chem. Today 25, 26 (2007).
15. Frączyk J, Kamiński Z.J.: J. Comb. Chem. 10, 934 (2008).
16. Fraczyk J., Kolesińska B., Czarnecka A., Malawska B., Więckowska A., Bajda M., Kamiński Z.J.: QSAR Comb. Sci. 28, 728 (2009).
17. Majchrzak J., Frączyk J., Kamiński Z.J.: Acta Pol. Pharm. Drug Res. 65, 703 (2008).

Acta Poloniae Pharmaceutica – Drug Research, Vol. 71 No. 6 pp. 954–958, 2014 ISSN 0001-6837
Polish Pharmaceutical Society

EFFECT OF GLY-HIS-LYS AND ITS COPPER COMPLEX ON TGF-β1 SECRETION IN NORMAL HUMAN DERMAL FIBROBLASTs

ARKADIUSZ GRUCHLIK*, EWA CHODUREK and ZOFIA DZIERŻEWICZ

School of Pharmacy with the Division of Laboratory Medicine in Sosnowiec,
Medical University of Silesia in Katowice, Chair and Department of Biopharmacy

Abstract : Transforming growth factor β (TGF-β) is a cytokine involved in a wide variety of biological processes such as cell growth, differentiation and proliferation, apoptosis and regulation of the immune response. It has an important role in wound healing process, fibrosis and scar tissue formation. Similarly to TGF-β1, insulin growth factor (IGF) family is expressed locally in response to tissue injury. Treatment of dermal fibroblasts with IGF-1 caused a substantial induction of TGF-β1 mRNA. Not a great deal of research so far has focused on IGF-2. Much attention has been focused on the tripeptides such as Gly-His-Lys (GHK) and their copper complexes, which have a high activity and good skin tolerance. Recent data suggest that their physiological role has been related to the process of wound healing, tissue repair and skin inflammation. In the present study, the influence of 1 nM solutions of GHK, GHK-Cu and $CuCl_2$, on IGF-2-dependent TGF-β1 secretion in normal human dermal fibroblasts cells was investigated. Fibroblasts were cultured in 24-well plates. Total TGF-β1 protein was evaluated using the ELISA kit. The Bradford reagent was used to determine the total quantity of cellular protein. Treatment of fibroblasts with 100 ng/mL IGF-2 resulted in a significant increase in TGF-β1 secretion. GHK and its copper complex and free copper ions decreased IGF-2-dependent TGF-β1 secretion. Our observations provide some new information on the potential use of that peptide contained in cosmetics to treat and prevent the formation of hypertrophic scars.

Keywords: normal human dermal fibroblasts, Gly-His-Lys, GHK-Cu, TGF-β1, IGF-2, fibrosis

Cosmeceuticals represent a marriage between cosmetics and pharmaceuticals (1). There is an increasing trend towards the use of these agents in skin care regimens. Cosmeceutically active products can be broadly classified into the following categories: antioxidants, oligopeptides, growth factors and pigment lightning agents (2). Much attention has been focused on the tripeptides such as Gly-His-Lys (GHK) and its copper complex, which have a high activity and good skin tolerance. Recent data suggested that their physiological role have been related to the process of wound healing, tissue repair and skin inflammation (3). GHK was isolated from human plasma, where it is present at concentration of about 200 ng/mL (4). It reveals high affinity to copper(II) ions exhibited in spontaneous formation of complex GHK-Cu. GHK may protect copper(II) ions against redox reaction, modulate copper intake into cell and increase the level of antioxidant enzymes and superoxide dismutase activity (5). It modulated an expression of both matrix metalloproteinases (MMP-1 and MMP-2) and their inhibitors (TIMP-1 and TIMP-2), improving wound healing and facilitating skin remodeling processes (6). GHK-Cu increased mRNA for collagen, dermatan sulfate, chondroitin sulfate, and a small proteoglycan decorin (7). Canapp et al. (8) showed that GHK-Cu improved healing of ischemic wounds and suppresses inflammation by lowering the level of acute-phase inflammatory cytokines such as transforming growth factor β (TGF-β) and tumor necrosis factor α (TNF-α).

TGF-β is a family of growth factors engaged in a number of essential cellular functions. The three isoforms of TGF-β (β1, β2 and β3) are secreted as inactive latent precursors that require activation prior to binding to the TGF-β receptors. TGF-β is a multifunctional cytokine involved in a wide variety of biological processes such as embryonic development, neoplastic growth and differentiation, cell proliferation, apoptosis and regulation of the immune response (9). It is an important regulator of the wound healing process. In particular, its interaction with dermal fibroblasts and the subsequent production of extracel-

* Corresponding author: Gruchlik Arkadiusz, Doctor in Pharmacy, Assistant. School of Pharmacy with the Division of Laboratory Medicine in Sosnowiec, Medical University of Silesia in Katowice, Chair and Department of Biopharmacy, Jedności 8, 41-200 Sosnowiec. Poland, e-mail: agruchlik@sum.edu.pl, mobile +48 32 3641061

lular products including collagen highlights its central role in abnormal scarring. Wang et al. (10) showed that hypertrophic scar derived fibroblasts produced more mRNA and protein for TGF-β1 than fibroblasts derived from normal skin, suggesting a possible role for TGF-β1 in hypertrophic scar formation. Similarly to TGF-β1, insulin growth factor (IGF) family is expressed locally in response to tissue injury. Expression of IGF-1 increased in parallel to the formation of granulation tissue after injury (11). Ghahary et al. (12) found greater expression of TGF-β1 and IGF-1 in post-burn hypertrophic scar tissues as compared to normal dermis from the same patients. Treatment of human dermal fibroblasts with IGF-1 caused a substantial induction of TGF-β1 mRNA. Although IGF-1 and IGF-2 exert their main effects through the IGF-1 receptor, their biological effects are different (13). According to Musselmann et al. (14), IGF-2 may serve as a mechanism to immediately activate keratocytes upon wounding and to ameliorate the scarring effects of TGF-β.

The present study investigated effect of IGF-2 on TGF-β1 secretion in normal human dermal fibroblasts and the influence of GHK and GHK-Cu on this process.

EXPERIMENTAL

Cell cultures

Normal human dermal fibroblasts (NHDF) were obtained from Clonetics™. The cells were cultured in minimum essential medium (MEM, Sigma-Aldrich) supplemented with 10% fetal bovine serum (FBS, Life Technologies), 100 IU/mL penicillin G (sodium salt), 100 μg/mL streptomycin (antibiotic solution, Sigma-Aldrich) and 10 mM HEPES (Gibco). The cell cultures were maintained at 37°C in 5% CO_2 atmosphere. In this study, we used cultures at passages 5 and 10. Fresh growth medium was added every 3 to 4 days and cells were kept subconfluent until used for experiments. Because of the significant content of TGF-β1 in FBS, it is recommended to culture cells in a medium without added serum or with its serum content decreased. Ninety percent confluent monolayer was rendered quiescent in media containing 0.2% fetal bovine serum FBS (Life Technologies) or ITS Premix (BD Biosciences) in dilution 1 : 100 for 24 h before use in experiments. ITS Premix contained insulin, human transferrin and selenous acid.

Modulators supply and their preparation

The solutions of GHK (liver cell growth factor, Sigma-Aldrich) and copper(II) chloride dihydrate ($CuCl_2 \times 2H_2O$, Sigma-Aldrich) were prepared by dissolving them in sterile-filtered water and were then diluted in a culture medium to the concentration of 1 nM. Complex of GHK with cooper (GHK-Cu) was prepared by mixing equimolar solutions of GHK and $CuCl_2$. The TNF-α and IGF-2 (lyophilizates) were diluted in water to 100 μg/mL.

TGF-β1 assay

The total TGF-β1 quantity in cultured medium was evaluated using the Legend Max enzyme-linked immunosorbent assay kit with pre-coated plates (BioLegend). Fibroblasts were cultured in 24-well plates (Sarsted). After 24 h, the medium is clarified by centrifugation and samples are stored at –70°C. To activate latent TGF-β1 to the immunoreactive form, the samples were acidified with 1 M HCl**.** The absorbance was measured at λ = 450 nm in a microplate reader (Triad LT Multimode Detector, Dynex Technologies). TGF-β1 concentration was determined from a standard curve and the resulting values were converted to the total amount of cellular protein.

Total protein assay

The Bradford reagent was used to determine the total quantity of protein in cell lysates. After removal of the culture medium, 24-well plates were placed in –70°C for 24 h, and then 100 μL 0.125% dodecyl sulfate sodium solution was added to each well. The cell lysates were centrifuged at 13000 rpm for 3 min. The absorbance was measured at λ = 595 nm by photometer Epoll-20. Bovine serum albumin was using as the standard protein.

Statistics

Statistical comparisons were made by the analysis of variance (ANOVA, *post hoc* Tukey's test) or by Student's *t*-test. A value of $p < 0.05$ was considered statistically significant. The results are expressed as the means ± standard deviation from number of experiments. Statistical analysis was performed using data analysis software system STATISTICA (StatSoft, Inc. 2011)

RESULTS AND DISCUSSION

Wound healing is a multi-stage process leading to the reconstruction of damaged tissue. It may be divided into inflammation, proliferation and maturation or remodeling. TGF-β1 is a well known cytokine to initiate the sequent wound healing phases of inflammation, angiogenesis, reepithelialization, and connective tissue regeneration. It is close-

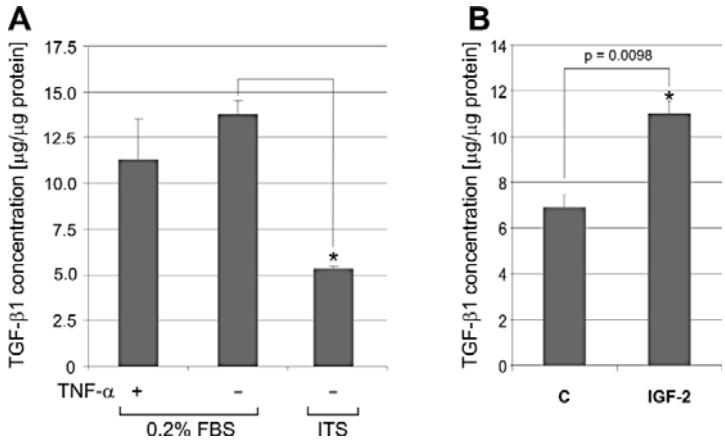

Figure 1. Influence of 100 ng/mL TNF-α, 100 ng/mL IGF-2 and type of medium on TGF-β1 secretion by NHDF cell line. (**A**) The cells were cultured for 24 h in medium containing 0.2% FBS and its Premix dilution 1 : 100. The results represent the mean ± SD (n = 3); * $p < 0.05$ (*t*-Student's test). (**B**) The cells were cultured for 24 h in serum-free medium containing ITS Premix in dilution 1 : 100. The results represent the mean ± SD (n = 4); * $p < 0.05$ (*t*-Student's test) compared with the control (**C**)

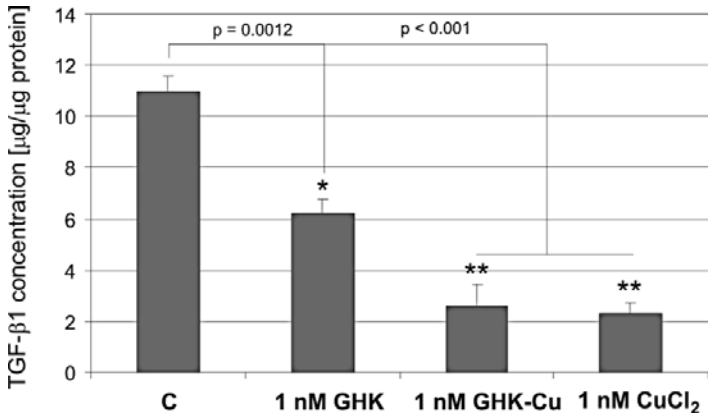

Figure 2. Influence of 1 nM GHK, GHK-Cu and $CuCl_2$ on IGF-2-dependent TGF-β1 secretion by NHDF cell line. The cells were cultured for 24 h in serum-free medium containing ITS Premix in dilution 1 : 100. The results represent the mean ± SD (n = 4); * $p < 0.05$ (ANOVA, *post hoc* Tukey's test) compared with the control (**C**)

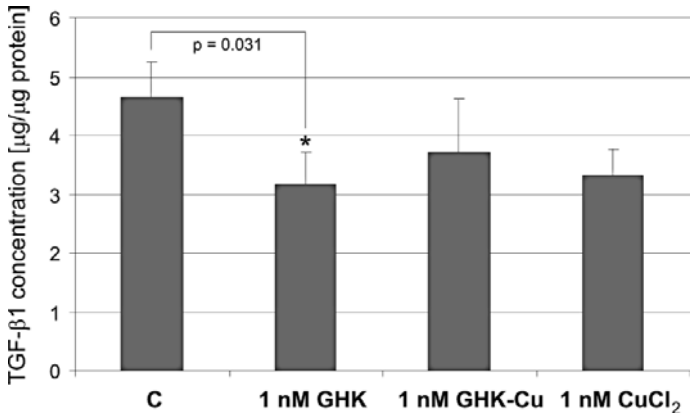

Figure 3. Influence of 1 nM GHK, GHK-Cu and $CuCl_2$ on TGF-β1 secretion by NHDF cell line. The cells were cultured for 24 h in medium containing 0.2% FBS. The results represent the mean ± SD (n = 4); * $p < 0.05$ (ANOVA, *post hoc* Tukey's test) compared with the control (**C**)

ly involved in the remodeling phase with function of stimulating the collagen synthesis and disposition by the sustained activation of fibroblasts. TGF-β1 can up-regulate the angiogenic growth factor like vascular endothelial growth factor (VEGF) and is also a potent inhibitor of MMP-1, MMP-3, and MMP-9 and a promoter of tissue inhibitor of MMP-1 synthesis (15). The action of TGF-β1 depended on its concentration and amount of active latent form. The proliferation of mink lung fibroblasts is stimulated by low concentrations of TGF-β1 (5–10 ng) and inhibited by higher concentrations (16). The chronic overexpression of TGF-β1 or one of its fellow family members β2 and β3 drives the formation of keloids and hypertrophic scars (17).

TGF-β1 production may be controlled at the levels of transcription, translation, secretion of preformed protein and activation of the latent protein to its active form (18). IGF-1 may directly increase secretion of TGF-β1 into extracellular matrix (12). IGF-1 and IGF-2 mainly exert their effects through the IGF-I receptor but their biological action are different (13). In contrast to IGF-1, poorly understood is the role of IGF-2 in this process. Two potential secretion inductors of TGF-β1, TNF-α and IGF-2 were used in this study. Similarly to IGFs family, TNF-α rapidly (at 4–6 h) upregulated expression of TGF-β1 mRNA resulting in increased production of TGF-β1 protein (18), while there are several studies that reported no increase in (or reduced) TGF-β1 expression consequent to TNF-α treatment (19, 20). We recorded almost twofold increase in TGF-β1 secretion in response to 100 ng/mL IGF-2 in contrast to 100 ng/mL TNF-α. NHDF cells released small amounts of TGF-β1 regardless of the inductor used (Fig. 1). All marked TGF-β1 most likely was coming from a latent complex. Its active form remained undetected in the studied samples or its concentration was below detection threshold. No significant effect of TNF-α on TGF-β secretion may be associated with the use of high concentrations of TNF-α (100 ng/mL). These conflicting data may be explained by differences in the experimental protocol or in the cell types used, regulation of TGF-β1 may be cell type-specific.

Much attention has been focused on the tripeptides such as GHK and its copper complex, which have a high activity and good skin tolerance. Recent data suggested their physiological role in process of wound healing, tissue repair and skin inflammation. Matalka et al. (21) demonstrated that GHK or its pegylated form at a very low, nontoxic concentration (1–10 nM) stimulated fibroblast proliferation. Cangula et al. (22) reported that open wounds in rabbits treated with GHK-Cu tend to heal faster than similar wounds treated with zinc oxide or kept untreated. They observed more granulation tissue formation in the GHK-Cu-treated wounds. According to Borkow et al. (23), this effect may be associated with the supply of copper to the wound tissue. This mechanism is poorly understood. In the present study, we investigated an effect not only GHK-Cu but also GHK and free copper (II) ions on IGF-2-dependent TGF-β1 secretion in NHDF cells. We observed that 1 nM GHK inhibited IGF-2-dependent (Fig. 2) and IGF-2-independent TGF-β1 secretion (Fig. 3), although in the second case we can say about a trend ($p = 0.31$). The addition of copper in the ions form ($CuCl_2$) and in the GHK complex form inhibited IGF-2-dependent TGF-β1 secretion more strongly than the use of the same peptide. The copper (II) ions effect was similar to the GHK-Cu action (Fig. 2). One nanomole of GHK-Cu and $CuCl_2$ have no effect on IGF-2-independent TGF-β1 secretion when the fibroblasts were treated with medium containing only 0.2% FBS (Fig. 3). McCormack et al. (24) obtained similar results. GHK-Cu reduced the secretion of TGF-β1 by normal fibroblasts and keloid producing fibroblasts. Although both cell types show sensitivity to GHK-Cu treatment, only keloid fibroblasts demonstrated statistically significant reductions (24). The simplest form of copper, an inorganic salt, cannot be a possible source of delivery of the metal ions to the low layers of skin because of its low bioavailability and its general toxicity to the organism. One of the widely used methods of delivering metal ions into the skin is their complexation with different ligands, among which peptides play a main role (25). Altering the availability of these peptides and its copper complexes at their target sites within the skin may offer new therapeutic approaches in skin disease and dermatology, wound healing and for cosmetic applications. Copper tripeptide therapy seems to suppress secretion of "fibrogenic" growth factor (TGF-β1) in fibroblasts and it may have application in decreasing excess scar formation.

Acknowledgment

This work was supported by the Medical University of Silesia (KNW-1-021/N/2/0).

REFERENCES

1. Malerich S., Berson D.: Dermatol. Clin. 32, 13 (2014).
2. Draelos Z.D.: Clin. Plast. Surg. 38, 397 (2011).

3. Pickart L., Margolina A.: JARCP 1, 13 (2012).
4. Pickart L., Thaler M.M.: Nat. New Biol. 243, 85 (1973).
5. Pickart L., Vasquez-Soltero J.M., Margolina A.: Oxid. Med. Cell Longev. 2012, 324832 (2012).
6. Siméon A., Emonard H., Hornebeck W., Maquart F.X.: Life Sci. 67, 2257 (2000).
7. Siméon A., Wegrowski Y., Bontemps Y., Maquart F.X.: J. Invest. Dermatol. 115, 962 (2000).
8. Canapp S.O. Jr., Farese J.P., Schultz G.S., Gowda S., Ishak A.M., Swaim S.F., Vangilder J. et al.: Vet. Surg. 32, 515 (2003).
9. Penn J.W., Grobbelaar A.O., Rolfe K.J.: Int. J. Burns Trauma 2, 18 (2012).
10. Wang R., Ghahary A., Shen Q., Scott P.G., Roy K., Tredget E.E.: Wound Repair Regen. 8, 128 (2000).
11. Pakyari M., Farrokhi A., Maharlooei M.K., Ghahary A.: Adv. Wound Care (New Rochelle) 2, 215 (2013).
12. Ghahary A., Shen Q., Shen Y.J., Scott P.G., Tredget E.E.: J. Cell Physiol. 174, 301 (1998).
13. Versteyhe S., Klaproth B., Borup R., Palsgaard J., Jensen M., Gray S.G., De Meyts P.: Front. Endocrinol. (Lausanne) 4, 98 (2013).
14. Musselmann K., Kane B.P., Alexandrou B., Hassell J.R.: Exp. Eye Res. 86, 506 (2008).
15. Werner S., Grose R.: Physiol. Rev. 83, 835 (2003).
16. Ghahary A., Tredget E.E., Ghahary A., Bahar M.A., Telasky C.: Wound Rep. Reg. 10, 328 (2002).
17. Campaner A.B., Ferreira L.M., Gragnani A., Bruder J.M., Cusick J.L., Morgan J.R.: J. Invest. Dermatol. 126, 1168 (2006).
18. Sullivan D.E., Ferris M., Pociask D., Brody A.R.: Am. J. Respir. Cell Mol. Biol. 32, 342 (2005).
19. Kwong K.Y., Literat A., Zhu N.L., Huang H.H., Li C., Jones C.A., Minoo P.: Life Sci. 74, 2941 (2004).
20. Hodge S., Hodge G., Holmes M., Flower R., Scicchitano R.: Respirology 6, 205 (2001).
21. Matalka L.E., Ford A., Unlap M.T.: J. Biotechnol. Biomater. 2, 144 (2012).
22. Cangul I.T., Gul N.Y., Topal A., Yilmaz R.: Vet. Dermatol. 17, 417 (2006).
23. Borkow G., Gabbay J., Zatcoff C.R.: Med. Hypotheses 70, 610 (2008).
24. McCormack M.C., Nowak K.C., Koch R.J.: Arch. Facial Plast. Surg. 3, 28 (2001).
25. Hostynek J.J., Dreher F., Maibach H.I.: Inflamm. Res. 60, 79 (2011).

Acta Poloniae Pharmaceutica – Drug Research, Vol. 71 No. 6 pp. 959–965, 2014 ISSN 0001-6837
Polish Pharmaceutical Society

SYNTHESIS OF PROTOESCIGENIN GLYCOCONJUGATES WITH O-28 TRIAZOLE LINKER

MARIUSZ GRUZA[1], KAMIL JATCZAK[1], KATARZYNA KOMOR[2], PIOTR ŚWIERK[2], WIESŁAW SZEJA[2] and GRZEGORZ GRYNKIEWICZ[1]*

[1] Pharmaceutical Research Institute, Rydygiera 8, 01-793 Warszawa, Poland
[2] Silesian University of Technology, Faculty of Chemistry, Chair of Organic Chemistry, Bioorganic Chemistry and Biotechnology, Krzywoustego 4, 44-100 Gliwice, Poland;

Abstract: New triazole linked conjugates were obtained from protoescigenin monopropargyl ethers and sugar azides, under Cu(II) salt promotion in good yield, without losing isopropylidene protection.

Keywords: protoescigenin propargyl ether, sugar azides, click reaction, copper acetate

Over 50 years ago, protoescigenin (PES, **1**; Scheme 1) was identified as the main aglycone of horse chestnut saponins (escins) and its structure has been firmly established (1–3). Unlike many other pentacyclic triterpene genins (particularly oleanolic, ursolic and lupeolic acids), which evoke continuous interest as prospective lead compounds for medicinal chemistry, this compound was completely absent from the life sciences research area until recent time. Although clinical position of escin is well established as venotonic and chronic venous insufficiency therapeutic (4), a challenge has been undertaken to examine single chemical entities – either constituents of the escin saponin complex or their new semi-synthetic derivatives, particularly in respect to their anti-inflammatory and endothelial activity (5). Consequently, **1** has emerged as the key chemical entity of the project, its isolation and purification had to be elaborated into technically viable and validated process (6) and its reactivity in terms of selective protection had to be re-examined (7). It turned out that selective ketalization is the most feasible, scalable process for effective partial protection of **1**, affording facile access to derivatives functionalized exclusively at C28-OH, such as the propargyl ether **2**.

This finding offers a chance to overcome persistent problems with semi-synthesis of triterpene saponin mimetics based on saccharide connection at C3-OH. Glycosylating reactions starting from **1** or its partially protected congeners, including Koenigs-Knorr and Schmidt protocols, were not successful and similarly, acid catalyzed procedures (e.g., involving thioglycosides or glycals) failed, indicating substrate inertness or instability.

Therefore, it has been decided to continue exploration of derivative **2** reactivity, in the format of click chemistry using custom synthesized novel sugar azide synthons. This decision was supported by recent findings that 1,2,3-triazoles, earlier considered pharmacologically and metabolically inert, may actually contribute some inherent biological activity (8). Since its introduction by Sharpless and coworkers at the turn of the century, *Click-Chemistry* have been applied in thousands of laboratories, in all fields of life sciences (9, 10). Azide – alkyne cycloadditions have been performed under variety of protocols, involving Cu(I) salt catalysis, Cu(II) salts in the presence or absence of a reducing agent, or metallic copper. Non-catalyzed versions have been recommended for application in biological chemistry (11, 12). Application of *Click-Chemistry* to carbohydrate chemistry and glycoscience has been so extensive that it has recently resulted in publishing an extensive monograph, which summarized over a decade of research (13).

Our first experiments on condensation of 28-*O*-propargyl PES ether **2** with monosaccharide derived azides were carried out according to well established procedure assuming CuAAC protocol –

* Corresponding author: e-mail: g.grynkiewicz@ifarm.eu

Cu(I) species were generating from Cu(II) by reduction with sodium ascorbate (7, 14, 15). Meanwhile, reports have appeared that use of Cu(II) salts (or in fact skipping additives acting as reducing agents) in an alkyne – azide click reaction protocols give just as satisfactory results as using ascorbate catalyzed version (16–20). We have confirmed these reports by obtaining new triazoles in reaction of sugar derived azides with **2** in the presence of copper(II) acetate without reducing agent, as depicted in Scheme 2. Azido-sugar substrates for these reactions fall in two distinct structural categories: 1) 1,6-anhydro-2-azido-2-deoxy-β-D-glucopyranoside **3** and 2) 3-azidopropyl 3,4,6-tri-*O*-acetyl-2-deoxy-α-D-galactopyranoside **5** and 3-azidopropyl-4-*O*-benzyl-3-*O*-[4'-*O*-benzyl-2',3',6'-trideoxy-α-D-*erythro*-hex-2'-enepyranosyl]-2,6-dideoxy-D-glucopyranoside **8**, which may be reflected by different chemical (primary and secondary azides) and metabolic stability (susceptibility to *in vivo* carbon – heteroatom cleavage). Compound **3** was obtained from well known levoglucosane epoxide, as described in the literature (21). The remaining azido-sugars **5** and **8** bearing terminal azido group were obtained from corresponding glycals **4** and **7** by addition of 3-azidopropanol to unsaturated bond under TPHB catalysis as described in Schemes 3 and 4.

EXPERIMENTAL

General

Chemical materials like solvents, sorbents, inorganic salts and organic reagents were of commercial origin, certified for laboratory use, and applied without purification. Protoescigenin derivative **2** was prepared as described (7). 1,6-Anhydro-2-azido-2-deoxy-β-D-glucopyranoside **3,** 3,4,6-tri-*O*-acetyl-D-galactal **4** and 4-*O*-benzyl-L-rhamnal **6** and **7** were prepared according to the published procedures (21–25).

Reactions were monitored by TLC on precoated plates of silica gel 60 F_{254} (Merck). Visualization was performed by UV light (λ = 254 and/or 365 nm), and by spraying with 10% sulfuric acid in ethanol or cerium molybdate stain (26, 27). Crude products were purified using column chromatography performed on silica gel 60 (70–230 mesh, Fluka).

Organic solvents were evaporated on a rotary evaporator under diminished pressure at 40°C.

The ^{1}H and ^{13}C-NMR NMR spectra were recorded in $CDCl_3$ and DMSO-d_6 solutions using TMS as an internal standard with an Agilent spectrometer 400 MHz, Varian spectrometer 300 MHz and 600 MHz, and Varian-NMR-vnmrs-500. NMR solvent was purchased from ACROS Organics (Geel, Belgium). The ^{1}H and ^{13}C-NMR chemical shifts are given relative to the TMS signal at 0.0 ppm (^{1}H) and DMSO-d_6 signal at 39.5 ppm (^{13}C). Chemical shifts (δ) are expressed in ppm and coupling constants (*J*) in Hz. Used abbreviations: s – singlet, d – doublet, t – triplet, q – quartet, q_{AB} – AB quartet, m – multiplet, ov – signals overlapped. Recorded signals were compared to 2D (HMBC, HSQC) solved spectra of protoescigenin and its derivatives (6, 7).

Optical rotations were measured on a JASCO 2000 polarimeter or a PERKIN ELMER 341 Polarimeter using a sodium lamp (589.3 nm).

Mass spectra were recorded with a WATERS LCT Premier XE system and 4000 QTrap (Applied Biosystems/MDS Sciex) using electrospray ionization (ESI) technique or on a MaldiSYNAPT G2-S HDMS (Waters) Spectrometer *via* electrospray ionization (ESI-MS).

Melting points were determined by differential scanning calorimetry (DSC) carried out by means of the DSC822 with IntraCooler (Mettler Toledo).

Synthesis of sugar azides 5 and 8

3-Azidopropyl 3,4,6-tri-*O*-acetyl-2-deoxy-α-D-galactopyranoside, 5

To a solution of 3,4,6-tri-*O*-acetyl-D-galactal **4** (1 mmol, 272.2 mg) in dry CH_2Cl_2 (5 mL) 3-azidopropanol (0.12 mL, 131.4 mg, 1.3 mmol) and molecular sieves 5Ĺ were added. Reaction mixture was cooled in water bath (0°C), then TPHB (triphenylphosphine hydrobromide, 36.3 mg, 0.1 mmol) was added. Reaction was monitored by TLC (hexane : ethyl acetate, 3 : 1, v/v). After 5 h, triethylamine (0.1 mL) was added, reaction mixture was filtered and then solvent was evaporated under reduced pressure. Crude product was purified by column chromatography on silica gel with hexane – acetone (20 : 1, v/v) elution system. Product **5** was obtained as a colorless syrup with 52% yield. $[a]_D^{20} = +113.8$ (c 1.0, $CHCl_3$). ^{1}H NMR (400 MHz, $CDCl_3$, δ, ppm): 5.33 (d, *J* = 3.0 Hz, 1H, H-4), 5.27 (ddd, *J* = 12.4, 5.0, 3.1 Hz, 1H, H-3), 5.01 (d, *J* = 3.0 Hz, 1H, H-1), 4.18–4.05 (m, 3H, H-5, H-$6_{a,b}$), 3.76 (dt, *J* = 9.9, 6.0 Hz, 1H, -$OCH_{2(a)}$-), 3.48 (dt, *J* = 9.9, 6.1 Hz, 1H, -$OCH_{2(b)}$-), 3.41 (dt, *J* = 6.5, 3.2 Hz, 2H, -CH_2N_3), 2.09 (m, 1H H-2_e), 2.14, 2.06, 1.99 (3s, 9H, 3 × -OAc), 1.91–1.81 (m, 3H, -CH_2-, H-2_e). ^{13}C NMR (100 MHz, $CDCl_3$, δ, ppm): 170.5, 170.3, 170.0 (3 × C=O), 97.6 (C1), 66.8 (C3, C4, C5), 66.6, 66.1, 64.3 (-OCH_2-), 62.5 (C6), 48.3 (-CH_2N_3), 30.1 (C2, CH_2), 28.8, 20.8 (-CH_3), 20.7. LRMS (ESI): calcd. for

$C_{15}H_{23}N_3O_8Na$ ([M + Na]$^+$): m/z 396.3482; found: m/z 396.3.

3-Azidopropyl-4-*O*-benzyl-3-*O*-[4'-*O*-benzyl-2',3',6'-trideoxy-α-D-*erythro*-hex-2'-enopyranosyl]-2,6-dideoxy-D-glucopyranoside, 8

To a solution of disaccharide **7** (450 mg, 1.06 mmol) in dry CH_2Cl_2 (5 mL) 3-azidopropanol (0.09 mL, 1.28 mmol) and molecular sieves 5Ĺ were added. Reaction mixture was cooled in water bath (0^{o}C), then TPHB (triphenylphosphine hydrobromide, 36 mg, 0.1 mmol) was added. Reaction was monitored by TLC (hexane : ethyl acetate, 3 : 1, v/v). After 5 h, trietylamine was added, reaction mixture was filtered and then solvent was evaporated under reduced pressure. Crude product was purified by column chromatography on silica gel with hexane : EtOAc (20 : 1, v/v) elution system. Product **8** (α:β 4:1) was obtained as a colorless syrup with 52% yield. ^{1}H NMR (400 MHz, $CDCl_3$, δ, ppm): 7.42–7.23 (m, 10H, H_{Ar}), 6.04 (d, *J* = 10.2 Hz, 1H, H-3'), 5.67 (ddd, *J* = 10.2, 2.6, 2.0 Hz, 1H, H-2'), 5.19–5.15 (m, 1H, H-1'), 4.82 (1/2 q_{AB}, *J* = 11.1 Hz, 1H, -C$\underline{H}_2$Ph), 4.78 (d, *J* = 2.7 Hz, 1H, H-1$_\alpha$), 4.67 (1/2 q_{AB}, *J* = 11.7 Hz, 2H, -C$\underline{H}_2$Ph), 4.65 (1/2 q_{AB}, *J* = 11.1 Hz, 1H, -C$\underline{H}_2$Ph), 4.54 (1/2q_{AB}, *J* = 11.7 Hz, 2H, -C$\underline{H}_2$Ph), 4.46 (dd, *J* = 9.8, 2.0 Hz, 1H, H-1$_\beta$), 4.07 (ddd, *J* = 11.5, 8.9, 5.3 Hz, 1H, H-3), 3.92 (dq, *J* = 8.8, 6.4 Hz, 1H, H-5'), 3.74 – 3.65 (m, 3H, H-4', H-5, H-1''$_a$); 3.44–3.31 (m, 3H, H-1''$_b$, H-3''$_{ab}$), 3.06 (dd~t, *J* = 9.2 Hz, 1H, H-4), 2.25 (ddd, *J* = 13.1, 5.3, 1.0 Hz, 1H, H-2$_{eq}$), 1.89–1.79 (m, 2H, H-2''$_{ab}$), 1.76 (ddd, *J* = 13.0, 11.5, 3.8 Hz, 1H, H-2$_{ax}$), 1.28 (d, *J* = 6.4 Hz, 3H, 6-CH_3), 1.27 (s, *J* = 6.4 Hz, 3H, 6'-CH_3). ^{13}C NMR (100 MHz, $CDCl_3$, δ, ppm): 138.5, 138.1 (C-1'', C-1''''', C_{Ar}), 130.60 (C-3'), 128.43, 128.41, 127.81, 127.77, 127.69 (10 × C_{Ar}), 126.84 (C-2'), 99.67 (C-1β), 97.27 (C-1α), 96.17 (C-1'α), 84.44 (C-4), 77.48 (C-3), 76.41 (C-4'), 75.31, 71.02 (2 × -C$\underline{H}_2$Ph), 67.31 (C-5), 65.62 (C-5), 63.76 (CH_2O), 48.51 (-CH_2N_3), 37.99 (C-2), 28.97 (CH_2), 18.25 (C-6'), 18.17 (C-6).

General procedure for PES triazoles synthesis

Without sodium ascorbate

To the solution of azidosugar (0.2 mmol) in 0.1 mL CH_2Cl_2 protected protoescigenin 28-*O*-propargyl ether **2** (0.2 mmol) in methanol (4 mL) and aquous solution of $Cu(OAc)_2$ (0.4 M, 0.025 mL) were added. Reaction mixture was stirred overnight in the room temperature. After that, solvents were evaporated under vacuum and product was separated by column chromatography (SiO_2).

PES triazole 9

From sugar **3.** Reaction mixture was stirred 10 days at room temperature. The crude reaction product was purified by column chromatography (SiO_2, CH_2Cl_2 : acetone, 6:1 → 2:1) with 76% yield as white solid. M.p. 223-232^{o}C (dec.), $[a]_D^{20}$ = +38.2^o (*c* 0.50, DMSO). ^{1}H NMR (600 MHz, DMSO, δ, ppm): 8.36 (s, 1H, H3'), 5.7 (d, *J* = 3.75 Hz, 1H, C3''OH, C4''OH), 5.68 (d, *J* = 4.2 Hz, 1H, C3''OH,C4''OH), 5.34 (s, 1H, H12), 5.03 (bs, 1H, H1''), 4.59 (d, *J* = 6.1 Hz, 1H), 4.56 (d, *J* = 16.1 Hz, 2H), 4.43 (d, *J* = 12.5 Hz, 1H), 4.24 (d, *J* = 4.7 Hz, 1H, C21-OH), 4.12 (d, *J* = 6.4 Hz, 1H), 3.93 (d, *J* = 11.6 Hz, 1H, H24), 3.8 (d, *J* = 9.2 Hz, 1H, H22), 3.74–3.69 (m, 1H), 3.69–3.62 (m, 2H), 3.63–3.58 (m, 1H), 3.44 (qd, *J* = 7.0,5.1 Hz, 2H, H16), 3.39–3.33 (m, 2H), 3.32 (s, 2H), 3.26 (d, *J* = 8.5 Hz, 1H), 3.14 (d, *J* = 11.5 Hz, 1H, H24), 2.41 (d, *J* = 11.3 Hz, 1H, H18), 1.98–1.84 (m, 3H), 1.84–1.74 (m, 1H), 1.69–1.58 (m, 2H), 1.57–1.40 (m, 5H), 1.40 (m, ov, 1H), 1.35 (s, 3H, CH_3), 1.33 (s, ov, 3H, CH_3), 1.33 (m, ov, 1H), 1.27 (s, 3H, CH_3), 1.25 (s, 3H, CH_3), 1.18 (dd, *J* = 13.0,3.2 Hz, 1H), 1.12 (s, 3H, CH_3), 1.11 (s, 3H, CH_3), 1.09–1.04 (m, 4H), 1.02 (m, 1H), 0.86 (d, *J* = 11.9 Hz, 1H), 0.75 (s, 3H, CH_3), 0.71 (s, 3H, CH_3). ^{13}C NMR (150 MHz, DMSO, δ, ppm): 143.9 (C2'), 140.3 (C13), 124.0 (C3'), 122.9 (C12), 99.8 (C1''), 98.03, 97.97, 76.3, 76.1, 75.6, 72.5, 71.3, 70.7, 70.5, 68.1 (C16), 64.9, 63.5, 62.9, 62.8, 53.1 (C5), 46.8, 44.4, 41.10, 41.06, 40.8, 36.8, 36.1, 35.8, 35.3, 34.8, 32.1 (C7), 30.32, 30.27, 27.9, 25.7, 25.4, 24.5, 23.6, 22.7, 18.5, 18.0, 17.4, 16.5. LRMS (ESI): calcd. for $C_{45}H_{69}N_3O_{12}Na$ ([M + Na]$^+$): *m*/*z* 835.0332; found: *m*/*z* 835.0.

PES triazole 10

The crude reaction product obtained from glycoside **5** was purified by column chromatography with gradient elution system CH_2Cl_2 : acetone (6 : 1 → 2 : 1) yielding colorless syrup with 74% yield. $[a]_D^{20}$ = +38.2 (*c* 1.00, $CHCl_3$). ^{1}H NMR (300 MHz, $CDCl_3$, δ, ppm): 7.53 (s, 1H, H3'), 5.36–5.20 (m, 3H), 4.99 (d, *J* = 2.7 Hz, 1H, H1''), 4.65 (s, 2H, H1'), 4.58–4.38 (m, 2H), 4.20–4.00 (m, 4H), 3.98–3.80 (m, 2H), 3.76–3.64 (m, 1H), 3.60–3.18 (m, 6H), 2.63 (dd, *J* = 14.3, 3.9 Hz, 1H), 2.37–2.18 (m, 1H), 3.25–2.18 (m, 2H), 2.14 (s, 3H, OAc), 2.12–2.04 (m, 1H), 2.04 (s, 3H, OAc), 2.00 (s, 3H, OAc), 1.99–1.48 (m, 12H), 1.46 (s, 3H, CH_3), 1.44 (s, 3H, CH_3), 1.37 (s, 3H, CH_3), 1.33 (s, 3H, CH_3), 1.22 (s, 3H, CH_3), 1.20^o–1.19 (m, 1H), 1.18 (s, 3H, CH_3), 1.12 (s, 3H, CH_3), 0.96–0.85 (m, 2H), 1.04 (s, 3H, CH_3), 0.85 (s, 3H, CH_3), 0.79 (s, 3H, CH_3). ^{13}C NMR (150 MHz, $CDCl_3$, δ, ppm): 170.48, 170.26,

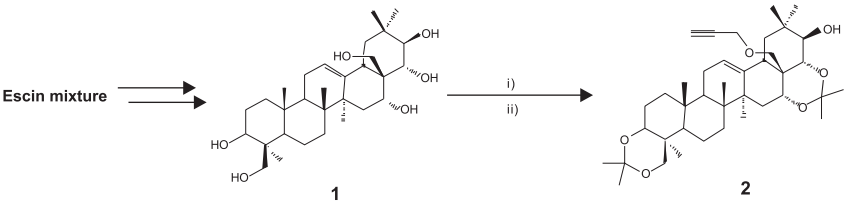

Scheme 1. Protoescigenin **1**, the main product of controlled hydrolysis of escin saponins and its partially protected 28-*O*-propargyl ether **2**. Conditions: i) 2,2-dimethoxypropane, acetone, *cat*. *p*-TSA, *RT*, overnight, ii) $BrCH_2C{\equiv}CH$, TBAB, KOH, THF, room temp., overnight

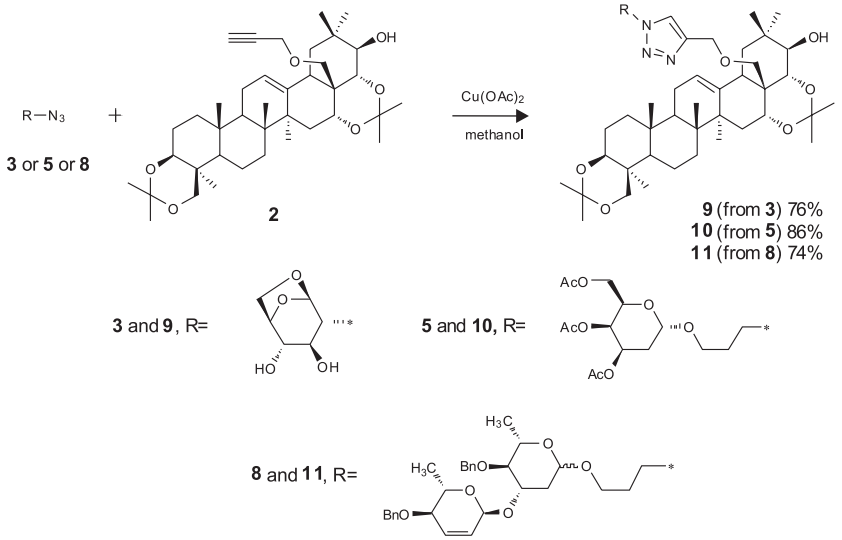

Scheme 2. General procedure of synthesis PES triazoles **9–11**

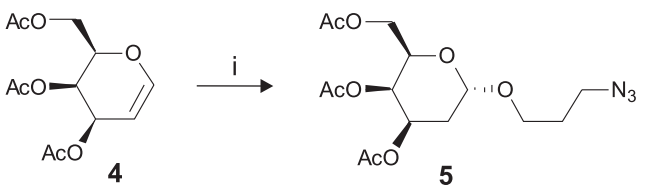

Scheme 3. Synthesis of 3-azidopropyl galactopyranoside **5**; i) 3-azidopropanol, TPHB, CH_2Cl_2, 0°C, 5 h

170.06 (3 × C=O); 140.12, 122.88, 99.2, 98.81, 97.71 (C1''), 77.19, 74.17, 71.27, 69.24 (C28), 66.83 (C16), 66.46 (C4''), 66.43 (C3''), 66.03 (C5''), 63.99, 63.67, 62.24, 53.74 (C5), 47.53, 44.25, 43.9, 41.8, 41.69, 40.15, 37.44, 36.58, 36.3, 36.26, 35.13, 32.41 (C7), 30.13, 30.06, 29.38, 28.83, 27.77, 26.06, 25.55, 25.53, 24.77, 24.53, 23.17, 20.94, 20.7, 20.68 (3 × OAc), 18.88, 17.93, 17.07, 16.69. LRMS (ESI): calcd. for $C_{54}H_{83}N_3O_{14}Na$ ($[M + Na]^+$): *m*/*z* 1021.2383; found: *m*/*z* 1021.0.

PES triazole 11

The crude reaction product obtained from sugar azide **8** was purified by column chromatography with gradient elution system CH_2Cl_2 : acetone (10 : 1›5 : 1) with 74% yield as light yellow syrup. ^{1}H NMR (400 MHz, $CDCl_3$, δ, ppm): 7.5 (s, 1H, H3'), 7.43–7.20 (m, 10H, H_{Ar}), 6.05 (d, J = 10.2 Hz, 1H, H3'''), 5.70–5.65 (m, 1H, H2'''), 5.25–5.20 (m, 1H, H12), 5.19 (bs, 1H, H1'''), 4.82 (1/2 q_{AB}, J = 11.9 Hz, 1H, -CH_2Ph), 4.78 (d, J = 3.1 Hz, 1H,

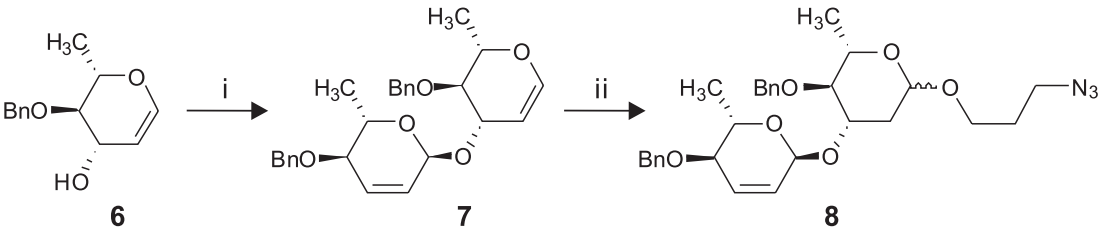

Scheme 4. Synthesis of 3-azidopropyl disaccharide **8**; i) *p*-TsCl, $NaOH_{aq}$, TBAI, toluene, room temp., 24 h; i) 3-azidopropanol, TPHB, CH_2Cl_2, 0°C, 5 h

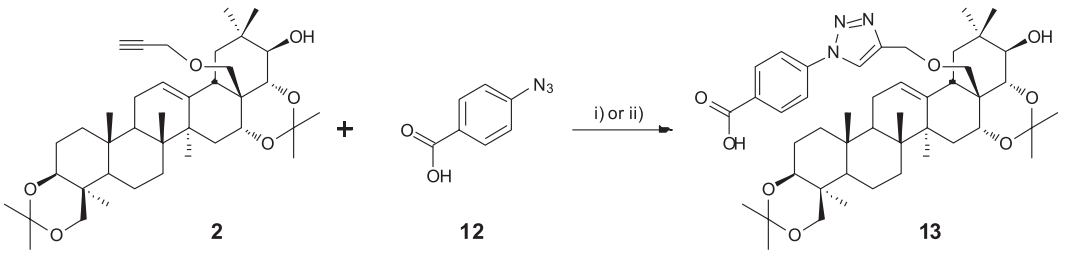

Scheme 5. Synthesis of PES triazoles **13**. Conditions: i) $Cu(OAc)_2$, AscNa, *t*-BuOH, water, room temp.; ii) $Cu(OAc)_2$, MeOH, room temp.

H1''), 4.67 (1/2 q_{AB}, J = 11.6 Hz, 1H, -CH_2Ph), 4.62 (1/2 q_{AB}, J = 11.9 Hz, 1H, -CH_2Ph), 4.67–4.63 (m, 2H, H1'), 4.54 (1/2 q_{AB}, J = 11.6 Hz, 1H, -CH_2Ph), 4.44 (ddd~dt, J = 13.5, 6.8 Hz, 2H, H4'), 4.08 (ddd, J = 11.3, 8.9, 5.0 Hz, 1H, H3''), 4.04 (d, J = 11.8 Hz, 1H), 3.96–3.90 (m, 1H, H5'''), 3.91 (d, J = 10.2 Hz, 1H), 3.86 (d, J = 10.2 Hz, 1H), 3.73–3.62 (m, 3H), 3.53 (d, J = 8.4 Hz, 1H), 3.45 (dd, J = 9.2, 4.5 Hz, 1H), 3.39–3.19 (m, 3H), 3.08 (dd~t, J = 9.2 Hz, 1H, H4''), 2.67–2.59 (m, 1H), 2.27 (dd, J = 12.5, 5.4 Hz, 1H, $H2''_{eq}$), 2.20–2.12 (m, 2H, H5'), 2.19–1.80 (m, 6H), 1.82–1.74 (m, 1H, $H2''_{ax}$), 1.74–1.3 (m, 20H), 1.3 (d, J = 6.2 Hz, 3H, C6'''-CH_3), 1.26 (d, J = 6.2 Hz, 3H, C6''-CH_3), 1.24–0.98 (m, 15H), 0.91–0.77 (m, 7H). ^{13}C NMR (100 MHz, $CDCl_3$), δ, ppm): 145.4 (C2'), 140.1 (C13), 138.4 (-Ph), 138.1 (-Ph), 130.6 (C3'''), 128.43 (-Ph), 128.41 (-Ph), 127.8 (-Ph), 127.7 (-Ph), 126.8 (C2'''), 122.9, 122.4, 99.2, 98.8, 97.3, 96.2 ($C1'''_a$), 84.3 (C4''), 77.5, 77.22, 77.06, 76.4, 75.3, 74.2, 71.1, 71.0, 69.3, 67.4, 65.7, 64.6, 63.8, 63.4, 53.8 (C5), 47.6, 47.4, 44.3, 43.9, 41.8, 41.7, 40.2, 37.9, 37.5, 36.6, 36.3, 35.1, 32.5 (C7), 30.9, 30.3, 29.7, 29.7, 28.9, 27.9, 26.1, 25.6, 24.6, 18.9, 18.3, 18.2, 18.0, 17.1, 16.7. LRMS (ESI): calcd. for $C_{68}H_{97}N_3O_{12}Na$ ($[M + Na]^+$): m/z 1171.5005; found: m/z 1171.4.

Reactions of 2 with 4-azidobenzoic acid 12

With sodium ascorbate

From azide **12**. Reaction mixture was stirred 8 days at room temperature. The crude reaction product was purified by column chromatography (SiO_2, $CH_2Cl_2 \rightarrow CH_2Cl_2$: MeOH 85 : 15) yielding white solid with 91% yield.

With sodium ascorbate

Ether **2** (110 mg, 0.17 mmol) and 4-azidobenzoic acid **12** (64 mg, 0.21 mmol) were dissolved in *t*-BuOH (7.5 mL) and water (4 mL) was added. Then was added solution of $Cu(AcO)_2$ (1.5 mL of soln. 280 mg of $Cu(AcO)_2$ in 10 mL of water) and solution of sodium ascorbate (AscNa, 1.5 mL soln. of 260 mg AscNa in 10 mL of water). Reaction mixture became brown immediately and then turbid. After two days, TLC control ($CHCl_3$: MeOH, 9 : 1, v/v, product R_F = 0.34) indicated complete depletion of the substrate. To the reaction mixture water (70 mL) was added and product was extracted with CH_2Cl_2 (3 × 20 mL). The combined organic phases were washed with 5% aqueous $NaHCO_3$ and dried over anhydrous Na_2SO_4. After filtration and concentration crude **13** was obtained, and purified by col-

umn chromatography with gradient elution system (SiO_2, $CH_2Cl_2 \rightarrow CH_2Cl_2$: MeOH 85 : 15) to give pure triazol **13** with yield 85% as a colorless solid. TLC: R_F = 0.34 ($CHCl_3$: MeOH 9 : 1, v/v); 0.40 (CH_2Cl_2 : MeOH 85 : 15, v/v); $[a]_D^{20}$ = +8.55 (*c* 1.0, THF). M.p. (DSC) 184.4°C (crystallized from THF). ^{1}H NMR (600 Hz, DMSO-d_6, d, ppm): 13.20 (bs, 1H, -CO_2H), 9.04 (s, 1H, H3'), 8.14 (d_{AB}, *J* = 8.8 Hz, 2H, Ar), 8.10 (d_{AB}, *J* = 8.7 Hz, 2H, Ar), 4.85 (bs, 1H, H12), 4.77 (d, *J* = 12.8 Hz, 1H, H1'), 4.47 (d, *J* = 12.9 Hz, 1H, H1'), 4.23 (d, *J* = 4.4 Hz, 1H, C21-OH), 3.82 (d, *J* = 9.6 Hz, 1H), 3.79 (d, *J* = 12.3 Hz, 1H), 3.68 (dd, *J* = 4.6, 9.2 Hz, 1H), 3.36–3.26 (m, ov, 4H), 3.14 (d, *J* = 8.3 Hz, 1H), 3.07 (d, *J* = 11.4 Hz, 1H), 2.40 (dd, *J* = 3.1, 14.2 Hz, 1H, H18), 1.89–1.75 (m, ov, 5H), 1.56–1.38 (m, ov, 7H), 1.35 (s, 3H, CH_3), 1.30 (s, 3H, CH_3), 1.28 (s, 3H, CH_3), 1.23 (s, 3H, CH_3), 1.18 (d, *J* = 11.0 Hz, 1H), 1.06 (s, 3H, CH_3), 1.04 (s, 3H, CH_3), 0.92 (s, 3H, CH_3), 0.88–0.85 (m, 1H), 0.77 (s, ov, 3H, CH_3), 0.75 (m, ov, 1H), 0.61 (s, 3H, CH_3), 0.53 (s, 3H, CH_3). ^{13}C NMR (150 Hz, DMSO-d_6, δ, ppm): 166.3 (C=O), 144.8 (C2'), 139.9 (C13), 139.5 (Ar), 131.1 (Ar), 130.5 (Ar), 122.7 (C3'), 121.8 (C12), 119.3 (Ar), 98.3, 97.7, 75.9, 75.6, 72.7, 69.7 (C28), 68.4 (C16), 62.7, 62.6, 52.8 (C5), 46.6, 44.2, 43.0, 41.0, 40.8, 39.6, 36.7, 35.7, 35.5, 35.4, 35.1, 31.9 (C7), 30.33, 30.16, 28.1, 27.8, 25.6, 25.2, 24.2, 24.0, 22.4, 18.0, 17.8, 17.4, 16.2. HRMS (ESI): calcd. for $C_{46}H_{65}N_3O_8Na$ $[M + Na]^+$ *m*/*z*: 810.4669; found: *m*/*z*: 810.4673.

RESULTS AND CONCLUSIONS

The four new triazole derivatives of protoescigenin were obtained – three of them containing a glycoside moiety. In all cases to perform the cycloaddition reaction there was no need of addition a reductant (e.g., sodium ascorbate). However, for the secondary azide, the reaction time was highly elongated.

It has been suggested that in Cu(II) catalyzed click reactions an alcohol used as the reaction solvent gets oxidized by copper salt to a sufficient degree to provide Cu(I) catalyst, which binds terminal acetylenic substrate by a covalent bond. Without entering a mechanistic dispute, it seems useful to sort out a situation in which Cu(I) and Cu(II) as well as non catalytic reaction pathways have been claimed, for purely practical purposes.

Thus, PES propargylic ether **13** has been subjected to click reactions with 4-azidobenzoic acid **12** (Scheme 5), side by side, under catalytic and non-catalytic conditions. It turned out that copper catalyzed reactions proceeded with comparable yield, while lack of reductant (sodium ascorbate, AscNa) resulted in significant prolongation of reaction time (from 1 day in the presence to 8 days in the absence of AscNa). Similar observation was done for the reaction of **2** with azidosugar **3**: in absence (presence) of AscNa product **9** was obtained with 76% (71%) yield after 10 days (1 day) of reaction time, respectively.

Acknowledgments

Work at the laboratory (PRI) was supported from European and Regional Funds under the Innovative Economy Programme POIG.0101.02-14-072/09-00 Grant. Katarzyna Komor (SUT) received a scholarship under the project "DoktoRIS – Scholarship Program for Innovative Silesia".

REFERENCES

1. Kuhn R., Löw I.: Justus Liebigs Ann. Chem. 669, 183 (1963).
2. Nakano T., Hasegawa M., Thomson J.B.: Tetrahedron Lett. 8, 1675 (1967).
3. Agrawal P.K., Thakur R.S., Shoolery J.N.: J. Nat. Prod. 54, 1394 (1991).
4. Sirtori C.R.: Pharmacol. Res. 44, 183 (2001).
5. Grynkiewicz G., Koziak K.: Acta Biochim. Pol. 56, 3 (2009).
6. Gruza M., Jatczak K., Zagrodzki B., Łaszcz M., Koziak K., Malińska M., Cmoch P. et al.: Molecules 18, 4389 (2013).
7. Jatczak K., Gruza M.M., Filip K., Cmoch P., Grynkiewicz G.: Cent. Eur. J. Chem. 12 (2014), *accepted manuscript, in press*.
8. Agalave S.G., Maujan S.R., Pore V.S.: Chem. Asian J. 6, 2696 (2011).
9. Kolb H.C., Finn M.G., Sharpless K.B.: Angew. Chem. Int. Ed. 40, 2004 (2001).
10. Zhang X., Zhang Y.: Molecules 18, 7145 (2013).
11. Bertozzi C.R., Baskin J.M.: Aldrichimica Acta 43 (2010).
12. Kloss F., Köhn U., Jahn B.O., Hager M.D., Görls H., Schubert U.S.: Chem. Asian J. 6, 2816 (2011).
13. Witczak Z.J., Bielski R. Eds.: Click Chemistry in Glycoscience: New Developments and Strategies, John Wiley & Sons, Hoboken, NJ 2013.
14. Meldal M., Tornře C. W.: Chem. Rev., 108, 2952 (2008).
15. Pérez-Labrada K., Brouard I., Morera C., Estévez F., Bermejo J., Rivera D.G.: Tetrahedron, 67, 7713 (2011).

16. Kirai N., Yamamoto Y.: Eur. J. Org. Chem. 2009, 1864 (2009).
17. Brotherton W.S., Michaels H.A., Simmons J.T., Clark R.J., Dalal N.S., Zhu L.: Org. Lett. 11, 4954 (2009).
18. Kuang G.-C., Michaels H.A., Simmons J.T., Clark R.J., Zhu L.: J. Org. Chem. 75, 6540 (2010).
19. Adzima B.J., Tao Y., Kloxin C.J., DeForest C.A., Anseth K.S., Bowman C.N.: Nat. Chem. 3, 256 (2011).
20. Ingale S.A., Seela F.: J. Org. Chem. 78, 3394 (2013).
21. Wei G., Cai C., Du Y.: Chin. J. Chem. 27, 1589 (2009).
22. Priebe W., Fokt I., Przewłoka T., Krawczyk M., Skibicki P., Grynkiewicz G., Perez-Soler R.: US Patent 6 673 907, filled 2004. 01. 04.
23. Hansen T., Daasbjerg K., Skrydstrup T.: Tetrahedron Lett. 41, 8645 (2000).
24. Dixon J.T., van Heerden F.R., Holzapfel C.W.: Tetrahedron Asymmetry 16, 393 (2005).
25. Komor K., Szeja W., Bieg T., Kuźnik N., Pastuch-Gawołek G., Komor R.: Tetrahedron Lett. *accepted manuscript, in press*.
26. Banaszek A., Krowicki K., Zamojski A.: J. Chromatogr. A 32, 581 (1968).
27. Pirrung M.C.: in The Synthetic Organic Chemist's Companion; pp. 171–172, John Wiley & Sons, Hoboken, NJ 2006.

Project co-financed by the European Regional Development Fund under the framework of the Innovative Economy Operational Programme.

POIG contract no 01.01.02-14-072/09 „Research on innovative endothelium medicine among novel escin analogues": www.ifarm.eu/poig/escyna/

Acta Poloniae Pharmaceutica – Drug Research, Vol. 71 No. 6 pp. 956–961, 2014 ISSN 0001-6837
Polish Pharmaceutical Society

INFLUENCE OF CYCLOSPORIN A ON EXPRESSION PATTERN OF GENES ASSOCIATED WITH DNA REPAIR IN HUMAN DERMAL FIBROBLASTS

GRZEGORZ HIBNER*, ALICJA ZAJDEL and ADAM WILCZOK

Department of Biopharmacy, Faculty of Pharmacy, Medical University of Silesia, Jedności 8, 41-200 Sosnowiec, Poland

Abstract: Cyclosporin A (CsA) is a cyclic nonribosomal peptide with immunosuppressive activity. Chronic immunosuppressive medication is associated with time distant side effects and is the cause of the different secondary diseases, including cancers (especially skin cancers). Anomalies in the functioning of DNA repair mechanisms are closely related to the processes of neoplastic transformation. The object of this study was to assess the impact of CsA exposure (8 h, early cell response) on expression of genes associated with DNA repair in normal human dermal fibroblasts (NHDF). NHDF from CC-2511 cell line were routinely maintained in FBM medium. Transcriptional activity of genes associated with DNA repair in NHDF after 8 h of cells exposition to CsA (C = 100 ng/mL) in relation to control cells was compared using Affymetrix HG–U133A 2.0 oligonucleotide microarray technique. GeneSpring GX fluorescence signals analysis of 1514 probes, which represented the expression of 875 genes selected from the NetAffx Analysis Center database for "DNA repair" query, demonstrated the inhibited expression of 32 probes (p-value < 0.05; Fold Change > 2.0), including: *BRCA1*, *RAD51*, *TOP2A*, *EXO1*, *RRM2*, *CDK1* and *POLE2*. The obtained results suggest that CsA can have a silencing effect on DNA repair genes. Therefore, the risk of skin cancer development during CsA therapy can result not only from immunosuppressive effects of the drug, but is also likely to arise from inhibition of DNA repair pathways.

Keywords: cyclosporin, DNA repair, NHDF, oligonucleotide microarray

Cyclosporin A (CsA) is a cyclic nonribosomal peptide composed of 11 amino acids, initially isolated from the fungus *Tolypocladium inflatum* (1). Immunosuppressive effects of CsA involve its binding to cyclophilin, a cytoplasmic protein of immunocompetent lymphocytes, especially T cells. CsA-cyclophilin complex is an inhibitor of calcineurin, a mediator of transcriptional activation pathway of interleukin 2 (IL-2). CsA-cyclophilin complex binds to calcineurin and prevents the dephosphorylation of the transcription factor NF-AT and its relocation to the cell nucleus, which excludes the increase in transcriptional activity of genes encoding IL-2 and related cytokines. CsA therapeutic activity takes place in the early phases of the cell cycle (G_0, G_1) and results from the inhibition of cellular and humoral immune responses and modification of inflammatory reactions. CsA affects the T_H cells activating process and thereby indirectly inhibits the production of antibodies and activation of macrophages. It also inhibits the B-lymphocytes to some extent (2–4). CsA also affects the mitochondria, preventing the opening of mitochondrial permeability transition pore – MPTP, thereby reducing the release of cytochrome C, which is an effective apoptosis-stimulating factor (5, 6).

CsA is widely used in patients after heart, kidney, liver, lung, pancreas, bone marrow, skin and small intestine transplants. Apart from transplant medicine, CsA is also used in psoriasis, severe atopic dermatitis, pyoderma gangrenosum, chronic autoimmune urticaria and, infrequently, in rheumatoid arthritis and related diseases, although it is only used in severe cases. In the United States, CsA is widely used in the form of eye drops for the treatment of dry eye (7). CsA was also studied for use as neuroprotective agent in case of traumatic brain injury. Experiments with animals demonstrated a reduction of damage associated with brain injury. It was shown that CsA blocks the formation of MPTP, which are responsible for the formation of neural tissue damage due to head injury or neurodegenerative diseases (8).

* Corresponding author: e-mail: ghibner@onet.eu

Eukaryotic cells developed specialized detectors of genome damage. DNA repair requires efficient lesion detection, which is one of the major early cell responses to DNA damage. Induction of this process is accompanied by mechanisms that stop the cell cycle, which prolongs the time needed for DNA repair before replication and division of chromosomes. This ensures the restoration of genetic information and maintenance of gene sequence. Until now, six major DNA repair pathways in living cells were described, including direct reversal, base excision repair, nucleotide excision repair, mismatch repair, non-homologous end joining, microhomology-mediated end joining and homologous recombination, which are represented by expression of over 850 genes (9, 10). It is well recognized that anomalies in the functioning of DNA repair mechanisms are closely related to the processes of neoplastic transformation (11).

Little is known about CsA molecular mechanism of action, particularly about its influence on gene expression and responses induced at the cellular level. Side effects and multidrug resistance alteration are frequently observed during the treatment with CsA. Furthermore, chronic immunosuppressive medication is associated with time distant side effects and is the cause of different secondary diseases, including cancers (especially skin cancers). The object of this study was to assess the impact of CsA exposure (8 h, early cell response) on expression of genes associated with DNA repair in normal human dermal fibroblasts (NHDF).

EXPERIMENTAL

Cell culture

Human dermal fibroblasts from CC-2511 cell line (Clonetics, San Diego, CA, USA), routinely grown in fibroblast basal medium (FBM – Lonza, Basel, Switzerland), were used as the material for the study. Cultures were incubated under conditions of constant temperature of 37^{o}C, constant humidity of 95% and 5% CO_2 enriched atmosphere. NHDFs were exposed to CsA at a concentration of 100 ng/mL for 8 h. CsA concentration of 100 ng/mL complied with an average therapeutic concentration of the drug in blood plasma of routinely treated renal transplant patients (12). The study used a base solution of CsA in 0.9% NaCl (Novartis, Basel, Switzerland) at a concentration of 50 mg/mL.

Extraction of total RNA

TRIzol reagent (Invitrogen Life Technologies, California, USA) was used to isolate total RNA from samples, according to the manufacturer's protocol. Total RNA extracts were treated with DNase I (Fermentas International Inc., Ontario, Canada) and purified with the use of RNeasy Mini Kit (Qiagen GmbH, Hilden, Germany), in accordance with manufacturer's instructions.

Qualitative and quantitative assessment of total RNA extracts

The quality of RNA was estimated by electrophoresis on a 1% agarose gel stained with ethidium bromide. RNA concentration was determined on the basis of absorbance at 260 nm using a GeneQuant pro RNA/DNA Calculator (Pharmacia LKB Biochrom Ltd., Cambridge, UK).

Oligonucleotide microarray gene expression analysis

To synthesize double-strand cDNA, 8 μg of total RNA was used (SuperScript Choice system; Invitrogen Life Technologies, CA, USA). The synthesis of biotinylated cRNA was carried out using BioArray HighYield RNA Transcript Labeling Kit (Enzo Life Sciences, New York, USA). Fragmentation of cRNA was performed with the use of Sample Cleanup Module Kit (Qiagen GmbH, Germany). Hybridization mixture was prepared using the GeneChip Expression 3'-Amplification Reagents Hybridization Control Kit and subjected to hybridization with HG-U133A 2.0 microarrays (Affymetrix Inc., California, USA). All steps were performed according to the Gene Expression Analysis Technical Manual (Affymetrix Inc., California, USA). Fluorescence intensity was measured with the use of Affymetrix GeneArray Scanner 3000 7G (Affymetrix Inc., California, USA).

Statistical analysis and prediction of differentially expressed genes

Six microarray plates were used: three for control and three for treated cells. For the analysis of NHDF transcriptomes, influenced by CsA exposure, among 22 277 mRNA probes present on the HG-U133A 2.0 microarray, transcripts associated with DNA repair were selected. The names of the probes were obtained from Affymetrix NetAffx Analysis Center database (13) after entering the query: "DNA repair". There were 1514 probes filtered, which represented the expression of 875 different genes.

Agilent GeneSpring GX software was used for statistical analysis of the data after microarrays scanning. Simultaneous normalization with RMA algorithm (Robust Multichip Average) of 22 277 fluorescence signal values for the six HG-U133A

2.0 chips was performed. Microarray quality control tests were carried out using: 3D Principal Component Analysis, analysis of the normalized fluorescence signal values for hybridization control probes and the 3'/5' ratios for internal controls. Differentially expressed genes were determined using T test unpaired and Fold Change (FC) filtering. P-values were computed using asymptotic method with 300 permutations and corrected using Benjamini-Hochberg multiple testing correction method. The standard cut-off of p-value < 0.05 was set to determine statistical significance of mRNA fluorescent signals. The criterion used for differentially expressed genes required the absolute value of FC to be greater than 2.0 (|FC| > 2.0) between compared samples.

RESULTS AND DISCUSSION

Cyclosporin A is known to inhibit nucleotide excision repair (NER) *via* downregulation of the xeroderma pigmentosum group A and G proteins, which is mediated by calcineurin inhibition (14, 15). The inhibition of NER mechanism is widely recognized to contribute to the skin cancer proneness in organ transplant patients. Also, CsA can induce DNA double-strand breaks (16) and it was shown that calcineurin inhibitors decrease DNA repair and apoptosis in human keratinocytes following ultraviolet B irradiation (17). Together, this suggests the potential role of CsA in carcinogenesis, which cannot be explained by immunosuppression alone.

Oligonucleotide microarray technique allows a detailed analysis of changes in transcriptional activity of tens of thousands of genes simultaneously. This technique is often used to study the impact of drugs on the cellular processes at the molecular level (18). Such study allows to perform the prediction of differentially expressed genes and also may help to understand how therapeutic agents modify the expression of specific genes of interest (19).

This study focused on investigating the transcriptional activity of genes associated with DNA repair in NHDF cells cultured in the presence of CsA for 8 h in comparison with control cultures. The use of HG-U133A 2.0 Affymetrix oligonucleotide microarray technology allowed to determine the gene expression parameters after obtaining normalized expression values for the individual probes. Comparison of gene expression in treated and control NHDFs was performed using Agilent GeneSpring GX software. Based on Affymetrix NetAffx Analysis Center database (13), the sets of probes associated with the pathway of interest were

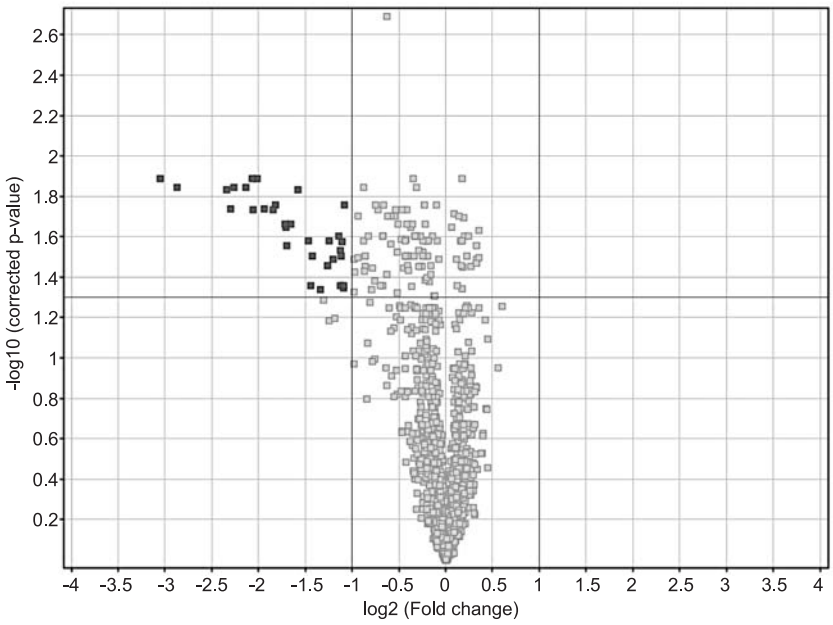

Figure 1. Volcano plot showing relationship between p-value (–log10 of p-value, y-axis) and fold change (x-axis, FC) as a result of T Test unpaired (1514 probes, n = 3). P-values were computed using asymptotic method with 300 permutations and corrected using Benjamini-Hochberg multiple testing correction method. Differential genes ($p < 0.05$; $|FC| > 2.0$) associated with DNA repair are shown in dark gray

Table 1. Probes for genes associated with DNA repair ($p < 0.05$; $|FC| > 2.0$), differentiating early cell response (8 h) of human dermal fibroblasts exposed to cyclosporin A (C = 100 ng/mL; n = 3) in relation to control cells.

Probe set ID	Gene symbol	Corrected p-value	FC Absolute	Regulation
201890_at	*RRM2*	0.0129	8.30	down
209773_s_at	*RRM2*	0.0143	7.33	down
210559_s_at	*CDK1*	0.0147	5.09	down
204126_s_at	*CDC45*	0.0181	4.94	down
203214_x_at	*CDK1*	0.0143	4.80	down
202503_s_at	*KIAA0101*	0.0143	4.39	down
203213_at	*CDK1*	0.0129	4.21	down
201291_s_at	*TOP2A*	0.0184	4.16	down
201292_at	*TOP2A*	0.0129	4.05	down
220651_s_at	*MCM10*	0.0181	3.85	down
204603_at	*EXO1*	0.0184	3.60	down
204146_at	*RAD51AP1*	0.0174	3.54	down
209642_at	*BUB1*	0.0216	3.30	down
206632_s_at	*APOBEC3B*	0.0225	3.28	down
218355_at	*KIF4A*	0.0278	3.26	down
204822_at	*TTK*	0.0216	3.16	down
220085_at	*HELLS*	0.0147	2.99	down
203145_at	*SPAG5*	0.0262	2.77	down
212949_at	*NCAPH*	0.0435	2.72	down
204033_at	*TRIP13*	0.0312	2.69	down
213007_at	*FANCI*	0.0458	2.54	down
208079_s_at	*AURKA*	0.0349	2.40	down
216237_s_at	*MCM5*	0.0262	2.37	down
219502_at	*NEIL3*	0.0323	2.30	down
205733_at	*BLM*	0.0249	2.22	down
203554_x_at	*PTTG1*	0.0292	2.19	down
204128_s_at	*RFC3*	0.0435	2.19	down
205909_at	*POLE2*	0.0312	2.18	down
204531_s_at	*BRCA1*	0.0266	2.16	down
213008_at	*FANCI*	0.0435	2.14	down
205024_s_at	*RAD51*	0.0448	2.14	down
202589_at	*TYMS*	0.0174	2.13	down

filtered. The aim of the analysis was to search for differences and similarities in the expression patterns of selected sets of genes. The set of 1514 probes, representing the expression of genes associated with DNA repair, in the form of values of the fluorescence signals, was used to determine differentially expressed genes characterized by the most significant fold change under the influence of CsA. T test unpaired, with a predetermined cut-off of p-value < 0.05, allowed to predict 128 mRNA probes,

Table 2. Genes associated with DNA repair, differentiating the response of NHDF exposed to CsA for 8 h.

Gene symbol	Encoded protein name
APOBEC3B	apolipoprotein B mRNA editing enzyme, catalytic polypeptide-like 3B
AURKA	aurora kinase A
BLM	Bloom syndrome, RecQ helicase-like
BRCA1	breast cancer 1, early onset
BUB1	BUB1 mitotic checkpoint serine/threonine kinase
CDC45	cell division cycle 45
CDK1	cyclin-dependent kinase 1
EXO1	exonuclease 1
FANCI	Fanconi anemia, complementation group I
HELLS	helicase, lymphoid-specific
KIAA0101	KIAA0101
KIF4A	kinesin family member 4A
MCM10	minichromosome maintenance complex component 10
MCM5	minichromosome maintenance complex component 5
NCAPH	non-SMC condensin I complex, subunit H
NEIL3	nei endonuclease VIII-like 3 (E. coli)
POLE2	polymerase (DNA directed), ε 2, accessory subunit
PTTG1	pituitary tumor-transforming 1
RAD51	RAD51 recombinase
RAD51AP1	RAD51 associated protein 1
RFC3	replication factor C (activator 1) 3, 38 kDa
RRM2	ribonucleotide reductase M2
SPAG5	sperm associated antigen 5
TOP2A	topoisomerase (DNA) II α 170 kDa
TRIP13	thyroid hormone receptor interactor 13
TTK	TTK protein kinase
TYMS	thymidylate synthetase

associated with DNA repair, with significantly altered transcriptional activity level in NHDF cells exposed to CsA compared to the control group. Filtering the absolute values of fold change between compared cells was performed in order to narrow down a set of differentially expressed genes. Probes with |FC| > 2.0 (minimum two-fold increase or decrease in signal intensity) were selected and formed a panel of 32 transcripts. Differentially expressed probes are shown in Figure 1 in the form of Volcano plot, describing relationship between p-value and FC as a result of statistical analysis.

Analysis of transcriptional activity of genes involved in DNA repair mechanisms, differentiating early NHDF response to CsA exposure in relation to control cultures, showed that all typed transcripts were inhibited, including: *BRCA1* (2.16-fold), three probes for *CDK1* (5.09-, 4.80- and 4.21-fold, respectively), *EXO1* (3.60-fold), *POLE2* (2.18-fold), *RAD51* (2.14-fold), two probes for *RRM2* (8.30- and 7.33-fold, respectively) and two probes for *TOP2A* (4.16- and 4.05-fold, respectively). Detailed data, illustrating the influence of CsA, including probe set IDs, symbols of genes, p-values, FCs and regulation are shown in Table 1. Names of the encoded proteins for differentially expressed genes along with gene symbols are presented in Table 2.

Under the influence of CsA, the most inhibited gene was *RRM2* encoding ribonucleotide reductase small subunit M2. This reductase catalyzes the formation of deoxyribonucleotides from ribonucleotides. Synthesis of the encoded protein (M2) is

regulated in a cell-cycle dependent fashion. It was recently shown that *RRM2* may be a facilitating factor in colorectal tumorigenesis and UV-induced DNA damage repair (20).

RAD51 encodes recombinase from RAD51 family, which members are highly similar to bacterial RecA and *Saccharomyces cerevisiae* Rad51. These proteins are known to be involved in DNA repair and homologous recombination. *RAD51* protein product can interact with the ssDNA-binding protein RPA and RAD52, and it is thought to play roles in homologous pairing and strand transfer of DNA. It was also found to interact with BRCA1 and BRCA2, which may be important for the cellular response to DNA damage (21).

BRCA1, which was also notably influenced by CsA, encodes a nuclear phosphoprotein involved in maintaining genomic stability and also acts as a tumor suppressor. The encoded protein interacts with other tumor suppressors, DNA damage sensors and signal transducers to form a large multi-subunit protein complex known as the BRCA1-associated genome surveillance complex (BASC) (22). *BRCA1* protein product cooperates with RNA polymerase II and also influences histone deacetylase complexes through its C-terminal domain. Thus, this protein plays a role in transcription, DNA repair of double-stranded breaks and recombination (23).

CONCLUSIONS

Together, the results suggest that CsA can have a silencing effect on DNA repair genes. Therefore, the risk of skin cancer development during CsA therapy can result not only from immunosuppressive effects of the drug, but is also likely to arise from inhibition of DNA repair pathways.

Acknowledgment

This study was supported by grant KNW-1-047/D/1/0 from the Medical University of Silesia (Poland).

REFERENCES

1. Tedesco D., Haragsim L.: J. Transplant. 2012, 1 (2012).
2. Colombo D., Ammirati E.: J. Biol. Regul. Homeost. Agents 25, 493 (2011).
3. Voskamp P., Bodmann C.A., Koehl G.E., Tensen C.P., Bavinck J.N., Willemze R., Geissler E.K., de Gruijl F.R.: Transplantation 96, 871 (2013).
4. Wimmer C.D., Angele M.K., Schwarz B., Pratschke S., Rentsch M., Khandoga A., Guba M. et al.: Transpl. Int. 26, 999 (2013).
5. Elrod J.W., Wong R., Mishra S., Vagnozzi R.J., Sakthievel B., Goonasekera S.A., Karch J. et al.: J. Clin. Invest. 120, 3680 (2010).
6. Wilkinson S.T., Johnson D.B., Tardif H.L., Tome M.E., Briehl M.M.: Oncol. Lett. 1, 227 (2010).
7. Tu E.Y., Rheinstrom S.: Dry eye, in Ophthalmology. Yanoff M., Duker J.S. Eds., Mosby Elsevier, St. Louis 2008.
8. Sullivan P.G., Thompson M., Scheff S.W.: Exp. Neurol. 161, 631 (2000).
9. Menck C.F., Munford V.: Genet. Mol. Biol. 37, 220 (2014).
10. Maginn E.N., de Sousa C.H., Wasan H.S., Stronach E.A.: Biochim. Biophys. Acta 1846, 45 (2014).
11. Herman-Edelstein M., Rozen-Zvi B., Zingerman B., Lichtenberg S., Malachi T., Gafter U., Ori Y.: Biomed. Pharmacother. 66, 111 (2012).
12. Abd A.Y., Aziz N.A., Hassan Y., Salih M.R.M., Ghazali R.: Int. J. Pharm. Sci. 2, 224 (2010).
13. http://www.affymetrix.com/ (accessed on 02.05.2014).
14. Kuschal C., Thoms K.M., Boeckmann L., Laspe P., Apel A., Schön M.P., Emmert S.: Exp. Dermatol. 20, 795 (2011).
15. Han W., Soltani K., Ming M., He Y.Y.: Cancer Prev. Res. (Phila) 5, 1155 (2012).
16. O'Driscoll M., Jeggo P.A.: Bone Marrow Transplant. 41, 983 (2008).
17. Yarosh D.B., Pena A.V., Nay S.L., Canning M.T., Brown D.A.: J. Invest. Dermatol. 125, 1020 (2005).
18. Aleksander E., Hibner G., Zajdel A., Paul-Samojedny M., Wilczok A.: Farm. Przegl. Nauk. 10, 47 (2010).
19. Hibner G., Aleksander E., Zajdel A., Paul-Samojedny M., Wilczok A.: Farm. Przegl. Nauk. 1, 35 (2011).
20. Lu A.G., Feng H., Wang P.X., Han D.P., Chen X.H., Zheng M.H.: World J. Gastroenterol. 18, 4704 (2012).
21. Nogueira A., Assis J., Catarino R., Medeiros R.: Pharmacogenomics 14, 689 (2013).
22. Knudsen N.Ø., Andersen S.D., Lützen A., Nielsen F.C., Rasmussen L.J.: DNA Repair (Amst) 8, 682 (2009).
23. Li M., Yu X.: Cancer Cell 23, 693 (2013).

Acta Poloniae Pharmaceutica – Drug Research, Vol. 71 No. 6 pp. 972–986, 2014 ISSN 0001-6837
Polish Pharmaceutical Society

EVALUATION OF GENISTEIN ABILITY TO MODULATE CTGF mRNA/PROTEIN EXPRESSION, GENES EXPRESSION OF TGFβ ISOFORMS AND EXPRESSION OF SELECTED GENES REGULATING CELL CYCLE IN KELOID FIBROBLASTS *IN VITRO*

MAGDALENA JURZAK[1]*, KATARZYNA ADAMCZYK[1], PAWEŁ ANTOŃCZAK[1], AGNIESZKA GARNCARCZYK[1], DARIUSZ KUŚMIERZ[2] and MAŁGORZATA LATOCHA[2]

Medical University of Silesia, School of Pharmacy with the Division of Laboratory Medicine,
[1]Department of Cosmetology, 3 Kasztanowa St., 41-200 Sosnowiec, Poland
[2] Department of Cell Biology, 8 Jedności St., 41-200 Sosnowiec, Poland

Abstract: Keloids are characterized by overgrowth of connective tissue in the skin that arises as a consequence of abnormal wound healing. Normal wound healing is regulated by a complex set of interactions within a network of profibrotic and antifibrotic cytokines that regulate new extracellular matrix (ECM) synthesis and remodeling. These proteins include transforming growth factor β (TGFβ) isoforms and connective tissue growth factor (CTGF). TGFβ1 stimulates fibroblasts to synthesize and contract ECM and acts as a central mediator of profibrotic response. CTGF is induced by TGFβ1 and is considered a downstream mediator of TGFβ1 action in fibroblasts. CTGF plays a crucial role in keloid pathogenesis by promoting prolonged collagen synthesis and deposition and as a consequence sustained fibrotic response. During keloids formation, besides imbalanced ECM synthesis and degradation, fibroblast proliferation and it's resistance to apoptosis is observed. Key genes that may play a role in keloid formation and growth involve: suppressor gene p53, cyclin-dependent kinase inhibitor CDKN1A (p21) and BCL2 family genes: antiapoptotic BCL-2 and proapoptotic BAX. Genistein (4',5,7-trihydroxyisoflavone) exhibits multidirectional biological action. The concentration of genistein is relatively high in soybean. Genistein has been shown as effective antioxidant and chemopreventive agent. Genistein can bind to estrogen receptors (ERs) and modulate estrogen action due to its structure similarity to human estrogens. Genistein also inhibits transcription factors NFκB, Akt and AP-1 signaling pathways, that are important for cytokines expression and cell proliferation, differentiation, survival and apoptosis. The aim of the study was to investigate genistein as a potential inhibitor of CTGF and TGFβ1, β2 and β3 isoforms expression and a potential regulator of p53, CDKN1A (p21), BAX and BCL-2 expression in normal fibroblasts and fibroblasts derived from keloids cultured *in vitro*. Real time RT-QPCR was used to estimate transcription level of selected genes in normal and keloid fibroblasts treated with genistein. Secreted/cell-associated *CTGF* protein was evaluated in cell growth's medium by ELISA. Total protein quantification was evaluated by fluorimetric assay in cells lysates (Quant-iT TM Protein Assay Kit). It was found that TGFβ1, β2 and β3 genes expression are decreased by genistein. Genistein suppresses the expression of CTGF mRNA and CTGF protein in a concentration dependent manner. p53 and p21 genes expression are modulated by genistein in concentration dependent manner. The agent also modulates BAX/BCL-2 ratio in examined cells *in vitro*.

Keywords: keloids, fibroproliferative disorders, genistein, connective tissue growth factor, transforming growth factor, cell cycle

Keloid disease is an abnormal cutaneous fibroproliferative disorder of unknown etiopathogenesis. Keloids present as benign fibroproliferative tumors are considered to be scars that occur when full thickness wounds heal abnormally (1–6). The molecular abnormalities in keloids that correlate with molecular mechanisms in normal wound healing can be categorized into the synthesis and degradation of extracellular matrix (ECM) components, cytokines and growth factors, and apoptotic pathways (6, 7). ECM deposition in any tissue is regulated by a balance between synthesis and degradation of individual components (8). The major component of keloids ECM is mainly either type III collagen (early) or type I collagen (late) because keloid is a type of scar which depends on its maturity (5, 6).

The synthesis of type I collagen is highly regulated by different cytokines at transcriptional level. Especially, isoforms β1 and β2 of transforming growth factor (TGFβ1 and TGFβ2), members of TGFβ family, enhance type I collagen gene expression. Moreover, they prevent collagen degradation

* Corresponding author: e-mail: magda@sum.edu.pl

by stimulating production of protease inhibitors (9). In contrast, TGFβ3, which is predominantly induced in the later stages of wound healing, has been found to reduce connective tissue deposition (10). Connective tissue growth factor (CTGF) is a cysteine-rich protein (CCN2) induced by TGFβ1 in connective tissue cells e.g., keloid fibroblasts which are implicated as mediators of elevated ECM deposition (11, 12). Elevated CTGF expression causes cell activation and tissue fibrosis (13–19). Sustained CTGF *s*ynthesis might be responsible for maintenance of the fibrotic phenotype in keloids (11, 16, 18, 19).

During keloids formation, besides imbalanced ECM synthesis and degradation, fibroblast proliferation and it's resistance to apoptosis is observed (2, 20–23). Key genes that may play a role in keloid formation and growth involve: suppressor gene p53, cyclin-dependent kinase inhibitor p21 (CDKN1A) and BCL2 family genes: antiapoptotic BCL-2 and proapoptotic BAX. The most crucial gene in the network of pathways governing cell's division and apoptosis is p53. The p53 tumor suppressor functions as transcription factor, by inducing or repressing different genes. It can also act as direct inducer of apoptosis by translocation into mitochondria (24). The p21 (also known as $p21^{WAF1/Cip1}$) is a negative regulator of cell divisions. It inhibits the kinase activity of the cyclin-dependent kinases (CDKs) CDK2 and CDK1 leading to growth arrest at specific stages in the cell cycle. In addition, by binding to proliferating cell nuclear antigen (PCNA), p21 interferes with PCNA-dependent DNA polymerase activity, thereby inhibiting DNA replication and modulating various PCNA-dependent DNA repair processes (25). BCL2 family genes are involved in intrinsic, mitochondrial pathway of apoptosis. In response to stress activation, BAX forms a homodimer and releases cytochrome c from the mitochondria, which results in caspase-9 activation and apoptosis. BCL-2 homodimers play opposite, protective role by stabilization of mitochondrial membrane (26).

Keloids are important problem in dermatology and esthetic dermatosurgery. In spite of long-lasting studies on keloid formation, there is no one satisfactory method to be successful in keloid prevention and treatment (14, 27, 28). There are some interesting perspectives with the use of genistein, which possesses antiproliferative and proapoptotic properties in many human cancer cell lines (29–36).

Genistein is a natural component of the plant belonging to isoflavones class. Soybean is the most abundant source of naturally occurring genistein. Genistein (4',5,7-trihydroxyisoflavone) exhibits antioxidant properties (37–40) and multidirectional action at the molecular level including i.a., estrogenic and antiestrogenic activity; inhibition of: protein tyrosine kinases (PTKs), topoisomerase II, phosphatidylinositol turnover and proteins involved in multidrug resistance of cancer cells. Genistein also interacts with other potential cellular target proteins (36, 41–50). Multidirectional molecular action of genistein led to its use as a modulator of cell proliferation, apoptosis, differentiation and cell cycle progression, particularly cancer cells. Recent report has shown that genistein is a potent cancer chemopreventive agent (51).

The aim of the study was to investigate genistein as a potential modulator of CTGF gene expression (mRNA and protein expression) and TGFβ1, β2 and β3 genes expression (mRNAs expressions) and was to enquire whether genistein exerts antiproliferative or apoptotic activity through effect on p53, p21 (CDKN1A), BCL-2 and BAX genes expression in keloid fibroblast and normal dermal fibroblasts cultured *in vitro*.

EXPERIMENTAL

Cell culture

Normal human dermal fibroblasts line (NHDF, Adult) was obtained from the tissue culture collection of Clonetics® (Lonza Walkersville Inc., Walkersville, MD, USA). Keloid fibroblasts line (KEL FIB) was obtained from the tissue culture collection of ATCC® (LGC Standards, Teddingtin, UK). Dulbecco's modified Eagle's medium (DMEM) with L-glutamine and fetal bovine serum (FBS) were purchased from ATCC® (LGC Standards, Teddington, UK). Antibiotic (penicillin-streptomycin solution), Dulbecco's phosphate buffered saline without Mg^{2+} and Ca^{2+} and 1x Trypsin with EDTA were purchased from Sigma Aldrich (St. Louis, USA). Nunc EasYFlasks with filter 25 cm^2 culture surface area was purchased from Thermo Scientific Nunc® (Roskilde, Denmark); 96-wells microplates and other plastic materials were purchased from Sarstedt (Nümbrecht, Germany).

Normal human dermal fibroblasts (NHDF) and keloid fibroblasts (KEL FIB) were cultured in DMEM with L-glutamine supplemented with 10% FBS and 1% pen/strep solution (100 U/mL penicillin, 200 μg/mL streptomycin). Cells were maintained at 37°C and 5% CO_2 atmosphere in a humidified incubator. At confluence, cells were routinely passaged. Cells from passages 4 to 6 were used in the study. For the quantitative determination of

examined mRNAs expression, the cells were seeded at the density of 5×10^5 per 5 mL medium in 25 cm^2 surface area culture flasks. For the quantitative determination of CTGF protein expression and total protein quantity, the cells were seeded at the density of 5×10^3/well per 300 µL medium in a 96-wells microplate. After 24 h, when cells adhered to the bottom of wells and started growing, the media were changed to media containing genistein.

Preparation of genistein dilutions

Genistein from *Glycine max* (soybean) used in the study was supplied by Sigma Aldrich® (cat. no. G6776). Genistein was dissolved in dimethyl sulfoxide (DMSO) as 1% stock solution (concentration of genistein 37 mM) and diluted in the growth medium (DMEM) with fetal bovine serum (FBS) and antibiotics for normal dermal fibroblast and keloid fibroblast cultures. Genistein in: 370, 185, 92.5, 37, 18.5, 3.7, 1.85, 0.37 µM and 0 µM (control) concentrations was used in the study to evaluate CTGF mRNA/protein expression and genes expression of TGFβ isoforms. For evaluation of the effect of soybean genistein on the expression of selected genes regulating cell cycle genistein in: 370, 37, 3.7, 0.37 µM and 0 µM (control) concentrations was used.

The expression of selected genes regulating cell cycle (p53, p21, BCL-2, BAX) and CTGF, TGFβ1, β2, β3 isoforms mRNAs expression in NHDF and KEL FIB cells treated with genistein

For the analysis of selected mRNAs expression, NHDF and KEL FIB cells were seeded at the density of 5×10^5 per 5 mL medium in 25 cm^2 surface area culture flasks. After 24 h of incubation under standard conditions (37°C, 5% carbon dioxide and 95% humidity), DMEM with L-glutamine, 10% FBS and 1% pen/strep in fibroblasts cultures were changed to proper mediums supplemented with genistein. Cells were treated with genistein for 72 h under standard conditions. Control groups of cells constituted NHDF and KEL FIB cells cultured 72 h in standard culture media described above.

RNA extraction and real-time RT-QPCR assay

Total RNA was extracted from control cell cultures and cell cultures incubated with genistein with the use of TRIZOL® reagent (Invitrogen, Carlsbad, CA, USA) according to the manufacturer's protocol. RNA concentration was determined spectrophotometrically, on the basis of absorbance values at the wavelength of 260 nm, using a Gene Quant II RNA/DNA Calculator (Pharmacia Biotech, USA). All RNA extracts were treated with DNase I (MBI Fermentas) according to the manufacturer's instruction.

Transcriptional activity of p53, p21, BCL-2, BAX, CTGF, TGFβ1, β2, β3 genes was evaluated by the use of real-time RT-QPCR technique with a SYBR Green I chemistry (SYBR Green Quantitect RT-PCR Kit, QIAGEN, Valencia, CA, USA). The analysis was carried out using an Opticon™ DNA Engine Sequence Detector (MJ Research, USA). Real-time RT-PCR assay was performed in triplicate for each sample. The thermal cycling conditions for one-step RT-QPCR assay were as follows: 50°C for 30 min for reverse transcription, 95°C for 15 min followed by 45 cycles at 94°C for 15 s, 60°C for 30 s and 72°C for 10 min.

mRNA (RT-QPCR) quantitative detection of CTGF, p53, p21, BCL-2, BAX were conducted on the basis of primer pairs designed for reference sequences (Gene Bank www.ncbi.nlm.nih.gov) with the following sequences:

CTGF mRNA: 5'-GTgACgAgCCCAAggACCAAACCT-3' (forward),
5'-TggACCAggCAgTTggCTCTAATCATAgTTg-3' (reverse);
p53 mRNA: 5'-TAACAgTTCCTgCATgggCggC-3' (forward),
5'-AggACAggCACAAACACg CACC-3' (reverse);
p21 mRNA: 5'-CACTCCAAACgC CggCTgATCTTC-3' (forward),
5'-TgTAgAgCgggCCTTTgAggCCCTC-3' (reverse);
BCL-2 mRNA: 5'-TTgTggCCTTCTTTgAgTTCggTg-3' (forward),
5'-ggTgCCggTTC AggTACTCAgTCA-3' (reverse);
BAX mRNA: 5'- CCTgTgCACCAA ggTgCCggAACT-3' (forward),
5'-CCACCCTggTCT TggATCCAgCCC-3' (reverse).

mRNA (RT-QPCR) quantitative detection of TGFβ1, β2 and β3 isoforms was conducted based on the published sequences (52).

The generally used housekeeping genes, β-actin and glyceraldehyde-3-phosphate dehydrogenase (GAPDH) were used as a potential, accessible endogenous controls for experimental conditions. The PCR primers for β-actin and GAPDH were purchased from PE Applied Biosystems (PE Applied Biosystems, Inc., Foster, CA, USA).

The mRNA copy numbers of examined genes were obtained by amplifying commercially available standard of β-actin cDNA (TaqMan® DNA Template Reagents Kit; PE Applied Biosystems, Inc., Foster, CA, USA). The control genes were amplified in triplicate under conditions applied for the target genes.

Following RT-PCR, the samples were subjected to temperature ramp from 60 to 95°C at the rate of 0.2°C/s with continuous fluorescence monitoring for melting curve analysis.

Specificity of real-time RT-QPCR reactions for analyzed genes was experimentally confirmed by 8% polyacrylamide gel electrophoresis and determination of the amplimer melting temperatures. No primer-dimers or unspecific by-products were generated during applied RT-QPCR amplification cycles.

Finally, specificity of RT-PCR reaction was confirmed by determining characteristic temperature of melting for each amplimer (p53 = 81.8°C; p21 = 83.3°C, BCL-2 = 82.6°C; BAX = 82.0°C; CTGF = 82.7°C; TGFβ1 = 85.5°C; TGFβ2 = 80.4°C; TGFβ3 = 80.8°C) and by 8% polyacrylamide gel electrophoresis of RT-PCR products with their visualization using silver staining (121 base pair (bp) for p53 amplimer, 101 bp for p21 amplimer, 114 bp for BCL-2 amplimer, 99 bp for BAX amplimer, 109 bp for CTGF amplimer, 152 bp for TGFβ1 amplimer, 201 bp for TGFβ2 amplimer and 121 bp for TGFβ3 amplimer).

Enzyme-linked immunosorbent assay (ELISA) quantitative measurement of CTGF protein

CTGF protein expression was measured by ELISA in cell culture media (NHDF and KEL FIB) according to the manufacturer's protocol (USCN Life Science Inc., Wuhan, P.R. China). The kit is a sandwich enzyme immunoassay for *in vitro* quantitative measurement of CTGF protein in human serum, plasma, cell culture medium and other biological fluids. ELISA was performed in triplicate for each sample and in duplicate for each standard and control. Optical density readings of each well (standards and samples) were taken at 450 ± 10 nm on the Asys UVM 340 Microplate Reader (Biogenet). The concentration of CTGF protein in the samples was determined by comparing the O.D. of the samples to the standard curve. The standard curve concentrations used for the ELISA's were: 30, 15, 7.5, 3.75, 1.88, 0.94 and 0.47 ng/mL. The minimum detectable concentration of human CTGF protein is typically less than 0.21 ng/mL.

The total protein concentration measurement in cell cultures

Total protein was extracted from control cells and cells treated with genistein (NHDF and KEL FIB) with the use of CellLytic™M kit (Sigma Aldrich®, Saint Louis, MO, USA) following the protocol of manufacturer. Total protein concentration (μg/mL) was determined in triplicate using a Qubit protein assay kit (no. Q3321; Invitrogen) on a Qubit 2.0 fluorometer (Invitrogen).

Statistical analysis

Statistical analysis was carried out using Statistica PL 8.0 software. The Shapiro-Wilk test for data normality was applied. Statistical analysis of the data showed their normality, therefore all the results are represented as the means ± SD. The one-way ANOVA followed by *post hoc* Dunnett's test was used to determine the significant differences between a control group (cells untreated with genistein) mean and the remaining genistein treatment group means in an analysis of variance setting. The difference between control cells (NHDF *vs*. KEL FIB) was analyzed using the Student's *t*-test. Values of $p < 0.05$ were considered statistically significant.

RESULTS

Housekeeping genes β-actin and glyceraldehyde-3-phosphate dehydrogenase GAPDH as potential candidates for endogenous control

The generally used housekeeping genes, β-actin and glyceraldehyde-3-phosphate dehydrogenase (GAPDH) were used as potential, accessible endogenous controls for experimental conditions. The transcriptional activity of β-actin (*ACTB*) and GAPDH genes were detected in both cell lines (NHDF and KEL FIB) untreated genistein.

The expression of β-actin gene exhibited significant differences between normal and keloid fibroblasts ($p = 0.004$, Student's *t*-test) and was lower in NHDF cells ($3.44 \times 10^7 \pm 4.81 \times 10^6$ copy number of mRNA per 1 μg of total RNA) compared to KEL FIB cells ($4.12 \times 10^7 \pm 2.03 \times 10^6$ copy number of mRNA per 1 μg of total RNA). Statistical analysis of the experimental data with the use of ANOVA revealed statistically significant differences ($p < 0.05$) in β-actin gene expression between control cells and cells treated with genistein, similarly as described previously (53). Moreover, expression of β-actin mRNAs changed, depending on genistein concentration, which excludes its application as endogenous control that might serve to normalize expression results of examined genes (54).

The expression of GAPDH mRNA exhibited no significant differences between normal and keloid fibroblasts ($p = 0.272087$, Student's *t*-test) and was lower in KEL FIB cells ($4.16 \times 10^4 \pm 3.5 \times 10^3$ copy number of mRNA per 1 μg of total RNA) compared to NHDF cells ($1.94 \times 10^5 \pm 2.04 \times 10^4$

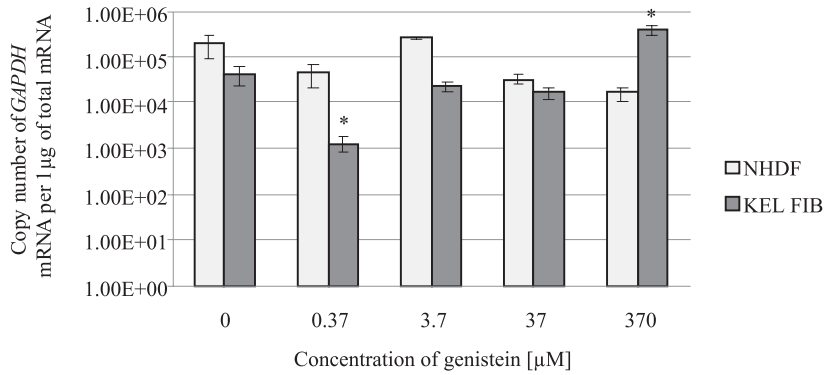

Figure 1. Comparison of the copy number of GAPDH mRNAs per 1 µg of total RNA in NHDF/KEL FIB cells treated with various genistein concentration *vs*. respective control NHDF/KEL FIB cells. * $p < 0.01$

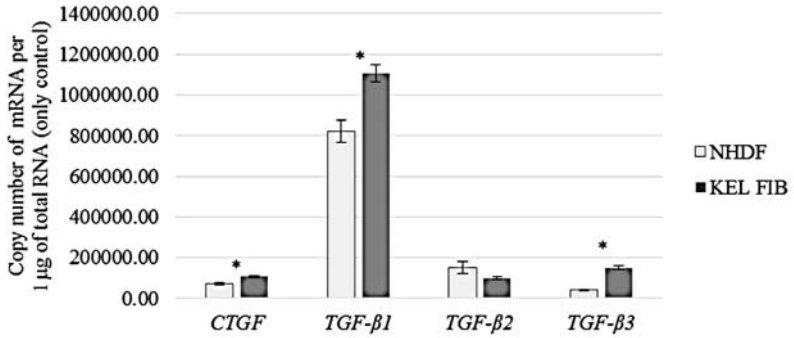

Figure 2. The native expression of *CTGF*, *TGFβ1*, *β2* and *β3* isoforms in NHDF control cells and KEL FIB control cells. * $p < 0.05$ (comparison between control NHDF cells and KEL FIB cells)

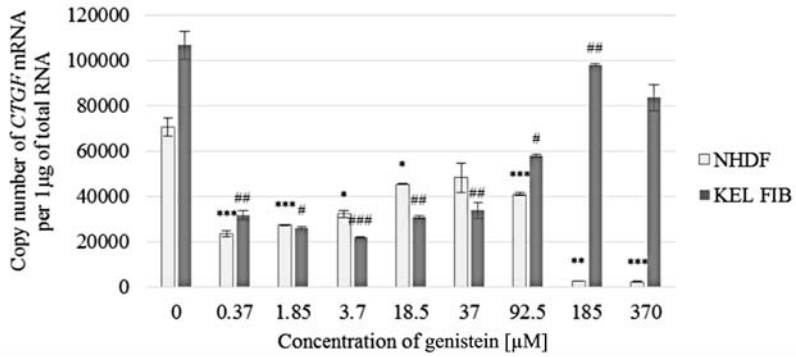

Figure 3. Expression of *CTGF* mRNA in NHDF cells and KEL FIB cells determined by real-time PCR. Comparison of the copy number of *CTGF* mRNAs per 1 µg of total RNA in NHDF cells treated with various genistein concentration *vs*. control NHDF cells (*p) and in KEL FIB cells treated with various genistein concentration *vs*. control KEL FIB cells (#p). */# $p < 0.01$, **/## $p < 0.001$, ***/### $p < 0.0001$ (*post hoc* Dunnett's test)

copy number of mRNA per 1 µg of total RNA) (Fig. 1). Statistical analysis of the experimental data revealed no statistically significant differences in GAPDH mRNA expression between NHDF control cells and NDHF cells treated with genistein ($p = 0.39094$, ANOVA). Statistical analysis of the experimental data with the use of ANOVA revealed statistically significant differences in GAPDH gene expression between KEL FIB control cells and KEL FIB cells treated with genistein ($p = 0.000022$, ANOVA). Expression of GAPDH mRNA in KEL FIB cells exposed to genistein in concentration 0.37 and 370 µM compared to control KEL FIB cells showed statistical significance ($p = 0.00059$ and $p =$

0.005634, respectively; *post hoc* Dunnett's test) (Fig.1).

The results of the statistical analysis showed no possibility of using *GAPDH* as endogenous control to normalize the results of examined genes expression.

The native mRNA expression of CTGF, TGFβ1, β2 and β3 isoforms in NHDF control cells and KEL FIB control cells

The transcriptional activity of all examined genes was detected in unstimulated (control) NDHF cells and KEL FIB cells. The expression of CTGF mRNA exhibited significant differences between normal and keloid fibroblasts ($p = 0.0154$, Student's *t*-test) and was lower in NHDF cells ($7.06 \times 10^4 \pm 7.92 \times 10^3$ copy number of mRNA per 1 μg of total RNA) compared to KEL FIB cells ($1.07 \times 10^5 \pm 1.26 \times 10^4$ copy number of mRNA per 1 μg of total RNA). Likewise, statistical analysis revealed significant differences in *TGFβ1* mRNA ($p = 0.0106$, Student's *t*-test) and *TGFβ3* mRNA ($p < 0.0001$, Student's *t*-test) between normal and keloid fibroblasts. The expression of *TGFβ1* mRNA and *TGFβ3* mRNA was lower in NHDF cells ($8.21 \times 10^5 \pm 8.67 \times 10^4$ and $4.0 \times 10^4 \pm 7.04 \times 10^3$ copy number of mRNA per 1 μg of total RNA, respectively), compared to KEL FIB cells ($1.11 \times 10^6 \pm 1.03 \times 10^5$ and $1.49 \times 10^5 \pm 1.87 \times 10^4$ copy number of mRNA per 1 μg of total RNA, respectively). No marked changes in *TGFβ2* mRNA were demonstrated between control NHDF cells ($1.50 \times 10^5 \pm 5.99 \times 10^4$ copy number of mRNA per 1 μg of total RNA) and control KEL FIB cells ($9.96 \times 10^4 \pm 1.36 \times 10^4$ copy

Table 1. The results of the statistical analysis (*post hoc* Dunnett's test) used to determine the differences between TGFβ1, β2, β3 mRNAs expression between control cells (cells untreated genistein) and cells treated with genistein in NHDF cells.

Genistein concentration [μM]	The results of *post hoc* Dunnett's test presented as *p* value		
	TGFβ1	**TGFβ2**	**TGFβ3**
0.37	0.000007	0.000005	0.000007
1.85	0.000005	0.012149	0.000416
3.7	0.000014	0.005199	0.007349
18.5	0.000023	0.000423	0.000246
37	0.000006	0.000006	0.000005
92.5	0.000044	0.000237	0.000124
185	0.000007	0.000042	0.000336
370	0.000005	0.000005	0.000006

Table 2. The results of the statistical analysis (*post hoc* Dunnett's test) used to determine the differences between TGFβ1, β2, β3 mRNAs expression between control cells (cells untreated with genistein) and cells treated with genistein in KEL FIB cell cultures.

Genistein concentration [μM]	The results of *post hoc* Dunnett's test presented as *p* value		
	TGFβ1	**TGFβ2**	**TGFβ3**
0.37	0.000006	0.000005	0.000005
1.85	0.000005	0.000005	0.000005
3.7	0.000006	0.000005	0.000005
18.5	0.000005	0.000005	0.000005
37	0.000005	0.000005	0.000005
92.5	0.000005	0.000005	0.000005
185	0.000005	0.000005	0.000005
370	0.000009	0.000005	0.000005

number of mRNA per 1 µg of total RNA) ($p > 0.05$, Student's *t*-test) (Fig. 2).

CTGF mRNA expression in NHDF and KEL FIB exposed to genistein

Treatment of NHDF cells and KEL FIB cells with genistein in each applied concentration resulted in downregulation of CTGF mRNA expression as compared with untreated cells in both lines ($p = 0.000004$, $p = 0.001009$, respectively; ANOVA) (Fig. 3).

Statistical analysis revealed no significant decrease in CTGF mRNA expression in NHDF cells exposed to genistein in concentration of 37 µM ($p = 0.064446$, *post hoc* Dunnett's test) (Fig. 3) and in KEL FIB cells exposed to genistein in concentration 370 µM ($p = 0.992769$, *post hoc* Dunnett's test) compared to the respective control cells, only. The other concentration of genistein showed significant differences compared to control NHDF cells and control KEL FIB cells, respectively (Fig. 3).

CTGF protein expression in NHDF and KEL FIB exposed to genistein

Statistical analysis revealed no significance differences between obtained CTGF protein concentration (ng/mL) (Fig. 4a) and CTGF protein concentration recalculated *per* total amount of protein in the cell lysates (Fig. 4b) ($p > 0.05$, Student's *t*-test), in both cells lines (NHDF and KEL FIB).

The expression of CTGF protein exhibited significant differences between normal and keloid fibroblasts ($p = 0.00001$, Student's *t*-test) and was about 5 times lower in NHDF cells (3.511 ± 1.046 ng/µL) compared to KEL FIB cells (26.133 ± 2.202 ng/µL).

Exposure of NHDF cells to genistein in each applied concentration resulted in downregulation of CTGF protein expression as compared with untreated NHDF cells ($p = 0.0261$, ANOVA). Statistical analysis revealed significant decrease in the CTGF protein expression in NHDF cells exposed to genistein in concentration 1.85 µM ($p = 0.024373$, *post*

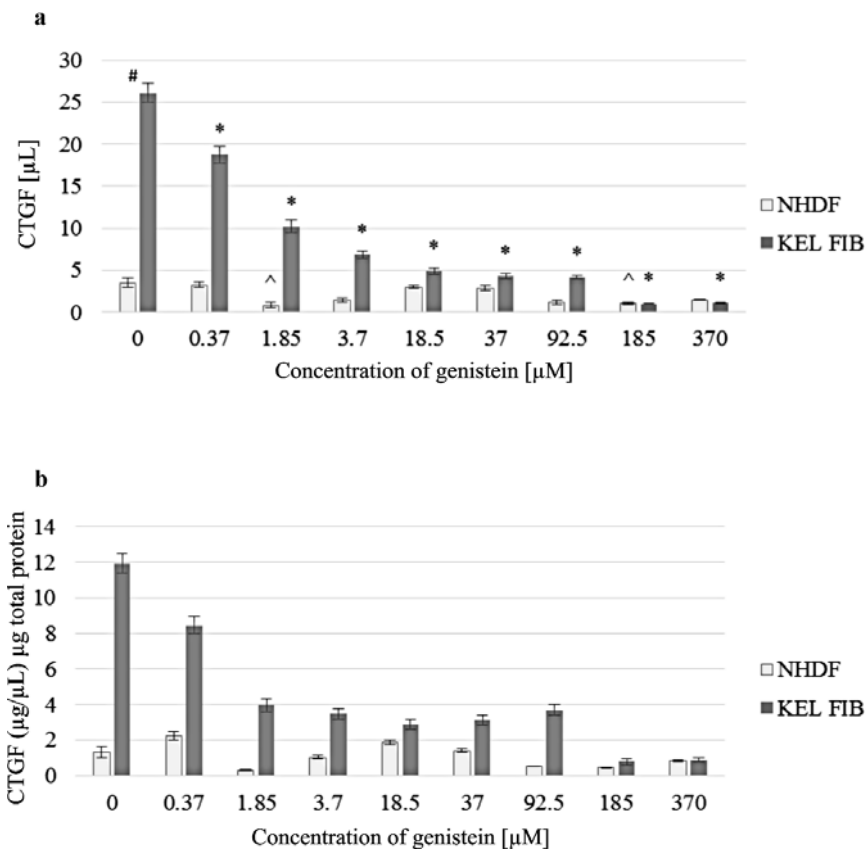

Figure 4. Expression of CTGF protein in NHDF cells and KEL FIB cells determined by ELISA. **a** Comparison of CTGF protein (µg/µL) between: control normal dermal fibroblasts (NHDF) and control keloid fibroblasts (KEL FIB) (# $p < 0.05$, Student's *t*-test), NHDF control cells and genistein treated NHDF cells (^ $p < 0.05$, Dunnett's test) and KEL FIB control cells and genistein treated KEL FIB cells (* $p < 0.00001$, Dunnett's test). **b** Comparison of CTGF protein (µg/µL) and CTGF protein (µg/µL) recalculated per µg of total protein (in each concentration $p > 0.05$, Student *t*-test)

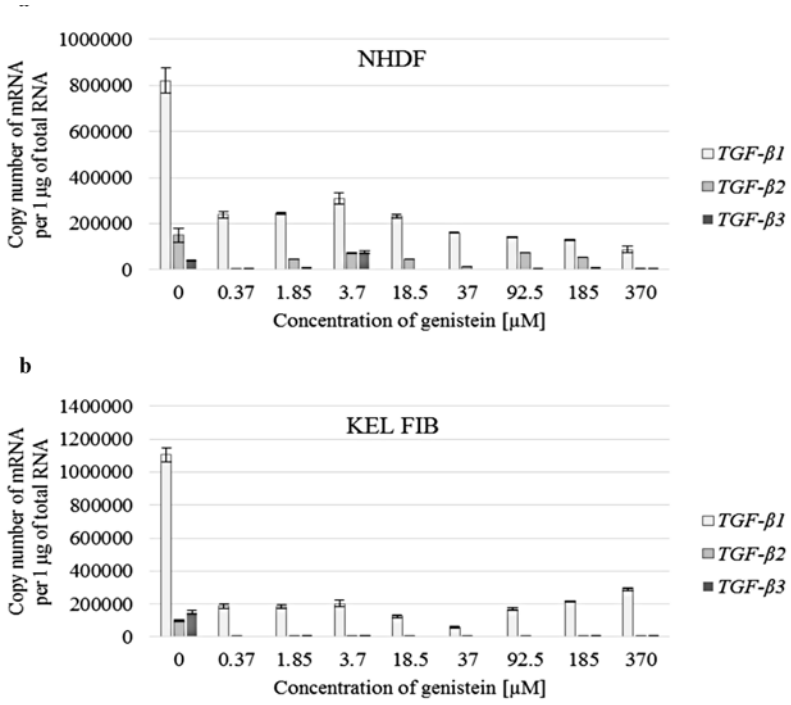

Figure 5. Expression of TGFβ1, β2, β3 mRNAs in cells treated with genistein determined by real-time PCR **a** – NHDF cells, **b** – KEL FIB cells

hoc Dunnett's test) and 185 µM ($p = 0.040428$, *post hoc* Dunnett's test), compared to NHDF control cells (Fig. 4a).

Similarly, genistein treatment of KEL FIB cells resulted in downregulation of CTGF protein expression as compared with untreated, control cells ($p < 0.0001$, ANOVA). Statistical analysis revealed significant decrease in the CTGF protein expression in KEL FIB cells exposed to genistein in each applied concentration, compared to control cells (Fig. 4a).

TGFβ1, β2, β3 mRNA isoforms expression in NHDF cells and KEL FIB exposed to genistein

Treatment of NHDF cells with genistein in each applied concentration resulted in downregulation of: TGFβ1 mRNA expression ($p < 0.000001$, ANOVA) and TGFβ2 mRNA expression ($p = 0.041047$, ANOVA), as compared with untreated control cells. Genistein downregulated TGFβ3 mRNA expression in NHDF cells ($p < 0.000001$, ANOVA), except for cells treated with 3.7 µM genistein ($7.5 \times 10^4 \pm 1.31 \times 10^4$ copy number of mRNA per 1 µg of total RNA) where an increase of expression was noted, as compared with untreated control cells ($4.00 \times 10^4 \pm 7.04 \times 10^3$ copy number of mRNA per 1 µg of total RNA) (Fig. 5a).

Statistical analysis (*post hoc* Dunnett's test) revealed significant differences in TGFβ1, β2, β3 mRNAs expression in NHDF cells exposed to various concentration of genistein compared to the untreated control cells (Tab. 1).

Exposure of KEL FIB cells to genistein in each applied concentration resulted in downregulation of TGFβ1 mRNA expression ($p < 0.000001$, ANOVA), TGFβ2 mRNA expression ($p < 0.000001$, ANOVA) and TGFβ3 mRNA expression ($p < 0.000001$, ANOVA), as compared with untreated control cells (Fig. 5b).

Statistical analysis (*post hoc* Dunnett's test) revealed significant differences in TGFβ1, β2, β3 mRNA expression in KEL FIB cells exposed to various concentrations of genistein compared to the untreated control cells (Tab. 2).

The effect of soybean genistein on the expression of selected genes regulating cell cycle in fibroblasts derived from keloids

The basal expression of p53, p21, BAX and BCL-2 mRNAs in NHDF and KEL FIB cells

The transcriptional activity of all examined genes was detected in unstimulated (control) NDHF cells and KEL FIB cells. No marked changes in p53

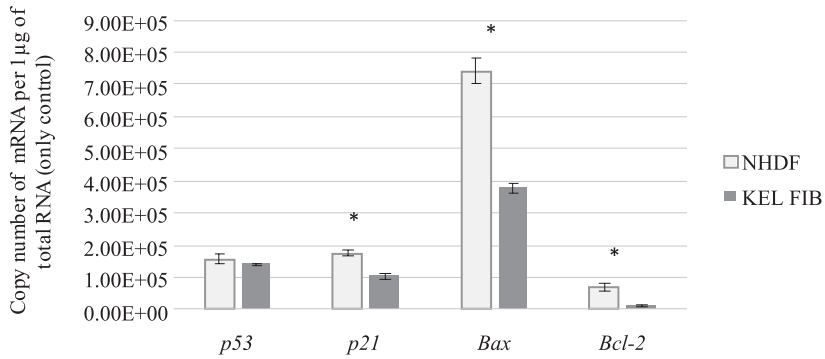

Figure 6. The native expression of p53, p21, BAX and BCL-2 in NHDF control cells and KEL FIB control cells. * $p < 0.05$ (comparison between control NHDF cells and KEL FIB cells)

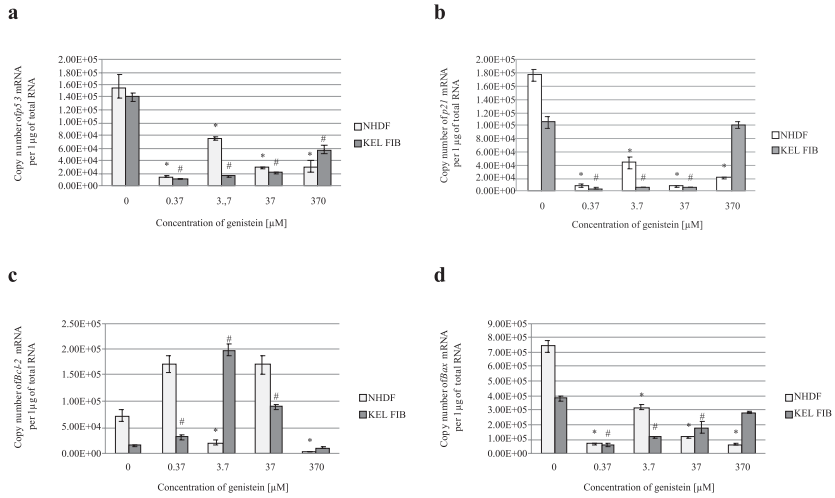

Figure 7. Expression of p53, p21, BCL-2 and BAX mRNAs in NHDF cells and KEL FIB cells determined by real-time PCR. Comparison of the copy number of mRNAs per 1 µg of total RNA: **a** p53, **b** p21, **c** BCL-2, **d** BAX (*$p < 0.05$ NHDF cells treated with various genistein concentration *vs*. control NHDF cells; #$p < 0.05$ KEL FIB cells treated with various genistein concentration *vs*. control KEL FIB cells)

gene activity were demonstrated in normal fibroblast ($1.56 \times 10^5 \pm 3.71 \times 10^3$ copy number of mRNA per 1 µg of total RNA) and keloid fibroblasts ($1.41 \times 10^5 \pm 1.11 \times 10^3$ copy number of mRNA per 1 µg of total RNA). ($p = 0.516160$, Student's *t*-test). Statistical analysis revealed significant reduction in p21 gene expression ($1.05 \times 10^5 \pm 1.78 \times 10^4$ copy number of mRNA per 1 µg of total RNA) ($p = 0.006554$, Student's *t*-test), BCL-2 gene expression ($1.42 \times 10^4 \pm 3.97 \times 10^3$ copy number of mRNA per 1 µg of total RNA) ($p = 0.012359$, Student's *t*-test) and BAX gene expression ($3.80 \times 10^4 \pm 2.53 \times 10^4$ copy number of mRNA per 1 µg of total RNA) ($p = 0.002177$, Student's *t*-test) in keloid fibroblasts as compared with normal fibroblast: p21 (CDKN1A) ($1.77 \times 10^5 \pm 1.61 \times 10^4$ copy number of mRNA per 1 µg of total RNA), BCL-2 ($7.19 \times 10^5 \pm 2.28 \times 10^4$ copy number of mRNA per 1 µg of total RNA), BAX ($7.42 \times 10^5 \pm 8.56 \times 10^4$ copy number of mRNA per 1 µg of total RNA) (Fig. 6).

P53 gene expression in NHDF and KEL FIB exposed to genistein

Treatment of NHDF cells and KEL FIB cells with genistein in each applied concentration resulted in downregulation of p53 mRNA expression as compared with untreated cells, both lines ($p = 0.000014$, $p = 0.000001$, respectively; ANOVA). Statistical analysis (*post hoc* Dunnett test) revealed significant decrease in the p53 mRNAs expression in NHDF cells exposed to genistein in concentration: 0.37 µM ($p = 0.000011$), 3.7 µM ($p = 0.001276$), 37 µM ($p = 0.000036$) and 370 µM ($p = 0.000042$) compared to NHDF control cells.

Genistein in concentrations: 0.37 μM (p = 000005, Dunnett's test), 3.7 μM (p = 000005, Dunnett's test), 37 μM (p = 000005, Dunnett's test) and 370 μM (p = 0.000019, Dunnett's test) downregulated constitutive transcriptional activity of p53 gene in KEL FIB cells (Fig. 7a).

P21 gene expression in NHDF and KEL FIB exposed to genistein

Exposure of NHDF cells and KEL FIB cells to genistein in each applied concentration resulted in downregulation of p21 mRNA expression as compared with untreated cells, both lines (p = 0.000002, p = 0.000001, respectively; ANOVA). Statistical analysis (*post hoc* Dunnett test) revealed significant decrease in the p21 mRNAs expression both in NHDF cells exposed to genistein in concentration: 0.37 μM (p = 0.000006), 3.7 μM (p = 0.000014), 37 μM (p = 0.000006) and KEL FIB cell exposed to genistein at the same concentration (p = 0.000005), (p = 0.000005), (p = 0.000006), respectively. Genistein in 370 μM concentration decreased expression of p21 mRNA in NHDF cells (p = 0.000069) compared to the NHDF control cells. Genistein in 370 μM concentration induced opposite effect in keloid fibroblasts cultured *in vitro,* where was noted increase of p21 expression ($1.01 \times 10^5 \pm 1.22 \times 10^4$ copy number of mRNA per 1 μg of total RNA) in comparison to control KEL FIB cells ($1.05 \times 10^5 \pm 1.78 \times 10^4$ copy number of mRNA per 1 μg of total RNA). Nevertheless, no statistically significant differences were revealed (p > 0.05, Dunnett's test) (Fig. 7b).

BCL-2 gene expression in NHDF and KEL FIB exposed to genistein

Exposure of NHDF cells to genistein in the concentration: 0.37, 3.7, 37 and 370 μM changed expression of BCL-2 gene in normal dermal fibroblast (p = 0.000003, ANOVA) and in keloid fibroblasts (p = 0.000002, ANOVA). The expression of BCL-2 revealed similar quantity in cells treated with 0.37 μM ($1.72 \times 10^5 \pm 3.32 \times 10^4$) and 37 μM genistein ($1.71 \times 10^5 \pm 3.41 \times 10^4$) to control cells ($7.19 \times 10^5 \pm 2.28 \times 10^4$) (p > 0.05, Dunnett's test). The expression of BCL-2 was significantly lower in cells treated with 3.7 μM genistein ($2.06 \times 10^4 \pm 8.28 \times 10^3$) and 370 μM genistein ($2.43 \times 10^3 \pm 3.75 \times 10^2$ copy number of mRNA per 1 μg of total RNA) compared to control NHDF cells (p = 0.025015, p = 0.00024, respectively; *post hoc* Dunnett's test). Expression of BCL-2 revealed similar quantity in cells treated with 370 μM genistein ($1.05 \times 10^4 \pm 1.20 \times 10^3$) compared to control KEL FIB cells (p > 0.05, Dunnett's test). Treatment of KEL FIB cells with 0.37, 3.7 and 370 μM genistein resulted in significant decrease (*post hoc* Dunnett's test) in BCL-2 expression in comparison to control KEL FIB cells (p = 0.042235, p = 0.000012, p = 0.00007, respectively) (Fig. 7c).

BAX gene expression in NHDF and KEL FIB exposed to genistein

Treatment of NHDF cells and KEL FIB cells with genistein in each applied concentration resulted in downregulation of BAX mRNA expression as compared with untreated cells, both lines (p = 0.000001, p = 0.000006, respectively; ANOVA). The expression of BAX in NHDF cells was significantly lower in cells treated with 0.37 μM genistein ($6.60 \times 10^4 \pm 1.94 \times 10^4$), 3.7 μM genistein ($3.19 \times 10^5 \pm 4.64 \times 10^4$), 37 μM genistein ($6.60 \times 10^4 \pm 1.94 \times 10^4$) and 370 μM genistein ($1.13 \times 10^5 \pm 1.22 \times 10^4$ copy number of mRNA per 1 μg of total RNA) compared to control NHDF cells (p = 0.000005, p = 0.000482, p = 0.000006, p = 0.000005, respectively;

Table 3. BAX/BCL-2 ratio for mRNA levels in normal fibroblasts (NHDF line) and fibroblast derived from keloid (KEL FIB) treated with genistein *p < 0.05 NHDF cells treated with various genistein concentration *vs*. control NHDF cells; #p < 0.05 KEL FIB cells treated with various genistein concentration *vs*. control KEL FIB cells.

Genistein concentration [μM]	BAX/BCL-2 mRNA ratio	
	NHDF	KEL FIB
0	10.31 ± 3.76	26.67 ± 6.40
0.37	0.38 ± 0.07 *	2.00 ± 0.22 #
3.7	15.48 ± 5.60	0.58 ± 0.07 #
37	0.66 ± 0.04 *	2.00 ± 0.09 #
370	25.76 ± 2.15 *	27.04 ± 1.89

post hoc Dunnett's test).The expression of BAX in KEL FIB cells was significantly lower in cells treated with 0.37 μM genistein ($6.04 \times 10^4 \pm 1.26 \times 10^4$), 3.7 μM genistein ($1.15 \times 10^5 \pm 8.15 \times 10^3$) and 37 μM genistein ($1.79 \times 10^5 \pm 7.73 \times 10^4$) compared to control KEL FIB cells ($p = 0.000008$, $p = 0.000145$, $p = 0.002822$, respectively; *post hoc* Dunnett's test). Although, expression of BAX gene was lower in cells treated with 370 μM genistein ($6.26 \times 10^4 \pm 8.07 \times 10^3$) compared to control KEL FIB cells, statistical analysis revealed no significant differences ($p > 0.05$, Dunnett's test) (Fig. 7d).

Proapoptotic ratio BAX/BCL-2 in normal and keloid fibroblasts

The BAX/BCL-2 ratio determines cell susceptibility to apoptosis. The BAX/BCL-2 mRNA ratio was determined based on real time RT-PCR results (Tab. 3).

Statistical analysis revealed significant increase in BAX/BCL-2 mRNA ratio in control fibroblasts derived from keloid ($p = 0.03621$, Student's *t*-test) compared to control normal fibroblasts. Treatment of NHDF cells with genistein resulted in statistically significant decrease of BAX/BCL-2 ratio in cells treated with 0.37, 37 and 370 μM genistein ($p = 0.003651$, $p = 0.004211$, $p = 0.002644$, respectively; Dunnett's test). No marked changes in BAX/BCL-2 mRNA ratio were demonstrated with 3.7 μM genistein stimulated cells ($p > 0.05$; Dunnett's test).

Keloid fibroblasts exposed to 0.37, 3.7 and 37 μM genistein revealed significant decrease of BAX/BCL-2 mRNA ratio compared to control KEL FIB cells ($p = 0.000211$, $p = 0.000055$, $p = 0.000200$, respectively; Dunnett's test). Keloid fibroblast exposed to 370 μM genistein revealed no differences in BAX/BCL-2 mRNA ratio in comparison to control fibroblast derived from keloids ($p > 0.05$; Dunnett's test).

DISCUSSION

Keloids are abnormal wound responses in predisposed individuals and represent a connective tissue response to skin injury. Treatment of keloids includes surgical, pharmacological and physical methods. Each of these methods can be applied as monotherapy, but combining them gives better results. Moreover, various modalities of therapy may be applied, but none of them has been proved entirely successful (55, 56). Keloids are abnormal cutaneous fibroproliferative disorders which grow beyond the confines of the original wound, invading the normal surrounding skin and they rarely regress over time (1, 6, 55). Cutaneous fibroproliferative disorders other than keloids include systemic sclerosis and hypertrophic scars (56, 57) and CTGF is their effective marker (57). Moreover, expression of CTGF in keloid fibroblast is dependent on fibroblast location and is more concentrated in keloid fibroblasts at the expanding invasive border of the keloid scar (6, 58). In the study, the keloid fibroblast culture revealed an increase of CTGF mRNA and an increase of CTGF protein expression compared to normal fibroblast confirming contribution of CTGF in keloid fibroblast pathology.

CTGF is up-regulated at the transcriptional level by a number of specific factors such as TGFβ and endothelin-1 (ET-1) or nonspecific factor (mechanicals stress, hypoxia) (16–19, 37, 57). Several studies describe the role of TGFβ in keloids and hypertrophic scars. CTGF expression increased more than 100-fold after stimulation with TGFβ1 and more than 75-fold after the addition of TGFβ2 and TGF-β3 (10).

TGFβ1 stimulation induces collagen synthesis in keloid and hypertrophic scar fibroblasts, but TGFβ1 upregulation alone seems not to be sufficient for excessive scarring (59, 60). In animal models, TGFβ2 induces cell proliferation and collagen production in scars (61, 62). The role of TGFβ3 in wound healing and pathological scarring is not fully understood, but TGF-β3 is both scar inducing and scar reducing in animals (63).

Our data revealed increased expression of TGFβ1 mRNA in keloid fibroblasts compared to normal dermal fibroblast, confirming results from other studies (64, 65). Lee et al. (64) describe increased TGF-β2 protein expression in keloid derived fibroblasts compared to normal skin fibroblasts. They did not define the biopsy site from which the fibroblasts were harvested and the time points for analysis of mRNA and protein expression may diverge. Our data reveal a decrease (no statistical significance) of TGFβ2 mRNA expression in keloids fibroblast compared to normal dermal fibroblasts, confirming Seiferts results (66). The study revealed increased expression of TGFβ3 mRNA in keloid fibroblasts compared to normal dermal fibroblast, in contrast to Lee's et al. study which revealed no difference between keloid derived fibroblasts and normal human skin fibroblasts. Seifert results revealed significantly decreased expression of TGFβ3 mRNA in keloids compared to hypertrophic scars to control skin (66).

Our study seems to confirm the thesis that the increased expression of CTGF by keloid fibroblasts

could be a response to TGFβ1 stimulation. The TGFβ signal is mediated by SMADs intracellular proteins. Changes in this signaling pathway regulate TGFβ expression and induce gene expression in the cell. The SMAD signaling pathway is crucial for simultaneous activation of several collagen genes by TGFβ and other ECM-related genes are identified as gene targets downstream of TGFβ (67). Moreover, functional Smad element resides within the CTGF promoter (68). However, the ability of TGFβ to fully induce the CTGF promoter and protein also requires protein kinase C and the ras/MEK/ERK MAP kinase cascade (69, 70).

Inhibitors of CTGF expression may be used as anti-fibrotic therapies (71) *via* TGFβ-dependent or TGFβ-independent mechanism. Inhibitors of TGFβ or endothelin receptors may be used to reduce CTGF expression in skin fibroproliferative disease such as scleroderma (72, 73). Ilprost, synthetic prostacyclin and 9-cis-retinoic acid reduced CTGF expression in scleroderma fibroblasts (74). One of the mechanisms of ilprost's action is antagonizing MEK/ERK signaling (75). U0126 is a highly selective inhibitor of both MEK1 and MEK2, a type of MAPK/ERK kinase, it reduces CTGF (CCN2) expression in response to TGFβ and ET-1 in scleroderma fibroblasts as well as constitutive over-expression of CTGF in the pancreatic cancer cell line (76). TNFα suppresses TGFβ-induced gene expression in fibroblasts but has no appreciable effect on the constitutive CTGF expression in scleroderma fibroblasts (77). Caffeine also reduces TGFβ-induced CTGF expression in hepatocytes by blocking Smad activation (78). Many *in vitro*, epidemiological and animal model studies proved application of genistein in the prophylaxis and treatment of i.a., menopause, cancer, cardiovascular disease and cystic fibrosis (79). Recent studies are focused on application of this natural isoflavone in fibroproliferative diseases. The results of the study revealed that genistein decreased mRNA and protein expression of CTGF in keloid fibroblast in a concentration-dependent manner. Moreover, genistein decreases TGFβ1, β2 and β3 genes expression (mRNA level) in keloid fibroblast. Han et al. (80) showed that genistein can effectively inhibit TGFβ1-induced invasion and metastasis in pancreatic cancer cell line Panc-1 and could partly suppress the expression of CTGF gene and its protein stimulated TGFβ1 in rat renal mesangial cells and probably decreases the accumulation of extracellular matrix (ECM) and has the potential ability of anti-fibrosis (81).

Keloid derived fibroblasts have a greater proliferative capacity than normal dermal fibroblasts (21, 82). Furthermore, the proliferation profile of fibroblasts in keloid *in vivo* has been properly documented (83) and clearly demonstrated differences in the proliferation of cells between the center and the edge of the lesion. Besides, proliferation, apoptosis, and necrosis occur simultaneously in keloids and these processes are distinctly compartmentalized, too. When keloid matures, apoptosis and necrosis result in selective removal of certain cellular populations resulting in the characteristic avascular fibrotic collagenous lesion, whereas proliferation of fibroblasts in the keloid dermis propagates the fibrosis (21). Moreover, keloid fibroblasts fail to undergo apoptosis and thus, continue to produce and secrete extracellular matrix components (20).

The induction of apoptosis is partly mediated, intracellularly, by several genes, such as p53, BCL-2, BAX, and p21. The p53 tumor suppressor gene is a cell cycle regulator able to induce cell cycle arrest to allow DNA repair or apoptosis. p21 is activated by the p53 protein, and an increased level of p21 is associated in cyclin-containing complexes with decreasing cyclin-dependent activity in damaged cells destined to apoptosis. BCL-2 functions as a suppressor of apoptotic death triggered by a variety of signals, and is negatively regulated by wild type p53. BCL-2 overexpression has been shown to inhibit apoptosis induced by a variety of stimuli, whereas, a predominance of BAX over BCL-2 accelerates apoptosis upon apoptotic stimuli (84). The aim of the study was to evaluate the influence of genistein on transcriptional activity of genes encoding p53, p21, BCL-2 and BAX in keloid fibroblasts. Results of the study reveal no marked changes in p53 gene expression between normal dermal fibroblast and fibroblast derived from keloid and marked decrease of p21 gene expression in keloid fibroblast compared to normal fibroblasts. De Felice et al. found that in keloid fibroblasts a p53 (TP53) under expression, due to the sequence mutations, in concert with ΔNp63 (an isoform of the p63 gene) activation, is central in the mechanism involved in keloid proliferation (85).

In the study, exposure of NHDF cells and KEL FIB cells to genistein in each applied concentration resulted in downregulation of p53 mRNA and p21 expression as compared with untreated cells, both lines. The effects of genistein may depend on the levels of endogenous p53 in the cells. p53 is known to induce DNA repair enzymes, and cells containing wildtype p53 may have repair of the DNA damage caused by genistein treatment. Tumor cells, either deficient in p53 or with very low doses of it, replicate through the damage and are more susceptible to genistein effects (34). The obtained results may indi-

cate that fibroblast derived from keloid compartment where cells proliferation and apoptosis were balanced, and keloid fibroblast not existed as malignant cells. Besides, in normal cells p53 is found at very low levels (86). The increase in the level of active p53 protein leads to an inhibition of entry into S-phase or the induction of apoptosis. Genistein has been identified as a protein tyrosine kinases (PTKs) inhibitor, which play a key role in oncogenesis, control of cell growth and apoptosis, therefore genistein is a potent inhibitor of cell proliferation, oncogenesis and clonogenic ability in animal and human cells (84).

P21 expression is usually controlled at the transcriptional level by both p53-dependent and p533-independent mechanisms. Cells lacking p21 appear to undergo apoptosis normally. The results of the study (decrease of p21 gene expression in cells KEL FIB cells and NHDF cells treated with genistein) are contrary to Upadhyay et al. results (87), which revealed that p21 is up-regulated by genistein treatment, and greatly induced at RNA and protein levels in normal breast epithelial cells, whereas its level was only slightly induced in malignant MDA-MB-231 breast epithelial cells and not detectable in malignant MCF10CA1a breast epithelial cells. Therefore, p21 is responsible for differential sensitivity of genistein among these cell lines (87). Li et al. revealed up-regulation of p21 and BAX expressions and down- regulation of p53 and BCL-2 expression in genistein-treated breast cancer cells MDA-MB-231 (84).

BAX and BCL-2 have been reported to play a major role in determining whether cells will undergo apoptosis under experimental conditions that promote cell death. Increased expression of BAX can induce apoptosis, while BCL-2 protects cells from apoptosis. Ratio of BAX/BCL-2 is important for the survival of drug-induced apoptosis in leukemia cell lines (84, 88). The study revealed significant reduction in BCL-2 and BAX genes expression in keloid fibroblasts as compared with normal fibroblast. Moreover, treatment of NHDF cells and KEL FIB cells with genistein in each applied concentration resulted in downregulation of BAX mRNA expression as compared with untreated cells, both lines. Expression of BCL-2 was dependent of genistein concentration. Genistein decreases BAX/BCL-2 ratio both, in normal fibroblast and keloid fibroblast, which may indicate its structural similarity to 17β-estradiol.

Genistein and 17β-estradiol may act by increasing the expression of BCL-2 and decreasing the expression of BAX, resulting in a protective effect (89). This protective effect may also come from the stimulation of estrogen receptor β, which activates the estrogen response element of the BCL-2 gene, and then increases transcription and translation to upregulate the expression of BCL-2 (90).

CONCLUSION

Summarizing the results of the study, genistein *in vitro* suppresses the expression of CTGF mRNA and CTGF protein probably in TGFβ-dependent mechanism in keloid fibroblasts but its potential application as a antifibrotic factor in keloids treatment requires further research.

Genistein does not induce the p53 and p21 genes expression, therefore it seems that it does not induce apoptosis in monoculture of keloids fibroblast. Genistein revealed cytoprotective effect stimulating BCL-2 gene expression in fibroblasts derived from keloids.

REFERENCES

1. Wolfram D., Tzankov A., Pülzl P., Piza-Katzer H.: Dermatol. Surg. 35, 171 (2009).
2. Gauglitz G.G., Korting H.C., Pavicic T., Ruzicka T., Jeschke M.G.: Mol. Med. 17, 113 (2011).
3. Barrientos S., Stojadinovic O., Golinko M.S., Brem H., Tomic-Canic M.: Wound. Rep. Reg. 16, 585 (2008).
4. Atiyeh B.S., Costagliola M., Hayek S.N.: Ann. Plast. Surg. 54, 676 (2005).
5. Marneros A.G., Krieg T.: J. Dtsch. Dermatol. Ges. 11, 905 (2004).
6. Ashcroft K.J., Syed F., Bayat A.: PLoS One 8, e75600 (2013).
7. Baum C.L., Arpey C.J.: Dermatol. Surg. 31, 674 (2005).
8. McCarty S.M., Percival S.L.: Adv. Wound Care (New Rochelle) 2, 438 (2013).
9. Leask A., Abraham D.J.: FASEB J. 18, 816 (2004).
10. Colwell A.S., Phan T.T., Kong W., Longaker M.T., Lorenz P.H.: Plast. Reconstr. Surg. 116, 1387 (2005).
11. Grotendorst G.R., Rahmanie H., Duncan M.R.: FASEB J. 18, 469 (2004).
12. Butler P.D., Longaker M.T., Yang G.P.: J. Am. Coll. Surg. 206, 731 (2008).
13. Leask A., Abraham D.J.: Biochem. Cell Biol. 81, 355 (2003).
14. Yang Q., Ma Y., Zhu R., Huang G., Guan M., Avram M.M., Lu Z.: Lasers Surg. Med. 44, 377 (2012).

15. Moussad E.E., Brigstock D.R.: Mol. Genet. Metab. 71, 276 (2000).
16. Gojniczek K., Jurzak M., Garncarczyk A.: Adv. Cell Biol. 1, 1 (2008).
17. Holbourn K.P, Acharya K.R., Perbal B.: Trends Biochem. Sci. 33, 461 (2008).
18. Shi-Wen X., Leask A., Abraham D.: Cytokine Growth Factor Rev. 19, 133 (2008).
19. Cicha I., Goppelt-Struebe M.: Biofactors 35, 200 (2009).
20. Sayah D.N., Soo C., Shaw W.W., Watson J., Messadi D., Longaker M.T., Zhang X., Ting K.: J. Surg. Res. 87, 209 (1999).
21. Appleton I., Brown N.J., Willoughby D.A.: Am. J. Pathol. 149, 1441 (1996).
22. Teofoli P., Barduagni S., Ribuffo M., Campanella A., Pita O.D., Puddu P.: J. Dermatol. Sci. 22, 33 (1999).
23. Chen W., Fu X., Sun X., Sun T., Zhao Z., Sheng Z.: J. Surg. Res. 113, 208 (2003).
24. Chumakov P.M.: Biochemistry (Mosc) 72, 1399 (2007).
25. Abbas T., Dutta A.: Nat. Rev. Cancer 9, 400 (2009).
26. Haupt S., Berger M., Goldberg Z., Haupt Y.: J. Cell Sci. 116, 4077 (2003).
27. Kelly A.P.: Dermatol. Ther. 17, 212 (2004).
28. Al-Attar A., Mess S., Thomassen J.M., Kauffman C.L., Davison S.P.: Reconstr. Surg. 117, 286 (2006).
29. Constantinou A.I., Kamath N., Murley J.S.: Eur. J. Cancer 34, 1927 (1998).
30. Davis J.N., Singh B., Bhuiyan M., Sarkar F.H.: Nutr. Cancer 32, 123 (1998).
31. Constantinou A.I., Kiguchi K., Huberman E.: Cancer Res. 50, 2618 (1990).
32. Lian F., Li Y., Bhuiyan M., Sarkar F.H.: Nutr. Cancer 33, 125 (1999).
33. Salti G.I., Grewal S., Mehta R.R., Das Gupta T.K., Boddie Jr A.W. Constantinou A.I.: Eur. J. Cancer 36, 796 (2000).
34. Rauth S., Kichina J., Green A.: Br. J. Cancer 75, 1559 (1997).
35. Markovits J., Linassier C., Fosse P., Couprie J., Pierre J., Jacquemin-Sablon A., Saucier J. et al.: Cancer Res. 49, 5111 (1989).
36. Schmidt F., Knobbe Ch.B., Frank B., Wolburg H., Weller M.: Oncol. Rep. 19, 1061 (2008).
37. Cai Q., Wei H.: Nutr. Cancer 25, 1 (1996).
38. Giles D., Wei H.: Nutr. Cancer 29, 77 (1997).
39. Ibrahim W.H., Habib H.M., Chow C.K., Bruckner G.G.: Int. J. Vitam. Nutr. Res. 78, 217 (2008).
40. Rasche M., Rowland I.R., Magee P.J., Pool-Zobel B.L.: Carcinogenesis 27, 2322 (2006).
41. Kraszewska O., Nynca A., Kaminska B., Ciereszko R.: Post. Biol. Kom. 34, 189 (2007) (Polish).
42. Muller F.J., Diel P., Zieran O., Hertrampf T., Maab J., Vollemer G.: Toxicol. Lett. 196, 142 (2010).
43. Schleipen B., Hertrampf T., Fritzemeir K.H., Kluxen F.M., Lorenz A., Molzbergen A., Velders M., Diel P.: Carcinogenesis 32, 1675 (2011).
44. Wang T.T.Y., Sathyamoorthy N., Phang J.M.: Carcinogenesis 17, 271 (1996).
45. Constantinou A., Huberman E.: Proc. Soc. Exp. Biol. Med. 208, 109 (1995).
46. Li Z., Li J., Mo B., Hu Ch., Liu H., Qi H., Wang X., Xu J.: Cell. Biol. Toxicol. 24, 401 (2008).
47. Park S.-Sh., Kim Y.-N., Jean Y.K., Kim Y.A., Kim J.E., Kim H., Kim Ch.W.: Cancer Chemother. Pharmacol. 56, 271 (2005).
48. Sandoval M.J., Cutini P.H., Rauschemberger Massheimer V.L.: Br. J. Nutr. 104, 171 (2010).
49. Marini H., Bitto A., Altavilla D., Burnett B.P., Polito F., Di Stefano V., Minutoli L. et al.: J. Clin. Endocrinol. Metab. 93, 4787 (2008).
50. Okura A., Arakawa H., Oka H., Yoshinari T., Monden Y.: Biochem. Biophys. Res. Commun. 157, 183 (1988).
51. Taylor Ch.K., Levy R.M., Elliott J.C., Burnett B.P.: Nutr. Rev. 67, 398 (2009).
52. Kapral M., Strzałka B., Kowalczyk M., Jurzak M., Mazurek U., Gierek T., Paluch J. et al.: Am. J. Otolaryngol. 29, 233 (2008).
53. Jurzak M., Adamczyk K.: Acta Pol. Pharm. Drug. Res. 70, 205 (2013).
54. Romanowski T., Markiewicz A., Bednarz N., Bielawski K.P.: Postepy Hig. Med. Dosw. 61, 500 (2007).
55. Slemp A.E., Kirschner R.E.: Curr. Opin. Pediatr. 18, 396 (2006).
56. Huang C., Ogawa R.: Connect. Tissue Res. 53, 187 (2012).
57. Leask A., Parapuram S.K., Shi-wen X., Abraham D. J.: J. Cell Commun. Signal. 3, 89 (2009).
58. Igarashi A., Nashiro K., Kikuchi K., Sato S., Ihn H., Fujimoto M., Grotendorst GR., Takehara K.: J. Invest. Dermatol. 106, 729 (1996).
59. Bettinger D.A., Yager D.R., Diegelmann R.F., Cohen I.K.: Plast. Reconstr. Surg. 98, 827 (1996).
60. Younai S., Nichter L.S., Wellisz T., Reinisch J., Nimni M.E., Tuan T.L.: Ann. Plast. Surg. 33, 148 (1994).

61. Polo M., Smith P.D., Kim Y.J., Wang X., Ko F., Robson M.C.: Ann. Plast. Surg. 43, 185 (1999).
62. Wang X., Smith P., Pu L.L., Kim Y.J., Ko F., Robson M.C.: J. Surg. Res. 87, 194 (1999).
63. Shah M., Foreman D.M., Ferguson M.W.: J. Cell Sci. 108, 985 (1995).
64. Lee T.Y., Chin G.S., Kim W.J. Chau D., Gittes G.K., Longaker M.T.: Ann. Plast. Surg. 43, 179 (1999).
65. Fujiwara M., Muragaki Y., Ooshima A.: Arch. Dermatol. Res. 297, 161 (2005).
66. Seifert O.: Linköping University Medical Dissertations no. 1023 (2008).
67. Verrecchia F., Chu M.L., Mauviel A.: J. Biol. Chem. 276, 17058 (2001).
68. Holmes A., Abraham D.J., Sa S., Shiwen X., Black C.M., Leask A.: J. Biol. Chem. 276, 10594 (2001).
69. Chen Y., Blom I.E., Sa S., Goldschmeding R., Abraham D.J., Leask A.: Kidney Int. 62, 1149 (2002).
70. Leask A., Holmes A., Black C.M., Abraham D.J.: J. Biol. Chem. 278, 13008 (2003).
71. Blom I.E., Goldschmeding R., Leask A.: Matrix Biol. 21, 473 (2002).
72. Leask A., Chen S., Pala D., Brigstock D.R.: J. Cell Commun. Signal. 2, 49 (2008).
73. Shi-Wen X., Renzoni E.A., Kennedy L., Howat S., Chen Y., Pearson J.D., Bou-Gharios G. et al.: Matrix Biol. 26, 625 (2007).
74. Stratton R., Shiwen X., Martini G., Holmes A., Leask A., Haberberger T., Martin G.R. et al.: J. Clin. Invest. 108, 241 (2001).
75. Stratton R., Rajkumar V., Ponticos M., Nichols B., Shiwen X., Black C.M., Abraham D.J., Leask A.: FASEB J. 16, 1949 (2002).
76. Pickles M., Leask A.: J. Cell Commun. Signal. 1, 85 (2007).
77. Abraham D.J., Shiwen X., Black C.M., Sa S., Xu Y., Leask A.: J. Biol. Chem. 275, 15220 (2000).
78. Gressner O.A., Lahme B., Rehbein K., Siluschek M., Weiskirchen R., Gressner A.M.: J. Hepatol. 49, 758 (2008).
79. Polkowski K. Mazurek A.P.: Acta Pol. Pharm. Drug Res. 57, 2 (2000).
80. Han L., Zhang H.W., Zhou W.P., Chen G.M., Guo K.J.: Chin. Med. J. 125, 2032 (2012).
81. Guo Y., Zhang A., Ding Y., Wang Y., Yuan W.: Arch. Med. Sci. 9: 724 (2013).
82. Calderon M., Lawrence W.T., Banes A.J.: J. Surg. Res. 61, 343 (1996).
83. Nakaoka H., Miyauchi S., Miki Y.: Acta. Derm. Venereol. 75, 102 (1995).
84. Li Y., Upadhyay S., Bhuiyan M., Sarkar F.H.: Oncogene 18, 3166 (1999).
85. De Felice B., Garbi C., Wilson R.R., Santoriello M., Nacca M.: Genomics 97, 265 (2011).
86. Toledo F., Wahl G.M.: Nat. Rev. Cancer. 6, 909 (2006).
87. Upadhyay S., Neburi M., Chinni S.R., Alhasan S., Miller F., Sarkar F.H.: Clin. Cancer Res. 7, 1782 (2001).
88. Hammes S.R., Levin E.R.: Endocr. Rev. 28, 726 (2007).
89. Peng Y., Jiang B., Huiling W., Ruchun D., Liming T.: Neural Regen. Res. 36, 2874 (2012).
90. Salomons G.S., Brady H.J., Verwijs-Janssen M., Van J.D., Hart A.A., Van H., Behren K., Smets L.A.: Int. J. Cancer 71, 959 (1997).

Acta Poloniae Pharmaceutica – Drug Research, Vol. 71 No. 6 pp. 987–993, 2014 ISSN 0001-6837
Polish Pharmaceutical Society

INFLUENCE OF INOSITOL HEXAPHOSPHATE ON THE EXPRESSION OF SELECTED PROLIFERATION MARKERS IN IL-1β-STIMULATED INTESTINAL EPITHELIAL CELLS

MAŁGORZATA KAPRAL*, STANISŁAW SOŚNICKI, JOANNA WAWSZCZYK and LUDMIŁA WĘGLARZ

Medical University of Silesia, School of Pharmacy with the Division of Laboratory Medicine, Department of Biochemistry, Jedności 8, 41-200 Sosnowiec, Poland

Abstract: The aim of the present study was to examine the influence of IP6, a naturally occurring phytochemical, on the expression of genes coding for proliferation markers, i.e., cyclin D1 (CCND1) and histone H3 in IL-1β-stimulated intestinal cancer cell line Caco-2. Quantification of genes expression was carried out using real time RT-QPCR technique in Caco-2 cells after treatment with IL-1β, 1 and 2.5 mM of IP6 for 3, 6 and 12 h. In separate cultures, cells were incubated with IL-1β for the indicated times. The untreated Caco-2 cells were used as the control. In a time course experiment, stimulation of cells with IL-1β only resulted in an overexpression of both CCND1 and histone H3 mRNAs as compared with control. IP6 had no influence on IL-1β-stimulated CCND1 expression for 3 and 6 h. After 12 h, statistically significant decrease in CCND1 mRNA was observed in cells exposed to IL-1β and IP6 (1 and 2.5 mM) in relation to cells treated with IL-1β only. The levels of H3 mRNA in IL-1β-stimulated cells and cells treated with IL-1β and IP6 revealed no statistically significant differences after 3 h. IP6 at 1 and 2.5 mM enhanced IL1β-stimulated transcription of H3 gene after 6 h. Subsequently (12 h), the combination of IP6 and IL-1β decreased H3 mRNA level compared to IL1β-treated cells. In conclusion, pro-inflammatory cytokine IL-1β up-regulates CCND1 and histone H3 mRNAs expression in Caco-2 cells. These results suggest that the ability of IP6 to inhibit colon cancer cells proliferation may be mediated through downregulation of genes encoding cyclin D1 and histone H3 at the mRNA level.

Keywords: IP6, proliferation, histone H3; cyclin D1; colon cancer; mRNA quantification

The loss of cell proliferation control is one of the major features of malignancy. Proliferation rate serves as a useful prognostic factor for tumor cells survival and response to treatment with anticancer drugs (1) and it can be expressed as the fraction of cells residing in the S-phase (2). There are a few methods for detecting proliferating cells including flow cytometry, immunostaining of cell cycle-restricted proteins like proliferating cell nuclear antigen (PCNA) and Ki-67, and incorporation of thymidine analogues or bromodeoxyuridine (BrdU) into DNA (1). Proliferating cells can also be distinguished from postmitotic cells by the detection of RNAs expressed differentially during cell cycle (3). Cyclin D1 and histone H3 mRNA genes are the ones expressed in a cell-cycle related pattern.

Histone H3 is a part of the nucleosome, the fundamental repeating unit of chromatin (4). There are two classes of histone H3 proteins – first that is produced concomitantly with S-phase DNA synthesis and the second produced independently of DNA synthesis. Genes encoding the first class of H3 are called canonical H3 genes. Their products are either H3.1 or H3.2 protein variants, which harbor cysteine or serine at position 96. Cells residing outside the S-phase also need newly synthesized histones, which involves production of the H3.3 variant (5). Histone mRNA metabolism is tightly coupled to cell cycle progression. As cells progress from G1 to S-phase, the rate of histone gene transcription and histone pre-mRNA processing increases resulting in a 35-fold increase in histone mRNA level. After the S-phase histone mRNA level rapidly decrease (6). In several studies it was found out histone H3 mRNA to be a reliable and accurate marker of S-phase cells in both normal and tumor human tissues (1, 2, 7–11).

Cyclin D1 (CCND1), forming complexes with cyclin dependent kinases CDK4 and CDK6, functions as a regulator of G1 to S-phase progression.

* Corresponding author: e-mail: mkapral@sum.edu.pl; phone: +48 32 364 10 72

Control of this stage is a crucial checkpoint for the cell fate (12). CCND1 accumulation begins in G1-phase and acquires the highest level during G1/S-phase transition. In the S-phase CCND1 nuclear level rapidly declines due to its increased turnover and relocation to the cytoplasm (13). Induction of its expression results from stimulatory influence of extracellular mitogens, such as growth factors, cytokines and hormones (14). Thus, cyclin D1 overexpression and nuclear accumulation is implicated in many cancers (11, 15, 16) and is associated with increased cell proliferation (17).

Chronic inflammation has been linked to the pathogenesis of tumors in up to 15% of human cancers (18). One of the most prevalent relationship between inflammation and cancer is inflammatory bowel disease associated colorectal cancer. Tumor growth is contributed by various cytokines and chemokines produced by immune cells (19). Interleukin-1β plays a central role in the pathogenesis of inflammatory bowel disease and experimental intestinal inflammation. It is upregulated in many cancer types, as it has strong impact on the expression of growth and transcription factors, proliferative and angiogenic proteins and adhesion molecules (18).

Several naturally occurring compounds are known to have antiproliferative effects on cancer cells. One of them is inositol hexaphosphate, an abundant intrinsic component of high fiber diets, such as cereals, grains, seeds and legumes (20). Its antiproliferative action was established in *in vitro* and *in vivo* models of various neoplasms such as colon, prostate, pancreatic and breast cancer (21–26).

The aim of the present study was to examine the influence of IP6 on the expression of genes coding for proliferation markers, i.e., CCND1 and histone H3 in IL-1β-stimulated intestinal cell line Caco-2.

EXPERIMENTAL

Cell culture and cell stimulation assays

The Caco-2 human intestinal epithelial cells (DSMZ, Braunschweig, Germany) were cultured in RPMI 1640 medium (Sigma Aldrich) supplemented with 10% fetal bovine serum (GibcoBRL), 100 U/mL penicillin and 100 μg/mL streptomycin (both from Sigma Aldrich) and 10 mM HEPES (GibcoBRL). They were maintained at 37°C in a 5% CO_2 atmosphere. Cells were seeded into six-well plates (Nunc International) at a density of 4.5×10^5 per well and allowed to grow to confluency in 3 mL of medium. After three days, the culture media were changed to media with 2% FBS and cells were then cultured for 2 days. They were then stimulated with 1 ng/mL IL-1β (Sigma Aldrich) for 30 min. Afterwards, cells were treated with 1 and 2.5 mM IP6 as dipotassium salt (dissolved in distilled water and adjusted to pH 7.4) (Sigma Aldrich) for 3, 6 and 12 h. In separate cultures, cells were incubated with 1 ng/mL IL-1β for the indicated times. The untreated Caco-2 cells were used as the control.

Real-time RT-QPCR assay

Total RNA was extracted from cells using TRIzol reagent (Invitrogen) and was treated with DNase-I (Fermentas) to remove DNA contamination. RNA concentration was determined spectrophotometrically on the basis of absorbance values at a wavelength of 260 nm using a GeneQuant pro spectrophotometer (Amersham Biosciences). The expression of genes encoding CCND1 and histone H3 was detected using a real-time RT-QPCR technique with a SYBR Green chemistry (SYBR Green Quantitect RT-PCR Kit, Qiagen) and Opticon™ DNA Engine Continuous Fluorescence detector (MJ Research). Oligonucleotide primers specific for CCND1 and H3 were previously described (11). The thermal profile for one-step RT-PCR was as follows: 50°C for 30 min for reverse transcription and 95°C for 15 min followed by 45 cycles at 94°C for 15 s, 55°C for 30 s and 72°C for 45 s for amplification. Specificity of RT-PCR reaction was confirmed by determining the characteristic temperature of melting for all amplimers. Each gene analysis was performed in triplicate. The mRNA copy numbers of examined genes were determined on the basis of the commercially available standard of β-actin (TaqMan DNA Template Reagent Kit, Applied Biosystems). The obtained results of mRNA copy number were recalculated per mg of total RNA. The expression level of genes in cultured cells was expressed as the fold change relative to the control. The value of fold change > 1 reflects increased expression of the target gene, and a value of fold change < 1 points to a decrease in the gene expression.

Statistical analysis

The results were collected from three independent experiments. Statistical analysis was performed with the use of Statistica PL 10.0 software. All the results are expressed as the means ± SD. Comparison of two data sets was performed by unpaired t-test. Comparison of more than two data sets was performed by one-way ANOVA followed

by *post-hoc* Tukey test. Significance level was assumed for $p < 0.05$.

RESULTS

Stimulation of Caco-2 with 1 ng/mL of IL-1β for 3–12 h resulted in an upregulation of CCND1 (Fig. 1A) and histone H3 (Fig. 2A) genes as compared with untreated cells ($p < 0.05$). In a time course experiment, the level of CCND1 mRNA in IL-1β-stimulated cultures remained relatively constant ($p = 0.171$) (Fig. 1A). Comparative analysis of H3 transcripts revealed statistically significantly diverse amounts in the cells treated with IL-1β for 3,

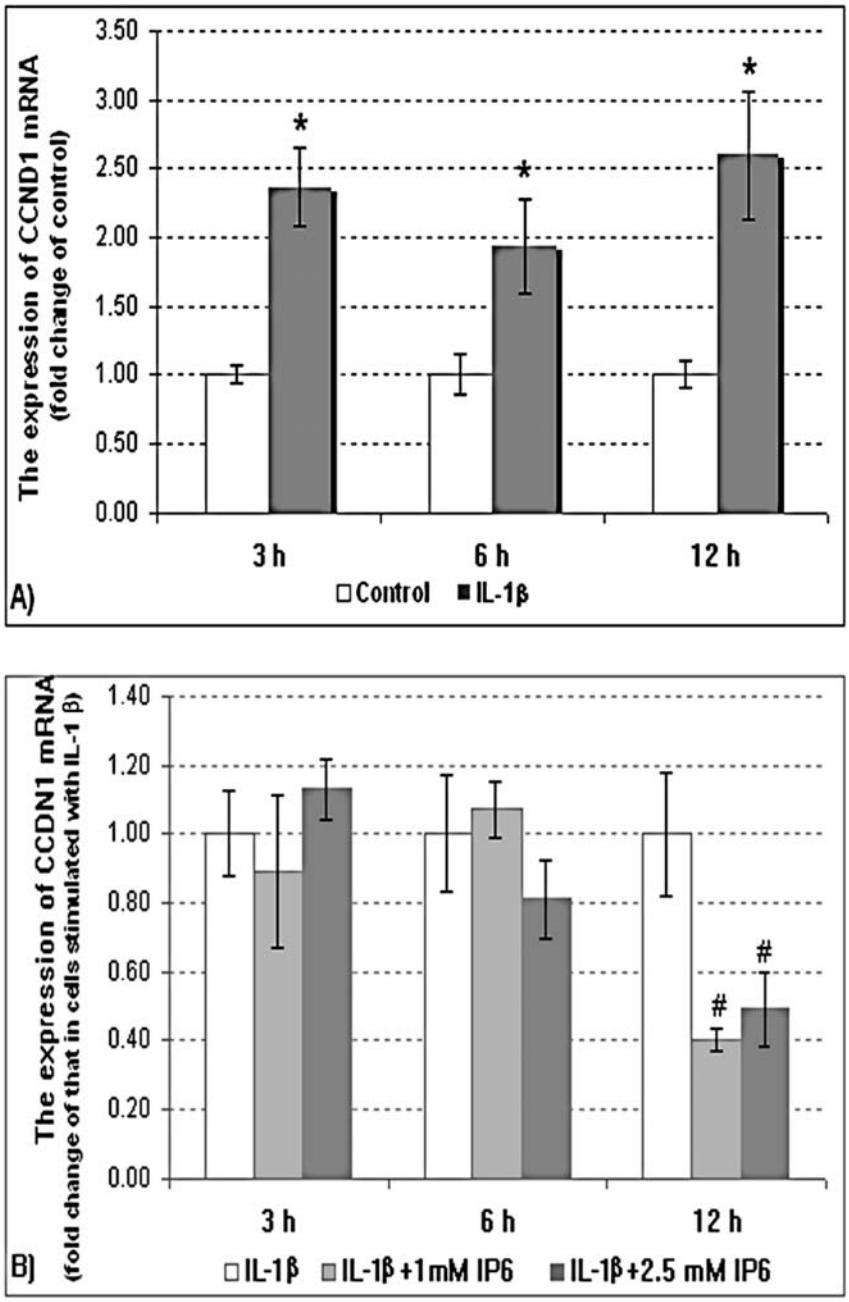

Figure 1. Expression of CCND1 gene in Caco-2 cells as determined by real-time RT-PCR. Changes in CCND1 mRNA expression in Caco-2 cells after treatment with A) IL-1β and B) IL-1β and 1 and 2,5 mM IP6 for 3, 6 and 12 h. The results are presented as the mean ± SD of three separate experiments; *$p < 0.05$ *vs.* control Caco-2 cells; #$p < 0.05$ *vs.* IL-1β-stimulated cells)

6 and 12 h ($p = 0.022$) (Fig. 2A). The highest level of this gene expression was determined in 3 h lasting cultures and subsequently the quantities of H3 mRNA were down-regulated within 3–12 h.

IP6 had no influence on IL-1β-stimulated CCND1 expression for both 3 and 6 h ($p > 0.05$). After 12 h, statistically significant decrease in CCND1 mRNA was observed in cells exposed to IL-1β and IP6 (1 and 2.5 mM) in relation to cells treated with IL-1β only ($p < 0.05$) (Fig. 1B).

The levels of H3 mRNA in IL-1β-stimulated cells and cells treated with IL-1β and IP6 revealed

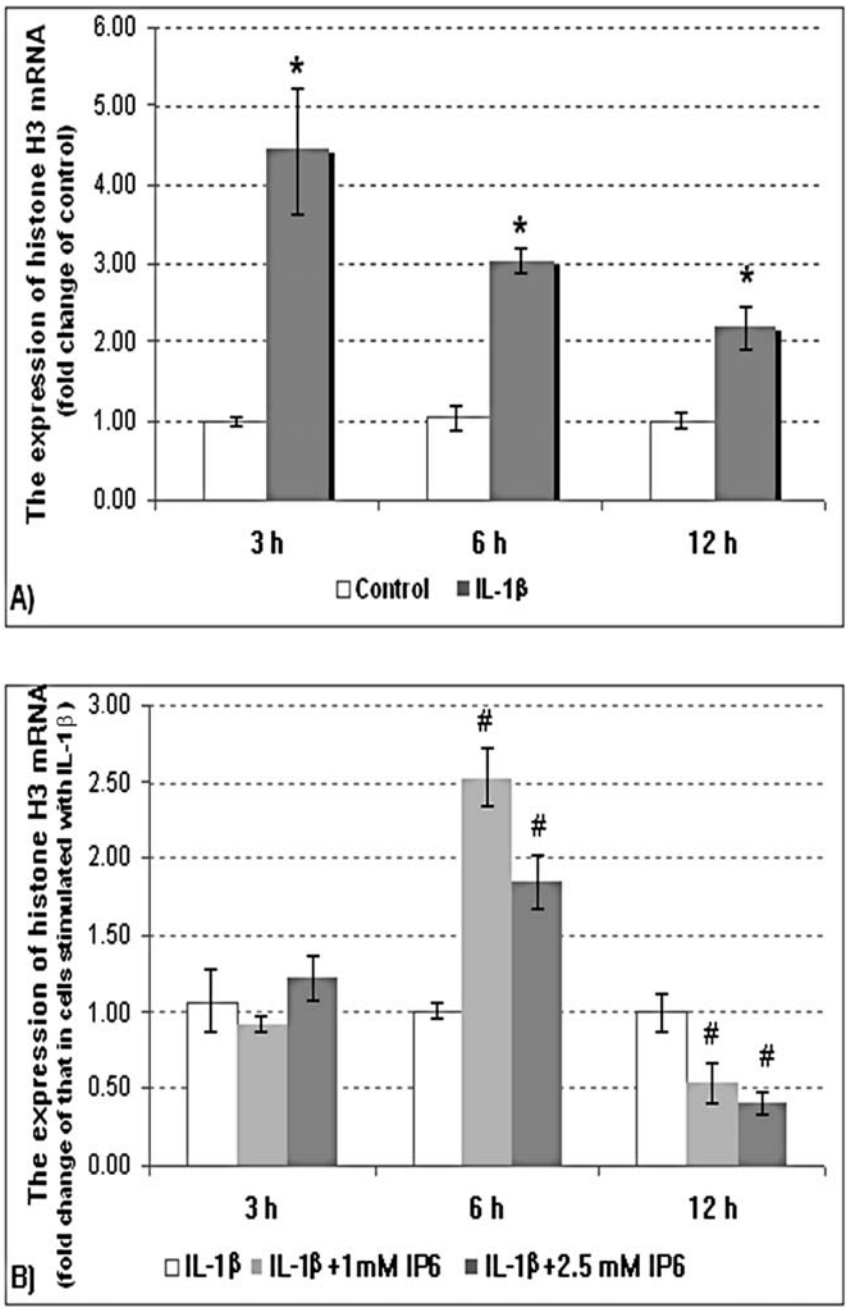

Figure 2. Expression of histone H3 gene in Caco-2 cells as determined by real-time RT-PCR. Changes in H3 mRNA expression in Caco-2 cells after treatment with A) IL-1β and B) IL-1β and 1 and 2,5 mM IP6 for 3, 6 and 12 h. The results are presented as the mean ± SD of three separate experiments; *$p < 0.05$ *vs.* control Caco-2 cells; #$p < 0.05$ *vs.* IL-1β-stimulated cells)

no statistically significant differences after 3 h. IP6 at a concentration of both 1 ($p < 0.001$) and 2.5 mM ($p = 0.003$) enhanced IL1β-stimulated transcription of H3 gene after 6 h and the stronger stimulatory effect was manifested by IP6 at lower concentration (1 mM). In longer-lasting cultures (12 h), transcriptional activity of this gene was suppressed about 2-fold by IP6 in a dose-independent manner in cells treated with IL-1β/IP6 as compared to those challenged with IL-1β alone ($p < 0.05$) (Fig. 2B).

DISCUSSION AND CONCLUSION

In the present study, the effect of IP6 on the expression of CCND1 and histone H3 genes in IL-1β-stimulated colon cancer cell line Caco-2 was evaluated. Colorectal cancer is one of the major causes of morbidity and mortality throughout the world, and its occurrence is frequently preceded by chronic inflammation. Several factors that are engaged in inflammatory response are also associated with increased proliferation of cells. Pro-inflammatory cytokines (INF-γ, TNF-α, IL-1 or IL-6) produced and secreted by macrophages, mast cells and neutrophils, may act as initiators and promoters of carcinogenesis by directly increasing the proliferation of epithelial cells (27). Our studies revealed that IL-1β induces transcription of both cyclin D1 and histone H3 genes in colon cancer cells. It is noteworthy that impact of this pro-inflammatory cytokine on histone H3 gene is most prominent for short-time incubation and diminishes in a time-dependent manner. The fact that both genes are known as proliferation markers indicates that IL-1 enhances cell proliferation. The exact mechanisms by which IL-1 promotes tumor growth is unclear, though it is known to contribute to activation of NF-κB and AP1 transcription factors (19). Both factors could be considered as mediators linking inflammation and cancer. These transcription factors have binding sequences in the promoter region of cyclin D1 gene (28). The results of the present study clearly support the connection between inflammation and enhanced proliferation.

According to Liao et al. (29), hyperproliferation under long-term chronic inflammation status is a critical condition in carcinogenesis and inhibition of uncontrolled cell proliferation is important for the prevention of carcinoma development. Moreover, they suggested that inhibition of both cell proliferation and inflammatory activity is crucial for the development of an efficient strategy to prevent colitis associated carcinogenesis. Inositol hexaphosphate is one of such agents that exhibit the immunomodulatory action and inhibit cell proliferation. Numerous reports indicate that anti-proliferative effect of IP6 is associated with cell growth inhibition and cell cycle progression halt, modulation of cell cycle regulators expression and cyclin-dependent kinases activation. Schröterová et al. (26) underline a more universal nature of IP6 since it has shown a similar inhibitory effect in many cell types including human colon cancer cell lines HT-29, SW-480, SW-620, breast cancer cell lines MCF-7 and MDA-MB231, prostate carcionoma cell lines PC-3, TRAMP-C1 and DU145.

El-Sherbiny et al. (21) found that in MCF-7 and MDA-MB 231 and HT-29 cells IP6 controls the progression of cells through the cycle by decreasing S-phase and arresting cells in the G0/G1-phase. Moreover, they observed a significant decrease in the expression of proliferation markers Ki-67 and PCNA in IP6-treated cells. The results of Singh et al. (22) indicated a significant dose- as well as time-dependent growth inhibition in IP6-treated prostate carcinoma DU145 cells, which was associated with an increase in G1 arrest. IP6 strongly enhanced the expression of cyclin-dependent kinase inhibitors (CDKIs), Cip1/P21 and Kip1/P27, and inhibited kinase activities associated with CDK 2, 4 and 6, and cyclin E and D1. Similarly, the growth inhibitory effect of IP6 and associated mechanisms have been investigated in human prostate carcinoma LNCaP cells. IP6 treatment of cells resulted in a strong growth inhibition and an increase in G1 cell population. IP6 caused an increase in CDKIs (P21 and P27) levels, together with a decrease in cyclin-dependent kinase (CDK4) and cyclin D1 protein levels (30). The immunohistochemical studies by Gu et al. (31) showed significant reduction of the expression of cyclin D1 and proliferating cell nuclear antigen by IP6 in prostate PC-3 cells. Vucenik et al. (23) hypothesized that IP6 modulates cell cycle by interacting with cytoplasmic signaling molecules based on the observation of blockage of proliferation of MCF-7 cells through an increase in the expression of anti-proliferative PKCδ. Furthermore, an *in vitro* administration of IP6 at doses of 0.5, 1.0, and 5.0 mM for 24 and 72 h to human pancreatic adenocarcinoma cells (MIA-PACA and PANC1) significantly reduced their proliferation (24). The cDNA microarray analysis demonstrated more than 2-fold down-expression of genes encoding cyclin H and PCNA in human leukaemic K562 cells treated with 5 mM IP6 for 24 h (32).

Several studies have also evaluated the role of IP6 in colon cancer cells proliferation. Tian et al.

(25) proved a potent inhibitory effect of IP6 on growth of HT-29 cells by modulating the expression of key cell cycle regulators. According to the authors, this compound reduced proliferation rate of cells and PCNA expression together with increasing the expression of P21 protein. Likewise, the results of Schröterová et al. (26) research indicated that IP6 at doses of 0.2–5 mM markedly inhibited DNA synthesis in cell lines HT-29, SW-480 and SW-620 derived from colorectal carcinoma. Our previous experiments, based on cellular DNA content determination, have also shown that IP6 at 5 mM inhibited the growth of colon cancer HT-29 and Caco-2 cells (33). Moreover, it stimulated P21 expression at the mRNA level in HT-29 cells, with the highest increase in P21 mRNA occurring at 24 h (34).

Currently, we investigated the influence of IP6 at a concentration of 1 and 2.5 mM on the expression of cyclin D1 and histone H3 at the transcription level in proliferating Caco-2 cells under inflammatory conditions. The results indicated that IP6 altered the transcriptional activity of CCND1 and H3 genes in time-dependent manner. We observed that 6 h incubation of Caco-2 with IP6 enhanced the level of H3 mRNA stimulated by IL-1β. This was inversely correlated with IP6 concentration. The longer treatment times with IP6 (12 h), independently of its concentration caused significant down-regulation in the expression of both CCND1 and histone H3 genes.

These results confirm previously published by us and others data that IP6, a dietary agent, possesses anti-proliferative efficacy against many cancer cell types including colon cancer cells. Based on these studies it may be concluded that the ability of IP6 to inhibit colon cancer cells proliferation may be mediated through down-regulation of genes encoding cyclin D1 and histone H3 at the mRNA level. Suppressive effect of IP6 on the CCND1 and histone H3 expression may be associated with cell arrest in G1-phase, decreasing the amount of cells in S-phase of the cell cycle and DNA content.

Acknowledgment

This work was supported by grant KNW-1-003/K/4/0 from the Medical University of Silesia (Katowice, Poland).

REFERENCES

1. Gown A.M., Jiang J.J., Matles H., Skelly M., Goodpaster T., Cass L., Reshatof M. et al.: J. Histochem. Cytochem. 44, 221 (1996).
2. Kotelnikov V., Cass L., Coon J.S., Spaulding D., Preisler D.: Clin. Cancer Res. 3, 669 (1997).
3. Barton K.M., Levine E.M.: Dev. Dynam. 237, 672 (2008).
4. Tachiwana H., Osakabe A., Shiga T., Miya Y., Kimura H., Kagawa W., Kurumizaka H.: Acta Cryst. 67, 578 (2011).
5. Ederveen T.H., Mandemaker I.K., Logie C.: Biochim. Biophys. Acta 1809, 577 (2011).
6. Marzluff W.F., Duronio R.J.: Curr. Opin. Cell Biol. 14, 692 (2002).
7. Orchel J., Slowinski J., Mazurek U., Wilczok T.: Biochim. Biophys. Acta 1689, 42 (2004).
8. Rautiainen E., Haapasalo H., Sallinen P., Rantala I., Helen P., Helin H.: Histopathology 32, 43 (1998).
9. Muskhelishvili L., Latendresse J.R., Kodell R.L., Henderson E.B.: J. Histochem. Cytochem. 51, 1681 (2003).
10. Sakamoto R., Nitta T., Kamikawa Y., Sugihara K., Hasui K., Tsuyama S., Murata F.: Med. Electron Microsc. 37, 52 (2004).
11. Kapral M., Strzalka-Mrozik B., Kowalczyk M., Paluch J., Gola J., Gierek T., Weglarz L.: Eur. Arch. Otorhinolaryngol. 268, 709 (2011).
12. Tsatsanis C., Spandidos D.A.: Int. J. Mol. Med. 5, 583 (2000).
13. Alao J.P.: Mol. Cancer 6, 24 (2007).
14. Assoian R.K., Klein E.A.: Trends Cell Biol. 18, 347 (2008).
15. Kim J.K., Diehl A.: J. Cell. Physiol. 220, 292 (2009).
16. Liu G., Luo Q., Xiong B., Pan C., Yin P., Liao H., Zhuang W., Gao H.: World J. Gastroenterol. 14, 7199 (2008).
17. Guller M., Toualbi-Abed K., Legrand A., Michel L., Mauviel A., Bernau D., Daniel F.: World J. Gastroenterol. 14, 6339 (2008).
18. Lewis A.M., Varghese S., Xu H., Alexander H.R.: J. Transl. Med. 4, 48 (2006)
19. Hu B., Elinav E., Flavell R.A.: Cell Cycle 10, 1936 (2011)
20. Matejuk A., Shamsuddin A.: Curr. Cancer Ther. Rev. 6, 1 (2010).
21. El-Sherbiny Y.M., Cox M.C., Ismail Z.A., Shamsuddin A.M., Vucenik I.: Anticancer Res. 21, 2393 (2001).
22. Singh R.P., Agarwal C., Agarwal R.: Carcinogenesis 24, 555 (2003).
23. Vucenik I., Ramakrishna G., Tantivejkul K., Anderson L.M., Ramljak D.: Breast Cancer Res. Treat. 91, 35 (2005).
24. Somasundar P., Riggs D.R., Jackson B.J., Cunningham C., Vona-Davis L., McFadden D.W.: J. Surg. Res. 126, 199 (2005).

25. Tian Y., Song Y.: World J. Gastroenterol. 12, 4137 (2006).
26. Schröterová L., Hasková P., Rudolf E., Cervinka M.: Oncol. Rep. 23, 787 (2010).
27. Eiro N., Vizoso F.J.: World J. Gastrointest. Surg. 4, 62 (2012).
28. Takahashi-Yanaga F., Sasaguri T.: Cell. Signal. 20, 581 (2008).
29. Liao J., Seril D.N., Yang A.L., Lu G.G., Yang G.Y.: Carcinogenesis 28, 446 (2007).
30. Agarwal C., Dhanalakshmi S., Singh R.P., Agarwal R..: Neoplasia 6, 646 (2004).
31. Gu M., Roy S., Raina K., Agarwal C., Agarwal R.: Cancer Res. 69, 9465 (2009).
32. Deliliers G.L., Servida F., Fracchiolla N.S., Ricci C., Borsotti C., Colombo G., Soligo D.: Br. J. Haematol. 117, 577 (2002).
33. Węglarz L., Parfiniewicz B., Orchel A., Dzierzewicz Z.: Acta Pol. Pharm. Drug Res. 63, 443 (2006).
34. Węglarz L., Molin I., Orchel A., Parfiniewicz B., Dzierżewicz Z.: Acta Biochim. Pol. 53, 349 (2006).

Acta Poloniae Pharmaceutica – Drug Research, Vol. 71 No. 6 pp. 994–1003, 2014 ISSN 0001-6837
Polish Pharmaceutical Society

SYNTHESIS OF CHIRAL TRIAZINE COUPLING REAGENTS BASED ON ESTERS OF *N*-ALKYLPROLINE AND THEIR APPLICATION IN THE ENANTIOSELECTIVE INCORPORATION OF D OR L AMINO ACID RESIDUE DIRECTLY FROM RACEMIC SUBSTRATE

KATARZYNA KASPEROWICZ-FRANKOWSKA, ANNA GZIK, MICHAŁ DZIEMIDKIEWICZ, BEATA KOLESIŃSKA and ZBIGNIEW J. KAMIŃSKI*

Institute of Organic Chemistry, Lodz University of Technology,
Żeromskiego 116, 90-924 Łódź, Poland

Abstract: Esters of *N*-methylproline and *N*-allylproline were prepared and used as component for synthesis of chiral triazine based coupling reagents. *N*-Triazinylammonium tetrafluoroborate obtained from methylester of L-*N*-methylproline, 2-chloro-4,6-dimethozxy-1,3,5-triazine and tetrafluoroboric acid in the coupling of *rac*-Z-Ala-OH with glycine methylester preferred formation of D-Z-AlaGly-OMe with L/D ratio 21/79. Coupling reagent prepared from D enantiomer of *N*-methylproline gave L-Z-AlaGly-OMe with L/D ratio 75/25.

Keywords: enantioselective condensation, 2-chloro-4,6-dimethoxy-1,3,5-triazine, 2,4-dichloro-6-methoxy-1,3,5-triazine, peptide synthesis

The majority of the biomolecules which are crucial for living systems are chiral e.g., amino acids, proteins, nucleic acids, sugars, isoprenoids etc. The interesting feature is that in the Nature in most cases there is existing only one of the two possible enantiomeric forms. Therefore, in the enantiospecific environment of biomolecules, for many of therapeutics, their enantiomers can provide diversified selectivity for their biological targets, different therapeutic indices, and/or pharmacokinetics. There are no doubts that the stereoselective pharmacokinetics and pharmacodynamics of chiral drugs has wide ranging implications in practical therapeutics, health care and pharmacy. According to the guidelines on the development of chiral drugs, presented by European Union (EU) in 1994 in a document entitled Investigation of Chiral Active Substances (1), it is recommended to recognize the occurrence of chirality in new drugs, attempts to separate the stereoisomers, assessed the contribution of the various stereoisomers to the activity of interest and finally made a rational selection of the stereoisomeric form that is proposed for marketing (2).

Even more complex relations are observed between living system and diastereomeric pharmaceutically active compounds (3). For the peptides, peptoids or other complex molecules prepared by condensation of a number of the chiral building blocks, the accurate composition of stereochemistry of all components is crucial factor determining activity, resistance to enzymatic degradation and all other pharmacological features and attributes. Therefore, ready access to a whole range of chiral building blocks is essential to acquire full profits from the systematic exploration of a structural diversity of such molecules.

In the search based on application methods of combinatorial chemistry and high throughput screening, the classical approach based on asymmetric synthesis or resolution of a racemic precursor seems to be non-optimal because most substrates are used in small amounts, in single experiments only and usually they are discarded after a preliminary selection procedure as not promising. More advantageous and less time-consuming would be evaluated an alternative approach based on the enantiodifferentiating transformation of racemic substrates, which are usually more easily available than enantiomerically pure equivalents. Such an approach would be considered particularly attractive for incorporation of non coded chiral amino acids into the peptide chain.

* Corresponding author: e-mail: zbigniew.kaminski@p.lodz.pl; phone: 48 42 6313224

Although several chiral coupling reagents and chiral acylation catalysts have been proposed for the enantioselective acylation and synthesis of enantiomerically enriched peptides directly from racemic substrates, including optically active 4-dimethylaminopyridine (DMAP) analogues (4), benzotetramisol (5), *N*-methylimidazole (6), *N*-hydroxysuccinimide (7), diacylamines (8), tertiary amines (9), phosphines (10) and others (11), until recently, none of the proposed enantioselective coupling methods has been accepted for peptide synthesis because of the unpredictable results of coupling experiments including configuration, enantiomeric purity, optimal coupling conditions and the yield of the final product. The unpredictability of the enantioselective synthesis of peptide bonds results from the complex mechanism of this process, consisting of two subsequent stages, e.g., activation of carboxylic group, followed by aminolysis proceeding *via* two independent tetrahedral intermediates and four independent transition states with additional stereogenic centers temporary formed on the carbon atom of the activated carboxylic group.

EXPERIMENTAL

Thin layer chromatography experiments (TLC) were carried out on silica gel (Merck; 60 Å F254), and spots were located with: UV light (254 and 366 nm), 1% ethanolic 4-(4-nitrobenzyl)pyridine (NBP) or, in the case of secondary amines, with a mixture of 2% solution of acetaldehyde in DMF and 2% solution of chloranil in DMF. Derivatives of *N*-methylproline were visualized by spraying plates with 1% $KMnO_4$ in 2% aqueous K_2CO_3 solution.

Analytical RP-HPLC was performed on a Waters 600S HPLC system (Waters 2489 UV/VIS detector, Waters 616 pump, Waters 717 plus autosampler, HPLC manager software from Chromax) using a Vydac C18 column (25 cm × 4.6 mm, 5 µm; Sigma). HPLC was performed with a gradient of 0.1% TFA in H_2O (A) and 0.08% trifluoroacetic acid in acetonitrile (B), at a flow rate of 1 mL/min with UV detection at 220 nm, t_R in min. Preparative column chromatography were performed on silica gel 60, 240–600 mesh (Merck).

LC/MS spectra were recorded on a Dionex UltiMate 3000. IR spectra were recorded in KBr pellets or film on a Bruker ALPHA spectrometer or a PerkinElmer Spectrum 100 apparatus. ^{1}H-NMR and ^{13}C-NMR, spectra were recorded on a Bruker Avance DPX 250 (250 MHz) and Varian (300 MHz) spectrometers. Chemical shifts (ppm) are relative to TMS used as an internal standard. Multiplicities are marked as s = singlet, d = doublet, t = triplet, q = quartet, qu = quintet, m = multiplet. Melting points were determined using a Büchi apparatus, model 510.

Synthesis of L-*N*-methylproline (1). Typical procedure

The vigorously stirred suspension of zinc dust (6.50 g; 100 mmol), L-proline (5.57 g; 50 mmol) and NaH_2PO_4 (11.90 g; 100 mmol) in water (22 mL) was treated with 35% aq. formaldehyde (2.10 mL). Stirring was continued for 48 h at 30°C. The suspension was discarded, the filtrate was neutralized with 2 M aq. ammonia to pH 8, concentrated under vacuum, the solid residue was dissolved in small amount of water and lyophilized. Dry residue was extracted with hot mixture of benzene-ethanol (1 : 1, v/v). Collected extracts were evaporated to dryness and then recrystallized from the mixture methanol/ether affording L-*N*-methylproline (**1**) (5.68 g; yield 88%) as white crystals m.p. 115–120°C, lit. (12) m.p. 115–116°C. IR (film, cm^{-1}): 3008–2978 (CH), 1738 (C=O), 1467 (CH), 1353 (CH), 1243 (C-N). ^{1}H-NMR (250 MHz, D_2O, δ, ppm): 1.9–2.1 (m, 4H, CH_2-CH_2-CH-), 2.5–2.7 (m, 1H, CH_2-N-), 2.8 (s, 3H, CH_3-N-), 3.0–3.2 (m, 1H, CH_2-N-), 3.6–3.7 (m, 1H, -CH-CO-).

L-*N*-Methylproline *n*-propyl ester hydrochloride (3b). General procedure

Stirred suspension of L-*N*-methylproline (6.45 g; 50 mmol) in *n*-propanol (100 mL) was cooled to –50°C and thionyl chloride (6 mL; 78 mmol) was added dropwise in such a rate to maintain the temperature below –45°C. Then, the solution was allowed to warm up and stirring was continued for 20 h at room temperature followed by boiling under reflux for additional 5 h. Clear solution was concentrated under vacuum and the solid residue was twice dissolved in dichloromethane (50 mL), and concentrated to oily residue. The residue was dissolved in dioxane and lyophilized yielding L-*N*-methylproline *n*-propyl ester hydrochloride (**3b**) as white plates (8.3 g; yield 86%). IR (film, cm^{-1}): 2957 (CH), 2849 (CH), 1737 (C=O), 1311 (C-O), 1231 (C-N). ^{1}H-NMR (250 MHz, CD_3OH, δ, ppm): 0.9–1.0 (m, 3H, CH_3-CH_2-), 1.6–1.8 (m, 2H, -CH_2-CH_3), 1.9–2.3 (m, 4H, -CH_2-CH_2-CH-), 2.5–2.7 (m, 1H, CH_2-N-), 2.9 (s, 3H, CH_3-N-), 3.2–3.3 (m, 1H, CH_2-N-), 3.6–3.8 (m, 1H, -CH-CO-), 4.2–4.4 (m, 2H, -O-CH_2-).

L-*N*-Methylproline methyl ester hydrochloride (3a)

L-*N*-Methylproline methyl ester hydrochloride was prepared according to the general procedure described above from L-*N*-methylproline (6.45 g;

50 mmol), methanol (100 mL) and thionyl chloride (6 mL; 78 mmol). The isolated product was dissolved in dioxane and lyophilized yielding L-*N*-methylproline methyl ester hydrochloride (**3a**) as white plates (8.12 g; yield 90%). IR (film, cm^{-1}): 2957 (CH), 2849 (CH), 1737 (C=O), 1311 (C-O), 1231 (C-N). ^{1}H-NMR (250 MHz, D_2O, δ, ppm): 1.90–2.20 (m, 4H, -CH_2-CH_2-CH-), 2.45–2.55 (m, 1H, CH_2-N-), 2.9 (s, 3H, CH_3-N-), 3.10–3.20 (m, 1H, CH_2-N-), 3.70 (s, 3H, O-CH_3), 4.20–4.30 (m, 1H, -CH-CO-).

Synthesis of L-proline *n*-propyl ester hydrochloride (H-Pro-OC_3H_7 × HCl) (2d). Typical procedure

A vigorously stirred suspension of L-proline (5.76 g; 50 mmol) in *n*-propanol (20 mL) was cooled to 0°C and thionyl chloride (6 mL; 78 mmol) was added dropwise in such a rate to maintain temperature below 5°C. The stirring was continued at room temp. for 21 h, then concentrated under reduced pressure. The oily residue was dissolved again with *n*-propanol (10 mL) and evaporated under reduced pressure. The treatment with *n*-propanol and evaporation was repeated twice to solidify the residue. After drying to the constant weight in vacuum desiccator under P_2O_5, proline *n*-propyl ester hydrochloride (**2d**) (9.29 g, 96% yield) was obtained as a white solid. IR (film, cm^{-1}): 3382 (NH), 2971–2881 (CH), 1732 (C=O), 1232 (C-O), 1102 (C-N). ^{1}H-NMR (250 MHz, $CDCl_3$, δ, ppm): 0.9–1.0 (m, 3H, CH_3-), 1.6–1.65 (m, 2H, -CH_2-CH_2-CH_3), 1.7–1.8 (m, 2H, -CH_2-CH_2-), 2.1–2.2 (m, 1H, -CH_2-CH_2-), 2.4–2.5 (m, 1H, -CH_2-CH_2-), 3.5–3.7 (m, 2H, -CH_2-CH_2-), 4.1–4.3 (m, 2H, -CH_2-CH_2-CH_3), 4.4–4.5 (m, 1H, -CH_2-CH-C-O).

Synthesis of L-*N*-allylproline methyl ester (3c). Typical procedure

To the stirred solution of proline methyl ester hydrochloride (6.45 g; 50 mmol) in DMF (20 mL) finely grounded anhydrous potassium carbonate (27.64 g; 200 mmol) was added and then allyl bromide was added dropwise (4.25 mL; 50 mmol). Stirring was continued at room temperature for 4 days. The slurry was filtered. The filtrate was diluted with water (100 mL) and extracted with ethyl acetate (4 × 50 mL). The filtrate cake was hashed with ethyl acetate (30 mL). Washing was combined with ethyl acetate extract, dried with anhydrous $MgSO_4$, filtered and concentrated under reduced pressure. The residue (7.5 g) was poured on silica gel column and eluted with hexane – ethyl acetate (8 : 1, v/v) to isolate first fraction (1.21 g; R_f = 0.46 in hexane : ethyl acetate), then eluted with hexane – ethyl acetate (4 : 1, v/v) to isolate *N*-allylproline methyl ester (**3c**) (3.14 g; 37% yield). R_f = 0.41 hexane : ethyl acetate (6 : 1, v/v). IR (film, cm^{-1}): 3078, 2951, 2876, 2796, 1731, 1681, 1643, 1435, 1420, 1356, 1275, 1195, 1167, 1086, 1038, 995, 917, 760, 706, 670, 606, 557, 442, 422. ^{1}H-NMR (250 MHz, $CDCl_3$, δ, ppm): 1.68 (m, 3H, -CH_2-CH_2-CH_2-), 2.10–2.15 (m, 1H, -CH_2-CH_2-CH-), 2.28–2.38 (m, 1H, -CH_2-CH_2-CH-), 3.02–3.14 (m, 3H, =CH-CH_2-N- + -CH_2-CH_2-CH_2-), 3.22–3.29 (m, 1H,-N-CH-CH-), 3.65 (s, 3H, -$COCH_3$), 5.00–5.16 (m, 2H, CH_2=CH-), 5.78–5.94 (m, 1H, CH_2=CH-). LC/MS: 170.0878 ([M + H]$^+$, $C_9H_{16}NO_2^+$, 170.23).

Synthesis of L-*N*-allylproline *n*-propyl ester (3d)

In the synthesis there were used proline *n*-propyl ester hydrochloride (10.08 g; 52 mmol) DMF (20 mL), anhydrous potassium carbonate (29.17 g; 211 mmol) and allyl bromide (4.50 mL; 52 mmol). Product was isolated by column chromatography on silica gel. The first fraction (0.623, R_f = 0.58) was eluted with hexane : ethyl acetate (10 : 1, v/v). *N*-Allylproline *n*-propyl ester (**3d**) (6.13 g, yield 78%). R_f = 0.28 (hexane : ethyl acetate 6 : 1, v/v) was eluted with hexane : ethyl acetate (10 : 1, v/v) as the second fraction. ^{1}H-NMR (250 MHz, $CDCl_3$, δ, ppm): 0.93 (t, 3H, J_1 = 7.48 Hz, CH_3-CH_2-), 1.59–1.73 (m, 2H, -CH_2-CH_2-CH_3), 1.8–2.02 (m, 3H, -CH_2-CH_2-CH-), 2.12–2.23 (m, 1H, -CH_2-CH_2-CH-), 2.44–2.53 (m, 1H, -CH_2-CH_2-CH-), 3.13–3.28 (m, 3H, -CH_2-CH_2-N- + -CH_2-CH_2-), 3.34–3.42 (m, 1H, -CH_2-CH_2-CH-), 4.10 (t, 2H, J_1 = 6.79 Hz, -O-CH_2-CH_2-), 5.08–5.23 (m, 2H, CH_2-CH=), 5.87–6.03 (m 1H, -CH_2=CH). IR (film, cm^{-1}): 3079, 2967, 2878, 2797, 1728, 1686, 1643, 1460, 1419, 1392, 1378, 1355, 1269, 1170, 1086, 1059, 1039, 992, 916, 766, 707, 659, 558, 424. LC-MS: 198.2 ([M + H]$^+$, $C_{11}H_{20}NO_2^+$, 198.28).

Synthesis of L-*N*-allylproline allyl ester (3e)

To the stirred solution of L-proline (11.50 g; 100 mmol) in DMF (40 mL) finely grounded anhydrous potassium carbonate (41.46 g; 300 mmol) was added and then allyl bromide was added dropwise (24 mL; 300 mmol). Stirring was continued at room temperature until all proline was consumed. The slurry was filtered. The filtrate was diluted with water (150 mL) and extracted with ethyl acetate (5 × 50 mL). The filtrate cake was hashed with ethyl acetate (50 mL). Washing was combined with ethyl acetate extract, dried with anhydrous $MgSO_4$, filtered and concentrated under reduced pressure. The

oily residue (18.31 g) was poured on silica gel column and eluted with hexane : ethyl acetate (8 : 1, v/v) to isolate first fraction (13.35 g) R_f = 0.27 in hexane : ethyl acetate (8 : 1, v/v), then eluted with hexane : ethyl acetate (4 : 1, v/v) to isolate *N*-allylproline allyl ester (**3e**) (3.87g, yield 21%) R_f = 0.35 (hexane : ethyl acetate, 4 : 1, v/v) as colorless oil. ^{1}H-NMR (250 MHz, $CDCl_3$, δ, ppm): 1.74–2.03 (m, 3H, -CH_2-CH_2-CH_2-), 2.10–2.19 (m, 1H, -CH_2-CH_2-CH-), 2.35–2.45 (m, 1H, =CH-CH_2-N-), 3.08–3.23 (m, 3H, CH_2=CH- + -CH_2-CH-), 3.3–3.38 (m, 1H, -CH_2-CH-), 4.6–4.63 (m, 2H, -O-CH_2-CH), 5.06–5.35 (m, 4H, CH_2=CH-CH_2-N), 5.84 (m, 2H, CH_2=CH-CH_2-N + CH_2=CH-CH_2-O). IR (film, cm^{-1}): 3080, 2950, 2876, 2797, 2026, 1730, 1680, 1646, 1443, 1419, 1384, 1356, 1269, 1166, 1087, 1035, 989, 918, 768, 717, 658, 554, 488. LC-MS: 196.1 ([M + H]$^+$, $C_{11}H_{18}NO_2^+$, 196.26).

Condensations of 4-methoxybenzoic acid (6) with 4-toluidine (8) mediated by CDMT (4) and *n*-propyl ester of L-*N*-allylproline 3d. Typical procedure

CDMT (0.044 g; 0.25 mmol) was added to the stirred and cooled to 0°C solution of L-*N*-allylproline *n*-propyl ester (0.049 g; 0.25 mmol) in acetonitrile (2 mL). Progress of activation was monitored by TLC (mobile phase: dichloromethane; visualization by spraying plate with 0.5% solution of 4,4'-nitrobenzylpyridine in ethanol). After formation of red spot R_f = 0, *p*-methoxybenzoic acid (0.038 g; 0.25 mmol) and DIPEA (45 µL; 0.25 mmol) were added. Stirring was continued until TLC confirmed disappearing of red spot R_f = 0.6 characteristic for CDMT. Then *p*-toluidine (0.026 g; 0.25 mmol) was added and stirring was continued for additional 24 h at room temperature and solvent was removed under reduced pressure. Dry solid residue was dissolved in dichloromethane (15 mL) and washed successively with water (15 mL), 1 M aq. HCl (15 mL), water (15 mL), 1 M aq. sodium bicarbonate (15 mL) and again with water (15 mL). Organic layer was dried with magnesium sulfate, filtered and the filtrate was concentrated to dryness. White solid residue was dried to constant mass in vacuum desiccator yielding **9** (0.055 g; yield 91.2%). M.p. = 140°C, lit. (13) m.p. = 150°C. ^{1}H-NMR (250 MHz, $CDCl_3$, δ, ppm): 2.34 (s, 3H, CH_3-), 3.87 (s, 3H, -OCH_3), 7.1 (dd, 4H, -C_6H_4, J_1 = 8.23 Hz, J_2 = 48.96 Hz), 7.65 (dd, 4H, -C_6H_4, J_1 = 8.93 Hz, J_2 = 48.96 Hz). IR (film, cm^{-1}): 3339, 3080, 3006, 2962, 2917, 2840, 1901, 1746, 1707, 1650, 1595, 1578, 1514, 1499, 1464, 1444, 1402, 1378, 1321, 1307, 1295, 1237, 1178, 1122, 1101, 1030, 967, 936, 898, 837, 811, 792, 760, 653, 639, 626, 610, 541, 504, 430, 399.

Synthesis of L-5b (DMT/L-*N*-MePro-OMe/BF_4^-) from L-*N*-methylproline methyl ester tetrafluoroborate and CDMT

To the solution of L-*N*-methylproline methyl ester (5.50 g; 39 mmol) in dichloromethane (50 mL) equimolar amount of HBF_4 in ether (4.02 mL; 39 mmol) was added. Solvent was removed under reduced pressure yielding quantitatively L-*N*-methylproline methyl ester tetrafluoroborate as white solid. Solid residue was dissolved in acetonitrile (100 mL), anhydrous $NaHCO_3$ (6.10 g; 72 mmol) and CDMT (6.30 g; 39 mmol) were added and suspension was vigorously stirred at room temperature until all CDMT was consumed as monitored by TLC. The suspension was filtered. The filter cake was washed several times with acetonitrile and combined filtrates were evaporated under reduced pressure affording **5b** (DMT/L-*N*-MePro-OMe/BF_4^-) (12.0 g, yield 83%) as pale oil. ^{1}H-NMR (250 MHz, CD_3CN, δ, ppm): = 1.77–1.81 (m, 4H, -CH_2-CH_2-), 3.01–3.33 (m, 2H, -N-CH_2-), 3.46–3.66 (m, 1H, -O-CH-), 3.70 (s, 3H, CH_3-N), 3.81 (s, 3H, CH_3O-), 3.96 (s, 6H, 2 × CH_3-O).

Synthesis of D-5b (DMT/D-*N*-MePro-OMe/BF_4^-) from D-*N*-methylproline methyl ester tetrafluoroborate and CDMT

The synthesis was performed according to general procedure (see above) from D-*N*-methylproline methyl ester (5.50 g; 39 mmol), dichloromethane (50 mL), HBF_4 in ether (4.02 mL; 39 mmol), acetonitrile (100 mL), anhydrous $NaHCO_3$ (6.10 g; 72 mmol) and CDMT (6.30 g; 39 mmol). Product **D-5b** (DMT/D-*N*-MePro-OMe/BF_4^-) (3.92 g, yield 88%) was obtained as yellow oil. Spectroscopic data identical as presented above for **L-5b.**

Synthesis of L-5d (DMT/L-*N*-MePro-OMe/ClO_4^-) from L-*N*-methylproline methyl ester, CDMT and silver perchlorate

To the vigorously stirred and cooled to 0°C solution of CDMT (0.840 g; 4.8 mmol) in acetonitrile (8 mL), the solution of L-*N*-allylproline allyl ester (0.936 g; 4.8 mmol) in acetonitrile (5 mL) and solution of silver perchlorate (0.995 g; 4.8 mmol) in acetonitrile (5 mL) were added dropwise. The reaction progress was monitored by TLC. After all CDMT was consumed (disappeared spot R_f = 0.6, mobile phase dichloromethane) a deposit of silver chloride was filtered off and the filtrate was concentrated to dryness under reduced pressure. Product **L-5d** (DMT/L-*N*-MePro-OMe/ClO_4^-) (0.437g, yield 21%) was obtained as solid, m.p. = 103°C. IR (film, cm^{-1}): 2965, 2877, 1573, 1551, 1516, 1474, 1455,

1400, 1364, 1312, 1236, 1214, 1185, 1086, 1048, 804, 682, 621, 556, 530, 492, 396. LC-MS: 179 ([M + Na]/2, $C_{16}H_{23}N_4O_4^+$, 335.37).

Enantioselective synthesis of Z-AlaGly-OMe from *rac*-Z-Ala-OH using L-5b (DMT/L-*N*-MePro-OMe/BF_4^-). General procedure

The vigorously stirred solution of **L-5b** (DMT/L-*N*-MePro-OMe/BF_4^-) (0.142 g; 0.5 mmol) in acetonitrile (5 mL) was cooled to 0°C and then *rac*-Z-Ala-OH (0.223 g; 1 mmol) and DIPEA(17.6 µL; 0.1 mmol) were added. Stirring was continued for 1 h and HCl × H-Gly-OMe (0.069 g; 0.5 mmol) and NMM (55 µL; 0.5 mmol) were added and the mixture was left at 0°C for 2 h. Then, it was allowed to warm-up to room temperature overnight. Solvent was removed under reduced pressure and residue was dissolved in dichloromethane (10 mL) and washed successively with water (3 mL), 1 M aq. HCl (3 mL), water (3 mL), 1 M aq. $NaHCO_3$ (3 mL) and again water (3 mL). Organic phase was dried with $MgSO_4$, filetered and evaporated to dryness yielding Z-D-Ala-Gly-OMe (99 µg, yield 67%), m.p. = 87–89°C; lit. m.p. = 94 – 96°C (14), $[\alpha]_D^{25}$ = (+) 18.5 (c = 1.0, MeOH); lit. $[\alpha]_D^{25}$ = (+) 26 (c = 1.0, MeOH) (14). IR (film/NaCl, cm^{-1}): 3321, 3017, 2966, 2937, 2903, 2274, 2143, 1984, 1815, 1759, 1695, 1666, 1586, 1536, 1480, 1448, 1410, 1374, 1362, 1320, 1247, 1191, 1168, 1127, 1072, 1054, 1017. ^{1}H-NMR (250 MHz, $CDCl_3$, δ, ppm): 1.41 (d, 3H, *J* = 6.5 Hz, CH_3-CH-), 3.78 (s, 3H, CH_3O-), 4.11 (q, 1H, *J* = 7 Hz, CH_3-CH-), 4.39 (m, 2H, -CH_2-CO-), 5.10 (s, 2H, -CH_2O-), 6.61 (broad s, 1H, NH), 7.40 (s, 5H, arom.).

Enantioselective synthesis of Z-AlaGly-OMe from *rac*-Z-Ala-OH using D-5b (DMT/D-*N*-MePro-OMe/BF_4^-).

Synthesis was carried out according to general procedure described above using **D-5b** (DMT/D-*N*-MePro-OMe/BF_4^-) (0.142 g; 0.5 mmol), rac-Z-Ala-OH (0.223 g; 1 mmol), DIPEA (17.6 µL; 0.1 mmol), HCl × H-Gly-OMe (0.069 g; 0.5 mmol) and NMM (55 µL; 0.5 mmol). Z-L-Ala-Gly-OMe (96 µg) was obtained (yield 65%), m.p. = 90–91°C; lit. m.p. = 94–96°C (15), $[\alpha]_D^{25}$ = (–) 17.2; lit. (15) $[\alpha]_D^{25}$ = (–) 23.2 (c = 1.0, MeOH). IR (film/NaCl, cm^{-1}): 3321, 3017, 2966, 2937, 2903, 2274, 2143, 1984, 1815, 1759, 1695, 1666, 1586, 1536, 1480, 1448, 1410, 1374, 1362, 1320, 1247, 1191, 1168, 1127, 1072, 1054, 1017. ^{1}H-NMR (250 MHz, $CDCl_3$, δ, ppm): 1.41 (d, 3H, *J* = 6.5 Hz, CH_3-CH-), 3.78 (s, 3H, CH_3O-), 4.11 (q, 1H, *J* = 7 Hz, CH_3-CH-), 4.39 (m, 1H, -CH_2-CO-), 5.10 (s, 2H, -CH_2O-), 6.61 (broad s, 1H, NH), 7.40 (s, 5H, aromatic).

RESULTS AND DISCUSSION

The problem of unpredictable results of enantioselective peptide synthesis from racemic substrates was resolved by designing the traceless enantioselective coupling reagents (16). According to this concept, traceless reagents are prepared by temporary attachment of the chiral fragment to a classic

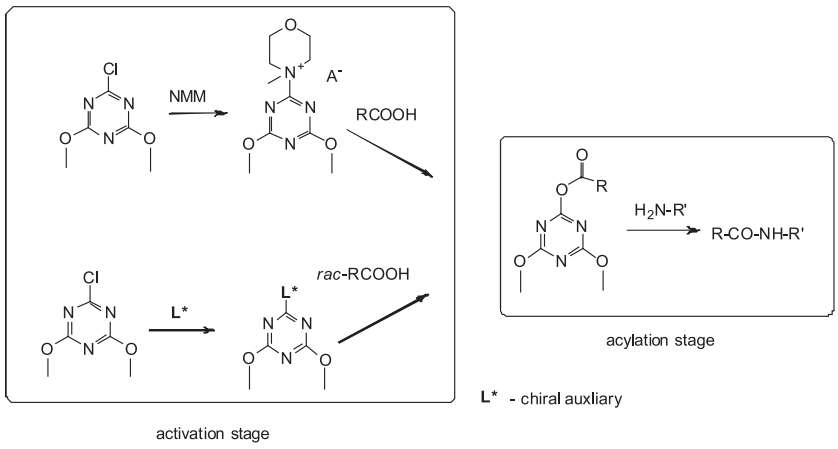

Scheme 1. Treatment of racemic carboxylic component with chiral traceless coupling reagent yields appropriate enantiomerically enriched activated derivative, the same for all chiral components in the whole family of enantioselective reagents as well as the entity identical with obtained using appropriate achiral counterpart

peptide-bond-forming agent. Thus, after selection of the enantiomer at the activation stage and departure of the chiral component, the activated intermediate is converted to a well-known form of a conventional achiral acylating species.

Moreover, it has been shown that configuration and enantiomeric enrichment once established at the activation stage remained intact and independent on the structure of acylated counterpart. This advantage is extremely important because all reaction parameters including configuration, optical purity of the product, optimal reaction conditions and the efficiency of coupling are predictable on the basis of a single experiment of the model reaction.

The first traceless enantioslective coupling reagents were designed based on chiral *N*-triazinylammonium salts derived from alkaloids (brucine, strychnine, quinine) (17). The versatility of the approach was fully confirmed by the high yield of peptide synthesis within up to 99% enantiomeric purity from racemic substrate, with expected configuration. However, until now, the main limitation in the broad application of chiral *N*-triazinylammonium salts are toxicity of the alkaloids and limited access to both enantiomeric forms of the chiral component of coupling reagent. To overcome this drawback, the search were undertaken for more versatile chiral components useful in enantioselective synthesis of peptide bond. In the introductory experiments it has been noticed that *N*-methylpyrrolidine is very versatile amino component in triazine mediated coupling reactions (18). Therefore, in order to open access to the representative collection of chiral nontoxic coupling reagents, the systematic studies were undertaken to develop procedures for synthesis of chiral *N*-methylpyrrolidines from proline which is readily available in both enantiomeric forms. In the first attempts an efforts were made to evaluate *N*-methyl and *N*-allylproline esters as chiral component in enantioselective activation of *N*-protected amino acids.

N-Methylproline (**1**) was prepared by treatment of proline with aqueous formaldehyde in the presence of zinc dust according to the modified procedure (12) with 92% yield. Methyl ester of *N*-methylproline (**3a**) and propyl esters of *N*-methylproline (**3b**) were obtained under classic conditions in reaction with appropriate alcohols and thionyl chloride in 90 and 86% yield, respectively. *N*-Allylproline methyl ester (**3c**) and *n*-propyl ester **3d** were

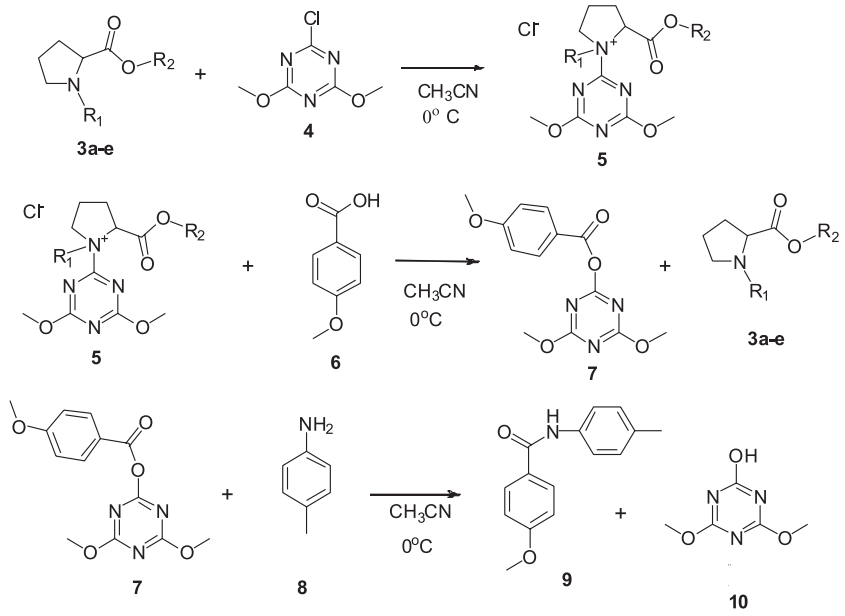

3a R_1= CH_3; R_2= CH_3
3b R_1= CH_3; R_2= $CH_2CH_2CH_3$
3c R_1= $CH_2CH{=}CH_2$; R_2= CH_3
3d R_1= $CH_2CH{=}CH_2$; R_2= $CH_2CH_2CH_3$
3e R_1= $CH_2CH{=}CH_2$; R_2= $CH_2CH{=}CH_2$

Scheme 2. Condensation of 4-methoxybenzoic acid (**6**) with 4-toluidine (**8**) mediated by 2-chloro-4,6-dimethoxy-1,3,5-triazine (**4**) in the presence of esters of *N*-alkylproline **3a-e**

obtained in 90% yield according to procedure of Hassner (18) in reaction of appropriate proline ester **2c** or **2d** with allyl bromide in the presence of potassium carbonate. The structure of **3c** was confirmed by MS analysis based on intensive (M + 1) signal m/z = 170.08 expected for *N*-allylproline methyl ester (M = 169.23). *N*-Allylproline allyl ester (**3e**) was prepared by direct *N*- *O*- dialkylation of proline with two equivalents of allyl bromide in the presence of potassium carbonate. Its structure was confirmed by the presence of double triplet at δ = 3.20 ppm and triplet at δ = 4.50 ppm in ^{1}H-NMR spectrum corresponding respectively to the allyl methylene fragment attached to nitrogen and oxygen and by the presence of $[M + 1]^+$ ion m/z = 196.1.

Model coupling reactions of 4-methoxybenzoic acid (**6**) with 4-toluidine (**8**) by 2-chloro-4,6-dimethoxy-1,3,5-triazine (**4**) in the presence of esters of *N*-alkylproline **3a-e** gave expected amide (**9**) with good yield (Scheme 2).

This confirmed that simple derivatives of *N*-alkylproline **3a-e** can be potentially used as chiral components in enantioselective condensations, although in all cases studied, progress of condensation was relatively slow and 24 h coupling time was necessary for reaction to be completed.

Careful examination of reacting mixture evidenced, that the rate limiting step is formation of *N*-triazinylammonium chloride **5a** in reaction of CDMT (**4**) with *N*-alkylproline ester **3a-e**. This circumstance is adverse for enantiodifferentiating procedures because prolonged contact of reactants forecast dealkylation of **5a**, racemization of chiral component **3a-e** and favors formation of *mezo*-anhydrides by acylation discriminated enantiomer of carboxylic acid with carboxylic acid enantiomer preferred in the activation step.

The remedy preventing this shortcoming is to separate the rate limiting quaternization of *N*-alkylproline ester **3a-e** in reaction with CDMT (**4**) and

Table 1. Condensations of 4-methoxybenzoic acid (**6**) with 4-toluidine (**8**) mediated by CDMT (**4**) and esters of *N*-alkylproline **3a-e**.

Entry	*N*-alkylproline ester **3a-e**	Solvent	Activation time [h]	Yield [%]
1	**3a**	acetonitrile	24	78.7
2	**3b**	acetonitrile	24	60
3	**3a**	THF	24	72.9
4	**3b**	THF	24	65.5
5	**3c**	acetonitrile	24	93
6	**3d**	acetonitrile	24	98
7	**3e**	acetonitrile	24	98

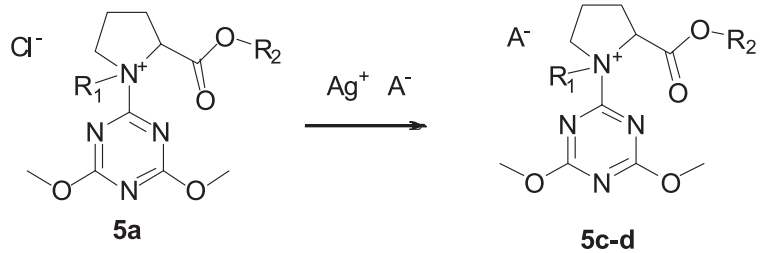

5c A$^-$ = 4-$CH_3C_6H_4$-SO_3^-

5d A$^-$ = ClO_4^-

Scheme 3. Stable salts of triazine based coupling reagents **5c-d**

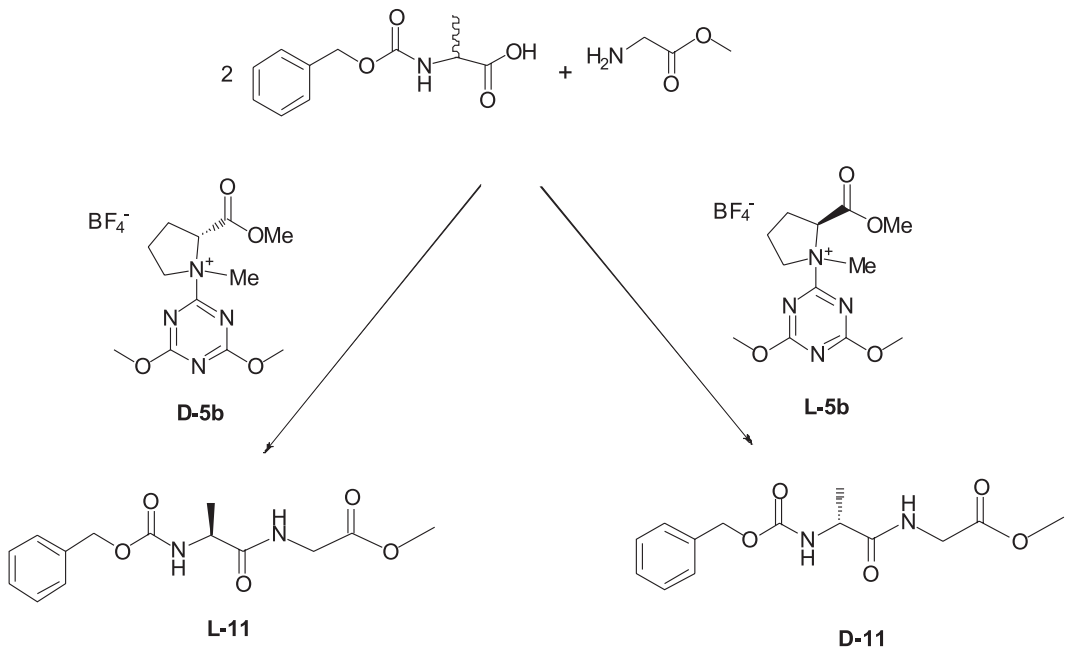

Scheme 4. Enantioselective coupling of racemic Z-Ala-OH with H-Gly-OMe to **11**, mediated by enantiomeric coupling reagents **L-5b** and **D-5b**

Table 2. Synthesis of Z-Ala-Gly-OMe from racemic Z-Ala-OH in the presence of chiral coupling reagents **L-5b** and **D-5b**.

Coupling reagent	Yield [%]	$[\alpha]_D^{25}$ (c = 1.0. MeOH)	Lit. $[\alpha]_D^{25}$ (c = 1.0, MeOH)	Preferred configuration	D/L [%]
L-5b	67	(+) 18.5	(+) 26 (14)	D	85/15
D-5b	65	(–) 17.2	(–) 23.2 (15)	L	13/87

substitute unstable *N*-triazinylammonium chlorides **5a** with stable salts of triazine based coupling reagents prepared in the form of appropriate salt with non-nucleophilic tetrafluoroborate, tosylate or perchlorate counterion **5b-d**. The treatment of L *N*-methylproline methyl ester (**3a**) with tetrafluoroboric acid solution and then reaction with CDMT gave appropriate tetrafluoroboric salt **L-5d** (DMT/L-*N*-MePro-OMe/BF_4^-) in 83% yield and **D-5b** (DMT/D-*N*-MePro-OMe/BF_4^-) in 88% yield, respectively. Appropriate perchlorate **L-5d** (DMT/L-*N*-MePro-OMe/ClO_4^-) was prepared by treatment of L-*N*-methylproline methyl ester (**3a**) with CDMT in the presence of silver perchlorate. Unfortunately, the poor solubility of **L-5d** in solvents used in peptide synthesis severely limited its synthetic applications. Furthermore, both procedures failed in the attempts to prepare 4-toluenesulfonate **5c** (DMT/L-*N*-MePro-OMe/TsO_3^-).

The versatility and selectivity of **5a-d** were studied both in model condensation of **6** with 4-toluidine (**8**) and in enantioselective coupling of racemic Z-Ala-OH with H-Gly-OMe.

It has been found that **L-5b** obtained from L enantiomer of methyl esters **3a** prefers formation of D dipeptide with L/D ratio 79/21, but enantiomeric form of **D-5b** prepared from D enantiomer of methyl esters **3a** prefers formation of L dipeptide with reverse L/D ratio 25/75. This demonstrated that relatively simple, non-toxic, non-expensive and readily accessible in both enantiomeric forms components for synthesis of traceless enantioselective coupling reagents can be obtained from proline.

CONCLUSION

The deteriorating effect of electron withdrawing ester group of proline severely reducing nucleophilicity of nitrogen in *N*-alkylproline esters in reaction with CDMT, as compared to not substituted *N*-alkylpyrrolidines, has been overcome by transformation of unstable quaternary chlorides into stable *N*-triazinyl-*N*-methylpyrrolidinium tetrafluoroborates **L-5b** and/or **D-5b.**

Acknowledgment

This study was supported by the Ministry of Science and High Education under the Reserch Project from National Science Center: project number: 2012/07/N/ST5/01883.

REFERENCES

1. Committee for Proprietary Medical Products (1993) Working parties on quality, safety and efficacy of medical products. Note for guidance: investigation of chiral active substances. III/3501/91.
2. Agranat I., Caner H., Caldwell J.: Nat. Rev. Drug Discov. 1, 753 (2002).
3. Hava C., Efrat G., Liron L., Israel A.: Drug Discov. Today 9, 105 (2004).
4. a) Garret C.E., Fu G.C.: J. Am. Chem. Soc. 120, 7479 (1998); b). Arai S., Bellemin-Laponnaz S., Fu G.C.: Angew. Chem. 113, 240 (2001); c). Arai S., Bellemin-Laponnaz S., Fu G.C.: Angew. Chem. Int. Ed. 40, 234 (2001); d) Shaw P., Aleman S.A., Christy J., Kampf J. ., Vedejs E.: J. Am. Chem. Soc. 128, 925 (2006); e) Mermerian. A.H., Fu G.C.: Angew. Chem. 117, 971 (2005); f) Mermerian A.H., Fu G.C.: Angew. Chem. Int. Ed. 44, 949 (2005); g) Spivey A.C., Zhu F., Mitchell M.B., Davey S.G., Jarvest R.L.: J. Org. Chem. 68, 7379 (2003); h) Kawabata T., Stragies R., Fukaya T., Nagaoka Y., Schedel H., Fuji K.: Tetrahedron Lett. 44, 1545 (2003); i) Priem G., Pelotier B., Madonald S.J.F., Anson M.S., Campbell I.B.: J. Org. Chem. 68, 3844 (2003); j) Dalaigh C.O., Hynes S.J., O'Brien J.E., McCabe T., Maher D.J., Watson G.W., Connon S.J.: Org. Biomol. Chem. 4, 2785 (2006); k) Anstiss M., Nelson A.: Org. Biomol. Chem. 4, 4135 (2006).
5. Birman V.B., Li X.: Org. Lett. 8, 1351 (2006).
6. a) Jarvo E.R., Miller S.J.: Tetrahedron 58, 2481 (2002); b) Sibi M.P., Maneyem S.: Tetrahedron 56, 8033 (2000); c) Copeland G.T., Jarvo E.R., Miller S.J.: J. Org. Chem. 63, 6784 (1998); d) Copeland G.T., Miller S.J.: J. Am. Chem. Soc. 121, 4306 (1999); e) Harris R.F., Nation A.J., Copeland G.T., Miller S.J.: J. Am. Chem. Soc. 122, 11270 (2000); f) Vasbinder M.M., Jarvo E.R., Miller S.J.: Angew. Chem. 113, 2906 (2001); g) Vasbinder M.M., Jarvo E.R., Miller S.J.: Angew. Chem. Int. Ed. 40, 2824 (2001); h) Birman V.B., Uffman E.W., Jiang H., Li X., Kilbane C.J.: J. Am. Chem. Soc. 126, 12226 (2004).
7. a) Takeda, K. Tsuboyama K., Suzuki A., Ogura H.T.: Chem. Pharm. Bull. 33, 2545 (1985); b) Teramoto T., Deguchi M., Kurosaki T.: Tetrahedron Lett. 22, 1109 (1981); c) Teramoto T., Kurosaki T.: Tetrahedron Lett. 18, 1523 (1977); d) Markowicz S.W., Karolak-Wojciechowska J.: Pol. J. Chem. 68, 1973 (1994); e) Kricheldorf H.R., Au M., Mang T.: Int. J. Pept. Protein Res. 26, 149 (1985); f) Kricheldorf H.R., Mang T.: Makromol. Chem. 183, 2093 (1982).
8. a) Murakami Y., Kondo K., Miki K., Akiyama Y., Watanabe T., Yokoyama Y.: Tetrahedron Lett. 38, 3751 (1997); b) Kondo K., Murakami Y.: Chem. Pharm. Bull. 46, 1217 (1998); c) Kondo K., Kurosaki T., Murakami Y.: Synlett 725 (1998); d) Al-Sehemi A.G., Atkinson R.S., Fawcett J., Russel D.R.: J. Chem. Soc., Perkin Trans. 1, 4413 (2000); e) Günster E.J., Scholtz R.C.: Makromol. Chem. 181, 643 (1980); f) Evans D.A., Andersen J.C., Taylor M.K.: Tetrahedron Lett., 34, 5563 (1993); g) Jencks P.W., Gilchrist M.: J. Am. Chem. Soc. 90, 2622 (1968); h) Maezaki N., Furusawa A., Uchida S., Tanaka T.: Tetrahedron 57, 9309 (2001).
9. a) Wegler R.: Liebigs Ann. Chem. 498, 62 (1932); b) Oriyama T., Hori Y., Imai K., Sasaki R.: Tetrahedron Lett. 37, 8543 (1996); c) Sano T., Imai K., Ohashi K., Oriyama T.: Chem. Lett. 265 (1999); d) Oriyama T., Imai K., Sano T., Hosoya T.: Tetrahedron Lett. 39, 3529 (1998); e) Terakado D., Koutaka H., Oriyama T.: Tetrahedron Asymmetry 16, 1157 (2005).
10. a) Vedejs E., Diner S.T.: J. Am. Chem. Soc. 115, 3358 (1993); b) Vedejs E., Bennett N.S., Conn L.M., Diver S.T., Gingras M., Lin S., Oliver P.A., Peterson M.J.: J. Org. Chem. 58, 7286 (1993); c) Bogatkov S.V., Golovina Z.P., Fild V.R. , Cherkasova E.M.: Zh. Org. Khim. 13, 2271 (1977); d) MacNeil P.A., Roberts N.K., Bosnisch B.: J. Am. Chem. Soc. 103, 2273 (1981); e) Gladiali S., Dore A., Fabbri D., De Lucchi O., Manassero M.: Tetrahedron:

Asymmetry 5, 511 (1994); f) Burk M.J., Feaster J.E., Harlow R.L.: Tetrahedron: Asymmetry 2, 569 (1991); g) Vedejs E., Daugulis O., Harper L.A., MacKay J.A., Powell D. R.: J. Org. Chem. 68, 5020 (2003); h) MacKay J.A., Vedejs E.: J. Org. Chem., 69, 6934 (2004); i) Methot J.L., Roush W.R.: Adv. Synth. Catal. 346, 1035 (2004).

11. a) Srseniyadis S., Valleix A., Wagner A., Mioskowski C.: Angew. Chem. 116, 3376 (2004); b) Srseniyadis S., Valleix A., Wagner A., Mioskowski C.: Angew. Chem. Int. Ed.: 43, 3314 (2004); c) Pelotier B., Priem G., Macdonald S.J.F., Anson M.S., Upton R.J., Campbell I.B.: Tetrahedron Lett. 46, 9005 (2005); d) Lewis C.A., Sculimbrene B.R., Xu Y., Miller S.J.: Org. Lett. 7, 3021 (2005); e) Birman V.B., Jiang H., Li X.: Org. Lett. 9, 3237 (2007); f) Kosugi Y., Akakura M., Ishihara K.: Tetrahedron 63, 6191 (2007); g) Stamatov S.D., Stawinski J.: Org. Biomol. Chem. 5, 3787 (2007); h) Karnik A.V., Kamath S.S.: J. Org. Chem. 72, 7435 (2007); i) Notte G.T., Sammakia T., Steel P.J.: J. Am. Chem. Soc. 127, 13502 (2005); j) Terakado D., Oriyama T.: Org. Synth. 83, 70 (2006); k) Moretto A., Peggion C., Formaggio F., Crisma M., Kaptein B., Broxterman Q.B., Toniolo C.: Chirality, 17, 481 (2005).
12. Moehrle R., Siekeor Z.: Arch. Pharm. (Weinheim) 309, 380 (1974).
13. Avenoza A, Pereprine J.: Tetrahedron 58, 10107 (2002).
14. Grzonka Z., Palacz Z., Baran L., Przegalinski E., Kupryszewski G.: Pol. J. Chem. 55, 1025 (1981).
15. Kawasaki K., Maeda M., Tamura, H., Ohashi S., Yoshimura T., Hatayama E.: Chem. Pharm. Bull. 32, 1717 (1984).
16. Kolesinska B., Kaminski Z.J.: Org. Lett., 11, 765 (2009).
17. a) Kolesinska B., Kasperowicz K., Sochacki M., Mazur A., Jankowski S., Kaminski Z.J.: Tetrahedron Lett. 51, 20 (2010); b) Kolesinska B., Kasperowicz-Frankowska K., Fraczyk J., Kaminski Z.J.: Helv. Chim. Acta 95, 2084 (2012); c) Kaminski, Z.J.; Kolesinska, B. Patent EPO 09001796,3-1211, priority PL/04. 02. 08/ PLA 384377608.
18. Kaminski Z. J, Kolesinska B, Kolesinska J, Jastrzabek K.: EP-05006473.2-2117 PCT, C07D 251/45, 18. 08. 2005.
19. da Silva R. A., Estevamb I. H. S., Bieber L. W.: Tetrahedron Lett. 48, 7680 (2007).
20. Hassner A., Maurya R.: J. Org. Chem. 56, 2775 (1991).

Acta Poloniae Pharmaceutica – Drug Research, Vol. 71 No. 6 pp. 1004–1012, 2014 ISSN 0001-6837
Polish Pharmaceutical Society

THE INTERACTION OF NEW PIROXICAM ANALOGUES WITH LIPID BILAYERS – A CALORIMETRIC AND FLUORESCENCE SPECTROSCOPIC STUDY

JADWIGA MANIEWSKA[1*], BERENIKA SZCZĘŚNIAK-SIĘGA[1], ANDRZEJ POŁA[2], KAMILA ŚRODA-POMIANEK[2], WIESŁAW MALINKA[1] and KRYSTYNA MICHALAK[2]

[1] Department of Chemistry of Drugs, Wroclaw Medical University, Borowska 211, 50-556 Wrocław, Poland;
[2] Department of Biophysics, Wroclaw Medical University, Chałubińskiego 10, 50-368 Wrocław, Poland

Abstract: The purpose of the present paper was to assess the ability of new piroxicam analogues to interact with the lipid bilayers. The results of calorimetric and fluorescence spectroscopic experiments of two new synthesized analogues of piroxicam, named PR17 and PR18 on the phase behavior of phospholipid bilayers and fluorescence quenching of fluorescent probes (Laurdan and Prodan), which molecular location within membranes is known with certainty, are shown in present work. The presented results revealed that, depending on the details of chemical structure, the studied compounds penetrated the lipid bilayers.

Keywords: piroxicam analogues, lipid bilayers, microcalorimetry, fluorescence spectroscopy, colon cancer chemoprevention

Piroxicam, from the group of the oxicams, is mainly known as a non-steroidal anti-inflammatory drug (NSAID), used in the treatment of chronic rheumatic diseases. The molecular target of NSAIDs is cyclooxygenase (COX), the enzyme that catalyzes the conversion from arachidonic acid to prostaglandins (PGs). There are three isoforms of COX (COX-1, COX-2 and COX-3).

Most solid tumors express the cyclooxygenase-2 (COX-2) protein, which is the target of NSAIDs, and that is why those drugs are evaluated as anticancer. They inhibit proliferation, invasiveness of tumors, and angiogenesis and overcome apoptosis resistance in a COX-2 dependent and independent manner (1). Moreover, chronic inflammatory processes affect all stages of tumor development, and there are many molecular and cellular pathways that participate in the crosstalk between cancer cells and inflammatory mediators (2). The incidence of colon, breast and prostate cancer is closely associated to the inflammation. The inflammation may play a role in tumor initiation by triggering the production of reactive oxygen species responsible for DNA damage, and also in tumor promotion, because it triggers the secretion of growth factors. COX-2 induction or overexpression is associated with an increased production of PGE2, one of the major products of COX-2 which is known to modulate cell proliferation, cell death and tumor invasion in many types of cancer (including colon cancer) (3). NSAIDs particularly decrease the incidence of, and mortality from, colon cancer, and therefore those drugs have been a major advance in chemoprevention, which is a strategy aimed at preventing tumor progression before irreversible changes to the proteome are in full progress (4, 5).

The trials of aspirin (*versus* control) and COX-2 inhibitors showed that those medicines reduce the risk of colon cancer. Unfortunately, prevention with COX-2 inhibitors is not possible because of an increased risk of vascular events, and, on the other hand, the greater risk of bleeding complications in patients on high-dose aspirin limits its chemoprevention potential in cases of colon cancer (6). That is why the other NSAIDs (e.g., sulindac) are examined for inhibiting colon cancer occurrence. However, all the studies strongly suggest a role for aspirin and other NSAIDs in the reduction of the

* Corresponding author: e-mail: jadwiga.maniewska@umed.wroc.pl

risk of colon cancer (7). Emerging evidence of as much as 40% reduction in mortality in patients undergoing curative treatment of colorectal cancer makes the concept of the use of NSAIDs as adjuvant treatment in high risk disease more compelling, when potential survival benefits may outweigh the risk of their use in cancer prophylaxis (8).

Lichtenberger et al. presume that one of the alternative mechanisms by which NSAIDs can be effective is by interacting with cellular membranes and altering their biophysical properties. Those drugs can induce changes in the fluidity, permeability and biophysical properties of cell membranes (9). Also Lúcio et al. consider the interaction of NSAIDs with membrane models concluding that in order to achieve their main target – membrane associated enzyme COX – NSAIDs have first to pass through the membranes, that is why understanding this interaction plays a key role in understanding the therapeutic effects of those drugs (10).

In the present work, we describe the results of calorimetric and fluorescence spectroscopic experiments of two new synthesized analogues of piroxicam, named PR17 and PR18 on the phase behavior of phospholipid bilayers and fluorescence quenching of two fluorescent probes which molecular location within membranes is known with certainty.

EXPERIMENTAL

Chemicals

Egg yolk phosphatidylcholine (EYPC) and 1,2-dipalmitoyl-n-glycero-3-phosphatidylcholine (DPPC) were purchased from Sigma-Aldrich (Poznań, Poland). All lipids were used as delivered, without further purification.

Fluorescent labels: 6-dodecanoyl-2-dimethylaminonaphthalene (Laurdan) and 6-propionyl-2-dimethylaminonaphthalene (Prodan) were purchased from Molecular Probes (USA).

All other chemicals used in this study were of analytical grade.

Synthesis

The proton nuclear magnetic resonance (^{1}H-NMR) spectra were measured on a Bruker 300 MHz NMR spectrometer using $CDCl_3$ as solvent and TMS as an internal standard. Spin multiplicities are given

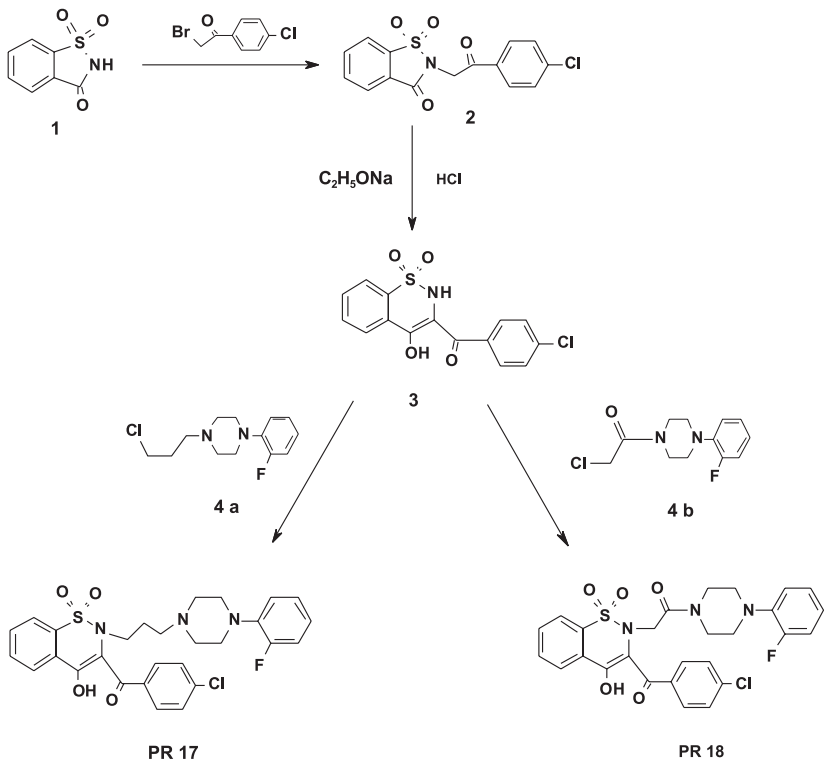

Scheme 1. General procedure for the preparation of **PR17** and **PR18**

as s (singlet), d (doublet), t (triplet) and m (multiplet) as well as b (broad). Coupling constants (*J*) are given in hertz. Infrared spectra (cm^{-1}) were recorded on a Perkin-Elmer Spectrum Two UATR FT-IR spectrometer. The samples were applied as neat solids. Melting points were determined in open capillary tubes and are uncorrected. Elemental analyses were performed by Carlo Erba NA 1500 analyzer and were within ± 0.4% of the theoretical value. Reactions were monitored by thin layer chromatography (TLC) on silica gel plates (Merck 60 F254), visualized with ultraviolet light. Flash chromatography was performed on silica gel column (230–400 mesh) using ethyl acetate.

General procedure for the preparation of PR17 and **PR18** (Scheme 1):

Compound **2** was obtained by alkylation of saccharine with 2-bromo-4'-chloroacetophenone in DMF with addition of a small amount of triethylamine at room temperature. Newly obtained compound was rearranged using sodium ethoxide to give compound **3**. The alkilation of **3** by 1-(chloroalkyl/acyl)-4-arylpiperazine resulted in products **PR17** and **PR18**.

2-(4-Chlorophenacyl)-2H-1,2-benzothiazol-3-on 1,1-dioxide (2)

A mixture of commercially available saccharine **1** (0.92 g, 5 mmol) with 5 mmol of 2-bromo-4'-chloroacetophenone in 7 mL of *N*,*N*-dimethylformamide (DMF) and triethylamine (0.7 mL, 5 mmol) was stirred at room temperature for 10 h, then poured into ice cooled water (50 mL) resulting in the formation of a white solid, which was filtered and washed with cold water. The solid was dried and crystallized from ethanol to give **2** with 99% yield. Analytical data for **2**: $C_{15}H_{10}ClNO_4S$ (m.w. 335.76); m.p. 179–181°C (EtOH). ^{1}H-NMR (δ, ppm): 5.11 (s, 2H, CH_2), 7.49–8.12 (m, 8H, Ar*H*). FT-IR (UATR): 1748, 1699 (CO), 1330, 1180 (SO_2) cm^{-1}.

3-(4-Chlorobenzoyl)-4-hydroxy-2H-1,2-benzothiazine 1,1-dioxide (3)

Three millimoles of **2** was dissolved in 7.5 mL of sodium ethoxide (2.3%) at 40°C and stirred with heating to 55–60°C for 5–10 min. Color changes from beige to deep red were observed. After this time and dissolution of all the substance, the mixture was rapidly cooled to 25°C and 7.5 mL HCl (9%) was added. Color changed from deep red to deep yellow and the product precipitated. The solid was filtered off, washed with cold water, dried and purified by crystallization from EtOH to give **3** (yield 92%).

Analytical data for **3**: $C_{15}H_{10}ClNO_4S$ (m.w. 335.76); m.p. 238–241°C (EtOH). ^{1}H-NMR (δ, ppm): 6.48 (s, 1H, NH), 7.47–8.24 (m, 9H, Ar*H*), 15.72 (s, 1H, OH_{enolic}). FT-IR (UATR): 3222 (NH), 1588 (CO), 1365, 1178 (SO_2) cm^{-1}.

1-(3-Chloropropyl)-4-(2-fluorophenyl)piperazine (4a)

Ten millimoles of 1-(2-fluorophenyl)piperazine and 11 mmol (1.1 mL) of 1-bromo-3-chloropropane were dissolved in acetone (3 mL) with addition of 25% NaOH (2 mL), stirred slowly at room temperature for 8 h and left overnight. After this time, diethyl ether (20 mL) was added and the mixture was stirred further for 30 min then was divided in a funnel into two parts. The ether part was dried with $MgSO_4$ and evaporated under vacuum. The residue was purified by flash silica gel chromatography, eluting with EtOAc to give **4a** (yield 74%).

Analytical data for **4a**: $C_{13}H_{18}ClFN_2$ (m.w. 256.75); ^{1}H-NMR (δ, ppm): 1.96–2.05 (m, 2H, $CH_2CH_2CH_2$), 2.56–2.68 (m, 6H, $CH_2N(CH_2)_2$), 3.11–3.14 (m, 4H, $N(CH_2)_2$), 3.61–3.65 (t, J = 6.6 Hz, 2H, $CH_2CH_2CH_2N_{piperazine}$), 6.92–7.26 (m, 4H, Ar*H*).

1-(2-Chloro-1-oxoethyl)-4-(2-fluorophenyl)piperazine (4b)

Ten millimoles of 1-(2-fluorophenyl)piperazine was dissolved in 40 mL of diethyl ether with the addition of 1.4 mL triethylamine and stirred slowly at room temperature for 10 min and then 1.6 mL (20 mmol) of chloroacetyl chloride in 20 mL of diethyl ether were slowly instilled and stirring was continued for another 2 h. After this time, diethyl ether was evaporated in vacuum, 10 mL of water and 60 mL of chloroform were added and the mixture was separated in a funnel. The chloroform part was dried with $MgSO_4$ and evaporated in a vacuum to give **4b** (yield 66%).

Analytical data for **4b**: $C_{12}H_{14}ClFN_2O$ (m.w. 256.70); ^{1}H NMR ($CDCl_3$ δ, ppm): 3.02–3.12 [m, 4H, $N(CH_2)_2$], 3.64–3.78 [m, 4H, $N(CH_2)_2$], 4.08 (s, 2H, CH_2), 6.87–7.06 (m, 4H, Ar*H*).

3-(4-Chlorobenzoyl)-2-substituted-4-hydroxy-2H-1,2-benzothiazine 1,1-dioxides (PR17, 18)

To the stirred mixture of 5 mmol of **3** in 20 mL of anhydrous EtOH 5 mL of EtONa (prepared from 0.115 g of Na and 5 mL of anhydrous EtOH) was added. Then, 5 mmol of corresponding piperazine (**4a** or **4b**) was added and refluxed with stirring for 10–12 h. When the reaction was completed, which was confirmed using TLC plates, ethanol was dis-

tilled off, the residue was treated with 50 mL of $CHCl_3$ and insoluble materials were filtered off. The filtrate was then evaporated and the residue was purified by crystallization from ethanol to give compounds **PR 17** or **18**.

Analytical data: **PR 17** $C_{28}H_{27}ClFN_3O_4S$ (m.w. 556.05); m.p. 135–138°C (EtOH). ^{1}H-NMR (δ, ppm): 1.22–1.26 (m, 2H, $CH_2CH_2CH_2$), 2.01 (brs, 2H, $CH_2CH_2CH_2N_{piperazine}$), 2.30 (brs, 4H, $N(CH_2)_2$), 2.97–3.65 (m, 6H, $CH_2N(CH_2)_2$), 6.93–8.20 (m, 12H, Ar*H*), 15.47 (s, 1H, OH_{enolic}); FT-IR (UATR): 1609 (CO), 1333, 1166 (SO_2) cm^{-1}. Analysis: calcd.: C 60.48; H 4.89; N 7.56; found: C 60.70; H 5.17; N 7.22. Yield 49%.

PR 18 $C_{27}H_{23}ClFN_3O_5S$ (m.w. 556,00); m.p. 200–203°C (EtOH). ^{1}H-NMR (δ, ppm): 2.82–3.75 (m, 10H, CH_2CO and $H_{piperazine}$), 6.83–8.27 (m, 12H, Ar*H*), 15.47 (s, 1H, OH_{enolic}). FT-IR (UATR): 1665, 1590 (CO), 1337, 1171 (SO_2) cm^{-1}. Analysis: calcd.: C 58.32; H 4.17; N 7.56; found: C 58.39; H 4.20; N 7.22. Yield 41%.

Microcalorimetry

For each calorimetric sample 2 mg of DPPC was dissolved in the appropriate amount of chloroform stock solution (5 mM) of the studied oxicam. The oxicam/lipid molar ratios in the samples were: 0.05, 0.10, 0.15, 0.20. After that, the solvent was evaporated by a stream of nitrogen and the residual solvent was removed under vacuum for 1.5 h. Samples were hydrated by 15 μL of Tris-EDTA-NaCl (20 mM Tris, 0.5 mM EDTA, 150 mM NaCl) buffer (pH 7.4). Hydrated mixtures were heated to 10°C higher than the main phase transition temperature of DPPC and vortexed until homogeneous dispersion was obtained. Then, the samples were transferred into aluminium sample pans and sealed. Calorimetric measurements were performed using a

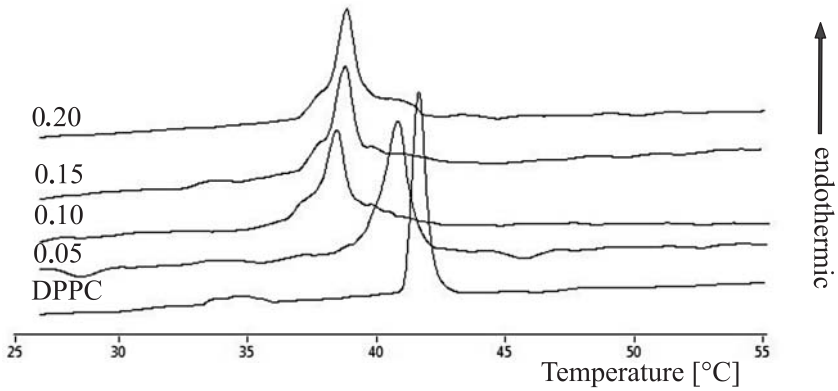

Figure 1. Thermograms of DPPC doped with **PR17**. Numbers in the Figure represent **PR17** : DPPC molar ratios. The thermograms were normalized to an equal amount of lipid for each profile

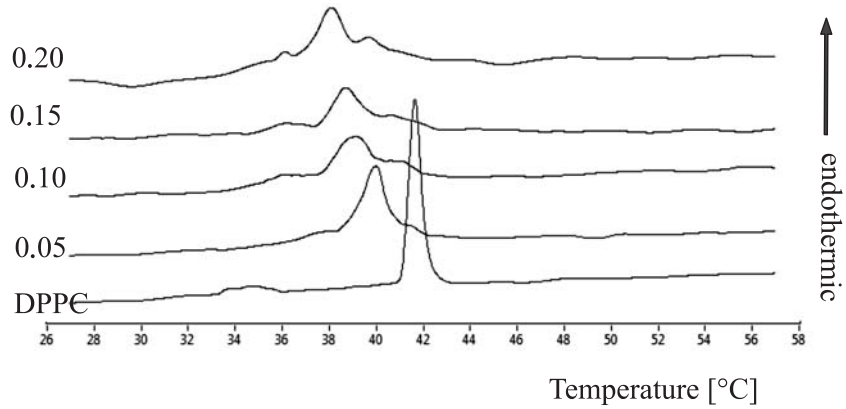

Figure 2. Thermograms of DPPC doped with **PR18**. Numbers in the figure represent **PR18** : DPPC molar ratios. The thermograms were normalized to an equal amount of lipid for each profile

Rigaku microcalorimeter. The samples were scanned at a rate of 1.25 °C/min. Data were stored on hard disk and analyzed off-line using software developed in our laboratory by Łukasz Fajfrowski.

Fluorescence spectroscopy

Unilamelar EYPC liposomes were obtained by sonification of 2 mM phospholipid suspension in Tris-NaCl-EDTA (20 mM Tris, 0.5 mM EDTA, 150 mM NaCl) buffer (pH 7.4) using UP 200s sonificator (Dr. Hilscher, GmbH, Berlin). Laurdan and Prodan stock solutions (1 mM) were prepared in DMSO. The stock solutions of the studied oxicams (30 mM) were prepared in DMSO. The liposomes were diluted and incubated with the fluorescent dye in darkness for 30 min at room temperature, then the studied oxicam was added and liposomes were incubated for another 20 min (also in darkness, at room temperature). In all of the experiments, the final phospholipid concentration was 200 μM. The concentration of the fluorescent dye (Laurdan or Prodan) was 5 μM. The oxicam concentration in samples was 25–125 μM. The fluorescence experiments were carried out with LS 50B spectrofluorimeter (Perkin-Elmer Ltd., Beaconsfield, UK) equipped with a xenon lamp using emission and excitation slits of 5 nm. The excitation wavelength for Laurdan was 390 nm and for Prodan – 360 nm. The recorded fluorescence spectra were processed with FLDM Perkin-Elmer 2000 software.

It was checked that the studied oxicams alone did not exhibit fluorescence in the spectral region of interest. All the experiments were performed in triplicate.

Molecular modelling

Theoretical calculations were performed using Spartan 10 software (Wavefunction, Inc., USA). The optimized molecular structure of all compounds and QSAR descriptors for them were calculated by *ab initio* DFT method with 6-31+G* basis set.

RESULTS

Microcalorimetry

In the calorimetric experiments we investigated the influence of the studied compounds on the thermal properties of DPPC bilayers. Since the pretransition was not detected in samples containing any of those compounds (see Fig. 1 and 2) we followed the dependencies of main transition temperature (T_m), enthalpy change (ΔH) and transition half-height width ($\Delta T_{1/2}$) on the oxicam analogues concentration. In Figures 1 and 2, showing the thermograms of DPPC mixed with **PR17** and **PR18** at different molar ratios, the impact of these oxicam derivatives on the lipid thermal behavior is exemplified. The addition of the studied compounds caused the disappearance of the DPPC pretransition (even at the lowest molar ratio used) and concentration-

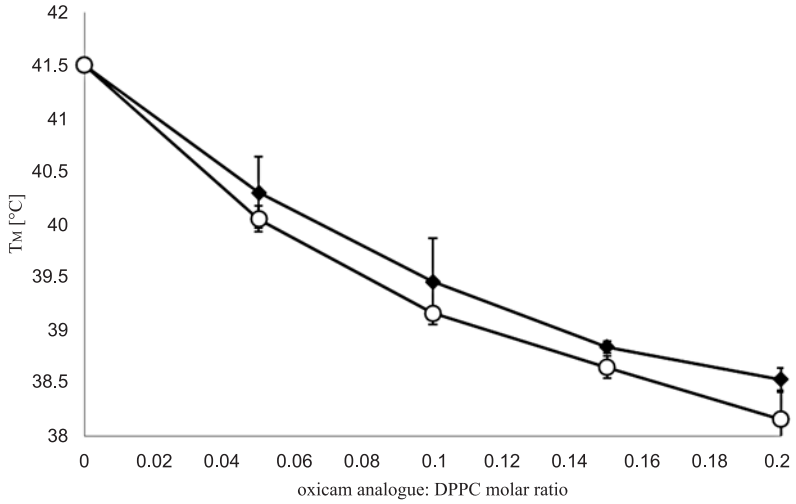

Figure 3. Influence of **PR17** (diamonds) and **PR18** (circles) on the DPPC main phase transition temperature (T_M). Bars represent standard deviations of eight measurements

dependent lowering of the main phase transition temperature accompanied by the decrease of the transition peaks area and the peak broadening. Additionally, at oxicam analogue: DPPC, molar ratios 0.10, 0.15 and 0.20, the peaks appeared to be composed of two overlapping peaks.

The dependencies of T_M, $\Delta T_{1/2}$ and ΔH on the oxicam analogue/lipid molar ratio obtained for mix-

Table 1. The molecular descriptors for **PR17** and **PR18**.

Compound	Log P	PSA [Å²]	HBD Count	HBA Count	E HOMO [eV]	E LUMO [eV]	Polarizability
PR 17	3.42	70.030	1	8	–6.00	–2.62	82.95
PR 18	2.23	80.328	1	9	–5.96	–2.68	81.62

Abbreviations: Log P – partition coefficient, PSA – polar surface area, HBD – hydrogen bond donor, HBA – hydrogen bond acceptor, E HOMO – energy of highest occupied molecular orbital, E LUMO – energy of lowest unoccupied molecular orbital.

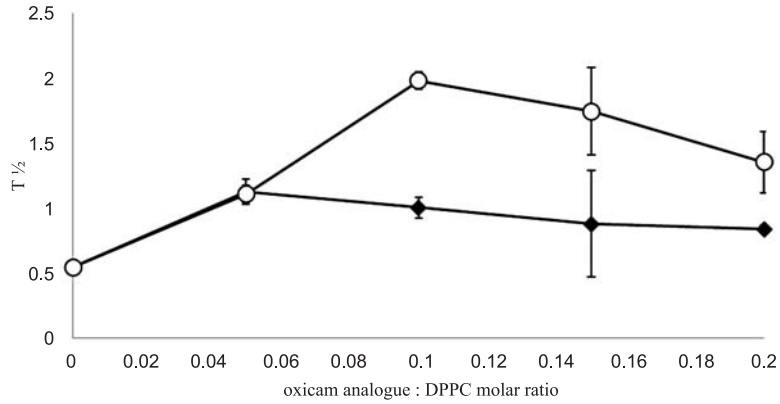

Figure 4. Influence of **PR17** (diamonds) and **PR18** (circles) on the DPPC peak half-height width ($T_{1/2}$). Bars represent standard deviations of eight measurements

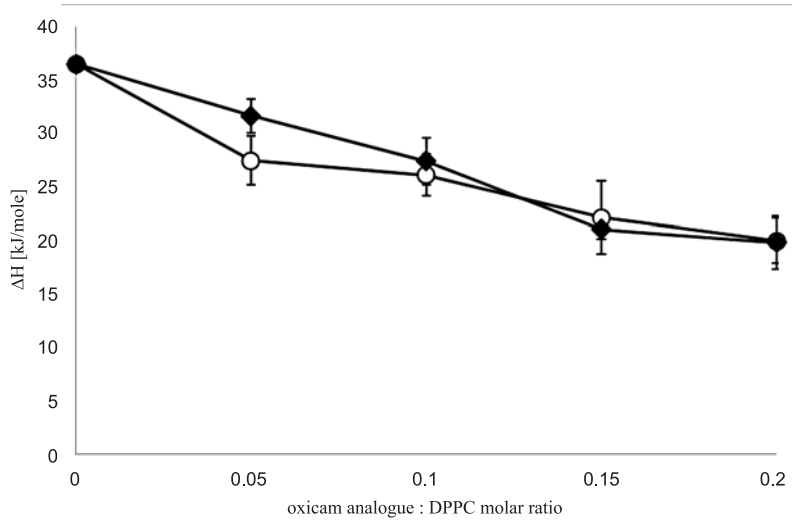

Figure 5. Influence of **PR17** (diamonds) and **PR18** (circles) on the DPPC transition entalpy (ΔH). Bars represent standard deviations of eight measurements

tures of DPPC with **PR17** and **PR18** are shown in Figures 3–5, respectively. In case of all DPPC gel–liquid crystalline phase transition parameters, the more pronounced effects were found for **PR18** than for **PR17**.

Fluorescence spectroscopy

To further study the effect of **PR17** and **PR18** on phospholipid bilayers, we have used two fluorescent probes localized in different membrane segments, and EYPC as unsaturated phospholipid. Laurdan and Prodan both possess the same fluorophore connected to an alkyl chain of different length (three carbon atoms in Prodan and twelve in Laurdan). Therefore, Prodan molecules locate closer to the hydrophilic surface of a bilayer than Laurdan whose fluorophore is positioned close to phospholipid glycerol groups (11, 12). The addition of studied oxicam analogues resulted in fluorescence quenching of both probes. Stern-Volmer plots are presented in Fig. 6 for **PR17** and in Fig. 7 for **PR18**. The studied compounds caused strong

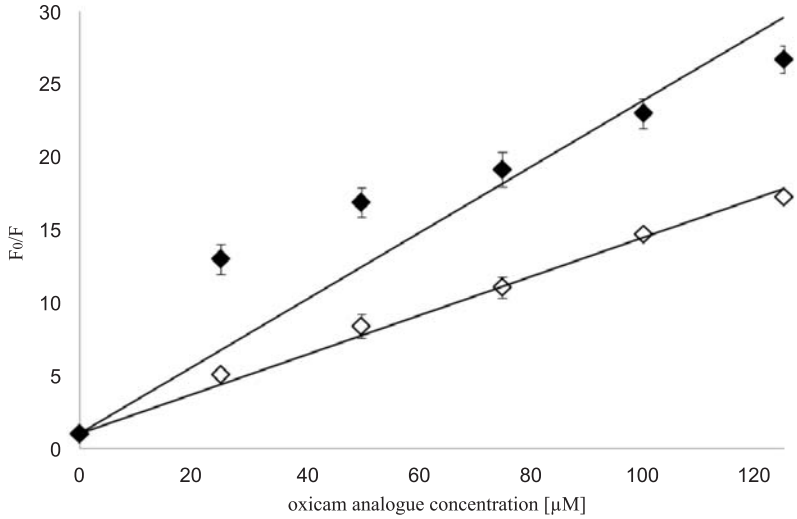

Figure 6. Stern-Volmer plots for quenching of Laurdan (open symbols) and Prodan (full symbols) by **PR17** (diamonds) in EYPC. Bars represent standard deviations of three independent experiments

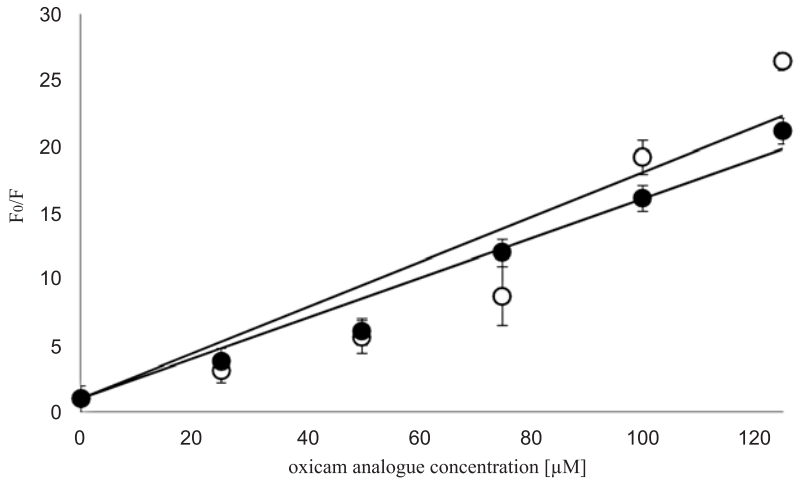

Figure 7. Stern-Volmer plots for quenching of Laurdan (open symbols) and Prodan (full symbols) by **PR18** (circles) in EYPC. Bars represent standard deviations of three independent experiments

quenching of both probes, although the effect was much more pronounced in case of Laurdan for **PR18**, and in case of Prodan for **PR17**.

Molecular modelling

Applying of QSAR methods allowed to describe electronic, structural and topological parameters and hydrophobicity of new compounds and to correlate these properties with their ability to affect phospholipid bilayers. Log P and polarizability of studied oxicam derivatives are ranked as follows: **PR17** > **PR18**, while PSA is inversed. The HOMO and LUMO energies are nearly the same for **PR17** and **PR18**. The HOMO level is at –6.00 for **PR17** and –5.96 for **PR18** with respect to the vacuum level, while the LUMO level is –2.62 and –2.68, respectively. Therefore, replacing the $(CH_2)_2$ group by carbonyl group (C=O) in the side chain in position 2 of the 1,2-thiazine ring did not significantly changed the HOMO and LUMO energy. The values of all molecular descriptors for newly synthesized oxicam derivatives are presented in Table 1. The obtained results may be related to the Lipinski's rule of five (RO5), which states that the poor absorption or permeation of newly synthesized compounds are more likely when: there are more than 5 H-bond donors, the MWT (molecular weight) is over 500, the LogP is over 5, there are more than 10-H bond acceptors (13). Compound classes that are substrates for biological transporters are exceptions to the rule. The new oxicam analogues fail the RO5 (although their MWT slightly exceed 500), that is why, we could except that they would be the drug-like compounds.

DISCUSSION AND CONCLUSION

To characterize the interaction of newly synthesized piroxicam analogues with lipid bilayers we employed the following techniques: microcalorimetry and fluorescence spectroscopy. The results obtained by these experimental approaches show that new piroxicam analogues interact with the model membranes under consideration. Calorimetric measurements showed that **PR17** and **PR18** interact with DPPC bilayer and changes the lipid phase behavior (Figs. 3–5) in a concentration-dependent manner. Abolishing of the pretransition from the thermograms, observed even at the lowest of oxicam analogue: DPPC molar ratios examined, suggests that the presence of small amounts of drug affects the packing of lipid molecules strongly enough to prevent formation of the ripple phase (14). The effects of **PR17** and **PR18** on DPPC gel-liquid crystalline phase transition parameters were stronger than observed by Kyrikou et al. for piroxicam and 3 other NSAIDs (15). As shown by the example thermograms presented in Figures 1 and 2, the increase in the oxicam analogue : lipid molar ratio is accompanied by the broadening of DSC peaks that suggests lower cooperativity of phospholipid main phase transition in the presence of studied compounds. Comparing the magnitude of changes induced by the studied oxicam analogues in thermotropic properties of DPPC bilayers the order **PR18** > **PR17** was observed.

According to the standard interpretation of calorimetric data proposed by Jain and Wu, the decrease of both transition temperature and enthalpy change suggests that lipid polar-heads as well as hydrocarbon chains regions were affected by the studied compounds (16). The character of observed changes (decrease of T_M, ΔH and increase of $T_{1/2}$) allows to conclude also that interactions between phospholipid molecules in the gel state became weaker in the presence of studied analogues of oxicams.

Alteration of the gel phase of model membranes by oxicam derivatives gives an improved picture when observed also by fluorescence spectroscopy. In spectroscopic measurements, we used two fluorescence dyes Laurdan and Prodan which are located in different membrane regions. In the present work, quenching of fluorescence of Laurdan and Prodan, by newly synthesized oxicam derivatives, was investigated. According to Joseph Lakowicz, if the molecular location of fluorescent probe within the lipid bilayer is known, quenching studies can be used to reveal the location of quenchers in the membrane (17). It was found that **PR17** quenched the fluorescence of Prodan to a higher extend than Laurdan in studied bilayers. It suggested that the regions close to the surface of the model membrane (where Prodan is located) were more affected by the presence of **PR17**. In the contrary, **PR18** affected the regions near phospholipid glycerol backbones, where Laurdan is located. Also in Figs. 6 and 7, the upward curvature of Stern-Volmer plots of quenching both fluorescent probes was noticed. It suggested that studied oxicam analogues were quenching the fluorescence of Laurdan and Prodan both by dynamic and static mechanism. What is more, **PR18** was identified as an effective multidrug resistance (MDR) modulator in LoVo/Dx multidrug-resistant colon cancer cells (data not shown – in press). That would confirm, that NSAIDs and related compounds, which induce the changes in biophysical properties of model mem-

branes, might also be used as adjuvant treatment to anticancer therapy.

The difference between studied oxicam analogues is the occurrence - in **PR18** - or the lack of - in **PR17** - the carbonyl group in the side chain in position 2 of the benzothiazine ring (see Scheme 1). The presented experiments revealed that the carbonyl group increased the ability of the compound (**PR18**) to interact with model membranes. It is also possible that the occurrence of three-carbon molecule chain in **PR17**, instead of two-carbon molecule chain with the carbonyl group (**PR18**), may allow the rotation of the side chain of molecule and changing of the shape of **PR17** compound, which may cause its worse diffusion into the lipid bilayers, although this hypothesis requires further verification.

Another studies, employing lipids of various headgroups are needed to fully understand the interaction of studied analogues of oxicams with model membranes.

Acknowledgments

This work was financed by Grant Pbmn176 from Polish Ministry of Science and Higher Education for Wroclaw Medical University.

REFERENCES

1. de Groot D.J.A., de Vries E.G.E., Groen H.J.M., de Jong S.: Crit. Rev. Oncol. Hematol. 61, 52 (2007).
2. Elinav E., Nowarski R., Thaiss Ch.A., Hu B., Jin Ch., Flavell R.A.: Nature Rev. Cancer 13, 759 (2013).
3. Sobolewski C., Cerella C., Dicato M., Ghibelli L., Diederich M.: Int. J. Cell Biol. 2010, 215158 (2010).
4. Gwyn K., Sinicrope F.A.: Am. J. Gastroenterol. 97, 13 (2002).
5. Boghossian S., Hawash A.: Surgeon 10, 43 (2012).
6. Rothwell P.M., Wilson M., Elwin C.E., Norrving B., Algra A., Warlow Ch.P., Meade T.W.: Lancet 376, 1741 (2010).
7. Umar A., Dunn B. K., Greenwald P.: Nature Rev. Cancer 12, 835 (2012).
8. Park J.H., McMillan D.C., Horgan P.G., Roxburgh C.S.: Cancer Treat. Rev. 40, 68 (2014).
9. Lichtenberger L.M., Zhou Y., Jayaraman V., Doyen J.R., O'Neil R.G., Dial E.J., Volk D.E. et al.: Biochim. Biophys. Acta 1821, 994 (2012).
10. Nunes C., Brezesinski G., Pereira-Leite C., Lima J.F.C., Reis S., Lúcio M.: Langmuir 27, 10847 (2011).
11. Krasnowska E.K., Gratton E., Parasassi T.: Biophys. J. 74, 1984 (1998).
12. Bagatolli L.A., Parasassi T., Fidelio G.D., Gratton E.: Photochem. Photobiol. 70, 557 (1999).
13. Lipinski Ch.A., Lombardo F., Dominy B.W., Feeney P.J.: Adv. Drug Deliv. Rev. 23, 3 (1997).
14. Heimburg T.: J. Biophys. 78, 1154 (2000).
15. Kyriokou I., Hadjikakou S.K., Kovala-Demertzi D., Viras K., Mavromoustakos T.: Chem. Phys. Lipids 132, 157 (2004).
16. Jain M.K., Wu N.M.: J. Membr. Biol. 34, 157 (1977).
17. Lakowicz J.R.: Principles of Fluorescence Spectroscopy. 3rd edn., Springer, Heidelberg, New York 2006.

Acta Poloniae Pharmaceutica – Drug Research, Vol. 71 No. 6 pp. 1013–1022, 2014 ISSN 0001-6837
Polish Pharmaceutical Society

DETERMINATION OF ORGANIC VOLATILE IMPURITIES IN NEPAFENAC BY GC METHOD

MARIOLA MUCHA[1]*, ALEKSANDRA GROMAN[1], JOANNA ZAGRODZKA[1] and MARCIN CYBULSKI[2]

[1]R&D Analytical Chemistry Department, [2]Chemistry Department, Pharmaceutical Research Institute, Rydygiera 8, 01-793 Warszawa, Poland

Abstract: The methods for controlling volatile impurities, including reagent and starting material, in Nepafenac active pharmaceutical ingredient, are reported. The proposed methods were developed using gas chromatography (GC) and gas chromatography with headspace injection (GC-HS) and validated according to the requirements of the ICH (International Conference of Harmonization) validation guidelines Q2R1 and the guideline for residual solvents Q3C.

Keywords: GC method, GC-HS method, validation, nepafenac, residual solvents, organic volatile impurities

Nepafenac, 2-amino-3-benzoylbenzeneacetamide (NF3), is non-steroidal anti-inflammatory drug (NSAID) formulated as an ophthalmic suspension. Nepafenac is a pro-drug of amfenac, a highly effective nonselective cyclooxygenase COX-1 and COX-2 inhibitor. It is used to prevent and treat ocular pain and inflammation that can occur after cataract surgery by reducing the production of prostaglandins in the eye (1, 2). Recently, our new method for nepafenac synthesis (Fig. 1.) and HPLC validated procedure for its purity and assay determination has been published (3, 4). To continue our studies on nepafenac active pharmaceutical ingredient, the GC and GC-HS methods for determination of organic volatile impurities and residual solvents has been elaborated and verified in validated analytical procedure. It is commonly known that residual solvents in active pharmaceutical ingredient are used or produced in manufacturing process and may stem from starting materials, reagents, intermediates, solvents etc. or can be formed in degradation process. It is assumed that the solvents and other volatile impurities may not be fully removable during API manufacturing. Therefore, their acceptable amounts are recommended due to patient safety and elimination of potential toxic risk (5, 6). Moreover, the presence of the particular solvent in production process effects the yield and quality of API and drug formulation. Thus, the selection of the solvents may be considered as one of the critical parameter of the process. According to *ICH Topic Q3C (R4) Impurities: Guideline for Residual Solvents* all sol-

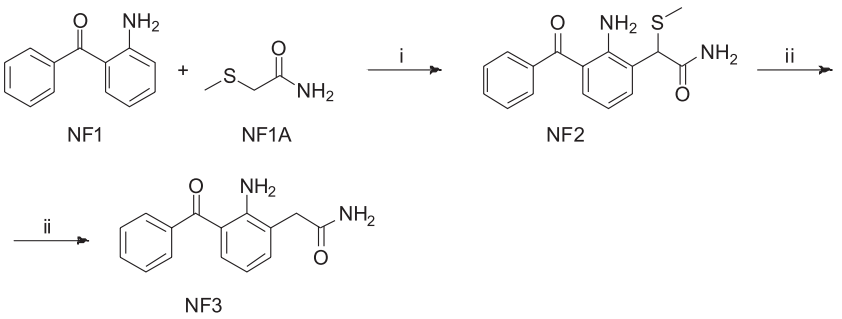

Figure 1. Nepafenac synthesis: i) N-chlorophthalimide, 1,4-dichloromethane (DCM), triethylamine (TEA), 1 M KOH_{aq} ii) Raneys type nickel, acetone, 2-propanol

* Corresponding author: e-mail: m.mucha@ifarm.eu; phone: +48 22 4563992

vents are classified into four classes based on their toxicity and potential environmental hazard (Class 1 – should be avoided; Class 2 – should be limited in pharmaceutical products because of their inherent toxicity; Class 3 – should be used only where it would be impractical to remove them and Class 4 – there is no adequate toxicological data and manufacturers should supply justification for the residual levels of these solvents in pharmaceutical products).

In the official monographs: USP (United States Pharmacopeial Convention) and EP (European Pharmacopoeia) there are no documents related to nepafenac. There are also no references to GC studies for the determination of: residual solvents, TEA and NF1A in active substance or purity control of the starting material NF1A, except the GC method disclosed for residual solvents in the patent document (7).

According to the method presented in this patent, the analyses were carried out using the gas chromatograph with FID, interfaced an auto-sampler and chromatographic separations were performed on the TRB-5 column. The main disadvantages of revealed procedure was the long analysis time.

In the present study, the residual solvents in nepafenac active substance were determined, using gas chromatographic techniques with headspace injection (GC-HS). For controlling the quality of the starting material NF1A (Fig. 1.) and the level thereof in final nepafenac API as well as triethylamine residual reagent, the gas chromatography methods with direct injection appeared to be more effective. The all revealed validation results meet the requirements of the ICH (International Conference of Harmonization) validation guidelines Q2R1 (5) and the guideline for residual solvents Q3C (6). Our analytical studies include the following validated methods: the full validation of a GC-HS analytical method for the determination of residual solvents (Class 3: acetone, 2-propanol); the limited validations of GC-HS analytical methods for the determination of solvents (Class 2: dichloromethane, methanol, toluene and Class 1: benzene); the limited validations of GC methods with direct injection analytical for the determination of triethylamine (TEA) and NF1A; the validation of the GC method with direct injection to control the quality of the starting material – NF1A (normalization method procedure).

MATERIALS AND METHODS

Chemicals and reagents

The active substance – nepafenac was synthesized at Pharmaceutical Research Institute (Warszawa, Poland). The solvents and starting material were purchased from commercial suppliers (acetone, 2-propanol, methanol, dichloromethane and toluene from POCH Avantor Performance Materials Poland S.A. (Poland), benzene and triethylamine from Fluka (Germany), N,N-dimethylacetamide from Sigma-Aldrich (Germany), 2-(methylthio)acetamide from Watson International Ltd. (China)).

Preparation of solutions and sample

All solutions were prepared directly before the analysis. In the methods I, II, IV and V the blanks were made up of N,N-dimethylacetamide (DMA); in the method III blank solution was formed from N,N-dimethylacetamide (DMA) and 1 mL of H_2O; and in the method VI the blank contained only methanol.

Method I (Determination of acetone, 2-propanol)

The test solution was prepared by dissolving the appropriate amounts of nepafenac in DMA to obtain the concentration of 4%. The standard solution I was prepared by dissolving the appropriate amounts of acetone and 2-propanol in DMA and then dilution to reach 5000 µg/mL of acetone and 2-propanol with respect to the sample preparation. The standard solution II was prepared by diluting the standard solution I to reach 500 µg/mL of acetone and 2-propanol.

Method II (Determination of methanol, dichloromethane and toluene)

The test solution was prepared by dissolving the appropriate amounts of nepafenac in DMA to obtain the concentration of 4%. The standard solution was prepared by dissolving the appropriate amounts of methanol, dichloromethane and toluene in DMA and dilution to reach 300 µg/mL of methanol, 60 µg/mL of dichloromethane and 89 µg/mL of toluene with respect to the sample preparation.

Method III (Determination of benzene)

The test solution was prepared by dissolving the appropriate amounts of nepafenac in DMA to obtain the concentration of 10%. The standard solution was prepared by dissolving the appropriate amounts of benzene in DMA and dilution to reach 0.6 µg/mL with respect to the sample preparation.

Method IV (Determination of triethylamine)

The test solution was prepared by dissolving the appropriate amount of nepafenac in DMA to obtain the concentration of 8%. The standard solu-

tion was prepared by dissolving the appropriate amount of triethylamine in DMA and dilution to reach 500 µg/mL with respect to the sample preparation. The reference solution was prepared by adding the standard solution to the sample.

Method V (Determination of 2-(methylthio)acetamide)

The test solution was prepared by dissolving the appropriate amount of nepafenac in DMA to obtain the concentration of 8%. The standard solution was prepared by dissolving the appropriate amount of 2-(methylthio)acetamide (NF-1A) in DMA followed by dilution up to 500 µg/mL with respect to the sample preparation. The reference solution was prepared by addition the standard solution to the sample.

Method VI (Purity control of the starting material NF-1A)

The test solution was prepared by dissolving the appropriate amount of 2-NF-1A in methanol to obtain the concentration of 10%.

Chromatographic conditions

Methods: I, II and III were performed using the Perkin Elmer CLARUS 500 gas chromatograph with a flame ionization detector interfaced with a Perkin Elmer headspace TURBOMATRIX 40 autosampler. Chromatographic separations were performed on a DB-624 column (phase composition: 6% cyanopropylphenyl – 94% dimethylpolysiloxane), film thickeness 1.8 µm, 60 m long and 0.32 mm ID. Method IV was carried out on the Shimadzu GC-2010 gas chromatograph with a flame ionization detector interfaced with a Shimadzu AOC-20i autosampler. Chromatographic separations were performed on a DB-624 column (phase composition: 6% cyanopropylphenyl – 94% dimethylpolysiloxane), film thickeness 1.8 µm, 60 m long, 0.32 mm ID. The other two methods (V and VI) were conducted on the same apparatus as Method IV, with the difference being that DB-5 column was used for chromatographic separations (phase composition: (5% phenyl methylpolysiloxane – 95% dimethylpolysiloxane), film thickeness 1.0 µm, 30 m long, 0.32 mm ID)

Method I and Method II (Determination of acetone, 2-propanol and methanol, dichloromethane, toluene)

These two methods used the same oven temperature programs: the initial temperature of 45°C was maintained for 9 min after the injection; then, it was ramped up at the rate of 10°C/min to 150°C and ramped up again at the rate of 40°C/min to 240°C, finally maintained for 3 min. The injection port temperature was 240°C and the detector temperature was 260°C. Nitrogen was used as the carrier gas at 100 kPa, split 5 : 1, attenuation – 5. The vial oven temperature was set at 100°C for 30 min. The needle temperature was 110°C, the transfer line was 120°C, injection: 0.05 min.

Method III (Determination of benzene)

The oven temperature program was as follows: the initial temperature 35°C was ramped up at the rate of 2°C/min to 70°C and it was maintained for 2 min then, it was ramped up again at the rate of 40°C/min to 240°C and maintained for 6 min. The injection port temperature was 240°C and the detector temperature was 260°C. Nitrogen was used as the carrier gas at 100 kPa, split 3 : 1, attenuation – 5. The vial oven temperature was set at 95°C for 30 min. The needle temperature was 110°C, the transfer line was 120°C, injecton: 0.07 min.

Method IV (Determination of triethylamine)

The oven temperature program was as follows: the initial temperature of 35°C; it was then ramped up at the rate of 2°C/min to 70°C and maintained for 3 min then, it was ramped up again at the rate of 40°C/min to 240°C and maintained for 10 min. The injection port temperature was 240°C and the detector temperature was 260°C. Nitrogen was used as the carrier gas at 100 kPa, split 5 : 1, injection 1 µL.

Method V (Determination of NF-1A)

The oven temperature program was as follows: the initial temperature of 120°C; it was ramped up at the rate of 10°C/min to 190 °C, then, ramped up again at the rate of 30°C/min to 280°C and maintained for 10 min. The injection port temperature was 260°C and the detector temperature was 290°C. Nitrogen was used as the carrier gas at 50 kPa, split 10 : 1, injection 1 µL.

Method VI (Purity control of the starting material NF-1A)

The oven temperature program was as follows: the initial temperature of 60°C; it was then ramped up at the rate of 5°C/min to 260°C. The injection port temperature was 260°C and the detector temperature was 290°C. Nitrogen was used as the carrier gas at 50 kPa, split 20:1, injection 0.5 µL.

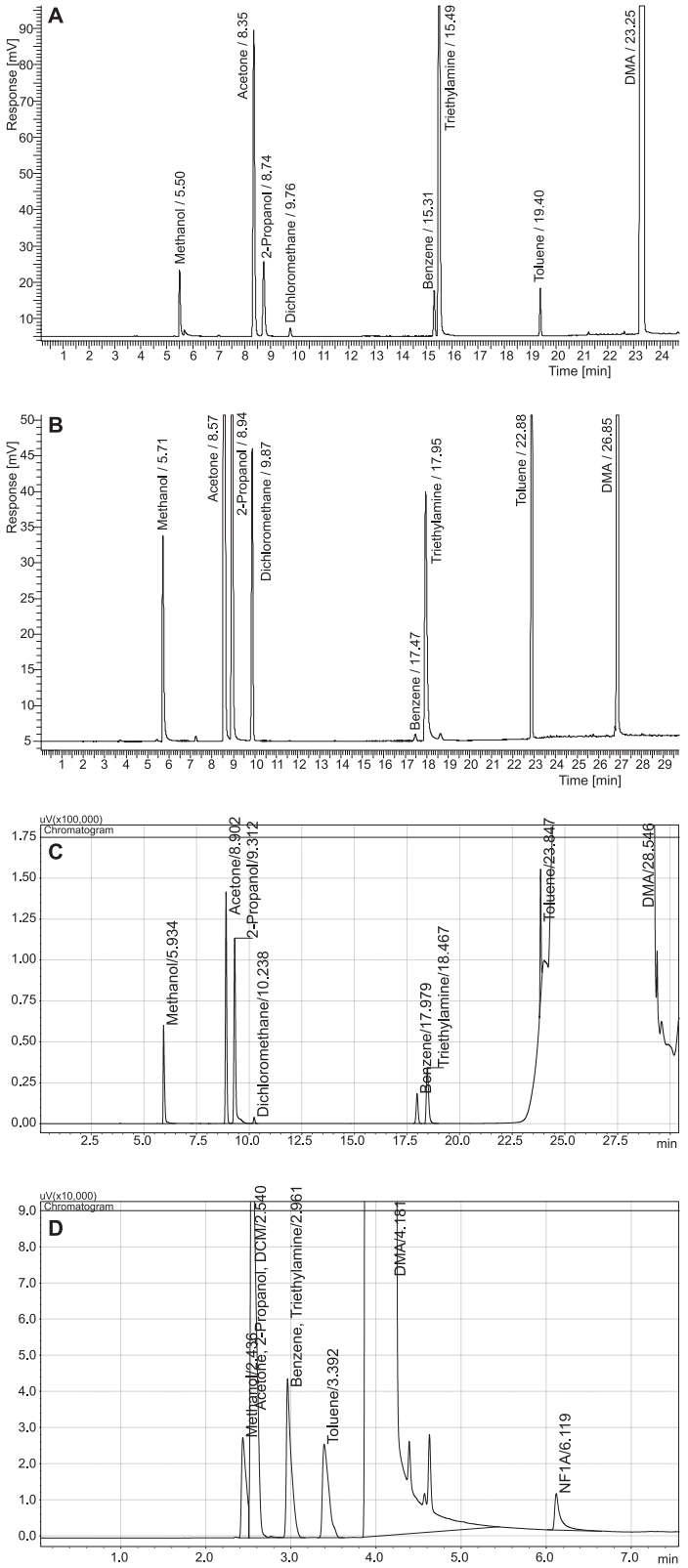

Figure 2. The chromatograms of the specificity solution: **A**) methods I and II; **B**) method III; **C**) method IV; **D**) method V

RESULTS AND DISCUSSION

Method I (Determination of acetone, 2-propanol – full validation procedure)

In this study, the HS-GC analytical method was developed and validated for the quantitative determination of acetone and 2-propanol i.e., the solvents used in the last step of the nepafenac synthesis. The method selectivity, limits of detection and quantitation, linearity, range, precision (system repeatability), recovery and robustness (changes in the GC conditions) were determined in consequence.

Specificity

The following solvents were used during the synthesis of nepafenc: acetone, 2-propanol, methanol, dichloromethane, toluene, triethylamine and a potential contaminant of acetone – benzene. The specificity of the method was evaluated by injecting the specificity solution containing the solvents from the synthesis route. The method was spe-

Table 1. Results of the method I (linearity, precision, SST, accuracy).

Parameters		Acetone	2-Propanol
Linearity of the method			
Statistical parameters of regression	R	0.9998	1.0000
	R^2	0.9995	0.9999
	y-intercept (b)	1504.6	–1218.3
	S_b	3685.08	423.05
	$t_{b, exp.}$	0.41	–2.88
	Slope (a)	77.819	21.852
	S_a	0.986	0.113
	$t_{a, exp.}$	78.95	193.02
	$t_{kr} = 3.18_{(\alpha = 0.05, n=5)}$	$t_r = 77.22$	$t_r = 173.2$
	y = ax + b	y = 77.819x + 1504.6	y = 21.852x – 1218.3
Precision			
Results of the precision	SD %	2.81%	2.60%
Results of 6 independent reference solutions	RSD %	4.98%	2.57%
Results of 6 independent reference solutions intermediate precision	RSD %	2.54%	2.28%
F-Snedecor test	F	3.31	1.10
System precision (SST)			
The solution containing 5000 µg/mL of the analytes	RSD% Peak area	1.66%	1.52%
	RSD% Retention time (min)	0.018%	0.017%
The solution containing 500 µg/mL of the analytes	RSD% Peak area	4.07%	4.14%
	RSD% Retention time (min)	0.027%	0.023%
Accuracy			
Recovery	[%]	105.33	108.63
RSD	[%]	2.81	2.72
CI	–	1.88	1.88

R – correlation coefficient, t_a , t_b , t_r , t_{kr} – parameters of Student's t-test, S_a, S_b – standard deviation of a and b, CI – confidence interval, RSD – relative standard deviation, F – parameters of Snedecor's F-test, SST – system suitability test.

cific for residual solvents (resolution R_s = 1.5; methanol/acetone – 27.28, acetone/2-propanol – 2.90, 2-propanol/dichloromethane – 8.01, dichloromethane/benzene – 51.08, benzene/triethylamine – 1.75, triethylamine/toluene – 39.66, toluene/DMA – 28.21). Spiking the sample with the analyte did not cause the peak splitting and the retention times remained the same as for the corresponding peak from the test solution (Fig. 2.).

Linearity and range

The linearity of the method was evaluated by analyzing five solutions ranging in concentrations from about 500 to 6000 µg/mL with respect to sample preparation. All concentrations were prepared in triplicate and the average was reported. The method is linear within a wide range for the solvents included in the validation; acceptance criteria (R^2 = 0.990, $y = ax + b$, $t_a = t_{kr,} | t_b | < t_{kr} , | t_r | > t_{kr}$ (α = 0.05, n – 2)) were confirmed. The plot of the concentration *versus* the response, the correlation coefficient, y-intercept and slope of the regression line were calculated and are presented in Table 1.

Precision

The precision of the method was established as repeatability, system and intermediate precision. Repeatability was performed by measuring triplicate independent preparations of four solutions – sample spiked with the analytes at 500, 2500, 5000 and 6000 µg/mL with respect to the sample preparation; 3 test solutions and 6 independent solutions – sample spiked with the analytes at about 5000 µg/mL with respect to the sample preparation, then the relative response (the relation of peak area to mass) was calculated. The intermediate precision was repeated on a different day by a different analyst by measuring 6 independent solutions – sample spiked with the analytes at about 5000 µg/mL with respect to the sample preparation, then the relative response (the relation of peak area to mass) was calculated. The comparison of the repeatability results and intermediate precision were performed using the F-Snedecor test. The results are expressed as a relative standard deviation (RSD%) and summarized in Table 1 and all criteria were fulfilled (RSD = 15%, $F = F_{kr}$ (α = 0.05, $f_1 = n_1 - 1$, $f_2 = n_2 - 1$) F_{kr} = 5.05 (n = 6)).

SST (system suitability test)

The system suitability test involves the examination of the system precision and resolution. The system precision was established by measuring the response of six replicate injections of the standard solution I and six replicate injections of the standard solution II. The results are presented as a relative standard deviation (RSD%) for the peak area and retention time (Table 1) and these were below 10% (peak area) and 1% (retention time).

Limit of quantitation (LOQ) and limit of detection (LOD)

The limit of quantitation (LOQ) and limit of detection (LOD) were evaluated by using the standard solutions containing the known low concentrations of solvents. The concentration which generated the peak about 10 times as high as the noise's height was stated as LOQ (acetone – 28 µg/mL, 2-propanol – 90 µg/mL). The concentration which generated the peak about 3 times as high as the noise's height was stated as LOD (acetone – 9 µg/mL, 2-propanol – 35 µg/mL).

Robustness

The robustness of the method was evaluated by injecting the specificity solution to ensure the separation of all the solvents from synthesis route with the use of different chromatographic conditions. The following parameters were tested: column temperature ± 5°C, rate ± 1°C/min, carrier gas pressure ± 10% and constant temperature time ± 1 min. The smallest resolution (Rs) was obtained between benzene and triethylamine Rs = 1.53 at carrier gas pressure 90 kPa. The changes in analytical conditions did not influence the resolution significantly and the method was robust.

Accuracy

The accuracy of the method was established by assaying 12 sample solutions (triplicate independent preparations of four solutions – sample spiked with the analytes at 500, 2500, 5000 and 6000 µg/mL of the specification limit). The results of the recovery, relative standard deviation (RSD%) and confidence interval (CI) are presented in Table 1. The acceptable criteria were set up as the RSD value below 15% and the recovery: 80–120%.

Method II (Determination of methanol, dichloromethane and toluene – limited validation procedure)

The control of residual methanol, dichloromethane and toluene in nepafenac by GC-HS method was elaborated as a limit test procedure, because these solvents were used prior to the last step in the synthesis and were not detected in the tested batches of the substance. The validation of this method included the examination of specificity, detection limit and additionally system precision.

Specificity

The specificity of the method was evaluated by injecting the specificity solution consisting of the solvents from the synthesis route (Fig. 2). The method was specific for residual solvents (R_s = 1.5, methanol/acetone – 27.28, acetone/2-propanol – 2.90, 2-propanol/dichloromethane – 8.01, dichloromethane/benzene – 51.08, benzene/triethylamine – 1.75, triethylamine/toluene – 39.66, toluene/DMA – 28.21).

SST (system suitability test)

The system precision was established by measuring the response of six replicate injections of the SST solution with the solvents at 300 µg/mL of methanol, 60 µg/mL of dichloromethane and 89 µg/mL of toluene with respect to the sample preparation. Results were presented as a relative standard deviation (RSD%) for the peak area (methanol – 1.46%, dichloromethane – 6.05%, toluene – 5.35%) and retention time (methanol – 0.025%, dichloromethane – 0.023%, toluene – 0.010%) and these were below 10% (peak area) and 1% (retention time).

Limit of detection (LOD)

The prepared solutions containing known low concentrations of solvents were injected into a chromatograph. The concentration which generated the peak about 3 times as high as the noise's height was stated as LOD (methanol – 28 µg/mL, dichloromethane – 25 µg/mL, toluene – 8 µg/mL).

Method III (Determination of benzene)

The validation of this method (limit test procedure) included the examination of the specificity, system precision and the detection limit. Benzene was not used during the synthesis but it is commonly considered as a potential contaminant of acetone and toluene. In the tested batches of nepafenac benzene was not detected.

Specificity

The specificity of the method was evaluated by injecting the specificity solution consisting of the solvents from the synthesis route (Fig. 2). The method was specific for residual solvents (R_s = 1.5, methanol/acetone – 23.81, acetone/2-propanol – 3.01, 2-propanol/dichloromethane – 7.49, dichloromethane/benzene – 53.06, benzene/triethylamine – 2.65, triethylamine/toluene – 36.44, toluene/DMA – 47.59).

SST (system suitability test)

The system precision was established by measuring the response of six replicate injections of the solution with benzene at the level of 0.6 µg/mL, with respect to the sample preparation. The results were presented as a relative standard deviation (RSD%) for the peak area and retention time and were: RSD% (peak area) – 4.54%; , RSD% (retention time) – 0.033%, respectively to acceptance criteria (RSD = 10% – peak area, RSD = 1% retention time).

Limit of detection (LOD)

The prepared samples containing known low concentrations of benzene were injected into a chromatograph. The concentration which generated the peak about 3 times as high as the noise's height was stated as LOD. In this method LOD was found as 0.2 µg/mL, with respect to the sample preparation.

Method IV (Determination of triethylamine)

The validation of a GC analytical method (limit test procedure) with direct injection for the determination of TEA involved the examination of the specificity, system precision as well as the detection limit, because triethylamine was used during the synthesis but not detected in the tested batches of nepafenac.

Specificity

The specificity of this method was examined by the use of the specificity solution. The specificity solution consists of the solvents from the synthesis route: acetone, 2-propanol, methanol, dichloromethane, toluene, triethylamine and benzene. The parameter measured included the resolution (Rs) and it was higher than 1.5 (methanol/acetone – 27.45, acetone/2-propanol – 3.34, 2-propanol/dichloromethane – 7.22, dichloromethane/benzene – 54.26, benzene/triethylamine – 2.71, triethylamine/toluene – 38.27, toluene/DMA – 12.91). The chromatogram of this solution is shown in Figure 2.

Limit of detection (LOD)

The determination of the signal-to-noise was performed by comparing the measured signals from the prepared samples containing known low concentrations of TEA with those of the blank samples and establishing the minimum concentration at which TEA can be reliably detected. The concentration which generated the peak about 3 times as high as the noise's height was stated as LOD and it amounted to 4 µg/mL (substance).

SST (system suitability test)

The system suitability test was analyzed by measuring the response of six replicate injections of

the reference solution (TEA at the level of 500 µg/mL, with respect to the sample preparation). The results were presented as a relative standard deviation (RSD%) for the peak area and retention time and were: RSD% (peak area) – 0.96%; RSD% (retention time) – 0.017%, respectively to acceptance criteria (RSD = 10% – peak area, RSD = 1% retention time).

Method V (Determination of NF-1A)

The method was validated for the examination of the specificity, system precision as well as the detection limit (limit test procedure), because NF-1A was used during the synthesis but not detected in the tested batches of nepafenac.

Specificity

The specificity of this method was examined by the use of the specificity solution. The specificity solution consists of the solvents from the synthesis route: acetone, 2-propanol, methanol, dichloromethane, toluene, triethylamine and a potential contaminant of acetone – benzene. The parameter measured included the resolution (Rs) and it was higher than 1.5 (methanol + acetone + 2-propanol + dichloromethane + benzene + triethylamine + toluene + DMA /NF1A – 8.38). The chromatogram of this solution is shown in Figure 2.

Limit of detection (LOD)

The determination of the signal-to-noise is performed by comparing the measured signals from the prepared samples containing known low concentrations of NF-1A with those of the blank samples and establishing the minimum concentration at which NF-1A can be reliably detected. The concentration which generated the peak about 3 times as high as the noise's height was stated as LOD and it was 180 µg/mL (substance).

SST (system suitability test)

The system precision was established by measuring the response of six replicate injections of the reference solution (NF-1A at level 500 µg/mL, with respect to the sample preparation). The results were presented as a relative standard deviation (RSD%) for the peak area and retention time and were: RSD% (peak area) – 3.95%; RSD% (retention time) – 0.031%, respectively to acceptance criteria (RSD = 10% – peak area, RSD = 1% retention time).

Method VI (Purity control of the starting material NF-1A)

The gas chromatography method with direct injection was applied to control the quality of this material. The validation of this method (normalization method procedure) included tests of the specificity, detection limit, linearity and range at the area normalization.

Specificity

The specificity of this method was examined by the use of the test solution. The parameter measured included resolution (Rs) and it was higher than 1.5 (methanol/impurity 1 – 7.6, impurity 1/impurity of methanol – 6.1, impurity of methanol/impurity 2

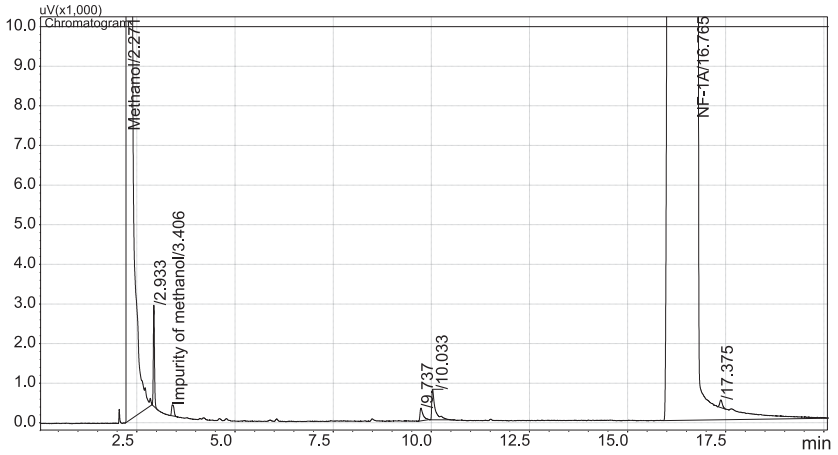

Figure 3. The chromatogram of test solution – method VI

Table 2. Results of the method VI (linearity and range of the area normalization method).

Parameters					**2-(methylthio)acetamide**
Linearity of the method					
Statistical parameters of regression		R R^2 y-intercept (b) S_b $t_{b, exp.}$ Slope (a) S_a $t_{a, exp.}$ $t_{kr} = 3.18_{(\alpha = 0.05, n=5)}$ y = ax + b			0.9997 0.9994 –20968 117209 –0.18 108419 1588 68.26 $t_r = 70.70$ y = 108419x – 20968
Range of the area normalization method					
Solution	Concentration (% of test solution)	Impurity 1 [%]	Impurity 2 [%]	Impurity 3 [%]	NF-1A [%]
1	120%	0.046 0.046	0.017 0.017	0.041 0.044	99.895 99.894
2	100%	0.047 0.045	0.016 0.016	0.043 0.042	99.894 99.897
3	50%	0.045 0.044	0.014 0.015	0.037 0.037	99.904 99.905
4	10%	0.017 0.012	0 0	0.025 0.025	99.958 99.964
Mean		0.038	0.012	0.037	99.914
SD		0.014	0.007	0.008	0.029
RSD		36.84%	58.33%	21.62%	0.03%
1	120%	0.046 0.046	0.017 0.017	0.041 0.044	99.895 99.894
2	100%	0.047 0.045	0.016 0.016	0.043 0.042	99.894 99.897
3	50%	0.045 0.044	0.014 0.015	0.037 0.037	99.904 99.905
Mean		0.046	0.016	0.041	99.898
SD		0.001	0.001	0.003	0.005
RSD		2.17%	6.25%	7.32%	0.005%

R – correlation coefficient, t_a , t_b , t_r , t_{kr} – parameters of Student's t-test, S_a, S_b – standard deviation of a and b.

– 52.8, impurity 2/impurity 3 – 2.3, impurity 3/NF-1A – 14.4, impurity 4 – on the tail of the main peak). The chromatogram of this solution is shown in Figure 3.

Limit of detection (LOD)

The solutions of different lowering concentrations of the examined substance were injected into a chromatograph. The concentration which generated the peak about 3 times as high as the noise's height was stated as LOD. In this method LOD was 0.05%.

Linearity

The linearity of the method was evaluated by analyzing the solutions ranging in concentrations from about 5 to 120% of the test solution. The method is linear within this range and acceptance criteria [$R^2 = 0.990$, y = ax + b , $t_a = t_{kr,} | t_b | < t_{kr ,} | t_r | > t_{kr} (\alpha = 0.05, n – 2)$] were confirmed. Two replicate injections were made for each concentration and the average result was reported. The correlation coefficient, y-intercept and slope of the regression line were calculated (Table 2).

Range of the area normalization method

The range of the area normalization method was evaluated by analyzing the solutions ranging in concentrations from about 120 to 10% of the test solution. Two replicate injections were made for each concentration. The acceptance criteria of this method: RSD = 15% for impurities; RSD = 0.05% for NF-1A were suitable for its intended purpose. The results of the assay (%) of the impurities and NF-1A, the mean, standard deviation (SD) and relative standard deviation (RSD%) are presented in Table 2.

DISCUSSION AND CONCLUSION

In the present report, a simple, rapid, sensitive, reliable, specific, accurate and precise GC methods for the determination of residual solvents (acetone, 2-propanol, methanol, toluene, dichloromethane, benzene), reagent (triethylamine) and starting material (2-(methylthio)acetamide) in nepafenac API batches and purity of starting material (NF-1A) were developed and validated. The complete validation of the GC-HS method to control the presence of solvent from the final synthetic step, acetone and 2-propanol, in nepafenac API was performed. The method turned out to be specific, accurate, linear, precise and the solvents were detected and quantified at a µg/mL level. Similarly, GC-HS limit test procedure for the solvents used in manufacturing process but not observed in nepafenac batches, i.e., methanol, dichloromethane, toluene and benzene as the potential contaminant of acetone, demonstrated adequate specificity, precision and allowed for the µg/mL detection. In course of triethylamine (reagent) and starting material NF-1A evaluation in nepafenac batches it was shown that GC analytical method with direct injection is suitable for its intended purpose i.e., limit test procedure. The satisfying results were achieved for the purity control of the starting material NF-1A. In conclusion, all the parameters for the demonstrated analytical methods fall within the expected limits, therefore, GC-HS and GC methods can be used for the routine QC analysis of nepafenac API.

Acknowledgment

The study was supported by European Union under European Regional Development Fund No. UDA-POIG.01.03.01-14-068/08 “Innovative technologies of ophthalmic medicines of special therapeutic and social importance”.

REFERENCES

1. Kim S.J., Flach A.J., Jampol L.M.: Surv. Ophthalmol. 55, 108 (2010).
2. http://www.emea.europa.eu/docs/en_GB/document_library/EPAR_-_Scientific_Discussion/human/000818/WC500027155.pdf
3. Cybulski M., Formela A., Mucha M., Kłos K., Roszczyński J., Winiarski J.: Lett. Org. Chem. 9, 461 (2012).
4. Lipiec-Abramska E., Jedynak Ł., Formela A., Roszczyński J., Cybulski M., Puchalska M., Zagrodzka J.: J Pharm. Biomed. Anal. 91, 1 (2014).
5. Harmonized Tripartite Guideline on Validation of Analytical Procedures: Text and Methodology (Q2(R1), International Conference on Harmonization of Technical Requirements for Registrations of Pharmaceuticals for Human Use (ICH), Geneva 2005.
6. Harmonized Tripartite Guideline on Impurities: Guideline for residual solvents (Q3C(R5), International Conference on Harmonization of Technical Requirements for Registration of Pharmaceuticals for Human Use (ICH), Geneva 1997.
7. Patent US 2009/0312575 A1.

Project co-financed by the European Regional Development Fund under the framework of the Innovative Economy Operational Programme.

UDA-POIG contract no 01.03.01-14-068/08 „Innovative technologies of ophthalmic medicines of special therapeutic and social importance:”: www.ifarm.eu/poig/oftal/

Acta Poloniae Pharmaceutica – Drug Research, Vol. 71 No. 6 pp. 1023–1028, 2014 ISSN 0001-6837
Polish Pharmaceutical Society

BIORESORBABLE COPOLYMER OF L-LACTIDE AND ε-CAPROLACTONE FOR CONTROLLED PACLITAXEL DELIVERY

MONIKA MUSIAŁ-KULIK[1]*, KATARZYNA GĘBAROWSKA[1], JANUSZ KASPERCZYK[1,2], MAŁGORZATA PASTUSIAK[1], HENRYK JANECZEK[1] and PIOTR DOBRZYŃSKI[1,3]

[1]Centre of Polymer and Carbon Materials, Polish Academy of Sciences, Skłodowska-Curie St. 34, 41-819 Zabrze, Poland
[2]Medical University of Silesia in Katowice, School of Pharmacy and Division of Laboratory Medicine, Department of Biopharmacy, Jedności 8, 41-200 Sosnowiec, Poland
[3]Faculty of Mathematics and Natural Science, Jan Dlugosz University, Al. Armii Krajowej 13/1, 42-200 Częstochowa, Poland

Abstract: Bioresorbable, aliphatic polyesters are known in medicine where serve as orthopedic devices (e.g., rods, pins and screws) or sutures and staples in wound closure. Moreover, such materials are extensively studied as scaffolds – three-dimensional structures for tissue engineering but also drug delivery systems (DDS). The aim of this study was to determine the release profile of paclitaxel, one of the anti-inflammatory, antiproliferative and anti-restenotic agent, from biocompatible copolymer of L-lactide and ε-caprolactone that seems to be very attractive especially for minimally invasive surgery due to its potential shape-memory property. The influence of drug on copolymer hydrolytic degradation was also analyzed. Three types of matrices (3%, 5% of PTX and without drug) were prepared by solvent-casting method and degraded *in vitro*. The physicochemical changes of copolymer were analyzed by means of nuclear magnetic resonance spectroscopy (NMR), gel permeation chromatography (GPC) and differential scanning calorimetry (DSC). The amount of drug released into media was monitored with the use of high-pressure liquid chromatography (HPLC). Similar drug release profiles were obtained for matrices with paclitaxel. The drug-containing matrices degraded slightly slower than drug free matrices, regardless PTX content. Results of this work may be helpful in designing new bioresorbable paclitaxel delivery system applied in anti-cancer therapy or drug-eluting stents technology.

Keywords: paclitaxel, drug delivery systems, bioresorbable polymers, poly(L-lactide-co-ε-caprolactone), hydrolytic degradation

Bioresorbable, aliphatic polyesters are known in medicine where serve as orthopedic devices (e.g., rods, pins and screws) or sutures and staples in wound closure. These materials are extensively studied as scaffolds – three-dimensional structures for tissue engineering but also drug delivery systems. They possess many desirable features as biodegradation to non-toxic products, biocompatibility and easy manufacturing/processing (1). Furthermore, it was established that some of aliphatic polyesters and polyestercarbonates have the ability to recover from temporary to permanent shape upon external stimulus such as temperature or irradiation. Shape-memory effect may be utilized in minimally invasive surgery when deformed device is implanted through natural orifices or small incisions, e.g., cardiovascular stents (2, 3).

Controlled drug delivery systems (CDDS) possess many advantages when compared to conventional dosage forms. They provide even, local or systemic, release profile of drug for a determined period of time, help to reduce or avoid side effects and, what is more important, increase patient comfort during the treatment (4).

Paclitaxel (Taxol™, PTX), a plant-derived anti-cancer and anti-restenotic agent, has been originally isolated from the bark of *Taxus brevifolia*. Its anti-proliferative activity is due to the inhibition of microtubule depolymerization, which results in a suppression of cell cycle and leads to apoptosis. PTX is widely used as an antineoplastic agent against breast, ovarian, lung, head, colon cancer and Kaposi's sarcoma but also as an anti-restenotic drug eluted from cardiovascular stents (Taxus™, Boston

* Corresponding author: e-mail: mmusial@cmpw-pan.edu.pl

Scientific). Highly hydrophobic nature of paclitaxel promotes its cellular uptake but presents substantial formulation challenges, especially concerning duration and rate of drug release (5, 6). Copolymers of L-lactide and ε-caprolactone may be interesting as alternative materials for paclitaxel delivery.

Poly(L-lactide) (PLLA) constitutes one of the most intensively studied polymers for a wide range of applications, including packaging, agriculture and disposable materials as well as medical devices or scaffolds for tissue regeneration (7). PLLA characterizes good mechanical properties but even though the polymer loses its strength in approximately 6 months when degraded *in vitro*. Therefore, in order to modify its mechanical features and also rate of degradation, PLLA is often blended with other polymers as poly(ethylene glycol) (PEG), collagen, chitosan or copolymerized with e.g., D,L-lactide or glycolide. Poly(ε-caprolactone) (PCL), a semicrystalline polyester with high drug permeability and good organic solvent solubility, is known as a polymer with slow degradation rate. It was applied as a contraceptive implant delivering levonorgestrel (Capronor®). PCL has a glass transition temperature of –54°C, low tensile strength and an extremely high elongation at breakage (4700%) (8). Copolymers of L-lactide with ε-caprolactone are obtained to meet requirements, dependent on application, for physicochemical and mechanical properties that influence degradation and drug release rate. It was reported that some of poly(L-lactide-co-ε-caprolactone)s (PLACap) possess shape-memory property and may be also considered as drug delivery systems (9, 10).

The aim of this study was to determine the release profile of paclitaxel from biocompatible PLACap that seems to be very attractive especially for minimally invasive surgery due to its potential shape-memory property. The influence of drug on copolymer hydrolytic degradation was also analyzed.

EXPERIMENTAL

Poly(L-lactide-co-ε-caprolactone) was synthesized with the use of $Zr(Acac)_4$ as a low toxic initiator of the ring-opening polymerization. The reaction was performed at 150°C for 25 h with the initiator to monomer molar ratio (I/M) of 1/1100. Paclitaxel (PTX) was purchased from LC Laboratories®.

Appropriate amount of PLACap and drug were dissolved separately in methylene chloride. Then, the two solutions were mixed, degassed under reduced pressure and cast on Teflon plates. All films were dried at ambient temperature and then under reduced pressure. Ten millimeters discs were cut from the films. The matrices without drug were obtained analogously.

Three kind of matrix: 0, 3 and 5% of PTX was hermetically packed and irradiated with the use of electron beam. The weighted matrices were immersed in phosphate buffered saline (PBS, pH 7.4) and incubated at 37°C under constant shaking for 15 weeks. Medium was renewed once a week and collected for HPLC analysis. At predetermined time points, each type of matrix was withdrawn, washed with distilled water, weighted then dried under reduced pressure until constant weight. Water uptake and weight loss were calculated according to the following equations:

$$\text{Water uptake } (\%) = [(W_{wet} - W_{dry})/W_{dry}] \times 100 \quad (1)$$

$$\text{Weight loss } (\%) = [(W_0 - W_{dry})/W_0] \times 100 \quad (2)$$

where W_{wet} = the weight of wet sample after withdrawn, W_{dry} = the weight of dried sample, W_0 = the initial weight of sample before degradation.

NMR spectroscope (AVANCE II Ultra Shield Plus, 600 MHz, Bruker) was employed to record ^1H spectra of copolymers in order to characterize comonomers composition and chain microstructure. The number average molecular weight (M_n) and molecular mass dispersity (D) were defined by means of gel permeation chromatograph (GPC, Physics SP 8800 chromatograph). The glass-transition temperature T_g, melting temperature T_m and melting enthalpy ΔH_m were determined with the use of differential scanning calorimetry (DSC, TA DSC 2010, TA Instruments, New Castle, DE). The matrices were scanned from of –50°C to 200°C with the heating rate of 20°C/min) then quenched to –100°C in liquid nitrogen and scanned again. DSC was calibrated with high purity gallium and indium standards.

High-performance liquid chromatography (VWR-Hitachi LaChrom Elite®) was used to assess amount of paclitaxel released into PBS. Measurements were carried out with the use of LiChrospher® RP-18 column (250 × 4 mm, 5 μm) and guard column LiChrospher® RP-18 column (4 × 4 mm, 5 μm). The mobile phase consisted of acetonitrile and water (60 : 40, v/v) with the flow rate of 1 mL/min. Paclitaxel was detected at 227 nm in the presence of internal standard – docetaxel (LC Laboratories®).

RESULTS AND DISCUSSION

Copolymer of L-lactide and caprolactone (PLACap) was synthesized in order to prepare matrices for controlled paclitaxel delivery as well as

drug free matrices. Table 1 presents molecular characteristic of PLACap. The comonomer molar ratio was 87 : 13 with the average length of lactidyl and caproil blocks of 5.6 and 3.0, respectively. M_n was 38600 g/mol with the dispersity index (D) of 2.3. PLACap was semicrystalline, the glass transition temperature T_g = 35.5°C and melting temperature T_m = 134°C (ΔH_m = 20 J/g). Signals shown in ^{1}H-NMR spectrum (Fig. 1) were assigned to the lactidyl and caproil units.

Degradation process of matrices with and without paclitaxel was monitored by measuring water uptake and weight loss. It was established that water uptake is one of the initial step during hydrolytic degradation. Water molecules penetrate amorphous regions and lead to cleavage of ester bonds in the polymer chains (11). The water uptake of all matrices was almost the same during 12 weeks. After 15 weeks of incubation, drug free matrix exhibited the highest water uptake of 31%, while water uptake of

Table 1 Characterization of copolymer applied to obtain matrices.

Poly(L-lactide-co-*Í*-caprolactone)	F_{LL}	F_{Cap}	l^e_{LL}	l^e_{Cap}	Tg (°C)[1]	T_m (°C)[2]	ΔH_m (J/g)[2]	M_n (g/mol)	D
	87	13	5.6	3.0	35.5	139	20	38 600	2.3

F_{LL}, F_{Cap} – the percentage content of lactidyl and caproil units; l^e_{LL}, l^e_{Cap} – the average length of lactidyl and caproil blocks; T_g – glass transition temperature; T_m – melting temperature; $\ddot{A}H_m$ – melting enthalpy; M_n – number average molecular mass; D – dispersity index
[1] – data obtained from the second DSC scan; [2] – data obtained from the first DSC scan.

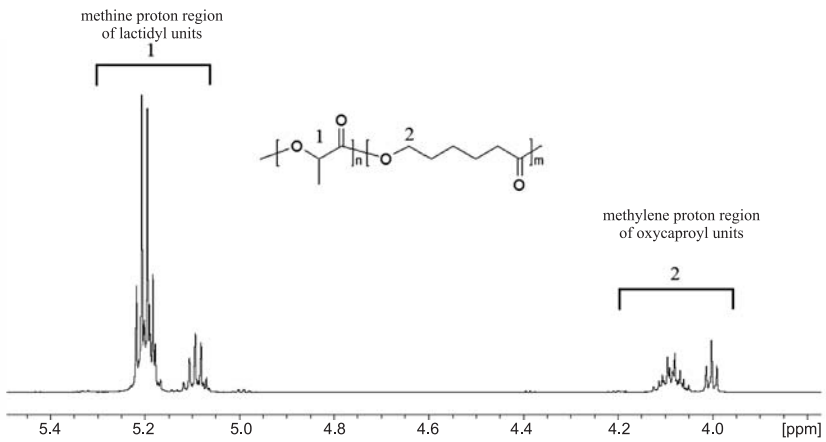

Figure 1. ^{1}H-NMR spectrum of poly(L-lactide-co-ε-caprolactone) recorded in $CDCl_3$

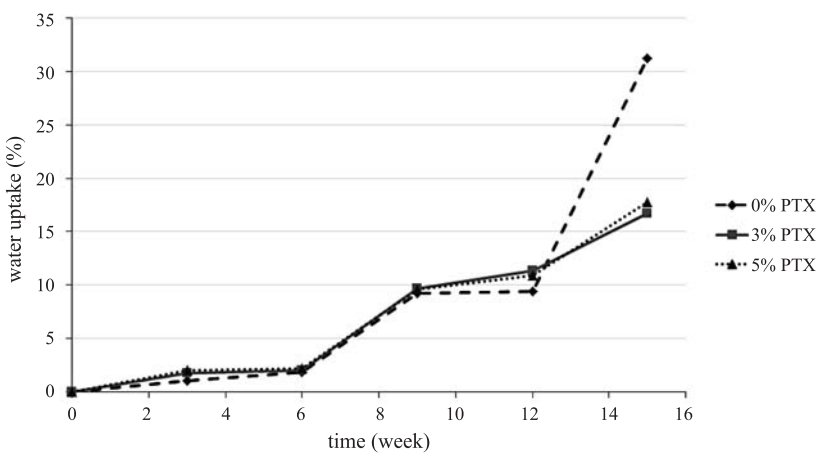

Figure 2. Water uptake of matrices during degradation

matrices with PTX reached 17 and 18% for matrix with 3 and 5% of PTX, respectively (Fig. 2). Weight loss of matrices is an effect of water-soluble oligomers and monomers release from the polymer bulk (12). The matrices with 3% and 5% of PTX lost their weight steadily to attain 29% after 15 weeks (Fig. 3). For matrix without drug, the weight loss profile was more unstable. Two rapid increases of weight loss was noticed after 9 weeks (from 3 to 18%) and 15 weeks (from 20 to 43%).

^{1}H-NMR spectra of PLACap were recorded in order to assess comonomer composition as well as the average length of lactidyl (l^e_{LL}) and caproil (l^e_{Cap}) blocks. The lactidyl units content increased and caproil units content decreased along with degradation. However, those changes were relatively small

Table 2. Changes in T_g of matrices during degradation.

Type of matrix	Degradation time (week)				
	3	6	9	12	15
0% PTX	32.5	28	24	26	35
3% PTX	34.5	28	25	25	29
5% PTX	33	28	27	24	30

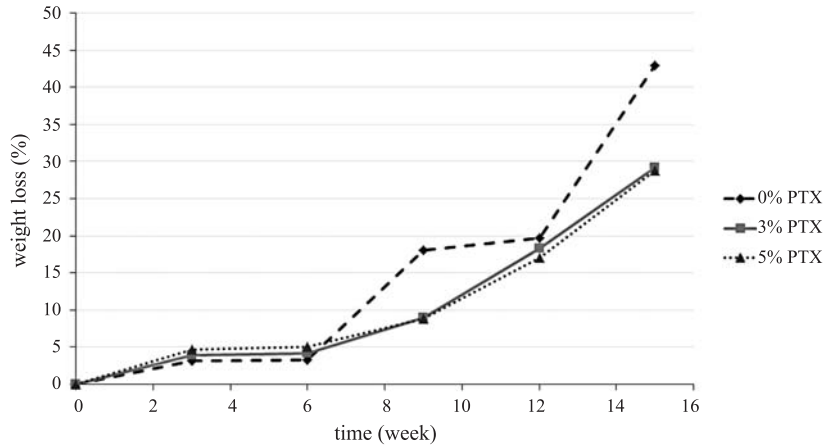

Figure 3. Weight loss of matrices during degradation

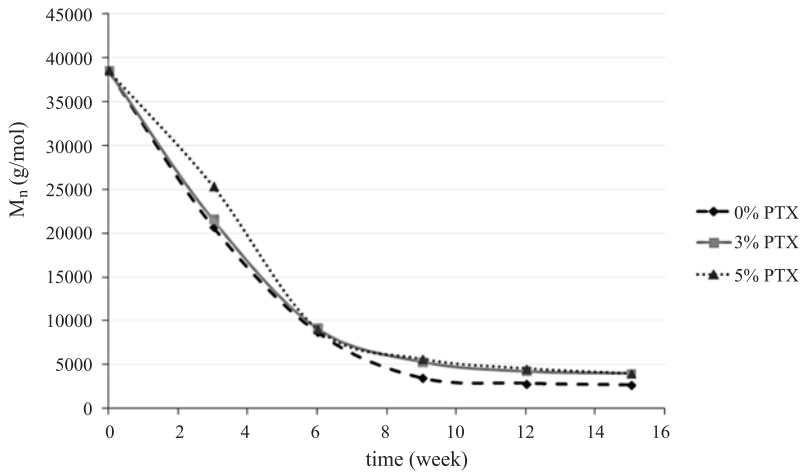

Figure 4. Changes of number average molecular weight M_n of matrices with and without PTX during degradation

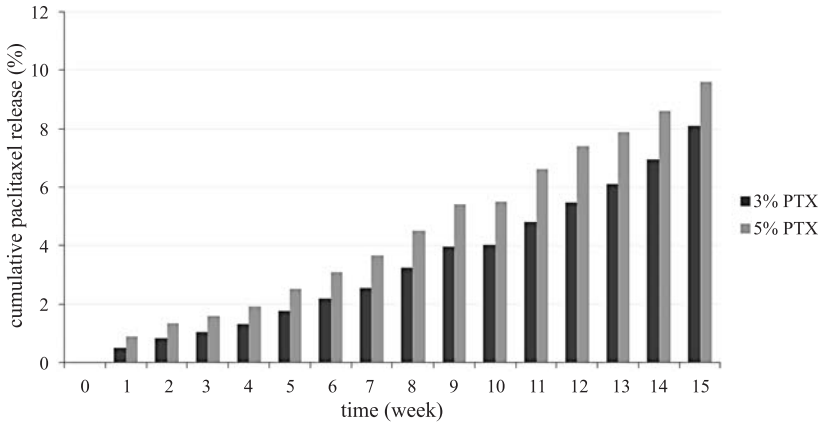

Figure 5. Cumulative release profiles of PTX from the matrices during degradation

since after 15 weeks comonomer molar ratio reached 90 : 10 (LA : Cap) for all matrices. The average lengths of caproil blocks remained stable during incubation. The l^e_{LL} decreased after 3 weeks, then increased gradually until 12 week in case of drug-containing matrices or 15 week for drug free matrix. A decrease of l^e_{LL} was observed at 15 week for both matrices with drug.

The changes in M_n and dispersity index (D) during degradation were followed by means of GPC. The highest M_n decrease was observed after 3 and 6 weeks in case of all types of matrices. After 15 weeks, M_n of drug free matrix was slightly lower than matrices with paclitaxel (Fig. 4). Dispersity index decreased after 3 weeks from initial 2.3 to 1.9, then increased to 2.0 after 6 weeks and decreased steadily to reach 1.9 (drug free matrix) and 1.7 (both matrices with PTX) after 12 weeks. It was previously reported that D decrease arises from scission of the polymer chains while its increase from release of soluble degradation products (13).

Thermal properties of matrices were analyzed with DSC. Table 2 shows changes of the glass transition temperature during degradation. In case of PTX containing matrices, T_g decreased steadily for 12 weeks and then increased to reach 29°C (3% PTX) and 30°C (5% PTX). T_g of drug free matrix started to increase after 6 weeks and attain 35°C. The increase of T_g may be attributed to the release of degradation products what corresponded to D decrease. First DSC scan revealed also melting temperature T_m that slightly decreased to 130°C after 15 weeks. It was assumed that PLACap matrices contained one type of crystalline form composed mainly of lactidyl units. The melting enthalpy ΔH_m increased from 20°C to 29°C for all matrices. This findings may be due to degradation of chains within amorphous regions and following crystallization, which was reported elsewhere (14). The ΔH_m increase was related with the l^e_{LL} and probably resulted from crystallization of long lactidyl blocks and degradation of short ones.

HPLC allowed to evaluate the amount of paclitaxel released from PLACap matrices. Both types of matrices provided even PTX release during degradation. It was noticed that PLACap matrices with 3% of PTX released less drug than matrices with 5% of PTX. After 15 weeks, 8.1% and 9.6% of PTX was released from matrices with 3% and 5% of PTX, respectively (Fig. 5).

The conducted study revealed regular degradation of matrices, regardless paclitaxel content, although degradation of drug-containing matrices was slightly slower than matrices without drug. Results of this work demonstrate the advantages of bioresorbable copolymer as material for controlled paclitaxel delivery.

CONCLUSION

The matrices of poly(L-lactide-co-ε-caprolactone) were degraded *in vitro* and studied for changes in physicochemical properties and paclitaxel release. The most noticeable was higher values of water uptake and weight loss for drug free matrices than matrices with PTX. Although paclitaxel did not affect significantly the physicochemical properties of PLACap during degradation when compared to drug free matrices, it seemed that PTX slightly slowed degradation rate of copolymer. Different

percentage content of PTX in PLACap matrices may be applied to design paclitaxel delivery systems tailoring specific clinical indications.

Acknowledgments

This study has been financially supported by a Grant from Polish Ministry of Science and Higher Education (N N405 682 340) and Centre of Polymer and Carbon Materials (Grant for Young Scientists 2013).

REFERENCES

1. Ulery B.D., Nair L.S., Laurencin C.T.: J. Polym. Sci. B Polym. Phys. 49, 832 (2011).
2. Zini E., Scandola M., Dobrzynski P., Kasperczyk J., Bero M.: Biomacromolecules 8, 3661 (2007).
3. Yu X., Wang L., Huang M. Gong T., Li W., Cao Y., Ji D. et al.: J. Mater. Sci. Mater. Med. 23, 581 (2012).
4. Bhowmik D., Gopinath H., Kumar B.P., Duraivel S., Kumar K.P.S.: J. Pharm. Innov. 1, 24 (2012).
5. Martin D.M., Boyle F.J.: Med. Eng. Phys. 33, 148 (2011).
6. Singla A.K., Garg A., Aggarwal D.: Int. J. Pharm. 235, 179 (2002).
7. Lopes M.S., Jardini A.L., Filho M.R.: Procedia Eng. 42, 1402 (2012).
8. Ulery B.D., Nair L.S., Laurencin C.T.: J. Polym. Sci. B Polym. Phys. 49, 832 (2011).
9. Lu X.L., Sun Z.J., Cai W., Gao Z.Y.: J. Mater. Sci. Mater. Med. 19, 395 (2008).
10. Jelonek K., Kasperczyk J., Li S., Dobrzynski P., Janeczek H., Jarzabek B.: BioMed. Res. Int. 2013, 607351 (2013).
11. Hofmann D., Entrialgo-Castańo M., Kratz K., Lendlein A.: Adv. Mater. 21, 3237 (2009).
12. Engineer C., Parikh J., Raval A.: Trends Biomater. Artif. Organs 25, 79 (2011).
13. Schliecker G., Schmidt C., Fuchs S., Wombacher R., Kissel T.: Int. J. Pharm. 266, 39 (2003).
14. Hua J., Gebarowska K., Dobrzynski P., Kasperczyk J., Wei J., Li S.: J. Polym. Sci. A Polym. Chem. 47, 3869 (2009).

Acta Poloniae Pharmaceutica – Drug Research, Vol. 71 No. 6 pp. 1029–1036, 2014 ISSN 0001-6837
Polish Pharmaceutical Society

SENSITIVE SINGLE QUADRUPOLE LC/MS METHOD FOR DETERMINATION OF LAPATINIB IN HUMAN PLASMA

JACEK MUSIJOWSKI*, MONIKA FILIST and PIOTR J. RUDZKI

Pharmaceutical Research Institute, Pharmacology Department, 8 Rydygiera St., 01-793 Warszawa, Poland

Abstract: A sensitive liquid chromatographic-single quadrupole mass spectrometric method was developed and validated for the determination of lapatinib in human plasma. Following a liquid-liquid extraction with methyl *t*-butyl ether, lapatinib and isotope labelled lapatinib, used as an internal standard (IS), were separated from the endogenous compounds on a Zorbax SB-C18 (150 × 3 mm, 3.5 μm) column. An isocratic elution with the mobile phase consisting of formic buffer and the mixture of acetonitrile, methanol and formic acid was used. Mass spectrometry with positive electrospray ionization in a single ion monitoring mode was applied. The proposed method provides the satisfactory recovery of lapatinib from human plasma and a sensitivity comparable to numerous tandem mass spectrometric methods, with a lower limit of quantification of 5 ng/mL. The validated method may be applied to pharmacokinetic studies in humans following a single 250 mg oral dose.

Keywords: lapatinib, liquid chromatography-mass spectrometry, bioanalytical method validation, liquid-liquid extraction, bioanalysis, pharmacokinetics

Breast cancer is the second most frequent cause of cancer related death in women in developed countries with over 1.67 million cases diagnosed worldwide in 2012 (1). It is recognized that in 15–20% of patients breast cancer exhibits an overexpression of the epidermal growth factor receptor 2 (HER2), which is associated with a more aggressive course of the disease (2). Lapatinib acting as a tyrosine kinase inhibitor is able to inhibit the HER2 receptors and therefore remains a valuable choice of treatment of the HER2-positive carcinoma. The addition of lapatinib to capecitabine in the treatment of HER2-positive advanced breast cancer significantly improves the median time to progression by 8.5 weeks. However, the estimated cost of introducing this tyrosine kinase inhibitor to the combination therapy is nearly $20,000 per patient (3). Considering the need for pharmaco-economic cancer treatments, it is essential to develop reliable and sensitive bioanalytical method for lapatinib determination in human plasma in order to conduct bioequivalence studies of new generic drug products.

Lapatinib is available as 250 mg tablets. After the oral administration of a single 250 mg dose, maximum lapatinib plasma concentrations occur within 3 to 6 h (mean 4 h) and range from 192 ng/mL to 524 ng/mL (mean – 317 ng/mL) (4). According to the European Medicines Agency guideline (5), a method designed for the application in bioequivalence studies should allow to assess maximum drug concentrations and analyze the area under the plasma concentration curve from the administration to the last observed concentration at a time t, $AUC_{(0\text{-}t)}$, which covers at least 80% of the area extrapolated to the infinity time, $AUC_{(0\text{-}\infty)}$. Taking into account the above recommendations and available pharmacokinetic data (4), the linearity range of 5.00–800.00 ng/mL seems to be suitable for bioequivalence studies.

Presently, several methods based on tandem mass spectrometry coupled with high-performance liquid chromatography (6–13), ultra-performance liquid chromatography (14) or without the separation technique (15) have been reported for lapatinib quantification in human plasma or serum samples. They were linear in the concentration ranges of 1–1000 ng/mL (6), 5–5000 ng/mL (8, 13), 10–5000 ng/mL (14), 20–10000 ng/mL (12), 25–10000 ng/mL (15), 50–3500 ng/mL (11), 50–5000 ng/mL (9), 100–5000 ng/mL (10) and 100–10000 ng/mL (7). However, a majority of the reported methods were designed for the measurement of lapatinib fol-

* Corresponding author: e-mail: j.musijowski@ifarm.eu

lowing higher doses used in routine clinical practice. Hence, only three methods seem to be sensitive enough for pharmacokinetic studies following a 250 mg dose (6, 8, 13). The triple quadrupole detector was also used for the determination of intracellular levels (16). A high cost of the instrumentation is the main limitation of these assays, making them unattainable to many routine biomedical laboratories. The application of ultraviolet detection was presented during the American Association for Cancer Research 103rd Annual Meeting. However, the poster presentation did not provide details concerning this assay (17). To the best of our knowledge, no method using a single quadrupole mass spectrometric detector has been reported for lapatinib quantification in human plasma so far.

The most widely employed sample preparation methodology was the precipitation of proteins (PP) (8, 9, 11, 12, 15). In spite of the high throughput of PP, large amounts of residual endogenous compounds may significantly contaminate instrumentation, especially if thousands of samples are to be measured. A more effective sample cleanup can be achieved by a solid-phase (7, 14) and liquid-liquid extraction (13). Solid-phase extraction methods, though very effective, significantly increase the cost of sample analysis and with high sample load they may require automated solution handling in order to obtain suitable sample throughput. Another alternative is the application of special on-line extraction columns (6, 10). However, this technique is available only to more complex equipment setups. Therefore, the liquid-liquid extraction seemed to be most practical for the present study.

The aim of the present study was to develop and validate a sensitive liquid chromatographic-single quadrupole mass spectrometric method for the determination of lapatinib in human plasma suitable for pharmacokinetic studies following a single 250 mg oral dose.

EXPERIMENTAL

Chemicals and reagents

Reference standards: lapatinib, N-[3-chloro-4-[(3-fluorophenyl)methoxy]phenyl]-6-[5-[[[2-(methylsulfonyl)ethyl]amino]methyl]-furan-2-yl]quinazolin-4-amine, as ditosylate monohydrate (CAS number: 388082-78-8) was synthesized at the Pharmaceutical Research Institute (Warszawa, Poland) (18), [^{13}C,$^{2}H_7$]-lapatinib was supplied by Alsachim (Strasbourg, France).

Methanol (HPLC and LC/MS grade), sodium carbonate and formic acid 98–100% (both of analytical grade) were purchased from POCH (Gliwice, Poland). Methyl *t*-butyl ether (HPLC grade) was obtained from Chem-Lab (Zedelgem, Belgium). Acetonitrile (HPLC and LC-MS grade) and 25% ammonium hydroxide solution (analytical grade) were purchased from J.T.Baker (Deventer, Netherlands). Purified water from Milli-Q system, Millipore (Molsheim, France), was used throughout the study.

Instrumentation

The Shimadzu LC/MS system (Duisburg, Germany), consisting of two LC–10AD*VP* pumps, an SIL–HTA autosampler, a CTO–10A column oven, a DGU–$20A_3$ degasser and an LCMS–2010 single quadrupole mass spectrometer, was used for lapatinib determination in human plasma. Data integration was performed with Shimadzu LCMS Solution software (version 2.05).

Chromatographic conditions

The chromatographic separation from endogenous compounds was performed on a Zorbax SB-C18 column (150 × 3 mm, 3.5 μm) from Agilent Technologies (Santa Clara, CA, USA). The HPLC column was preceded by a SecurityGuard C-18 guard column (4 × 3 mm) purchased from Phenomenex (Torrance, CA, USA). The mobile phase, consisting of 10 mM formic buffer pH 4.0 (phase A) and acetonitrile/methanol/formic acid (25 : 75 : 0.1, v/v/v) (phase B) mixed in the ratio A : B 25 : 75, v/v, was delivered at the flow rate of 0.45 mL/min. The sample volume of 50 μL was injected onto the column. The column and the autosampler were maintained at 35 ± 2°C and 20 ± 5°C, respectively. The total chromatographic run time was 11.0 min with the retention time of lapatinib was approximately 3.5 min.

Mass spectrometric conditions

The mass spectrometer was equipped with an electrospray ionization source operated in the positive mode, using single ion monitoring (SIM) as the data acquisition mode. Ions of lapatinib and the IS were monitored at *m*/*z* ratio of 581.0 and 589.1, respectively. The probe high voltage was 3.0 kV and nitrogen at 4.0 L/min was used as the nebulizer gas. The block temperature was 280°C, whereas the curved desolvation line temperature and voltage were 290°C and 75 V, respectively. The Q-Array lens voltages were 74 V, 55 V, 32 V, respectively. The detector voltage was 1.2 kV. Data were collected in 0.4 s intervals.

Solution preparation

Stock solutions of lapatinib and the IS were prepared by dissolving the appropriate amounts of the substances in methanol. The stock solutions were further diluted with 75% methanol to the working solutions. The working solutions used to prepare the calibration standards and quality control samples were obtained from different stock solutions. The stock solutions were stored in a freezer at temperature = –6°C and in a refrigerator at temperature = 12°C and the working solutions were stored in a refrigerator at temperature = 12°C.

Preparation of the calibration standards and quality control samples

The calibration standards contained lapatinib at the following concentration levels: 5.00, 15.00, 50.00, 100.00, 200.00, 400.00, 600.00 and 800.00 ng/mL. The quality control samples contained lapatinib at the concentration levels: 15.00, 200.00 and 600.00 ng/mL. The calibration standards and quality control samples were prepared by spiking blank human plasma with the appropriate working solution of lapatinib. The calibration standards were prepared directly before the analysis and the quality control samples were stored in a freezer at temperature = –14°C.

Sample preparation

Twenty microliters of the IS solution and 250 mL of the 2M sodium carbonate solution were added to the 250 mL aliquot of human plasma and vortex mixed in a glass, screw cap extraction tube. Then, 2 mL of methyl *t*-butyl ether were added and shaken on a vibrax mixer for 10 min. After centrifugation, the aqueous phase was frozen and the organic layer was transferred to a glass tube and evaporated to dryness under the stream of nitrogen. The dry residue was reconstituted in 200 mL of the mobile phase and mixed. After centrifugation, the supernatant was transferred into an autosampler vial.

Method validation

The validation parameters were defined according to the European Medicines Agency as well as the Food and Drug Administration guidelines (19, 20). The study was performed in compliance with the principles of Good Laboratory Practice. For the calculation of the precision, accuracy, calibration curve parameters and selected stability results, a normal distribution of measurements was assumed. The statistical analysis of the stability included the comparison of two sets of experimental data, assuming the log-normal distribution of mea-

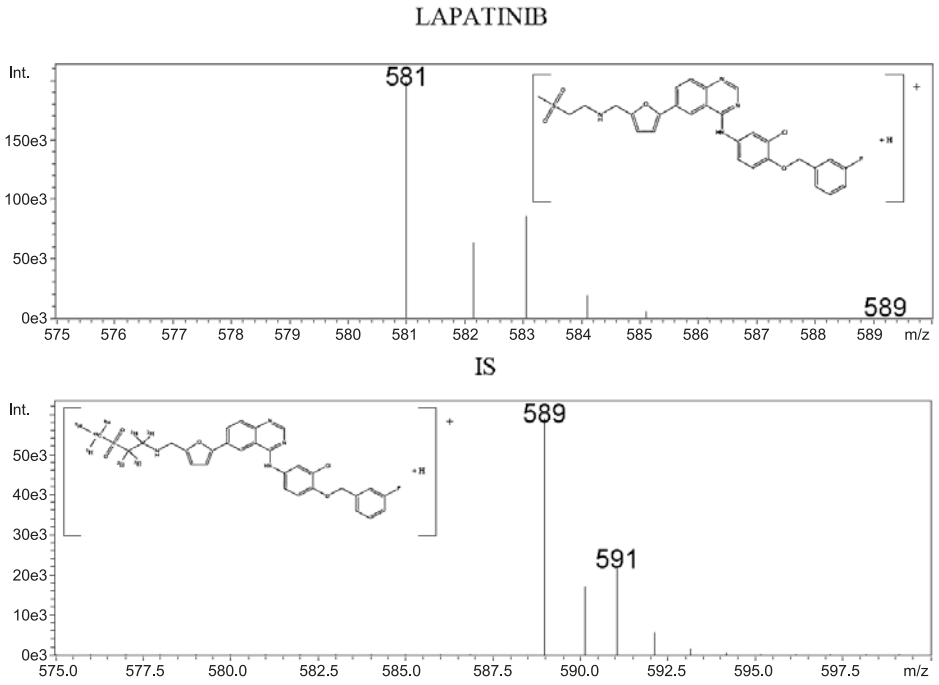

Figure 1. Positive ion electrospray mass scan spectra of lapatinib and IS. As reported previously (7, 9), the $[M + H]^+$ peak of m/z 581 was the most abundant one for lapatinib

surements' results and it was based on the application of confidence intervals (21, 22). The construction of confidence intervals depends on the variance equality, therefore the F-Snedecor test (significance level 0.01) was applied to test the hypothesis on the variance equality.

RESULTS

Method development

Manufacturing method of lapatinib of pharmaceutical purity was recently developed in Chemistry Department of the Pharmaceutical Research Institute (18). In this work, the chromatographic conditions, especially the chromatographic column and the composition of the mobile phase, were selected by subsequent iterations in order to achieve a suitable lapatinib retention and acceptable peak shape. To improve the peak shape a number of different mobile phases, sample solvents and reversed-phase columns including several brands of octadecyl and C6-phenyl phases were tested. Mobile phases consisted of acetonitrile and methanol mixed with 0.1% acetic acid or 10 mM formic buffer (pH 4.0) in various ratios changed to modify lapatinib retention or limit the back-pressure. Four sample solvents were used acetonitrile/0.1% formic acid and methanol/0.1% formic acid in two ratios 75 : 25 and 25 : 75 (v/v). It was found that the greatest influence on the peak shape had the composition of the sample solvent and no acceptable shape could be obtained unless the solvent was identical with the mobile phase. The selected mobile phase, which was used throughout the validation, consisted of a 10 mM formic buffer (pH 4.0) and acetonitrile/methanol/formic acid (25 : 75 : 0.1, v/v/v) in the ratio 25 : 75, v/v. Among tested reverse-phase columns, the best sensitivity with acceptable retention was obtained for a Zorbax SB-C18 column (150 × 3 mm, 3.5 μm, Agilent Technologies). Lapatinib and the IS were eluted at 3.5 min.

Positive ion electrospray mass scan spectra of lapatinib and the IS are shown in Figure 1. The $[M + H]^+$ peak of m/z 581.0 and $[M + H]^+$ peak of m/z 589.1 were the most abundant for lapatinib and the IS, respectively, and were selected for the analysis.

During the development of sample preparation, the extraction efficiencies using various extracting solvents were tested. Polar solvent like methyl *t*-butyl ether provided a much higher lapatinib recovery than the non-polar mixture of hexane and isopropanol and was selected for the sample cleanup. The influence of a modifier on extracting conditions was also studied. Saturated (2 M) sodium carbonate solution and 10 mM formic buffer pH 4.0 were tested as modifiers. The best results were achieved for the sodium carbonate. Finally, the optimization of the extraction time and extracting solvent volume led to the conclusion that shaking time of 10 min and the volume of 2 mL of methyl *t*-butyl ether are sufficient to obtain the high recovery (71–82%) of both lapatinib and the IS.

Method validation

Linearity and lower limit of quantification

The calibration curve was linear within the range of 5.00–800.00 ng/mL regarding the peak area ratio of lapatinib to the IS *versus* the nominal concentration of lapatinib. The curve was obtained by a weighted linear regression analysis with the weighting factor of $1/y^2$ selected according to the minimum sum of percentage relative errors (23). The values of regression parameters for the curve, described by the equation: $y = ax + b$, were: $a = 2.727e^{-3}$, $b = 2.016\ e^{-3}$ and $r = 0.9997$ ($n = 6$), where x was the lapatinib nominal concentration, y was the lapatinib/IS instrument response ratio, a and b were slope and

Table 1. Validation summary.

Linear range [ng/mL]	5.00 – 800.00			
Lapatinib concentration [ng/mL]	5.00	15.00	200.00	600.00
Extraction recovery of lapatinib [%]	–	82.0	82.4	71.4
Matrix effect – RSD [%]	–	6.22	5.31	2.55
Within-run precision [%]*	4.75–11.37	4.33–10.38	2.19–5.26	1.80–4.32
Within-run accuracy [%]*	89.3–99.9	91.0–100.7	96.9–101.8	94.2–98.2
Between-run precision [%]*	2.37–11.37	3.02–10.38	2.19–14.69	1.11–5.34
Between-run accuracy [%]*	89.3–100.9	90.4–100.7	93.2–106.9	92.9–98.2

*The accuracy and precision results are expressed as the 90% confidence intervals.

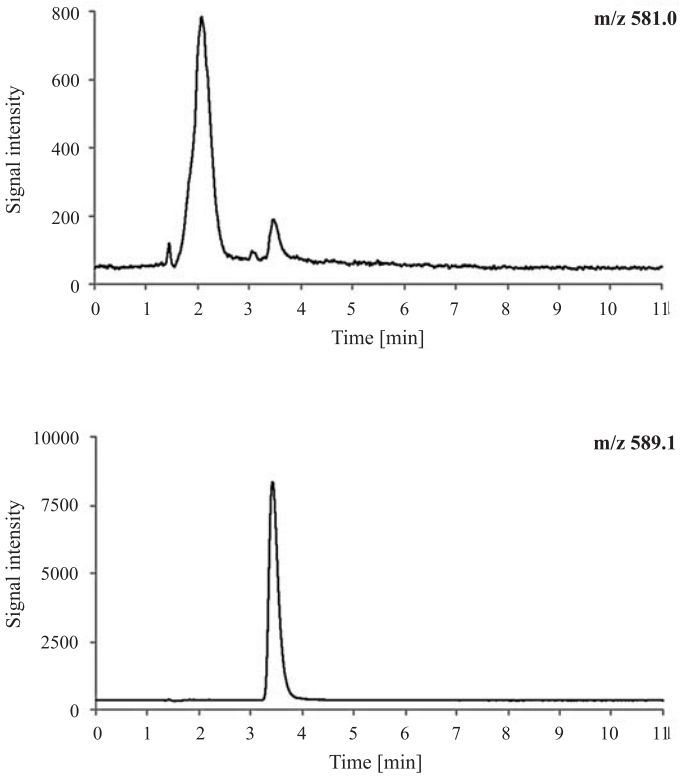

Figure 2. Chromatogram of the extracted plasma sample containing lapatinib at 5.00 ng/mL and the working concentration of the IS (the retention time of lapatinib and the IS – 3.5 min)

intercept, respectively (Table 1). All regression parameters were statistically significant (significance level 0.05, df = n –2).

The lower limit of quantification was determined at 5.00 ng/mL and met international acceptance criteria for the accuracy and precision (Table 1, Fig. 2).

Selectivity and carry-over

To confirm the method selectivity, blank human plasma from six different sources, including hemolyzed and lipophilic plasma, was analyzed. The chromatograms showed no peaks influencing the quantification near the retention times of lapatinib and the IS (Fig. 3).

The carry-over experiment, in which blank human plasma samples were analyzed immediately after the highest concentration calibration standards (procedure repeated six times), showed no peaks influencing the quantification.

Matrix effect and recovery

To determine the extraction recovery of lapatinib for three quality control sample levels, blank human plasma samples from six different sources, including hemolyzed and lipophilic plasma, were spiked with both lapatinib and the IS before the extraction (pre-extraction spiked plasma samples) and after the extraction of the plasma sample (post-extraction spiked plasma samples). The calculation of the lapatinib and IS recovery was based on the ratio of the peak areas determined in the pre- and post-extraction spiked plasma samples (24). The extraction recovery of lapatinib was stable across the studied concentration range and did not influence the recovery of the IS (Table 1).

The matrix factor was studied for lapatinib at three concentration levels and for the IS at the working concentration. It was calculated as the ratio of the instrument response for the substance in the presence of the matrix (post-extraction spiked plasma samples) to the instrument response in the absence of the matrix (standard solutions) (19). The matrix effect was evaluated from the RSD of the IS-normalized matrix factor (i.e., the ratio of the matrix factors calculated for lapatinib and the IS) calculated for six different sources of plasma, including hemolyzed and lipophilic plasma. The calculated

RSD did not exceed 15%, which confirmed the absence of matrix effects (Table 1).

Accuracy and precision

The results of the within-run (one sequence, n = 6 for each concentration) and between-run (three sequences, n = 6 for each concentration) accuracy and precision for the lower limit of quantification and three quality control sample levels are presented in Table 1. For the lower limit of quantification, the accuracy was within the acceptance criteria range of 80–120% and the precision was below the acceptance limit of 20%. For each quality control sample level, the accuracy was within the acceptance criteria range of 85–115% and the precision was below the acceptance limit of 15% (Table 1).

Stability

The results of the stability tests: autosampler, freeze and thaw, short-term and long-term at two storage temperatures for 53 days, are presented in Table 2. For each concentration level, the 90% confidence interval for the mean stability met the acceptance criteria falling within the range of 85–115%. Moreover, respective stability tests confirmed the stability of lapatinib and the IS in the stock and working solutions (Table 3).

DISSCUSION AND CONCLUSION

To the best of our knowledge, the method developed is the first application of a single quadrupole mass spectrometry for the determination of lapatinib in human plasma. It offers an attractive lower limit of quantification of 5.00 ng/mL. Previously published tandem mass spectrometric methods presented wide linearity ranges, however, only one of them provided better sensitivity (6). Based on pharmacokinetic data (4), the upper limit of quantification proposed in this paper seems to be sufficient for the determination of lapatinib in plasma following a

Table 2. The stability of lapatinib in plasma expressed as the 90% confidence intervals (n = 6).

Stability		Short-term	Freeze-thaw	Autosampler	Long-term	Long-term
Temperature		Ambient temperature	≤ –14°C	20 ± 5°C	≤ –14°C	≤ –65°C
Storage period		4 h	3 cycles	18 h	53 days	53 days
Lapatinib concentration [ng/mL]	15.00	96.4–109.9	98.7–110.2	91.3–100.8	96.2–112.7	96.2–109.7
	600.00	101.3–105.4	90.3–100.2	99.1–100.3	91.8–98.8	92.1–99.5

Table 3. The stability of lapatinib and the IS in the solutions expressed as the 90% confidence intervals (n = 6).

	Analyte	Concentration	Temperature	Storage period	Stability
Stock solutions	Lapatinib	1.00 mg/mL	≤ –6°C	64 days	104.2–109.4
			≤ 12°C	7 days	103.3–104.8
			Ambient temperature	24 h	101.6–103.9
	IS	0.10 mg/mL	≤ –6°C	64 days	95.3–98.9
			≤ 12°C	7 days	98.2–100.9
			Ambient temperature	24 h	98.7–102.3
Working solutions	Lapatinib	100.00 µg/mL	≤ 12°C	57 days	99.4–102.5
			Ambient temperature	24 h	100.4–106.7
		62.50 ng/mL	≤ 12°C	64 days	91.7–102.1
			Ambient temperature	24 h	94.2–105.4
	IS	5.00 µg/mL	≤ 12°C	57 days	97.7–103.7
			Ambient temperature	24 h	101.0–105.5

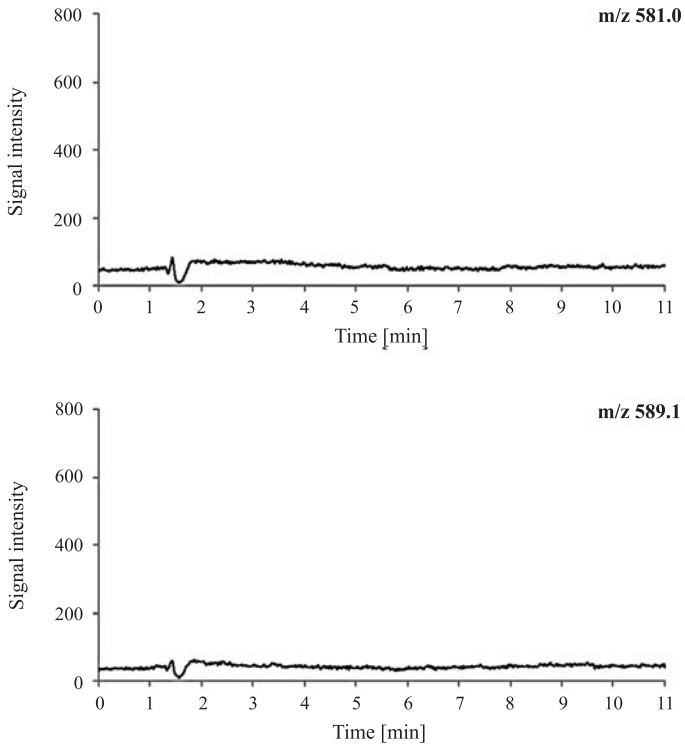

Figure 3. Chromatogram of the extracted blank plasma sample

250 mg oral dose. For economic reasons triple quadrupole mass spectrometers are not so widely available as the single quadrupole detectors. Therefore, the present method expands the list of instrumental setups applicable to the analysis of the drug and represents an attractive alternative approach for many biomedical laboratories.

Sample preparation is a critical part of the quantitative bioanalysis. Selecting a proper technique is always a good practice even with mass spectrometric detectors, as it limits matrix effects, improves the selectivity and sensitivity, extends column life as well as protects the liquid chromatographic system and the ion source from impurities. Protein precipitation is less effective in the removal of endogenous compounds compared to the extraction techniques and thus carries the highest risk of ion suppression (25–27). It also makes necessary a frequent ion source cleaning. Although a solid-phase extraction provides a selective sample cleanup, the use of expensive columns limits its availability. The liquid-liquid extraction procedure described in this paper allowed to obtain high sensitivity and good recovery (above 70%) of the method as well as avoid significant matrix effects.

The method was fully validated with respect to the European Medicines Agency and the Food and Drug Administration requirements, proving its reliability, and may be applied to pharmacokinetic studies in humans following a single 250 mg oral dose.

Acknowledgments

The present study was supported by the European Union (European Regional Development Fund) under the Innovative Economy Operational Programme 2007-2013 (project No. UDA-POIG.01.03.01-14-069/08). The sponsor was not involved in conducting the study.

The authors are grateful to Mrs. Krystyna Serafin-Byczak and Mrs. Magdalena Troć for their excellent technical assistance. The authors wish to thank Mr. Wojciech Łuniewski and his synthetic and analytical teams from the Chemistry Department and R&D Analytical Chemistry Department of Pharmaceutical Research Institute (Warsaw, Poland) for supplying the lapatinib reference standard.

REFERENCES

1. Ferlay J., Soerjomataram I., Ervik M., Dikshit R., Eser S., Mathers C., Rebelo M. et al.: Lyon, France: International Agency for Research on Cancer (2013) (http://globocan.iarc.fr, accessed on 05/05/2014).
2. Baselga J.: Ann. Oncol. 21 (Suppl. 7), vii36 (2010).
3. Le Q.A., Hay J.W.: Cancer 115, 489 (2009).
4. Bence A.K., Anderson E.B., Halepota M.A., Doukas M.A., DeSimone P.A., Davis G.A., Smith D.A. et al.: Invest. New Drugs 23, 39 (2005).
5. European Medicines Agency. Guideline on the investigation of bioequivalence (CPMP/EWP/QWP/1401/98 Rev. 1/ Corr **). London, 20 January, 2010.
6. Hsieh S., Tobien T., Koch K., Dunn J.: Rapid Commun. Mass Spectrom. 18, 285 (2004).
7. Bai F., Freeman B.B. III, Fraga C.H., Fouladi M., Stewart C.F.: J. Chromatogr. B Analyt. Technol. Biomed. Life Sci. 831, 169 (2006).
8. Haouala A., Zanolari B., Rochat B., Montemurro M., Zaman K., Duchosal M.A., Ris H.B. et al.: J. Chromatogr. B Analyt. Technol. Biomed. Life Sci. 877, 1982 (2009).
9. Götze L., Hegele A., Metzelder S.K., Renz H., Nockher W.A.: Clin. Chim. Acta 413, 143 (2012).
10. Couchman L., Birch M., Ireland R., Corrigan A., Wickramasinghe S., Josephs D., Spicer J., Flanagan R.J.: Anal. Bioanal. Chem. 403, 1685 (2012).
11. Andriamanana I., Gana I., Duretz B., Hulin A.: J. Chromatogr. B Analyt. Technol. Biomed. Life Sci. 926, 83 (2013).
12. Lankheet N.A.G., Hillebrand M.J.X., Rosing H., Schellens J.H.M., Beijnen J.H., Huitema A.D.R.: Biomed. Chromatogr. 27, 466 (2013).
13. Wu J., Wiegand R., LoRusso P., Li J.: J. Chromatogr. B Analyt. Technol. Biomed. Life Sci. 941, 100 (2013).
14. Bouchet S., Chauzit E., Ducint D., Castaing N., Canal-Raffin M., Moore N., Titier K., Molimard M.: Clin. Chim. Acta 412, 1060 (2011).
15. Mičová K., Friedecký D., Faber E., Adam T.: Talanta 93, 307 (2012).
16. Roche S., McMahon G., Clynes M., O'Connor R.: J. Chromatogr. B Analyt. Technol. Biomed. Life Sci. 877, 3982 (2009).
17. Escudero V., Valenzuela B., Rebollo J., Sureda M., Brugarolas A.: Cancer Res. 72 (Suppl. 1) abstract 757 (2012).
18. Łuniewski W., Krzeczyński P., Kłos K., Trzcińska K.: Przem. Chem. 91, 276 (2012) (Polish).
19. European Medicines Agency. Guideline on Bioanalytical Method Validation (EMEA/CHMP/EWP/192217/2009). London, 21 July, 2011.
20. Department of Health and Human Services. Food and Drug Administration. Center for Drug Evaluation and Research (CDER). Center for Veterinary Medicine (CVM). Bioanalytical Method Validation. May, 2001.
21. Timm U., Wall M., Dell D.: J. Pharm. Sci. 74, 972 (1985).
22. Rudzki P.J., Leś A.: Acta Pol. Pharm. Drug Res. 65, 743 (2008).
23. Almeida A.M., Castel-Branco M.M., Falcão A.C.: J. Chromatogr. B Analyt. Technol. Biomed. Life Sci. 774, 215 (2002).
24. Matuszewski B.K., Constanzer M.L., Chavez-Eng C.M.: Anal. Chem. 75, 3019 (2003).
25. Bonfiglio R., King R.C., Olah T.V., Merkle K.: Rapid Commun. Mass Spectrom. 13, 1175 (1999).
26. Müller C., Schäfer P., Störtzel M., Vogt S., Weinmann W.: J. Chromatogr. B Analyt. Technol. Biomed. Life Sci. 773, 47 (2002).
27. Taylor P.J.: Clin. Biochem. 38, 328 (2005).

Project co-financed by the European Regional Development Fund under the framework of the Innovative Economy Operational Programme.

UDA-POIG contract no 01.03.01-14-069/08 „Innovative technologies of oncological medicines of special therapeutic and social importance:": www.ifarm.eu/poig/onko/

Acta Poloniae Pharmaceutica – Drug Research, Vol. 71 No. 6 pp. 1037–1044, 2014 ISSN 0001-6837
Polish Pharmaceutical Society

ABSORPTION AND METABOLISM OF BIOLOGICALLY ACTIVE GENISTEIN DERIVATIVES IN COLON CARCINOMA CELL LINE (CACO-2)

KATARZYNA PAPAJ[1]*, ALEKSANDRA RUSIN[2], WIESŁAW SZEJA[1] and GRZEGORZ GRYNKIEWICZ[3]

[1] Silesian University of Technology, Faculty of Chemistry, Department of Organic Chemistry, Bioorganic Chemistry and Biotechnology, Krzywoustego 4, 44-100 Gliwice, Poland
[2] Maria Skłodowska-Curie Memorial Center and Institute of Oncology, Department of Tumor Biology, Wybrzeże Armii Krajowej 15, 44-101 Gliwice, Poland
[3] Pharmaceutical Research Institute, Rydygiera 8, 01-793 Warszawa, Poland

Abstract: Several genistein derivatives comprising an isoflavonoid skeleton substituted with an alkyl chain and a sugar moiety show ability to inhibit proliferation of cancer cells *in vitro* at the concentration several-fold lower than genistein. In our previous studies we shown that these compounds influenced the mitotic spindle, blocked the cell cycle and induced apoptosis. The purpose of this study was to determine the relationship between structural modifications of genistein molecule and the intestinal disposition of its derivatives. Transport and metabolism of these compounds were studied in the human intestinal Caco-2 model. The results of our study indicate that transport and metabolism of genistein derivatives depend both, on the structure of the carbonyl linker and position of genistein molecule substitution. All new compounds showed higher permeability coefficient in comparison to genistein. Moreover, genistein derivatives described in this work were transformed in Caco-2 cells into glucuronide and sulfate metabolites.

Keywords: genistein, metabolism, Caco-2, LC-MS/MS

Genistein (5,7-dihydroxy-3-(4-hydroxyphenyl)chromen-4-one) is considered as a useful compound for prophylaxis or treatment of many pathological conditions, such as cancer, menopausal syndrome, cardiovascular disease, osteoporosis and diabetes. The most promising applications of this isoflavonoid are associated with cancer chemoprevention. Many *in vitro* and *in vivo* studies demonstrating antiproliferative activity of genistein go along with epidemiological data, linking genistein rich diet with reduced risk of some types of cancer. Genistein inhibits proliferation of tumor cells due to inhibition of activity of several molecular targets, including transcriptional factor NF-κB, tyrosine kinases and topoisomerase II (1–4).

However, despite many beneficial properties, the use of this compound *in vivo* is limited due to weak solubility in water, fast biotransformation to inactive metabolites, poor accumulation in tissues and target cells, and low concentration in blood after administration *per os* (5). In order to improve pharmacological properties and antitumor potency of genistein, new derivatives were designed and synthesized by different laboratories (6). Very promising class of compounds, synthesized on the base of genistein, that exhibit anticancer potential are glycoconjugates and 2,3 unsaturated mono- or disaccharides of this isoflavonoid, described in our previous work. Our screening studies revealed several glycoconjugates of genistein inhibiting cancer cell proliferation at the concentration several fold lower than the parent compound. Depending on the structure of a sugar moiety and the type of substitution, new glycoconjugates of genistein inhibited cancer cell proliferation through different molecular mechanisms (7, 8). Some of them acted in a different manner than genistein and targeted mitotic spindles.

Next, we decided to correlate structural features of genistein derivatives with their bioavailability. To address this question, we decided to use Caco-2 model, regarded as an *in vitro* surrogate for studying intestinal absorption. This paper presents *in vitro* bioavailability parameters of genistein derivatives and discusses correlation between structural features and bioavailability of compounds.

* Corresponding author: e-mail: katarzyna.papaj@polsl.pl

EXPERIMENTAL

Synthesis of genistein derivatives

Synthesis of tested compounds (Fig. 1) was described previously in (7–9).

Determination of absorption

General

Cancer cell line

Human Caucasian colon adenocarcinoma cell line (Caco-2) was obtained from ECACC (European Collection of Cell Cultures, UK). Cells were cultured in Dulbecco's modified Eagle medium – high glucose 4.5 g/L (Sigma Aldrich, USA), supplemented with 20% (v/v) inactivated fetal bovine serum [iFBS] (PAA Laboratories GmbH, Austria) and 1% (v/v) non-essential amino acids (Biological Industries, Israel). Additionally, gentamycin (KRKA, Slovenia) was added to culture media at the concentration 0.04 mg/mL. Cells were cultured at 37°C in humidified atmosphere of 5% CO_2.

MTT assay

Toxicity of tested compounds in Caco-2 cell line was estimated using an MTT (3-(4,5-dimethylthiazol-2-yl)-2,5-diphenyltetrazolium bromide) (Sigma Aldrich, USA) assay.

Caco-2 cells were plated in 96-well plates (Thermo Fisher Scientific, Nunc, Denmark) at the density of 6×10^4 cells per cm^2 and grown for 72 h. Then, the medium was aspirated and cells were treated for 24 h with the solution of tested compounds in growth medium. In the experiment, we used a series of concentrations: 5, 10, 25 and 50 µM. After 24 h, medium was removed and cells were incubated with 0.5 mg/mL MTT solution (50 µL) in Dulbecco's modified Eagle medium without phenol red (Sigma Aldrich, USA) for 3 h. Then, medium was aspired and crystals of formazan were solubilized in 0.04 M solution of HCl in 2-propanol (Avantor Performance Materials, Poland). The absorbance of samples was measured spectrophotometrically with a microplate reader BioTek Synergy II (BioTek Instruments, USA) at 570 nm wavelength.

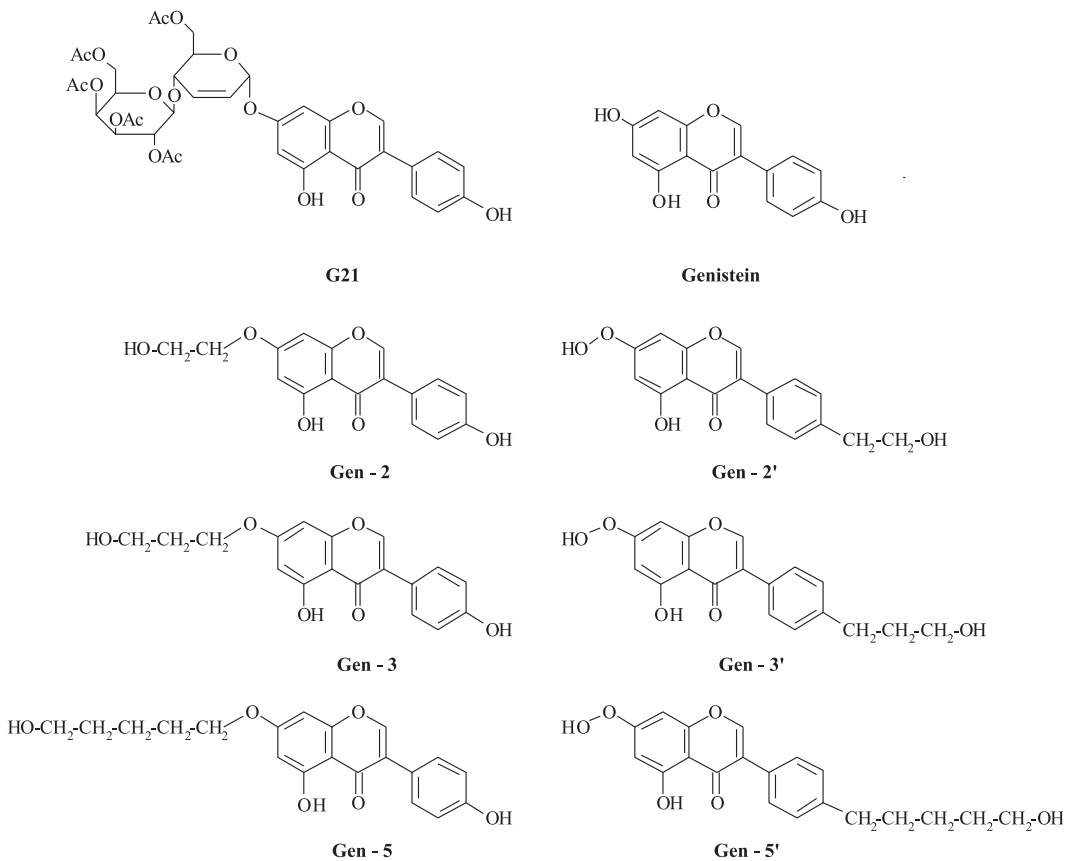

Figure 1. Structure of the tested compounds

Moreover, for two concentrations of compounds (25 and 50 µM), the additional experimental variant was performed, using Hanks' Balanced Salt (Sigma Aldrich, USA) solution with calcium and magnesium instead of MEM for preparation of compounds solution.

For each compound in a single experiment, every concentration was tested in quadruplicate. Experiments were repeated at least three times. The percentage of cell viability was calculated using the following equation:

% of cell viability in relation to untreated control

$$= \left(\frac{A - B}{C - B}\right) \cdot 100\%$$

where A = average of absorbance measured for wells with cells treated with a tested compound, B = average of absorbance measured for wells without cells (blank) C = average of absorbance for wells with cells non-treated cells (control).

Transport experiments

The experiment was based on protocols described in (10).

In the first step, Caco-2 cell line was cultivated on 24-well plates with porous membranes (Millicell PCF, 0.4 µm pore size) (Merck Millipore, Germany). The apical volume was 0.4 mL and basolateral volume was 0.6 mL. The cells were seeded at a density of 4.4×10^5 cells per cm^2. The culture medium consisted of:

- 1 to 3 day: DHEM-HG + 1% (v/v) non-essential amino acids + 0.04 mg/mL of gentamycin + 20% (v/v) iFBS;
- 3 to 7 day: DHEM-HG + 1% (v/v) non-essential amino acids + 0.04 mg/mL of gentamycin + 15% (v/v) iFBS;
- 7 to 22 day: DHEM-HG + 1% (v/v) non-essential amino acids + 0.04 mg/mL of gentamycin + 10% (v/v) iFBS.

Confluent monolayers of differentiated cells were obtained after 20–22 days. The culture medium was changed twice a week. The integrity of Caco-2 monolayers was monitored twice a week by measuring transepithelial electrical resistance (TEER) using Millicell – ERS (Electrical Resistance System) (Merck Millipore, Germany).

When the confluent monolayer was obtained (after 20–22 days), the medium was removed and cells were washed three times with the warm Hanks' Balanced Salt solution containing calcium and magnesium [HBSS, pH 7.4] (Sigma Aldrich, USA), and then the cells were pre-incubated with a buffer at 37°C for 30 min. Then, TEER values were measured for each well, and those with TEER values less than 500 ohms/cm^2 were discarded.

After pre-incubation, the buffer was removed, and the proper solutions of genistein or its derivatives (25 µM) were added either to the apical (transport A-B), or to the basolateral (transport B-A) compartment. Stock solutions of compounds were prepared in DMSO. The concentration of DMSO (Acros Organics, USA) in transport medium did not exceed 0.01% (v/v). Fresh HBSS without analyzed compounds was added to basolateral (transport A-B) or apical (transport B-A) compartment in a well serving as a blank sample.

The samples were collected from basolateral (transport A-B) or apical (transport B-A) chambers after 1, 2, 4, 8 and 24 h incubation of cells with the tested substances. Moreover, after 24 h, samples were collected from apical (transport A-B) and basolateral (transport B-A) chamber. Each time after collecting the samples, the volume of HBSS, equal to the volume of the sample collected was added to culture solution. After 24 h, TEER value was measured to confirm the integrity of the monolayer.

Afterwards, the samples were centrifuged (2000 × g, 2 min). Supernatant (100 µL) was filtered through a syringe filter (0.22 µL, 4 mm, nylon) (Thermo Scientific, USA), and then the filter membrane was washed by acetonitrile (100 µL) (Merck Millipore, Germany). The filtrates were mixed and transferred to an autosampler vial. The concentrations of tested compound were determined by HPLC-MS/MS.

The experiments evaluating the rate of transport in apical-basolateral (AP-BL) and basolateral-apical direction were performed in triplicates.

The permeability of a compound was calculated using the following equation:

$$P_{app} = \frac{\frac{dC}{dt}}{C_0 \cdot A},$$

where dC/dt is the rate of drug transport (mol/s), A is the surface area of membrane (cm^2), C_o is the initial concentration in the donor chambers (mol/L). Efflux ratio was calculated according to the following equation (11, 12):

$$P_{ratio} = \frac{P_{app,\ B\ A}}{P_{app,\ A–B}}$$

Chromatographic conditions for determination of genistein and its derivatives

Liquid chromatography

The LC separation was performed using a Dionex UHPLC system (Dionex Corporation, USA)

consisting of an UltiMate 3000 RS pump, an UltiMate 3000 autosampler, an UltiMate 3000 column compartment and an UltiMate 3000 variable wavelength detector. UHPLC system was operated using Dionex Chromaleon ™6.8 software.

Chromatography was performed using a C18 ACE column (150 × 4.6 mm, 3.0 µm) (Advanced Chromatography Technologies, UK) connected by the integral holder (3.2 × 4.6 mm) with the guard column of the same material. Isocratic conditions were: 30% of 0.1% solution of formic acid (Sigma Aldrich, Fluka, Germany) in water (v/v) (Merck Millipore, Germany) and 70% of acetonitrile (Merck Millipore, Germany) for genistein, Gen-X and Gen-X' or 15% of 0.1% solution of formic acid in water (v/v) and 85% of acetonitrile for G21, the flow rate for all compounds was set at 1.0 mL/min and sample injecion volume was 5 µL. The HPLC column was thermostated at 25°C. Samples were kept in the autosampler at 10°C.

Mass spectrometry

For determination of compound mass, the UHPLC system was connected to a 4000 Q TRAP triple quadrupole, linear ion trap mass spectrometer (Applied Biosystem/ MDS SCIEX, USA). For data acquisition, Analyst software (version 1.5.1.) was used. The mass spectrometer was operated in the negative (for genistein) or positive (for Gen-X, Gen-X' and G21) electrospray ionization (ESI) mode.

In order to obtain the best performance of mass spectrometer analysis of genistein derivatives, the parameters dependent on the source, such as: ion source gas 1 (GS1), ion source gas 2 (GS2), curtain gas (CUR), ion spray voltage (IS) and temperature of the heater gas (TEM) were optimized. The high-pressure nitrogen was used as ion source gas, curtain gas and collision gas.

Moreover, to get the good sensitivity and the peak shape, the compound dependent parameters, such as: declustering potential (DP), entrance poten-

Table 1. MS/MS conditions for determination of genistein and its derivatives.

Analyte	**t_r** (min)	**Q1** (m/z)	**Q3** (m/z)	**DP** (V)	**EP** (V)	**CE** (V)	**CXP** (V)	**CUR** (ř)	**IS** (V)	**TEM** (°C)	**GS1** (ψ)	**GS2** (ψ)
Genistein	1.90	268.9	132.9	-95	-10	-44	-5	10	-4000	600	70	50
Gen-2	1.85	314.9	271.2	100	6	30	20	10	4500	600	70	50
Gen-3	1.96	329.0	271.2	100	7	35	16	10	4500	600	70	50
Gen-5	2.21	357.0	271.1	100	10	29	6	10	4500	600	70	50
Gen-2'	1.87	315.0	271.1	90	9	30	20	10	4500	600	70	50
Gen-3'	1.98	329.0	270.8	100	7	35	16	10	4500	600	70	50
Gen-5'	2.22	357.1	270.8	100	10	29	6	10	4500	600	70	50
G21	1.84	771.3	331.2	100	7	20	10	10	5500	550	70	50

t_r _ retention time, Q1- precursor ion, Q3 – fragment ion

Table 2. MRM transitions for determination of metabolites of genistein and its derivatives.

Analyte	**Q1** (m/z)	**Q3**(m/z)
Genistein sulfate	349	269
Genistein glucuronide	445	269
Gen-2, Gen-2' sulfates	395	315
Gen-2, Gen-2' glucuronide	491	315
Gen-3, Gen-3' sulfates	409	329
Gen-3, Gen-3' glucuronide	505	329
Gen-5, Gen-5' sulfates	437	357
Gen-5, Gen-5' glucuronide	533	357
G21 sulfate	851	271or 771
G21 glucuronide	947	271 or 771

tial (EP), collision energy (CE), and collision cell exit potential (CXP) were tuned up for individual compounds. Optimized parameters are summarized in Table 1. Final analysis was performed in a selected reaction monitoring mode, using the precursor ions and the corresponding product ions.

Chromatographic conditions for detection of metabolites

Sample preparation

To determine the possible metabolites, samples collected after 24 h of incubation were mixed and lyophilized. Residues were dissolved in 100 µL mixture of acetonitrile : water, 4 : 1 (v/v) and filtered through a syringe filter. The filter membrane was washed with acetonitrile (100 µL). Mixed filtrates were transferred to an autosampler vial and analyzed by HPLC-MS/MS.

Liquid chromatography

The analysis of metabolites was performed using HPLC system, software and column described previously. The eluents were composed of 0.1% solution of formic acid in water (A) and acetonitrile (B). The elution conditions were as follows: 0 min 10% B, 0–3 min 20% B, 3–6 min 40% B, 6–10 min 50% B, 10–11 min 60% B, 11–12 min 70% B, 12–15 min 80% B for genistein, Gen-X and Gen-X' or 0 min 10% B, 0–3 min 20% B, 3–6 min 40% B, 6–8 min 50% B, 8–10 min 60% B, 10–12 min 70% B, 12–15 min 80% B for G21, The flow rate for all compounds was set at 0.8 mL/min and sample injecion volume was 10 µL. The HPLC column was thermostated at 25°C. Samples were kept in the autosampler at 10°C.

Mass spectrometry

Analyses of conjugates with glucuronic or sulfuric acid were performed on a selected reaction monitoring mode. The MRM transitions for genistein was found in the literature (13). In case of genistein derivatives, analyses were performed on theoretical MRM transitions determined based on data available for genistein (Table 2). The MS/MS con-

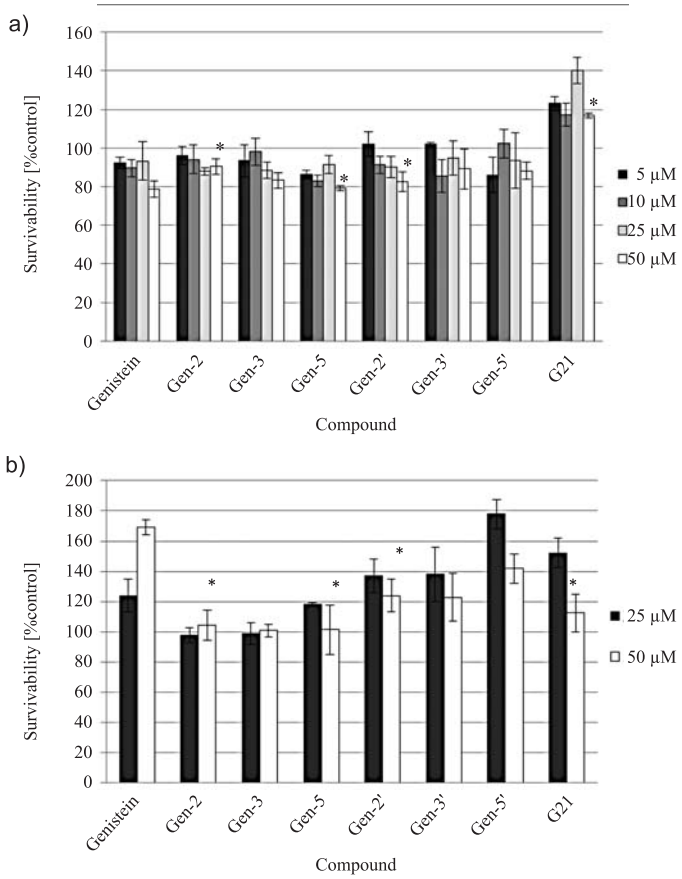

Figure 2. Percent of cell proliferation in relation with concentration of compound; a) compound solution in medium b) compound solution in HBSS; "*" compound precipitated in solution

ditions were described previously. Moreover, for identification of metabolites the LightSight software (version 2.2.1.) was used.

RESULTS AND DISCUSSION

Cells cultures are playing very important role in drug bioavailability studies. Many papers show a good correlation between transport of compounds by the intestinal epithelium *in vitro*, and by the intestinal wall *in vivo*. One of the most common cell line used in drug transport studies is Caco-2. This cell line shows many characteristics of human small intestine epithelium and serves as an *in vitro* model of drug transport through the intestine wall (14). Caco-2 cells form tight junctions on lateral side of plasma membrane, produce enzymes, taking part in transport and metabolism of compounds, and excrete small amounts of intestinal mucus on the apical surface (14, 15).

In this study, the bioavailability and metabolism were determined for six genistein derivatives, in which genistein is linked at C-7 or C-4' position with an alkyl chain containing two, three or five carbon atoms by *O*-glycosidic bond and one pyranosyl derivative of genistein (G21). The study was started with determination of cytoxicity of the tested compounds in Caco-2 cells, which allowed us to determine the highest nontoxic concentration of the tested compounds. The highest non-toxic concentration of the drug was used in experiments aiming at evaluation of transport through cell monolayer measured with HPLC-MS/MS. The toxicity of the tested compounds in Caco-2 cell line was determined with use of MTT assay.

MTT assay (Fig. 2) showed, that the analyzed compounds used in concentration up to 50 μM (solutions prepared in culture medium) affected cell viability only by about 10%, compared to untreated control. Due to low solubility of certain compounds and their precipitation in culture medium, Gen-2, Gen-5, Gen-2' and G21 were used at 25 μM. MTT assay showed that 25 μM solutions of these drugs were safe for Caco-2 cell monolayer and it was selected for absorption and metabolism experiments. Interestingly, when cells were incubated with HBSS solution of the tested genistein derivatives, the metabolic activity exceeded the control values, suggesting that these compounds stimulated cell metabolism.

We found that all the analyzed compounds permeated across the membrane to the acceptor compartment in both the apical to basolateral and the basolateral to apical direction and they were highly permeable. P_{app} values obtained for both directions of transport were greater than 1×10^{-6} cm/s, suggest-

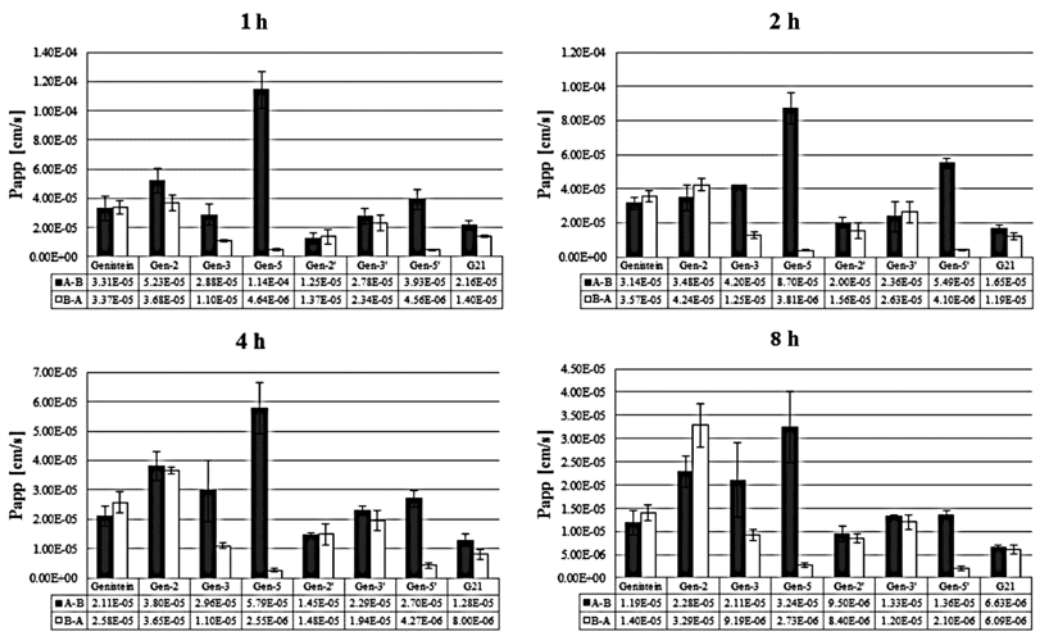

Figure 3. Apparent permeability values obtained for AP-BL and BL-AP directions in the Caco-2 after 1, 2, 4 and 8 h of incubation

Table 3. Retention times for glucuronide and sulfate conjugates of genistein and its derivatives.

	Retention time [min]		
	Parent	**Glucuronide**	**Sulfate**
Genistein	12.51	8.98	11.28
Gen-2	11.91	9.0	10.49
Gen-3	13.09	9.61	11.37
Gen-5	14.61	11.39	12.94
Gen-2'	12.20	8.89	10.90
Gen-3'	13.31	9.48	11.33
Gen-5'	14.69	10.49	13.63
G21	14.17	–	12.75

Table 4. Values of efflux ration for genistein and derivatives after 1, 2, 4 and 8 h of incubation.

	Efflux ratio			
	1 h	**2 h**	**4 h**	**8 h**
Genistein	1.02	1.13	1.22	1.18
Gen-2	0.70	1.22	0.96	1.44
Gen-3	0.38	0.30	0.37	0.44
Gen-5	0.04	0.04	0.04	0.08
Gen-2'	1.10	0.78	1.02	0.88
Gen-3'	0.84	1.12	0.85	0.90
Gen-5'	0.12	0.07	0.16	0.15
G21	0.65	0.72	0.63	0.92

ing that these compounds will be completely absorbed in human after administration per os. According to the literature (16), absorption of drugs in human is correlated with permeability coefficient in the following way:

- P_{app}: > 1.0×10^{-6} cm/s – drugs are absorbed in 100%
- P_{app}: $0.1–1.0 \times 10^{-6}$ cm/s – drugs are absorbed to a greater than 1% but less than 100%
- P_{app} coefficient: 1.0×10^{-7} cm/s – drugs are absorbed less than in 1%.

The values of P_{app} obtained for genistein were similar to values found in the literature (17, 18). Calculated $P_{app, A-B}$ values for most of genistein derivatives (except for Gen-2' and G21) were higher in comparison with P_{app} value for genistein. For derivatives of Gen-X and Gen-X' series, the value of coefficient increased with increasing number of carbon atoms in a linker (except for Gen-3). The highest value of $P_{app, A-B}$ was obtained for Gen-5. Of note, this compound showed the best anticancer properties (the lowest IC_{50} value) (7, 8), among both, Gen-X and Gen-X' series.

Apparent permeabilities in the mucosal direction ($P_{app, B-A}$) were for most derivatives lower than the values obtained for genistein. They were also lower than the $P_{app,A-B}$ values obtained for the transport in the opposite direction. It is also worth to note that derivatives of Gen-X series (substituted at C-7 position of genistein) have higher values of $P_{app, A-B}$ and $P_{app, B-A}$ coefficients when compared to their analogs of Gen-X' series (substituted at C-4' of genistein).

The results presented in Figure 3 show clearly that P_{app} values changed depending on duration of incubation with drugs. This observation can be explained by the metabolic changes of the analyzed compounds that occurred in Caco-2 cells. On the base of literature data, Caco-2 cells are known to secrete enzymes capable to metabolize drugs by connecting to their structure glucuronic acid or sulfuric acid (14).

Following this assumption, we analyzed the samples collected 24 h after addition of a drug, and we found that genistein and its derivatives were metabolized, and the type of derivatization was dependent on the type of molecule. Genistein and its derivatives containing the alkyl chain were metabolized by conjugation of sulfuric acid or glucuronic acid. (Table 3). The only metabolite of G21 detected in our analysis was its sulfate. The obtained results are only of qualitative character; quantitative analysis of the metabolites formed in Caco-2 cells was not possible due to the lack of appropriate standards.

Determination of $P_{app, A-B}$ and $P_{app, B-A}$ coefficient for the tested drugs allowed us to determine the P_{ratio} values, helpful in predicting drug transport back into the intestinal lumen. It is assumed that a P_{ratio} greater than 2 is predictive of relevant efflux (active drug transport back into the intestinal lumen) (11, 19). The P_{ratio} of genistein derivatives (Table 4) were lower than for genistein and lower than 2. The smallest values of these coefficient were obtained for Gen-5 and Gen-5' (after 1 h of incubation: 0.04 and 0.12, respectively). It means that this drug may become a useful leader in the future drug development.

In conclusion, modifications introduced to genistein structure influenced not only antitumor activity of compounds (lower IC_{50} values in comparison to genistein), but also improved their availability parameters (increased permeability coefficient and decreased P_{ratio} values).

In the perspective, we plan to study permeability and metabolism of new analogs of Gen-X and Gen-X', which contain a sugar moiety – rhamnal, connected with an isoflavone by a glycosidic bond. These derivatives showed higher antitumor activity in comparison to compounds of Gen-X or Gen-X' series. Since the sugar moiety may influence the biological properties of a compound remarkably, it can be assumed that this type of derivatization will alter transport and bioavailability of genistein derivatives.

Acknowledgments

This work was financed by the grant from Polish National Science Centre funds allocated with the decision no. DEC-2011/01/N/NZ4/01141. Katarzyna Papaj received a scholarship under the project DoktoRIS – Scholarship Program for Innovative Silesia.

REFERENCES

1. Polkowski K., Mazurek A.P.: Acta Pol. Pharm. Drug Res. 57, 135 (2000).
2. Prasain J.K., Carlson S.H., Wyss J.M.: Maturitas 66, 163 (2010).
3. Kampa M., Nifli A.P., Notas G., Castanas E.: Rev. Physiol. Biochem. Pharmacol. 159, 79 (2007).
4. Middleton E., Kandaswami C., Theoharides T.C.: Pharmacol. Rev. 52, 673 (2000).
5. Polkowski K., Popiołkiewicz J., Krzeczyński K., Ramza J., Pucko W., Zegrocka-Stendel O., Boryski J. et al.: Cancer Lett. 203, 59 (2004).
6. Rusin A., Krawczyk Z., Grynkiewicz G., Gogler A., Zawisza-Puchałka J., Szeja W.: Acta Biochim. Pol. 57, 23 (2010).
7. Rusin A., Zawisza-Puchałka J., Kujawa K., Gogler-Piglowska A., Wietrzyk J., Świtalska M., Głowala-Kosińksa M. et al.: Bioorg. Med. Chem. Lett. 19, 259 (2011).
8. Byczek A., Zawisza-Puchałka J., Gruca A., Papaj K., Grynkiewicz G., Szeja W., Rusin A.: J. Chem. 2013, Article ID 191563 (2013).
9. Rusin A., Gogler A., Głowala-Kosińska M., Bochenek D., Gruca A., Grynkiewicz G., Zawisza J. et al.: Bioorg. Med. Chem. Lett. 19, 4939 (2009).
10. Wise C., in Epithelial Cell Culture Protocols, Tavelin S., Gråsjö J., Taipalensuu G.O. Artursson P. Eds., p. 233, Humana Press, Totowa, New Jersey 2002.
11. Seera H., Mendes T., Bronze M. R., Simplicio L.: Bioorg. Med. Chem. 16, 4009 (2008).
12. Chen Y., Wang J., Wang L., Chen L., Wu Q.: Molecules 17, 14908 (2012).
13. Prasain J.K., Barnes S.: Mol. Pharm. 40, 846 (2007).
14. Shah P., Jogani V., Bagchi T., Misra A: Biotechnol. Prog. 22, 186 (2006).
15. Artursson P., Palm K., Luthman K: Adv. Drug Deliv. Rev. 22, 67 (1996).
16. Artursson P., Karlsson J.: Biochem. Biophys. Res. Commun. 175, 880 (1991).
17. Liu Y., Hu M.: Drug Metab. Dispos. 30, 370 (2002).
18. Kobayashi S., Shinohara M., Nagai T., Konishi Y.: Biosci. Biotechnol. Biochem. 77, 2210 (2013).
19. Faassen F., Vogel G., Spanings H., Vromans H.: Int. J. Pharm. 263, 113 (2003).

Acta Poloniae Pharmaceutica – Drug Research, Vol. 71 No. 6 pp. 1045–1050, 2014 ISSN 0001-6837
Polish Pharmaceutical Society

SYNTHESIS OF NEW PIROXICAM DERIVATIVES AND THEIR INFLUENCE ON LIPID BILAYERS

BERENIKA SZCZĘŚNIAK-SIĘGA[1*], JADWIGA MANIEWSKA[1], ANDRZEJ POŁA[2], KAMILA ŚRODA-POMIANEK[2],WIESŁAW MALINKA[1] and KRYSTYNA MICHALAK[2]

[1] Department of Chemistry of Drugs, Wroclaw Medical University, Borowska 211, 50-556 Wrocław, Poland
[2] Department of Biophysics, Wroclaw Medical University, Chałubińskiego 10, 50-368 Wrocław, Poland

Abstract: A novel series of potentially biologically active 1,2-benzothiazine 1,1-dioxides – analogs of piroxicam (a recognized non-steroidal anti-inflammatory drug) were synthesized from commercially available saccharin. All of the synthesized compounds were subjected to preliminary evaluation for their ability to interact with lipid bilayers. The influence of the new derivatives of piroxicam on liposomes made of EYPC was investigated by fluorescence spectroscopy with two fluorescent probes – Laurdan and Prodan. All the studied compounds showed an interaction with model membranes.

Keywords: synthesis, piroxicam, lipid bilayers, fluorescence spectroscopy, multitarget drugs, benzothiazines, MDR

The discovery of drugs these days is based upon a "one molecule – one target – one disease" philosophy, but modulating multiple protein targets simultaneously can be more beneficial for treating complex diseases, for instance, cancer, diabetes or neurodegenerative diseases like Alzheimer's disease (1). Our understanding of systems biology and the molecular complexity of human diseases has substantially shifted current therapeutic thinking towards drugs acting upon many molecular targets, i.e., multitarget drugs. Moreover, to fully understand the actions of a drug, knowledge of its polypharmacology is clearly essential (2, 3).

Since it is becoming well understood that chronic inflammation in any form can initiate and accelerate the cancer process, NSAIDs (non-steroidal anti-inflammatory drugs), which inhibit inflammation, became anti-cancer drugs (4, 5). The molecular target of NSAIDs is cyclooxygenase (COX), the enzyme which catalyzes the conversion from arachidonic acid to prostaglandins (PGs). There are three isoforms of COX (COX-1, COX-2 and COX-3) (6). The inhibition of COX-2 is responsible for the decrease in colorectal, breast, prostate and lung cancer incidence. That is why NSAIDs have been reported to reduce the risk of some solid tumors and are one of the most promising chemopreventive agents for cancer. Among the many NSAIDs studied as chemopreventive agents, there is a distinguished group of *oxicams* (e.g. piroxicam, meloxicam, tenoxicam), identified by their benzene(thieno)thiazine heterocyclic system containing an enolic group in position 4 (7).

Lichtenberger et al. presume that one of the alternative mechanisms by which NSAIDs can be effective is by interacting with cellular membranes and altering their biophysical properties (8). What is more, Peetla et al. prove that biophysical changes in membrane lipids in multidrug resistance (MDR) of cancer cells influence the transport and delivery of anticancer drugs. Recent advances in membrane lipid research show the varied roles of lipids in regulating membrane P-glycoprotein (P-gp) function, membrane trafficking, apoptotic pathways, drug transport and endocytic functions. Therefore, understanding the relationship between biophysical aspects of the cell membrane in drug-resistance mechanisms and drug delivery processes is crucial to overcome the phenomenon of MDR (9). It is proved that a lipid bilayer's composition and fluidity affect P-gp function, which efflux system occurs in drug-resistant cancer cells (10).

We designed new piroxicam (4-hydroxy-2-methyl-N-(pyridin-2-yl)-2*H*-1,2-benzothiazine-3-

* Corresponding author: berenika.szczesniak-siega@umed.wroc.pl

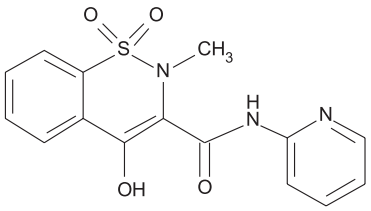

Figure 1. Structure of piroxicam

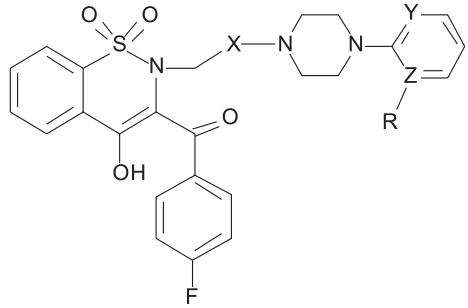

X = $(CH_2)_2$, C=O
Y = Z = C, N
R = F, OCH_3

Figure 2. Structures of new piroxicam analogues – **PD 28–31**

carboxamide 1,1-dioxide), (Fig. 1) derivatives as potentially multitarget drugs. They would be an analgesic, anti-inflammatory and, at the same time, chemopreventive in cancer. And, what is more, it might be the modulator overcoming the MDR phenomenon in resistant cancer cells. In our present work, we describe the procedure of synthesis of four new piroxicam derivatives, named **PD 28–31** (Fig. 2), and the results of studies of the interaction of new compounds with lipid bilayers by means of fluorescence spectroscopic methods. Also molecular structures of all compounds were optimized by molecular mechanics calculations *in silico*.

EXPERIMENTAL

Chemicals

The reagents and solvents used for synthesis were purchased from commercial suppliers and used as received. Homogeneity of the compounds was checked by TLC on silica gel plates. Flash column chromatographic purifications were performed using Sigma-Aldrich 60A silica gel 230–400 mesh. The proton nuclear magnetic resonance (^{1}H-NMR) spectra were measured on a Brucker 300 MHz NMR spectrometer using $CDCl_3$ as solvent and TMS as an internal standard. Melting points were determined in open capillary tubes and are uncorrected. Elemental analyses were performed with Carlo Erba NA 1500 analyzer and were within ± 0.4% of the theoretical value. IR spectra (cm^{-1}) were recorded on a Perkin-Elmer Spectrum Two UATR FT-IR spectrometer. The samples were applied as neat solids.

Phospholipid: egg yolk phoshphatidylcholine (EYPC) was purchased from Sigma-Aldrich (Poznań, Poland). The lipid was used as delivered, without further purification.

Fluorescent labels: 6-dodecanoyl-2-dimethylaminonaphthalene (Laurdan) and 6-propionyl-2-dimethylaminonaphthalene (Prodan) were purchased from Molecular Probes (USA).

All other chemicals used in this study were of analytical grade.

General procedure for the preparation of PD 28–31

2-(4-Fluorophenacyl)-2H-1,2-benzothiazol-3-on 1,1-dioxide (**2**)

A mixture of commercially available saccharine **1** (0.92 g, 5 mmol) with 5 mmol of 2-bromo-4'-fluoroacetophenone in 7 mL of *N*,*N*-dimethylformamide (DMF) and triethylamine (0.7 mL, 5 mmol) was stirred at room temperature for 10 h, then poured over ice cooled water (50 mL) resulting in the formation of a white solid, which was filtered and washed with cold water. The solid was dried and crystallized from ethanol to give **2**.

Analytical data for **2**: $C_{15}H_{10}FNO_4S$ (m.w. 319.31); m.p. 165–168°C (EtOH). ^{1}H-NMR (δ, ppm): 5.11 s (2H, CH_2), 7.16–8.01 m (8H, Ar*H*). FT-IR (UATR): 1738, 1693 (CO), 1330, 1183 (SO_2) cm^{-1}. Yield 94%.

3-(4-Fluorobenzoyl)-4-hydroxy-2H-1,2-benzothiazine 1,1-dioxide (**3**)

Three millimole of **2** was dissolved in 7.5 mL of EtONa (prepared from 0.17 g of Na and 7.5 mL of anhydrous EtOH) at 40°C and stirred with heating to 55–60°C for 5–10 min. Color changes from beige to deep red were observed. After this time and after dissolving all of the substance, the mixture was rapidly cooled to 25°C and 7.5 mL HCl (9%) was added. Color changed from deep red to deep yellow and the product precipitated. The solid was filtered off, washed with cold water, dried and purified by crystallization from EtOH to give **3**.

Analytical data for **3**: $C_{15}H_{10}FNO_4S$ (m.w. 319.31); m.p. 193–195°C (EtOH). ^{1}H-NMR (δ, ppm): 5.91 s (1H, NH), 7.13–8.20 m (8H, Ar*H*), 15.80 s (1H, OH_{enolic}). FT-IR (UATR): 3151 (NH), 1590 (CO), 1280, 1158 (SO_2) cm^{-1}. Yield 81%.

***1-(2-Chloro-1-oxoethyl)-4-arylsubstituted-piperazine* (4a, b)**

Ten millimoles of 1-(2-fluorophenyl)piperazine (for **4a**) or 1-(2-pyrimidin)piperazine (for **4b**) was dissolved in 40 mL of diethyl ether with addition of 1.4 mL of triethylamine and stirred slowly at room temperature for 10 min. Then, 1.6 mL (20 mmol) of chloroacetyl chloride in 20 mL of diethyl ether were slowly instilled, and stirring was continued for another 2 h. After this time, diethyl ether was evaporated in vacuum and 10 mL of water and 60 mL of chloroform were added. The organic phase was separated, dried with $MgSO_4$ and evaporated in vacuum to give **4a** or **4b**.

Analytical data for **4a**: $C_{12}H_{14}ClFN_2O$ (m.w. 256.70); ^{1}H-NMR ($CDCl_3$, δ, ppm): 3.02–3.12 (m, 4H, $N(CH_2)_2$), 3.64–3.78 (m, 4H, $N(CH_2)_2$), 4.08 (s, 2H, CH_2), 6.87–7.06 (m, 4H, Ar*H*). Yield 70%.

Analytical data for **4b**: $C_{10}H_{13}ClN_4O$ (m.w. 240.69); ^{1}H-NMR ($CDCl_3$, δ, ppm): 3.56–3.70 (m, 4H, $N(CH_2)_2$), 3.82–3.92 (m, 4H, $N(CH_2)_2$), 4.11 (s, 2H, CH_2), 6.53–6.56 [t, *J* = 4.8 Hz, 1H, $CH(5)_{pyrimidine}$], 8.31–8.33 [d, *J* = 4.8 Hz, 2H, $CH(4\text{ and }6)_{pyrimidine}$]. Yield 66%.

***1-(3-Chloropropyl)-4-(2-substituted-phenyl)piperazine* (5a, b)**

Ten millimoles of 1-(2-fluorophenyl)piperazine (for **5a**) or 1-(2-methoxyphenyl)piperazine (for **5b**) and 11 mmol (1.1 mL) of 1-bromo-3-chloropropane were dissolved in acetone (3 mL) with addition of 25% NaOH (2 mL), stirred slowly at room temperature for 8 h and left overnight. After this time, ether (20 mL) was added and stirred for further 30 min. Then, the mixture was divided in a separatory funnel into two parts. The ether part was dried with $MgSO_4$ and evaporated under vacuum. The residue was purified by flash silica gel chromatography, eluting with EtOAc to give **5a** or **5b.**

Analytical data for **5a**: $C_{13}H_{18}ClFN_2$ (m.w. 256.75); ^{1}H-NMR (δ, ppm): 1.96–2.05 (m, 2H, $CH_2CH_2CH_2$), 2.56–2.68 (m, 6H, $CH_2N(CH_2)_2$), 3.11–3.14 (m, 4H, $N(CH_2)_2$), 3.61–3.65 (t, *J* = 6.6 Hz, 2H, $CH_2CH_2CH_2N_{piperazine}$), 6.92–7.26 (m, 4H, Ar*H*). Yield 85%.

Analytical data for **5b**: $C_{14}H_{21}ClN_2O$ (m.w. 268.78); ^{1}H-NMR (δ, ppm): 1.94–2.04 (m, 2H, $CH_2CH_2CH_2$), 2.49–2.66 (m, 6H, $CH_2N(CH_2)_2$), 3.09 (brs, 4H, $N(CH_2)_2$), 3.59–3.63 (t, *J* = 6.6 Hz, 2H, $CH_2CH_2CH_2N_{piperazine}$), 3.85 (s, 3H, OCH_3), 6.83–7.02 (m, 4H, Ar*H*). Yield 74%.

***3-(4-Fluorobenzoyl)-2-substituted-4-hydroxy-2H-1,2-benzothiazine 1,1-dioxides* (PD 28–31)**

To the stirred mixture of 5 mmol **3** in 20 mL of anhydrous EtOH 5 mL of EtONa (prepared from 0.12 g of Na and 5 ml of anhydrous EtOH) was added. Then, 5 mmol of corresponding piperazine (**4a, b** or **5a**, **b**) was added and refluxed with stirring for 10–12 h. When the reaction was complete, which was confirmed on TLC plates, ethanol was distilled off, the residue was treated with 50 mL of $CHCl_3$ and insoluble materials were filtered off. The filtrate was evaporated and the residue was purified by crystallization from ethanol to give compounds **PD 28-31**.

Analytical data for **PD 28–31**:

PD 28: $C_{27}H_{23}F_2N_3O_5S$ (m.w. 539.55); m.p. 165–166°C (EtOH). ^{1}H-NMR (δ, ppm): 2.80–4.23 (m, 10H, CH_2CO and $H_{piperazine}$), 6.79–8.25 (m, 12H,

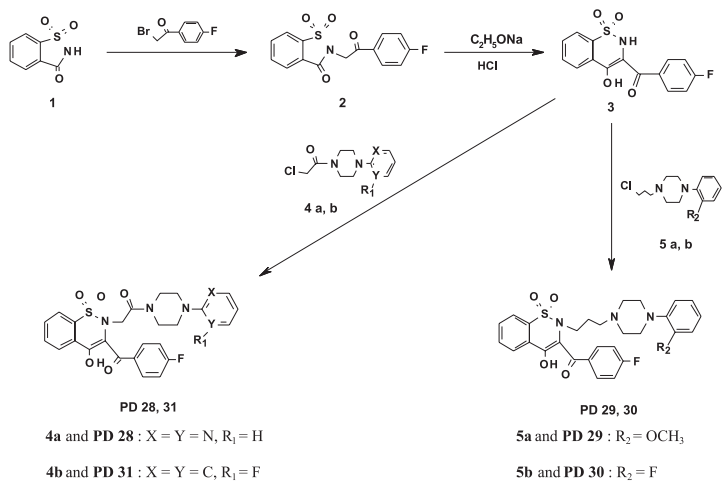

Scheme 1. General procedure for preparation of **PD 28-31**

Ar*H*), 15.49 (s, 1H, OH_{enolic}). FT-IR (UATR): 1644, 1591 (CO), 1336, 1175 (SO_2) cm^{-1}. Analysis: calcd.: C 60.10, H 4.30, N 7.79%; found: C 59.97, H 4.40, N 7.59%. Yield 45%.

PD 29: $C_{25}H_{22}FN_5O_5S$ (m.w. 523.54); m.p. 210–213°C (EtOH). ^{1}H-NMR (δ, ppm): 3.13–4.31 (m, 10H, CH_2CO and $H_{piperazine}$), 6.51–8.29 (m, 11H, Ar*H*), 15.50 (s, 1H, OH_{enolic}). FT-IR (UATR): 1660, 1586 (CO), 1344, 1175 (SO_2) cm^{-1}. Analysis: calcd.: C 57.35, H 4.24, N 13.38%; found: C 57.39, H 4.28, N 13.46%. Yield 44%.

PD 30: $C_{28}H_{27}F_2N_3O_4S$ (m.w. 539.59); m.p. 145–148°C (EtOH). ^{1}H-NMR (δ, ppm): 1.24 (brs, 2H, $CH_2CH_2CH_2$), 1.99 (brs, 2H, $CH_2CH_2CH_2N_{piperazine}$), 2.28 (brs, 4H, $N(CH_2)_2$), 2.95–3.42 (m, 6H, $CH_2N(CH_2)_2$), 6.91–8.19 (m, 12H, Ar*H*), 15.50 (s, 1H, OH_{enolic}). FT-IR (UATR): 1607 (CO), 1331, 1174 (SO_2) cm^{-1}. Analysis: calcd.: C 62.32, H 5.04, N 7.79%; found: C 62.67, H 5.37, N 7.51%. Yield 55%.

PD 31: $C_{29}H_{30}FN_3O_5S$ (m.w. 551.63); m.p. 121–123°C (EtOH). ^{1}H-NMR (δ, ppm): 1.39 (brs, 2H, $CH_2CH_2CH_2$), 2.10 (brs, 2H, $CH_2CH_2CH_2N_{piperazine}$),

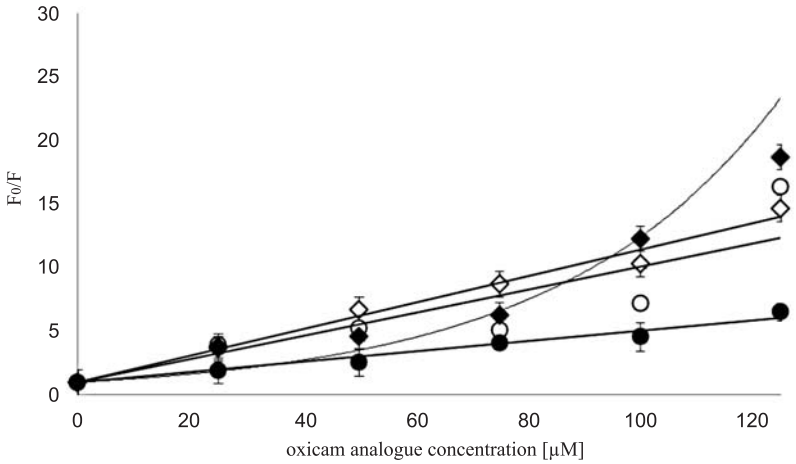

Figure 3. Stern-Volmer plots for quenching of Laurdan (open symbols) and Prodan (full symbols) by **PD28** (circles) and **PD29** (diamonds) in EYPC. Bars represent standard deviations

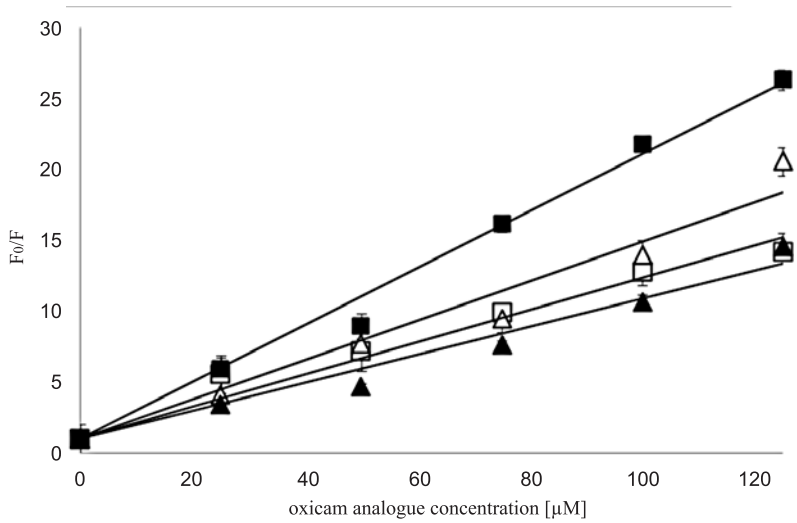

Figure 4. Stern-Volmer plots for quenching of Laurdan (open symbols) and Prodan (full symbols) by **PD30** (squares) and **PD31** (triangles) in EYPC. Bars represent standard deviations

2.44 (brs, 4H, $N(CH_2)_2$), 3.03–3.40 (m, 6H, $CH_2N(CH_2)_2$), 3.84 (s, 3H, OCH_3), 6.84–8.18 (m, 12H, Ar*H*), 15.48 (s, 1H, OH_{enolic}). FT-IR (UATR): 1614 (CO), 1329, 1175 (SO_2) cm^{-1}. Analysis: calcd.: C 63.14, H 5.48, N 7.62%; found: C 63.36, H 5.63, N 7.54%. Yield 42%.

Fluorescence spectroscopy

Small unilamellar liposomes, prepared by sonification of 2 mM EYPC suspension in 20 mM Tris–HCl buffer (20 mM Tris, 0.5 mM EDTA, 150 mM NaCl pH 7.4) using UP 200s sonificator (Dr. Hilscher GmbH, Berlin, Germany), were used for fluorescence spectroscopy measurements. Final phospholipid concentration in a sample was 200 μM. Laurdan and Prodan were dissolved in DMSO in order to obtain 1 mM stock solutions. Liposomes were incubated with a fluorescent probe (final concentration 5 μM) for 30 min in darkness at room temperature. Then, the appropriate amount of oxicam stock solution (30 mM DMSO) was added and the sample was further incubated for 20 min in darkness. The oxicam concentration in samples was 25–125 μM in concentration-dependence experiments. All spectroscopic experiments were carried out at room temperature with LS 50B spectrofluorimeter (Perkin–Elmer Ltd., Beaconsfield, UK) equipped with a xenon lamp using emission and excitation slits of 5 nm. The excitation wavelength for Laurdan was 390 nm and for Prodan 360 nm. The recorded fluorescence spectra were processed with FLDM Perkin-Elmer 2000 software.

It was checked that the studied oxicam analogues alone did not exhibit fluorescence in the spectral region of interest. All the experiments were performed three times.

Molecular modelling

Theoretical calculations were performed using Spartan 10 software (Wavefunction, Inc., USA). The optimized molecular structure of all compounds and QSAR (quantitative structure–activity relationship) descriptors for them were calculated *ab initio* by DFT method with 6-31+G* basis set.

RESULTS

Synthesis

Compound **2** was obtained by alkylation of saccharin with 2-bromo-4'-fluoroacetophenone in DMF with addition of a small amount of triethylamine in room temperature. Then, newly obtained compound was rearranged using sodium ethoxide to give compound **3**. The alkilation of **3** by 1-(chloroalkil/acyl)-4-arylpiperazine resulted in products **PD 28–31**.

Fluorescence spectroscopy

Laurdan and Prodan, two fluorescent probes, were used to characterize the interaction of the studied compounds with EYPC liposomes. Both probes possess the same fluorophore but connected to the propionyl chain in case of Prodan and to the lauryl chain in Laurdan (11). Laurdan fluorophore is located deeper in the lipid bilayer at the level of the phospholipid glycerol backbone, whereas Prodan, in contrast, is anchored to the lipid bilayer more loosely and resides closer to the membrane surface. In the studies it was initially checked if the addition of any of the studied compounds would result in fluorescence quenching of the probes. Stern–Volmer plots are presented in Figure 3 for **PD 28** and **PD 29** and in Figure 4 for **PD 30** and **PD 31**. The studied compounds caused very strong quenching of both probes, although the effect was much more pronounced in case of Laurdan for **PD 28** and **PD 31**, and in case of Prodan for **PD 29** and **PD 30**.

Molecular modelling

Applying of QSAR methods allowed to describe electronic, structural and topological parameters and hydrophobicity of new compounds and to correlate these properties with their ability to interact with model membranes. LogP of studied oxicam derivatives is ranked as follows: **PD 30** > **PD 29** > **PD 31** > **PD 28** and PSA: **PD 28** > **PD 31** > **PD 29** > **PD 30**, while polarizability is ranked as follows: **PD 29** > **PD 30** > **PD 31** > **PD 28**. Values of all molecular descriptors for newly synthesized oxicam derivatives are presented in Table 1.

Presented results revealed that newly synthesized compounds pass the Lipinski's Rule of five (RO5), because LogP < 5, H-bond donors < 5, and H-bond acceptors < 10 (12). These physicochemical parameters are associated with acceptable aqueous solubility and intestinal permeability so comprise the first steps in oral bioavailability and ability to interact with lipid bilayers.

DISCUSSION AND CONCLUSION

Our group has focused on synthesis of new chemical analogues of piroxicam with potential analgesic, anti-inflammatory and chemopreventive or anti-MDR activity as multitarget drugs. In the present work, we have shown that new compounds **PD 28–31** interact with the model membranes under consideration. Quenching of fluorescence of two probes, Laurdan and

Table 1. The molecular descriptors for **PD 28–31** (Spartan 10).

Compound	Log P	PSA [Å²]	HBD Count	HBA Count	E HOMO [eV]	E LUMO [eV]	Polarizability
PD 28	0.32	91.799	1	10	–6.04	–2.65	79.47
PD 29	2.73	75.592	1	9	–5.79	–2.57	84.08
PD 30	3.02	70.503	1	8	–6.00	–2.54	82.20
PD 31	1.83	80.632	1	9	–5.95	–2.61	80.88

PSA = polar surface area, HBD = hydrogen bond donor, HBA = hydrogen bond acceptor, E HOMO = energy of highest occupied molecular orbital, E LUMO = energy of lowest unoccupied molecular orbital

Prodan, by four newly synthesized oxicam derivatives (**PD 28–31**) was investigated. According to Lakowicz, the extent of quenching expressed by the values of Stern-Volmer constants can reveal the accessibility of fluorophores to quenchers. That is why, if the location of fluorescent probe (fluorophore) within the model membranes is known, quenching studies can be used to reveal the location of quenchers in membranes or the permeability of membrane to quenchers (13). It was found that **PD 28** and **PD 31** quenched the fluorescence of Laurdan to a higher extent than Prodan in model membranes. On the contrary, **PD 29** and **PD 30** turned out to be weaker quenchers of Laurdan than Prodan fluorescence. The decreased fluorescence intensity in the presence of the studied compounds may be the result of their interaction with fluorescent probes affecting e.g., their influence on fluorophore's microenvironment or their molecular organization within the phospholipid bilayer. The more pronounced quenching of Laurdan than Prodan fluorescence for **PD 28** and **PD 31** in comparison to **PD 29** and **PD 30** suggested that the bilayer region occupied by Laurdan (the level of the phospholipid glycerol backbone) is more affected by their presence. The regions close to the surface of the model membrane, where Prodan is localized, were more affected by the presence of **PD 29** and **PD 30**. Quenching of the fluorescence of another fluorescent probe -DPH by NSAIDs (two oxicams - lornoxicam and meloxicam - and nimesulide) was examined by Sousa et al. (14). Their DPH fluorescence quenching studies revealed that studied NSAIDs were able to quench the fluorescene of the probe located in phospholipid bilayer hydrocarbon region - even deeper than Laurdan. Their fluorescence anisotropy measurements were also made to investigate the effects on membrane fluidity resulting from the interaction between the drugs and lipid bilayers. The efficiency of NSAIDs to increase the membrane fluidity and to penetrate into the hydrocarbon chain region was ordered as: lornoxicam > meloxicam > nimesulide. The deeper penetration of **PD 28** and **PD 31** into the lipid bilayer, reveled in our studies, may be related to the presence of the additional carbonyl group in the side chain in position 2 of benzothiazine ring, which might increase their ability to interact with model membranes. However, the precise determination of the nature of new oxicam analogues interaction with phospholipid membranes would require further studies.

REFERENCES

1. Morphy R., Rankovic Z.: Drug Discov. Today 12, 156 (2007).
2. Hopkins A.L.: Nature 12, 462 (2009).
3. Bojanowski P., Lipiński P., Czekała P., Plewczyński D.: Biul. Wydz. Farm. WUM 1, 1 (2013) (Polish).
4. Steele V.E., Hawk E.T., Viner J.L., Lubet R.A.: Mutat. Res. 523, 137 (2003).
5. Grivennikov S., Greten F., Karin M.: Cell 19, 883 (2010).
6. Sobolewski C., Cerella C., Dicato M., Ghibelli L., Diederich M.: Int. J. Cell Biol. 2010, 215158 (2010).
7. Wang D., DuBois R.N.: Nature Rev. Cancer 10, 181 (2010).
8. Lichtenberger L.M., Zhou Y., Jayaraman V., Doyen J.R., O'Neil R.G., Dial E.J., Volk D.E. et al.: Biochim. Biophys. Acta 1821, 994 (2012).
9. Bamburowicz-Klimkowska M., Szutowski M.: Biul. Wydz. Farm. WUM 1, 1 (2012).
10. Peetla Ch., Vijayaraghavalu S., Labhasetwar V.: Adv. Drug Deliv. Rev. 65, 1686 (2013).
11. Parasassi T., Krasnowska E.K., Bagatolli L., Gratton E.: J. Fluoresc. 8, 4 (1998).
12. Lipinski Ch., Drug Discov. Today Technol. 1, 337 (2004).
13. Lakowicz J.R.: Principles of Fluorescence Spectroscopy. 3rd edn., Springer, Heidelberg, New York 2006.
14. Sousa C., Nunes C., Lúcio M., Ferreira H., Lima J.L.F.C., Tavares J., Cordeiro-da-Silva A., Reis S.: J. Pharm. Sci. 97, 8 (2008).

Acta Poloniae Pharmaceutica – Drug Research, Vol. 71 No. 6 pp. 1051–1055, 2014 ISSN 0001-6837
Polish Pharmaceutical Society

IN VITRO EVALUATION OF ANTIPROLIFERATIVE AND CYTOTOXIC PROPERTIES OF PTEROSTILBENE AGAINST HUMAN COLON CANCER CELLS

JOANNA WAWSZCZYK*, MAŁGORZATA KAPRAL, ANDRZEJ HOLLEK and LUDMIŁA WĘGLARZ

Medical University of Silesia, School of Pharmacy with the Division of Laboratory Medicine, Department of Biochemistry, Jedności 8, 41-200 Sosnowiec, Poland

Abstract: Colon cancer has been remaining the second leading cause of cancer mortality in Poland in the last years. Epidemiological, preclinical and clinical studies reveal that dietary phytochemicals may exert chemopreventive and therapeutic effect against colorectal cancer. There is a growing interest in identifying new biologically active agents from dietary sources in this respect. Pterostilbene (trans-3,5-dimethoxy-4-hydroxystilbene) is a naturally occurring stilbene, that has been found to have antioxidative, anti-inflammatory and antiproliferative properties. Compared to other stilbenes, pterostilbene has greater bioavailability, and so, a greater potential for clinical applications. Recent studies showed that pterostilbene exhibits the hallmark characteristics of an anticancer agent. The aim of this study was to analyze antiproliferative and cytotoxic effects of pterostilbene on human colon cancer Caco-2 cells. They were cultured using standard techniques and exposed to increasing doses of pterostilbene (5–100 μM) for 48 and 72 h. Cell proliferation was determined by sulforhodamine B assay. The growth of treated cells was expressed as a percentage of that of untreated control cells. Pterostilbene decreased proliferation rate of Caco-2 cells in a dose- and time-dependent manner. Its concentrations = 25 μM did not affect cell growth after 48 h treatment period. Significant growth inhibition was observed in cultures incubated with higher concentrations of pterostilbene (40–100 μM). Pterostilbene at all concentrations used (5–100 μM) caused significant inhibition of cell proliferation when the experimental time period was elongated to 72 h. The maximum growth reduction was observed at 100 mM pterostilbene. The cytotoxicity of pterostilbene was evaluated in 48 h cultures based on lactate dehydrogenase (LDH) leakage into the culture medium and showed dose-related pattern. The findings of this study showed significant dose-dependent antiproliferative and cytotoxic effects of pterostilbene against human colon cancer cells *in vitro*.

Keywords: pterostilbene, colon cancer, proliferation, Caco-2 cell line

Colon cancer remains the second leading cause of cancer mortality in Poland in the last years (1). Epidemiological, preclinical and clinical studies reveal that dietary phytochemicals may exert chemopreventive and therapeutic effect against colorectal cancer (2, 3). There is a growing interest in identifying new biologically active agents from dietary sources in this respect.

Pterostilbene (trans-3,5-dimethoxy-4-hydroxystilbene) is a naturally occurring stilbene, found in fruits such as grapes and berries (4). It is a structural analogue of another highly studied stilbene, resveratrol (5). The structural difference between these compounds is that pterostilbene contains one hydroxy group and two methoxy groups while resveratrol has three hydroxy groups. Due to the presence of methoxy groups pterostilbene exhibits an increased oral absorption, better metabolic stability, greater lipophilicity and higher potential for cellular uptake. Pterostilbene administered orally, shows 95% bioavailability while resveratrol has only 20% bioavailability (4, 6). Compared to other stilbenes, pterostilbene has greater bioavailability, and so, a greater potential for clinical applications (7). Pterostilbene has been found to possess several pharmacological activities such as antioxidative, anti-inflammatory and antiproliferative (5, 8). Recent studies showed that pterostilbene exhibits the hallmark characteristics of a valuable anticancer agent (9).

The aim of this study was to evaluate antiproliferative and cytotoxic effects of pterostilbene on human colon cancer Caco-2 cells *in vitro*.

* Corresponding author: e-mail: jwawszczyk@sum.edu.pl; phone : +48 32 3641072

EXPERIMENTAL

Cell line and culture conditions

The Caco-2 human colon adenocarcinoma cell line was purchased from the American Type Culture Collection (ATCC). Cells were grown routinely in medium containing the following composition: 90% modified Eagle's medium (MEM, Sigma Aldrich), 10% fetal bovine serum (FBS, PAA), 100 U/mL penicillin, 100 µg/mL streptomycin (Sigma Aldrich), and 10 mM HEPES (Sigma Aldrich). The cell cultures were cultivated as a monolayer at 37°C in a humidified atmosphere containing 5% CO_2.

Cell growth determination

The effect of pterostilbene on Caco-2 cell proliferation was analyzed by *In Vitro* Toxicology Assay Kit, Sulforhodamine B (SRB) based (Sigma Aldrich). The SRB is a dye staining cellular proteins and thus the amount of the incorporated dye is an indirect measure of total biomass and consequently, cell number and proliferation (10). Pterostilbene was purchased from Sigma Aldrich. Stock solution of pterostilbene was prepared in dimethyl sulfoxide (DMSO) and further diluted in sterile culture medium to desired concentrations immediately before use. The final DMSO concentration in the working solutions was 0.01%.

To study the cell proliferation, colonocytes were seeded at an initial density of 1×10^3 cells/well in 200 µL MEM medium complemented with the components given above and allowed to attach and grow. After 24 h, the medium was aspirated and cells were exposed to the freshly prepared medium containing pterostilbene (5; 10; 25; 40; 50; 60; 75 and 100 µM) for 48 or 72 h. Subsequently, cells were washed with PBS and fixed in 10% trichloroacetic acid (4°C, 1 h), followed by 5 washes with deionized water. Cells were stained by the addition of 0.4% SRB in 1% acetic acid at room temperature for 30 min. Afterwards, plates were washed with 1% acetic acid and air-dried. After the liberation of the incorporated SRB by the addition of 10 mM Tris-HCl, absorbance was measured at 570 nm and 690 nm (reference wavelength) using the MRX Revelation plate reader (Dynex Technologies). The growth of treated cells was expressed as a percentage of untreated control cells.

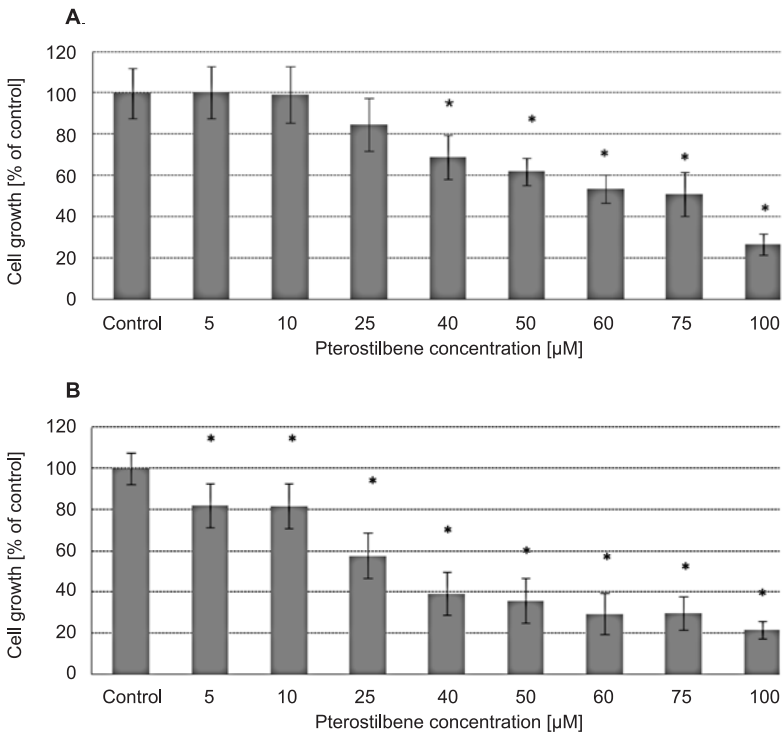

Figure 1. Growth inhibitory effect of various concentrations of pterostilbene on Caco-2 cells after 48 (**A**) and 72 (**B**) hours treatment. The results are expressed as percentage of untreated control (the means ± SD; *p < 0.05 *vs.* control).

LDH cytotoxicity assay

Cytotoxicity induced by pterostilbene was assessed by lactate dehydrogenase (LDH) leakage into the culture medium by a commercially available *In Vitro* Toxicology Assay Kit, Lactic Dehydrogenase based (Sigma Aldrich). Increased LDH activity in the supernatants of cell cultures is a result of a damage to the cellular membrane and correlates with the percentage of dead cells. For the cytotoxicity test, Caco-2 cells were seeded at a density of 1×10^4 cells per well in 200 µL culture medium in a 96-well plate and cultured for 24 h. Afterwards, media were replaced with the fresh ones containing various concentrations of pterostilbene (5–100 µM). Following a 48 h period, LDH activity was measured in both culture media and cell lysates according to manufacturer's instruction. Colorimetric results were read on a multiplate reader MRX Revelation (Dynex Technologies) at 492 nm and 690 nm (reference wavelength). The results were shown as percentage of total LDH released into the medium. The LDH release (%) was calculated using the following equation:

LDH release (%) = Extracellular LDH / Total LDH × 100%.

Statistical analysis

Statistical analysis was performed with the use of Statistica PL ver. 9.0 Software (StatSoft). The examined parameters were first evaluated for normal distribution (Shapiro-Wilk test). One-way analysis of variance (ANOVA) with NIR's *post-hoc* test was used to evaluate significances between examined groups. Comparison of two data sets was performed by t-test. Results were expressed as the means ± standard deviation (SD). Differences were considered statistically significant when the probability value p was lower than 0.05.

RESULTS

In the present study, Caco-2 cells were used as the colon cancer cell model *in vitro*. The effect of pterostilbene on their growth was evaluated using the SRB assay. Cells were incubated in the presence of different concentrations of pterostilbene (5; 10, 25; 40; 50; 60; 75 and 100 µM) for 48 and 72 h (Fig. 1). The effect of this compound on Caco-2 cell proliferation after 48 h is shown in Figure 1A. Its concentrations = 25 mM did not affect cell growth and higher concentrations (40–100 mM) significantly decreased cellular density. Pterostilbene at all concentrations used (5–100 µM) caused significant inhibition of cell proliferation when the experimental time period was elongated to 72 h (Fig. 1B) and the maximum growth reduction (78%) was observed at 100 mM. The effect of DMSO on the growth of Caco-2 cell line was also evaluated by culturing cells in medium containing 0.01% DMSO but no influence of this compound was found (data not shown). Taken together, this data demonstrated that pterostilbene decreased proliferation rate of Caco-2 cells in a time- and dose-dependent manner.

The effect of pterostilbene on Caco-2 cell membrane integrity was examined by determining the percentage of LDH released into the culture medium following 48 h treatment. As seen in Fig. 2, pterostilbene at concentrations up to 40 µM did not cause significant increase in the LDH release and at higher concentrations (= 50 µM) statistical-

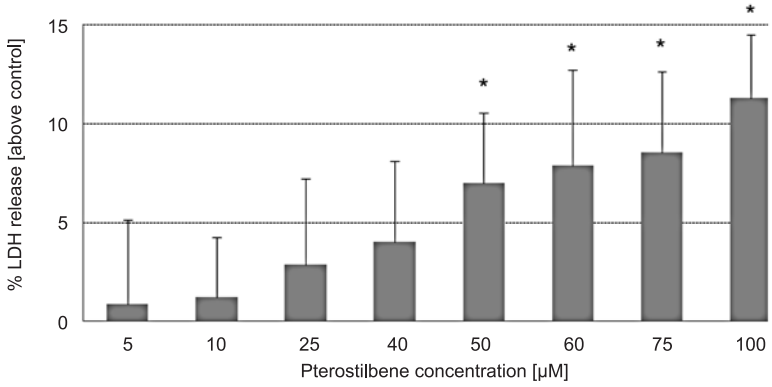

Figure 2. Cytotoxicity of pterostilbene evaluated by lactate dehydrogenase (LDH) release from Caco-2 cells after 48 h of incubation. Data are expressed as the % LDH release above control, *p < 0.05 *vs.* control.

ly significant increase in LDH release as compared with control cells (7–11.3% LDH released above control). The highest accumulation of LDH in media was observed after treatment of Caco-2 cells with 100 μM pterostilbene. DMSO at concentration of 0.01% did not affect LDH release in this model (data not shown). The study indicated that pterostilbene exerted cytotoxic activity on colon cancer cells, but this effect depended on its concentration

DISCUSSION

Colorectal cancer is one of the most common tumors in the industrialized countries. Diet strongly influences the risk of this cancer, and changes in food habits might reduce up to 70% of colon cancer incidence rate (11). In addition, a number of studies point to an increased risk of colorectal cancer with low consumption of vegetables and fruits (12). Recently, pterostilbene found in fruits such as grapes, berries, has been a subject of intense investigation as cancer chemopreventive agent. The latest clinical trial showed that pterostilbene is well-tolerated and safe for use in humans (13).

Several studies in animal models have demonstrated that dietary administration of pterostilbene inhibited colon tumor development. Diet containing pterostilbene has been shown to significantly reduce colon tumor multiplicity when treatment of rats with pterostilbene was commenced after injection of colon-specific carcinogen – azoxymethane (AOM) (14). Supplementation of a diet with pterostilbene inhibited formation of AOM-induced colonic aberrant crypt foci and adenomas also in mice (15). Furthermore, colon tumors from pterostilbene-fed animals showed reduced expression of a cell proliferation marker, proliferating cell nuclear antigen (PCNA) (14).

In cancer biology, cell proliferation is an important and commonly studied parameter reflecting cellular vitality. Dysregulation of cell proliferation is a hallmark of cancer cells and assessment of cellular proliferation is a key component in discovery and development of anticancer drugs (16). As observed in this study, pterostilbene demonstrated time- and dose-dependent growth inhibitory effect on human colon cancer cells Caco-2. Significant decrease of cell proliferation was observed in cultures incubated with the concentrations of pterostilbene = 40 mM for 48 h treatment period. The prolongation of cells exposure to stilbenoid up to 72 h resulted in their considerable growth inhibition compared to untreated control cells at all concentrations used (5–100 mM). These data concur with the results published by Paul et al. (17), who observed reduced cell proliferation of colon cancer cells HT-29 after 24, 48 and 72 h incubation with pterostilbene in a dose-dependent manner and the most pronounced growth inhibition after 72 h treatment. In addition, pterostilbene revealed greater inhibitory potency toward HT-29 cells proliferation than resveratrol.

Furthermore, in the current study, the cytotoxic effect of pterostilbene was evaluated by measuring the LDH leakage out of cells. This method is commonly used as an indicator of cell membrane integrity and serves to assess cytotoxicity of chemical compounds (18). Percentage of LDH released to the medium was measured to find out whether the growth inhibitory effect of pterostilbene on Caco-2 cells was due to its cytotoxicity. Pterostilbene at concentrations up to 40 μM did not cause increase in the percentage of LDH release after 48 h treatment. Higher concentrations of this stilbene (= 50 μM) statistically significantly enhanced the leakage of enzyme resulting from a loss of membrane integrity. Pterostilbene was reported to reduce cell viability in colon cancer cells HT-29, HCT116 and Caco-2 and its concentration required to achieve 50% inhibition of cell viability after 48 h incubation period was about 15 μM in HT-29, 12 μM in HCT116 and 65 μM in Caco-2 cells (19). These results differ from the findings by Harun and Ghazali (20), who did not observe toxic effects of pterostilbene at concentrations up to 100 μM against HT-29 cells. This might be, however, due to the shorter incubation period (24 h) with pterostilbene.

In conclusion, the present study show antiproliferative and cytotoxic properties of pterostilbene against colon cancer cells *in vitro*. Hence, it can be suggested that pterostilbene, an active constituent of berries, holds great promise in the field of chemoprevention of colon cancer.

Acknowledgment

This work was supported by the Medical University of Silesia, Katowice, Poland (Grant No. KNW-2-001/N/4/N).

REFERENCES

1. Wojciechowska U., Didkowska J., Zatoński W.: Cancer in Poland in 2008. National Cancer Registry of Poland, the Maria Sklodowska-Curie Memorial Cancer Center and Institute of Oncology, Warszawa 2010.

2. Rimando A.M., Suh N.: Planta Med. 74, 1635 (2008).
3. van Duijnhoven F.J., Bueno-De-Mesquita H.B., Ferrari P., Jenab M., Boshuizen H.C., Ros M.M., Casagrande C. et al.: Am. J. Clin. Nutr. 89, 1441 (2009).
4. Estrela J.M., Ortega A., Mena S., Rodriguez M.L., Asensi M.: Crit. Rev. Clin. Lab. Sci. 50, 65 (2013).
5. Remsberg C.M., Yáñez J.A., Ohgami Y., Vega-Villa K.R., Rimando A.M., Davies N.M.: Phytother. Res. 22, 169 (2008).
6. Lin H.S., Yue B.D., Ho P.C.: Biomed. Chromatogr. 23, 1308 (2009).
7. Wang Y., Ding L., Wang X., Zhang J., Han W., Feng L., Sun J. et al.: Am. J. Transl. Res. 4, 44 (2012).
8. Chakraborty A., Gupta N., Ghosh K., Roy P.: Toxicol. In Vitro 24, 1215 (2010).
9. McCormack D., McFadden D.: J. Surg. Res. 173, 53 (2012).
10. Logan P., Burnier J., Burnier M.N.: Ecancermedicalscience 7, 336 (2013).
11. Haggar F.A., Boushey R.P.: Clin. Colon Rectal Surg. 22, 191(2009).
12. Gingras D., Béliveau R.: Cancer Microenviron. 4, 133 (2011).
13. Riche D., McEwen C., Riche K, Sherman J., Wofford M., Deschamp D., Griswold M.: J. Toxicol. 2013, 463595 (2013).
14. Paul S., DeCastro A.J., Lee H.J., Smolarek A.K., So J.Y., Simi B., Wang C.X. et al.: Carcinogenesis 31, 1272 (2010).
15. Chiou Y.S., Tsai M.L., Wang Y.J., Cheng A.C., Lai W.M., Badmaev V., Ho C.T., Pan M.H.: J. Agric. Food Chem. 58, 8833 (2010).
16. Hanahan D., Weinberg R.A.: Cell 100, 57 (2000).
17. Paul S., Rimando A.M., Lee H.J., Ji Y., Reddy B.S., Suh N.: Cancer Prev. Res. 2, 650 (2009).
18. Johnson J., Mukhtar H.: Cancer Lett. 255, 170 (2007).
19. Nutakul W., Sobers H.S., Qiu P., Dong P., Decker E.A., McClements D.J., Xiao H.: J. Agric. Food Chem. 59, 10964 (2011).
20. Harun Z., Ghazali A.R.: Asian Pac. J. Cancer Prev. 13, 6403 (2012).

Acta Poloniae Pharmaceutica – Drug Research, Vol. 71 No. 6 pp. 1056–1059, 2014 ISSN 0001-6837
Polish Pharmaceutical Society

ANTIPROLIFERATIVE EFFECT OF VALPROIC ACID AND 5,7-DIMETHOXYCOUMARIN AGAINST A2058 HUMAN MELANOMA CELLS

DANIEL WOLNY, EWA CHODUREK and ZOFIA DZIERŻEWICZ

Medical University of Silesia in Katowice, School of Pharmacy with the Division of Laboratory Medicine, Department of Biopharmacy, Jedności 8 St., 41-200 Sosnowiec, Poland

Abstract: Melanoma is one of the most malignant tumors of a dangerous high incidence and high metastatic potential. It grows quickly and in an advanced stage is resistant to radio-, chemo- and immunotherapy, which makes it difficult to cure. Therefore, research efforts are focused on the development of new therapeutics or chemopreventive strategies. The aim of the study was to investigate whether the valproic acid and 5,7-dimethoxycoumarin have an antiproliferative activity against A2058 human melanoma cell line. Investigated compounds inhibited the proliferation of cells, however, no synergistic effect of their co-administration was observed.

Keywords: melanoma, A2058 human melanoma cells, valproic acid, 5,7-dimethoxycoumarin

Melanoma (*melanoma malignum*) is a malignancy originating from melanocytes, the cells synthetizing pigment called melanin. This cancer develops predominantly in the skin but also in mucous membrane or the uvea. Melanoma is a highly aggressive tumor of a dangerous high incidence and high metastatic potential. Its occurrence and mortality rates are constantly growing worldwide (1, 2). Malignant melanoma is responsible for 65% of skin malignancy-related deaths and long-term survival rate for patients with metastatic melanoma is only 5% (3).

Due to its significant unresponsiveness to conventional treatments, especially at advanced stages of disease, prophylaxis and early detection seems to be crucial in fight against melanoma. Recently, a several chemopreventive strategies for treatment of this tumor have been proposed (4–7). Cancer chemoprevention involve the use of natural or synthetic substances to reverse, suppress, or prevent the development of cancer. One of such strategies is to use therapeutic agent that is capable of inducing differentiation of tumor cells and their conversion to normal melanocytes (8, 9).

Valproic acid (VPA) (Fig. 1a), currently used as an anti-convulsant and anti-depressant, is one of the histone deacetylase inhibitors (HDACis). HDACis alter acetylation of chromatin influencing gene expression in such a way that tumor suppressive genes are activated, whereas oncogenes expression is suppressed (10–12). VPA, by inhibition of HDAC1 and HDAC2, elongates the G_1 phase of cell cycle and influences many cell growth and replication processes. As a result, it exhibits antiproliferative, proapoptopic and differentiation-stimulating properties (12–14). Moreover, it seems that VPA sensitizes certain cancers to the standard chemotherapeutic (15).

5,7-Dimethoxycoumarin (DMC) (Fig. 1b) is another compound with chemopreventive potential. This natural product, also called citropten, is found in the essential oils of lime, lemon and bergamot. DMC influences phosphorylation of Mek1/2/ERK1/2 proteins, which are components of mitogen activated protein kinase (MAPK) signalling pathway. Consequently, cell cycle is blocked in the G_0/G_1 phase, leading to tumor cells growth reduction and differentiation (16).

The aim of the study was to investigate the influence of VPA and DMC on proliferation of A2058 human melanoma cells. It was also examined whether these compounds have a synergistic antiproliferative activity against the investigated cells.

* Corresponding author: e-mail: dwolny@sum.edu.pl

EXPERIMENTAL

Cell cultures

Human malignant melanoma cell line A2058 were obtained from American Type Culture Collection. The cells were cultured in minimum essential medium (MEM, Sigma-Aldrich) supplemented with 10% fetal bovine serum (FBS, Sigma-Aldrich), 100 IU/mL penicillin G, 100 µg/mL streptomycin and 10 mM HEPES (Gibco). The cell were cultured at standard condition (37°C, humidified atmosphere of 95% air and 5% CO_2).

Proliferation assays

The XTT (*In Vitro* Toxicology Assay Kit, XTT Based, TOX-2, Sigma-Aldrich) and sulforhodamine B (*In Vitro* Toxicology Assay Kit, Sulforhodamine B Based, TOX-6, Sigma-Aldrich) assays were used to assess cell proliferation in the presence of tested compounds.

Tetrazolium ring of XTT (2,3-bis[2-methoxy-4-nitro-5-sulfophenyl]-2H-tetrazolium-5-carboxyanilide inner salt) is cleaved by mitochondrial dehydrogenases of viable cells and soluble in water formazan crystals are formed. Cell were seeded in 96-well plates at initial density of 8×10^3 per well and cultured in MEM for 24 h. Next medium was exchanged for medium containing VPA (concentration range: 0.1–10 mM), DMC (10–500 mM) and mixture of 1 mM VPA and 10, 50, 100 and 150 mM DMC. After 72 h of incubation cells were washed three times with RPMI (without phenol red dye) then 100 µL XTT solution was added into each well for 4 h. The absorbance was measured at 450 nm (reference 690 nm) using a MRX Revelation plate reader (Dynex) and was directly proportional to amount of the living cells.

Sulforhodamine B is a dye capable of binding to basic amino acid residues of cell proteins. A2058 cell were cultured in 96-well plates (initial density of 10^3 per well) for 24 h. Subsequently, cells were treated with VPA, DMC and their mixture at the same concentration as in XTT assay. Following 72 h of incubation, cells were washed with PBS (Sigma-Aldrich), fixed with 10% trichloroacetic acid (Sigma-Aldrich) and incubated with sulforhodamine B for 30 min. Next, unbound dye was washed off using 1% acetic acid (Sigma-Aldrich). Protein-bounded sulforhodamine B was quantitatively liberated with 10 mM Tris base solution and absorbance was measured at 565 nm (reference 690 nm).

Statistics

To evaluate the influence of VPA and DMC on the A2058 cells proliferation the arithmetic mean as a measure of the average and standard deviation as a measure of dispersion were used. Differences in cells proliferation were analyzed for statistical significance using analysis of variance (ANOVA) followed by Tukey test. Normality was verified by Shapiro-Wilk test, and homogeneity of variance by Brown-Forsythe test. The p-value of less than 0.05 was considered significant. Analysis was performed using Statistica 10.0 software (StatSoft).

RESULTS AND DISCUSSION

Melanoma is a cancer difficult to treat. The prognosis for patient at the late-stage of disease are very poor. Therefore, it is crucial to develop new therapies. Histone deacetylase inhibitors (HDACis) are very promising new antitumor agents. HDACis restore the equilibrium between the acetylation and deacetylation of histones, resulting in selective activation of the genes responsible for the inhibition of proliferation and the induction of tumor cells differentiation (17).

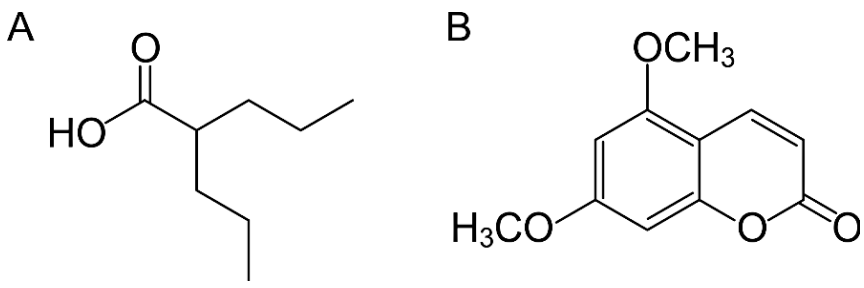

Figure 1. The chemical structure of valproic acid (A) and 5,7-dimethoxycoumarin (B)

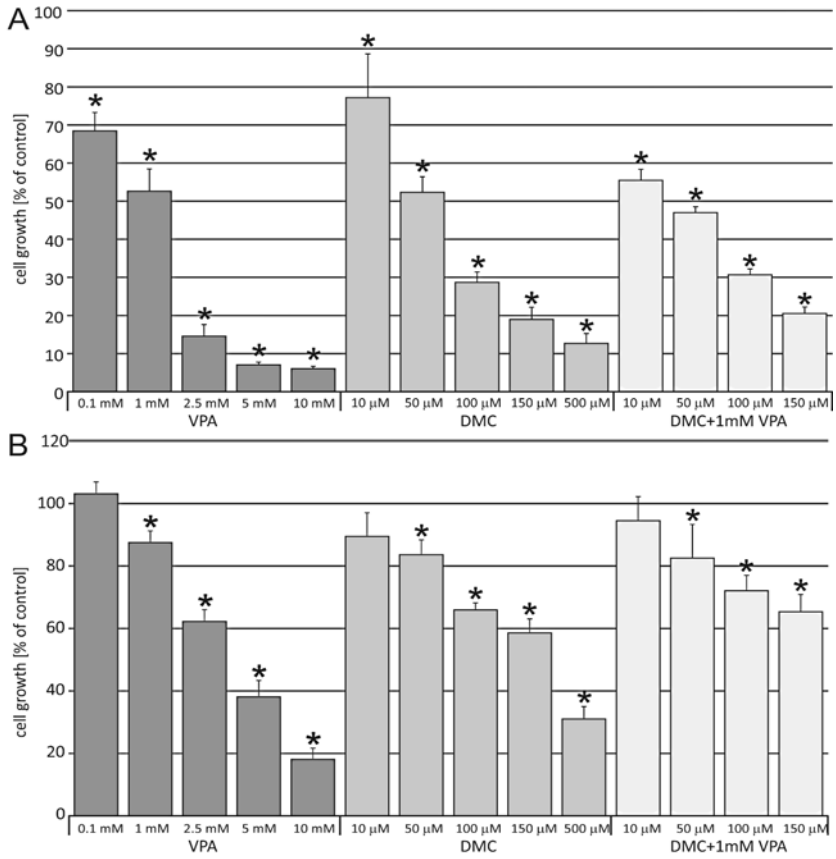

Figure 2. The effect of VPA and DMC on the proliferation of the human melanoma A2058 cell line evaluated by sulforhodamine B (**A**) and XTT assay (**B**). Each bar represents the mean ± SD; * $p < 0.05$ *versus* untreated cells

Cytotoxic effect of valproic acid, 5,7-dimethoxycoumarin and a combination of these two compounds on A2058 human melanoma cell line was investigated. The effect was measured using two colorimetric test after the cells had been treated for 72 h with various concentration of investigated compounds. Both XTT and sulforhodamine B based test revealed that VPA, DMC and their mixture inhibited the proliferation of A2058 cells in a concentration depended manner (Fig. 2). This findings are consistent with results of Chodurek et al. (18, 19) concerning the influence of VPA and DMC on A-375 and G-361 human melanoma cell lines. The statistically significant inhibition of cells proliferation was observed even at the lowest concentrations. After supplementation of investigated cells with VPA, DMC and their mixture, the growth of dendrites and formation of star-shape cells were observed. These morphological changes may be a result of melanoma cell differentiation to normal melanocytes.

There are evidences that VPA makes tumor cells more sensitive to standard chemotherapy. Hubaux et al. (20) investigated the effect of VPA on small cell lung carcinoma (SCLC) cells in combination with cisplatin and etoposide. The 1 mM VPA significantly increased apoptosis induced by 10 µM cisplatin or 10 µM etoposide. Valentini et al. (21) also observed similar effect on M14 melanoma cells when VPA was co-administrated with standard chemotherapeutics. They observed that 1 mM VPA combined with 2.5 µM cisplatin or 0.5 µM etoposide inhibited the proliferation of cells by 50% in comparison to cells treated by these compounds alone. Finding of Chodurek et al. (18, 19) revealed that valproic acid increased the apoptosis of G-361 and A-375 human melanoma cells caused by 5,7-dimethoxycoumarin. As observed in Figure 2, although VPA and DMC caused the inhibition of A2058 melanoma cell proliferation, their co-administration did not increase this effect.

CONCLUSION

The results of our study showed that valproic acid and 5,7-dimethoxycoumarin inhibited the proliferation of A2058 human melanoma cells. However, no synergistic effect of combined compounds have been observed.

Acknowledgment

This study was supported by SUM grant KNW-1-002/K/4/0.

REFERENCES

1. Markovic S.N., Erickson L.A., Rao R.D., Weenig R.H., Pockaj B.A., Bardia A., Vachon C. M. et al.: Mayo Clin. Proc. 82, 364 (2007).
2. Siegel R., Naishadham D., Jemal A.: CA Cancer J. Clin. 62, 10 (2012).
3. Cummins D.L., Cummins J.M., Pantle H., Silverman M.A., Leonard A.L., Chanmugam A.: Mayo Clin. Proc. 81, 500 (2006).
4. Sigalotti L., Covre A., Fratta E., Parisi G., Colizzi F., Rizzo A., Danielli R. et al.: J. Transl. Med. 8, 56 (2010).
5. Westekemper H., Freistuehler M., Bornfeld N., Steuhl K.P., Scheulen M., Hilger R.A.: Graefes Arch. Clin. Exp. Ophthalmol. 251, 279 (2013).
6. Julia F., Thomas L., Dalle S.: Dermatol. Ther. 25, 452 (2012).
7. Eggermont A.M., Robert C.: Eur. J. Cancer 47, 2150 (2011).
8. Alcazar O., Achberger S., Aldrich W., Hu Z., Negrotto S., Saunthararajah Y., Triozzi P.: Int. J. Cancer 131, 18 (2012).
9. Triozzi P.L., Aldrich W., Achberger S., Ponnazhagan S., Alcazar O., Saunthararajah Y.: Cancer Immunol. Immunother. 61, 1441 (2012).
10. Di Gennaro E., Bruzzese F., Pepe S., Leone A., Delrio P., Subbarayan P. R., Avallone A., Budillon A.: Cancer Biol. Ther. 8, 782 (2009).
11. Richon V.M., Sandhoff T.W., Rifkind R.A., Marks P.A.: Proc. Natl. Acad. Sci. USA 97, 10014 (2000).
12. Wagner J.M., Hackanson B., Lubbert M., Jung M.: Clin. Epigenetics 1, 117 (2010).
13. Batty N., Malouf G.G., Issa J.P. J.: Cancer Lett. 280, 192 (2009).
14. Bacon C.L., Gallagher H.C., Haughey J.C., Regan C.M.: J. Neurochem. 83, 12 (2002).
15. Hubaux R., Vandermeers F., Crisanti M.C., Kapoor V., Burny A., Mascaux C., Albelda S. M., Willems L.: Eur. J. Cancer 46, 3127 (2010).
16. Alesiani D., Cicconi R., Mattei M., Montesano C., Bei R., Canini A.: Int. J. Oncol. 32, 425 (2008).
17. Cunneen T.S., Conway R.M., Madigan M.C.: Arch. Ophthalmol. 127, 414 (2009).
18. Chodurek E., Dzierzega-Lecznar A., Kurkiewicz S., Stepien K.: J. Anal. Appl. Pyrolysis 104, 567 (2013).
19. Chodurek E., Orchel A., Orchel J., Kurkiewicz S., Gawlik N., Dzierzewicz Z., Stepien K.: Cell. Mol. Biol. Lett. 17, 616 (2012).
20. Hubaux R., Vandermeers F., Crisanti C., Kapoor V., Burny A., Mascaux C., Albelda S. M., Willems L.: Eur. J. Cancer 46, 1724 (2010).
21. Valentini A., Gravina P., Federici G., Bernardini S.: Cancer Biol. Ther. 6, 185 (2007).

Acta Poloniae Pharmaceutica – Drug Research, Vol. 71 No. 6 pp. 1060–1065, 2014 ISSN 0001-6837
Polish Pharmaceutical Society

POLYUNSATURATED FATTY ACIDS POTENTIATE CYTOTOXICITY OF CISPLATIN IN A549 CELLS

ALICJA ZAJDEL[1]*, ADAM WILCZOK[1], MAŁGORZATA LATOCHA[2], MICHAŁ TARKOWSKI[1], MIROSŁAWA KOKOCIŃSKA[1] and ZOFIA DZIERŻEWICZ[1]

[1] Medical University of Silesia, School of Pharmacy with the Division of Laboratory Medicine in Sosnowiec, Department of Biopharmacy, [2] Department of Cell Biology, Jedności 8, 41-200 Sosnowiec, Poland

Abstract: In normal and tumor cells, polyunsaturated fatty acids (PUFAs) act as intracellular second messengers, which play a role in signaling, proliferation and cell death. PUFAs have selective tumoricidal action and may alter sensitivity of tumor cells to cisplatin (CDDP), a commonly used anticancer agent. The aim of this study was to evaluate the influence of arachidonic acid (AA, 20:4 n-6), eicosapentaenoic acid (EPA, 20:5 n-3), docosahexaenoic acid (DHA, 22:6 n-3) and CDDP on autophagy and apoptosis in A549 human lung adenocarcinoma cells. Viability of A549 cells treated with CDDP and PUFAs was measured using the XTT tetrazolium salt based assay. Caspase-3/7 activity was estimated using ApoTox-Glo kit (Promega). Autophagic vacuoles were detected by Cyto-ID Autophagy Detection Kit (Enzo). The results were compared to control cultures maintained in the absence of CDDP and PUFAs. PUFAs, in particular EPA and DHA, added to the cultivation medium, increased the antitumor activity of CDDP in A549 cells in a concentration dependent manner. In case of AA this effect was observed at the highest of the concentrations tested only (100 μM). Both, EPA and DHA, but not AA, significantly increased the amount of autophagic vacuoles and induced caspase-3/7 activity. The obtained results suggest that the antiproliferative effect of CDDP in A549 cells can be enhanced by AA and in particular by EPA and DHA through their influence on autophagic and apoptotic cell death. It is likely that EPA and DHA incorporated to the tumor cells may improve outcomes in lung cancer patients.

Keywords: polyunsaturated fatty acids, cisplatin, autophagy, apoptosis

Cisplatin [cis-diamminedichloroplatinum (II); CDDP] is one of the most potent and widely used anticancer drugs for the treatment of lung cancer. However, the treatment with CDDP and its analogs is often limited by their side-effects including nephrotoxicity, neurologic damage, and ototoxicity. Furthermore, both primary and acquired resistance to platinum-based drugs limits their application (1–3). Administration of larger doses of CDDP to overcome the resistance may lead to severe organ toxicities.

It has been reported that acquired CDDP resistance in human lung adenocarcinoma cells is associated with enhanced autophagy (4). Macroautophagy (hereafter referred to as autophagy) is an evolutionarily conserved catabolic process by which cells destruct their cytoplasmic content and organelles through the lysosomal machinery. Autophagy is initiated by the formation of the double-membrane bound short lived vacuoles (autophagosomes), which sequester cytosolic proteins and organelles such as mitochondria and endoplasmic reticulum. Autophagosomes fuse with acidic lysosomes to produce autolysosomes where the sequestered content is degraded by lysosomal enzymes, and amino acids and sugars are recycled into the cytosol for reuse (5). Emerging evidence shows that autophagy is important in the regulation of cancer development and progression. However, the role of autophagy is complicated and autophagy may cause divergent effects in cells. Autophagy may protect tumor cells from nutrient deficiency and hypoxia; but on the other hand, autophagy defects are associated with development of cancer (6, 7). The fact that autophagy can have both suppressive and promoting roles in carcinogenesis, makes it an attractive target in cancer research. As a tumor suppressing mechanism, autophagy serves as an alternative to apoptosis to eliminate transformed cells. Nevertheless, autophagy may facili-

* Corresponding author: e-mail: azajdel@sum.edu.pl; phone: +48 32 364 12 48

tate tumor cells resistance to certain anticancer drugs (6, 7).

It is well documented that polyunsaturated fatty acids (PUFAs) found in fish oil, in particular eicosapentaenoic acid (EPA, 20 : 5, n-3) and docosahexaenoic acid (DHA, 22 : 6, n-3), exert selective cytotoxicity against various types of cancer cells. Moreover, PUFAs can enhance their sensitivity to anticancer therapy and reverse the resistance (8, 9). This led us to investigate the effect of arachidonic acid (AA, 20 : 4, n-6), EPA, and DHA on autophagy and apoptosis in A549 human lung adenocarcinoma cells treated with CDDP.

EXPERIMENTAL

Cell culture

A549 human lung adenocarcinoma cells were obtained from the American Type Culture Collection (ATCC) and cultured (25000 cells/cm^2) in Modified Eagle's Medium (MEM) supplemented with 10% heat inactivated fetal bovine serum (FBS;PAA The Cell Culture Company), 10 mM buffer HEPES (Sigma), 100 U/mL penicillin and 100 μg/mL streptomycin (Sigma). Cells were maintained at 37^{o}C in a humidified atmosphere of 95 % air and 5 % CO_2.

Cell exposure to CDDP and PUFAs

CDDP, AA, EPA, and DHA were purchased from Sigma. The fatty acids were dissolved in 99% ethanol and stored as stock solutions (100 mM) under nitrogen at –20^{o}C. To achieve experimental conditions, PUFAs and CDDP were prepared freshly from stock solutions and diluted with the appropriate volumes of the growth medium. Twenty-four hours after cell seeding (96-well plates; 1×10^4 cells/well), the medium was replaced with the media supplemented with CDDP (5 μg/mL) and AA, EPA or DHA (25, 50, 100 μM). The CDDP concentration was chosen on the basis of the viability tests results obtained in our laboratory prior to the experiment. Control cells were cultured in the medium containing the same concentration of ethanol (v/v, 0.1%) as the experimental cultures for another 24 h. Previous observations showed, that ethanol at this concentration had not been toxic to the cells.

Viability assay

Survival of cells exposed to CDDP (5 μg/mL) or PUFAs (25, 50, 100 μM) and CDDP (5 μg/mL) together was assessed by the XTT method (In Vitro Toxicology Assay Kit XTT Based, TOX-2, Sigma) with a commercial kit according to the manufacturer's instruction. The method based on the ability of mitochondrial dehydrogenases of viable cells to cleave the tetrazolium ring of XTT (2,3-bis[2-methoxy-4-nitro-5-sulfophenyl]-2H-tetrazolium-5-carboxyanilide inner salt), yielding orange formazan crystals, which are soluble in aqueous solutions. Absorbance of formazan was measured at 450 nm with the plate reader (Triad LT Multimode Detector, Dynex Technologies). Cell viability was expressed as a percentage of absorbance measured in the treated wells relative to that in the untreated control wells.

ApoTox-Glo Triplex assay

The ApoTox-Glo Triplex Assay (Promega) was used to measure A549 cells viability, cytotoxicity and apoptosis in the same sample following manufacturer's protocols. Briefly, viability and cytotoxicity are measured by fluorescent signals produced when either live-cell or dead-cell proteases cleave added substrates GF-AFC (viability) and bis-AAF-R110 (cytotoxicity). GF-AFC can enter cells and is therefore cleavable by live-cell protease only, which incidentally becomes inactive when cell membrane activity is lost; bis-AAF-R110 cannot enter the cell, and is cleaved only by dead-cell protease leaked from cells lacking membrane integrity. Both cleaved substrates have different excitation and emission spectra. Apoptosis is measured by the addition of a luminogenic caspase-3/7 substrate (Caspase-Glo 3/7) which is cleaved in apoptotic cells to produce a luminescent signal. Fluorescence at 365 Ex/500 Em (viability), 485 Ex/535 Em (cytotoxicity) and luminescence (apoptosis) were measured with a plate reader (Triad LT Multimode Detector, Dynex Technologies).

Cyto-ID autophagy detection assay

Cyto-ID kit (Enzo) was used according to the manufacturer's protocol for fluorescence microplate reader. Cyto-ID Autophagy Detection Kit measures autophagic vacuoles and monitors autophagic flux in live cells using a novel dye that selectively labels autophagic vacuoles. The dye has been optimized through the identification of titratable functional moieties that allow for minimal staining of lysosomes while exhibiting bright fluorescence upon incorporation into pre-autophagosomes, autophagosomes, and autolysosomes (autophagolysosomes). The assay offers a rapid and quantitative approach to monitoring autophagy in live cells without the need for cell transfection. Rapamycin and tamoxifen, typical inducers of autophagy, were used as a positive control and 3-methyladenine (3-MA) as inhibitor of autophagy (negative control).

Fluorescence was measured at 365 Ex/465 Em (Hoechst 33342 nuclear stain) and 485 Ex/535 Em (Cyto-ID green autophagy detection reagent) with a plate reader (Triad LT Multimode Detector, Dynex Technologies).

Statistical analysis

The data obtained from 4 independent series of experiments were expressed as the mean values ± standard deviations. Statistical comparisons were made by analysis of variance (ANOVA), followed

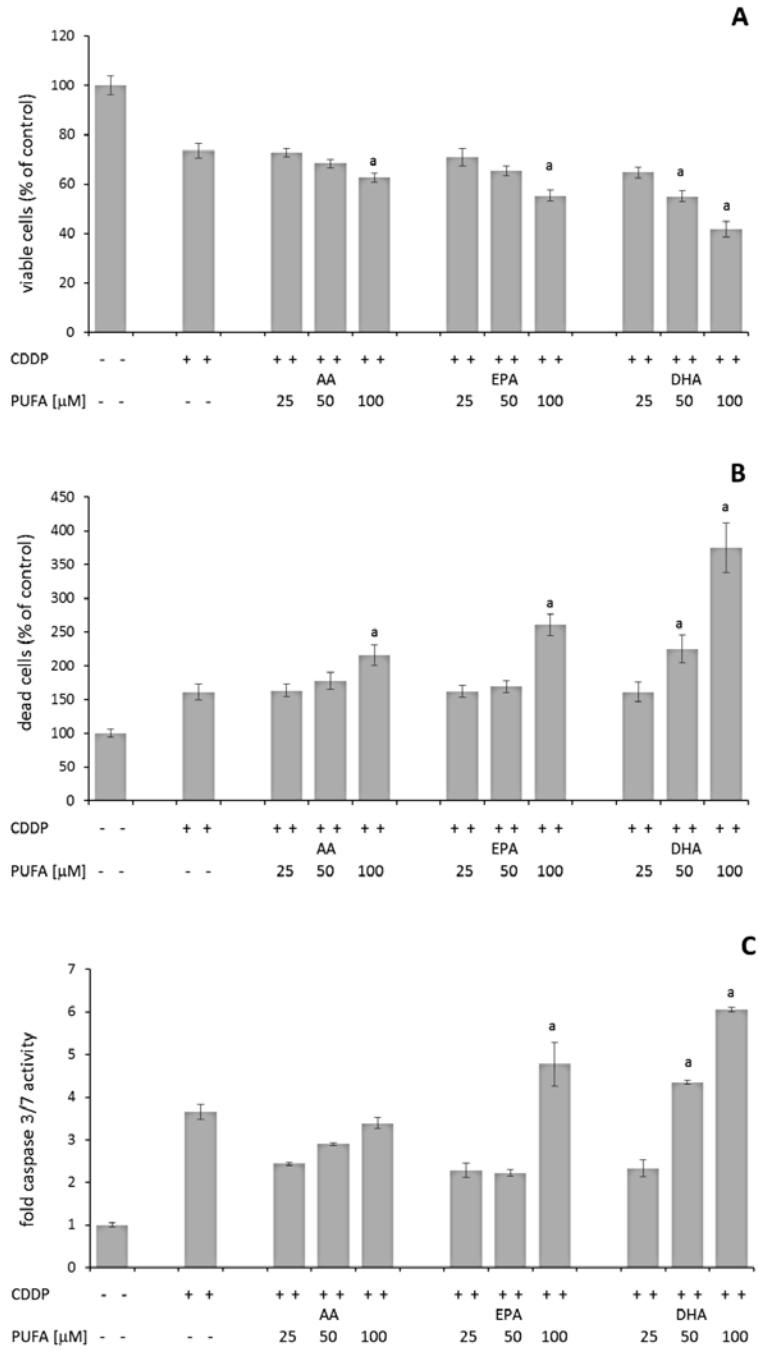

Figure 1. Concentration-dependent (25–100 μM) effect of arachidonic acid (AA), eicosapentaenoic acid (EPA) or docosahexaenoic acid (DHA) on cisplatin (CDDP, 5 μg/mL) cytotoxicity in A549 cells. The viability (**A**), cytotoxicity (**B**) and apoptosis (**C**) of A549 cells exposed to cisplatin (CDDP) in the absence or presence PUFAs were detected by the ApoTox-Glo Triplex Assay. Data were calculated as the means ± SD from four independent experiments. [a] statistically significant differences ($p < 0.05$) *vs*. CDDP

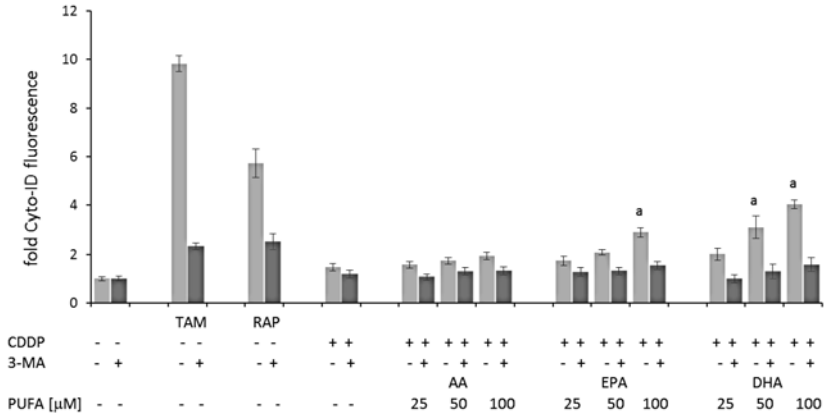

Figure 2. Cyto-ID fluorescence in A549 cells exposed to cisplatin (CDDP, 5 μg/mL) in the absence or presence of arachidonic acid (AA), eicosapentaenoic acid (EPA), and docosahexaenoic acid (DHA) at various concentrations (25–100 μM) detected by the Cyto-ID autophagy detection assay. Rapamycin and tamoxifen, the typical inducers of autophagy, were used as a positive control and 3-methyladenine (3-MA; 5 mM) as inhibitor of autophagy (negative control). Data were calculated as the means ± SD from four independent experiments. [a] statistically significant differences ($p < 0.05$) *vs.* CDDP

by Tukey's HSD test. The p-value of less than 0.05 was considered significant. Statistical analysis was performed using Statistica 10 PL software for Windows (StatSoft, Poland).

RESULTS AND DISCUSSION

Cisplatin treatment is known to promote tumor cell resistance to apoptosis induction *via* multiple mechanisms involving gene expression, modulation of oncogenes, tumor suppressors and blockade of pro-apoptotic mitochondrial membrane permeabilization. Many cancers have disrupted intrinsic (mitochondrial dependent) and extrinsic (death receptor mediated) apoptosis signaling pathways. The consequential insufficient activation of caspases is thought to contribute to resistance to chemotherapy. Many papers have presented data suggesting that tumor cell autophagy induced by anticancer treatment inhibits tumor cell killing. However, it has also been proposed that autophagy is a cell death mechanism that could function as a backup when apoptosis is disabled. The form of cell death initiated by autophagy (autophagic cell death) is caspase independent. Moreover, an increasing number of studies have demonstrated that apoptosis and autophagy share some common signaling pathways and are mutually regulated (10, 11).

There is increasing interest in the new therapeutic approaches based on the knowledge of structure, function, and alteration of membrane lipids (12). Supplementation of tumors with long-chained ω-3 PUFAs results in enrichment of tumor phospholipid fractions with these PUFAs. As components of membrane phospholipids, PUFAs cause changes of membrane fluidity and membrane structure, which may influence receptor-ligand interactions, signal transduction properties and various membrane mediated cellular functions (13). Such cells have membranes with increased fluidity, an elevated unsaturation index, enhanced transport capabilities that result in accumulation of selective anticancer agents and alteration of signaling pathways important for cancer progression. (10).

Several *in vivo* and *in vitro* studies have reported the increased efficacy of CDDP against human tumors after DHA supplementation. It has been shown that both, EPA and DHA downregulated SOD1, SOD2, GPx-4 and GST-π genes expression in CDDP treated A549 cells, which may explain the increased efficacy of this drug against these cells (14). Moreover, incubation of CDDP-sensitive (GLC-4) and resistant (GLC-4-CP) small cell lung carcinoma cells with non-toxic levels of DHA resulted in an increased accumulation of DHA in the tumor membranes and a three-fold decrease in the resistance of GLC-4-CP cells toward CDDP, but had no influence on the cytotoxicity of CDDP toward the susceptible GLC-4 cells. DHA enhanced the sensitivity of drug resistant tumor cells to CDDP by increasing the intracellular platinum levels, total platinum bound to DNA and inter- strand cross-link-

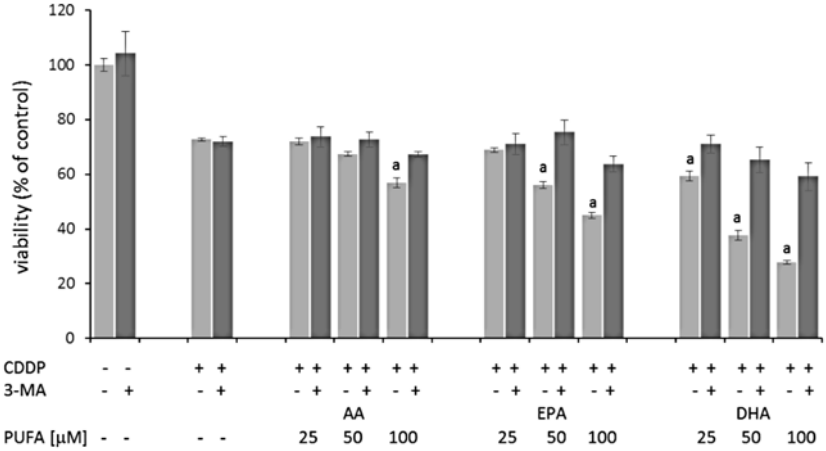

Figure 3. Viability (% of control) of A549 cells exposed to cisplatin (CDDP, 5 μg/mL) in the absence or presence of arachidonic acid (AA), eicosapentaenoic acid (EPA), and docosahexaenoic acid (DHA) at various concentrations (25–100 μM) and the effect of 3-methyladenine (3-MA; 5 mM) on CDDP and PUFAs toxicity measured by XTT. Data were calculated as the means ± SD from four independent experiments. [a] statistically significant differences ($p < 0.05$) *vs*. CDDP

ing in the both cell lines (15). Similarly, the CDDP resistant ovarian cell line 2780- CP was sensitized to CDDP by pre-incubation with EPA, whereas, the parent ovarian line 2780 was not (16). Elmesary et al. evaluated the antitumor effects of DHA, alone or in combination with CDDP, in the EAC solid tumor mice model (17). The study found that DHA reduced the size of tumors, enhanced the positive effects of the CDDP chemotherapy, and limited its harmful side effects. In addition, DHA eradicated lethal CDDP-induced nephrotoxicity and renal tissue injury. In agreement with the *in vitro* and *in vivo* studies on human cancer cells, the presented results demonstrated that AA (100 μM), EPA (100 mM) and DHA (50, 100 μM), caused a significant decrease in cell viability and a significant increase in cytotoxicity of CDDP (5 μg/mL) in A549 cells (Figs. 1A, 1B). Several studies have documented that DHA simultaneously induced both autophagy and apoptosis in cancer cells by activating intrinsic and extrinsic apoptotic pathways (18, 19). Exposure of A549 cells to CDDP in the presence of EPA (100 μM) or DHA (50, 100 μM) significantly increased caspase activity and apoptosis (Fig. 1C).

To examine the possibility that PUFAs and CDDP induce autophagy in A549 cells, autophagy was monitored in live cells by measuring the fluorescence intensity using a novel dye (Cyto-ID) that exhibits bright green fluorescence when selectively labeling autophagic vacuoles including pre-autophagosomes, autophagosomes and autophagolysosomes. Recently, this assay has been recognized to be a rapid and quantitative approach to monitor autophagy in live cells (20). Figure 2 shows the Cyto-ID fluorescence in A549 cells exposed to CDDP in the presence or absence of PUFAs. 3-MA, as an inhibitor of autophagy, blocks the formation of autophagosomes, by controlling class I and class III phosphatidylinositol 3-kinases (PI3K) (21, 22). As expected, it caused a reduction in the cytoplasm vacuolization and therefore a decrease of Cyto-ID fluorescence intensity. As shown in Figure 2, the treatment of A549 cells with CDDP did not induce autophagy. These results are in agreement with some previous observations in A549 cells, indicating that 3-MA enhanced growth inhibition and apoptotic effect of CDDP in cells with acquired resistance (A549/DDP) and did not alter its cytotoxic effect to the parent A549 cell line (4, 23). After CDDP treatment in the presence of EPA (100 μM) or DHA (50, 100 μM) the Cyto-ID fluorescence intensity significantly increased (Fig. 2), what suggests that autophagic vacuolization in response to PUFAs treatment occurred. The effect was reverted when the autophagy inhibitor was applied (Fig. 2). Statistically significant differences were observed between CDDP and EPA or DHA treated cells and CDDP and EPA or DHA plus 3-MA treated cells ($p < 0.01$), confirming the reduction of autophagy (Fig. 2). Moreover, the inhibition of the autophagic process induced an increase in cell viability, what confirms the occurrence of cell death by autophagy (Fig. 3). 3-MA did not alter the viability of A549 cells. These results indicate that CDDP toxicity, at

least in part, is increased by EPA or DHA-induced autophagy. It is likely that EPA and DHA incorporated to the tumor cells may improve outcomes in lung cancer patients.

Acknowledgment

This work was supported by SUM grant KNW-1-002/M/4/0.

REFERENCES

1. Siddik Z.H.: Oncogene 22, 7265 (2003).
2. Wang D., Lippard S.J.: Nat. Rev. Drug Discov. 4, 307 (2005).
3. Ohmichi M., Hayakawa J., Tasaka K., Kurachi H., Murata Y.: Trends Pharmacol. Sci. 26, 113 (2005).
4. Ren J.H., He W.S., Nong L., Zhu Q.Y., Hu K., Zhang R.G., Huang L.L. et al.: Cancer Biother. Radiopharm. 25, 75 (2010).
5. Mizushima N., Levine B., Cuervo A.M., Klionsky D.J.: Nature 451, 1069 (2008).
6. Chen N., Karantza-Wadsworth V.: Biochim. Biophys. Acta 1793, 1516 (2009).
7. Yang Z.J. , Chee C.E., Huang S., Huang S., Sinicrope F.A.: Mol. Cancer Ther. 10, 1533 (2011).
8. Berquin I.M., Edwards I.J., Chen Y.Q.: Cancer Lett. 269, 363 (2008).
9. Siddiqui R.A., Harvey K., Stillwell W.: Chem. Phys. Lipids 153, 47 (2008).
10. Kozubík A., Vaculová A., Soucek K., Vondrácek J., Turánek J., Hofmanová J.: Met. Based Drugs 2008, 417897 (2008).
11. Shao Y., Gao Z., Marks P.A., Jiang X.: Proc. Natl. Acad. Sci. USA 101, 18030 (2004)
12. Escribá P.V.: Trends Mol. Med. 12, 34 (2006).
13. Los D. A., Murata N.: Biochim. Biophys. Acta 1666, 142 (2004).
14. Zajdel A., Wilczok A., Gruchlik A., Paduszyński P., Dzierżewicz Z.: Adv. Clin. Exp. Med. 19, 585 (2010).
15. Timmer-Bosscha H., Hospers G.A., Meijer C., Mulder N.H., Muskiet F.A., Martini I.A., Uges D.R., de Vries E.G.: J. Natl. Cancer Inst. 81, 1069 (1989).
16. Plumb J.A., Luo W., Kerr D.J.: Br. J. Cancer 67, 728 (1993).
17. El-Mesery M., Al-Gayyar M., Salem H., Darweish M., El-Mowafy A.: Cell Div. 4, 6 (2009).
18. Shin S., Jing K., Jeong S., Kim N., Song K.S., Heo J.Y., Park J.H. et al.: Biomed. Res. Int. 568671, (2013).
19. Serini S., Piccioni E., Merendino N., Calviello G.: Apoptosis 14, 135 (2009).
20. Lee J.S., Lee G.M.: Methods 56, 375 (2012).
21. Klionsky D.J., Abeliovich H., Agostinis P., Agrawal D.K., Aliev G., Askew D.S., Baba M. et al.: Autophagy 4, 151 (2008).
22. Chen Y., Azad M.B., Gibson S.B.: Can. J. Physiol. Pharmacol. 88, 285 (2010).
23. Liu F., Liu D., Yang Y., Zhao S.: Oncol. Lett. 5, 1261 (2013).

Acta Poloniae Pharmaceutica – Drug Research, Vol. 71 No. 6 pp. 1066–1072, 2014 ISSN 0001-6837
Polish Pharmaceutical Society

EPR STUDIES OF FREE RADICALS IN A-2058 HUMAN MELANOMA CELLS TREATED BY VALPROIC ACID AND 5,7-DIMETHOXYCOUMARIN

MAGDALENA ZDYBEL[1*], EWA CHODUREK[2] and BARBARA PILAWA[1]

Medical University of Silesia in Katowice, School of Pharmacy with the Division of Laboratory Medicine, [1]Department of Biophysics, [2]Department of Biopharmacy, Jedności 8, 41-200 Sosnowiec

Abstract: Free radicals in A-2058 human melanoma cells were studied by the use of electron paramagnetic resonance (EPR) spectroscopy. The aim of this work was to determine the changes in relative free radical concentrations in tumor A-2058 cells after treatment by valproic acid (VPA) and 5,7-dimethoxycoumarin (DMC). The influences of VPA and DMC on free radicals in A-2058 cells were compared with those for human *melanoma malignum* A-375 and G-361 cells, which were tested by us earlier. Human malignant melanoma A-2058 cells were exposed to interactions with VPA, DMC, and both VPA and DMC. The tumor cells A-2058 were purchased from LGC Standards (Lomianki, Poland), and they were grown in the standard conditions: at 37°C and in an atmosphere containing 95% air and 5% CO_2, in the Minimum Essential Medium Eagle (MEM, Sigma-Aldrich). The A-2058 cells were incubated with VPA (1 mM) and DMC (10 μM) for 4 days. The first-derivative EPR spectra of the control A-2058 cells, and the cells treated with VPA, DMC, and both VPA and DMC, were measured by the electron paramagnetic resonance spectrometer of Radiopan (Poznań, Poland) with microwaves from an X-band (9.3 GHz). The parameters of the EPR lines: amplitudes (A), integral intensities (I), line widths (ΔB_{pp}), and g-factors, were analyzed. The changes of amplitudes and line widths with microwave power increasing from 2.2 to 70 mW were drawn evaluated. o-Semiquinone free radicals of melanin biopolymer are mainly responsible for the EPR lines of A-2058 *melanoma malignum* cells. The amounts of free radicals in A-2058 cells treated with VPA, and both VPA and DMC, were lower than in the untreated control cells. Application of the tested substances (VPA, and both VPA and DMC) as the antitumor compounds was discussed. DMC without VPA did not decrease free radicals concentration in A-2058 cells. The studies confirmed that EPR spectroscopy may be used to examine interactions of free radicals with antitumor compounds.

Keywords: valproic acid, 5,7-dimethoxycoumarin, A-2058 human melanoma cells, free radicals, EPR spectroscopy

The pharmacologically active compounds may produce and interact with free radicals in cells (1–7). Free radicals are formed in tumor cells during pathological process (8–11). The modern antitumor compounds should decrease the amount of free radicals in cells to stop the toxic biochemical reactions during cancer transformation. Our earlier studies concentrate on changes in free radicals in melanin biopolymer isolated from A-375 and G-361 human *melanoma malignum* cells (12) after application of valproic acid (VPA), 5,7-dimethoxycoumarin (DMC), and free radicals in melanin isolated from A-375 cells exposed on valproic acid (VPA) and cisplatin (CPT) (13). Melanins are strongly paramagnetic and they contain the high amounts of o-semiquinone free radicals (12–21), so their free radicals are mainly responsible for polymer-drug interactions. The strong decrease of free radicals concentrations in melanin from A-375 and G-361 cells after treatment with both VPA and DMC was observed (12). Such effect was not obtained after A-375 cells treated with both VPA and CPT (13). Valproic acid, 5,7-dimethoxycoumarin and cisplatin were recommended as the antitumor compounds (12, 13). Their effect on free radicals in the whole tumor cells was not tested.

The aim of this work was to determine the changes in relative free radical concentrations in A-2058 human *melanoma malignum* cells after interactions with valproic acid (VPA) and 5,7-dimethoxycoumarin (DMC). The influences of VPA, DMC, and both VPA and DMC on free radicals in A-2058 cells were compared. The results were discussed relative to our earlier conclusions

* Corresponding author: e-mail: mzdybel@sum.edu.pl

(12, 13) about the effectiveness of VPA and DMC as the antitumor compounds. Free radicals in melanin from tumor A-2058 cells were detected by the use of electron paramagnetic resonance (EPR) spectroscopy (12, 13). The same method of free radical examination in cells was used by now. EPR spectroscopy is the useful method in examination of drugs (22, 23) and the melanin complexes with drugs (18, 20, 21, 24, 25).

EXPERIMENTAL

Tumor cells

The human malignant melanoma cell line A-2058 was purchased from LGC Standards (Łomianki, Poland). The cell line was grown in the medium containing the following composition: 90% Minimum Essential Medium Eagle (MEM, Sigma-Aldrich), 10% fetal bovine serum (FBS, PAA), 100 U/mL penicillin, 100 μg/mL streptomycin (Sigma-Aldrich) and 10 mM HEPES (Sigma-Aldrich). The cells were cultivated in standard conditions (at 37°C, in a humidified atmosphere containing 5% CO_2).

Tested compounds

Synthetic valproic acid (VPA) and 5,7-dimethoxycoumarin (DMC) were purchased from Sigma-Aldrich.

Cells A-2058 were incubated with test compounds (1 mM VPA, 10 mM DMC or their combination) for 4 days.

EPR measurements

Free radicals in A-2058 tumor cells were examined by the use of an X-band (9.3 GHz) electron paramagnetic resonance (EPR) spectrometer with magnetic modulation of 100 kHz produced by Radiopan (Poznań, Poland). The EPR spectra were measured for the cell samples located in thin walled glass tubes with the external diameter of 1 mm. The empty tubes were free of paramagnetic impurities, and they did not reveal EPR signals. The EPR spectra as the first derivative of absorption curves were recorded by the Rapid Scan Unit from Jagmar (Kraków, Poland). The numerical acquisition (100) of EPR spectra for each sample was done. The total microwave power (M_o) produced by klystron of the EPR spectrometer was 70 mW. The microwave power was changed by different attenuation in the range from 2.2 to 70 mW. Additionally, the influence of microwave power on the parameters of the EPR spectra was drawn.

Spectroscopic programs of Jagmar (Kraków, Poland) and LabVIEW 8.5 by National Instruments were used to measure and to analyze the EPR spectra. g-Factors, line widths (ΔB_{pp}), amplitudes (A), and integral intensities (I) of the examined EPR spectra were obtained. g-Factors were calculated according to the formula (26, 27):

$$g = h\nu/\mu_B B_r$$

where: h – Planck constant, ν – microwave frequency, μ_B – Bohr magneton, B_r – induction of resonance magnetic field. Microwave frequency (ν) was directly measured by MCM101 recorder of EPRAD (Poznań, Poland). The induction of resonance magnetic field (B_r) was determined from the EPR line. ΔB_{pp} depend on magnetic interactions in the samples (1, 26).

Amplitudes (A) and integral intensities (I) increase with increasing amount of free radicals in the sample (26). Free radical concentration is proportional to integral intensity of the EPR line, which is defined as the area under the absorption curve (26). Integral intensities were calculated by double integration of the first derivative EPR spectra. To compare the relative concentrations of free radicals in the tested samples, the values of integral intensities were divided by the volume of the cells in the glass tube, and the integral intensities were done in the arbitrary units. Integral intensities reflect the concentrations in the cells. The integral intensities of the analyzed samples were compared with those for the free radical reference. Ultramarine was the reference which was used. The second reference permanently placed in a resonance cavity – a ruby crystal (Al_2O_3: Cr^3) was used to rise the accuracy of the measurements.

The effect of microwave power (2.2–70 mW) on amplitudes (A) and line widths of the EPR spectra of the cell samples was examined. Type of broadening (homogeneous or inhomogeneous) of EPR lines was determined from the correlations between microwave powers and both amplitudes (A) and line widths. The spin-lattice relaxation processes were evaluated from the changes of amplitudes (A) with microwave power. The faster spin-relaxation processes give EPR lines, which saturate at the higher microwave powers (26).

RESULTS

In the present study, we have assessed the morphology of human malignant melanoma cells A-2058 incubated in the presence of 1 mM VPA, 10 μM DMC or their combination. In the control culture (Fig. 1a) large aggregates of spindle-shaped cells were visible, which were readily adhere to the surface of the culture vessel. At low concentrations

of VPA (0.1 and 0.3 mM) there was no difference in the appearance of cells in comparison to the control. In contrast, in cultures exposed to 1 mM VPA (Fig. 1b), the number of cells was decreased. The cells were most often found separate from one another and their shape was irregular. Part of the cells was taken a round shape, which indicates their poor adhesion to the surface of the culture vessel. A similar effect was observed in cultures exposed to 10 μM DMC (Fig. 1c) and mixture of 1 mM VPA and 10 μM DMC (Fig. 1d).

For all the tested A-2058 tumor cells: the control cells and the cells treated with valproic acid and 5,7-dimethoxycoumarin, EPR spectra were obtained (Fig. 2). The spectra without microwave saturation effect were observed. In Figure 2, the EPR spectra measured with microwave power of 62 mW are compared.

Free radicals exist in all the tested cell samples, but their amounts and their EPR parameters differed for the cells treated with the individual compounds.

g-Factors characteristic for o-semiquinone free radicals were obtained for the examined A-2058 human *melanoma malignum* cells (Table 1). The broad EPR spectra with line widths in the range: 1.86-1.91 mT were measured (Table 1). Integral intensities indicated that VPA, and VPA together with DMC decrease free radical concentrations in the cells. The lower values of integral intensities, so the lower free radical concentrations, revealed A-2058 cells treated with VPA, and VPA and DMC together (Table 1). The lowest integral intensities were measured for the tested cells treated with both VPA and DMC. Integral intensity of the EPR spectrum of A-2058 cells interacting with VPA is lower than integral intensity of the spectrum for these cells treated with DMC. Integral intensity of the EPR spectrum of A-2058 cells interacting only with DMC revealed similar integral intensity as the control A-2058 cells (Table 1), so DMC did not quenched free radicals in the tested tumor cells.

The spectral amplitudes and line widths depend on microwave power. The changes of the parameters of the EPR spectra of A-2058 cells are shown in Figures 3 and 4. The influence of microwave power (M/M_o) on linewidths of EPR spectra of the control A-2058, and the cells treated with VPA, DMC, and both VPA and DMC, shows the broadening of all the spectra with an increase of microwave power (Fig. 3). This correlation indicates homogeneous broadening of EPR lines of the examined tumor cells.

Amplitudes (A) of EPR lines of all the studied A-2058 human malignant melanoma cells increase with increasing microwave power, and these lines are not saturated (Fig. 4). Only for A-2058 cells treated with both VPA and DMC at the beginning of

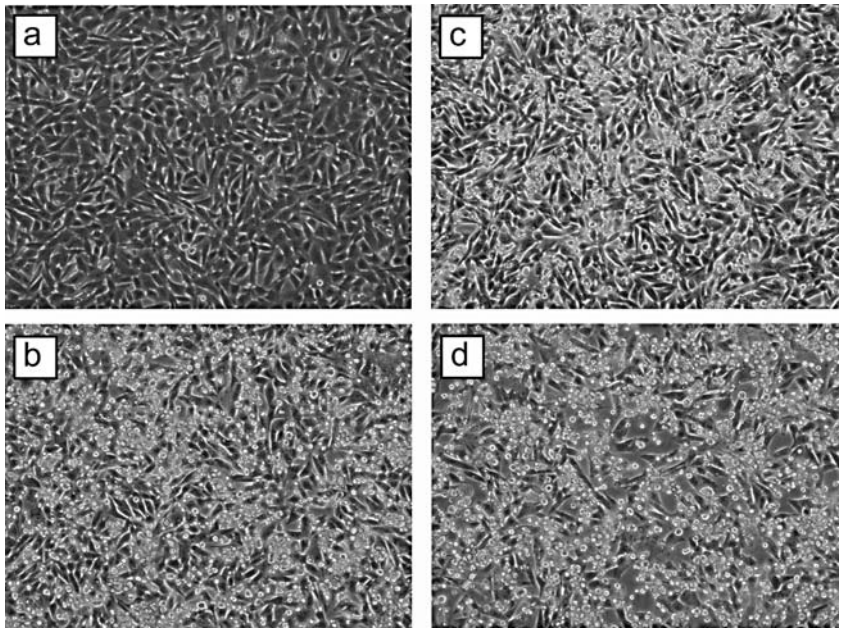

Figure 1. Morphology of malignant melanoma A-2058 cells: control (a), cells treated with 1 mM VPA (b), cells treated with 10 mM DMC (c), cells treated with 1 mM VPA and 10 mM DMC (d)

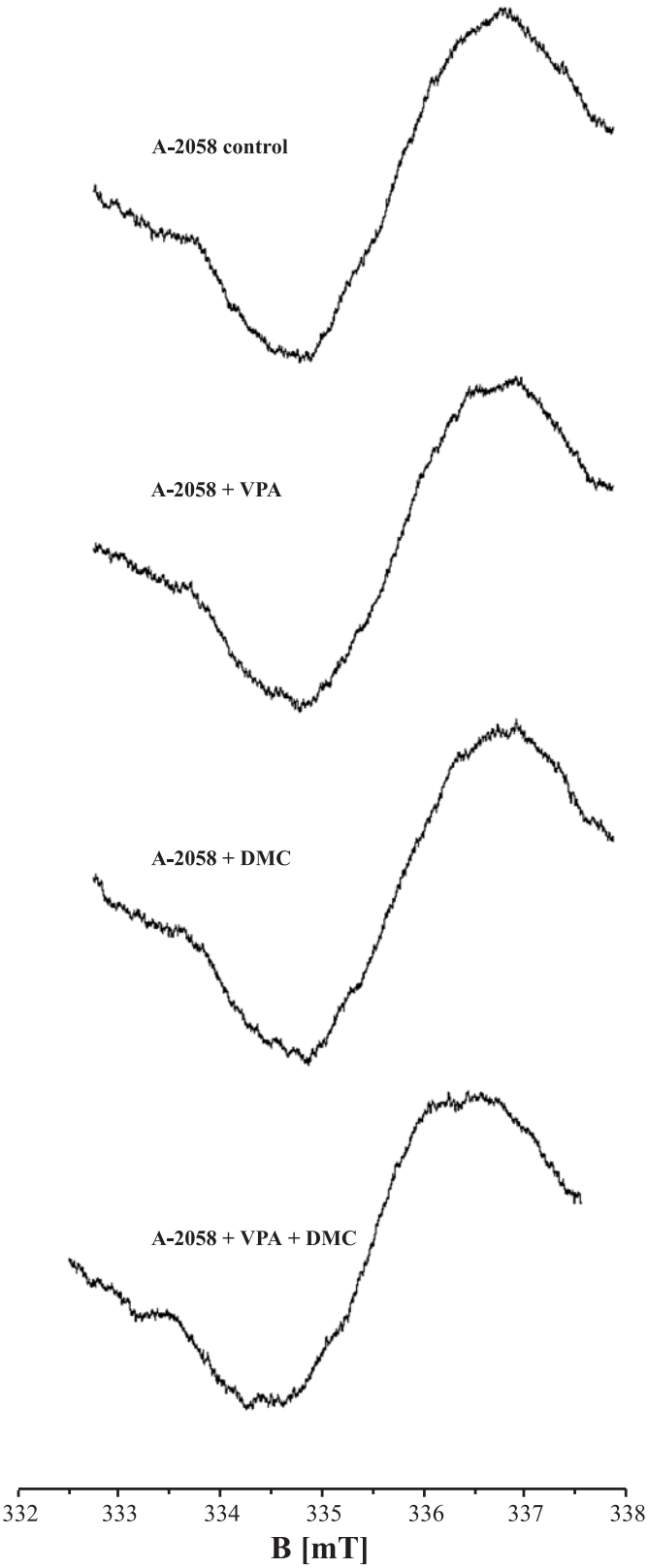

Figure 2. EPR spectra of control A-2058 human *melanoma malignum* cells, and the cells treated with VPA, DMC, and both VPA and DMC. The spectra were measured with microwave power of 62 mW. B – magnetic induction

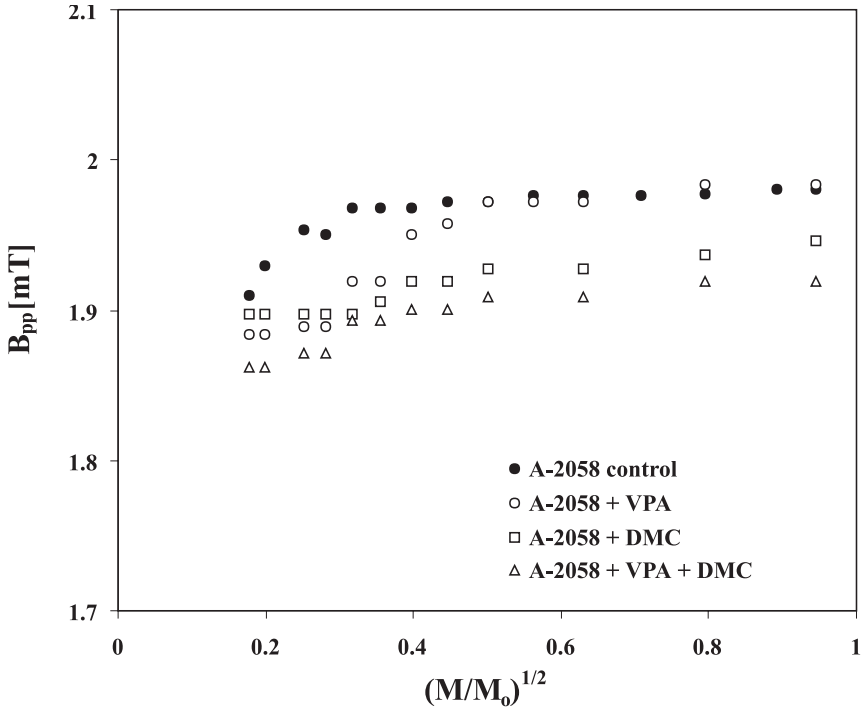

Figure 3. Influence of microwave power (M/M_o) on line widths (ΔB_{pp}) of EPR spectra of A-2058 control cells (●), and the cells treated with VPA (○), DMC (□), and both VPA and DMC (△). M, M_o – the microwave power used during the measurement of the spectrum and the total microwave power produced by klystron (70 mW), respectively

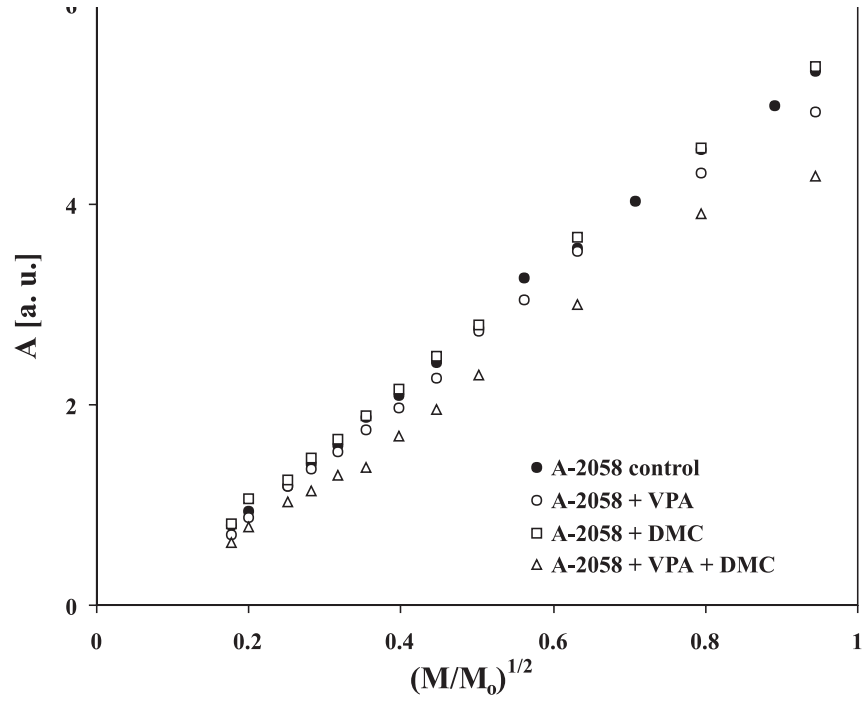

Figure 4. Influence of microwave power (M/M_o) on amplitudes (A) of EPR spectra of A-2058 control cells (●), and the cells treated with VPA (○), DMC (□), and both VPA and DMC (△). M, M_o – the microwave power used during the measurement of the spectrum and the total microwave power produced by klystron (70 mW), respectively

Table 1. Integral intensities (I), g-factors, and line widths (ΔB_{pp}) of EPR spectra of the studied A-2058 human *melanoma malignum* cells. Free radicals concentrations in the cells are proportional to the integral intensities (I). The data for the control cells and cells treated with VPA, DMC, and both VPA and DMC, are shown. The EPR spectra were measured with microwave power of 2.2 mW.

Sample	I [a. u.] ± 0.2	g ± 0.0002	ΔB_{pp} [mT] ± 0.02
A-2058 control	18.0	2.0060	1.91
A-2058 + VPA	15.3	2.0060	1.88
A-2058 + DMC	17.9	2.0058	1.90
A-2058 + VPA + DMC	13.3	2.0060	1.86

EPR line the saturation effect is observed. These correlations (Fig. 4) are characteristic for fast spin-lattice relaxation processes in the samples.

DISCUSSION AND CONCLUSIONS

Electron paramagnetic resonance (EPR) measurements indicated that o-semiquinone free radicals exist in both untreated and treated with VPA and DMC A-2058 human *melanoma malignum* cells. Microwaves were absorbed for all the samples located in magnetic field, and EPR spectra were detected (Fig. 2). The characteristic values of g-factors (Table 1) for such type of free radicals (14, 18–21, 24–26) were obtained.

Free radicals in A-2058 tumor cells are located near each others, because their EPR lines are very broad (Table 1). Such located o-semiquinone free radicals strongly dipolar interact, what is responsible for the measured line broadening (26). Strong dipolar interactions were also found in the melanin biopolymers (14–21). EPR lines of the A-2085 cells are homogeneously broadened (Figs. 3 and 4), similar to EPR lines of melanin biopolymers (14, 18–21, 24, 25). Spin-lattice relaxation processes in A-2058 tumor cells were different than those in melanin biopolymers of A-375 and G-361 human *melanoma malignum* cells (12). Spin-lattice interactions in A-2058 cells were fast (Fig. 4), and slow spin-lattice relaxation processes were detected in melanin of A-375 and G-361 cell (12). Probably, these differences results from the magnetic interactions of o-semiquinone free radicals of melanin with the whole structures in A-2085 cells.

Free radicals have unpaired electrons, which are responsible for their biochemical activity (1). Effective drugs should quench free radicals content in cells to avoid pathological transformation. Such positive interactions were observed for the tested VPA (Table 1). Because of the lowest intensities of EPR lines of A-2058 cells after VPA used together with DMC (Table 1), it seems better to use them both. VPA and DMC used together strongly decrease the amount of o-semiquinone free radicals in melanin biopolymers from A-375 and G-361 cells (12). In this study, we obtained the next proof of the effectiveness of VPA, and VPA used together with DMC as the antitumor compounds by the use of electron paramagnetic resonance.

Reports in the literature indicate that DMC and VPA can be a new strategy in the treatment of melanoma (28, 29). 5,7-Dimethoxycoumarin, which is a natural substance widely distributed in the plant kingdom, has a wide spectrum of biological activities. It is a natural chemopreventive agent (28). Furthermore, valproic acid, applied in the treatment of epilepsy, can be used in the chemoprevention and cancer chemotherapy (29).

Taking into account our spectroscopic results for free radicals, it can be concluded that VPA, and VPA applied with DMC together may be used as the antitumor compounds in A-2058 human malignant melanoma cells therapy, because they decrease free radical concentrations in these cells. It is expected that VPA is more effective than DMC, because it strongly quenches free radicals in A-2058 tumor cells, while such effect was not observed for DMC. The lower amounts of free radicals exist in A-2058 cells after treatment with VPA, and VPA applied with DMC together, so the optimal for antitumor therapy is to use VPA or VPA and DMC together. The similar conclusions were obtained by us earlier (12) for VPA, and VPA and DMC combination applied in therapy of G-361 human *melanoma malignum* cells. The usefulness of DMC without the other substance was not confirmed in the case of A-2058 human malignant melanoma cells.

Acknowledgment

These studies were financially supported by Medical University of Silesia in Katowice (grant no. KNW-1-005/K/4/0).

REFERENCES

1. Eaton G.R., Eaton S.S., Salikhov KM.: Foundations of modern EPR. World Scientific, Singapore 1998.
2. Kim H.J., Bae S.C.: Am. J. Transl. Res. 3, 166 (2011).
3. Buszman E.: Habilitation thesis. Medical University of Silesia in Katowice 1994.
4. Hegedus Z.L.: Toxicology 145, 85 (2000).
5. Smit N.P., van Nieuwpoort F.A., Marrot L., Out C., Poorthuis B., van Pelt H., Meunier J.R., Pavel S.: Photochem. Photobiol. 84, 550 (2008).
6. Desbois N., Gardette M., Papon J., Labarre P., Maisonial A., Auzeloux P., Lartigue C. et al.: Bioorg. Med. Chem. 16, 7671 (2008).
7. Larsson B.S.: Pigment Cell Res. 6, 127 (1993).
8. Bartosz G. The second face of oxygen. Free radicals in nature (Polish), PWN, Warszawa 2006.
9. Godechal Q., Gallez B.: J. Skin Cancer 2011, 273280 (2011).
10. Wang S.Q., Setlow R., Berwick M., Polsky D., Marghoob A.A., Kopf A.W., Bart R.S.: J. Am. Acad. Dermatol. 44, 837 (2001).
11. Noonan F.P., Zaidi M.R., Wolnicka-Glubisz A., Anver M.R., Bahn J., Wielgus A., Cadet J. et al.: Nat Commun. 6, 884 (2012).
12. Chodurek E., Zdybel M., Pilawa B.: J. Appl. Biomed. 11, 173 (2013).
13. Chodurek E., Zdybel M., Pilawa B., Dzierżewicz Z.: Acta Pol. Pharm. Drug Res. 69, 1334 (2012).
14. Sarna T.: Current Topics in Biophysics (Polish) 6, 201 (1981).
15. Pasenkiewicz-Gierula M., Sealy R.C.: Biochim. Biophys. Acta 884, 510 (1986).
16. Plonka P.M., Michalczyk D., Popik M., Handjiski B., Paus R.: J. Dermatol. Sci. 49, 227 (2008).
17. Krzywda A., Petelenz E., Michalczyk D., Płonka P. M.: Cell. Mol. Biol. Lett. 13, 130 (2008).
18. Najder-Kozdrowska L., Pilawa B., Buszman E., Więckowski A. B., Świątkowska L., Wrześniok D., Wojtowicz W.: Acta Phys. Pol. A 118, 613 (2010).
19. Zdybel M., Chodurek E., Pilawa B.: Appl. Magn. Reson. 40, 113 (2011).
20. Zdybel M., Pilawa B., Buszman E., Witoszyńska T.: Nukleonika 58, 401 (2013).
21. Zdybel M., Pilawa B., Buszman E., Wrześniok D.: Chem. Phys. Lett. 556, 278 (2013).
22. Ramos P., Pilawa B., Stroka E.: Nukleonika 58, 413 (2013).
23. Skowrońska A., Wojciechowski M., Ramos P., Pilawa B., Kruk D.: Acta Phys. Pol. A 121, 514 (2012).
24. Beberok A., Zdybel M., Pilawa B., Buszman E., Wrześniok D.: Chem. Phys. Lett. 592, 41 (2014).
25. Beberok A., Buszman E., Zdybel M., Pilawa B., Wrześniok D.: Chem. Phys. Lett. 497, 115 (2010).
26. Wertz J.E., Bolton J.R.: Electron spin resonance: elementary theory and practical applications. Chapman and Hall, London 1986.
27. Stankowski J., Hilczer W.: Introduction to magnetic resonance spectroscopy (Polish). PWN, Warszawa 2005.
28. Musa M.A., Cooperwood J.S., Khan M.O.: Curr. Med. Chem. 15, 2664 (2008).
29. Federico M., Bagella L.: J. Biomed. Biotechnol. 2011, 475641 (2011).

Acta Poloniae Pharmaceutica – Drug Research, Vol. 71 No. 6 pp. 1073–1078, 2014 ISSN 0001-6837
Polish Pharmaceutical Society

SHORT COMMUNICATIONS

FULLERENES AS THE CARRIERS OF COMPOUNDS WITH AMIDE BOND

MONIKA K. GRUDZIEŃ[1]*, MARCIN SUSKIEWICZ[1], EDITA AJMANOVIČ[1], FRANCISZEK A. PLUCIŃSKI[2] and ALEKSANDER P. MAZUREK[1,2]

[1] Department of Drug Chemistry, Faculty of Pharmacy, Medical University of Warsaw, 1 Banacha St., 02-097 Warszawa, Poland
[2] National Medicines Institute, 30/34 Chełmska St., 00-725 Warszawa, Poland

Keywords: fullerene C_{60}, endohedral fullerene, amide bond

Fullerenes are molecules created solely of carbon and have a highly unusual attributes. The smallest structure in the fullerene family is conformation C_{20}, which consists of pentagonal rings only, resulting in its instability. The C_{60} is the first fullerene containing 12 pentagonal and 20 hexagonal rings in which pentagons do not share an edge. It results in good stability of the carbon cage. The structure of C_{60} is a truncated icosahedron, with two different bond lengths: the ones between two hexagons are shorter (bond C–C, length 1.44 Å), then between a hexagon and a pentagon (double-bond C=C, length 1.39 Å); average bond length is 1.4 Å (1–3). The attributes like structure, geometry, size and shape of carbon cages yield the possibility to use them as vehicles to carry substances with pharmacological activity to molecular target.

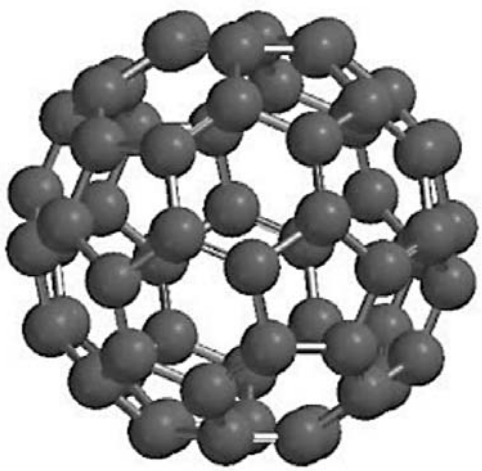

Figure 1. The structure of fullerene C_{60}

The derivatives of fullerenes are classified into following categories according to their functionalization: endohedral fullerenes with active molecules residing inside the carbon cage, exohedral with wide variety of both inorganic and organic groups existing outside and connected to the fullerenes' exterior and heterofullerenes – when one or more carbon atoms that form the fullerene carbon cage are replaced by a non-carbon atom, i.e., a heteroatom.

EXPERIMENTAL

The aim of this investigation was to analyze possibilities to use fullerenes as the potential carriers of compounds with peptide bond.

The N-aminoformamide (a), N-hydroxyformamide (b), N-methylformamide (c) and also their phosphorous analogues, where nitrogen atom from amide bond was replaced by phosphorus atom, were chosen for empirical studies (Fig. 2.). All these compounds were trapped into a carbon cage of fullerene C_{60}.

The energies of inclusion, deformation and interaction as well as absolute energy of each examined compound and their complexes with fullerene C_{60} were calculated with the use of the molecular modeling technique. The calculations for all the structures were carried out using DFT/B3LYP method at the level 6-31G** implemented in

* Corresponding author: e-mail: monika.grudzien@wum.edu.pl

Spartan 08 and Gaussian 03 software (4, 5). The chosen basis set takes into consideration polarization functions on carbon and hydrogen atoms. The first calculation stage was geometry optimization, establishing the most stable conformation and the absolute energy (in energetic minimum) of each examined compound. After that, all the lowest energy conformers were placed into carbon cage of fullerene C_{60} and each complex geometry was optimized. The next step was delimitation of total energy of endohedral complexes (E_{cx}). Finally, the energy values in geometry from endohedral complex – compound@C_{60} for N-aminoformamide, N-hydroxyformamide, N-methylformamide and their phosphorous analogues (E_{comp}) and empty carbon cage (E_{cage}) were calculated.

Stabilization energy (ΔE_{stab}) of the endohedral complexes was calculated as follows:

$$\Delta E_{stab} = E_{cx} - (E_{cage} + E_{comp})$$

where E_{cx} – complex energy, E_{cage} – fullerene C_{60} carbon cage energy, E_{comp} – every examined compound energy.

The energy of compound deformation (E_{def}) was calculated as a difference between encapsulated optimized structure energy and total energy of the most stable conformation. The deformation energy of fullerenes' C_{60} carbon cage was analogically estimated. The inclusion energy was calculated as a difference between complex energy in energetic minimum and sum of total energies of particular components. The interaction energy was calculated as the difference between complex energy in energetic minimum and the sum of total energies of particular components in the complex geometry (in single-point calculations – SP).

RESULTS AND DISCUSSION

The results of the calculations are presented in Tables below.

Table 1 shows total energies of examined systems and energies of inclusion as well as interaction energy, respectively. The presented data reveal that complexes compound@C_{60} are thermodynamically unstable. It refers both to endohedral fullerenes, including compounds with nitrogen atom, and their phosphorous analogues. Nevertheless, nitrogen derivatives have higher stability. It results both from van der Waals volumes of trapped molecules and electron stability. The methyl group in both nitrogen compound and in its phosphorous analogue destabilizes the system the most, while hydroxy one – the

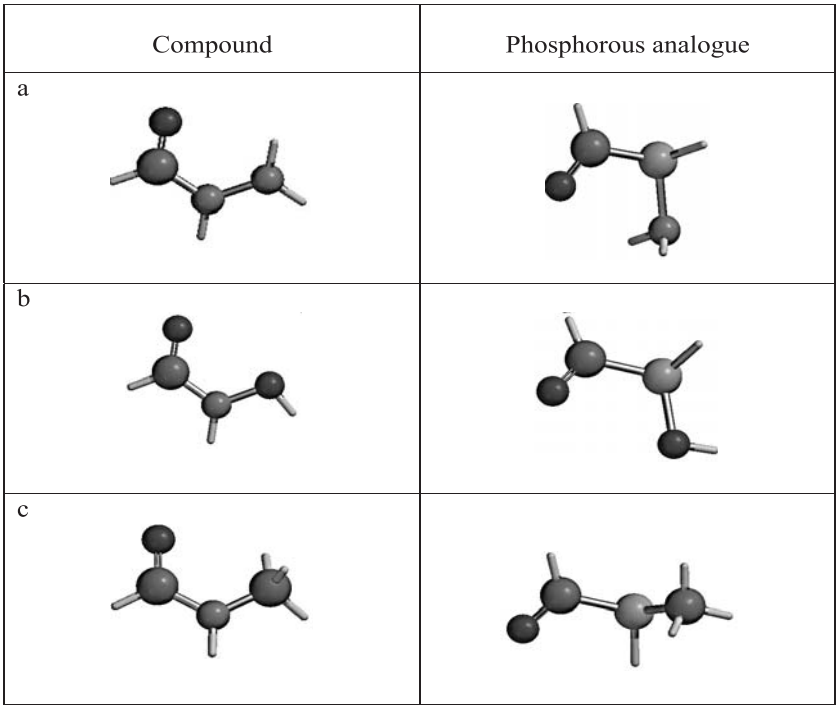

Figure 2. The structures of examined compounds

Table 1. Total energies of studied systems.

Compound	Complex energy (E_{cx}) [hartree]	Inclusion energy (E_{inc}) [kcal/mol]	Interraction energy (E_{int}) [kcal/mol]
CHO-NH-NH_2	–2511.165396	141.7	109.8
CHO-NH-OH	–2531.057702	106.7	86.0
CHO-NH-CH_3	–2495.082799	188.8	139.8
CHO-PH-NH_2	–2797.626637	204.0	148.0
CHO-PH-OH	–2817.557307	191.0	152.3
CHO-PH-CH_3	–2781.489139	292.5	207.3

Table 2. The total energy and energy of deformation of studied compounds.

Compound	Total energy [hartree]	SP [hartree]	Energy of deformation (E_{def}) [kcal/mol]
CHO-NH-NH_2	–225.216830	–225.186915	18.8
CHO-NH-OH	–245.053341	–245.035131	11.4
CHO-NH-CH_3	–209.209250	–209.162445	29.4
CHO-PH-NH_2	–511.777230	–511.719734	36.1
CHO-PH-OH	–531.687195	–531.652959	21.5
CHO-PH-CH_3	–495.780854	–495.684091	60.7

Table 3. The total energy and energy of deformation of fullerene C_{60}.

Fullerene C_{60} „guest" molecule	Total energy [hartree]	SP [hartree]	Energy of deformation [kcal/mol]
CHO-NH-NH_2	–2286.174447	–2286.153464	13.2
CHO-NH-OH	–2286.174447	–2286.159638	9.3
CHO-NH-CH_3	–2286.174447	–2286.143197	19.6
CHO-PH-NH_2	–2286.174447	–2286.142816	19.8
CHO-PH-OH	–2286.174447	–2286.147069	17.2
CHO-PH-CH_3	–2286.174447	–2286.135481	24.4

least, probably due to the size of functional groups in examined compounds. The inclusion energies range from 106.7 to 292.5 kcal/mol. Therefore, it could be concluded that these systems can be created at higher temperature (e.g., plasma) and their disintegration time will depend, in the first approximation, on the energetic barrier defined by inclusion energy.

Tables 2 and 3 show the total energies of compounds and fullerenes C_{60} after their geometry optimization and their complex geometry energy values, as well as their deformation energies. They reveal the level of deformation energy of disturbed structures, which are molecules of fullerenes C_{60} and the examined compounds, as the result of complex formation.

The phosphorous analogues are more destabilized except for compounds with hydroxy group – its energy of deformation value is smaller than for N-methylformamide. It probably results from the tendency for intermolecular hydrogen bond formation. The nitrogen derivative with hydroxy group of high possibility to form this type of bond (size of molecule, distance between atoms) is relatively less destabilized.

Tables 4 and 5 contain bond lengths of examined compounds after their geometry optimization –

before (G_B) and after (G_A) inside fullerenes' cage placement. In the case of derivatives with hydroxy group, when the tendency for intermolecular hydrogen bond formation is high, the angle values between atoms were also analyzed. The α is the angle between atoms: oxygen (O') and hydrogen of hydroxy group and oxygen of formyl group. The β angle is defined as between carbon and oxygen of formyl group and hydrogen of hydroxy group. The distances between the atoms: hydrogen and nitrogen (N') as well as hydrogen and carbon (C') in amine and methyl groups, respectively, were expressed as the average value of those bond lengths.

The lengths in amide bond atoms are succumb to disturbances, the angle alteration is observed and total geometry of encapsulated molecules undergoes deformation. The most significant changes are observed between the atom lengths in CHO-PH-CH_3 (phosphorous analogue of N-methylformamide) molecule, the least in CHO-NH-OH (N-hydroxyformamide) based on difference between lengths of particular bonds in investigated compounds. It is not surprising if the molecule sizes are taken into consideration. The placement of compounds with hydroxy group inside of carbon cage of fullerene C_{60} elicited significant shortening of bond lengths between hydrogen atoms of hydroxy group and oxygen atom of formyl group. In contrast, the probability of intermolecular hydrogen bond formation increased molecule deformation. Together with O—

Table 4. The comparison of particular bond lengths [Å] and angles of nitrogen compounds.

Bond	CHO-NH-N'H_2		CHO-NH-O'H		CHO-NH-C'H_3	
	G_B	G_A	G_B	G_A	G_B	G_A
C=O	1.219	1.213	1.226	1.224	1.219	1.209
C-N	1.362	1.306	1.353	1.308	1.362	1.302
N-N'	1.409	1.361				
N-O'			1.402	1.351		
N-C'					1.453	1.392
O'-H			0.981	1.002		
N'-H (śr.)	1.021	1.011				
C'-H (śr.)					1.093	1.051
O—-H			2.023	1.495		
α			119.09°	128.83°		
β			81.41°	88.84°		

Table 5. The comparison of bond lengths [Ĺ] and angles of phosphorous analogues.

Bond	CHO-PH-NH_2		CHO-PH-O'H		CHO-PH-C'H_3	
	G_B	G_A	G_B	G_A	G_B	G_A
C=O	1.210	1.252	1.209	1.215	1.212	1.199
C-P	1.872	1.803	1.873	1.705	1.868	1.702
P-N	1.715	1.756				
P-O'			1.665	1.578		
P-C'					1.861	1.760
O'-H			0.966	1.006		
N-H (aver.)	1.011	1.005				
C'-H (aver.)					1.092	1.050
O—-H			3.493	1.410		
α			53.60°	136.92°		
β			73.05°	95.64°		

Table 6. The bond lengths [Å] changes [$G_B - G_A$] in compounds studied. (+) depicts elongation of bond, (–) depicts shortening of bond (based on Tables 4 and 5).

Bond	CHO-NH-N$^{\bullet}$H$_2$	CHO-NH-O$^{\bullet}$H	CHO-NH-C$^{\bullet}$H$_3$	Bond	CHO-PH-NH$_2$	CHO-PH-O$^{\bullet}$H	CHO-PH-C$^{\bullet}$H$_3$
C=O	(–) 0.006	(–) 0.002	(–) 0.010	C=O	(+) 0.052	(+) 0.006	(–) 0.013
C-N	(–) 0.056	(–) 0.045	(–) 0.060	C-P	(–) 0.069	(–) 0.168	(–) 0.166
N-N’	(–) 0.048			P-N	(+) 0.041		
N-O’		(–) 0.051		P-O’		(–) 0.087	
N-C’			(–) 0.061	P-C’			(–) 0.101
O’-H		(+) 0.021		O’-H		(+) 0.040	
N’-H (aver.)	(–) 0.010			N-H (aver.)	(–) 0.005		
C’-H (aver.)			(–) 0.042	C’-H (aver.)			(–) 0.042
O—-H		(–) 0.528		O—-H		(–) 2.083	

-H distance shortening the α and β angles increase, as well as the distance between the hydroxy group atoms. The biggest changes are observed in CHO-PH-OH (phosphorous analogue of N-hydroxyformamide).

CONCLUSIONS

The results reveal that examined systems consisting of compounds with amide bond and their phosphorous analogues build into carbon cage of fullerene C_{60} are thermodynamically unstable. However, calculation with the use of DFT method suggests that those systems could exist despite positive energies of inclusion values. The energy related barrier of fullerene breaking results in retention of the compound inside the carbon cage in spite of angles and bond lengths deformation in molecules of examined compounds.

The values of deformation, inclusion and interaction energies are higher in case of phosphorous analogues, which can be, in the first approximation, explained by the phosphorous atom size compared with the replaced nitrogen atom and consequently larger so-called van der Waals volume of entire molecules.

Comparing the results obtained for formamide incorporated into spherical cap of fullerene C_{60} by H. Dodziuk et al. (6) the analogies are apparent. Energy of stabilization value, calculated with the use of molecular mechanics (MM) (INSIGHT program package (version 98.0) with CVFF and ESFF force fields), was 62.7 kcal/mol, which is an evidence of complex formamide@fullerene C_{60} instability. The stability of complexes with fullerenes C_{70}, C_{80}, C_{76}, C_{82} was also studied. It turned out that the system $CHONH_2@C_{82}$ has achieved the highest stability, in which energy of stabilization was –24.5 kcal/mol. According to the authors of „Molecular mechanics study of endohedral fullerene complexes with small molecules” (6) fullerene energy of stabilization depends on many weak interactions between „host” and „guest”, respectively, fullerenes carbon cage and molecules „guest” sizes as well as symmetry of fullerene.

The results of analysis performed indicate the possible use of fullerenes as the carriers of compounds with peptide bond. The study on model structures: N-aminoformamide, N-hydroxyformamide, N-methylformamide and their phosphorous analogues suggest that fullerene C_{60} could serve as a carrier for peptide nature substances not provoking danger of amide bond structure disturbance. The geometry deformation of structures trapped in car-

bon cage could only have influence on properties and reactivity during their transport to molecular target.

REFERENCES

1. Greer J.C.: Chem. Phys. Lett. 326, 567 (2000).
2. Huczko A., Bystrzewski M.: Fullerenes – 20 Years After Discovery, 1st edn., UW, Warszawa 2007.
3. Ghua S., Nakamoto K.: Coordination Chem. Rev. 249, 1111 (2005).
4. Wavefunction Inc. Spartan 08; Wavefunction Inc.: 18401 Von Karman Avenue, suite 370, Irvine, CA 92612, 2009.
5. Frisch M.J., Trucks G.W., Schlegel H.B., Scuseria G.E, Robb M.A., Cheeseman J.R., Montgomery J.A., Vreven Jr. T., Kudin K.N., Burant J.C., Millam J.M., Iyengar S.S., Tomasi J., Barone V., Mennucci B., Cossi M., Scalmani G., Rega N., Petersson G.A., Nakatsuji H., Hada M., Ehara M., Toyota K., Fukuda R., Hasegawa J., Ishida M., Nakajima T., Honda Y., Kitao O., Nakai H., Klene M., Li X., Knox J.E., Hratchian H.P., Cross J.B., Adamo C., Jaramillo J., Gomperts R., Stratmann R.E., Yazyev O., Austin A.J., Cammi R., Pomelli C., Ochterski J.W., Ayala P.Y., Morokuma K., Voth G.A., Salvador P., Dannenberg J.J., Zakrzewski V.G., Dapprich S., Daniels A.D., Strain M.C., Farkas O., Malick D.K., Rabuck A.D., Raghavachari K., Foresman J.B., Ortiz J.V., Cui Q., Baboul A.G., Clifford S., Cioslowski J., Stefanov B.B., Liu G., Liashenko A., Piskorz P., Komaromi I., Martin R.L., Fox D.J., Keith T, Al-Laham M.A., Peng C.Y., Nanayakkara A., Challacombe M., Gill P.M.W., Johnson B., Chen W., Wong M.W., Gonzalez C., Pople J.A.: Gaussian 03, Rev A.1. Gaussian Inc., Pittsburgh, PA 2003.
6. Dodziuk H., Dolgonos G., Lukin O.: Carbon 39, 1907 (2001).

Acta Poloniae Pharmaceutica – Drug Research, Vol. 71 No. 6 pp. 1079–1082, 2014 ISSN 0001-6837
Polish Pharmaceutical Society

APPLICATION OF NEW DATA PROCESSING METHOD FOR THE PHOTODIODE ARRAY DETECTOR IN THE DRUG SUBSTANCE ANALYSIS

ŁUKASZ JEDYNAK[1]*, MARIA PUCHALSKA[1], JOANNA ZAGRODZKA[1], WOJCIECH ŁUNIEWSKI[2] and ŁUKASZ KACZMAREK[2]

[1]R&D Analytical Chemistry Department, [2]Chemistry Department,
Pharmaceutical Research Institute, 8, Rydygiera St., 01-793 Warszawa, Poland

Keywords: temozolomide, drug substance, HPLC, photodiode array detector, i-DReC

While analyzing active pharmaceutical ingredients (APIs) it is necessary to determine both the assay of the drug substance itself and the content of impurities in a drug substance. The ideal situation is when both assay of drug substance and content of related substances can be determined simultaneously (1). However, as the impurities must be determined at relatively low levels, it is often impossible to select such analytical conditions, which allow to determine both the API assay and the content of impurities in one chromatographic run. Drug substance concentration in a method for the determination of its purity is often outside the linear range of the applied detector and an additional analytical procedure for the drug substance assay must be developed (2, 3).

An Intelligent Dynamic Range Extension Calculator (i-DReC) is a new data processing method for the photodiode array detector, available in the LabSolutions software by Shimadzu. It allows to extend the linear range of chromatographic method by shifting the chromatographic profile to the wavelength where the target signal is not saturated. The peak area of the acquired chromatogram is corrected by the factor of the absorption ratio between the original target wavelength and the wavelength used by the i-DReC function. The i-DReC is applied automatically when the intensity of the target peak exceeds the user-defined threshold value (4, 5).

Temozolomide (3,4-dihydro-3-methyl-4-oxoimidazo-[5,1-*d*]-as-tetrazine-8-carboxamide; TZ) is an oral alkylating drug used for the treatment of primary brain tumors (6, 7). The temozolomide signal is saturated in the method for the determination of temozolomide related substances used for the assessment of the chemical purity of temozolomide samples manufactured by Pharmaceutical Research Institute (PRI), which imposed the necessity of using separate methods for the temozolomide API assay and purity determination (2).

The aim of the study was to apply the i-DReC data analysis function of the LabSolutions software to the determination of temozolomide assay using a method for the chemical purity determination. It was possible in spite of the temozolomide signal being saturated.

EXPERIMENTAL

Reagents and equipment

Acetonitrile (ACN) and methanol (MeOH) of HPLC grade (Super Gradient) were obtained from POCh (Poland). Acetic acid (HAc, > 99.8%) was purchased from Fluka (Germany). Demineralized water (< 0.0055 µS/cm) from Polwater system (Poland) was used throughout the investigation. All analyses were performed using the UHPLC Shimadzu Nexera X2 with LC-30AD pumps, an SIL-30AC autosampler, a CTO-20AC column oven, a DGU-20A5R degasser, an SPD-30AD DAD detector and the LabSolutions 5.54 SP5 software (Shimadzu, Japan). The separations were carried out using an Aqua C18, 250 × 4.6 mm, 5 µm column

* Corresponding author: e-mail: l.jedynak@ifarm.eu; phone +48 22 456 39 18, fax +48 22 456 38 38

(Phenomenex, USA). The temozolomide samples were manufactured by PRI.

Analytical procedures

The method for the determination of the temozolomide chemical purity was as follows: eluent A: 0.5% acetic acid in water, eluent B: acetonitrile, gradient elution program: t (min)/%B: 0/8; 8/8; 28/40; 31/8; 36/8, column temperature: 25°C; autosampler temperature: 5 ± 2°C; flow rate: 1 mL/min; injection volume: 20 µL; UV detection wavelength: λ = 254 nm; diluent: water with 0.5% HAc : ACN (4 : 1, v/v); concentration of temozolomide in the investigated sample solutions: 1 mg/mL. The validation of the method for the determination of the temozolomide chemical purity as well as important notes on the sample preparation were described in the previous publication (2). The reference method for the temozolomide assay was as follows: mobile phase: 0.5% HAc in water : MeOH (9 : 1, v/v); isocratic elution; duration of analysis: 20 min; column temperature: 25°C; autosampler temperature: 5 ± 2°C; flow rate: 1 mL/min; injection volume: 10 µL; UV detection wavelength: λ = 254 nm; diluent: 0.5% HAc : ACN (9 : 1, v/v); concentration of temozolomide in the investigated sample solutions: 0.25 mg/mL.

The applied i-DReC settings were as follows: threshold: 500 mAU; wavelength for correction: 500 mAU (Auto); direction: +; intensity to extract: 500 mAU.

RESULTS AND DISCUSSION

The chromatographic procedure used for the determination of related substances in temozolomide is not suitable for the determination of the temozolomide assay. The concentration of TZ in the samples used for the determination of related substances is relatively high (1 mg/mL), so the TZ sig-

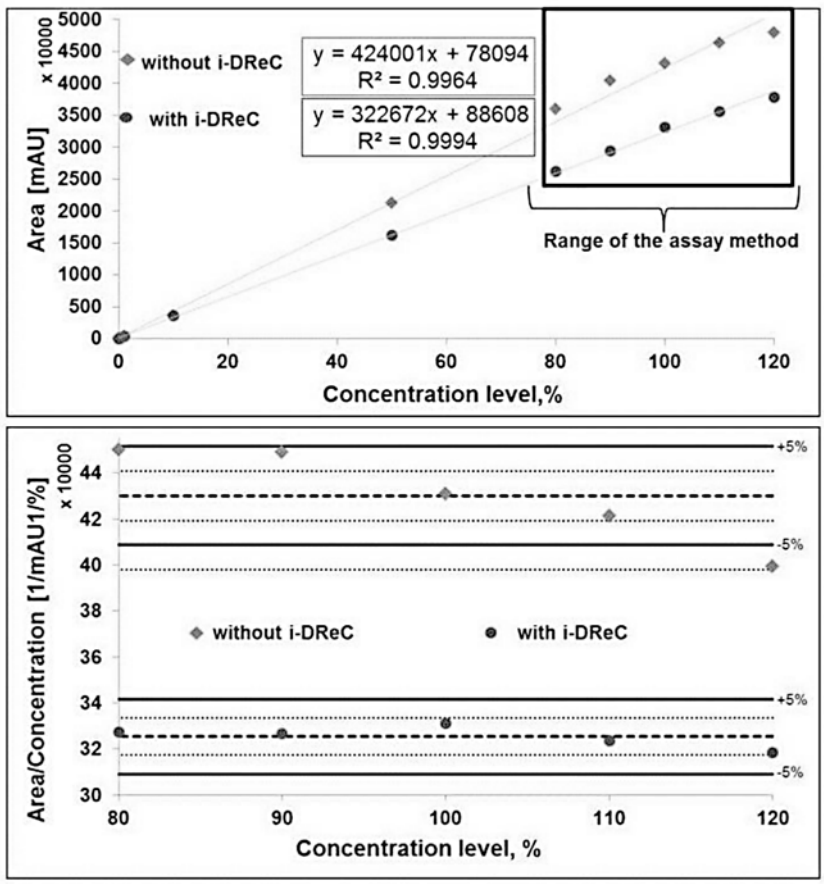

Figure 1. Comparison of calibration curves with application of i-DReC function (circles) and without application of i-DReC (squares) and comparison between the ratio of intensity/ concentration and concentration of temozolomide in the range used for assay determination (80–120% i.e., 0.8–1.2 mg/mL)

Table 1. Comparison of the results of temozolomide assay determined using the method for chemical purity with and without i-DReC and the reference assay method

	No. of sample	Reference assay method [%]	Assay determined using the method for chemical purity without i-DReC [%]	Assay determined using the method for chemical purity with i-DReC [%]
	1	100.6	76.2	100.0
	2	99.0	75.3	98.9
	3	100.0	76.5	100.4
	4	99.1	75.2	98.7
	5	99.6	75.8	99.6
	6	99.7	75.7	99.4
	7	98.5	75.6	99.3
	8	98.6	76.0	99.8
Statistical analysis comparison of the results of temozolomide assay				
	$\bar{x}$	**99.4**	**75.8**	**99.5**
	SD	0.7	0.4	0.6
Snedecor`s F-test	***F***	–	0.37	0.61
$F = SD_2^2/SD_1^2$ $F_{cr(\alpha = 0.05,\ f = n-1)}$	$\boldsymbol{F_{cr} = 3.79}$	$F \le F_{cr}$ – the difference between the standard deviations is not significant		
Student's *t*-test	***t***	-	79.156	0.310
$t = \frac{\lvert \bar{x}_1 - \bar{x}_2 \rvert}{\sqrt{s_1^2 + s_2^2}} \cdot \sqrt{n}$ $t_{cr(\alpha = 0.05,\ f = 2n-2)}$	$\boldsymbol{t_{cr} = 2.149}$		$t >> t_{cr}$ – the difference between the average results is significant	$t \le t_{cr}$ – the difference between the average results is not significant
Statistical analysis comparison of the results of linearity				
n			13	13
Regression line			y = 424002x + 78094	y = 322672x + 88608
Standard deviation			SD_a = 7733 SD_b = 496533 SD_{xy} = 1324961	SD_a = 2385 SD_b = 153165 SD_{xy} = 408708
R^2			0.9964	0.9994

nal is saturated. Therefore, it was necessary to develop another procedure for the determination of the TZ assay to perform routine analyses of the TZ samples manufactured by PRI (2). As the i-DReC function allows to perform a quantitative analysis even outside the linear range of the method, an attempt to determine the TZ assay with the use of the method destined for the determination of the TZ purity was undertaken. Calibration curves were plotted in the range from 0.30 µg/mL (0.03% in relation to the initial TZ concentration) to 1.2 mg/mL (120% in relation to the initial TZ concentration). Thus, the chosen calibration range covered the concentrations used for the determination of related substances according to the guidelines (8), i.e., from the limit of quantitation, which was formerly set at 0.30 µg/mL (0.03% in relation to the initial TZ concentration) level (2) to 120% of the specification limit for both unknown and known impurities, i.e., 1.2 µg/mL and 1.5 µg/mL, respectively (0.12% and 0.15% in relation to the initial TZ concentration, respectively). The calibration curve also contained the concentration range required for the assay determination, i.e., 80–120% of the test concentration (0.8–1.2 mg/mL).

The results of the temozolomide assay determination with and without the use of the i-DReC function were compared with the results obtained with the reference assay method (Table 1). The tests were carried out for eight independent temozolomide samples. As it is shown in Table 1, the assay of temozolomide is significantly underestimated when the calibration curve without the i-

DReC correction is used for the calculation of the results. On the other hand, the results calculated with the use of the calibration curve with the i-DReC correction are consistent, compared to the results acquired with the reference assay method. The performed statistical tests (Snedecor's F-test and Student's *t*-test) confirmed that the application of the i-DReC procedure allows to obtain valid results of the temozolomide assay in contrast to the procedure without the application of the i-DReC. The comparison of the calibration curves plotted for the results obtained with and without the application of the i-DReC clearly denotes that the linearity is lost at higher TZ concentration levels (Fig. 1). The application of the i-DReC function allowed to correct the linearity and carry out quantitative measurements even at high TZ concentrations. The comparison between the ratio of intensity/concentration and the concentration of temozolomide in the range used for the assay determination (80–120% i.e., 0.8–1.2 mg/mL) shows that the application of the i-DReC function allows to maintain the ratio within the ± 5% confidence level.

As the i-DReC is a relatively new function, there is a scarcity of literature data referring to this feature's application. However, there are two technical notes released by Shimadzu where the application of the i-DReC in pharmaceutical analyses is presented (6, 7). It was demonstrated that it is possible to simultaneously quantify both the major component at a high concentration level and the impurities at low levels with the application of the i-DReC. The results described in the current paper also confirm that the use of the i-DReC function allows to quantify the major component in pharmaceutical samples, even at high concentrations.

CONCLUSION

The comparison of the determination results of the temozolomide assay with the use of the analytical procedure for the purity determination and the application of the i-DReC function with the results obtained for the separate reference assay method revealed a good coherence between them. It is thus possible to use only one chromatographic run instead of two procedures to quantify both the major component and related substances, which allows to reduce the solvent consumption, lower the costs of the analysis and save time.

Acknowledgments

The study was supported by the European Union under the European Regional Development Fund No. UDA-POiG.01.03.01-069/08-00 "Innovative technologies of oncological medicines of special therapeutic and social importance".

The authors would like to kindly acknowledge Shim-Pol for the opportunity to test the UHPLC Nexera X2 system with the LabSolutions software.

REFERENCES

1. Lipiec-Abramska E., Jedynak Ł., Formela A., Roszczyński J., Cybulski M., Puchalska M., Zagrodzka J.: J. Pharm. Biomed. Anal. 91, 1 (2014).
2. Jedynak Ł., Puchalska M., Zezula M., Łaszcz M., Łuniewski W., Zagrodzka J.: J. Pharm.. Biomed. Anal. 83, 19 (2013).
3. Official Monographs – Paricalcitol, US Pharmacopoeia 36, 4691 (2013)
4. Newlands E.S., Stevens M.F.G., Wedge S.R., Wheelhouse R.T., Brock C.: Cancer Treat. Rev. 25, 35 (1997).
5. Wesolowski J.R., Rajdev P., Mukherji S.K.: AJNR Am. J. Neuroradiol. 31, 1383 (2010).
6. Yanagisawa T.: Shimadzu Journal 2, 43 (2013).
7. http://www.shimadzu.com/an/literature/hplc/jpl213039.html
8. ICH Harmonised Tripartite Guideline. Validation of Analytical Procedures: Text and Methodology, Q2(R1), 1994.

Acta Poloniae Pharmaceutica – Drug Research, Vol. 71 No. 6 pp. 1083–1089, 2014 ISSN 0001-6837
Polish Pharmaceutical Society

SYNTHESIS OF FUCOSYLATED URIDINE CONJUGATES AS POTENTIAL GLYCOSYLTRANSFERASE INHIBITORS

KATARZYNA KOMOR[1*], WIESŁAW SZEJA[1], ROMAN KOMOR[1], GABRIELA PASTUCH-GAWOŁEK[1] and JOACHIM THIEM[2]

[1]Silesian University of Technology, Faculty of Chemistry, Chair of Organic Chemistry, Bioorganic Chemistry and Biotechnology, 44-100 Gliwice, Krzywoustego 4, Poland
[2]University of Hamburg, Faculty of Sciences, Department of Chemistry, D-20146 Hamburg, Martin-Luther-King-Platz 6, Germany

Keywords: glycosyltransferase inhibitor, L-fucose, glycosylation

The role glycans play in protein function, receptor binding and cell adhesion has spawned a great deal of research toward the identification of molecules that alter their structures. The development of improved methods for carbohydrate synthesis and particularly glycosidic bond formation is therefore crucial (1). The key role played by L-fucose in glycoprotein and cellular function has prompted significant research toward identifying recombinant and biochemical approaches for blocking its incorporation into proteins and membrane structures (2, 3). Also deoxyfucose anologues such as L-rhodinose (2,3,6-trideoxy-L-*threo*-hexopyranose), and L-oliose (2,6-dideoxy-L-*lyxo*-hexopyranose), occur as structural moieties of many bioactive natural products and often play an important role in their mechanism of action, in particular for DNA interaction of anti-cancer drugs (4, 5). Therefore, utilization of L-fucal derivatives as building blocks for the total synthesis of various deoxy glycosides is of great interest in bioorganic and medicinal chemistry.

In connection with our own studies in this area (6–9) we became interested in the prospect of developing a simple method that would lead to various L-fucosyl derivatives of uridine as a potential GTs inhibitors (10). Glycosyltransferases (GTs) are family of enzymes that are responsible for the biosynthesis of glycoconjugates such as glycolipids and glycoproteins as well as oligo- and polysaccharides which are crucial factors in bacterial and viral infections (11). Thus, the development of new selective inhibitors is of great importance in dealing with bacterial and fungal diseases (12, 13).

EXPERIMENTAL

NMR spectra were recorded on Agilent spectrometer 400 MHz and Bruker AV spectrometer 400 MHz using TMS as internal standard and $CDCl_3$ as a solvent. NMR solvent was purchased from ACROS Organics (Geel, Belgium). Chemical shifts (δ) are expressed in ppm and coupling constants (*J*) in Hz. Optical rotations were measured with a JASCO 2000 polarimeter using a sodium lamp (589.3 nm) at room temperature. Electrospray-ionization mass spectrometry was performed on a 4000 QTrap (Applied Biosystems/MDS Sciex) mass spectrometer. Reactions were monitored by TLC on precoated plates of silica gel 60 F254 (Merck). TLC plates were inspected under UV light (λ = 254 nm) or charring after spraying with 10% sulfuric acid in ethanol. Crude products were purified using column chromatography performed on silica gel 60 (70–230 mesh, Fluka) developed with hexane/EtOAc and $CHCl_3$/MeOH as solvent systems. Organic solvents were evaporated on a rotary evaporator under diminished pressure at 40°C.

All selectively protected substrates: 4-*O*-benzyl-L-fucal **1** (14), 2',3'-bis-*O*-(*tert*-butyldimethylsilyl)uridine **3** (15) and 2',3'-*O*-isopropylidene-uridine-5'-carboxylic acid **11** (16) were prepared according to published procedures. Other chemicals were purchased from Acros and POCh Chemical Companies and were used without purification.

* Corresponding author: e-mail: katarzyna.komor@polsl.pl

3-*O*-[4-*O*-Benzyl-2,3,6-trideoxy-α-L-*threo*-hex-2-enopyranosyl]-1,5-anhydro-4-*O*-benzyl-2,6-dideoxy-2,6-dideoxy-L-*lyxo*-hex-1-enitol (2)

To a solution of the sugar **1** (1 g, 4.5 mmol) in toluene (40 mL) sat. aq. NaOH (4 mL) was added. The mixture was stirred for 20 min, then a catalytic amount of $Bu_4N^+I^-$ (84 mg, 0.23 mmol) and *p*TsCl (438 mg, 2.3 mmol) were added. The reaction was stirred at room temperature until TLC (hexane : ethyl acetate, 3 : 1, v/v) showed complete consumption of the starting material. The solution was then diluted with toluene (50 mL) and quenched with H_2O (100 mL). The aqueous layer was extracted with toluene (60 mL). The combined organic phases were washed with brine (2 × 100 mL), dried over anhydrous $MgSO_4$ and concentrated to give a crude residue, that was purified by column chromatography on silica gel with hexane : EtOAc (20 : 1, v/v) to give disaccharide **2αβ** as a colorless syrup (α : β 4 : 1), yield 645 mg (65%). Diastereoisomer α was separated by crystallization from diethyl ether-hexane. Disaccharide **2α** was obtained as white solid in 40% yield, m.p. 106–108 C, = 228.1 (*c* 0.4, $CHCl_3$). ^{1}H-NMR (400 MHz, $CDCl_3$, δ, ppm): 7.40–7.23 (m, 10H, H_{arom}), 6.33 (dd, *J* = 6.2, 1.6 Hz, 1H, H-1), 6.13 (ddd, *J* = 10.0, 5.2, 0.7 Hz, 1H, H-3'), 5.97 (dd, *J* = 10.1, 3.0 Hz, 1H, H-2'), 5.23 (d, *J* = 2.9 Hz, 1H, H-1'), 4.84, 4.67 (qAB, *J* = 11.9 Hz, 2H, 4-O-Bn), 4.76 (ddd, *J* = 6.2, 3.1, 1.1 Hz, 1H, H-2), 4.66, 4.57 (qAB, *J* = 12.0 Hz, 2H, 4'-O-Bn), 4.52 (ddd, *J* = 5.7, 2.9, 1.4 Hz, 1H, H-3), 4.23 (qd, *J* = 6.6, 2.6 Hz, 1H, H-5'), 4.14 (dq~q, *J* = 6.1 Hz, 1H, H-5), 3.72 (dd, *J* = 2.9, 1.3 Hz, 1H, H-4), 3.52 (dd, *J* = 5.3, 2.6 Hz, 1H, H-4'), 1.36 (d, *J* = 6.6 Hz, 3H, 6'-CH_3), 1.29 (d, *J* = 6.7 Hz, 3H, 6-CH_3); ^{13}C-NMR (101 MHz, $CDCl_3$, δ, ppm): 144.2 (C1), 138.6 (C_{IV}-Ph),, 138.4 (C_{IV}-Ph), 129.4 (C-2'), 128.4, 128.4, 128.05, 127.8, 127.7, 127.6 (10 C_{arom}), 127.4 (C-3'), 101.2 (C-2), 94.4 (C-1'α), 73.6 ($\underline{C}H_2$Ph), 73.5 (C-4), 72.5 (C-5), 70.9 ($\underline{C}H_2$Ph), 70.2 (C-3), 69.4 (C-4'), 66.4 (C-5'), 16.4 (C-6'), 16.0 (C-6).

Addition reaction of uridine derivative 3 to unsaturated disaccharide 2

To the mixture of disaccharide **2** (100 mg, 0.237 mmol) and the uridine derivative **3** (123 mg, 0.260 mmol) in dry CH_2Cl_2 (5 mL) molecular sieves 4Å were added and the mixture was cooled to 0°C in ice-water (Table 1, entry 2). Then, a catalytic amount (8 mg, 0.024 mmol) of triphenylphosphine hydrobromide (TPHB) in CH_2Cl_2 (1 mL) was added dropwise *via* syringe. The reaction was monitored by TLC (hexane : AcOEt, 2 : 1, v/v) and finally finished by addition of Et_3N (0.05 mL). Molecular sieves were filtered off and solvents were evaporated under reduced pressure. The residue was purified by column chromatography (hexane : AcOEt, 4 : 1, v/v) to yield the glycoconjugates: **4** (55 mg, 26%), **5** (46 mg, 29%) and **6** (10%, in a mixture with uridine **3**).

Glycoconjugate 4

Colorless syrup, α : β = 5 : 1; selected NMR data: ^{1}H-NMR (400 MHz, $CDCl_3$, δ, ppm): 8.34 (s, 1H, NH_{ur}), 8.15 (d, *J* = 8.2 Hz, 1Hβ, H-6_{ur} β-isomer), 7.80 (d, *J* = 8.2 Hz, 1H, H-6_{ur} α-isomer), 7.41–7.23 (m, 10H, H_{arom}), 6.15 (dd, *J* = 10.0, 5.3 Hz, 1H, H-3'), 5.98–5.92 (m, 2H, H-2', H-5_{ur}), 5.75 (d, *J* = 1.6 Hz, 1H, H-1'$_{ur}$), 5.22 (d, *J* = 2.8 Hz, 1H, H-1' α-isomer), 5.08 (d, *J* = 2.9 Hz, 1Hβ, H-1' β-isomer), 4.96 (d, *J* = 3.5 Hz, 1H, H-1α), 4.87, 4.64 (qAB, *J* = 11.7 Hz, 2H, CH_2Ph), 4.67, 4.57 (qAB, *J* = 11.9 Hz, 2H, CH_2Ph), 4.25–4.14 (m, 2H, H-5', H-4'$_{ur}$), 4.11–4.02 (m, 3H, H-3, H-2'$_{ur}$, H-3'$_{ur}$), 4.04 (dd, *J* = 11.8, 2.7 Hz, 1H, H-5a'$_{ur}$), 3.80 (q, *J* = 6.5 Hz, 1H, H-5), 3.58 (dd, *J* = 5.4, 2.7 Hz, 1H, H-4'), 3.57–3.53 (m, 1H, H-4), 3.48 (dd, *J* = 11.8, 2.6 Hz, 1H, H-5b'$_{ur}$), 2.32–2.21 (m, 1H, H-2_{eq}), 1.98 (dd, *J* = 12.9, 5.0 Hz, 1H, H-2_{ax}), 1.32 (d, *J* = 6.7 Hz, 3H, 6'-CH_3), 1.18 (d, *J* = 6.5 Hz, 3H, 6-CH_3), 0.91, 0.90 (2 × s, 18H, 2 × $C(CH_3)_3$), 0.16, 0.10, 0.08, 0.07 (4 × s, 12H, 2 × $Si(CH_3)_2$). ^{13}C-NMR (101 MHz, $CDCl_3$, δ, ppm): 162.69 (C=O), 149.92 (C=O), 139.51 (C-6_{ur}), 138.68, 138.49 ($2C_{IV}$), 129.31 (C-2'), 128.45,

Table 1. Reaction conditions for addition of uridine **1** to unsaturated disaccharide **4**.

Entry	Reaction	Temp. conditions	Time [°C]	Products / Yield [%]		
				4	**5**	**6***
1.	TPHB, CH_2Cl_2	10	10 min	11	49	~20
2.		0 3	0 min	26	29	~10
3.		–20	4 h	13**	12**	–

* in a mixture with **3**; ** consumption rate of **2** only 38%

128.34, 128.32, 128.28, 127.88, 127.81, 127.72, 127.68, 127.56 (C_{arom}, C-3'), 102.27 (C-5_{ur}), 98.58 (C-1), 93.47 (C-1'), 90.16 (C-1'$_{ur}$), 81.67 (C-4'$_{ur}$), 76.04 (C-4), 75.63, 73.45, 70.33 (C-3, C-2'$_{ur}$, C-3'$_{ur}$), 74.82, 70.23 (2 × CH_2Ph), 69.12 (C-4'), 67.09 (C-5'), 66.93 (C-5), 65.06 (C-5'$_{ur}$), 31.88 (C-2), 25.85, 25.78 (2 × C($\underline{C}H_3)_3$), 18.11, 18.03 (2 × $\underline{C}(CH_3)_3$), 17.29 (6-CH_3), 16.38 (6'-CH_3), –0.00, –4.17, –4.46, –4.85, –5.00 (2 × Si($\underline{C}H_3)_2$).

Glycoconjugate 5

Colorless syrup, α : β = 10 : 1; selected NMR data: ^{1}H-NMR (400 MHz, $CDCl_3$, δ, ppm): 8.91 (br.s, 1H, NH_{ur}), 8.15 (d, *J* = 8.2 Hz, 1H, H-6_{ur} α-isomer), 7.80 (d, *J* = 8.2 Hz, 1Hβ, H-6_{ur} β-isomer), 7.41–7.28 (m, 5H, H_{arom}), 6.20 (dd, *J* = 10.3, 5.1 Hz, 1H, H-3), 5.95 (dd, *J* = 10.1, 3.0 Hz, 1H, H-2), 5.75 (d, *J* = 1.6 Hz, 1H, H-1'$_{ur}$ β-isomer), 5.72 (d, *J* = 1.5 Hz, 1H, H-1'$_{ur}$ α-isomer), 5.48 (dd, *J* = 8.2, 2.3 Hz, 1H, H-5_{ur}), 5.08 (br.d, *J* = 2.9 Hz, 1H, H-1α), 4.98–4.95 (m, 1Hβ, H-1β) 4.66, 4.59 (qAB, *J* = 11.9 Hz, 2H, CH_2Ph), 4.27–4.17 (m, 2H, H-3'ur, H-5a'$_{ur}$), 4.10–4.00 (m, 1H, H-2'$_{ur}$, H-4'$_{ur}$), 4.03 (dq, *J* = 6.6, 2.6 Hz, 1H, H-5), 3.55–3.52 (m, 1H, H-5b'$_{ur}$), 3.51 (dd, *J* = 5.4, 2.7 Hz, 1H, H-4), 1.36 (d, *J* = 6.6 Hz, 3H, 6-CH_3), 0.91, 0.90 (2 × s, 18H, 2 × C($C\underline{H}_3)_3$), 0.17, 0.09, 0.08, 0.06 (4 × s, 12H, 2 × Si($C\underline{H}_3)_2$); ^{13}C-NMR (101 MHz, $CDCl_3$, δ, ppm): 163.37 (C=O), 150.11 (C-6_{ur}), 140.56 ($C_{IV\ arom}$), 138.26, 128.49, 128.44, 128.13, 127.81 (C_{arom}, C-2, C-3), 101.01 (C-5_{ur}), 94.08 (C-1), 90.16 (C-1'$_{ur}$), 81.82 (C-3'$_{ur}$), 76.15 (C-2_{ur}), 71.23 (CH_2), 70.10 (C-4'$_{ur}$), 68.94 (C-4), 66.97 (C-5), 64.49 (C-5'$_{ur}$), 25.83, 25.80 (2 × C($\underline{C}H_3)_3$), 18.11, 18.04 (2 × $\underline{C}(CH_3)_3$), 16.36 (6-CH_3), –4.23, –4.48, –4.91, –5.09 (2 × Si($\underline{C}H_3)_2$); LRMS (ESI): calcd. for $C_{34}H_{54}N_2O_8Si_2Na$ ($[M + Na]^+$): *m*/*z* 697.9619; found: *m*/*z* 697.7.

Glycoconjugate 6

Compound **6** (α-isomer, 16 mg, 10%) was isolated as an inseparable mixture (27 mg) with substrate **3** (mol ratio 1:1 – according to ^{1}H-NMR); ^{1}H-NMR (400 MHz, $CDCl_3$, δ, ppm): 8.93 (s, 1H, NH_{ur}), 8.88 (s, 1H, NH_{ur}), 7.92 (d, *J* = 8.2 Hz, 1H, H-6_{ur}), 7.61 (d, *J* = 8.1 Hz, 1H, H-6_{ur}), 7.41–7.28 (m, 5H, H_{arom}), 5.75 (dd, *J* = 8.2, 2.1 Hz, 1H, H-5_{ur}), 5.72 (dd, *J* = 8.3, 2.4 Hz, 1H, H-5_{ur}), 5.71 (d, *J* = 2.1 Hz, 1H, H-1'$_{ur}$), 5.47 (d, *J* = 5.3 Hz, 1H, H-1'$_{ur}$), 4.95 (d, *J* = 3.0 Hz, 1H, H-1α), 4.84, 4.69 (qAB, *J* = 11.6 Hz, 1H), 4.58–4.53 (m, 1H, H-2'$_{ur}$), 4.22–4.15 (m, 2H, H-3'ur, H-4'$_{ur}$), 4.11–4.07 (m, 2H, H-2'ur, H-4'$_{ur}$), 4.05 (dd, *J* = 12.1, 2.3 Hz, 1H, H-5a'$_{ur}$), 4.04 (dd, *J* = 7.3, 4.0 Hz, 1H, H-3'$_{ur}$), 3.94 (dd, *J* = 12.3, 2.1 Hz, 1H, H-5a'$_{ur}$), 3.93–3.87 (m, 1H, H-3), 3.85 (dq, *J* = 13.5, 6.8 Hz, 1H, H-5), 3.72 (br.dd, *J* = 12.2, 1.3 Hz, 1H, h-5b'$_{ur}$), 3.55 (d, *J* = 2.8 Hz, 1H, H-4), 3.47 (dd, *J* = 11.7, 2.4 Hz, 1H, H-5b'$_{ur}$), 3.02 (br.s, *J* = 15.6 Hz, 1H, 3-OH), 1.96 (dd, *J* = 12.1, 3.5 Hz, 1H, H-2_{eq}), 1.87 (dd, *J* = 12.8, 5.1 Hz, 1H, H-2_{ax}), 1.73–1.55 (m, 1H, OH), 1.28 (d, *J* = 6.6 Hz, 3H, H-6), 0.91, 0.89, 0.88 (3 × s, 36H, 2 × C($C\underline{H}_3)_3$), 0.17, 0.10, 0.09, 0.07, 0.07, 0.05, 0.04 (7 × s, 24H, 4 × Si($C\underline{H}_3)_2$); ^{13}C-NMR (101 MHz, $CDCl_3$, δ, ppm): 163.24, 163.08, 150.26, 149.97 (4 × C=O), 143.03, 139.84 (2 × C-6_{ur}),, 138.13 ($C_{IV\ arom}$), 128.61, 128.08, 128.07 (C_{arom}), 102.11, 101.53 (2 × C-5_{ur}), 98.40(C-1), 94.02, 90.34 (C-1), 86.16 81.66 (2 × C-4'$_{ur}$), 79.18 (C-4), 76.00 (C-2'$_{ur}$), 75.89 ($\underline{C}H_2$Ph), 73.56 (C-2'$_{ur}$), 71.71, 70.03 2 × (C-3'$_{ur}$), 67.06 (C-5), 66.19 (C-3), 65.04, 61.67 (2 × C-5'$_{ur}$), 33.61 (C-2), 25.81, 25.80, 25.78 (4 × C($\underline{C}H_3)_3$), 18.06, 18.05, 18.02, 17.94 (4 × $\underline{C}(CH_3)_3$), 17.31 (6-CH_3), –4.19, –4.44, –4.45, –4.63, –4.80, –4.87, –4.93, –5.11 (4 × Si($\underline{C}H_3)_2$).

General procedure for deprotection of *tert*-butyldimethylsilyl groups

To the solution of anhydrous Bu_4NF (87 mg, 0.340 mmol) in CH_3CN (1 mL) the solution of glycoconjugate **4** or **5** (0.034 mmol) in CH_3CN (1 mL) was added. The reaction mixture was stirred at room temperature for 30 min and monitored by TLC ($CHCl_3$: MeOH, 10 : 1, v/v). Then, the mixture was dissolved in chloroform (15 mL) and washed with saturated aq. solution of $NaHCO_3$ (20 mL) and water (20 mL). The organic phase was dried over anhydrous $MgSO_4$ and concentrated to give a crude residue, that was purified by column chromatography on silica gel with $CHCl_3$: MeOH (25 : 1, v/v) elution system to give corresponding products **7** and **8** (isolated only the α anomers).

Glycoconjugate 7

Colorless syrup, 67% yield, α-isomer, = 30.5 (*c* 0.4, MeOH). ^{1}H-NMR (400 MHz, $CDCl_3$, δ, ppm): 9.35 (s, 1H, NH_{ur}), 7.73 (d, *J* = 8.1 Hz, 1H, H-6_{ur}), 7.40–7.23 (m, 10H, H_{arom}), 6.15 (dd, *J* = 10.3, 4.9 Hz, 1H, H-3'), 5.91 (dd, *J* = 10.1, 3.0 Hz, 1H, H-2'), 5.82 (dd, *J* = 8.2, 1.4 Hz, 1H, H-5_{ur}), 5.78 (d, *J* = 3.6 Hz, 1H, H-1'$_{ur}$), 5.13 (d, *J* = 2.9 Hz, 1H, H-1'), 4.96 (d, *J* = 3.2 Hz, 1H, H-1α), 4.85, 4.61 (qAB, *J* = 11.6 Hz, 2H, CH_2Ph), 4.65, 4.57 (d, *J* = 11.9 Hz, 2H, CH_2Ph), 4.29–4.11 (m, 4H, H-5', H-2'$_{ur}$, H-3'$_{ur}$, H-4'$_{ur}$), 4.01 (m, 1H, H-3), 3.95 (dd, *J* = 11.7, 2.4 Hz, 1H, H-5a'$_{ur}$), 3.77 (q, *J* = 6.6 Hz, 1H, H-5), 3.56–3.49 (m, 3H, H-4, H-4', H-5b'$_{ur}$), 3.27 (s, 1H, OH), 2.23 (ddd, *J* = 12.7, 3.8 Hz, 1H, H-2_{eq}), 1.86 (dd, *J* = 12.9, 4.7 Hz, 1H, H-2_{ax}), 1.67 (s, 1H, OH),

1.31 (d, J = 6.7 Hz, 3H, 6'-CH_3), 1.18 (d, J = 6.5 Hz, 3H, 6-CH_3). ^{13}C-NMR (101 MHz, $CDCl_3$, δ, ppm): 182.67 (C=O), 163.11 (C=O), 139.58 (C-6_{ur}), 138.44, 138.43 (2 $C_{IV\ arom}$), 129.20 (C-2'), 128.39, 128.31, 128.27, 128.10, 127.79, 127.70, 127.68 ($C_{arom,}$ C-3'), 102.20 (C-5_{ur}), 98.95 (C-1), 93.53 (C-1'), 91.64 (C-$1'_{ur}$), 84.46 (C-$4'_{ur}$), 77.20, 76.00, 75.78, 74.82 (C-3, C-4, C-$2'_{ur}$, C-$3'_{ur}$), 73.20, 70.81 (2 ×x CH_2), 69.38 (C-4'), 67.32 (C-5'), 66.89 (C-5), 66.69 (C-$5'_{ur}$), 31.95 (C-2), 17.27 (6-CH_3), 16.44 (6'-CH_3); LRMS (ESI): calcd. for $C_{35}H_{42}N_2O_{11}Na$ ($[M + Na]^+$): m/z 689.7045; found: m/z 689.8.

Glycoconjugate 8

Colorless syrup, 85% yield, α-isomer, = 163.3 (*c* 0.73, MeOH); ^{1}H-NMR (400 MHz, $CDCl_3$, δ, ppm): 10.10 (br.s, 1H, NH_{ur}), 8.00 (d, J = 8.2 Hz, 1H, H-6_{ur}), 7.37–7.25 (m, 5H, H_{arom}), 6.18 (dd, J = 10.1, 5.1 Hz, 1H, H-3), 5.98 (dd, J = 10.1, 2.9 Hz, 1H, H-2), 5.86 (d, J = 2.1 Hz, 1H, H-$1'_{ur}$), 5.56 (dd, J = 8.2, 1.2 Hz, 1H, H-5_{ur}), 5.11 (d, J = 2.8 Hz, 1H, H-1), 4.65, 4.57 (qAB, J = 11.8 Hz, 2H, C$\underline{H_2}$Ph), 4.25–4.12 (m, 3H, H-$2'_{ur}$, H-$3'_{ur}$, H-$5a'_{ur}$), 4.03 (qd, J = 6.5, 2.6 Hz, 1H, H-5), 3.65 (dd, J = 11.2, 2.0 Hz, 1H, H-$5b'_{ur}$), 3.55–3.46 (m, 1H, H-$4'_{ur}$), 3.51 (dd, J = 5.2, 2.6 Hz, 1H, H-4), 1.78 (s, 1H, OH), 1.36 (d, J = 6.6 Hz, 3H, H-6). ^{13}C-NMR (101 MHz, $CDCl_3$, δ, ppm): 163.83 (C=O), 151.09 (C=O), 140.52 (C-6_{ur}), 138.24 ($C_{IV\ arom}$), 128.64 (C-2), 128.42, 127.98, 127.80 ($C_{arom,}$ C-3), 101.82 (C-5_{ur}), 94.54 (C-1), 90.63 (C-$1'_{ur}$), 83.42 (C_3'$_{ur}$), 75.29 (C-$2'_{ur}$), 71.15 (CH_2), 69.76 (C-$4'_{ur}$), 69.03 (C-4), 66.91 (C-5), 65.90 (C-$5'_{ur}$), 16.35 (6-CH_3); LRMS (ESI): calcd. for $C_{22}H_{26}N_2O_8Na$ ($[M + Na]^+$): m/z 469.4402, found: m/z 469.6.

(3-Azidopropyl) 3-*O*-[4-*O*-benzyl-2,3,6-trideoxy-α-L-*threo*-hex-2-enopyranosyl]-4-*O*-benzyl-2,6-dideoxy-L-*lyxo*-hexopyranoside (9)

To the mixture of disaccharide **2** (100 mg, 0.237 mmol) and 3-azidopropane-1-ol (0.02 mL, 0.284 mmol) in dry CH_2Cl_2 (3 mL) molecular sieves 4Å were added and the mixture was cooled to –10°C. Then, a catalytic amount (8 mg, 0.024 mmol) of triphenylphosphine hydrobromide (TPHB) in CH_2Cl_2 (1 mL) was added dropwise *via* syringe. After 15 min, the mixture was allowed to warm up to room temperature. The reaction was monitored by TLC (hexane : AcOEt, 2 : 1, v/v) and finally finished by addition of Et_3N (0.05 mL). Molecular sieves were filtered and solvent was evaporated under reduced pressure. The residue was purified by column chromatography (hexane : AcOEt, 10 : 1, v/v) to yield glycoside **9** (49 mg, 40%) as a colorless syrup; α : β 5 : 1; selected NMR data for the major α-isomer: ^{1}H-NMR (400 MHz, $CDCl_3$, δ, ppm): 7.42–7.23 (m, 10H, H_{arom}), 6.14 (ddd, J = 10.1, 5.3, 0.8 Hz, 1H, H-3'), 6.09–5.93 (m, 2Hβ, H-2', H-3' β-isomer), 5.91 (dd, J = 10.1, 3.1 Hz, 1H, H-2'), 5.20 (d, J = 3.0 Hz, 1H, H-1'), 5.16 (dd, J = 3.2, 1.5 Hz, 1H, H-1' β-isomer), 4.91 (d, J = 3.2 Hz, 1H, H-1α), 4.85, 4.64 (qAB, J = 11.7 Hz, 1H), 4.65, 4.57 (qAB, J = 11.9 Hz, 1H), 4.22 (ddd, J = 12.3, 4.8, 2.7 Hz, 1H, H-3), 4.17 (dq, J = 6.6, 2.7 Hz, 1H, H-5'), 3.81 (q, J = 6.6 Hz, 1H, H-5), 3.73–3.66 (m, 1H, C$\underline{H}$HO), 3.56–3.50 (m, 2H, H-4, H-4'), 3.42 (ddd, J = 7.8, 6.5, 5.1 Hz, 1H, CH$\underline{H}$O), 3.37 (ddd~td, J = 6.7, 1.7 Hz, 2H, C$\underline{H_2}N_3$), 2.20 (ddd~td, J = 12.4, 3.8 Hz, 1H, H-2_{eq}), 1.88 (ddd, J = 12.7, 5.0, 1.1 Hz, 1H, H-2_{ax}), 1.87–1.75 (m, 2H, CH_2), 1.35 (d, J = 6.7 Hz, 3H, 6'-CH_3), 1.18 (d, J = 6.5 Hz, 3H, 6-CH_3). ^{13}C-NMR (101 MHz, $CDCl_3$, δ, ppm): 138.70, 138.58 (2 $C_{IV\ arom}$), 129.41 (C-2'), 128.31, 128.25, 128.18, 128.00, 127.67, 127.59, 127.53 ($C_{arom,}$ C-3'), 97.88 (C-1), 92.86 (C-1'), 75.74 (C-4), 74.62 (CH_2Ph), 72.94 (CH_2Ph), 70.78 (C-3), 69.33 (C-4'), 66.66 (C-5), 66.52 (C-5'), 63.82 (CH_2O), 48.53 (CH_2N_3), 32.09 (C-2), 28.94 (CH_2), 17.30 (6-CH_3), 16.30 (6'-CH_3).

(3-Aminopropyl) 3-*O*-[4-*O*-benzyl-2,3,6-trideoxy-α-L-*threo*-hexopyranosyl]-4-*O*-benzyl-2,6-dideoxy-L-*lyxo*-hexopyranoside (10)

A solution of **9** (49 mg, 0.095 mmol) in methanol (4 mL) was hydrogenated in a Paar shaker flask at 1.5 atm. over 10% Pd/C (10 mg) for 30 min. After removal of the catalyst by filtration, the solvent was evaporated under reduced pressure. The crude product **10** was used in the next step without further purification.

Glycoconjugate 12

To the solution of 3-aminopropyl glycoside **10** (29 mg, 0.040 mmol) and the uridine derivative **11** (18 mg, 0.060 mmol) in dry THF (2 mL), 2-chloro-4,6-dimethoxy-1,3,5-triazine (11 mg, 0.060 mmol) was added. After 1 min, 4-methylmorpholine (0.009 mL, 0.080 mmol) was added and the reaction mixture was stirred for 30 min at room temperature. The reaction was monitored by TLC ($CHCl_3$: MeOH, 20 : 1, v/v). After completion, the reaction mixture was concentrated under reduced pressure, remaining solid was dissolved in CH_2Cl_2 (15 mL) and washed with sat. aq. $NaHCO_3$ (10 mL) and brine (10 mL). The organic layer was dried over anhydrous $MgSO_4$, the adsorbent was filtered off and the filtrate was concentrated to give a crude product. This was purified by column chromatography ($CHCl_3$: MeOH,

100 : l, v/v) to give **12** as a colorless syrup in 83% yield; α : β 4 : 1. Selected NMR data for the major α-isomer: ^{1}H-NMR (400 MHz, $CDCl_3$, δ, ppm): 9.28 (s, 1Hβ, NH_{ur}β), 9.20 (s, 1H, NH_{ur}), 7.43 (d, *J* = 8.1 Hz, 1H, H-6_{ur}), 7.40–7.19 (m, 10H, H_{arom}), 6.81 (t, *J* = 5.4 Hz, 1H, CH_2N<u>H</u>), 5.75–5.71 (m, 1Hβ, H-5_{ur}β), 5.68 (dd, *J* = 8.0, 2.0 Hz, 1H, H-5_{ur}), 5.51 (s, 1H, H-1'$_{ur}$), 5.31 (dd, *J* = 6.3, 2.2 Hz, 1H, H-3'$_{ur}$), 5.23 (dd, *J* = 6.3, 2.6 Hz, 1Hβ, H-2'$_{ur}$ β-isomer), 5.17 (dd, *J* = 6.3, 1.2 Hz, 1H, H-2'$_{ur}$), 5.13–5.09 (m, 1H, H-1'), 4.87, 4.64 (qAB, *J* = 11.6 Hz, 2H, CH_2Ph), 4.84 (d, *J* = 3.2 Hz, 1H, H-1), 4.68, 4.44 (qAB, *J* = 12.1 Hz, 2H, CH_2Ph), 4.57 (d, *J* = 2.2 Hz, 1H, H-4'$_{ur}$), 4.11 (ddd, *J* = 12.2, 4.6, 2.5 Hz, 1H, H-3), 4.02 (dq, *J* = 6.6, 1.3 Hz, 1H, H-5'), 3.78–3.71 (m, 1H, H-5), 3.68–3.58 (m, 1H, C<u>*H*</u>HO), 3.51 (br. s, 1H, H-4), 3.45–3.33 (m, 2H, CH<u>*H*</u>O, C<u>*H*</u>HNH), 3.29 (br.s, 1H, H-4'), 3.27–3.16 (m, 1H, CH<u>*H*</u>NH), 2.20 (ddd~td, *J* = 12.5, 3.8 Hz, 1H, H-2_{eq}), 2.15–1.64 (m, 5H, H-2_{ax}, H-2', H-3', CH_2), 1.53, 1.35 (2 × s, 6H, C(CH_3)$_2$), 1.29 (d, *J* = 6.5 Hz, 3Hβ, 6'-CH_3 β-isomer), 1.20 (d, *J* = 6.6 Hz, 3H, 6'-CH_3), 1.15 (d, *J* = 6.5 Hz, 3H, 6-CH_3), 1.07 (d, *J* = 6.5 Hz, 3Hβ, 6-CH_3 β-isomer). ^{13}C-NMR (101 MHz, $CDCl_3$, δ, ppm): 168.98 (<u>C</u>ONH), 162.88 (C=O), 150.01 (C=O), 144.32 (C-6_{ur}), 138.77, 138.54 (2 × C_{IV}Ph), 128.70, 128.23, 128.16, 128.12, 128.10, 127.87, 127.75, 127.55, 127.51, 127.45, 127.35 (C_{arom}), 113.62 (<u>C</u>(CH_3)$_2$), 102.51 (C-5_{ur}), 98.28 (C-1'$_{ur}$), 97.85 (C-1), 96.65 (C-1'), 88.21(C-4'$_{ur}$), 83.68 (C-3'$_{ur}$), 83.31 (C-2'$_{ur}$), 76.19 (C-4), 74.57 (C-3), 73.55 (CH_2Ph), 73.48 (C-4'), 70.85 (CH_2Ph), 66.98 (C-5), 66.80 (C-5'), 66.06 (CH_2O), 37.66 (CH_2NH), 31.76 (C-2), 28.72 (CH_2), 26.71, 24.92 (2 × C(<u>C</u>H_3)$_2$), 24.54, 21.24 (C-2', C-3'), 17.34 (6-CH_3), 17.18 (6'-CH_3); LRMS (ESI): calcd. for $C_{41}H_{53}N_3O_{12}Na$ ([M + Na]$^+$): *m*/*z* 802.8622; found: *m*/*z* 802.8.

RESULTS AND DISCUSSION

This contribution focuses on a design of potential GT inhibitors, mainly based on modifications of central building blocks of their natural donors. In our research, we decided to use L-fucal as glycosyl donor, which easily allows to obtain a number of 2,6-dideoxy-glycosides, by simple addition to 1,2-unsaturated bond. Deoxysaccharides ubiquitously occur in a number of structural fragments of natural products having biological activity and often play a key role in their mechanism of action.

We recently developed a novel approach for the synthesis of new doubly unsaturated disaccharides (17). This approach utilizes *in situ* generation of an active glycosyl donor *via* Ferrier-type rearrangement under phase-transfer conditions and subsequent reaction with a nucleophile. This concept was put into practice employing 4-*O*-benzyl-L-fucal **1** and afforded a disaccharide product containing 1,2- and 2,3-unsaturated hexoses **2** (Scheme 1). This moiety can be easily functionalized to give various deoxy saccharide derivatives such as L-oliose (2-deoxy-L-fucose) and L-rhodinose (2,3-dideoxy-L-fucose). These deoxy sugar units can be found in the structure of many biologically active natural products such as anthracycline antibiotics, cardiac glycosides, and aminoglycosides (18).

One of the most convenient methods for obtaining 2-deoxy-glycosides under mild conditions

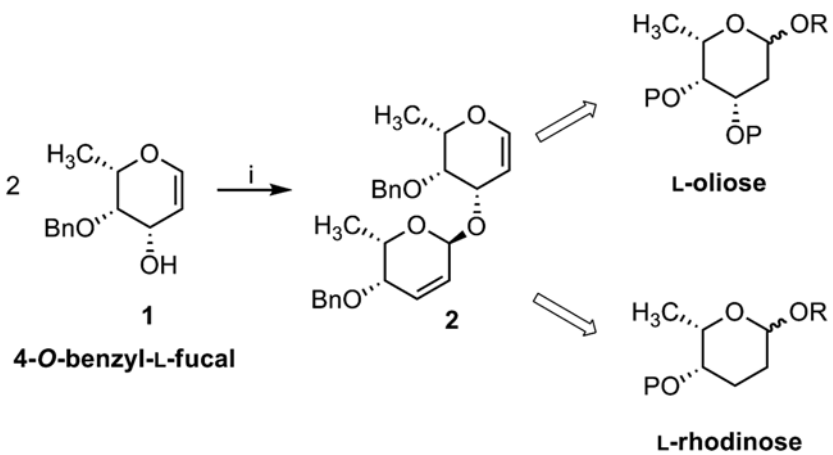

Scheme 1. Reagents and conditions: i) *p*TsCl, toluene, sat. aq NaOH, Bu_4NI, 40%

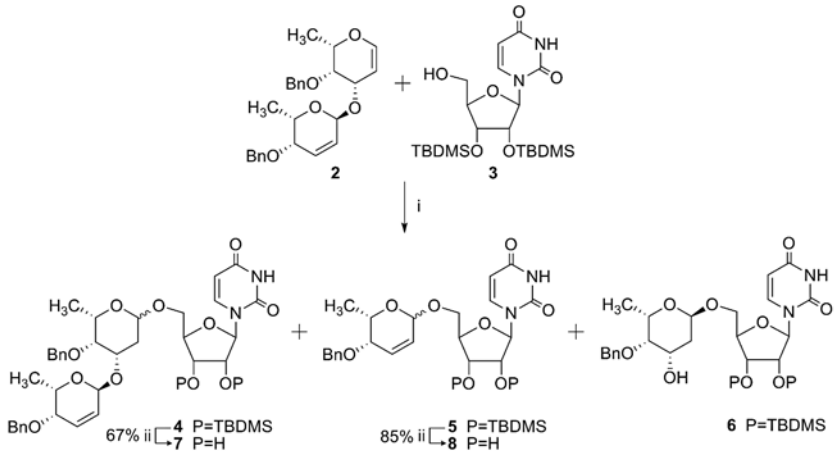

Scheme 2. Reagents and conditions: i) TPHB, CH_2Cl_2; ii) Bu_4NF, CH_3CN

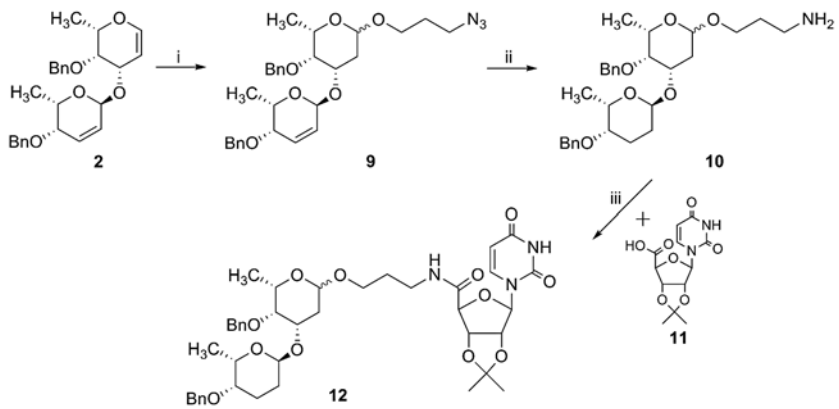

Scheme 3. Reagents and conditions: i) TPHB, CH_2Cl_2, r.t., 40%, α : β 5 : 1; ii) H_2, Pd/C, methanol; iii) DMTMM, THF, r.t., 83%

is addition of a nucleophile to the 1,2-unsaturated sugar bond in the presence of the triphenylphosphine hydrobromide (TPHB) (19). The addition of the uridine derivative **3** to the disaccharide glycal **2** was carried out in anhydrous CH_2Cl_2 in an ice-bath (Scheme 2, Table 1). The reaction gave a mixture of three glycoconjugates **4**, **5** and **6**. It can be assumed that products **5** and **6** are subsequent cleavage products of 2,3-unsaturated sugar unit from **4** and/or substrate **2**, and their reaction with another molecule of uridine derivative **3**. Probably the observed results can be explained by the high reactivity of the glycosidic bond of the disaccharide. The addition was carried out under different temperature conditions (Table 1). Evidently, with diminishing temperature an increase of the stability of the disaccharide is observed. However, with a substantial reduction of temperature (to –20°C) the reaction rate was significantly reduced resulting in incomplete conversion of the substrate. After deprotection of *tert*-butyldimethylsilyl groups the final uridine glycoconjugates **7** and **8** were isolated.

In order to obtain an amide bond with an uridine unit it was decided to attach it to the sugar using a three-carbon linker. Addition of 3-azidopropanol to the unsaturated disaccharide **2** and follow-up reduction led to obtain (3-aminopropyl) 3-*O*-[4-*O*-benzyl-α-L-rhodinosyl]-4-*O*-benzyl-2-deoxy-L-fucopyranoside **10**. The last step was condensation of **10** with uridine acid derivative **11** in the presence of (4,6-dimethoxy-1,3,5-triazin-2-yl)-4-methylmorpholinium chloride (DMTMM) generated *in situ* (20, 21) This final glycoconjugate **12** was obtained in excellent yield of 83%.

This novel approach provides ample opportunities for facile syntheses to various glycoconjugates as well as derivatives of natural biologically active products containing labile, multi-functional natural compounds as acceptors. All novel glycoconjugates are presently subject of further studies to evaluate their activity in enzymatic reactions of GTs.

Acknowledgment

Katarzyna Komor and Roman Komor gratefully acknowledge the receipt of scholarships under the project "DoktoRIS – Scholarship Program for Innovative Silesia".

REFERENCES

1. Glycoscience, Chemistry and Chemical Biology; Fraser-Reid B. O., Tatsuta K., Thiem J., Eds., Vols. 1–3, 2nd edn., Springer, Berlin 2008.
2. Becker D.J., Lowe J.B.: Glycobiology 13, 41R (2003).
3. Baisch G., Ohrlein R.: Bioorg. Med. Chem. 5, 383 (1997).
4. McDonald F.E., Wu M.: Org. Lett. 4, 3979 (2002).
5. Rohr J., Wohlert S.-E., Oelkers C., Kirschning A., Ries M.: Chem. Commun. 973 (1997).
6. Rusin A., Zawisza-Puchałka J., Kujawa K., Gogler-Pigłowska A., Wietrzyk J., Świtalska M., Głowala-Kosińska M. et al.: Bioorg. Med. Chem. 19, 295 (2011).
7. Goj K., Rusin A., Szeja W., Kitel R., Komor R., Grynkiewicz G.: Acta Pol. Pharm. Drug Res. 69, 1239 (2012).
8. Pastuch-Gawolek G., Bieg T., Szeja W., Flasz J.: Bioorg. Chem. 37, 77 (2009).
9. Krol E., Wandzik I., Szeja W., Grynkiewicz G., Szewczyk B.: Antiviral Res. 86, 154 (2010).
10. Kączkowski J.: Pol. J. Food Nutr. Sci. 12 (53), 3 (2003).
11. Weijers C., Franssen M., Visser G.: Biotechnol. Adv. 26, 436 (2008).
12. Berg S., Kaur D., Jackson M., Brennan P. J.: Glycobiology 17, 35R (2007).
13. Behr J.-B., Gainvors-Claisse A., Belarbi A.: Nat. Prod. Res. 21, 76 (2007).
14. Priebe W., Fokt I., Przewloka T., Krawczyk M., Skibicki P., Grynkiewicz G., Perez-Soler R.: PCT Int. Appl. WO 2000056267 A2 (2000).
15. Nomura M., Shuto S., Tanaka M., Sasaki T., Mori S., Shigeta S., Matsuda A.: J. Med. Chem. 42, 2901 (1999).
16. Meurillon M., Chaloin L., Périgaud C., Peyrottes S.: Eur. J. Org. Chem. 3794 (2011).
17. Komor K., Szeja W., Bieg T., Kuźnik N., Pastuch-Gawołek G., Komor R.: Tetrahedron Lett. (2014); DOI: 10.1016/j.tetlet.2014.05.025 (accepted manuscript).
18. Szeja W., Grynkiewicz G.: Top. Curr. Chem. 282, 249 (2008).
19. Bolitt V., Mioskowski C., Lee, S.-G.. Falck J.R.: J. Org. Chem. 55, 5812 (1990).
20. Kunishima M., Kawachi C., Hioki K., Terao K., Tani S.: Tetrahedron 57, 1551 (2001).
21. Kaminski Z.J.: Biopolymers 55, 140 (2000).

Acta Poloniae Pharmaceutica – Drug Research, Vol. 71 No. 6 pp. 1090–1094, 2014 ISSN 0001-6837
Polish Pharmaceutical Society

DETERMINATION OF THE VISCOSITY AND DENSITY OF VETERINARY VACCINES

DOROTA M. KRASUCKA[1], KATARZYNA KOS[1]*, ANETA D. WOŹNIAK[1] and WOJCIECH A. CYBULSKI[2]

[1]Department of Veterinary Pharmacy, [2]Department of Pharmacology and Toxicology, National Veterinary Research Institute, Al. Partyzantów 57, 24-100 Puławy, Poland

Keywords: dynamic viscosity, relative density, veterinary vaccines, monitoring

The quality of veterinary vaccines is monitored by physicochemical, microbiological and biological tests. Two of the most important physicochemical parameters are viscosity and density, which are determined in the three different types of matrices: emulsions, suspensions and solvents.

Viscosity, known as internal friction or viscose medium, is a feature of fluids and plastic solids characterized by their internal resistance against flowing. Viscosity is one of the most important property of fluids (1). Newton's law states that the force of the impact (friction) between layers of flowing liquid depends on their ratio, and the viscosity are directly proportional to the difference in flowing velocity of layers, and inversely proportional to the distance between them. Shear rate (Fig. 1) is the quotient of the velocity of liquid layers and the distance between them (2). According to the European Pharmacopoeia (3), there are two types of viscosity: dynamic and kinematic. The unit of dynamic viscosity (which is described in this paper) is the pascal × second (Pa·s). The most commonly used submultiple is the millipascal × second (mPa·s = cP).

According to the European Pharmacopoeia (4), the relative density of a substance is the ratio of the mass of a certain volume of a substance at tempera-

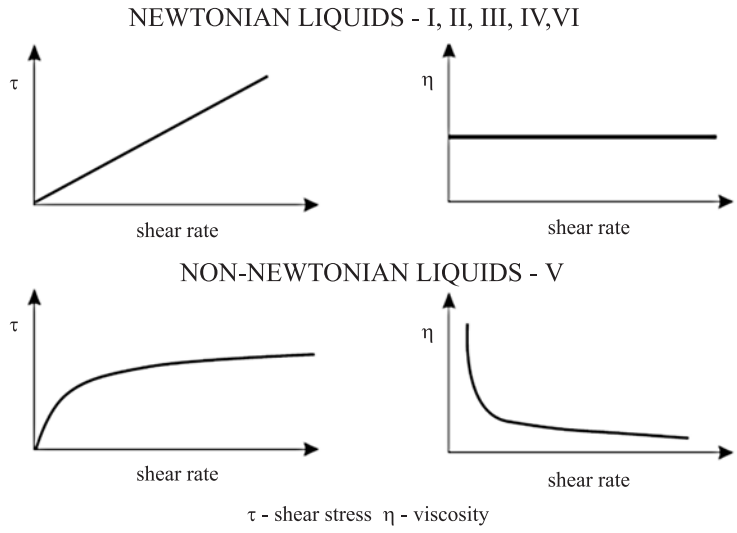

Figure 1. Shear stress. shear rate. and viscosity inter-relationship for vaccines as Newtonian and non-Newtonian liquids (explanation of vaccines symbols are in Table 1)

* Corresponding author: e-mail: katarzyna.pasik@piwet.pulawy.pl

ture t_1 to the mass of an equal volume of water at temperature t_2. Unless otherwise indicated, the relative density is used. Relative density is also commonly presented as density ρ20, defined as the mass of a unit volume of the substance at 20°C, expressed in kilograms per cubic meter or grams per cubic centimeter (1 kg/m^3 = 10^{-3} g/cm^3).

Viscosity and density are two of the most important parameters of vaccines' adjuvants like aluminium hydroxide or aluminium phosphate (5). The gels of this adjuvants are commonly used as adsorbents for antigens. All pre-formed gels are controlled by using internal standard methods, for example, determination of viscosity (6). Vaccine adjuvants improve immune responses to numerous antigens. Veterinary vaccines may contain a large number of adjuvants.

There are three types of emulsions used in veterinary medicine today. The first one are water-in-oil emulsions (W/O) that have a continuous oil phase. High viscosity makes these products difficult to inject. This emulsions induce a strong and long term immune response. The second type are oil-in-water emulsions (O/W). They have lower viscosity and thus are easier to inject. This emulsions are well tolerated and induce a short term immune response. The third type are the double emulsions: water-in-oil-in-water emulsions (W/O/W). These products are characterized by low viscosity but are less stable than the other two types. This multiphasic emulsions can induce short or long term immune responses depended on various antigens (7, 8). Burrel et al. studied the effect of sterilization on adjuvants without an antibody, which resulted in a decrease of the pH and a reduction of viscosity (9).

Beebe et. al. also monitored viscosity level in emulsion of vaccines. Measurements run at 0.1 intervals up to 3 months. A Brookfield RVDV-II Digital Viscometer with cone CP40 and sample cup CP-44Y equipped with a Neslab RTE-111 Refrigerated Bath Circulator were used to maintain a temperature of 25°C. The initial viscosity was 231 cP and remained stable over time, with a minimal decrease to 197 cP by 3 months and the results were expressed in centipoise units (cP). Analyses were carried out during the research on immunotherapy (10). Other findings proved that the viscosity of oily emulsions can reduce bacterial retention and filter capacity (11).

Yeu-Chun Kim et. al. reported that vaccine stability, as measured by an *in vitro* hemagglutination assay, was increased by decreased concentration of viscosity-enhancing compounds**.** They found that the influenza VLP vaccine could be coated onto microneedles and rapidly released into the skin or into solution. They also found that the inclusion of carboxymethylcellulose (CMC) used to increase viscosity of microneedles coating solution decreased vaccine activity (12).

In medicine, viscosity is an important parameter in the case of blood tests. Rajzer et al. described abnormal blood viscosity, accompanied by hypertension, atherosclerosis and stroke (2). There are scarce data found in the available literature devoted to stability of the veterinary vaccines in respect to methodological issues.

The aim of this study was to validate the method for determination of the viscosity and density of different types of veterinary vaccines.

MATERIALS AND METHODS

The linearity, repeatability, precision and uncertainty were comprised. Linearity was made at four levels of viscosity (within range 3.902–1110 mPa·s) and density (within range 0.81213–0.84262 g/cm^3) using Anton Paar company standards – SH L 122, M 116, H 120, C 120. Standards were used to check the instrument before each the day measurements. Six determinations of viscosity and density for each of six different vaccines were performed. All tested vaccines were of viral origin, except for the vaccine no. V, which was of bacterial origin.

Measurements of the viscosity and density were carried out by means of a rotational viscometer SVM 3000 with a density measurement, from Anton Paar (USA) with a fixed shear rate at 20°C. Rotating viscometers with simultaneous density measurement were used for measuring the viscosity of Newtonian (shear-independent viscosity, e.g., emulsions and solvents) or non-Newtonian liquids (shear dependent viscosity or apparent viscosity, e.g., suspensions) (13). The measurements were performed under the following conditions: ambient temperature of 18 to 25°C and relative humidity of 20 to 80% at the laboratory environment. The minimum quantity of sample dispensed into the measuring cell was optimized (2 mL).

The viscosity was measured in rotational viscometer with a cylinder geometry. It is based on a modified Couette principle with a rapidly rotating outer tube and an inner measuring bob which rotates more slowly. Rotational viscosity measurement is based on a torque and speed measurement. A rotating magnet in SVM 3000 produces an eddy current field with an exact speed dependent brake torque. The eddy current torque is measured with extremely high resolution. Combined with the integrated ther-

moelectric thermostating, this ensures unparalleled precision. The torque resolution is an unmatched 50 pico-Nm. That's why it only requires a very compact measuring cell. The very small measuring cell contains a tube which rotates at a constant speed. This tube is filled with the sample. A measuring rotor with a built-in magnet is floating in the sample. The low density of the rotor allows it to be centered by the centrifugal force. The freely swimming rotor requires no bearing – as it is not followed by a friction. This also makes the instrument insensitive to vibration. The small sample volume allows extremely quick temperature changes (Peltier) and very short equilibrium times. Shortly after the start of the measurement, the rotor reaches a stable speed. This is determined by the equilibrium between the effect of the eddy current brake and the shear forces at work in the sample. The dynamic viscosity is calculated from the rotor speed.

In order to calculate the kinematic viscosity from the dynamic viscosity, the density of the sample must be known. For this reason, SVM 3000 also has a density measuring cell that employs the well-known oscillating U-tube principle. Both cells are filled in one cycle. The measurements are carried out simultaneously (14).

All vaccines materials used in this studies are presented in Table 1. Before tests, the samples were stored at 2 to 8^{o}C. Tests were performed on six vaccines: (I) the vaccine against egg drop syndrome EDS'76, inactivated; (II) vaccine against feline rhinotracheitis birds, inactivated; (III) the vaccine against birds' reovirus infections, inactivated; (IV) rabies vaccine, calcivirose, viral rhinotracheitis and feline panleucopenia; (V) the vaccine against fungal infection of the skin of cattle, inactivated; (VI) the vaccine against myxomatosis and rabbit hemorrhagic disease of rabbits.

RESULTS AND DISCUSSION

Optimization of viscosity and density determination let to obtain very reproducible results. The maximum scatter of results (CV) for the viscosity was 3.87%, while the density was 0.261%. These results of measurements were for the suspension. It was the only bacterial vaccine in this study. For other types of vaccines, scattering measurements of viscosity did not exceed 1.7% and for a density did not exceed 0.09%. Based on the validation and subsequent monitoring studies, it was observed that the viscometer with a density measurement did not allow to obtain reliable results of viscosity and density determination of the suspensions (non-Newtonian liquids). The reason for this situation was the inability to change the settings of shear rate. Parameters of repeatability and precision of the viscosity and density determination are presented in Tables 2 and 3. The uncertainty of the viscosity were determined at 3.26% and density at 0.25% level. The method of dynamic viscosity was linear with r^2 = 1.000000. The method of relative density was linear with r^2 = 0.999995.

The main challenge in this research was to eliminate contamination of measuring apparatus after each analysis. Vaccines are an extremely diverse group of matrices. Each vaccine is an individual composition so that it was necessary to select of appropriate organic solvents for cleaning the instrument. Isopropanol, acetone and hexane were the most effective solvents. A sign of an effective apparatus purification were density less than 0.001

Table 1. Form of vaccines used in analysis.

Symbol	Form of vaccine	The commonly used name
I	emulsion for injection for chickens	the vaccine against egg drop syndrome EDS'76, inactivated
II	emulsion for injection for chickens	vaccine against feline rhinotracheitis birds, inactivated
III	emulsion for injection for chickens	the vaccine against birds' reovirus infections, inactivated
IV	lyophilizate and solvent for emulsion for injection for cats	rabies vaccine, calcivirose, viral rhinotracheitis and feline panleukopenia
V	suspension for injection	the vaccine against fungal infection of the skin of cattle, inactivated
VI	lyophilized, and suspension for injection	the vaccine against myxomatosis and rabbit haemorrhagic disease of rabbits

Table 2. Analytical and validation parameters of dynamic viscosity determination. Results of analysis for six different vaccines (explanation of vaccines symbols are in Table 1).

VALIDATION FEATURE		**VALIDATION RESULTS OF DYNAMIC VISCOSITY**					
LINEARITY	y = ax + b	y = 0.9980x – 0.4055 x – the level of plasma concentrations of analyte					
	r^2	1.000000					
	RANGE [mPa·s]	3.902 – 1110					
VETERINARY VACCINES		I	II	III	IV	V	VI
REPEATABILITY	$\bar{x}$	101.143	89.671	99.610	4.330	1.412	1.193
	s	0.728	0.774	0.969	0.070	0.055	0.013
	CV	0.720	0.863	0.972	1.611	3.870	1.130
PRECISION	$\bar{x}$	89.671	89.717	90.133	-	-	-
	S	0.774	0.205	0.400	-	-	-
	CV	0.863	0.228	0.444	-	-	-
UNCERTAINTY	$u_c(y)$ 1	1.63 %					
	k	2					
	U	3.26 %					

Table 3. Analytical and validation parameters of relative density determination. Results of analysis for six different vaccines (explanation of vaccines symbols are in Table 1).

VALIDATION FEATURE		**VALIDATION RESULTS OF RELATIVE DENSITY**					
LINEARITY	y = ax + b	y = 0.9765x + 0.0193 x – the level of plasma concentrations of analyte					
	r^2	0.999995					
	RANGE [mPa·s]	0.81213 – 0.84262					
VETERINARY VACCINES		I	II	III	IV	V	VI
REPEATABILITY	$\bar{x}$	0.918	0.916	0.914	0.964	1.006	1.007
	s	0.001	0.001	0.001	0.001	0.003	0.001
	CV	0.085	0.070	0.086	0.074	0.261	0.077
PRECISION	$\bar{x}$	0.916	0.917	0.917	-	-	-
	S	0.001	0.001	0.001	-	-	-
	CV	0.070	0.075	0.063	-	-	-
UNCERTAINTY	$u_c(y)$ 1	0.125 %					
	k	2					
	U	0.25 %					

g/cm^3 in dried measuring cell. Analysis of the literature data presented maximum values for the viscosity and density of veterinary vaccines – maximum 450 mPa·s and maximum of 1.05 g/cm^3.

Viscosity and density are two of the most important quality parameters of liquid vaccines that determine their stability. These parameters are officially controlled in Poland during the market monitoring research. The above-described method was set up, validated and used in this monitoring in years 2011–2013 and till now. Test specimens were randomly sampled from the market by inspection officers of pharmacovigilance from various pharmaceutical wholesalers across the country. Bioproducts

were intended to different animal species vaccination – poultry, cats, cattle and rabbits. Twenty seven vaccines were analyzed for density and six vaccines were analyzed for viscosity according to official EU actual guidelines.

Further investigation will be viscometry with a density measurement to explore dependence of viscosity and density on temperature.

REFERENCES

1. Bańkowski Z., Gajewski W.: Encyclopedia of Technics. Chemistry. (Polish). WNT, Warszawa 1965
2. Rajzer M., Palka I., Kawecka-Jaszcz K.: Arterial Hypertension 11, 1 (2007).
3. European Pharmacopoeia 1, p. 27 (2014).
4. European Pharmacopoeia 1, p. 25 (2014).
5. Sesardic D., Dobbelaer R.: Vaccine 22, 2452 (2004).
6. Matheis W., Zott A., Schwanig M.: Vaccine 20, 67 (2002).
7. Macy D.W.: Vaccine Adjuvants, Semin. Vet. Med. Surg. 12, 206 (1997).
8. Aucouturier J., Dupuis L., Ganne V.: Vaccine 19, 2666 (2001).
9. Capelle M.A.H., Brugger P., Arvinte T.: Vaccine 23, 1686 (2005).
10. Beebe M., Qin M., Moi M., Wu S., Heiati H., Walker L, Newman M. et. al.: Hum. Vaccin. 4, 210 (2008).
11. Carbrello C., Rogers M.: BioPharm Int. suppl. Vaccine development and manufacturing: pandemics and beyond. pp. 21–26 (2010).
12. Kim Y.-C., Quan F-S., Compans R.W., Kang S.-M., Prausnitz M.R.: AAPS PharmSciTech, 11, 1193 (2010).
13. European Pharmacopoeia 1, p. 28 (2014).
14. Manufacturer's operating instructions of SVM 3000. Copyright Anton Paar GmbH, Graz, Austria (2002).

Acta Poloniae Pharmaceutica – Drug Research, Vol. 71 No. 6 pp. 1095–1102, 2014 ISSN 0001-6837
Polish Pharmaceutical Society

TRANSCRIPIONAL ACTIVITY OF GENES ENCODING MMPs AND TIMPs IN BREAST CANCER CELLS TREATED BY GENISTEIN AND IN NORMAL CANCER-ASSOCIATED FIBROBLASTS – *IN VITRO* STUDIES

MAŁGORZATA LATOCHA[1]*, JUSTYNA PŁONKA[1], DARIUSZ KUŚMIERZ[1], MAGDALENA JURZAK[2], RENATA POLANIAK[3] and ADA NOWOSAD[1]

[1]Medical University of Silesia in Katowice, School of Pharmacy with the Division of Laboratory Medicine, Department of Cell Biology, Jedności 8, 41-200 Sosnowiec, Poland
[2]Medical University of Silesia in Katowice, School of Pharmacy with the Division of Laboratory Medicine, Department of Cosmetology, Kasztanowa 8, 41-200 Sosnowiec, Poland
[3]Medical University of Silesia in Katowice, School of Public Health, Department of Nutrition, Jordana 19, Zabrze 41-808, Poland

Keywords: genistein, matrix metalloproteinases (MMPs), tissue inhibitors of metalloproteinases (TIMPs)

Abbreviations: *BCL-2*, *BCL-XL*, *IAP*, *XIAP* – inhibitors of apoptosis genes; *BRCA1*, *BRCA2*, *CHEK*, *TP53* – human tumor suppressor genes; CDK1 – cyclin-dependent kinase 1; EMMPRIN – extracellular matrix metalloproteinase inducer; ERα, ERβ – estrogen receptors (α, β); HB-EGF – heparin-binding EGF-like growth factor; HER2 – epidermal growth factor receptor 2; IGFBP-3 – insulin-like growth factor binding protein 3; IL-1β – interleukin 1β; MAPK – mitogen-activated protein kinases; MMP-1 – matrix metalloproteinase-1 (collagenase-1) encoded by the *MMP-1* gene; MMP-2 – matrix metalloproteinase-2 (gelatinase A) encoded by the *MMP-2* gene; MMP-3 – matrix metalloproteinase-3 (stromelysin-1) encoded by the *MMP-3* gene; MMP-9 – matrix metalloproteinase-9 (gelatinase B) encoded by the *MMP-9* gene; MMP-13 – matrix metalloproteinase-13 (collagenase-3) encoded by the *MMP-13* gene; MMP-14 – matrix metalloproteinase-14 (membrane-inserted, interact with TIMP-2) encoded by the *MMP-14* gene; MMP-15 – matrix metalloproteinase-15 (membrane-inserted) encoded by the *MMP-15* gene; $P21^{WAF1}$, $P27^{KIPI}$, $P16^{INK4a}$ – regulators of cell cycle progression; PGR – progesterone receptor; PTK – protein tyrosine kinase; Real-Time RT-QPCR – Real Time Reverse Transcription Quantitative Polymerase Chain Reaction; TIMP-1 – metalloproteinase inhibitor 1 encoded by the *TIMP-1* gene; TIMP-2 – metalloproteinase inhibitor 2 encoded by the *TIMP-2* gene; TIMP-3 – metalloproteinase inhibitor 3 encoded by the *TIMP-3* gene; TGF-β – transforming growth factor β; TNF-α – tumor necrosis factor α; VEGF – vascular endothelial growth factor; Wee-1 – CDK1 inhibitor

According to National Cancer Registry, breast cancer is one of the most common cancer among women in Poland, accounting for 23% of all new cases of cancer in females and it is the leading cause of cancer death in women (1). The highest incidence rates occur in females in 25–50 age group. Its etiology is very complex and the molecular mechanisms involved are still poorly understood. Around 5–10% of cases is linked to familial (hereditary) breast cancer (2). Most inherited cases of breast cancer are associated with abnormal genes: *BRCA1, BRCA2, TP53, CHEK* (3, 4). The deregulation of expression of proteins from BCL-2 family which control apoptosis process is also very common during tumorigenesis (5). The heterogeneity in breast cancer includes a diversity between clinical parameters such as tumor size, lymph node involvement, histological grade, biomarkers like estrogen receptor (ER), progesterone receptor (PGR) and epidermal growth factor receptor 2 (HER2) routinely used in the diagnosis and treatment of patients (6). The standard treatment used in breast cancer is surgery. Anyway, the chemotherapy and hormonotherapy is often a necessary step because of the spread of a tumor from one organ to another non-adjacent organ. Thus, the scientists are still looking for the new efficient therapeutic methods of treatment which allow to kill cancer cells and avoid metastasis.

Phytoestrogens are currently in the center of attention because of their therapeutic and preventive

* Corresponding author: e-mail: mlatocha@sum.edu.pl; phone: +48 32 364 12 11

proprieties. Genistein (Fig. 1) is a naturally occurring plant compound from the group of phytoestrogens which possess many therapeutic activities, such as antioxidant and anticancer properties. It is well known that genistein is capable of inducing the programmed cell death, inhibiting the proliferation, stimulating of differentiation and reducing metastasis (7). Its mechanisms of action include inhibition of topoisomerase I and II, DNA polymerase II and downexpression of genes encoding cyclins: B1 and D1, as well as CDK-1 and Wee-1. Furthermore, it suppress expression of anti-apoptotic genes: *BCL-2*, *BCL-XL*, *IAP*, *XIAP*, *survivin* (8, 9). What is more, genistein upmodulates P53, $P21^{WAF1}$, $P27^{KIPI}$, $P16^{INK4a}$ in many cancer cells (9, 10). It acts also as a non-specific inhibitor of tyrosine kinases which are the factors involved in many signaling pathways controlling cell proliferation and survival (11). It was confirmed that it is able to promote differentiation in cancer stem-like cells (12). The similarity in chemical structure to natural 17β-estradiol leads to the high affinity to hormone-binding proteins and to both isoforms of estrogen receptors (ERα and ERβ) (13). It was demonstrated that at physiological concentration (around 10^{-9} M), genistein acts as an agonist of estrogens but it causes biological effects through both: ER- and non-ER-mediated pathways, which contributes to decreasing the estrogens level in blood *via* inhibition of aromatase activity which is responsible of converting androgens to females hormones (13). The ability of inducing angiogenesis by cancer cells seems essential in the metastatic spread of cancer. New growth in the vascular network provides oxygen and nutrients to the tumor tissues and allows malignant cells to disseminate to other parts of the body where they form secondary tumor. The experiments with xenograft tumors have demonstrated that genistein supress angiogenesis though regulation of genes encoding VEGF, PTK, MAPK and decreases proteolysis of cancer-associated tissue (14). This mechanism is linked to activity of matrix metalloproteinases and their tissues inhibitors.

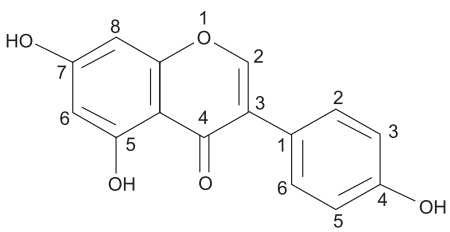

Figure 1. Chemical structure of genistein

Matrix metalloproteinases (MMPs) and their tissues inhibitors (TIMPs) are synthesized, by many cells – the normal and the cancer ones. The mutual interactions between neoplastic cells and their stroma are a well known phenomenon which leads to promote tumor development and progression.

It is well known that the transcritptional activity of genes encoding MMP-1 is correlated with molecular subtype of breast cancer cell. Thus, *MMP-1* is overexpressed in cancer associated stromal cells in Luminal B but not in Luminal A or ER- breast cancer, while the synthesis of *MMP-1* in tumor cells seems to be independent from their immunophenotypic characterization (15). It was demonstrated that the level of mRNA *MMP-1* in tumor cells had an independent prognostic value as a marker of disease outcome (16). Metalloproteinases -2 and -9, which belong to gelatinases family, share similar proteolytic activity against denatured collagens, gelatins and various extracellular matrix molecules and their overexpression is associated with acquisition of invasive potential by cancer cells (17). Metalloproteinase 3 is a member of the stromelysin subfamily which have a large repertoire of ECM and non-matrix substrates (18). *MMP*-3 is expressed in many types of cells including keratinocytes, fibroblasts and chondrocytes. Thus, it contributes to remodeling microenvironement and it could be a key player in breast cancer progression (19). Futhermore, MMP-3 is able to activate many factors involved in cell growth and proliferation like TGF-b, HB-EGF, IGFBP-3, TNF-a and IL-1b (20).

The regulation of metalloproteinases is complex and occurs at many levels (expression, activa-

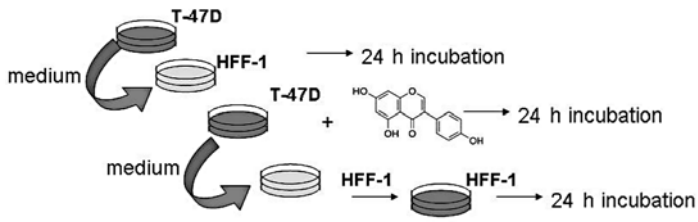

Figure 2. Experiment scheme

tion, inhibition of proteolytic activity). One of many factors involved in regulation of their expression is glycoprotein EMMPRIN (extracellular matrix metalloproteinase inducer) that is enriched on the surface of tumor cells. EMMPRIM stimulates production of several matrix metalloproteinases, mostly MMP-1, MMP-2 and MMP-3 by adjacent stromal cells (21).

Tissue inhibitors of metalloproteinases (TIMPs) are endogenous protein regulators of the matrix metalloproteinases. Four members of TIMPs family have been characterized so far, designated as TIMP-1, TIMP-2, TIMP-3 and TIMP-4. All of them are capable of inhibiting the activities of all known metalloproteinases but with different substrate specificity. They bind to the zinc catalytic site of MMPs, thus they inhibit their proteolytic activity. On the other hand, they can also bind to zymogen forms of MMPs and activate them. Recently, it was demonstrated that TIMPs are involved in regulation of cell fate by MMP-independent mechanism. Their role in induction or prevention of apoptosis was confirmed by many *in vitro* and *in vivo* studies (22).

The aim of this study was to examine the impact of genistein on genes involved in MMPs and TIMPs synthesis in breast cancer cells and normal fibroblasts stimulated by medium derived from T-47D cultures.

EXPERIMENTAL

Cell culture

T-47D (human breast cancer cells) and HFF-1 (normal newborn human foreskin fibroblasts) were purchased from the American Type Culture Collection (ATCC). T-47D is slightly invasive hormone-dependent breast cancer cell line, subtype Luminal A, that responds to hormonotherapy. The low level of the Ki-67 antigen implies their low proliferation index. This line express also progesterone receptor (PR+), calcitonin, androgen receptor (AR+), prolactin and normal levels of HER2 (HER2 0/1+).

T-47D and HFF-1 cells were cultured in Nunc 75 cm flasks. As a cell culture medium, DMEM (LONZA, Switzerland) with glutamine, containing 10% heat inactivated FBS (Biological Industries, Israel), penicillin (10000 u/mL) and streptomycin (10 mg/mL) (Biological Industries, Israel) was used. T-47D cells were incubated 24 h, then they were treated with genistein at a concentration of 50 μM (Sigma-Aldrich, USA) for 24 h. In parallel, HFF-1 culture was performed, to which DMEM derived from T-47D cells were added for 24 h (Fig. 2).

RT-QPCR

After the incubation, the cells were proceeded to RNA isolation and purification using Quick-RNA™ MiniPrep Zymo-Spin™ columns (Zymo Research Corporation, USA)**.** The concentration and quality of isolated RNA was determined by measuring the absorbance at 230, 260, 280 and 320 nm in a spectrophotometer HP8452A (Hewlett Packard, USA). Quantitation of the genes encoding MMP-1, -2, -3 -9, -13, -14, -15 and tissue inhibitors of metalloproteinases: TIMP-1, -2, -3 was done using RT-QPCR (DNA Engine OPTICON™ (MJ Research, USA)) with kit QuantTect® SYBR® Green RT-PCR (Qiagen GmbH, Germany).

Statistical analysis

Statistica PL 9.0 software was used to carry out statistical analysis. The amounts of mRNA copies of genes of interest were presented as a mean value of 3 samples. To compare the results, Student's *t*-test for unpaired samples was used. The equality of variances were verified by the F-test (Fisher's test), whereas the normal distribution was confirmed by Shapiro-Wilk test.

RESULTS

The results of analysis of genes in T-47D and HFF-1 cells after 24 h of treatment with genistein at concentration of 50 μM are illustrated in Figures 3 and 4. The mRNA copy numbers of *MMP-1, MMP-2, MMP-3, MMP-9, MMP-13, MMP-14, MMP-15, TIMP-1, TIMP-2, TIMP-3* were compared between: A) T-47D control cells and T-47D treated by genistein; B) HFF-1 control cells (24 h in medium derived from T-47D control cells) and HFF-1 in medium from T-47D treated by genistein. Statistical significance is indicated with star ($p \leq 0.05$). In T-47D culture, the presence of genistein downregulated expression of genes encoding: MMP-2, MMP-3, MMP-13, MMP-15, TIMP-1, TIMP-2, TIMP-3, but the statistical significance was observed only for *MMP-2* and *TIMP-1, TIMP-2, TIMP-3*. The similar effects were observed in HFF-1 cells but, in this case, the significant differences were obtained for genes encoding MMP-1, MMP-3, MMP-13, MMP-14 and MMP-15.

DISCUSSION and CONCLUSION

One of the most important properties of cancer cells is their ability to spread from their original site. During this process, cells need to cross many barriers formed by ECM. First, they must break away

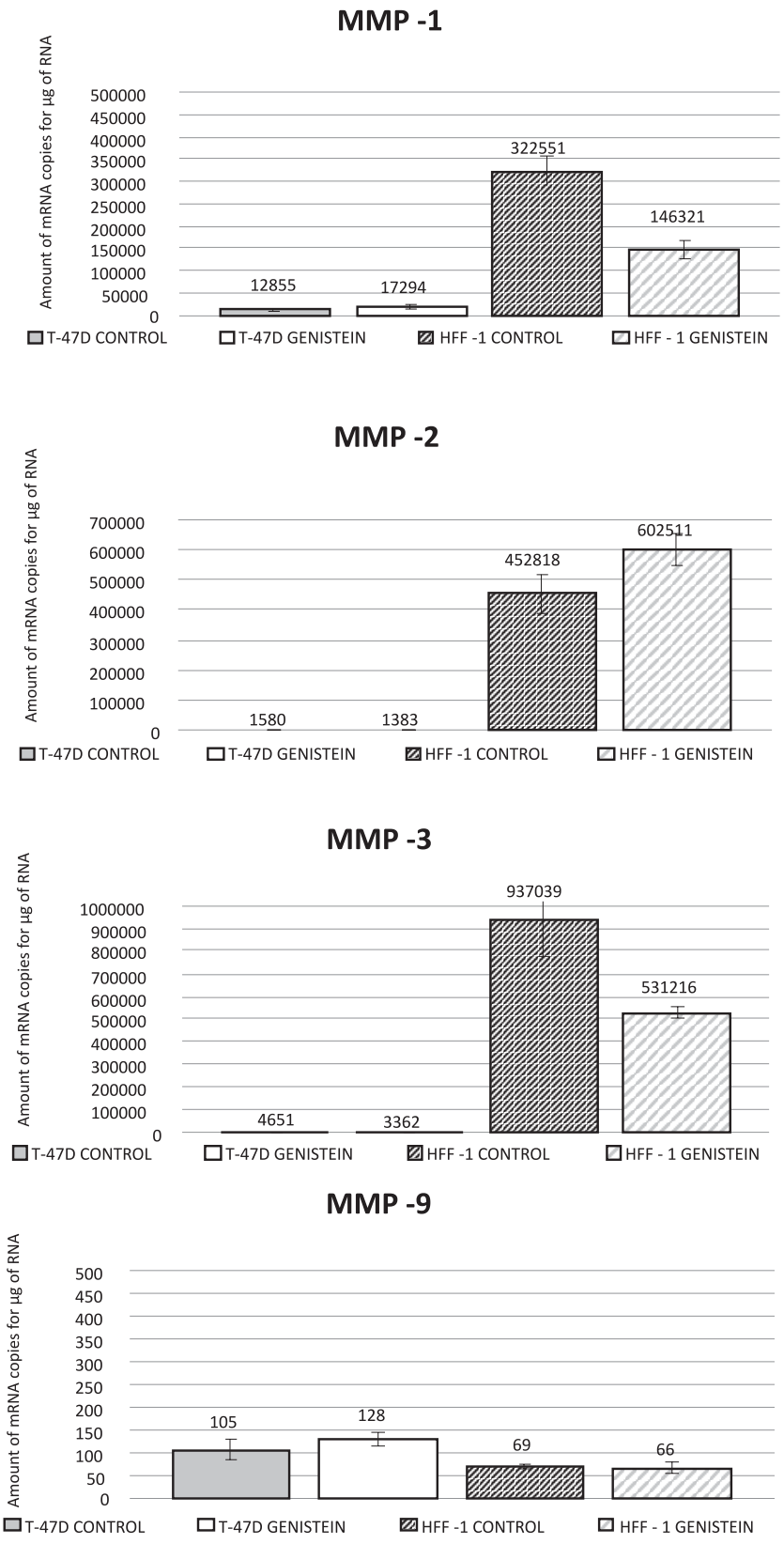

Figure 3. The influence of genistein on expression of genes encoding MMPs in breast cancer cells T-47D and in fibroblasts HFF-1 incubated with culture medium derived from T-47D treated by genistein

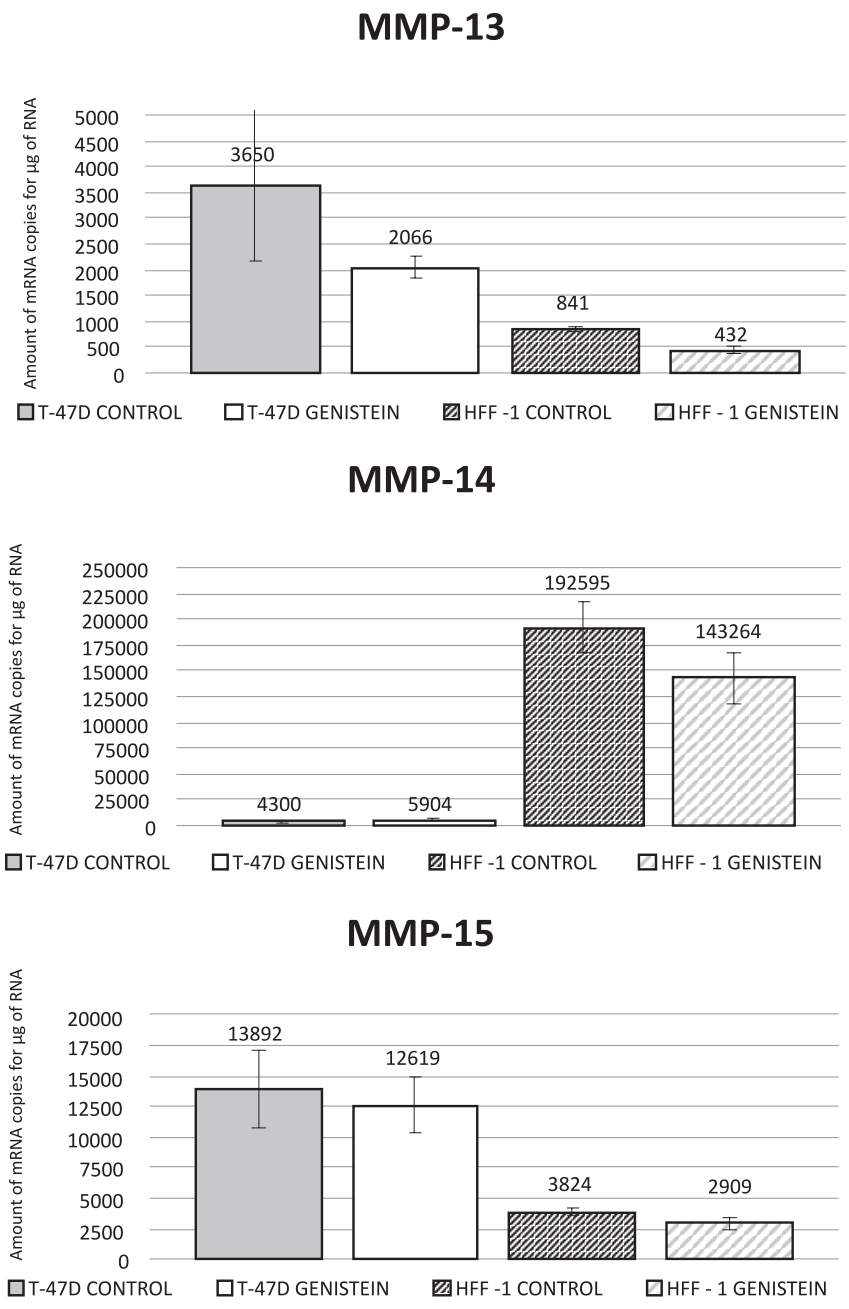

Figure 3. cont.

from its stroma, then navigate through the basal lamina of mesenchymal cells and invade either the circulatory or lymph system (intravasation), migrate through the vessel's walls to the new location (extravasation) and establish secondary tumors, capable of proliferation. Matrix metalloproteinases contribute in metastasis *via* their proteolytic activity which is responsible for degradation of ECM proteins such as fibronectin, vitronectin, laminin, collagen fibrils, entacin, tenascin, aggrecan. Thus, they participate in cleavage and remodeling of basal lamina and ECM components (17).

To determinate the ability of genistein to suppress metastasis process, its influence on expression of genes encoding MMPs (MMP-1, MMP-2, MMP-3, MMP-9, MMP-13, MMP-14, MMP-15) and TIMPs (TIMP-1, TIMP-2, TIMP-3) in breast cancer ductal carcinoma and in cancer-associated fibro-

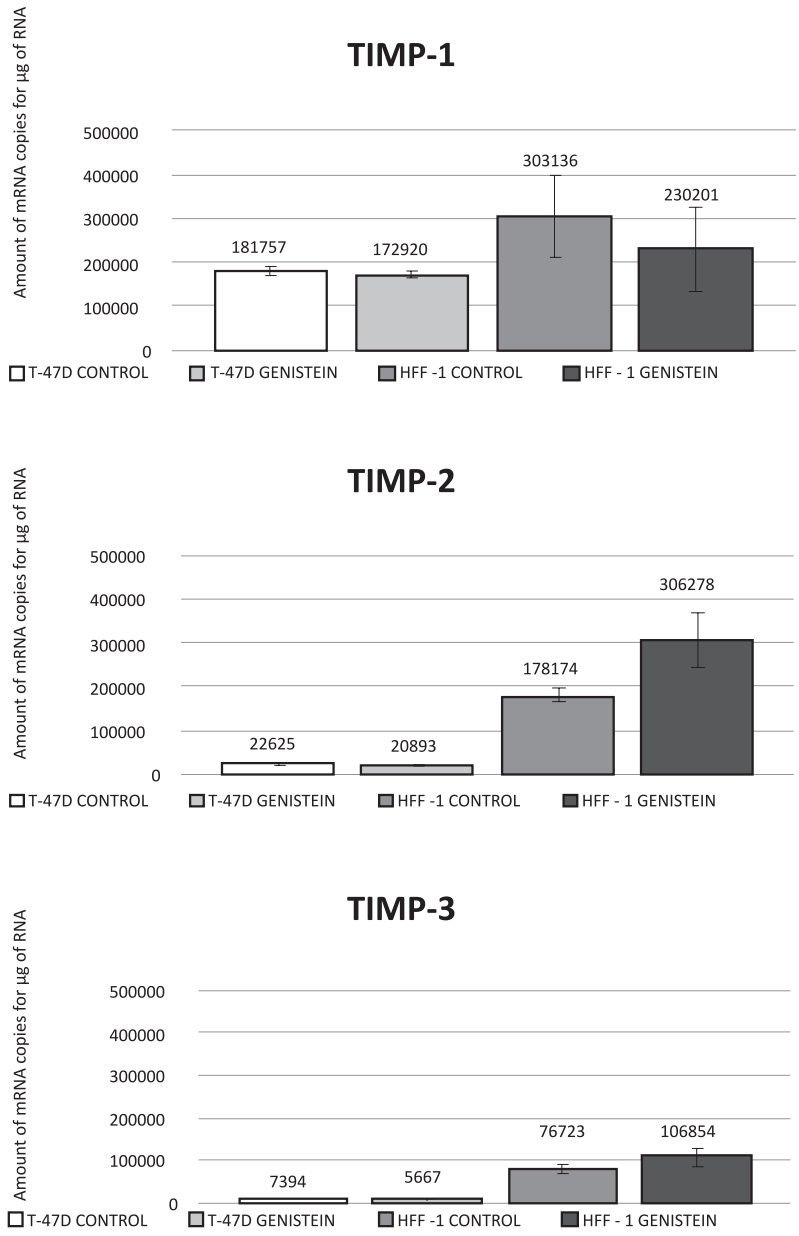

Figure 4. The influence of genistein on expression of genes encoding TIMPs in breast cancer cells T-47D and in fibroblasts HFF-1 incubated with culture medium derived from T-47D treated by genistein

blasts (normal fibroblasts exposed to factors excreted by cancer cells treated by genistein (50 µM for 24 h) to their culture medium) was investigated.

In this study, was used T-47D breast cancer cell line, which derived from metastatic site, thus the metalloproteinases level was increased regarding to the early stages of cancer. Anyway, the low level of antigen Ki-67 implicates the low invasive potential of these cells.

After 24 h of incubation with genistein, a non-statistically significant increase of *MMP-1* expression in cancer cells was observed, whereas the expression of *MMP-1* in HFF-1 was downregulated when they were treated by genistein. The expression of *MMP-1* has a prognostic value in breast cancer and *in vitro* studies showed that a high *MMP-1* mRNA level is associated with poor prognosis and development of metastasis (15). The ability of

genistein to down express MMP-1 in stromal cells could be used in treatment of advanced disease to avoid metastases, especially to bone tissues (23).

Many previous studies indicated MMP-9 as a main target of genistein (16). Results of this study revealed a significant difference in the amount of mRNA *MMP-2* copies in cancer cells exposed to genistein but the expression of both genes in control cells was relatively low regarding other metalloproteinases.

Metalloproteinase 3 (MMP-3) contributes to remodeling microenvironment and it could be a key player in breast cancer progression (19). In the present work, it was demonstrated that genistein can decrease *MMP-3* expression in both: T-47D and HFF-1 cells but the statistically significant result was observed only in fibroblasts.

MMP-13, also known as collagenase-3, has large substrate specificity, including type II of collagen and gelatin (24). The exposure to genistein was responsible for downregulation of *MMP-13* transcription in both cells type.

MMP-14 (MT1-MMP) and MMP-15 (MT2-MMP) are classified as membrane-type matrix metalloproteinases. They are involved in the regulation of cell-ECM interaction and the activation of the pro-MMPs by their cleavage (18). They initiate the activation of pro-MMP-2 and pro-MMP-13. The overexpression of MT-MMPs (especially MT1-MMP) is observed in many types of cancer cells as well as stromal cells. Results of this study indicated, that genistein induces the expression of *MMP-14* and *MMP-15* in fibroblasts cultured with medium derived from T-47D with genistein.

In this study, the expression of genes encoding extracellular tissue inhibitors of metalloproteinases (TIMP-1, TIMP-2, TIMP-3) was also investigated. Genistein downregulated expression of all three members of TIMPs family analyzed in this work: *TIMP-1*, *TIMP-2* and *TIMP-3* in T-47D cells. According to an analysis of previous studies, TIMP-1 has been clearly demonstrated to exert a protective effect on breast cancer cells against apoptosis. Hence, overexpression of TIMP-1 is correlated with poor prognosis in patients (25). What is more, TIMP-1 is responsible of activation of pro-MMP-9 to its active form, which promote angiogenesis and progression of disease (25–27). The mechanisms by which TIMP-1 inhibit programmed cell death are still poorly understood but its effect can be mediated by phosphorylation (activation) of Akt kinase and an increase of expression of anti-apoptotic proteins such as BCL-X_L and BCL-2 (27). The decrease of TIMP-1 expression caused by genistein is consistent with hypothesis that genistein exert its anticancer functions *via* intrinsic pathway of apoptosis and suppress angiogenesis mediated by MMP-9. Futhermore, its role as inhibitor of Akt activation (28) leads to decrease in tumor cell proliferation induced by TIMP-1. In fibroblasts exposed to medium derived from T-47D treated by genistein, it was observed the downregulation of expression of *TIMP-1* but upregulation of *TIMP-2* and *TIMP-3* (no statistically significant differences). TIMP-2 was confirmed to restrain metastasis though inhibition of MMPs activity, but on the other side, TIMP-2 has confirmed anti-apoptotic activity (29). TIMP-3 also participate in signaling pathways controlling programmed cell death, but unlike TIMP-1 and TIMP-2, it induces apoptosis in tumor cells. It acts *via* stabilization of TNFR1 on the cell surface that is involved in TNF-α-mediated apoptosis (26). In many breast cancer cases, the genes encoding TIMP-3 acquire abnormal hypermethylation, which results in transcriptional silencing of this factor (30).

In the present work, it was demonstrated that genistein has the influence on the expression of MMP-1, -3, -13, -14 -15 and TIMP-1 in T47D and in HFF-1 cells in the way that implies its capacity to inhibit the process of angiogenesis and metastasis. Though this effect *in vitro* is not unequivocal, it can be helpful in clinical practice to decrease the risk of angiogenesis and increase survival of patients with breast cancer. Thus, it seems extremely important to continue the research on genistein to fully understand all mechanisms of action by which it exerts its anticancer effects.

Acknowledgment

This work was supported by grant KNW-1-023/K/3/0 from the Medical University of Silesia in Katowice (Poland).

REFERENCES

1. Bączek I.: Rynek Zdrowia [doi: 19-03-2013] [http://www.rynekzdrowia.pl/Uslugi-medyczne/Nowotwory-zlosliwe-w-Polsce-znamy-najnowsze-dane-epidemiologiczne, 128987,8,0.html] (Polish).
2. Janssens J., Vandeloo M.: Nowotwory – J. Oncology 59, 159 (2009) (Polish).
3. Arnold A.G., Otegbeye E., Fleischut M.H., Glogowski E.A., Siegel B., Boyar S.R., Salo-Mullen E. et al.: Breast Cancer Res. Treat. 145, 625 (2014).

4. Manoukian S., Peissel B., Frigerio S., Lecis D., Bartkova J., Roversi G., Radice P. et al.: Breast Cancer Res. Treat. 130, 207 (2011).
5. Hamed E.A., Zakhary M.M., Maximous D.W.: J. Cancer Res. Clin. Oncol. 138, 999 (2012).
6. Eroles P., Bosch A., Pérez-Fidalgo J.A., Lluch A.: Cancer Treat. Rev. 38, 6, 698 (2012).
7. Tiulea C., Peev C., Brezovan D., Dehelean C., Motoc A.: Rom. J. Morphol. Embryol. 52 (Suppl. 3), 1065 (2011).
8. Nichols J.A., Katiyar S.K.: Arch. Dermatol. Res. 302, 71 (2010).
9. Tarkowski M., Latocha M., Kokocińska M.: Pol. Merkur. Lekarski 34 (199), 54 (2013) (Polish).
10. Das A., Banik N.L., Ray S.K.: Cancer 116, 164 (2010).
11. Li Y.S., Wu LP., Li K.H., Liu Y.P., Xiang R., Zhang S.B., Zhu L.Y., Zhang L.Y.: J. Int. Med. Res. 39, 2141 (2011).
12. Rajah T.T., Du N., Drews N., Cohn R.: Pharmacology 84, 68 (2009).
13. Dai S.Y., Burris T.P., Dodge J.A., Montrose-Rafizadeh C., Wang Y., Pascal B.D., Chalmers M.J., Griffin P.R.: Biochemistry 13, 48, 9668 (2009).
14. Yu X., Zhu J., Mi M., Chen W., Pan Q., Wei M.: Med. Oncol. 29, 349 (2012).
15. Boström P., Söderström M., Vahlberg T., Söderström K.O., Roberts P.J., Carpén O., Hirsimäki P.: BMC Cancer 11, 348 (2011).
16. Roy R., Yang J., Moses M.A.: J. Clin. Oncol. 27, 31, 5287 (2009).
17. Lewandowska U., Owczarek K., Szewczyk K., Podsedek A., Koziołkiewicz M., Hrabec E.: Post. Hig. Med. Dosw. 68, 110 (2014).
18. Ra H.J., Parks W.C.: Matrix Biol. 26, 587 (2007).
19. Slattery M.L., John E., Torres-Mejia G., Stern M., Lundgreen A., Hines L., Giuliano A., Baumgartner K., Herrick J., Wolff R.K.: PLoS One 16, 8, e63165. [doi: 10.1371/journal.pone.0063165] (2013).
20. Tvorogov D., Anisimov A., Zheng W., Leppänen V.M., Tammela T., Laurinavicius S., Holnthoner W. et al.: Cancer Cell 14, 18, 630 (2010).
21. Siu A., Chang J., Lee C., Lee S., Lee C., Ramos D.M.: J. Calif. Dent. Assoc. 41, 831 (2013).
22. Fink K., Boratyński J.: Post. Hig. Med. Dosw. 66, 609 (2012).
23. Eck S.M., Hoopes P.J., Petrella B.L., Coon C.I., Brinckerhoff C.E.: Breast Cancer Res. Treat. 116, 79 (2009).
24. Vandenbroucke R.E., Dejonckheere E., Van Hauwermeiren F., Lodens S., De Rycke R., Van Wonterghem E., Staes A. et al.: EMBO Mol. Med. 5, 932 (2013).
25. Bigelow R.L., Williams B.J., Carroll J.L., Daves L.K., Cardelli J.A.: Breast Cancer Res. Treat. 117, 31 (2009).
26. Monroy A., Kamath S., Chavez A.O., Centonze V.E., Veerasamy M., Barrentine A., Wewer J.J. et al.: Diabetologia 52, 2169 (2009).
27. Nalluri S., Gayatri S., Ohja J., Rojiani A.M., Rojiani M.V.: Cancer Res. 72 (8), (Suppl.) , abstract 4955 (2012).
28. Pavese J.M., Farmer R.L., Bergan R.C.: Cancer Metastasis Rev. 29, 3, 465 (2010).
29. Londero A.P., Calcagno A., Grassi T., Marzinotto S., Orsaria M., Beltrami C.A., Marchesoni D., Mariuzzi L.: Virchows Arch. 461, 589 (2012).
30. Rivenbark A.G., Coleman W.B.: Exp. Mol. Pathol. 93, 391 (2012).

Acta Poloniae Pharmaceutica – Drug Research, Vol. 71 No. 6 pp. 1103–1106, 2014 ISSN 0001-6837
Polish Pharmaceutical Society

CYP2C9 GENE POLYMORPHISM IN THE PHARMACOLOGICAL TREATMENT OF LONG QT PATIENTS

SŁAWOMIR SMOLIK*, EWA MORIC-JANISZEWSKA and LUDMIŁA WĘGLARZ

Department of Biochemistry, Medical University of Silesia,
Jedności 8, 41-200, Sosnowiec, Poland

Keywords: CYP2C9, genetic polymorphism, long QT syndrome

The family of cytochrome CYP450 enzymes consists of more than 30 enzymes which are the major mediators of phase I metabolism of drugs and endogenous compounds. Genetic polymorphism of CYP450 enzymes can lead to adverse drug reaction or inadequate response to commonly prescribed doses of the therapeutic agents (1). CYP2C9 represents the most abundant form among human CYP2C isoforms and comprises approximately 20% of the total hepatic CYP450 content. It participates in the metabolism of number of drugs including non-steroidal anti-inflammatory agents, S-warfarin, phenytoin, tolbutamide and losartan (2). Polymorphism in the CYP2C9 gene seriously affects the toxicity of drugs, with S-warfarin in particular, and may lead to severe and life-threatening bleeding episode (3). Three variants of the CYP2C9 allele denominated as CYP2C9*1, CYP2C9*2 and CYP2C9*3 have been found in Caucasian population,. The mutant alleles CYP2C9*2 and CYP2C9*3 differ from the wild-type CYP2C9*1 by a point mutation, i.e., CYP2C9*2 is characterized by a C416T exchange in the exon 3 resulting in Arg144Cys substitution, whereas CYP2C9*3 has an exchange of A1061C in exon 7 causing Ile359Leu substitution. Both allelic variants are associated with reduced catalytic activity compared to the wild type; they are reported to show approximately 12% (CYP2C9*2) and less than 5% (CYP2C9*3) of the wild-type enzyme activity (4, 5).

Long QT syndrome is a rare inherited disorder of ion channels that may cause dangerous heart rhythms in response to exercise or stress. Inherited long QT syndrome affects about 1 among 7000 people. To date, mutations in 11 genes have been discovered and described as being relevant for this disease. The LQT1 type is caused by mutation in the KCNQ1 gene and is found in approximately 50–60% of cases. The LQT2 type can be caused by mutations in HERG gene and it is found in 30–35% of clinical cases (6, 7). The treatment of long QT syndrome is intended to prevent abnormal heartbeats, decrease hypertension and improve lipid profile and function of platelets. The treatment options include antiarrhythmic and antihypertensive agents (i.e., losartan), cholesterol lowering drugs, supplementation of potassium and anticoagulants (i.e., S-warfarin) (8).

The metabolism of the anticoagulant drug S-warfarin was found to be markedly lowered in patients having mutant CYP2C9 alleles. Moreover, a strong association was demonstrated between CYP2C9 variant alleles and low S-warfarin dose requirement, as well as a higher risk of bleeding complications, so it was suggested that dose adjustment of S-warfarin in patients carrying 2C9 allelic variants might be worthwhile in order to lower the risk of drug intoxication and bleeding (9). CYP2C9 genotype contributes to inter-individual differences in losartan activation and its hypotensive effect (10). Evaluation of losartan in the elderly showed that losartan reduced the QT dispersion in elderly patients with heart failure, so it may reduce mortality of long QT patients (11). Polymorphism of CYP2C9 has strong influence on long QT patients drug therapy and its allelic variants may cause severe adverse reaction. The purpose of the present study was to investigate the prevalence of the

* Corresponding author: e-mail: epimer@wp.p

CYP2C9*2 and CYP2C9*3 allelic variants in the group of 104 patients with long QT and discuss their clinical implication in the modern pharmacotherapy of long QT syndrome.

EXPERIMENTAL

Clinical study

A group of 104 patients sufferngi from long QT syndrome (58 males and 46 females, mean age 49 ± 12 years) were recruited for genotyping study after approval by the local ethics committee. The diagnosis of syndrome was based on clinical examination of patients, which was performed according to guidelines issued by Polish Cardiology Society. All patients had QTc interval > 440 ms for men and 450 ms for women. The exclusion criteria were QTc at baseline and history of additional risk factor (hypokalemia, heart failure, left ventricular hypertrophy).

ASA-PCR genotyping

Genomic DNA was extracted from the 5 mL whole blood samples with the use of Genomic Prep Plus method (A&A Biotechnology, Gdynia, Poland). Allele-specific amplification (ASA-PCR) was developed for genotyping CYP2C9*2 and CYP2C9*3 alleles. Each reaction mix included an external pair of primers (named forward and reverse) and two allele-specific primers, carrying either the wild type nucleotide or the mutant nucleotide in the 3' position. PCR would amplify the region between the wild type primer and the reverse external primer only if the wild type allele was present. Inversely, amplification of the region between the internal mutation specific primer and the forward external primer would occur only if the mutant allele was present. Wild type and mutant amplicons can be distinguished by a fragment size. A third fragment, which represents the region between the two external primers, was also generated and served as an internal control. The following reaction mixture was prepared for tetra-primer PCR assay to genotype CYP2C9*2: 100 ng of genomic DNA, 0.5 U of Taq DNA polymerase (Novazym, Poznań, Poland), a final concentration 1 × PCR buffer, 1.5 mM of $MgCl_2$, 100 μM of each dNTP, and primers as follows: CYP2C9E3-F (0.24 μM), CYP2C9E3-R (0.16 μM), CYP2C9E3-T-F (0.16 μM), CYP2C9E3-C-R (0.24 μM) (Genomed, Warszawa, Poland). The mixture volume was adjusted to 25 μL with water. Primer sequences are listed in Table 1. The following thermal conditions were used: 95°C for 2 min for initial denaturation, and then 10 cycles at 95°C for 20 s, 66°C for 45 s and 72°C for 45 s, 20 cycles at 95°C for 20 s, 63°C for 45 s and 72°C for 45 s, and a final extension at 72°C for 5 min. In order to genotype the CYP2C9*3 polymorphism four primers were combined in one tetra-primer PCR assay. These were: CYP2C9E7-F (0.2 μM), CYP2C9E7-R (0.2 μM), CYP2C9E7A-F (0.2 μM) and CYP2C9E7C-R (0.2 μM) (Genomed, Warszawa, Poland. The other reaction mixture ingredients were identical to the ones applied for CYP2C9*2. The following thermal conditions were used: 95°C for 2 min for initial denaturation, 10 cycles at 95°C for 20 s, 59°C for 45 s and 72°C for 45 s, 20 cycles at 95°C for 20 s, 57°C for 45 s and 72°C for 45 s, and a final extension at 72°C for 5 min (12, 13). Primer sequences are listed in Table 1. The PCR products were separated by polyacrylamide gel electrophoresis and visualized by silver staining. The length of the ASA-PCR products were established based on the comparison with marker DNA with the use of BAS SYS 1D program (Biotec Fisher, Perth, Australia).

Table 1. Primers used for ASA-PCR.

Target	Primer	Sequence 5'→ 3'
CYP2C9*2	CYP2C9E3-F	AATAGTAACTTCGTTTGCTGTTATCTC
	CYP2C9E3-R	CAGTAGAGAAGATAGTAGTCCAGTAAGGT
	CYP2C9E3T-F	GGAAGAGGAGCATTGAGGACT
	CYP2C9E3C-R	GGGCTTCCTCTTGAACACG
CYP2C9*3	CYP2C9E7-F	GCCATTTTTCTCCTTTTCCAT
	CYP2C9E7-R	GGAGAACACACACTGCCAGA
	CYP2C9E7A-F	GCACGAGGTCCAGAGATACA
	CYP2C9E7C-R	TGGTGGGGAGAAGGTCAAG

All data were analyzed using the Statistica version 10 software. Differences in the distribution of all analyzed CYP genotypes were performed with χ^2 test. Differences were considered statistically significant at p value ≤ 0.05.

RESULTS

Amplification of CYP2C9*2 with the use of the external forward and external reverse primers yielded a 581 bp PCR product, amplification with CYP2C9E3T-F and external reverse primers indicating the presence of a T allele yielded a 127 bp product, amplification with CYP2C9E3C-R and external forward primers, indicating the presence of a C allele, yielded a 493 bp product. Amplification of CYP2C9*3 with the use of external forward and external reverse primers yielded a 434 bp product, amplification with CYP2C9E7A-F and external reverse primers, presenting the A allele, yielded a 295 bp product, amplification with CY2C9E7C-R and external forward primers presenting the C allele, yielded a 177 bp product.

Genotyping of CYP2C9*2 revealed that 2 persons were homozygous for the defective CYP2C19*2 allele, heterozygosity for CYP2C19*2 was found in 17 individuals. For the CYP2C9*3 polymorphism, 10 of 104 individuals carried the CYP2C9*3 allele (one of them was homozygous, 9 showing heterozygosity).

The allelic frequencies and final genotype distribution in investigated group of patients are shown in Table 2. Statistical analysis did not reveal any significant statistical differences between observed in European population and predicted genotype frequencies, however, the study group is too small to evaluate the frequency of CYP2C9 *2 and * 3 alleles in the Polish population. In statistical analysis, the British frequency of CYP2C9*2 and *3 alleles was used (14).

DISCUSSION AND CONCLUSION

CYP2C9 exhibits a genetic polymorphism and to date more than 35 allelic variants have been described. The two most common allelic variants are CYP2C9*2 and CYP2C9*3 which occur in approximately 85% of poor metabolizers and their frequencies are reported to range 10% to 14% and 6 to 7%, respectively, for Caucasian population, but are relatively rare in Asian and African populations (15). Both of these polymorphisms lead to reduced activity of CYP2C9 which can influence on the therapy with S-warfarin and losartan, the drugs commonly prescribed for long QT patients.

Warfarin is a natural product and given as racemic mixture of the R and S stereoisomers of the drug. S-warfarin is 3–5 times more potent an inhibitor of the vitamin K epoxide reductase complex, the target of action, than R-warfarin. The stereoisomers are metabolized by different phase 1 enzymes; the predominant metabolism of the S isomer is *via* CYP2C9 whereas metabolism of R-warfarin is mainly *via* CYP3A4 with involvement of CYP1A1, CYP1A2, CYP2C8, CYP2C9, CYP2C18 and CYP2C19 (16). Both CYP2C9*2 and CYP2C*3 cause a reduction in S-warfarin clearance with 10-fold variation observed from the genotype with the highest (CYP2C9*1/*1) to the one with the lowest (CYP2C9*3/*3) activity (*1/*1 > *1/*2 >*1/*3 > *2/*2 > *2/*3 > *3/*3). The effect of CYP2C9*3/*3 genotype is the most severe one with clearance of S-warfarin being 10% of the wild type genotype (17). According to the clinical studies, individuals with CYP2C9*1/*2 and *1/*3 genotypes require 10–20% and 20–50% lower average maintenance doses of warfarin, respectively, compared to wild type individuals. The CYP2C9*2 allele seems to have less influence on the dose of acenocoumarol or phenprocoumon compared to warfarin. It is important to identify the subjects having both polymor-

Table 2. Number and frequencies of variant alleles of CYP2C9*2 and CYP2C9*3 in a cohort of long QT patients.

Genotype	Number of individuals	Observed frequency (%)	Frequency in European population (%)
CYP2C9*1/*1	75	72	80.9
CYP2C9*1/*2	17	16	19.1
CYP2C9*2/*2	2	2	0.2
CYP2C9*1/*3	9	9	8.5
CYP2C9*3/*3	1	1	0.05

phisms as poor metabolizers because of them having the highest susceptibility to severe and life-threatening episodes when treated with anticoagulants. Numerous guidelines have been published on the use of pharmacogenomic test in dosing of S-warfarin, two algorithms are recommended that both provide reliable and very similar results (18).

Losartan is a selective angiotensin II receptor antagonist used in the treatment of hypertension in long QT patients. After oral administration, approximately 14% of the losartan dose is converted to E-3174. The E-3174 metabolite is at least 10-fold more potent than losartan. *In vitro* and *in vivo* studies have demonstrated that losartan is metabolized by CYP3A4 and CYP2C9 to E-3174 (19). Oxidation of losartan was significantly reduced in liver microsomes from individuals homozygous for the CYP2C9*3 allele or homozygous for the CYP2C9*2 allele compared with CYP2C9*1 (approximately 30- and 4-fold, respectively). Individuals with slow CYP2C9 metabolism showed an impaired therapeutic response to losartan, but still there is no algorithm of pharmacogenomic dosing of this drug (20, 21).

The presented assay allow rapid genotyping of CYP2C9 alleles and decrease the chance of contamination intrinsic to the generally used two-step procedures. The method used in the study is very simple and provides results of genotyping theoretically within 3 h. To increase the efficiency and facilitate genotyping, a real-time PCR method with fluorometric melting point analysis of PCR product was developed. The real-time PCR method produced 100% reliable results as confirmed by sequencing, however the costs of genotyping with use the hybridization probe are higher than the costs for conventional PCR genotyping. Method presented in this paper is more time-consuming but less expensive than sequencing and real-time PCR assays (22).

Molecular genetic analysis constitutes a determinative tool for the definitive validation of the right dose of the drug to the right patient. Genotyping for CYP2C9 allelic variants can be carried out rapidly and at low cost by ASA-PCR based assays. When genotyping is to be performed in all patients before starting treatment with losartan or S-warfarin, drugs often used in some of long QT patients, it should be adjusted in the high-risk individuals at the initiation of treatment. This procedure, together with serum drug concentration monitoring, will facilitate and accelerate a proper drug dosing, with a lower risk of intoxications, which contributes to the individualization and optimalization of pharmacotherapy patients with long QT syndrome.

REFERENCES

1. Samer C., Lorenzini K., Rollason V., Daali Y., Desmeules J.: Mol. Diagn. Ther. 17, 165, (2013).
2. Yip V., Pirmohamed M.: Am. J. Cardiovasc. Drugs 151, 13 (2013).
3. Eby C.: Semin. Thromb. Hemost. 661, 38 (2012).
4. Flachsbart F., Ufer M., Kleindorp R., Nikolaus S., Schreiber .S, Nebel A.: J. Gerontol. A Biol. Sci. Med. Sci. 66, 1186 (2011).
5. Hiratsuka M.: Drug Metab. Pharmacokinet. 27, 68 (2012).
6. Priori S., Cerrone M.: Ital. Heart J. 6, 241 (2001).
7. Goldenberg I., Zaręba W., Moss A.: Curr. Probl. Cardiol. 33, 629 (2008).
8. Visscher H., Amstutz U., Sistonen J., Ross C., Hayden M., Carleton B.: J. Cardiovasc. Pharmacol. 58, 228 (2011).
9. Hamberg A., Wadelius M.: Pharmacogenomics 15, 361 (2014).
10. Bae J., Choi C., Lee H., Lee Y., Jang C., Lee S.: Int. J. Clin. Pharmacol. Ther. 50, 683 (2012).
11. Feichao X., Caiping M., Yali H., Can R., Zhice X., Lubo Z.: Curr. Med. Chem. 16, 3841 (2009).
12. Spohn G., Geisen C., Luxembourg B., Sittinger K., Seifried E., Bonig H.: Mol. Diagn. Ther. 13, 15 (2011).
13. Arvanitidis K., Ragia G., Iordanidou M., Kyriaki S., Xanthi A., Tavridou A., Manolopoulos V.: Fundam. Clin. Pharmacol. 21, 419 (2007).
14. Xie H., Prasad H., Kim R., Stein M.: Adv. Drug Deliv. Rev. 54, 1257 (2002).
15. Smires F., Habbal R., Moreau C., Assaidi A., Loriot M., Nadifi S.: Pathol. Biol. 61, 88 (2013).
16. Rettie A., Korzekwa K., Kunze K., Lawrence R., Eddy A., Aoyama T., Gelboin H. et al.: Chem. Res. Toxicol. 5, 1 (1992).
17. Daly A.K.: Arch. Toxicol. 87, 407 (2013).
18. Cavallari L., Kittles R., Perera M.: N. Eng. J. Med. 18, 1763 (2014).
19. Stearns R., Chakravarty P., Chen R., Chiu S.: Drug Metab. Dispos. 2, 207 (1995).
20. Yasar U., Forslund-Bergengren C., Tybring G., Dorado P., Llerena A., Sjöqvist F., Eliasson E., Dahl M.: Clin. Pharmacol. Ther. 71, 89 (2002).
21. Hatta F., Teh L., Helldén A., Hellgren K., Roh H., Salleh M., Aklillu E., Bertilsson L.: Eur. J. Clin. Pharmacol. 68, 1033 (2012).
22. Kim S., Lee H., Lee W., Um T., Cho C., Chun S., Min W.: Thromb. Res. 130, 104 (2012).

Acta Poloniae Pharmaceutica – Drug Research, Vol. 71 No. 6 pp. 1107–1113, 2014 ISSN 0001-6837
Polish Pharmaceutical Society

DEVELOPMENT AND VALIDATION OF THE GC METHOD FOR THE QUANTITATIVE DETERMINATION OF SEMI-VOLATILE SOLVENTS IN THE PHARMACEUTICAL SUBSTANCE BOSENTAN

ELŻBIETA U. STOLARCZYK*, ALEKSANDRA GROMAN and WOJCIECH ŁUNIEWSKI

Pharmaceutical Research Institute, 8 Rydygiera St., 01-793 Warszawa, Poland

Keywords: Bosentan (BO), dimethyl sulfoxide (DMSO), ethylene glycol (EG), acetic acid (AA), GC method, validation

Bosentan is an active substance in the orphan drugs used to treat pulmonary artery hypertension (PAH). It is a dual endothelin receptor antagonist (ERA) with the affinity for both receptors of the A and B: endothelin-A (ET_A) and endothelin-B (ET_B). Under normal conditions, ET_A or ET_B receptors cause constrictions of the pulmonary blood vessels. By blocking this interaction, bosentan decreases pulmonary vascular resistance (1).

During the synthesis of bosentan the following solvents were used: ethanol, methanol, acetone, toluene, ethylene glycol, acetic acid, DMSO. Benzene is a potential contaminant of acetone. The acetic acid and ethylene glycol were used in the last stage of the bosentan synthesis. The DMSO was used prior to the last step in the synthesis. According to the International Conference on Harmonization (ICH) guidelines (2), all these residual solvents should be controlled to ensure the safety and quality of the finished product. Ethanol, acetone, methanol, toluene and benzene are determined by static headspace gas chromatography (HS-GC) methods. Volatile organic components (VOCs) are often determined by static headspace gas chromatography. This technique is very robust and combines easy sample preparation with good selectivity and low detection limits (high sensitivity). The HS technique is characterized by low sample matrix interference. The European Pharmacopoeia (Ph. Eur.) (3), describing a general HS procedure for Identification and Control of Residual Solvents in a drug substance, classifies solvents into three classes on the basis of their toxicity level and the degree to which they can be considered an environmental hazard (4). The AA and DMSO fall into Class 3 with the permissible daily exposure (PDE) of 50 mg/day (2). The EG is classified into Class 2 with the permissible daily exposure (PDE) of 6.2 mg/day (2). According to the Guideline Q3C (R5) 11 (2) the acceptable limits – maximum allowable limits in respect to sample preparation – are as follows: 620 ppm for the ethylene glycol, 5000 ppm for the acetic acid and 5000 ppm for the DMSO.

Headspace technique is not suitable for less volatile solvents because they cannot reach the injector and the column. As a consequence, the determination of high boiling/semi-volatile solvents becomes challenging. Therefore, the described method for the determination of high boiling VOCs like the acetic acid (AA), dimethyl sulfoxide (DMSO) and ethylene glycol (EG) presents an interesting example of dealing with high boiling/semi-volatile solvents.

In the literature there is a lack of descriptions of the methods for the simultaneous determination of the AA, DMSO and EG in bosentan and other substances. However, AA, DMSO and EG were determined separately, with other analytes and in different matrices (5–7). If a sample is not liquid, first, it has to be dissolved in a suitable medium to obtain a clear, homogeneous solution. This implies that residual VOCs have to be determined in the simultaneous presence of the sample matrix and dilution medium.

The development and validation of the gas chromatographic method with direct injection for

* Corresponding author: e-mail: e.stolarczyk@ifarm.eu; phone:+48 22 4563992; fax: +48 22 4563838

the quantitative determination of residual AA, DMSO and EG in the pharmaceutical active substance bosentan has been described in this work.

EXPERIMENTAL

Chemicals

Chemicals of an analytical grade were used for the validation. The active substance – bosentan – was synthesised in PRI (Pharmaceutical Research Institute, Warsaw, Poland). The 99.7% AA and 99.7% DMSO were provided by Sigma-Aldrich (Steinheim, Germany), the 99.5% EG and acetonitrile were provided by POCH (Gliwice, Poland).

Method optimization

In order to analyze the high boiling VOCs in a short time, so that the method could be implemented as a routine method of analysis, a further optimization was needed. The mixture of three high boiling point (b.p.) VOCs, namely AA (b.p. 118°C), DMSO (b.p. 189°C) and EG (b.p. 198°C), was used as the standard solution in order to generate data. A higher initial temperature and a faster ramp were selected. Thus, the analysis time of the optimized temperature program was reduced to 30 min. Working standard solutions were prepared based on different sample sizes to investigate the effect of the sample size. Different split ratios were also studied. The injector port temperature was considered to be a very important parameter. In order to investigate whether the bosentan decomposition was the reason of an unknown impurity at the retention time of the etylene glycol, the analyses under different injector temperatures were performed. The results of these investigations are presented in Figure 1. Stable injections have been achieved as the injector temperature was changed from 220 to 160°C. If the injector temperature is too low, the AA, DMSO and EG in the sample matrix may not vaporize completely before they are transferred into the column. Therefore, lower injector temperatures were not investigated. Complete GC parameters can be found in *Method description*.

Method description

Chromatographic conditions

Chromatographic separations were performed on a DB-WAX column (poly(ethylene glycol) film thickeness 0.5 μm, 60 m long, 0.32 mm ID). The experiments were performed on a Shimadzu GC-2010 gas chromatograph (GC) equipped with a Shimadzu AOC -20i autosampler and a flame ionization detector (FID).

GC parameters: inlet heater 160°C, detector 260°C, oven initial temperature 60°C, raised at the rate of 5°C/min to 185°C, then raised at the rate of 30°C/min to 240°C, 3 min at the final temperature. Nitrogen was used as the carrier gas at 100 kPa (constant flow, approximately 3.48 mL/min) and the split flow of 10 mL/min. The air flow rate of 400 mL/min, the hydrogen flow rate of 40 mL/min were used for FID and 1 μL was used for injection.

Preparation of standard and test solutions

All solutions were prepared directly before the analysis.

The acetonitrile (ACN) was used for the standard and test solution preparation as the diluent.

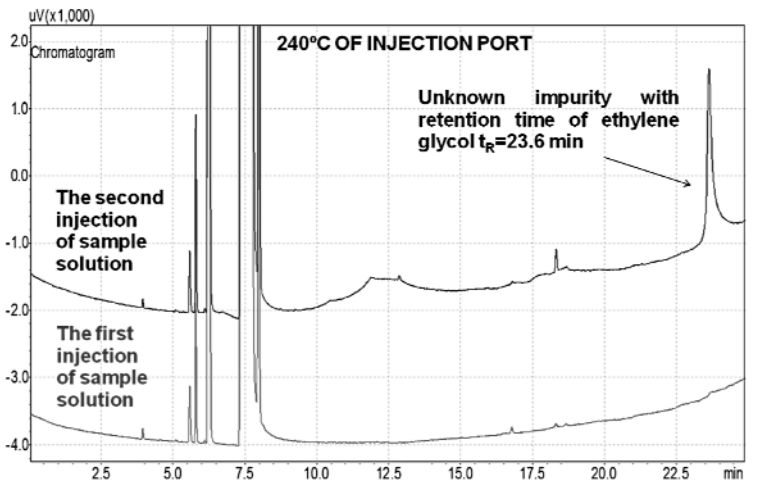

Figure 1. Overlain chromatograms of the first and second injection of the sample solution in temperature 240°C of the inlet heater

Standard solutions were prepared from the standard stock solutions by diluting an appropriate volume in the diluent to reach 100% of the specification limit concentrations – 620 µg/mL of EG, 5000 µg/mL of AA and 5000 µg/mL of DMSO (the SST solution) and to reach 10% of the specification limit concentrations – 62 µg/mL of EG, 500 µg/mL of the AA and 500 µg/mL of DMSO.

Test solutions were prepared by dissolving approximately 100 mg of bosentan in 1.0 mL of diluent.

Additional validation solutions were prepared as follows:

Specificity solution

The specificity solution was prepared by dissolving the appropriate amounts of all solvents from the synthesis route and a potential contaminant in the ACN to reach 100% of the specification limit concentrations: (ethanol (5000 µg/mL), methanol (3000 µg/mL), acetone (5000 µg/mL), toluene (890 µg/mL), EG (620 µg/mL), AA (5000 µg/mL), DMSO (5000 µg/mL), benzene (20 µg/mL).

Reference solutions

Spiked test solutions (Solution I, Solution II, Solution III, Solution IV) were prepared by dissolving 100 mg of bosentan in 1.0 mL of the corresponding standard solutions. Solution I contains 50 µg/mL of AA, 50 µg/mL of DMSO and 6.2 µg/mL of EG, that corresponds to 500 µg/mL of AA, 500 µg/mL of DMSO and 62 µg/mL of EG in the tested substance. Solution II contains 250 µg/mL of AA, 250 µg/mL of DMSO and 31 µg/mL of EG, that corresponds to 2500 µg/mL of AA, 2500 µg/mL of DMSO and 310 µg/mL of EG in the tested substance. Solution III contains 500 µg/mL of AA, 500 µg/mL of DMSO and 62 µg/mL of EG, that corresponds to 5000 µg/mL of AA, 5000 µg/mL of DMSO and 620 µg/mL of EG in the tested substance. Solution IV contains 74.4 µg/mL of AA, 60 µg/mL of DMSO and 6.2 µg/mL of EG, that corresponds to 6000 µg/mL of AA acid, 6000 µg/mL of DMSO and 744 µg/mL of EG in the tested substance.

Chromatographic procedure

For the GC analysis, a portion of each solution was transferred into a crimp-top vial with a fixed insert. The vial was closed with a PTFE/rubber crimp cap. One microliter of the blank (ACN), 1.0 µL of the test solution and six 1.0 µL replicate injections of the standard solution (SST solution) were chromatographed separately. Under the described conditions, the retention time is about 18.1 min, about 22.7 min and about 23.1 min for AA, DMSO and EG, respectively. The resolution of not less than 1.5 between the determined solvents was set as the system suitability requirement for the system suitability solution. To verify the system precision, six replicate injections of the system suitability solution were injected and the relative standard deviation (RSD) for the area peak of the residual solvents from six injections was calculated. The RSD of not more than 10.0% was set as the system precision acceptance criterium for the determined solvents peak areas. The acetic acid, DMSO and ethylene glycol in the test sample were determined against the mean areas of respective solvents obtained from the replicate injections of the system suitability solution.

Evaluation

In order to establish the validation parameters, the peak area (x), mean peak area ($\bar{x}$), relative standard deviation (RSD), and confidence interval $\bar{x} \pm \Delta x$ were evaluated.

The recovery was calculated using the following formula (1):

$$\text{Recovery} = \frac{W_{std} \cdot A_{sol}}{A_{std} \cdot W_{sol}} \times 100\% \qquad (1)$$

where: W_{std} – weight of the analytes in mg in 1 mL of the standard solution; W_{sol} – weight of the analytes in mg in 1 mL of the solution I, II, III or IV; A_{std} – peak area of the analytes in the chromatogram of the standard solution; A_{sol} – peak area of the analytes in the chromatogram of the solution I, II, III or IV.

For intermediate precision, the Snedecor F-test was performed using the following formula (2):

$$F = \frac{SD_1^2}{SD_2^2} \qquad SD_1 > SD_2 \qquad (2)$$

where: SD_1 – standard deviation from the results obtained by the first analyst. SD_2 – standard deviation from the results obtained by the second analyst.

RESULTS AND DISCUSSION

The validation procedure was performed based on the ICH requirement (8). During the validation, the specificity, precision, linearity, accuracy, limits of detection (LODs) and quantitation (LOQs) and robustness were investigated.

Specificity

The specificity of the method was evaluated by injecting the following samples: the blank (ACN –

diluent), test solution, reference solution, specificity solution, solvent solutions (ethanol solution, methanol solution, acetone solution, toluene solution, EG solution, AA solution, DMSO solution, benzene solution).

The peak area of the analytes in the chromatogram of the reference solution (spiked test solution) was greater than the corresponding peak area in the chromatogram of the test solution. The retention times of the analytes in the chromatogram of the reference solution correspond with the retention times of the analytes in the chromatogram of the solvent injected separately. Spiking the sample with the analyte did not cause the peak to split. In the chromatogram of the blank there were no peaks with the retention time of the analytes. All peaks in the chromatogram of the specificity solution are separated, $R_s \geq 1.5$ between the determined solvents (Table 1).

Table 1. Specificity results of the acetic acid, DMSO and ethylene glycol determination.

Compound name	Specificity solution		Solvent solutions injected separately
	Retention time [min]	R_s	Retention time [min]
Acetone	4.97	-	4.98
Methanol	5.62	5.21	5.62
Ethanol	6.03	3.70	6.03
Benzene	6.22	1.39	6.21
ACN	7.23	5.51	7.27
Imp. of ACN	7.60	2.43	7.62
Toluene	7.82	2.11	7.83
Acetic acid	18.13	93.09	18.01
DMSO	22.74	46.19	22.73
Ethylene glycol	23.14	3.84	23.14

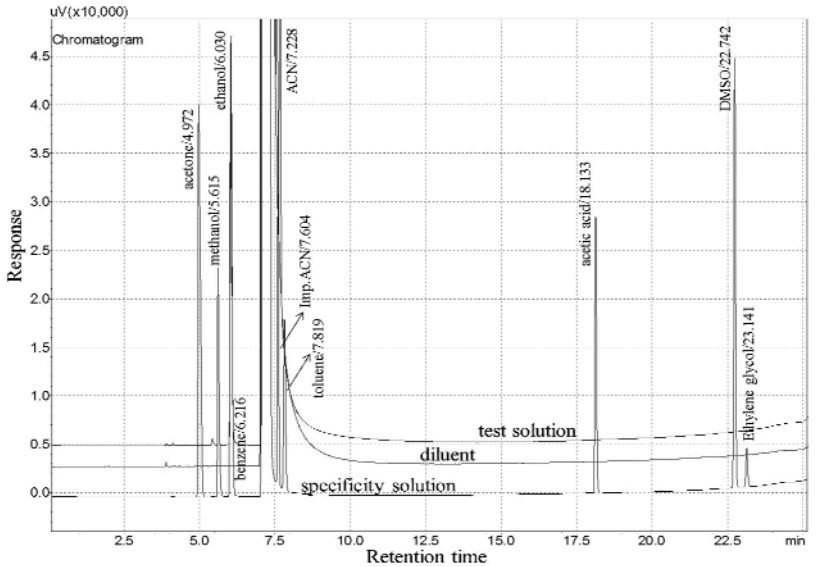

Figure 2. Overlain chromatograms of the diluent, test solution and specificity solution

Table 2. Validation results of the acetic acid, DMSO and ethylene glycol determination.

Parameter			Acetic acid	DMSO	Ethylene glycol
System precision	6 × 10% of spec. limit, RSD%	peak area	1.13	0.57	1.50
		t_R	0.01	0.07	0.08
	6 × 100% of spec. limit, RSD%	peak area	0.49	0.50	0.72
		t_R	0.006	0.009	0.007
Method precision – repeatability	3 × 10%, 50%, 100%, 120% of spec. limit, RSD%		6.39	6.38	6.54
	6 × 100% of spec. limit, RSD%		6.29	8.08	4.87
Method precision – intermediate precision	6 × 100% of spec. limit, RSD%		2.42	3.44	4.79
	Snedecor's F-test ($F_{5,5,exp.}$)		3.17	2.01	1.63
Accuracy	3 × 10%, 50%, 100%, 120% of spec. limit	$\overline{x} \pm \Delta x$	91.6 ± 3.7%	97.0 ± 3.9%	99.4 ± 4.1%
		RSD%	6.39	6.37	6.54

Table 3. The characteristic of regression lines ($y = ax + b$).

Parameter	Acetic acid	DMSO	Ethylene glycol
R^2	0.9994	0.9994	0.9991
SD_{xy}	1061.23	1716.30	190.91
y-intercept, b	–1612.13	–841.45	–183.62
SD_b	717.25	1159.98	129.03
$t_{b,exp.}$	2.25	0.73	1.42
Slope, a	216.97	351.50	252.55
SD_a	1.86	2.99	2.63
$t_{a,exp.}$	116.89	117.60	96.08

Figure 2 presents the comparison of the chromatograms obtained from the blank, test solution and specificity solution, respectively.

Precision

The precision of the method was established as the repeatability, system and intermediate precision. The repeatability was established by measuring triplicate independent preparations of the solutions I–IV with the analytes at 10, 50, 100 and 120% of the specification limit, 6 independent preparations of the solution III with the analytes at about 100% of the specification limit – prepared according to the solution preparation presented in *Additional validation solutions*. The system precision was established by measuring the response of six replicate injections of the standard solution – the solution with the AA, DMSO and EG at 100% of the specification limit – and six replicate injections of the standard solution – the solution with AA, DMSO and EG at 10% of the specification limit. The intermediate precision was established by performing a repeatability test on a different day and by a different analyst. The intermediate precision was determined by comparing the results obtained by both analysts using Snedecor's F-test.

The acceptance criteria were set up as the RSD value below 15, 10 and 15%, respectively. An additional criterium based on Snedecor's F-test was set up as: if $F_{experimental} \leq F_{critical}$ (for $\alpha = 0.05$, $f_1 = n_1 - 1$, $f_2 = n_2 - 1$), then, the difference between the results obtained by both analysts is insignificant. The criti-

cal parameter F (α = 0.05; f_1, f_2 = 5) is 5.05. The results of the method precision are presented in Table 2. It has been pointed out that all criteria were fulfilled and the method is precise.

Accuracy

The accuracy was assessed on the samples spiked with known amounts of the analytes (sample spiked with the analytes at 10, 50, 100 and, 120% of the specification limit). The accuracy of the method was established by assaying 12 sample solutions (triplicate independent preparations of solutions I–IV), blank (ACN) and test solution against the standard solution (three replicate injections). Then, the recovery results were calculated. The acceptance criteria were set up as the RSD value below 15% and the recovery value 100% ± 20%. The recovery results are presented in Table 2. All set up criteria were fulfilled. The method is accurate.

Limits of detection and quantitation

The sensitivity of the method was demonstrated by low LOD values obtained for the analytes. The limit of detection (LOD), calculated as the concentration which generated a peak about 3 times as high as the noise's height, and the limit of quantitation (LOQ) calculated as the concentration which generated a peak about 10 times as high as the noise's height, were found as 14 and 46 µg/mL for AA, 6.3 and 20 µg/mL for DMSO and 9.2 and 29.2 µg/mL for the EG, respectively.

Linearity

The linearity of the method was evaluated by analyzing 3 replicates of the standard solutions at ten concentration levels in the range between 10 to 120% of the specification limit. The AA concentrations ranged from 50.22 to 602.64 µg/mL, which corresponds with approximately 502.2–6026.4 µg/mL in the tested substance. The DMSO concentrations ranged from 50.44 to 605.28 µg/mL, which corresponds with approximately 504.4–6052.8 µg/mL in the tested substance and for EG they ranged between 6.38–76.56 µg/mL, which corresponds to approximately 63.8–765.6 µg/mL in the tested substance. The results of the statistical evaluation of the linearity experiments (correlation coefficient, y-intercept (b), slope of regression line (a), residual standard deviation (SD_{xy}), standard deviation of b (SD_b), standard deviation of a (SD_a) are all summarized in Table 3. The obtained correlation coefficients (R^2) of the linear regression for the determined solvents were above 0.999. This indicates a linear relationship between the analyte concentrations and the detector response. The critical parameter t (95%, 8) is 2.306. Our results show that the parameters a and b are statistically important, the method is characterized by a very good precision and is free from systematic errors.

Robustness

In order to evaluate the robustness of the method, the influence of the variations of such method parameters as the pressure, temperature and rate were investigated to ensure the separation of the solvents with the use of different chromatographic conditions. System suitability (SST) requirements were checked for the variations of ± 10 kPa on the carrier gas flow, ±5°C on the initial oven temperature, ± 1°C/min on the rate. Under all the deliberately changed chromatographic conditions, all system suitability criteria were within the limits (the resolutions (R_s) between two analyte peak > 1.5, and RSD < 10.0%). The obtained results indicate that the studied variations of the GC conditions do not cause any significant changes in the resolutions and the method is robust.

CONCLUSIONS

A direct injection GC is the preferred method to determine AA, DMSO and EG. A preliminary direct injection GC method was developed using a DB-WAX column (stationary phase: (poly(ethylene glycol); 60 m × 0.32 mm i.d., 0.5 µm film thickeness) at 240°C of the inlet heater. During the method, evaluation matrix effects were observed, resulting in an unknow impurity – a decomposition peak with the retention time of EG. Reports on drug matrix effects in the determination of residual solvents are rare. Kersten (9) reported a study on matrix effects in the GC determination of residual solvents in a drug substance (acidic, basic and neutral). It was claimed that no matrix effects were observed. In this paper, attempts were made to overcome the matrix effects and it was found that they can be eliminated by changing the inlet heater temperature. Bosentan is a polar compound that contains hydroxy group. The melting point of bosentan is 110°C and it is therefore possible that a higher injector temperature results in the decomposition of bosentan, which represents itself as a peak with the retention time of EG. The method described above represents an interesting tool for the analysis of high boiling VOCs, namely A, DMSO and EG in matrices which are unstable at higher temperatures. Its considerable advantage is that the specificity enormously increased for the investigated solvents after reducing

the injector temperature. This is the first method ever reported in the literature, which concerns the separation and quantitation of AA, DMSO and EG.

In this study, the validation of a new GC method for the simultaneous control of residual AA, DMSO and EG in bosentan was performed. During the validation procedure, which was carried out according to the ICH guidelines Q2R1, the specificity, precision, accuracy, limits of detection and quantitation and robustness were evaluated. All set up criteria were fulfilled. The method is specific, accurate, linear and shows a satisfactory level of precision. The determined solvents can be detected and quantified at µg/mL level. As a consequence, these solvents can be quantified in substance bosentan far below their respective official limit concentrations. The validation procedure shows that the method is suitable for its intended purpose.

Acknowledgments

The study was supported by the European Union under the European Regional Development Fund No. UDA-POiG.01.03.01-14-062/09-00 "Innovative technologies of cardio-vascular medicines of special therapeutic and social importance". We wish to thank Ms. Maria Puchalska, Ph.D., Ms. Joanna Zagrodzka, Ph.D. and Ms. Katarzyna Sidoryk, Ph.D. from PRI for their support in this study.

REFERENCES

1. http://www.ema.europa.eu/docs/pl_PL/document_library/EPAR__Product_Information/human/000401/WC500041597.pdf
2. Harmonized Tripartite Guideline on Impurities: Guideline for residual solvents (Q3C(R5), International Conference on Harmonization of Technical Requirements for Registration of Pharmaceuticals for Human Use (ICH), Geneva 1997.
3. Identification and Control of Residual Solvents (2.4.24). European Pharmacopoeia, 8th edn., European Directorate for the Quality of Medicines & HealthCare, Strasbourg, France 2014.
4. Residual solvents (5.4). European Pharmacopoeia, 8th edn., European Directorate for the Quality of Medicines & HealthCare, Strasbourg, France 2014.
5. Tian J., Chen G., He Z.: J. Chromatogr. Sci. 52, 36 (2014).
6. Kialengila D.M., Wolfs K., Bugalama J., Vanschepdael A., Adams E.: J Chromatogr. A 1315, 167 (2013).
7. Molever K.: J. Cosmet. Sci. 61, 225 (2010).
8. Harmonized Tripartite Guideline on Validation of Analytical Procedures: Text and Methodology (Q2(R1), International Conference on Harmonization of Technical Requirements for Registrations of Pharmaceuticals for Human Use (ICH), Geneva 2005.
9. Kersten, B.S: J. Chromatogr. Sci. 30, 115 (1992).

Project co-financed by the European Regional Development Fund under the framework of the Innovative Economy Operational Programme.

UDA-POIG contract no 01.03.01-14-062/09 „Innovative technologies of cardio-vascular medicines of special therapeutic and social importance": www.ifarm.eu/poig/cardio

Acta Poloniae Pharmaceutica – Drug Research, Vol. 71 No. 6 pp. 1114–1118, 2014 ISSN 0001-6837
Polish Pharmaceutical Society

MEASUREMENT OF THE RADIOACTIVITY OF ^{137}Cs IN MATERIALS OF PLANT ORIGIN WITH POTENTIAL RADIOACTIVE CONTAMINATION

MAREK WASEK[1]*, PIOTR WROCZYŃSKI[1], SYLWIA SOŁOBODOWSKA[1], KAMIL SZEWCZAK[2] and ZUZANNA JAROSZ[2]

[1]Department of Drug Bioanalysis and Analysis, Faculty of Pharmacy with the Laboratory Medicine Division, Medical University of Warsaw, 61 Żwirki and Wigury St., 02-091 Warszawa, Poland
[2]Laboratory of Individual and Environmental Doses, Central Laboratory for Radiological Protection, 7 Konwaliowa St., 03-194 Warszawa, Poland

Keywords: radioactive contamination of medicinal plants, environmental ^{137}Cs

One of the most dangerous phenomena of the XX century was the introduction of radionuclides into the (natural) environment what, when uncontrolled, can lead to a radioactive contamination. Serious contamination may be a consequence of the release of radioactive gases during nuclear power plants disasters, tests of nuclear weapons and to smaller extent, improper storage of radioactive materials as well as radioactive fallouts from nuclear power plants. Raw materials used in different industry branches that were acquired/collected from contaminated areas pose a risk to human health. One example of such materials are plants used in medicinal preparations. They are mainly contaminated with ^{137}Cs. The half-life of this radionuclide is long enough to allow it to be deposited in plants and soil for a very long time. Nuclear tests in the atmosphere contributed to the wide spread of fission and activation products of this isotope. It was estimated that the activity of about 9.6×10^{17} Bq ^{137}Cs was introduced this way to the atmosphere, since 76% was deposited in the northen hemisphere and 24% in the southern (1). Another important source of ^{137}Cs contamination are nuclear power plants accidents. Chernobyl disaster released the greatest amount of ^{137}Cs (activity around 7×10^{16} Bq) (2.) Even though it has been 28 years ago, because of the close geographic vicinity, ^{137}Cs contamination can be still observed in Poland. Figure 1 shows the average deposition of the ^{137}Cs concentration in soil in particular provinces of Poland in 2010 (3). These measurement results indicate that the concentration of ^{137}Cs radioisotope in particular samples taken from 10 cm thick soil layer oscillated from 0.22 to 23.78 kBq/m^2. The highest levels – registered in the South of Poland – are caused by intensive local rainfall which occurred in those territories at the time of Chernobyl accident. The highest soil average concentration of the ^{137}Cs ranging from 3 to 6 kBq/m^2 was found in Opole, Silesian and Lower Silesian voivodeships.

The ^{137}Cs undergoes radioactive decay with the emission of β particles with a mean energy of 0.52 MeV and γ rays of energy 661.7 keV. Its presence in soil has substantial effect on the contamination of human food chain. Cesium gets to the plants through the passive deposition on the aerial parts of plants as well as *via* roots. The latter way of ^{137}Cs uptake has long-term effects.

Many plant and food products may be contaminated with ^{137}Cs. According to Polish Informacyjna Agencja Radiowa (Information broadcasting agency), Belorussian Sanitary Inspection found that some types of wines are produced using radioactively contaminated fruits. Higher than allowed radioactive concentrations were also detected in many other food products. Areas heavily affected by Chernobyl accident (including Poland) still suffer from the consequences of this nuclear plant disaster. It can be suspected that companies trading with groundcover products and wanting to reduce costs, may be looking for lower quality products from unknown

* Corresponding author: e-mail: marek.wasek@wum.edu.pl

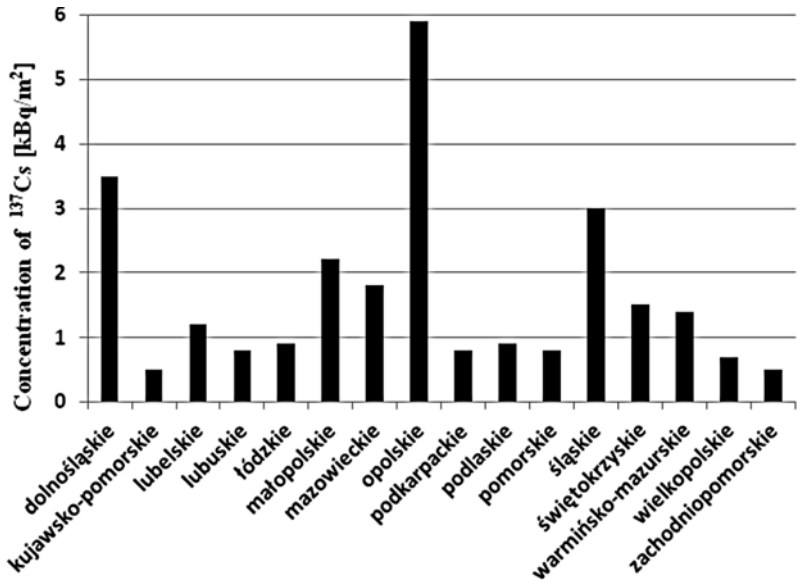

Figure 1. Average surface concentration of ^{137}Cs (10 cm-thick soil layer) in 2010 in particular provinces of Poland

Table 1. Plant-based raw materials used in the study along with the site of collection.

Plant-based raw material	Site of collection
Vaccinium vitis-idaea fruits *Vaccinium myrtillus* fruits	1. Solska Wilderness (Hamernia vicinity, near Józefów) 2. Kuźnica Ligocka – Bory Niemodlińskie 3. Bory Dolnośląskie 4. Suche Rzeki – Bieszczady
Vaccinium oxycoccus fruits	1. Solska Wilderness (Hamernia vicinity, near Józefów) 2. Przemyśl vicinity 3. Gmina Lutowiska – Bieszczady 4. Lasy Stobrawsko-Turawskie

Table 2. Dietary supplements used in the study.

Main component	Supplement brand name
Vaccinium vitis-idaea fruits	1.Biotta 2. Dried lingonberry – Biofit
Vaccinium myrtillus fruits	1. Lutein plus 2. Solgar bilberry 3. Pryzmin
Vaccinium oxycoccus fruits	1.Urinal 2. Urinatin Megafryt 3. Dried swamp cranberry – Biofit 4. Colfarm swamp cranberry 5. Solgar swamp cranberry 6. Żurawinea Max

sources. Sanitary Inspection in Belarus and Ukraine came across radioactive frozen raspberries and currants. Contaminated products very often came to European Union countries, where limits are lower than those in Belarus. Regarding the total cesium radionuclides concentration in foodstuff, the European Union limit stands at 600 Bq/kg. The importance of this issue is evidenced by the fact that

one of the European Parliament debates, taking place in Strasburg (14 February 2011), entitled „Radioactive contamination of foodstuff", was devoted to the subject of this article (4).

EXPERIMENTAL

Tables 1 and 2 show herbal medicines and dietary suplements, respectively, that were used in this study.

Radioactivity of ^{137}Cs was measured using γ-ray spectroscopy, which enables to quantify radioactivity ranging from 0.5 to 4000 Bq/kg or Bq/l in food and environmental samples such as soil, grass and ground water. Canberra γ-ray spectroscopy system coupled with three semi-conductor HPGe detectors and Genie 2000 software were used. The γ-ray spectrometric method for determining ^{137}Cs is based on the measurement of the intensity of γ radiation at 661.6 keV in both, sample and standard. Multi-γ

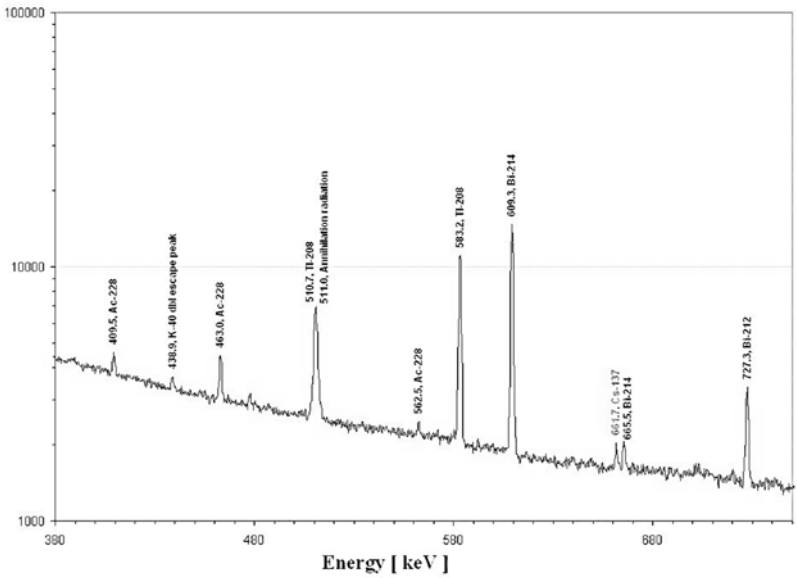

Figure 2. γ-Ray spectrum of background. Time of measurement – 60 h

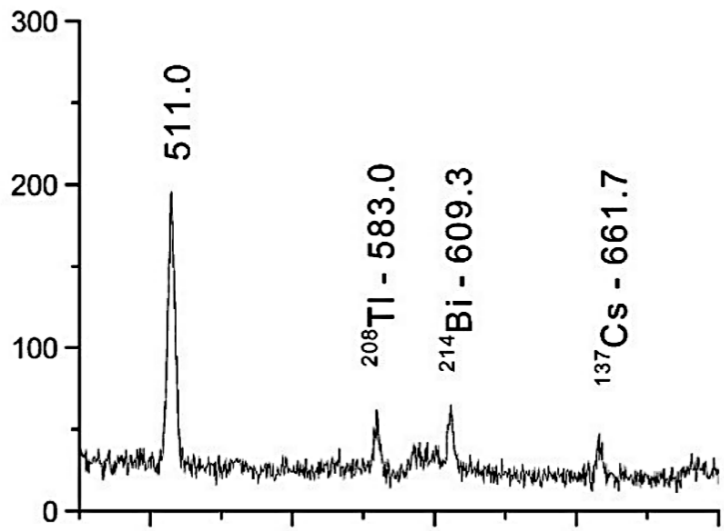

Figure 3. γ-Ray spectrum for dietary supplement Urinal. Time of measurement – 24 h

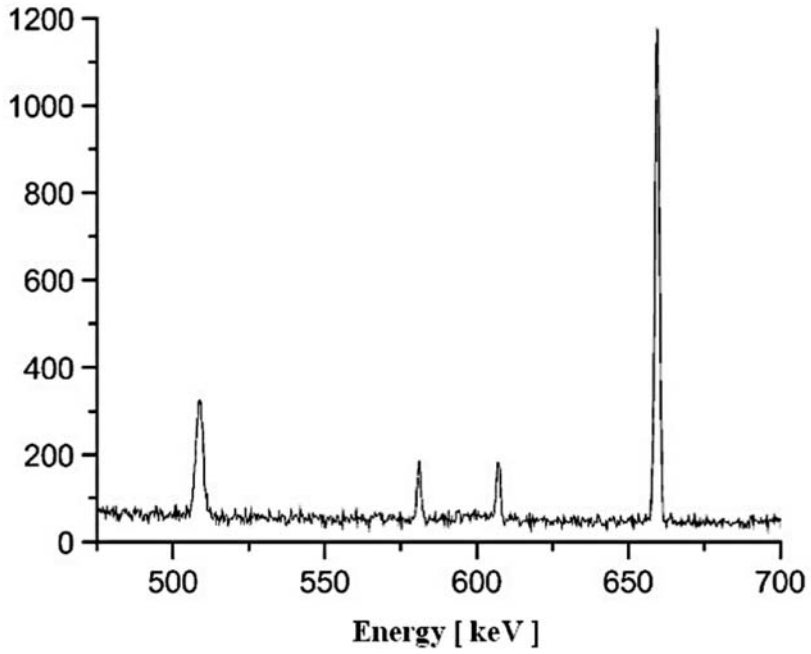

Figure 4. γ-Ray spectrum of *Vaccinium vitis-idaea* L. fruits collected in Bory Niemodlińskie. Time of measurement – 24 h

Table 3. Concentration of ^{137}Cs in plant-based raw materials with the site of collection.

Plant-based raw material Site of collection	Total activity of ^{137}Cs [Bq/kg]
Vaccinium vitis-idaea fruits	
1.Solska Wilderness (Hamernia vicinity, near Józefów)	5 ± 1*
2. Kuźnica Ligocka – Bory Niemodlińskie	30 ± 5
3. Bory Dolnośląskie	25 ± 4
4. Suche Rzeki – Bieszczady	3 ± 1
Vaccinium myrtillus fruits	
1. Solska Wilderness (Hamernia vicinity, near Józefów)	4 ± 1
2. Kuźnica Ligocka – Bory Niemodlińskie	27 ± 4
3. Bory Dolnośląskie	20 ± 4
4. Suche Rzeki – Bieszczady	1.0 ± 0.2
Vaccinium oxycoccus fruits	
1. Solska Wilderness (Hamernia vicinity, near Józefów)	4 ± 1
2. Przemyśl vicinity	8 ± 2
3. Gmina Lutowiska – Bieszczady	6 ± 1
4. Lasy Stobrawsko-Turawskie	9 ± 2

* – Expanded uncertainty; Coverage factor k = 3

mixtures in Marinelli beakers with 100 and 450 mL acitive volumes and 1.0, 1.14 and 1,15 g/cm^3 active densities were used covering the γ energy range from 88 to 1836 keV.

The 100 or 450 mL Marinelli beakers were weighted and filled with samples. If the sample volume was lower than the active volume of the beaker, distilled water was added in case of liquid samples.

In case of solid and semi-solid samples, non-reactive and easily mixible material (such as talk) was added.

The energy dependence on the detection efficiency was determined with reference standard and used to calculate the concentration of radionuclides in the samples..

RESULTS

Figure 2 shows the level of background γ radiation measured using Canberra spectrometric system. It was used as an analytical blank. The 661.6 keV line corresponding to ^{137}Cs had intensity of 3×10^{-4} cps. This value was taken into account in determination of ^{137}Cs radioactivity in all samples and standards. Other lines present in the spectra are of natural origin and had no influence on the results. Figure 3 shows the γ-ray spectrum obtained for dietary supplement Urinal. ^{137}Cs activity was below the detection limit.

Figure 4 shows the γ-ray spectrum of *Vaccinium vitis-idaea* L. fruits collected in Bory Niemodlińskie. Elevated radioactivity of ^{137}Cs (around 30 Bq/kg) is clearly visible.

The ^{137}Cs radioactivity was below the detection limit in all dietary supplements tested. Table 3 shows the activity of ^{137}Cs found in other raw materials tested.

CONCLUSIONS

None of the dietary supplements analyzed contained radioactive ^{137}Cs isotope, what indicates proper collection of raw plant materials or low concentration of these raw materials in analyzed samples.
Concentrations of radioactive cesium found in *Vaccinium vitis-idaea* L. and *Vaccinium myrtillus* are variable and depend on the site of raw material collection. They are 8 times greater for materials collected in southern voivodeships (Opole and Lower Silesian) than for those acquired in Bieszczady, what correlates with the soil contamination of these regions.

Much lower activity was found in case of *Vaccinum oxycoccos* samples (4–9 Bq/kg). There were no differences for samples collected at different areas.

The activity levels measured (maximum 30 Bq/kg) lead to negligibly low effective doses (around 0.03 mSv) even after single consumption of 1 kg. Such equivalent doses correspond to the single chest x-ray and can be considered as hormetic dose.

REFERENCES

1. UNSCEAR: Ionizing Radiation: Levels and Effects. Volume I: Levels, Volume II: Effects. United Nations Scientific Committee on the Effects of Atomic Radiation, Report to the General Assembly, with scientific annexes, E.72.IX.17 (1972).
2. UNSCEAR: Sources and Effects of Ionizing Radiation: Official Records of the General Assembly, Nineteen Session, Suplement No. 14. (1995).
3. Activities of the President of National Atomic Energy Agency (PAA) and Assessment of Nuclear Safety and Radiological Protection in Poland in 2012; p. 90 (2013).
4. http://www.europarl.europa.eu/sides/getDoc.do?pubRef=-//EP//TEXT+TA+P7-TA-2011-0055+0+DOC+XML+V0//EN

Erratum

In the paper: “Influence of spray drying manufacturing parameters on quality of losartan potassium microspheres.” Acta Pol. Pharm. Drug Res., Vol. 71, No. 5, pp. 833–841 (2014), the correct authorship should read:
Andrzej Jankowski, Radosław Balwierz, Dominik Marciniak, Dariusz Łukowiec, Janusz Pluta

In Acta Pol. Pharm. Drug Res. Vol. 71, issue 5 (2014), in Table 3, p. 805, in the last column and line 9 the letters "FTMFTM" should be removed.